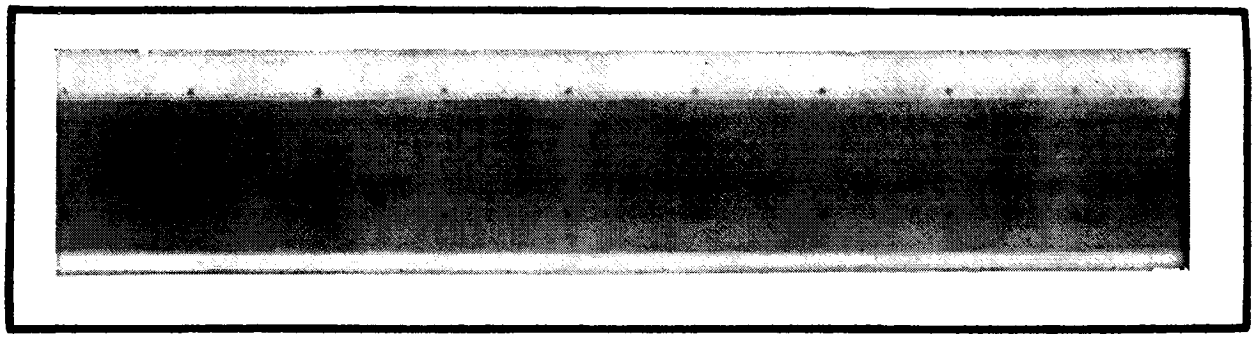

Axiomatix

SHUTTLE COMMUNICATION AND TRACKING SYSTEMS SIGNAL DESIGN AND INTERFACE COMPATIBILITY ANALYSIS

Final Report
Contract No. NAS9-17384

Prepared for
NASA Lyndon B. Johnson Space Center
Houston, Texas 77058

Axiomatix
9841 Airport Boulevard
Suite 912
Los Angeles, California 90045

Axiomatix Report No. R8606-3
June 16, 1986

Table of Contents

List of Figures

EXECUTIVE SUMMARY

Axiomatix has been tasked by NASA/JSC to provide analysis for the Space Shuttle Program in the areas of:

1) S-band antenna system enhancements
2) S-band payload communication system enhancements
3) Advanced communication and tracking system conceptual design and analysis

In addition to the above tasks, Axiomatix was directed by JSC to support the Shuttle Orbiter Radar Test and Evaluation (SORTE) mission at the White Sands Missile Range (WSMR).

Axiomatix was given the assignment of evaluating various options for the Dedicated Payload Communication Link (DPCL) under Task 1. Appendix A is an annoted viewgraph presentation given by Axiomatix on the subject of the DPCL. Specific subjects addressed include:

1) Payload to DPCL power transfer in the proximity of the payload,
2) DPCL antenna pointing considerations,

and

3) DPCL transceiver implementations which can be mounted on the deployed antenna boom.

Preliminary conclusions of the study to date indicate that a limiter will be required at the input to the DPCL preamplifier. Suggestions that a man-in-the-loop pointing scheme using a power meter to peak the beam would not be practical unless a highly nonlinear calibration curve (near vertical at the operating point) is used. Finally a transceiver design was evaluated, and it was concluded that such a design is feasible provided that a careful evaluation of all components within the loop is performed.

Additional analysis of the Space Telescope performance was conducted under Task 2 of this contract. It is shown that the Space Telescope may have a BER so poor that the data would be unusable at the proposed 500 bps data rate of Bi-ϕ-L data. This problem, however, would not occur at 4 kbs, 32 kbs or 1 Mbs due to the diminished effect

of the PI loop on the data. The basis for this problem lies in the fact that the data is heavily filtered by the action of the PI phase locked loop whose nominal bandwidth is 1000 Hz. Whether or not the link would work depends upon knowing the exact operational PI loop bandwidth.

The effect of the bit synchronizer in the PSP is not included, but rather ideal unfiltered bit synchronization is assumed. If it were included, then probably the threshold effect would be more pronounced.

It is recommended that 500 bps not be considered a viable data rate, due to the fact that the link may or may not work depending on the actual PI loop bandwidth. This work is documented in Appendix B of this final report, which is a copy of Axiomatix Report No. R8509-1.

The feasibility of using GPS for attitude determination and control for large spacecraft was examined by Axiomatix under Task 3. GPS signals from a particular Navstar satellite can be simultaneously received by three (or more) antennas aboard the host vehicle. Phase comparison of two received signals can yield the angle of the baseline between the two antennas and the transmitting Navstar. If the angles are measured with respect to different Navstars, the absolute orientation of the spacecraft can be determined. Through observation of the attitude or attitude rates (or some combination thereof) experience by the baselines between antennas, the vehicle can be stablized or re-oriented. Two orthogonal baselines, one along the attitude and one perpendicular to it, can be used to determine the attitude and rotational position. Preliminary analysis indicates that use of a standard GPS link would produce an RMS error of about 0.5° using the P code, while tracking the carrier would yield an error of about 0.003°. This work was documented in Axiomatix Report No. R8605-2, which is included as Appendix C of this final report.

The SORTE support task involved Axiomatix participation in all phases of the SORTE tests. The objective of the SORTE program was to quantify the Ku-band radar tracking accuracy using calibrated WSMR radar and optical tracking equipment, with

helicopter and balloon targets. As an adjunct to the SORTE accuracy tests, a series of Tethered Satellite System (TSS) tests were conducted to prove the feasibility of using the Ku-band radar with a conductive tether. Prior to the TSS tests, Axiomatix evaluated the tether effect by analysis using the radar cross section of the tether as a measure of performance. This analysis concludes that the tether should not be a problem, and is documented in an Axiomatix memo included as Appendix D of this report. Finally, the availability of the Ku-band radar in a system configuration allowed us to run a series of servo performance tests to determine the limits of radar stability and scan degradation at extreme angles. This is relevant to the TSS mission, during which acquisition may be required to angles off zenith.

The Axiomatix tasks for SORTE and TSS included the following:

- Participate in the sell-off of the Qual System and System Test Equipment (STE) to NASA.
- Write test plans and Trouble Shooting Sequences (TSS).
- Act as stand-in test director during absense of NASA personnel at WSMR.
- Review test data.
- Conduct servo tests
- Participate in sell-off equipment to HAC at completion of tests.

Results of the servo tests comprise significant portion of the report.

SORTE

Introduction

Axiomatix was tasked to participate in the Shuttle Orbiter Radar Test and Evaluation (SORTE) at the White Sands Missle Range (WSMR). The Axiomatix test experience, gained during the Baldwin Hills System Design Verification Test (SDVT) was deemed extremely helpful toward the success of the SORTE tests. The objective of the SORTE program was to quantify the Ku-band radar tracking accuracy using calibrated WSMR radar and optical tracking equipment, with helicopter and balloon targets. As an adjunct to the SORTE accuracy tests, a series of Tethered Satellite System (TSS) tests were conducted to prove the feasibility of using the Ku-band radar with a conductive tether. Finally, the availability of the Ku-band radar in a system configuration allowed us to run a series of servo performance tests to determine the limits of radar scan stability and scan degradation at extreme angles. This is relevant to the TSS mission, during which acquisition may be required at angles off zenith.

The Axiomatix tasks for SORTE and TSS included the following:

- Participate in the sell-off of the Qual System and System Test Equipment (STE) to NASA.
- Write test plans and Trouble Shooting Sequences (TSS).
- Act as stand-in test director during absence of NASA/JSC personnel at WSMR.
- Review test data.
- Conduct servo tests
- Participate in sell-off of equipment to HAC at completion of tests.

Portions of these tasks were covered under a prior contract, and documented in Axiomaitx report No. R8604-4, April 24, 1986, forNASA/JSC contract No. NAS9-17139. Generally,tasks performed during the first half of 1985 were covered under the prior contract and tasks or portions of tasks performed during the latter half of 1985 were

covered by this contract. The only task performed exclusively under the prior contract was the system sell-off to NASA. Most other tasks, other than the sell-off back to HAC, were performed during the whole year. Those tasks charged to NASA/JSC contract No. NAS9-17389 are documented in this report.

Servo Performance Test

In order to quantify the servo scan performance outside zone 1 (a 30° cone centered at zenith), a series of scans were performed centered at the angles depicted in Figure 1. Thirty five scans were run with the designates as shown by large dots at 20° increments of roll and pitch. Figure 1, supplied by JSC, is a template of the Ku-band obscuration zone in roll/pitch space. In addition, two sets of three concentric "circles" are centered, one set each, at the positive and negative beta stops. The inner circle is the locus of the beam center at the representative beta stop as alpha is rotated. The middle circle represents a beta of ±71°, the angle at which a radar scan is presumed to go unstable. The outer circle represents a beta of ±41°,the angle within which, if a scan is initiated, the ±71° critical angle will be entered. Note, that several of the test scans were inititated at angles greater than 41°. The subsequent instability is evidenced in subsequent scan patterns. (See Figure 2 for example). A normal radar scan at close or intermediate range searches a ±30° cone in one minute: in the proximity of the payload bay, denoted by the heavy outline near 60° roll, a slow, long-range scan is used. This prevents the radar beam from coasting into the payload bay before obscuration logic can shut off the transmitter. Time-on-target (TOT) for such a scan is large. For example, Figure 3, which is a plot of cumulative probability that time-on-target is exceeded, shows a $P(TOT \geq 100 \text{ msec}) = 1$.

Scan data, in the form of alpha vs. beta vs. time, was recorded on disc in the STE, and was subsequently transferred to floppy disc for use by Axiomatix. The HAC plotting routine "SERVO" was used to make plots of roll vs. pitch, x vs. y, time-on-target vs. time, and scan overlap vs. time. The x vs. y plot is a polar plot of the scan spiral in inertial space, e.g., the projection of the scan onto a unit sphere. Inertial coordinates are

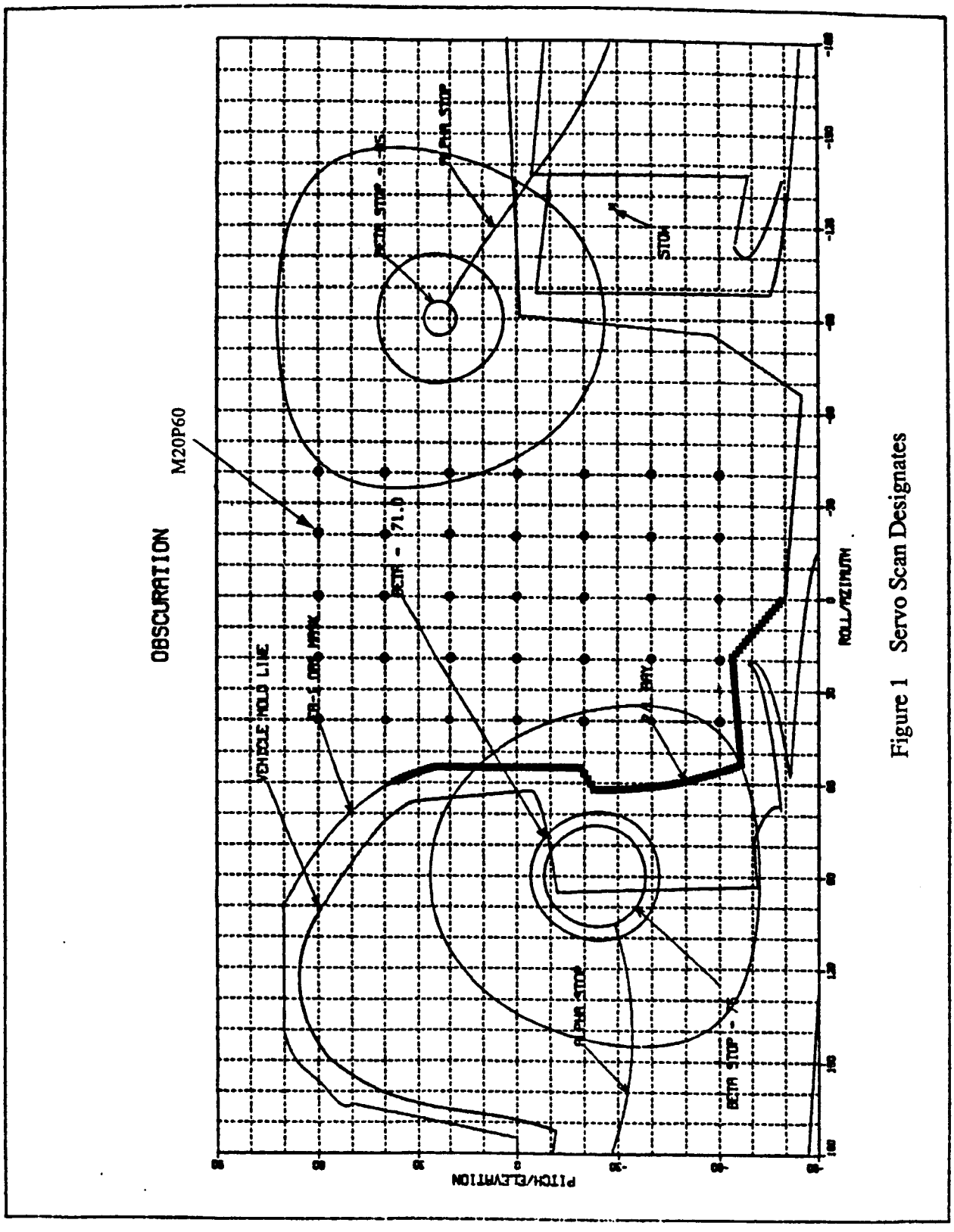

Figure 1 Servo Scan Designates

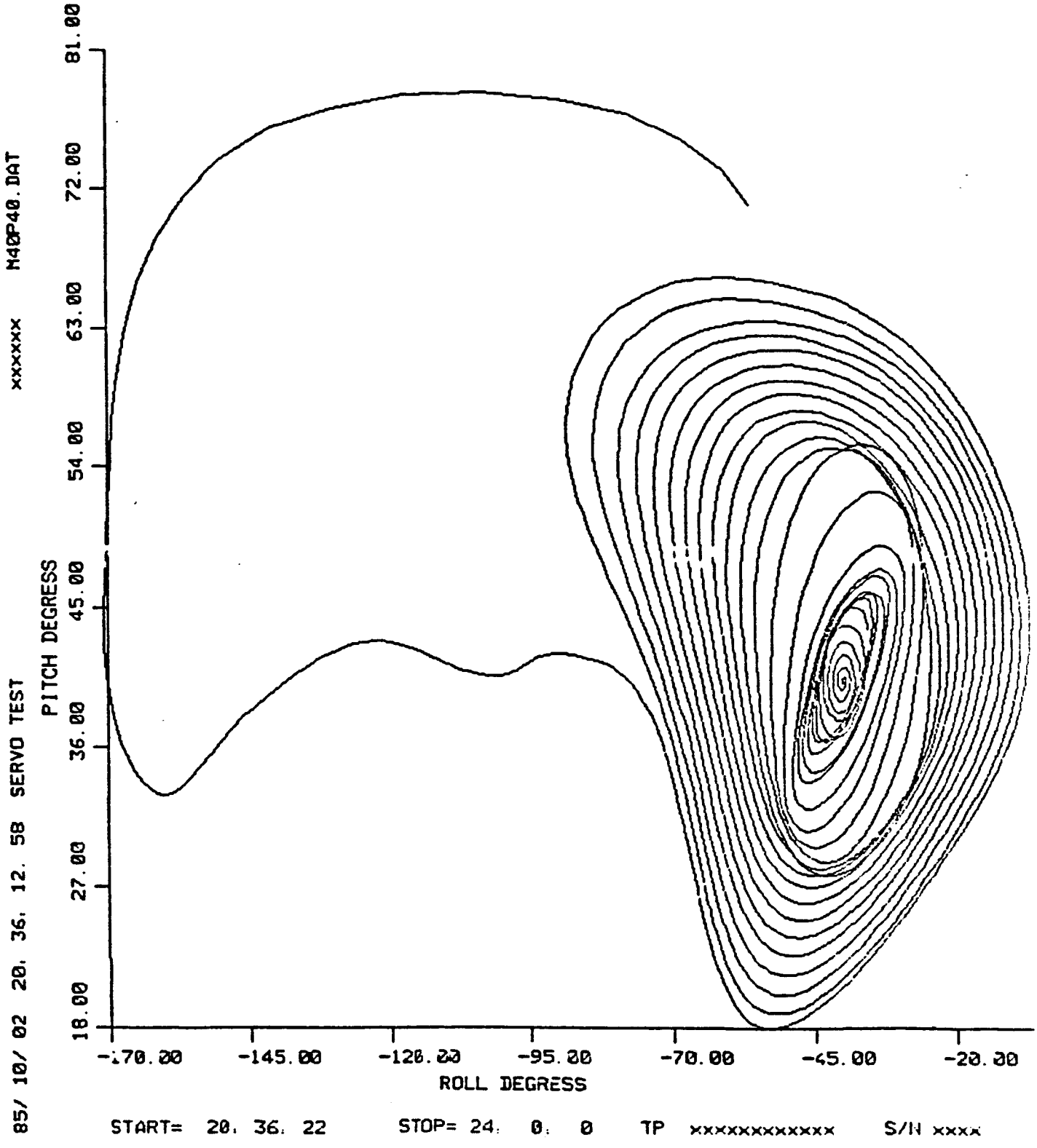

Figure 2 Servo Runaway

Figure 3 TOT Greater than 100 msec for Slow Scan

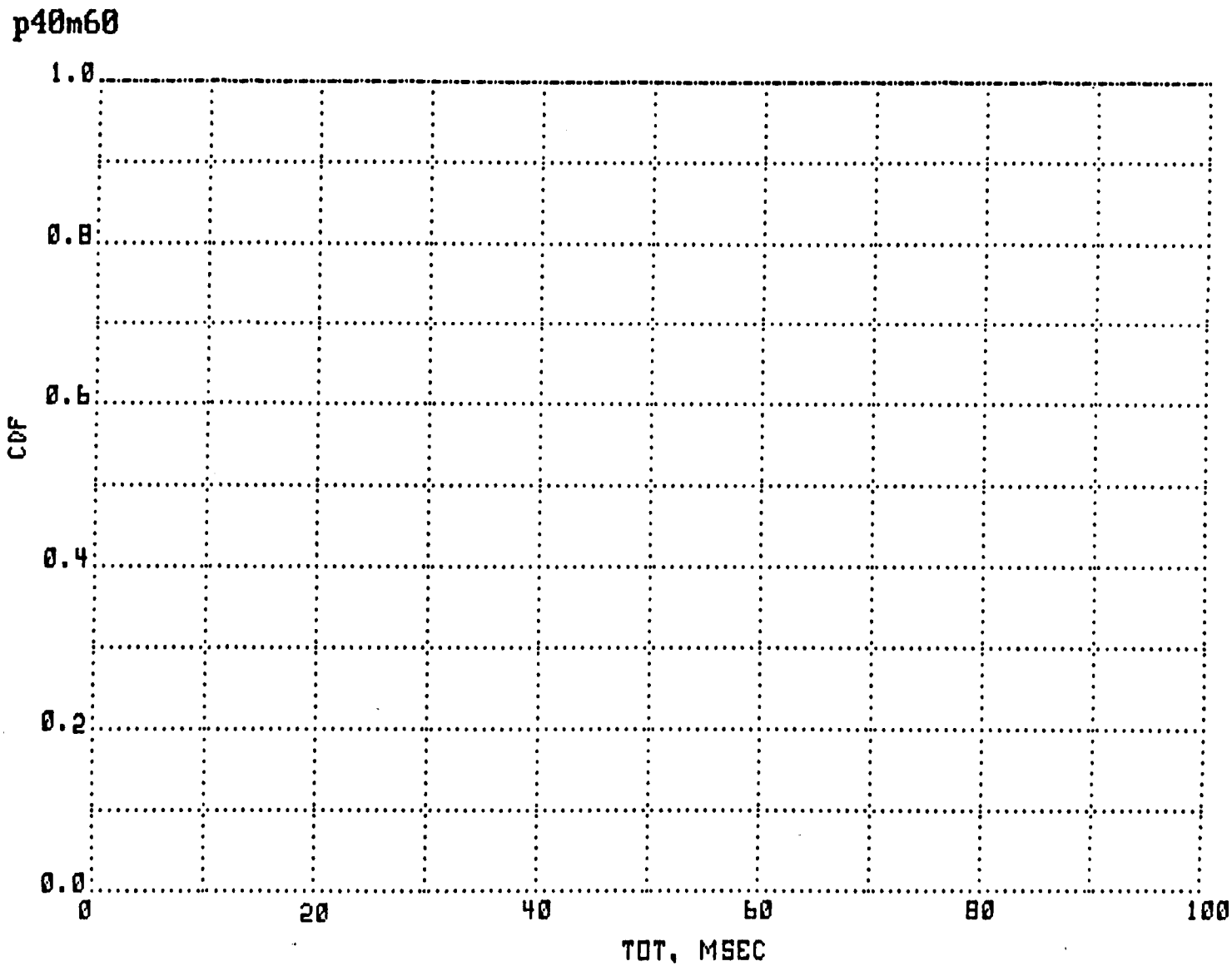

calculated from α and β as shown in Figure 4. The inertial scan is centered at α_0 and β_0, and ρ and Θ are derived as shown. The inertial angles x and y are then calculated from $\rho \cos(\Theta)$ and $\rho \sin(\Theta)$. The quality of the scan can be estimated by comparing the spiral with a "model" scan centered at zenith. In addition to scan patterns, the HAC "SERVO" program plots time-on-target vs. time and scan overlap vs. time. "SERVO" plots TOT and overlap at 45° increments of Θ.

Time-on-target is calculated from ρ and Θ as shown in Figure 5. The radial vectors ρ_1 and ρ_2, represent arcs on a unit sphere pointing to two adjacent 25 msec samples separated by an arc ℓ. Time-on-target is given as $\Delta t/\ell$ times antenna 3dB beamwidth (BW). The scan overlap shown in Figure 6 as $0' = \rho 3 - (\rho_2 + \rho_1)/2$ with overlap = $100^* (1 - 0'/B)$. If 0' is greater than BW, we set 0' equal to BW, so that overlap is 0%. This is an approximation to scan overlap; a more accurate but cumbersome representation would calculate overlap based on an arc perpendicular to the arc betweeen two data points, as shown in Figure 7. Both measures were implemented by Axiomatix. Sample plots show no significant difference in accuracy, but the simple approximation is much faster to calculate, and is the one used. The time-on-target and scan overlap vs. time plots provide another measure of scan quality, but still do not provide a firm delineation between "good" scans and "bad" scans.

In an effort to provide a more quantitative measure of scan performance, we have calculated TOT and scan overlap at every data point, and computed a histogram of these parameters. In lieu of plotting the histograms, which are probability density functions, the cumulative distribution (CDF) is plotted, which is the integral of the point density function. The form we have chosen to plot is CDF is one minus the traditional distributiion function, i.e., we have plotted the probability that TOT and overlap are exceeded vs. TOT and overlap. In order to determine if a particular value TOT is exceeded, the ordinate value for the TOT of interest is read from the plot. Note, that these plots are parameters in ρ the angular distance from the center of the scan. The first curve in each

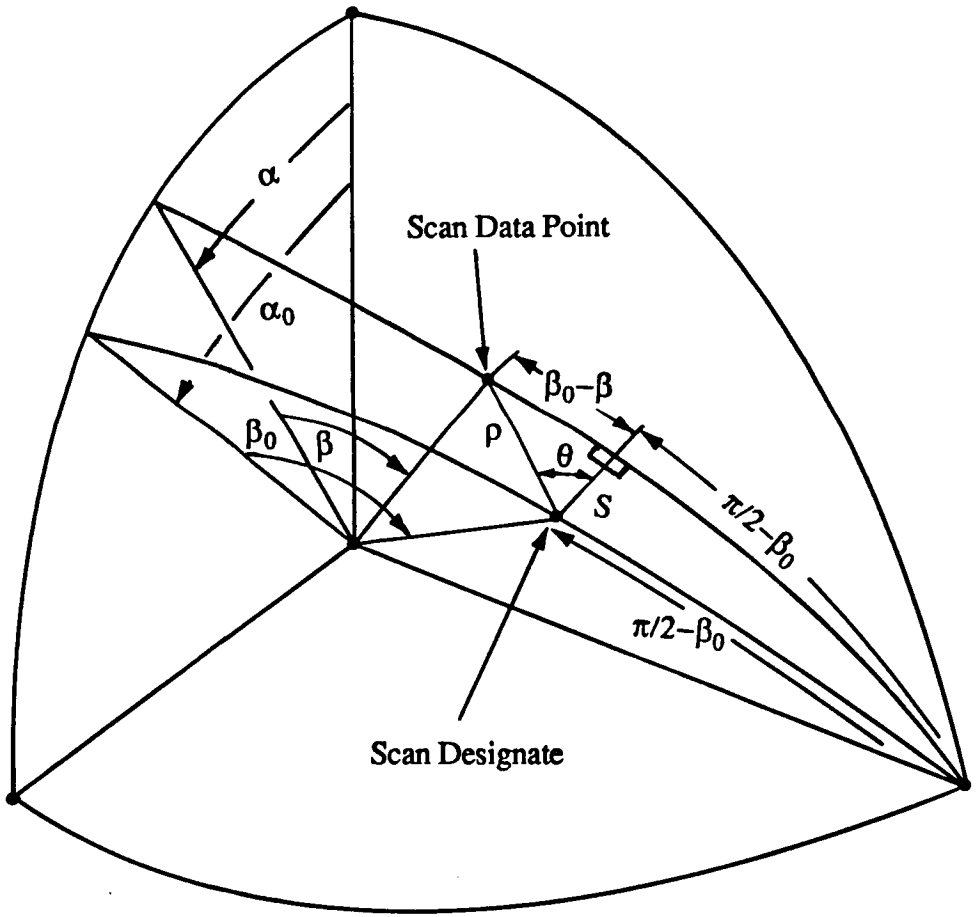

From Spherical Trigonometry:

$$\frac{\sin(S)}{\sin(\alpha_0-\alpha)} = \frac{\sin(\pi/2-\beta_0)}{\sin(\pi/2)}$$

$$S = \sin^{-1}\{\sin(\alpha_0-\alpha)\cos(\beta_0)\}$$

$$\cos\rho = \cos(\beta_0-\beta)\cos(S) + \sin(\beta_0-\beta)\sin(S)\cos(\pi/2)$$

$$\boxed{\rho = \cos^{-1}\{\cos(\beta_0-\beta)\cos(S)\}}$$

$$\frac{\sin\Theta}{\sin(\beta_0-\beta)} = \frac{\sin(\pi/2)}{\sin\rho}$$

$$\boxed{\Theta = \sin^{-1}\left\{\frac{\sin(\beta_0-\beta)}{\sin(\rho)}\right\}}$$

Figure 4 Derivation of ρ, θ as Function of α, β

$$\cos \ell = \cos \rho_1 \cos \rho_2 + \sin \rho_1 \sin \rho_2 \cos \Theta$$

$$\text{TOT} = \frac{\Delta t}{\ell} \times \text{BW}$$

(BW = Beam Width = 1.68°)

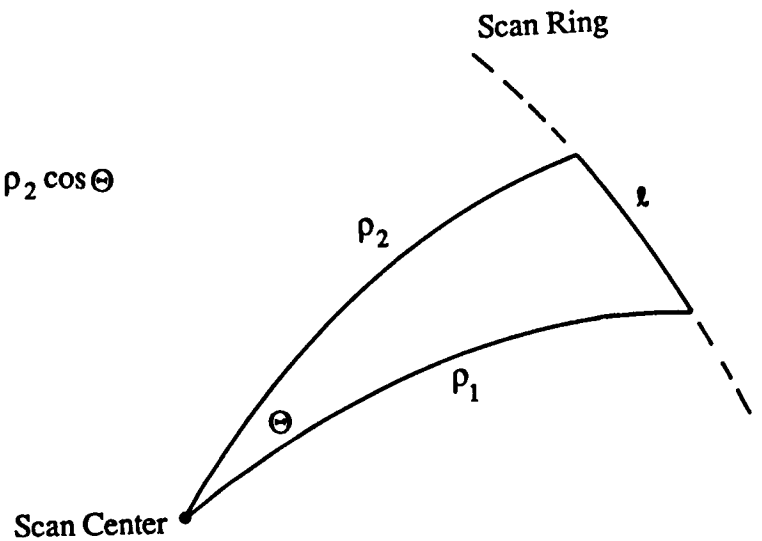

Figure 5 Definition of Time-on-Target

$$d = \rho_3 - (\rho_1 + \rho_2)/2$$

$$\text{Overlap} = \left(1 - \frac{d}{\text{BW}}\right) \times 100 : d \leq \text{BW}$$

$$= 0 \qquad : d > \text{BW}$$

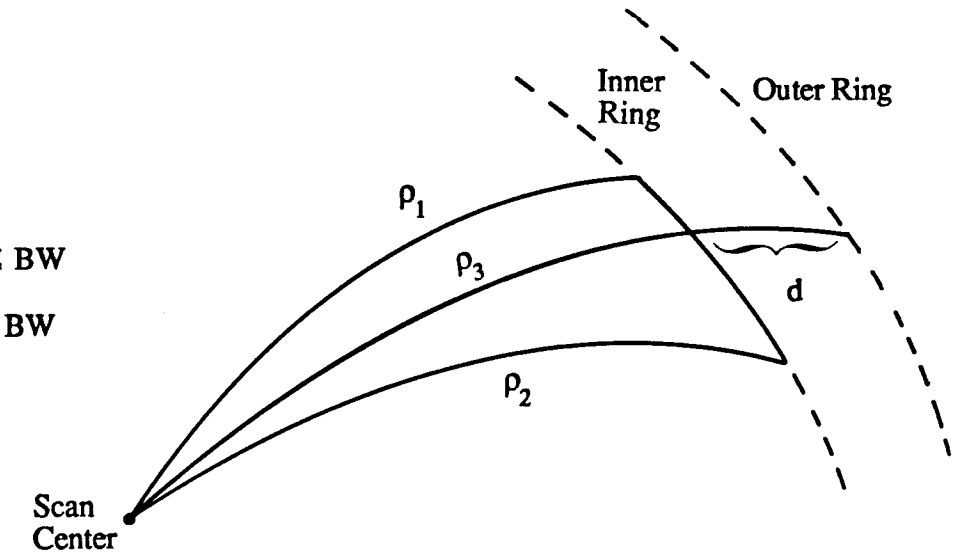

Figure 6 Definition of Scan Overlap

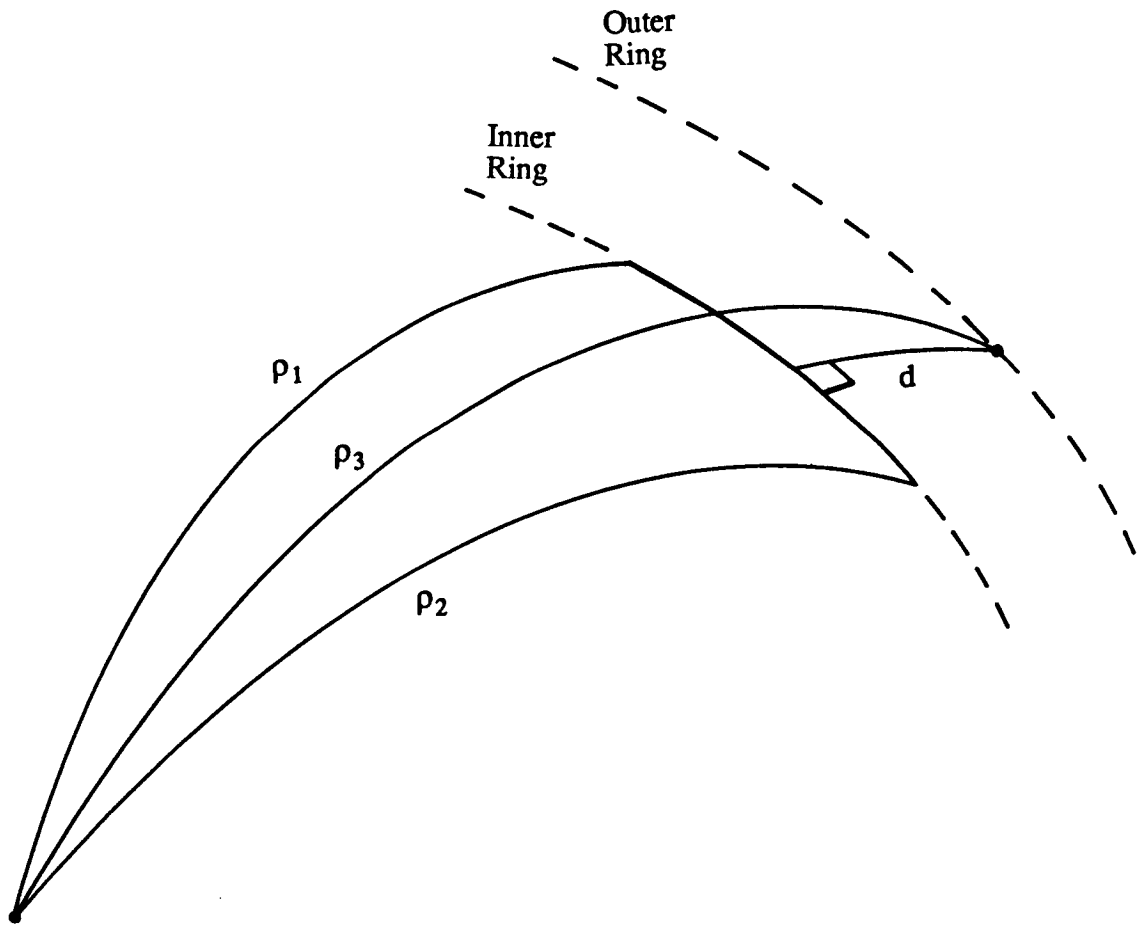

Figure 7 Alternate Definition of Scan Overlap

figure represents an angular distance of 8° , which is just inside the changeover limit from constant angular rate to constant velocity. Some of the figures have TOT and overlap plotted at 7° increments of ρ after the first 8°, for example 8°, 15°, 22°, and so on, to the maximum ρ. Some of these plots appeared "busy", so the rest of the figures were plotted at ρ = 8° and at the maximum ρ at which the scan terminates. The point was to show how scan performance degraded as radial distance from the designate increased. Since it appears that the most significant degradation occurs just past 9°, it was deemed adequate just to plot ρ = 8° and the maximum ρ. These figures are included as Appendix D of this report.

The plots of scan patterns, TOT and overlap vs. time, and CDF's of TOT and overlap, are labeled to indicate the roll and pitch of the scan designate. The alphbetic characters indicate plus or minus (P/M) and the numeric characters indicate roll angle and pitch angle in degrees, with roll first. For example, the scan labeled P40P20 indicates a roll designate of +40° and a pitch of desingate of +20°, while P20M40 indicates a roll designate of +20° and a plot designate of –40°. With a few exceptions, as explained in a subsequent paragraph, there are six plots per designate in the order of roll vs. pitch, x vs. y (inertial), TOT vs. time, scan overlap vs. time, cumulative distribution function vs. TOT and CDF vs scan overlap. The plots are ordered by decreasing roll angel from P40xxx to M40xxx, and within any given roll angle from decreasing pitch angle from xxxP60 to xxxM60. P00 P00 is a scan centered at zenith. As was discussed in a prior paragraph, some scans do not follow the normal 60 second, 30° standard due to proximity of the designate the obscuration profile. These will be discussed on an individual basis below:

P40P60, P40P40, P40P20, P40P00 and P40M20 are nominal high speed scans which are prematurely terminated upon entry into the obscuration zone. Note the distortion in P40M20 due to torque limitations at high beta angles.

P40M40 is commanded to a long range double scan (spiral out then spiral in) by the EA-1, which senses that the designate is close to the payload bay.

P40M60 is a long range slow scan for the same reason. Note that the TOT is always greater than 100msec. This scan was not plotted on the STE, so an x vs. y. plot was generated on the AT&T. This plot does not have a set of axes, however the scan is so benign that it was not considered worthwhile to spend the time to write a special plotting routine (the data for the inertial plots are stored as and Θ vs time).

P20M60 is a slow scan, similar to P40M60. TOT and scan overlap were not plotted for this scan, as the data was incompatible with the plot routine: multiple data points had identical values which gives a divide by zero for the TOT calculation. This scan is so slow, it is not a concern vis-a-vis TOT and overlap, so no attempt was made to excise the redundant points.

M20P60 and M20M60 scans were not plotted on the STE, so x vs. y plots were made on the AT&T.

M20P00 has data dropout on the eleventh scan ring which is an artifact, not a real scan phenomenon.

M20M20 and M20M40 also have similar data dropouts.

M40P60 and M40M60 were not plotted on the STE, and hence x vs. y plots were generated on the AT&T. M20M60 is a reduced volume scan due to the proximity to the obscuration zone.

M40P40 and M40P20 both exhibit servo runaway. They are designates within the 41° circle, and there is no obscuration zone to stop the scan prior to runaway. Note also that the scan pattern is dramatically altered at the transmition from constant angular rate to constant velocity.

Conclusions

The Ku-band radar system is fully capable of supporting radar missions within the specified zone 1 region. Performance to β angles greater than about 50° is degraded in the constant velocity region. That is, if the target is outside the 9° crossover from constant angular rate to constant velocity, there are holes in the scan. However, while

not recommended, if the target is actually within 9° of the designate, but less than 70° in β, the scan can be initiated as long as the target can be detected prior to the servo going unstable. The advantage of having the target within 9° of the designate can be shown dramatically by looking at a suboptimum scan, for example the CDF's of M40P40. Note that within 8° of designate, more than 90% of the scan has a TOT of 35 msec or greater, and more than 70% of the scan has an overlap greater than 50%. However, the entire scan has a TOT of 35 msec or more only 55% of the time, and an overlap of 50% only 30% of the time.

In the event the that the target is within the 30° radar scan volume but no detection is evident, the target may well have fallen into one of the holes in the scan. Since scan patterns are essentially deterministic, repeated trials with the same designate will most likely yield the same results; in this case, the designate should be shifted slightly. This will alter the probability that a scan ring overlaps the target.

Once the geometry of the TSS is known, and the designation accuracy established, the CDF curves of TOT and scan overlap can be used to estimate radar acquisition performance. If the target is close (within 49°) to the pitch axis of the Orbiter, acquisition should not be a problem from the standpoint of servo performance. If the target will be outside of a 49° roll angle, designation accuracy should be maintained to within 9° for optimum performance.

Test Plans, Trouble Heating Sequence, and System Anomalies

The primary Axiomatix responsibility during SORTE was to provide expertise in the area of Ku-band system test. This includes experience in system test at Baldwin Hills writing test plans and test procedures, conducting tests, writing trouble shooting sequence, and researching anomalies. This experience was carried over to SORTE, during which Axiomatix participated in all phases of testing, and was present at every live helicopter and balloon test during which data was recorded.

Axiomatix provided software for the AT&T PC 6300 to assist in acquiring a target as a backup mode. This software was used in conjunction with the optical tracker. Azimuth and elevation readouts from the tracker were converted to alpha/beta designates for the Ku-band system. This software was used when WSMR tracking data was not available.

During the course of generating scan patterns for the servo performance tests, a system anomaly in the encoder readouts was discovered. This was manifested by regular jumps at a fixed gimbal angle (see Figure 8). Subsequent troubleshooting using the slew switches indicated encoder pulse dropouts in the region of alpha = 21°. This was determined by fast slewing and slow slewing and observing that the antenna did not stop during the period of time that the encoder pulses dropped out. Figure 9 is a plot of alpha vs. time. The region of constant alpha is expanded in Figure 10 and shows minimal change in alpha even though the gimbal is moving at a constant rate.

Physical inspection of the shaft angle encoders revealed a foreign substance on the alpha encoer disc. This substance was removed, and the encoder returned to normal operation.

The underlying problem with occluded optical discs is not that the scan is affected since the apparent scan anomaly is an artifact, but rather that designates in the region past the bad area on the disc will result in the antenna overshooting the designate by an angle equal to the occluded angle. This would preclude designating to the TDRS.

The problem of how to ascertain if a disc is dirty at the cape, in situ on the Orbiter, is currently being investigated. It would be desirable to automate a procedure to detect a dirty optical disc, thereby removing any human uncertainty, but connection of the Radar Test Set (RTS) to the Ku-band LRU's would probably be necessary. One such procedure would be to generate a series of scans, similar to the procedure used to generate the servo test scans. Visual comparison of a normal scan and a scan with a dirty optical disc (see Figures 11 and 12) readily reveals a problem. The normal servo test scan of

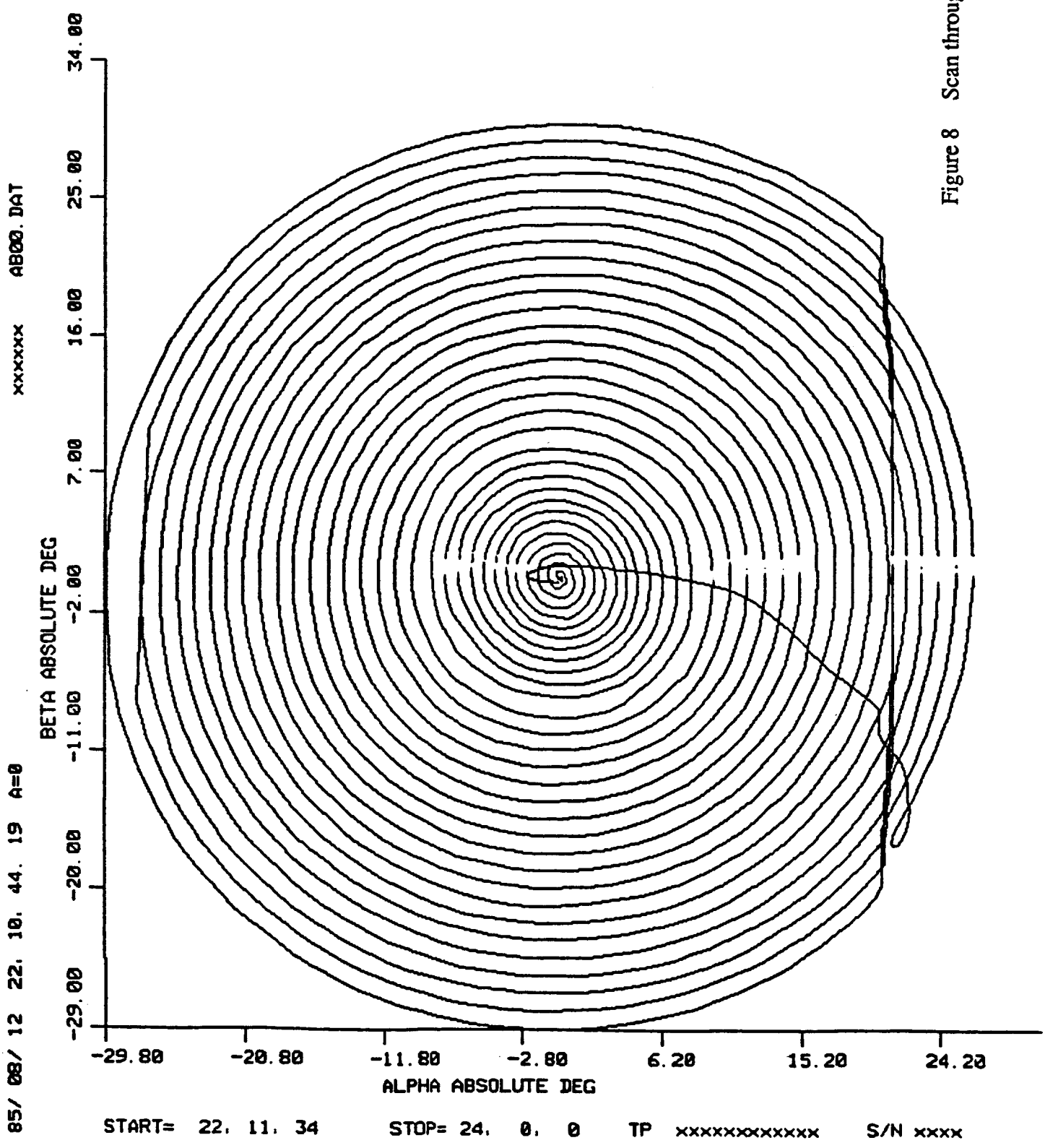

Figure 8 Scan through Anomaly

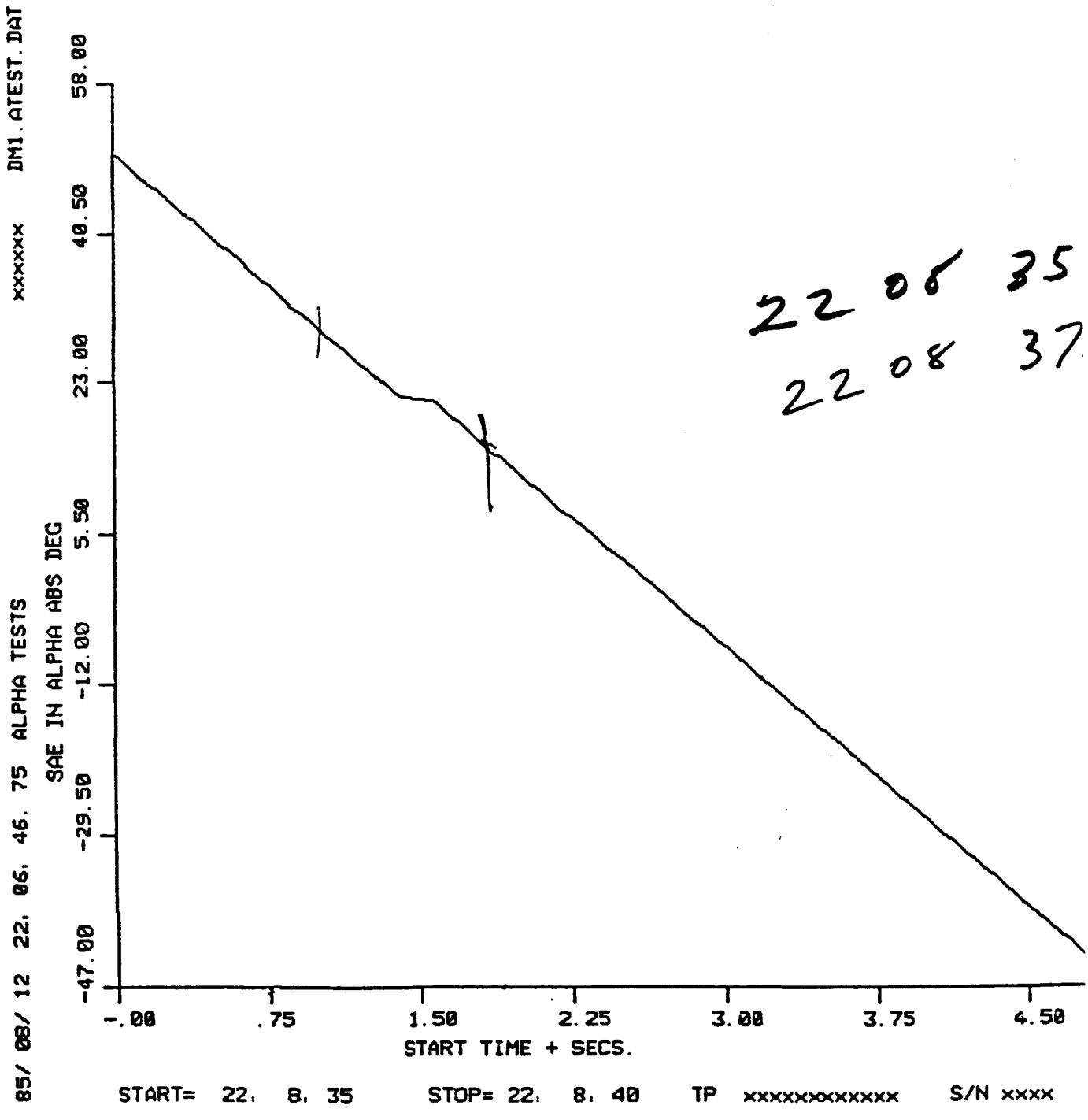

Figure 9 Fast Slew through Anomaly

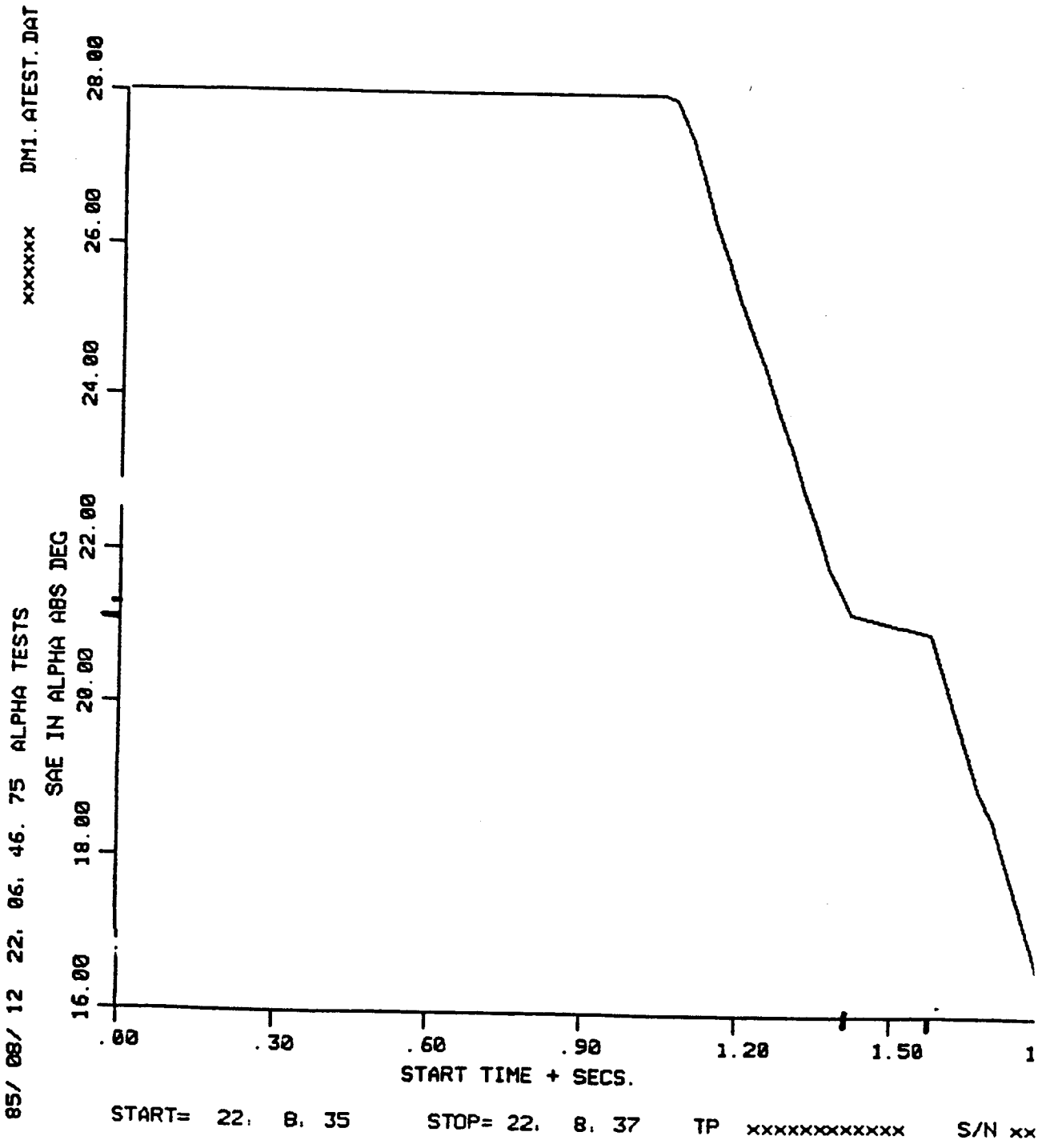

Figure 10 Fast Slew through Anomaly with Expanded Time Scale

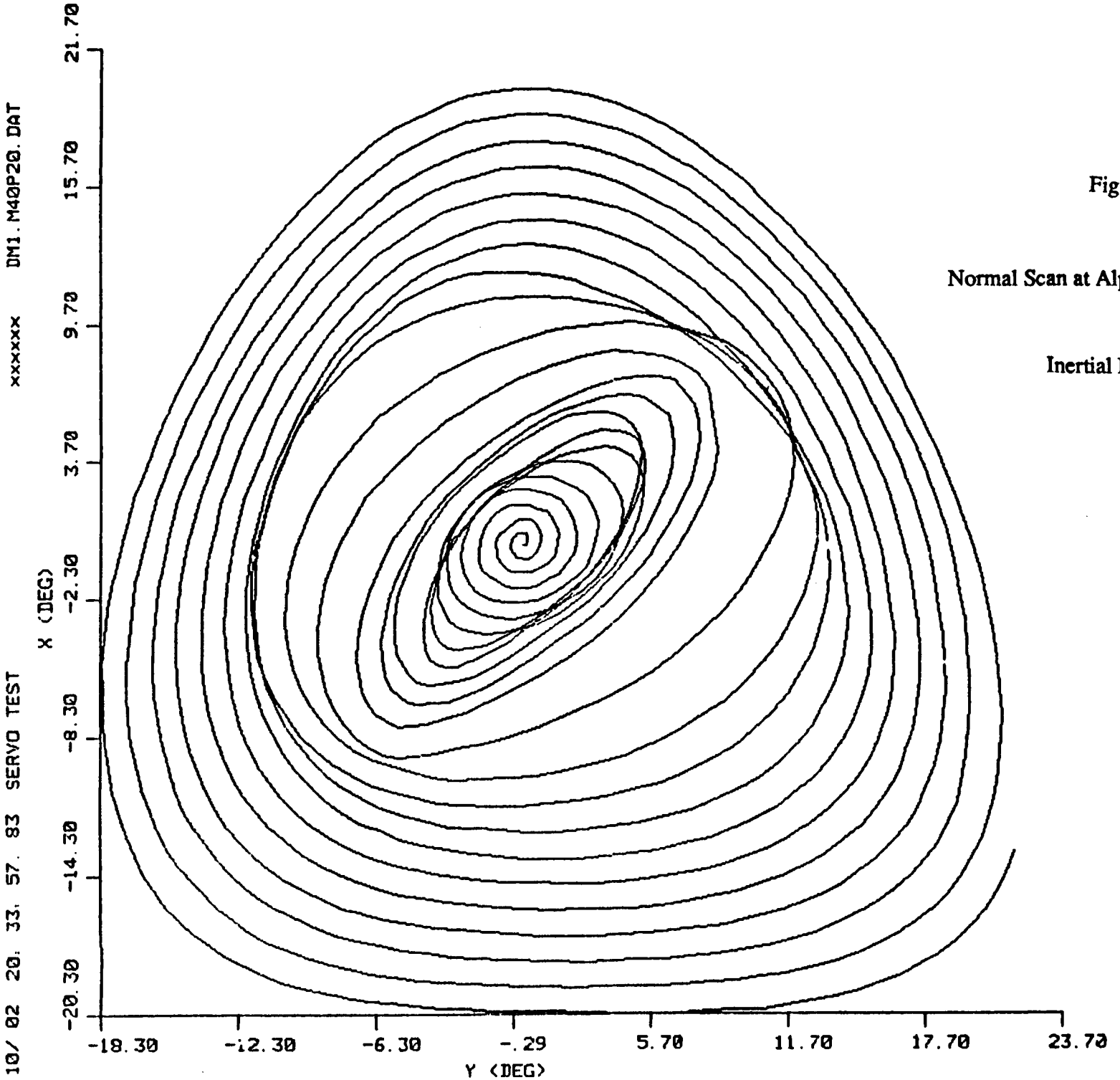

Figure 11

Normal Scan at Alpha = –6, Beta = –44

Inertial Projection

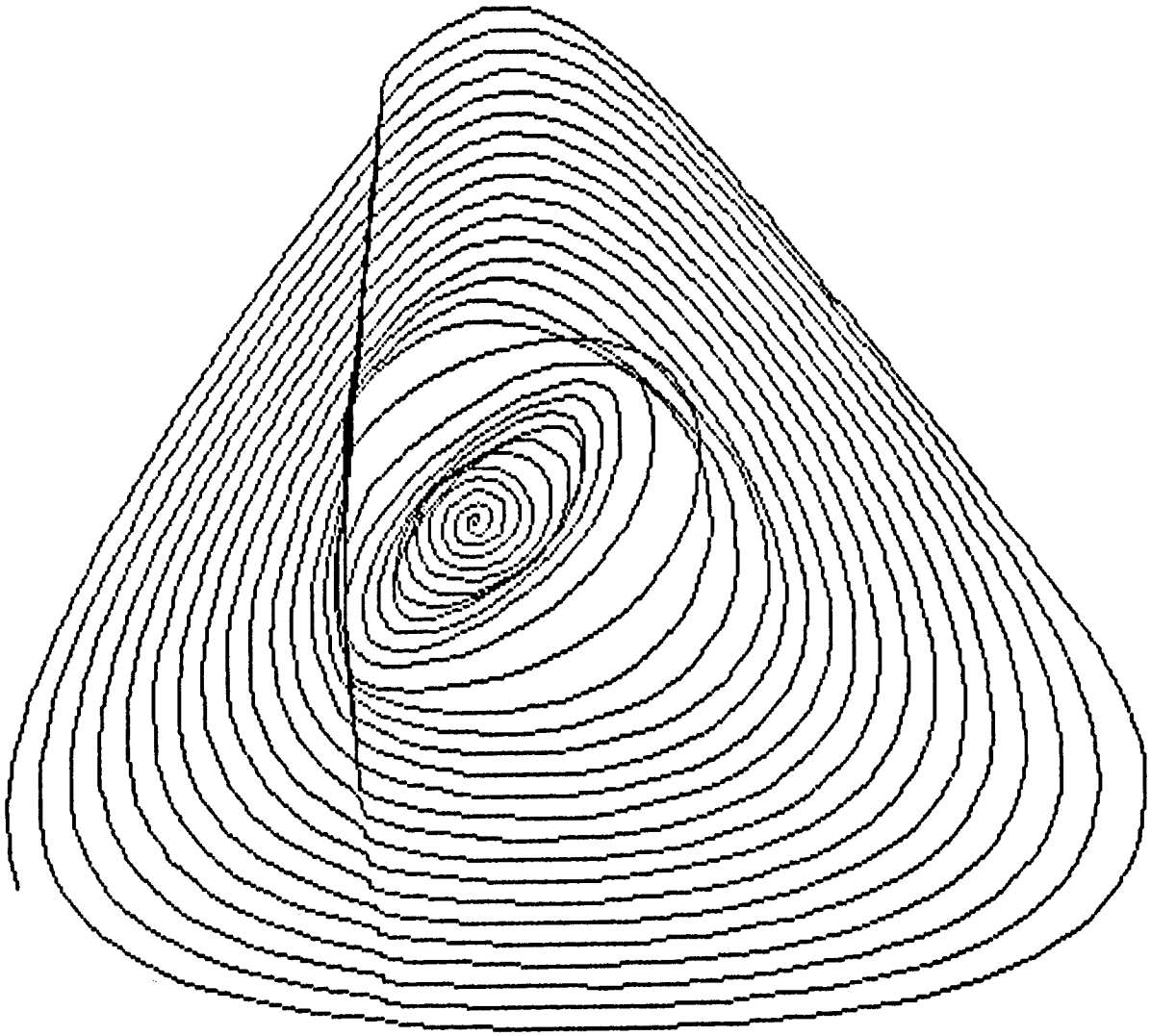

Figure 12 Scan through Anomaly Inertial Projection at Alpha = 7, Beta = –40

Figure 11 is the one designate closest to the occluded scan. Note that in regions where the anomaly is evident, excessive scan overlap is evidenced. Figure 13 is a plot of scan overlap vs. time for the normal scan. No overlap of 100% is evident past the changeover region from constant angular rate to constant velocity, whereas Figure 14, which is the occluded scan, shows a large number of 100% overlap points. The recommended procedure, should an automated procedure be required, would be to generate a family of scans, with each scan having a threshold value of the number of 100% (or 70% - 80%) hits of scan overlap. The calculations are rather simple, and a simplified version of the RTS based on a microcomputer could be used.

A simpler approach, which could be used to trigger the more time consuming scan approach, is to physically move the gimbals from stop-to-stop. The total indicated gimbal travel should be a constant if no encoder pulses are missing. Preliminary investigation by Rockwell indicates that there is a variability in the indicated travel, but other factors contributing to this variability have not yet been tracked down.

Tethered Satellite System Tests

As a prelude to the TSS portion of the SORTE tests, Axiomatix evaluated the effect of the tether on the Ku-band radar using the tether radar cross section (RCS) as a measure. The analysis indicates that the RCS of the tether is negligible unless the tether is perpendicular to the radar beam. This analysis is included as Appendix E of this report. Subsequent TSS tests at WSMR initially indicated a significant effect of the tether, a result at variance with the RCS analysis. Follow on testing after the encoder fix, and with a target less sensitive to angle of incidence, did not substantiate the initial tests, and a deleterious effect due to the tether has not been demonstrated.

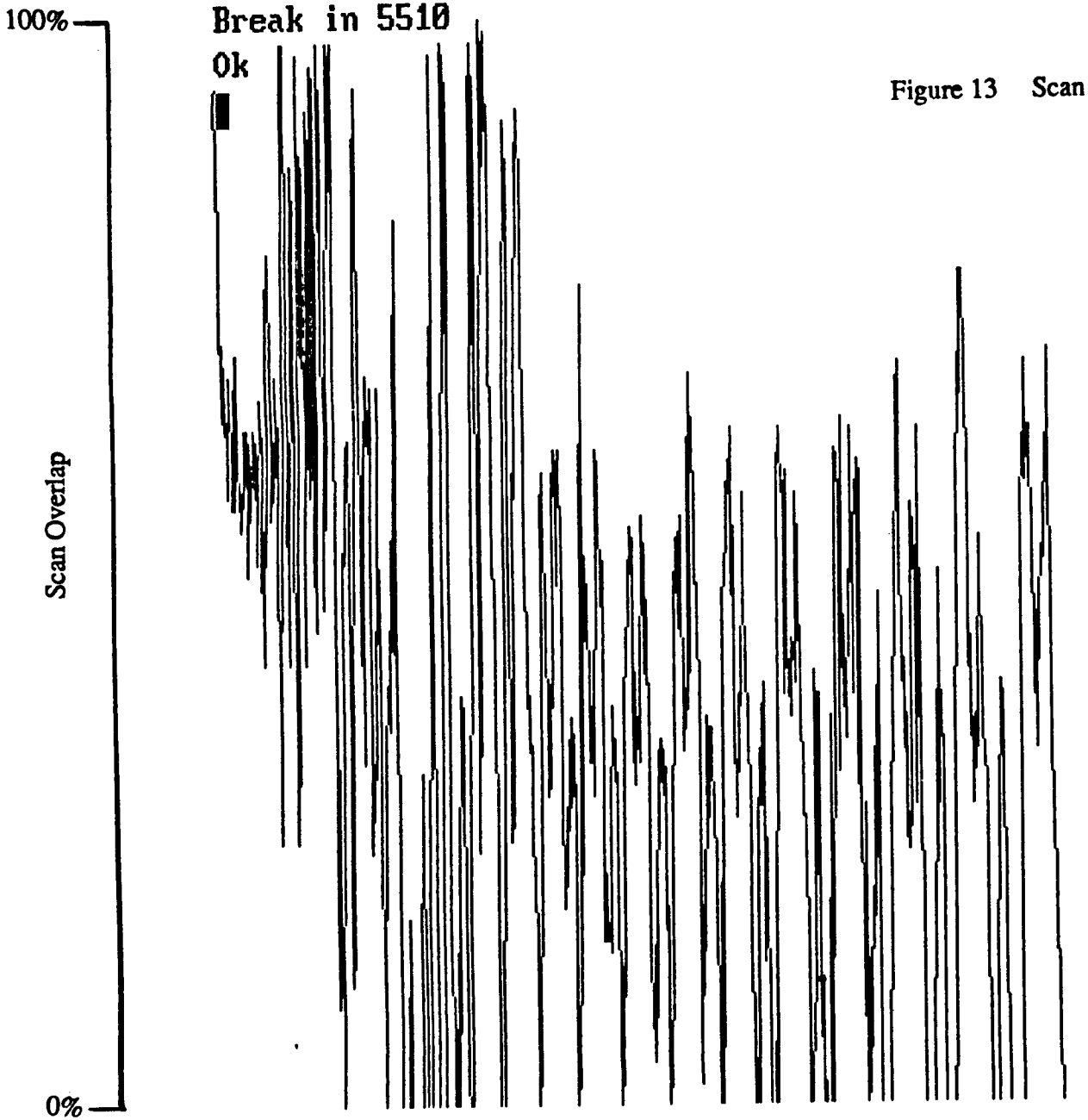

Figure 13 Scan Overlap vs. Time, Normal Scan of Figure 11

OF POOR QUALITY

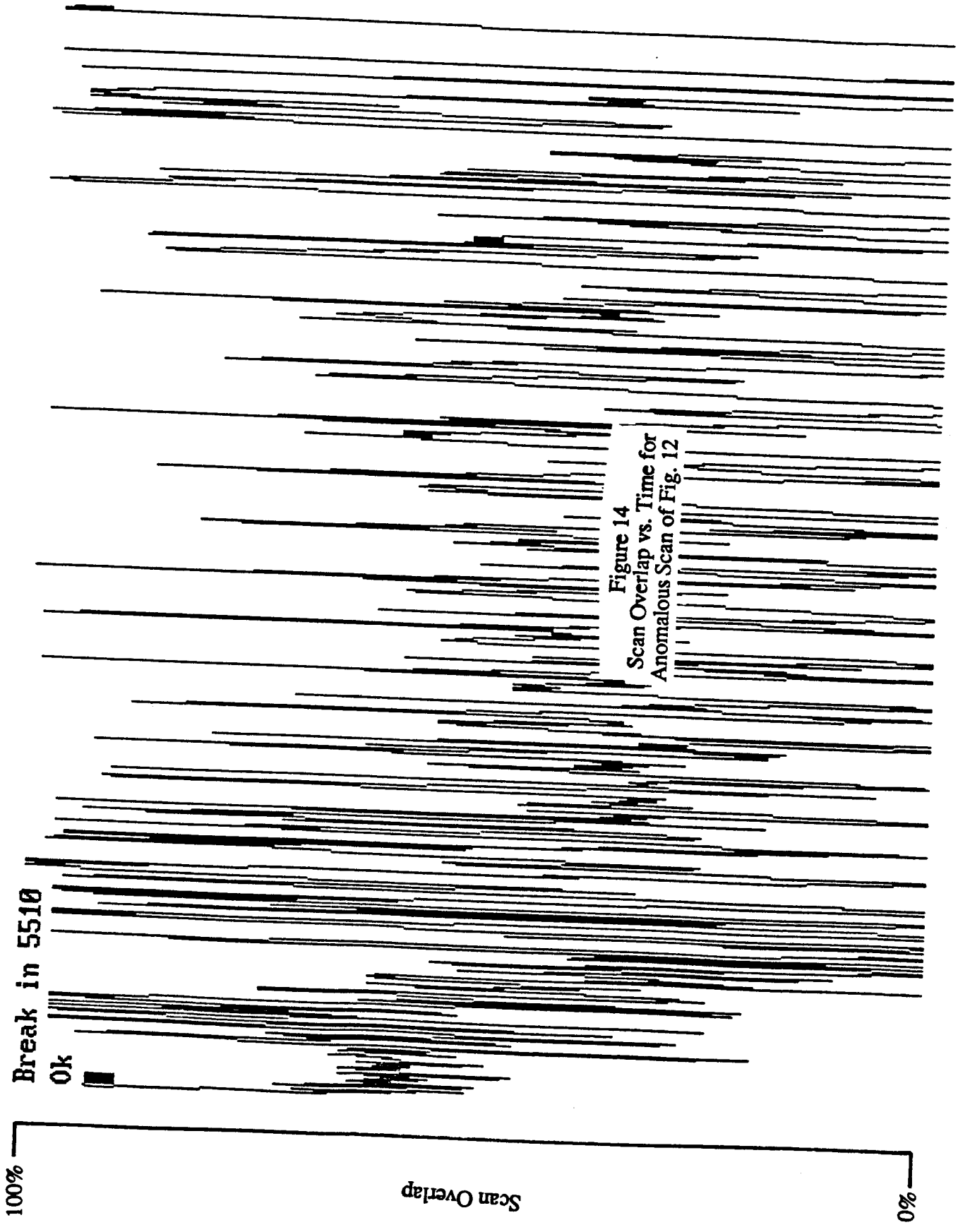

Figure 14
Scan Overlap vs. Time for
Anomalous Scan of Fig. 12

APPENDIX A

DEDICATED PAYLOAD COMMUNICATION LINK (DPCL) DESIGN CONSIDERATIONS

APPENDIX A

Dedicated Payload Communication Link (DPCL) Design Considerations

1.0 INTRODUCTION

With the present equipment making use of the payload interrogator (PI) and its associated antenna, the RF range to a detached payload is limited to about 10 to 20 nautical miles depending on a payload. However, the use of the Dedicated Payload Communication Link (DPCL) kittable communication system, which is being considered for DOD missions, may increase the effective range of PI mani-fold. Specifically, it is expected that the range of telemetry reception may be increased out to approximately 1000 nautical miles or greater depending on payload EIRP and data rate. Furthermore, by use of DPCL, the Orbiter's PI system should be able to command deployed payloads out to approximately 300 nautical miles or greater depending on payload sensitivity and command data rate. Figure 1 shows a general DPCL scenario.

Another function for which DPCL is intended in the later phases is to provide direct TDRS/Orbiter communication on a "stand alone" basis, i.e., independent of other S-band or Ku-band systems. In this mode, the Orbiter will be employing a payload-type transponder and by means of a dedicated computer, the Orbiter may provide the pointing information to the DPCL antenna.

With the DPCL upgrade kit, all the basic functions of the PI will be retained. The additional DPCL equipment will only increase the EIRP and G/T of the system. One of the main components of the DPCL is an S-band antenna kit. The kit consists of a 2-foot dish which at the nominal S-band frequency of 2 GHz has a beamwidth of approximately 16 degrees and a gain of approximately 20 dB. This dish is mounted on a Pan/Tilt type of pedestal which can be articulated either mannually or by a programmed track. This S-band dish antenna can be used in either of two modes: (1) Receive only or

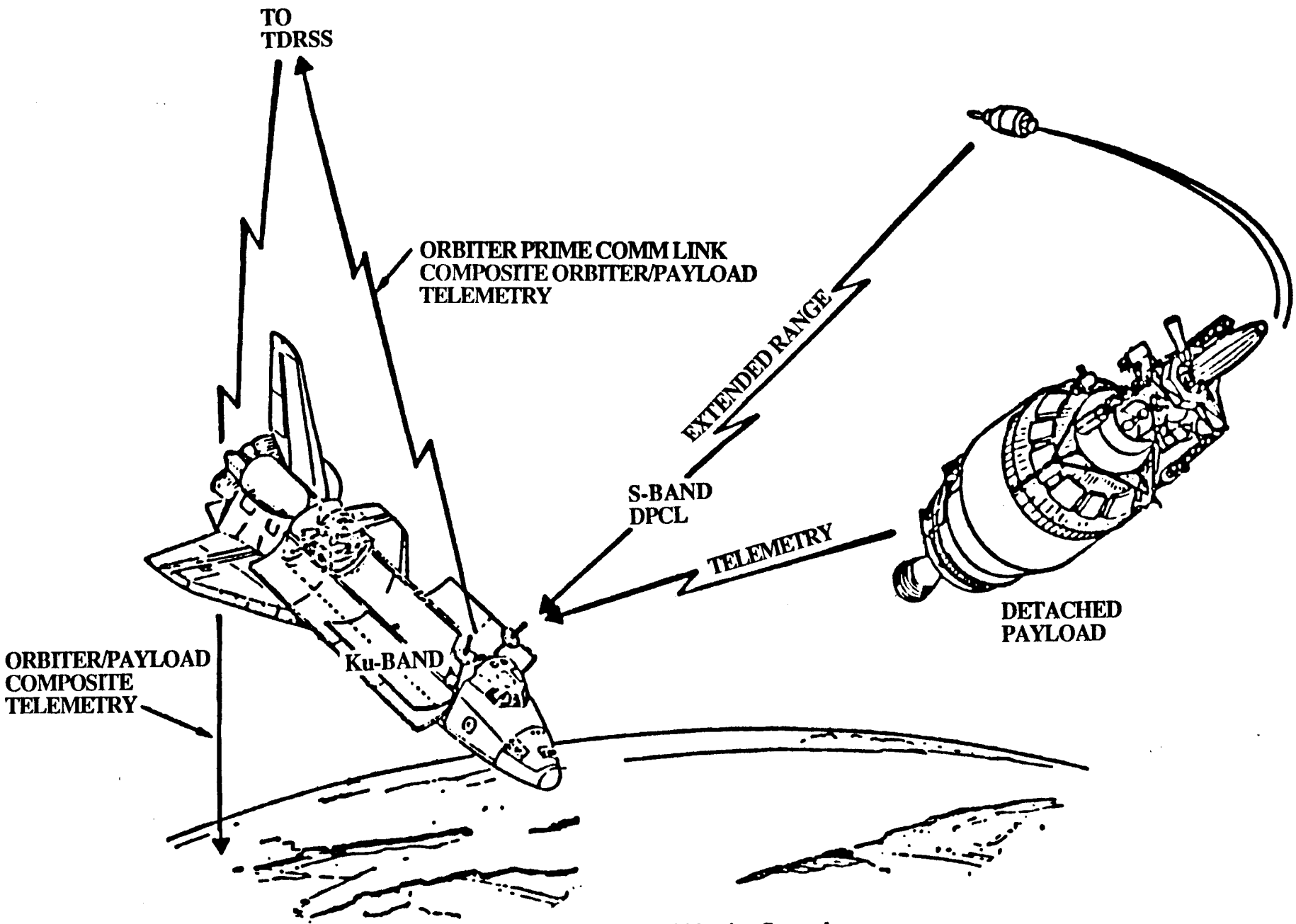

Figure 1 DPCL Utilization Scenario

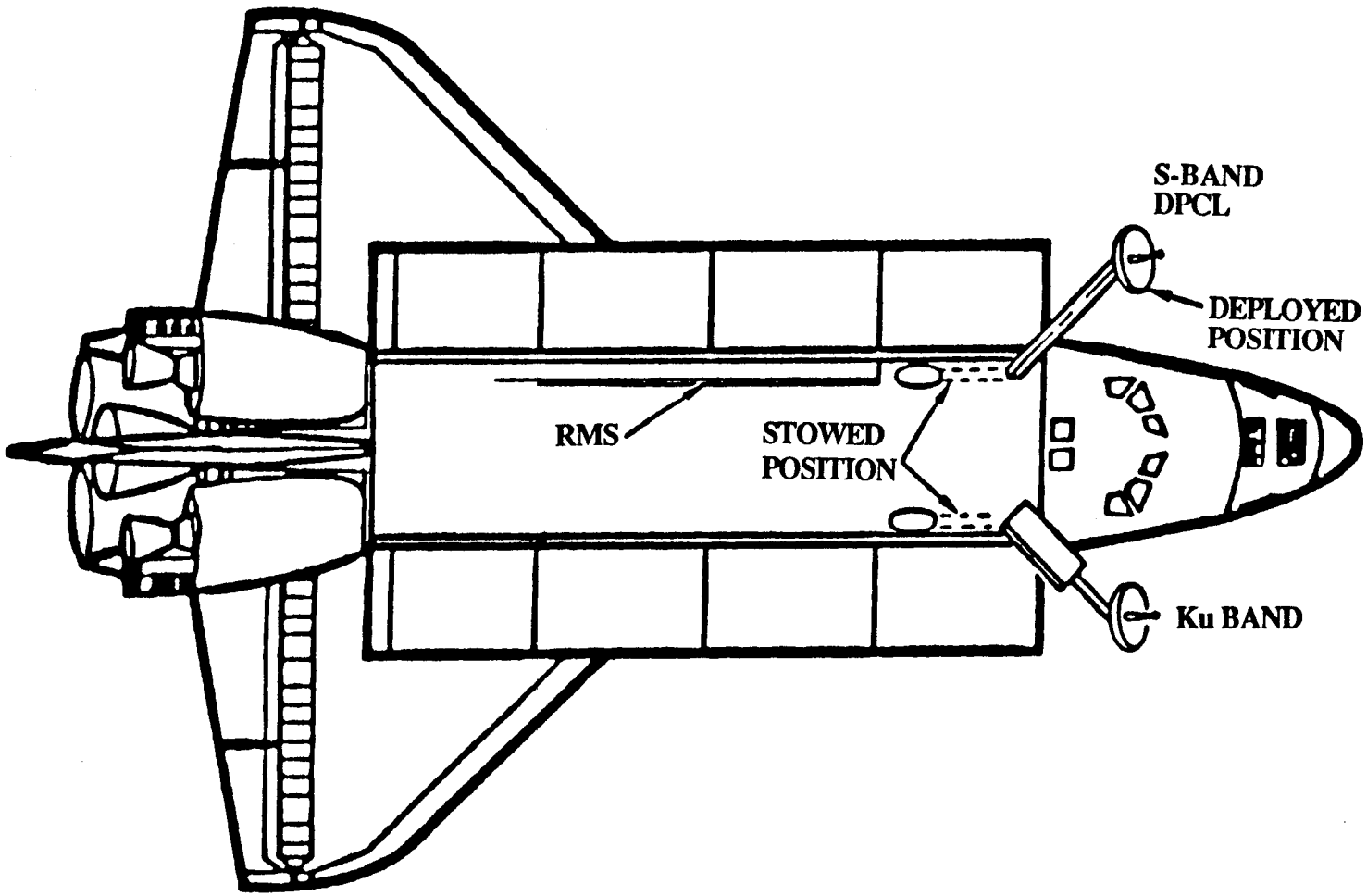

Figure 2 DPCL Deployment Concept

(2) Receive/Transmit. In either case, the dish works with the payload interrogator (PI) unit. The antenna is deployable from the port-side location, a mirror image of the location of the Ku-band system. Figure 2 shows the DPCL deployment concept.

2.0 SUMMARY

This appendix contains some design considerations pertaining to the Dedicated Payload Communication Link (DPCL) system. Specific subjects addressed are:

1) Payload to DPCL power transfer in proximity to a payload
2) DPCL antennas pointing considerations

and

3) DPCL transceiver implementation which can be mounted on the deployed antenna boom.

With respect to the power transfer from the payload to DPCL antenna, we have shown that with such payloads as Centaur and IUS saturation of DPCL preamplifier may occur at distances from 6 to 10 meters. This saturation is not envisioned as a problem. However, the input to the DPCL preamplifier may be as high as 0.25 watts at 1 meter distance from the payload. Thus, a limiter similar to the one at input to the PI should be provided at the input to the DPCL amplifier.

Some of the current thinking on DPCL antenna pointing involves the use of signal strength meter which monitors the AGC voltage of the PI. This voltage is displayed on the panel in Orbiter's cockpit so that manual stearing of the DPCL antenna can be performed. Our considerations indicate that this method results in a rather low visual sensitivity to antenna pointing. For example, 3 dB change in signal strength corresponds to about 3% displacement of the pointer on the meter scale. Thus, some means of automatic antenna pointing should be used. One method consists of nutating the antenna by some small angle along the pan and tilt axes. From this nutation pointing error can be derived and used for correcting antenna direction. This method of antenna pointing appears to be most easily implementable for the DPCL.

The present concept of transceiver mode uses DPCL antenna to enhance the performance of the PI's transmitter. For transmission of commands to payloads, the effectiveness of the PI transmitter is decreased, however, by the 8 to 9 dB loss in the RF cable between the PI transmitter and the antenna.

A different concept of a transceiver may employ a transmitter, placed close to the DPCL antenna, and located physically close the low-noise preamplifier. Electrically, such configuration would result in a closed loop between the transmitter and the low-noise amplifier (LNA). The closed loop in this case results in because both the input and the output of the transceiver must have common circulators which connect to DPCL antenna on one end and the PI input on the other end. We have examined a typical loop gain of such a configuration and determined it to be feasible provided that a careful design is performed on all of the components within the loop.

DCPL DESIGN CONFIGURATIONS

by

AXIOMATIX

FIGURE A-1

DPCL Functional Block Diagram
(Basic System)

Figure A-1 shows a functional block diagram for the basic DPCL system. As shown in the figure, the PI can be connected either to the conventional PI antenna or to the DPCL preamplifier assembly. The preamplifier assembly, in turn, is connected to the DPCL antenna dish. The antenna dish is steared by a pan and tilt unit mounted on the antenna deployment mechanism. The pointing of the DPCL antenna can be accomplished either by uplink commands (designate inputs) or manually via a panel control. For pointing, by means of panel control, the signal strength meter, which displays the AGC signal generated by PI, is used to indicate optimum antenna direction. The panel mounted mode select switch provides for selection of either Mode 1 (telemetry receive only) or Mode 2 (commands transmit and telemetry recieve). In Mode 2, the DPCL antenna is connected directly to PI via an existing RF cable which may have from 8 to 9 dB attenuation. Thus, in this mode, the performance of the DPCL system is essentially that of the existing PI enhanced by the gain of the DPCL antenna.

DPCL FUNCTIONAL BLOCK DIAGRAM (BASIC SYSTEM)

Axiomatix

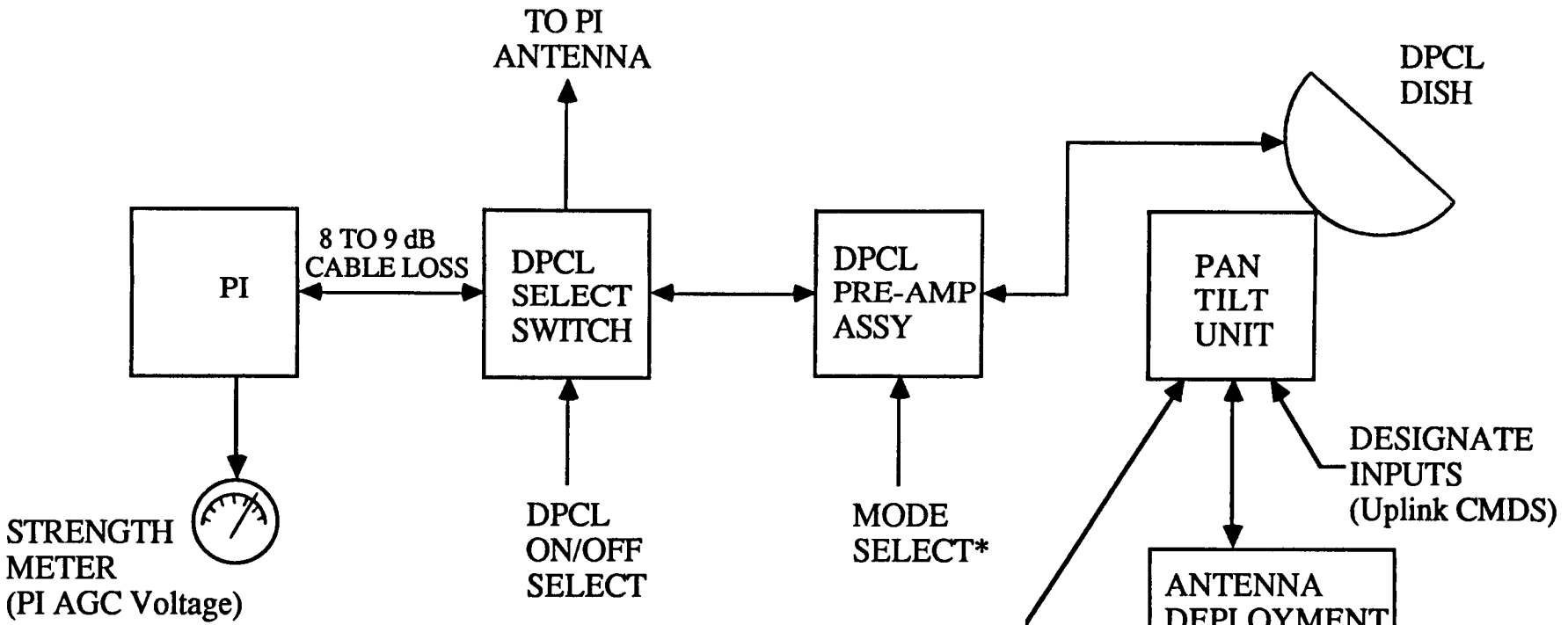

* MODES ARE: 1) TELEMETRY RECEIVE ONLY
OR
2) COMMANDS TRANSMIT AND TELEMETRY RECEIVE

Figure A-1

FIGURE A-2

DPCL Pre-Amp Configuration for PI Overload Protect

The baseline preamplifier assembly consists of a low-noise amplifier and the associated RF circuitry. The nominal (baseline) noise figure of this preamplifier is 2dB and the small signal gain is 25 dB. As shown in the figure, the preamplifier is protected by an RF limiter at its input. The limiter may be of design similar to that of PI which can take up to +36 dBm (4 watts) without damage. Note that the maximum output power of the preamplifier should be such it does not overload the PI.

In Figure A-2, a maximum level of 4 watts is indicated to be consistent with the PI maximum input spec of +36 dBm. One must keep in mind, however, that even if 4 watts were generated at the output of the preamplifier, which is highly unlikely, there would be additional loss of about 8 dB in the RF cable between the pre-amplifier and the input of the PI. The circulator placed at the output of the preamplifier actually acts as an isolator which provides proper termination for pre-amplifier, particularly in view of the fact that the pre-amplifier has to feed a long RF cale as well as the switching networks.

As shown in the figure, for Mode 2 the preamplifier assembly is completely bypassed and the DPCL antenna is connected to the RF cable which feeds the PI.

DPCL PRE-AMP CONFIGURATION FOR PI OVERLOAD PROTECT

Axiomatix

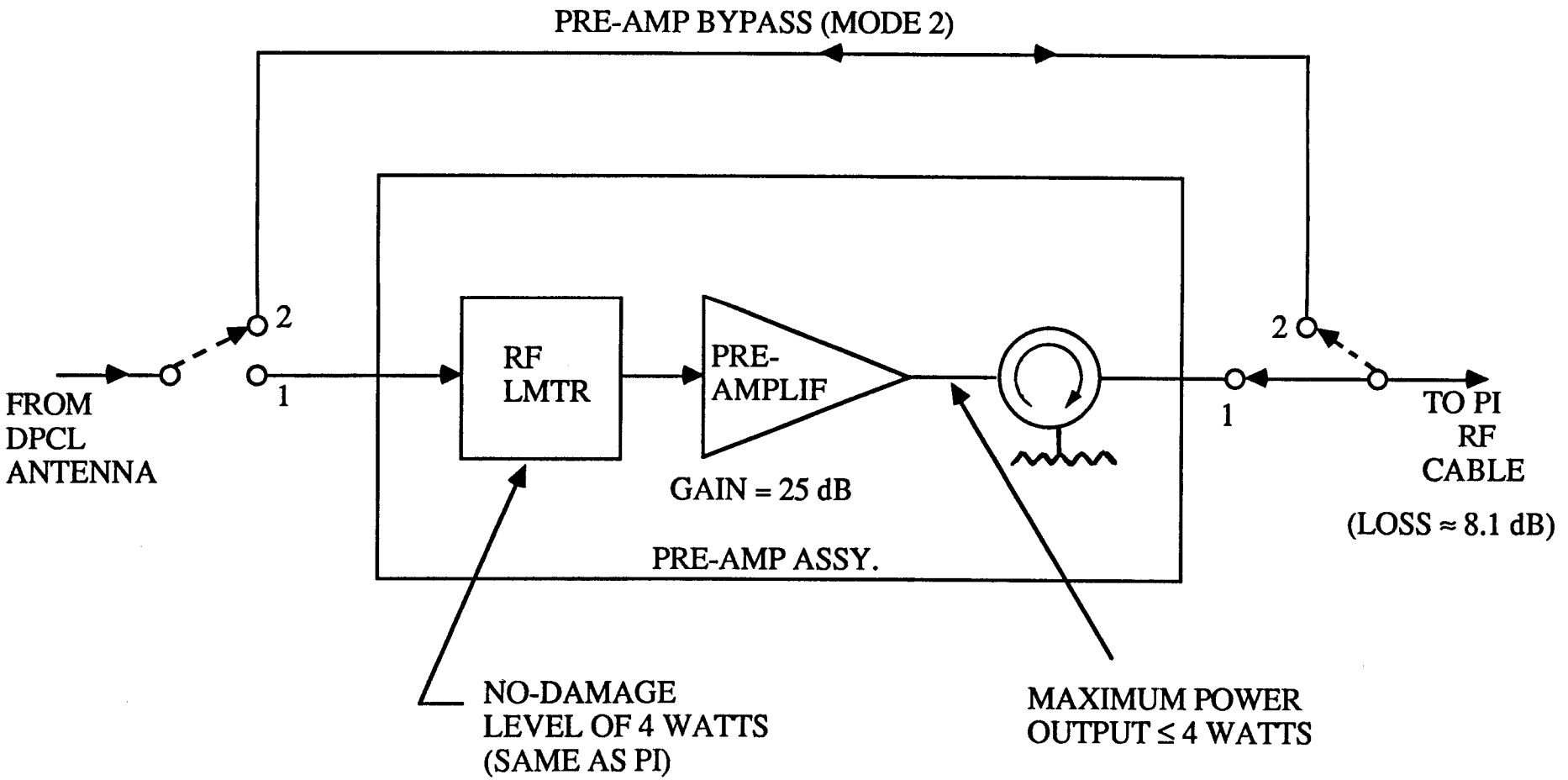

MODE 1 : RECEIVE ONLY

MODE 2 : TRANSCEIVE

Figure A-2

FIGURE A-3

DPCL Performance Factors

In this figure are listed various factors which affect the performance of a DPCL system. Some of these factors are design parameters such as G/T's, EIRP's and implementation losses. Other parameters are variable, such as modulation indexes and data rates (command and telemetry rates).

The purpose of listing all of factors is to provide awareness that the range performance in both modes (Mode 1 and 2) is a function of many system parameters, both fixed and mission-dependent. Thus, to get a better definition of DPCL system performance, the user should generate a set parametric curves by means of which he can place boundaries on the performance of the DPCL system

TELEMETRY RECEIVE (MODE 1) RANGE ≥ 1000 NMI

FUNCTION OF:

1) PAYLOAD EIRP
2) TLM DATA RATE
3) MOD INDEX AT PL
4) DPCL G/T
5). BER
6). IMPLEMENTATION LOSSES

COMMAND TRANSMIT (MODE 2) + TLM RECEIVE RANGE ≥ 300 NMI

FUNCTION OF:

1) DPCL EIRP AND DPCL G/T
2) CMD DATA RATE AND TLM DATA RATE
3) MOD INDEX AT PI AND MOD INDEX AT PL
4) PAYLOAD G/T
5) BER
6) IMPLEMENTATION LOSSES

Figure A-3

PAYLOAD TO DPCL POWER TRANSFER

FIGURE A-4

Payload to DPCL Antenna Power Transfer

With a high gain antenna connected to the input of the PI, there arises the question of exessive power pick-up from a nearby payload. The analytical assumptions for this model are shown in Figure A-4. For this model, it is assumed that the payload antenna has a relatively low gain and thus at a distance of about 1 meter, or beyond, its EIRP falls off as free space propagation, i.e., at the "inverse range" (R^{-2}) rate.

It is also assumed that the DPCL antenna intercepts the payload power density with its entire physical aperture. The assumption of physical aperture is a most conservative one, because if the efficiency of the antenna is less than 100%, which is the case for most antennas, the power intercepted and delivered to the output of the antenna will be smaller.

PAYLOAD TO DPCL ANTENNA POWER TRANSFER

Axiomatix

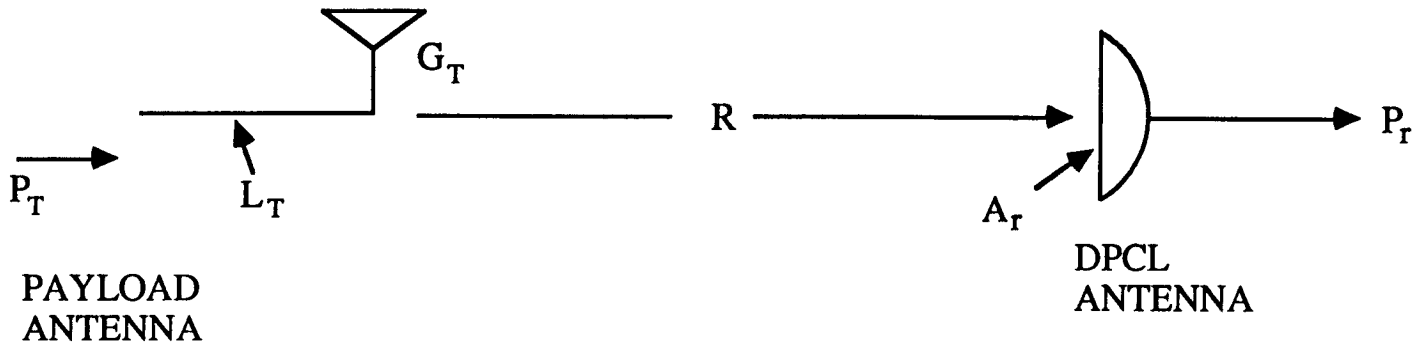

$$P_r = P_T L_T G_T \left(\frac{1}{4\pi R^2}\right) A_r$$

WHERE

P_r = POWER RECEIVED AND OUTPUTTED BY DPCL ANTENNA

P_T = PAYLOAD TX POWER

L_T = PAYLOAD RF AND ANTENNA LOSSES

G_T = PAYLOAD ANTENNA GAIN

R = RANGE TO DPCL ANTENNA

A_r = AREA OF DPCL ANTENNA (PHYSICAL OR EFFECTIVE)

Figure A-4

FIGURE A-5

Payload to DPCL Antenna Power Transfer at Close Range

Figure A-5 presents a table of functional dependence of payload power intercepted by the DPCL antenna as a function of range to the nearby payload radiator. For computing this table, the mathematical model explained in Figure A-4 was used. Note that the physical area of the DPCL antenna ($A_r = 0.29\ m^2$) was used for the calculations.

The conclusions are presented in the figure. Perhaps the most important area of further investigation should deal with the saturation behavior of the LNA. Such saturation, unless handled properly in the design of the LNA may create undesirable harmonics and crossproducts at the input to the PI, thus, affecting close range performance of DPCL.

PAYLOAD TO DPCL ANTENNA POWER TRANSFER AT CLOSE RANGE

Axiomatix

PAYLOAD	P_T(w)	L_T(dB)	G_T(dB)	R(m)	P_r (w)	COMMENTS
CENTAUR	27	-2.3	-1.5	1	0.26	
				2	0.065	P IS BASED ON $A_r = 0.29m^2$ (PHYSICAL AREA OF A 24" DIAM. DPCL ANTENNA)
				10	0.0026	
IUS	20	-3.2	-2.6	1	0.122	
				2	0.031	
				10	0.0012	

CONCLUSIONS

- AT 1m RANGE POWER OUT OF DPCL ANTENNA IS LESS THAN 1 WATT
- PI HAS ADDITIONAL PROTECTION OF ≈ 8 dB CABLE ANTENNA
- FOR RECEIVE ONLY MODE, PRE-AMPLIFIER MUST BE PROTECTED BY AN RF LIMITER SIMILAR TO PI
- OUTPUT POWER OF PRE-AMPL. AT SATURATION SHOULD BE LESS THAN 4 WATTS, I.E., MAXIMUM POWWER TO PI (ACTUAL VALUE IS TBD)
- FOR LNA GAIN OF 25 dB, OUTPUT POWER OF 4 WATTS WILL BE CAUSED BY CENTAUR AT 4.4 METERS AND IUS AT 3 METERS. (MOST LIKELY LNA OUTPUT WILL BE LESS THAN 4 WATTS AT SATURATION).

Figure A-5

DPCL ANTENNA POINTING CONSIDERATIONS

FIGURE A-6

Signal Strength Meter Display Scale Factor for DPCL Antenna Pointing

The idea expressed by Figure A-6 is that the use of the signal strength meter, which displays the AGC voltage generated by the PI, may be rather ineffective in view of the fact a 3 dB change in signal strength is displayed only as about 3% of the full scale of the meter. A change of 3 dB due to antenna mispointing can wipe out a link margin as shown by the example in the figure.

A possible solution which may alleviate this problem is to employ a nonlinear scale for the strength meter. With such a scale, signals from targets at further range will occupy a larger fraction of the scale of the signal strength meter.

SIGNAL STRENGTH METER DISPLAY SCALE FACTOR FOR DPCL ANTENNA POINTING

Axiomatix

EXAMPLE: DOD IUS-DPCL S-BAND LINK (MODE 2)
64 KBPS TLM CHANNEL
(1.024 MHz SC, FDM WITH 1.7 MHz SC)

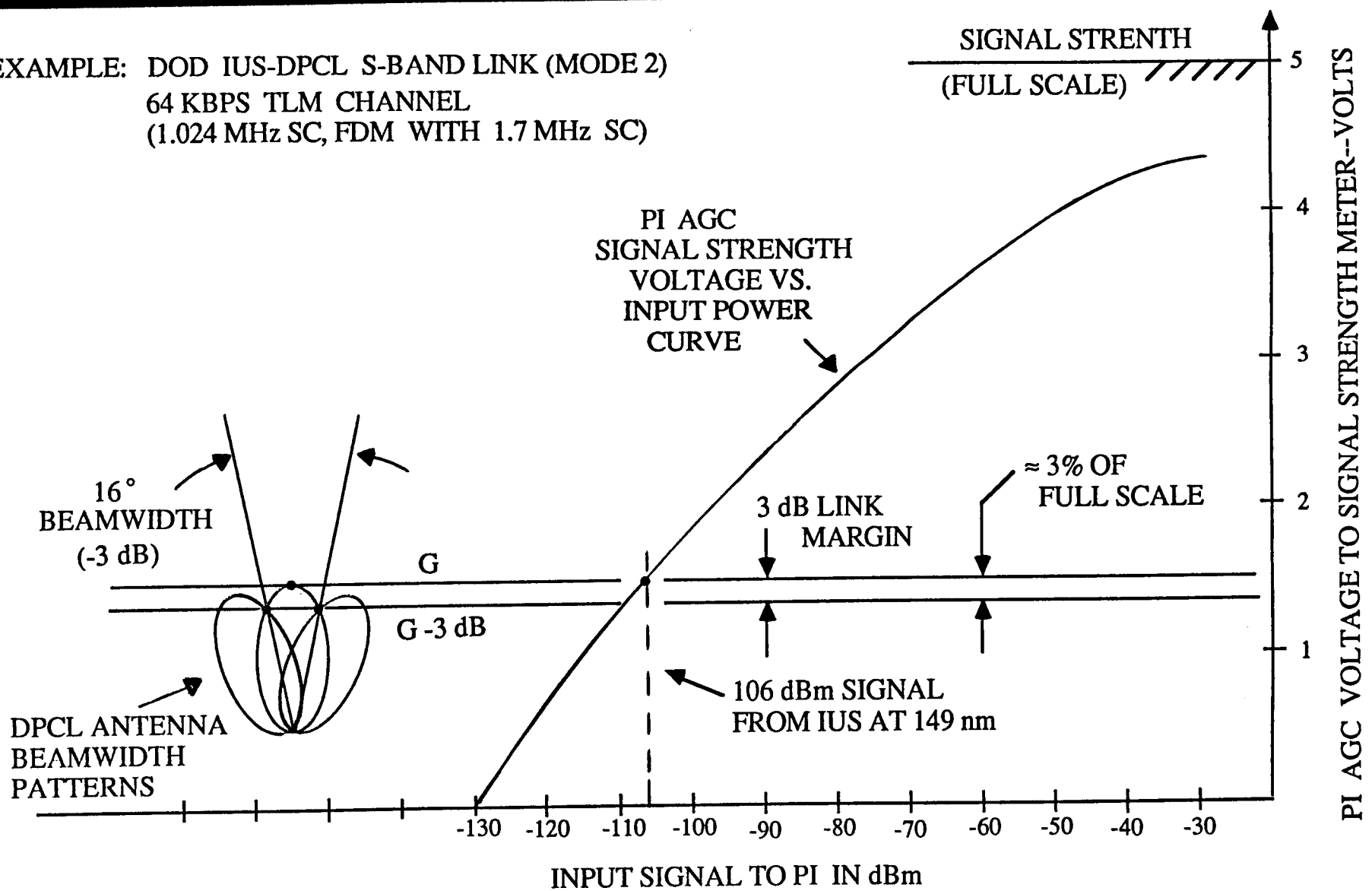

Figure A-6

FIGURE A-7

DPCL Antenna Pointing Methods Comparison

In addition to using the signal strength meter for manually pointing the DPCL antenna other alternatives are available. These alternatives are listed in the order of increasing complexity in Figure A-7. The comments associated with these alternatives, i.e., advantages vs. disadvantages are presented.

DPCL ANTENNA POINTING METHODS COMPARISON

Axiomatix

METHOD	ADVANTAGES	DISADVANTAGE
1). USE SIGNAL STRENGTH METER TO MANUALLY UPDATE ANTENNA POINTING	1). SIMPLIEST IMPLEMENTATION	1). POINTING ACCURACY IS VERY POOR. MARGINAL LINKS CAN BE EASILY LOST (SEE EXAMPLE)
2). DEVELOP PAN AND TILT ERRORS BY OFF-BEAM DISPLACING DPCL ANTENNA AND USE ERRORS TO KEEP ANTENNA POINTED	1). DOES NOT REQUIRE MONOPULSE FEED ON DPCL ANTENNA 2). IF CLOSED LOOP IS PROVIDED THEN A SIMPLE FORM OF AUTO-TRACKING CAN BE PROVIDED	1). REQUIRES AUTO-DRIVE ON PAN/TILT MOUNT 2). REQUIRES ANGLE POINT LOOPS IN PAN AND TILT 3). SMALL SIGNAL LOSS (0.5 TO 1 dB) MAY BE INCURRED DUE TO ANTENNA POINTING OFF-BEAM TO DEVELOP ANGLE TRACKING ERRORS
3). PROVIDE MONOPULSE FEED AND DISPLAY ANGLE ERROR SIGNAL ON SIGNAL STRENGTH METER	1). DOES NOT REQUIRE ANGLE TRACKING SERVO LOOPS 2). PROVIDES RELATIVELY HIGH ACCURACY OF ANTENNA POINTING USING SIGNAL STRENGTH METER	1). REQUIRES DEVELOPMENT OF A MONOPULSE FEED ON DPCL ANTENNA 2). REQUIRES ADDITIONAL RECEIVER(S) FOR ERROR (Δ-PAN AND Δ-TILT) AMPLIFICATION

Figure A-7

FIGURE A-8

DPCL Antenna Pointing Method Comparison (Cont.)

This figure is a continuation of comparison of DPCL antennas pointing methods.

DPCL ANTENNA POINTING METHODS COMPARISON (CONT.)

Axiomatix

METHOD	ADVANTAGES	DISADVANTAGES
4). PROVIDE MONOPULSE FEED AND USE MONOPULSE CONVERTER TO PERMIT USE OF PI FOR ANGLE TRACK ERROR AMPLIFICATION	1). PI RECEIVER CAN BE USED FOR AMPLIFYING ANGLE TRACK ERRORS	1). REQUIRES MODIFICATION OF SOME UNITS OF PI RECEIVER TO PERMIT EXTRACTION OF ANGLE TRACK DATA 2). INTRODUCES SOME DEGRADATION TO RECEPTION OF PI SIGNAL
5). DEVELOP A MONOPULSE ANTENNA AND USE A SEPARATE RECEIVER CHANNEL FOR ANGLE ERROR AMPLIFICATION	1). TRUE MONOPULSE ANGLE TRACKING CAN BE OBTAINED WITH THIS METHOD	1). REQUIRES SEPARATE RECEIVER WHICH MAY BE AS COMPLICATED AS THE RECEIVER PORTION OF THE PI 2). REQUIRES CONSIDERABLE AMOUNT OF NEW DEVELOPMENT--MAY BE A COSTLY OPTION

Figure A-8

DPCL TRANSCEIVER IMPLEMENTATION CONSIDERATION

FIGURE A-9

Closed Loop Gain/Attenuation Budget

The original system concept has the DPCL electronics on a deployable boom with a modified television pan-tilt unit pointing a 2 foot S-band high gain antenna. This antenna would be installed in the forward payload bay opposite the Ku-band antenna. The RF portion has two configurations: Mode 1 (receive only) with a low-noise amplifier (LNA) at the output of the S-band antenna, and Mode 2 (transmit/receive) in which the LNA is bypassed and the antenna output is connected to the payload interrogator with a resulting 8 to 9 dB loss.

An alternate design proposed by JSC has the same deployable assembly configuration except the RF electronics (low noise amplifier and power amplifier) are both located on the boom (possibly behind the feed into the antenna). Locating the RF electronics near the antenna terminals provides approximately 10 dB of performance improvement because of reduced RF cables losses. A block diagram of the proposed design is shown in Figure A-9. In closed proximity to the feed of the antenna is placed a low noise amplifier (LNA) with a noise figure of less than 2 dB over the receive frequency band. This provides a system gain/temperature (G/T) such that the telemetry range capabilities can be greatly extended over the present Orbiter system. Co-located with the LNA is a power amplifier (PA) of approximately 5 watts. This will provide sufficient radiated power such that the range objectives for commanding payloads can be met. The LNA, PA, and associated electronics can be provided as one package mated to the antenna.

The advantage of this system over the baseline DPCL system is the 10 dB gain provided by the PA in the transmit/receive Mode 2. As can be seen in Figure A-9, the transmit/receive module is now a closed loop system with a single input and output.

FIGURE A-9 (Continued)

Care must be taken in the system design to ensure that the closed loop gain does not exceed the losses at all frequencies.

An oscillatory condition would exist if the net closed loop gain exceeded unity. Accordingly, a number of bandpass filters are inserted both before and after the amplifiers to provide isolation between the transmit and receive freeqnencies. The transmit circuitry has to accommodate a 360 MHz bandwidth since the L-band lower frequency is 1763 MHz and the S-band upper frequency is 2120 MHz. The receive circuitry has only a 100 MHz bandwidth to cover the S-band 2200 to 2300 Mhz range.

The factors which determine the loop stability are defined in Figure A-9.

CLOSED LOOP GAIN/ATTENUATION BUDGET

Axiomatix

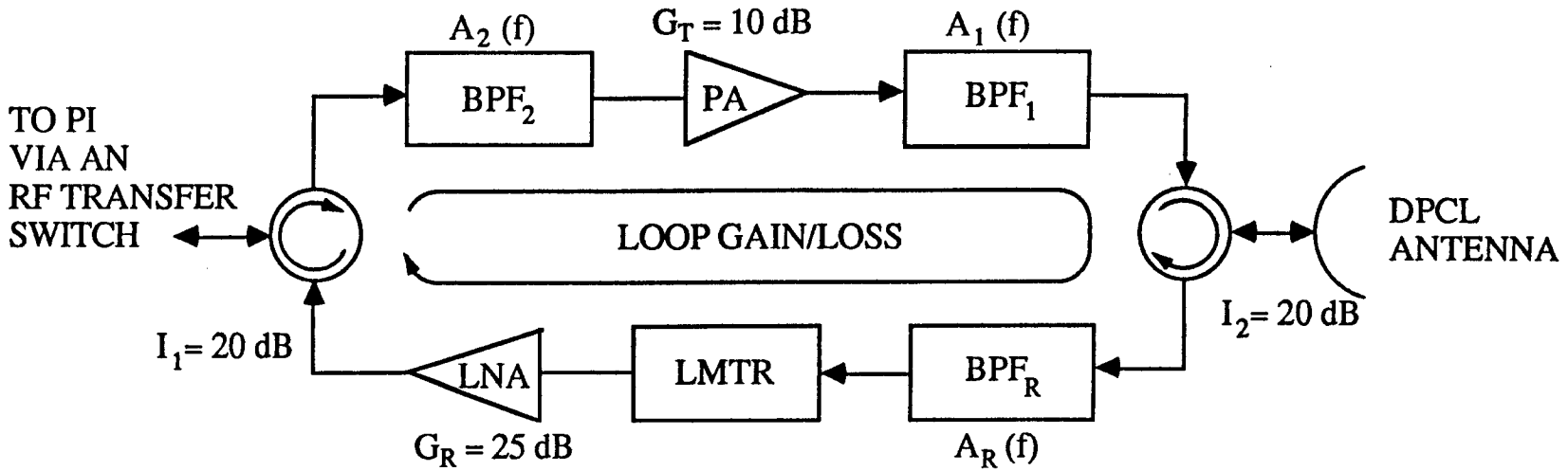

LOOP/GAIN LOSS IS A <u>FUNCTION OF FREQUENCY</u> AND DEPENDS ON:

G_T = TRANSMITTER GAIN (MAY OR MAY NOT BE FREQUENCY DEPENDENT)

$A_1(f)$ = ATTENUATION OF BPF_1 (FUNCTION OF FREQUENCY)

I_2 = ISOLATION OF CIRCULATOR # 2 (ASSUMED FLAT)

$A_R(f)$ = ATTENNATION OF BPF_R (FUNCTION OF FREQUENCY)

G_R = RECEIVER LNA GAIN (MAY OR MAY NOT BE FREQUENCY DEPENDENT)

I_1 = ISOLATION OF CIRCULATOR # 1 (ASSUMED FLAT)

$A_2(f)$ = ATTENUATION OF BPF_2 (FUNCTION OF FREQUENCY)

FOR WIDEBAND PA AND LNA:

$$\text{LOOP GAIN/LOSS} = G_T + G_R - (I_1 + I_2) - [A_1(f) + A_R(f) + A_2(f)]$$
$$= 10 + 25 - (20 + 20) - \Sigma A(f) = -5 - \Sigma A(f) < 0 \text{ (LOOP STABLE)}$$

Figure A-9

FIGURE A-10

Closed Loop Gain/Attenuation Budget (Continued)

In this figure, we summarize the loop stability considerations presented in the previous figure. Thus, there are at least 5 dB of margin available due to circulators. This, however, may not be sufficient for a practical system and, consequently, additional margin should be obtained via frequency-selective filtering.

As indicated, however, a detailed knowledge of the gain vs. frequency characteristics of all of the components comprising the loop must be obtained to define the actual margin available at each frequency.

CLOSED LOOP GAIN/ATTENUATION BUDGET (CONT.)

Axiomatix

SUMMARY

- AT LEAST 5 dB OF LOSS IS PROVIDED IN THE LOOP OF A TRANSRECEIVER TYPE DPCL (LOOP STABLE)
- ADDITIONAL LOSS MARGIN CAN BE PROVIDED BY TRANSMIT AND RECEIVER FILTERS WITHIN THE LOOP

ISSUES

- ATTENUATION PROVIDED BY FILTERS IS FREQUENCY-SELECTIVE AND MUST BE PRECISELY KNOWN OVER THE FREQUENCY RANGE WHERE LNA AND PA HAVE GAIN
- FOR EXAMPLE, ASSUMING:

  1) WIDE-BAND LNA AND PA
  2) BPF_1 IS 3-POLE, 1dB CHEBYCHEV

  AND 3) BPF_R IS 6-POLE, 1dB CHEBYCHEV

THE COMBINATION MINIMUM ATTENUATION OF -12 dB APPEARS AT ABOUT 2200 MHz JUST ABOVE THE CROSS-OVER OF THE SELECTIVITY CURVES OF THE TWO FILTERS.

CONCLUSIONS

- THE TRANSCEIVER DESIGN BASED ON CLOSED LOOP IS STABLE IN PRINCIPLE PROVIDED THAT FILTER CHARACTERISTICS ARE CAREFULLY DESIGNED
- TRANSCEIVER DESIGN REQUIRES PRECISE KNOWLEDGE OF FREQUENCY DEPENDENT GAIN/LOSSES OF ALL COMPONENTS COMPRISING THE LOOP

Figure A-10

APPENDIX B

SPACE TELESCOPE PERFORMANCE AT 500 BPS

SPACE TELESCOPE PERFORMANCE AT 500 BPS

Prepared for

Contract No. NAS9-17384
Lyndon B. Johnson Space Center
Houston, Texas 77058

Prepared by

Jack K. Holmes

Axiomatix
9841 Airport Boulevard, Suite 912
Los Angeles, California 90045

Axiomatix Report No. 8509-1
October 28, 1985

Table of Contents

Summary

It is shown that the Space Telescope may have a BER so poor that the data would be unusable at the proposed 500 bps data rate of Bi-ϕ-L data. This problem, however, would not occur at 4 kbs, 32 kbs or 1 Mbs due to the diminished effect of the PI loop on the data. The basis for this problem lies in the fact that the data is heavily filtered by the action of the PI phase locked loop whose nominal bandwidth is 1000 Hz. Whether or not the link would work depends upon knowing the exact operational PI loop bandwidth.

This report does not include the effect of the bit synchronizer in the PSP, but rather assumes ideal unfiltered bit synchronization. If it were included, then probably the threshold effect would be more pronounced.

It is recommended that 500 bps not be considered a viable data rate, due to the fact that the link may or may not work depending on the actual PI loop bandwidth.

List of Figures

List of Tables

1.0 INTRODUCTION

The purpose of this analysis is to determine whether the Space Telescope can transmit 500 bps Bi-ϕ-L data to the Shuttle Orbiter without major problems. The basic concern is the fact that the data rate is 500 bps and the Payload Interrogator closed loop carrier tracking bandwidth is 1000 Hz. Thus, it appears that considerable distortion would occur with this scenario.

In this report we will determine the bit error rate for various loop bandwidths around B_L=1000 Hz.

2.0 ANALYSIS

2.1 Signal Structure

The Space Telescope signal modulation is based on direct digital phase modulation of the carrier. The signal can be described by

$$y(t) = \sqrt{2}A \sin(\omega_c t + \theta\, d(t)) \tag{1}$$

$$y(t) = \overbrace{\sqrt{2}A \cos\theta \sin\omega_c t}^{\text{carrier}} + \overbrace{\sqrt{2}Ad(t) \sin\theta \cos\omega_c t}^{\text{data}} \tag{2}$$

with the power in the carrier and the data tabulated in Table I.

Table 1. Suppression vs. Modulation Angle

	Modulation Index		
	NOMINAL	MIN	MAX
	0.78 rad	0.5 rad	1.06 rad
CARRIER SUPPRESSION	-2.96 dB	-1.13 dB	-6.22 dB
DATA SUPPRESSION	-3.06 dB	-6.38 dB	-1.19 dB

Thus, we see from Table I that the power in the carrier and the data can vary significantly as the modulation angle varies from 0.5 to 1.06 radians.

2.2 Response of the Loop to One Manchester Symbol

The data demodulation model is shown in Figure 1.

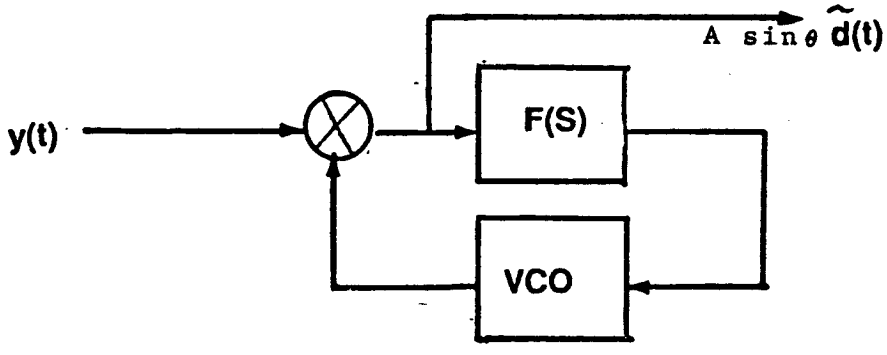

Figure 1. Payload Interrogator Data Demodulation

Figure 1: Payload Interrogator Data Demodulation

It was shown in Reference 1 that the demodulated output $e_o(t)$ is given by

$$e_o(t) = A \sin \theta \, \tilde{d}(t) = A \sin \theta (1-H(S))d(t) \qquad (3)$$

where

θ = the phase modulation angle, radians
A = rms input signal amplitude
H(S) = closed loop transfer function of the PI (in operator notation)
d(t) = unmodulated data stream (Bi-ϕ-L)

The closed loop transfer function of the second order loop is given by

$$H(S) = \frac{2\zeta\omega_n S + \omega_n^2}{S^2 + 2\zeta\omega_n S + \omega_n^2} \qquad (4)$$

where

ζ = damping factor
ω_n = natural frequency

To determine the bit error rate performance we must determine the data response at the output of the loop as described by equation (3). We model a Manchester (Bi-ϕ-L) bit, p(t), by the sum of three terms:

$$p(t) = U(t)-2U(t-T/2) + U(t-T) \tag{5}$$

where

$U(t) = 1$ $t \geq 0$ and zero, otherwise
T = Manchester symbol duration

It follows, using inverse La Place Transforms, that the distorted single pulse is given by

$$e_o(t) = \mathcal{L}^{-1}\left\{\frac{1}{s}\,\frac{s^2}{s^2 + 2\zeta\omega_n s + \omega_n^2}\,A \sin\theta\right\} \tag{6}$$

By using the La Place Transform Tables, we determine that the output signal is given by ($t \geq 0$)

$$e_o(t) = A \sin\phi\left[\cos\left(\sqrt{1-\zeta^2}\,\omega_n t\right) - \frac{\zeta}{\sqrt{1-\zeta^2}}\sin\left(\sqrt{1-\zeta^2}\,\omega_n t\right)\right].\exp[-\zeta\omega_n t] \tag{7}$$

for a single pulse (not the Manchester symbol).

2.3 Response of the Loop to the Data Sequence

In order to determine the overall data sequence response, the influence of previous bits must be allowed for. Based on some preliminary calculations we shall consider two bits prior to the bit under discussion. Consider Figure 2.

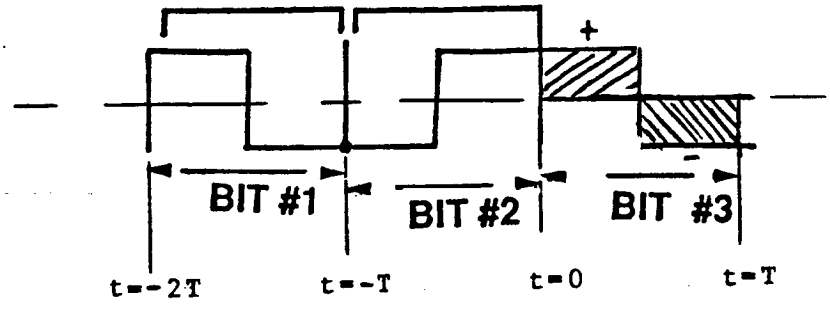

Figure 2. Intersymbol Interference Model

Now consider the output during bit #3 with t = 0 corresponding to the start of bit #3. For $t\varepsilon(0, T/2)$ we have,

$$e(t) = \frac{e_o(t)}{A \sin A} = [\cos(.707\,\omega_n t) - \sin(.707\,\omega_n t)]e^{-.707\omega_n t}$$

$$+ d_1[\cos(.707\,\omega_n(t+T)) - \sin(.707\,\omega_n(t+T)]e^{-.707\omega_n(t+T)}$$

$$- 2d_1[\cos(.707\,\omega_n(t+\tfrac{1}{2}T) - \sin(.707\,\omega_n(t+\tfrac{1}{2}T))]e^{-.707\omega_n(t+\frac{1}{2}T)}$$

$$+ d_1[\cos(.707\,\omega_n(t))) - \sin(.707\,\omega_n(t)]e^{-.707\omega_n(t)}$$

$$+ d_2[\cos(.707\,\omega_n(t+2T)) - \sin(.707\,\omega_n(t+2T)]e^{-.707\omega_n(t+2T)}$$

$$-2d_2[\cos(.707\,\omega_n(t+3/2T)) - \sin(.707\,\omega_n(t+3/2T))]e^{-.707\omega_n(t+3/2T)}$$

$$+ d_2[\cos(.707\,\omega_n(t+T)) - \sin(.707\,\omega_n(t+T))]e^{-.707\omega_n(t+T)} \qquad (8)$$

and for $t\varepsilon(T/2, T)$ we have

$$e(t) = \frac{e_T(t)}{A \sin\theta} = [\cos(.707\,\omega_n(t+T/2) - \sin(.707\,\omega_n(t+T/2))]e^{-.707\omega_n(t+T/2)}$$

$$- 2[\cos(.707\,\omega_n t) - \sin(.707\,\omega_n t)]e^{-.707\omega_n t}$$

$$+ d_1[\cos(.707\omega_n(t+3/2T)) - \sin(.707\omega_n(t+3/2T)]e^{-.707\omega_n(t+3/2T)}$$

$$- 2d_1[\cos(.707\,\omega_n(t+T)) - \sin(.707\,\omega_n(t+T))]e^{-.707\omega_n(t+T)}$$

$$+ d_1[\cos(.707\,\omega_n(t+\tfrac{T}{2})) - \sin(.707\,\omega_n(t+\tfrac{T}{2}))]e^{-.707\omega_n(t+T/2)}$$

$$+ d_2[\cos(.707\,\omega_n(t+\tfrac{5}{2}T)) - \sin(.707\,\omega_n(t+\tfrac{5}{2}T))]e^{-.707\omega_n(t+5/2T)}$$

$$- 2d_2[\cos(.707\,\omega_n(t+2T)) - \sin(.707\,\omega_n(t+2T))]e^{-.707\omega_n(t+2T)}$$

$$+d_2[\cos(.707\,\omega_n(t+\tfrac{3}{2}T)) - \sin(.707\,\omega_n(t+\tfrac{3}{2}T))]e^{-.707\omega_n(t+3/2T)} \qquad (9)$$

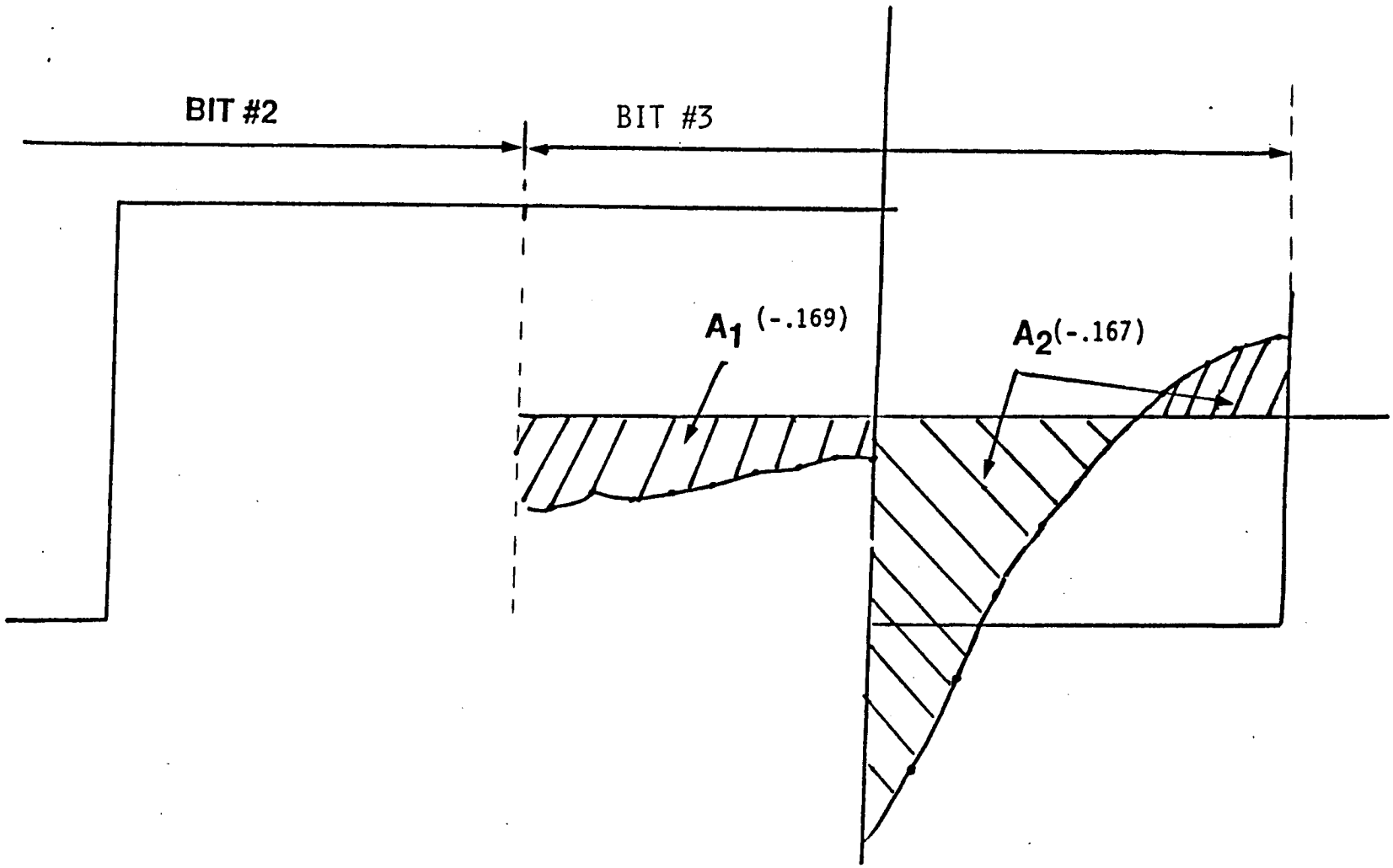

Figure 3. Effect of Intersymbol Interference on the Detected Bit Showing Irreducible Error

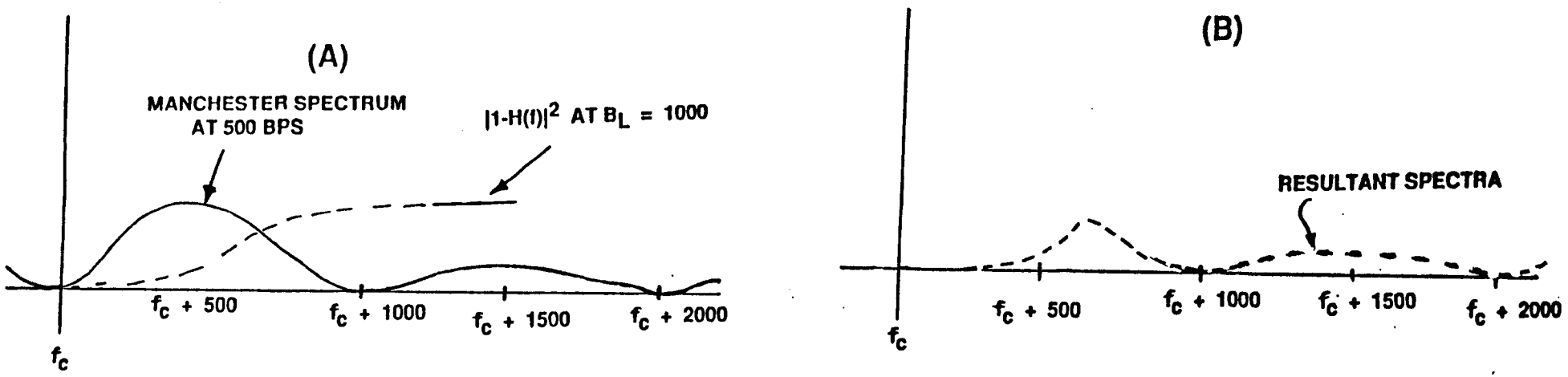

Figure 4. Data Spectra and Loop Response

As the bandwidth of the loop increases relative to the data rate, the distortion increases until the area in the first half of the bit #3, minus the area in the latter half of bit #3, becomes zero for a particular bit #1 - bit #2 sequence. At that point no amount of signal power can cause the BER to reduce below 1/4. Hence, an irreducible or catastropic error occurs.

Figure 3 illustrates the actual waveform when bit #1 is plus one, bit #2 is negative one, and of course bit #3 is plus one. (It is only necessary to consider the case when bit #3 is plus one due to the symmmetry involved).

We note in Figure 3 that the relative area in the first half of bit #3 is negative (-.169) and not positive as it would be if no distortion occurred. Furthermore, the area in the second half of the bit has two components one negative and one positive. In the case shown $A_1 - A_2 < 0$ and hence the irreducible error occurs for the 1, -1, 1 bit sequence.

Another way to look at the distortion is to consider the effect in the frequency domain. Figure 4 illustrates how the PI loop response causes severe distortion on the Bi-ϕ-L spectra to the bit synchronizer.

The appendix lists a Basic program which is capable of computing the BER for this 3 bit sequence with bit #3 the bit to be detected. It has been assumed that ideal bit synchronization occurs. However, this is probably not a valid assumption as the bit synchronizer architecture was not available when it was decided that it was a reasonable approach.

2.4 BER Performance Calculation

In order to determine the Bit Error Probability (BER) it is necessary to determine the BER for each of the four possible sequences. Thus, the average BER is given by $P(d_1 = i, d_2 = j) = 1/4$ for all i,j

$$\overline{PE} = 1/4 \operatorname{erfc}\left(\sqrt{\frac{2E_1}{N_o}}\right) + 1/4 \operatorname{erfc}\left(\sqrt{\frac{2E_2}{N_o}}\right) + 1/4 \operatorname{erfc}\left(\sqrt{\frac{2E_3}{N_o}}\right) + 1/4 \operatorname{erfc}\left(\sqrt{\frac{2E_4}{N_o}}\right) \quad (10)$$

where

$$\operatorname{erfc}(x) = \frac{2}{\sqrt{\pi}} \int_{x}^{\infty} e^{-z^2} dz \tag{11}$$

with

$$E_1 = \left| A \int_0^T e(t \mid d_1 = 1,\ d_2 = 1)\ dt \right|^2 / T \tag{12}$$

$$E_2 = \left| A \int_0^T e(t \mid d_1 = 1,\ d_2 = -1)\ dt \right|^2 / T \tag{13}$$

$$E_3 = \left| A \int_0^T e(t \mid d_1 = -1,\ d_2 = 1)\ dt \right|^2 / T \tag{14}$$

$$E_4 = \left| A \int_0^T e(t \mid d_1 = -1,\ d_2 = -1)\ dt \right|^2 / T \tag{15}$$

The resulting BER is illustrated in Figure 5 for the case when B_L = 800, 850,900, 950, 1000, 1100, and 1200 H_z. Also, the NASA measured BER is shown with a dark line. Note, as the PI loop BW increases the BER deteriorates until at $B_L \cong 1200\ H_z$ the BER becomes 1/2!

We have not considered the bit synchronizer in this analysis. It is probable that the bit synch would make the BER performance even more of a threshold effect.

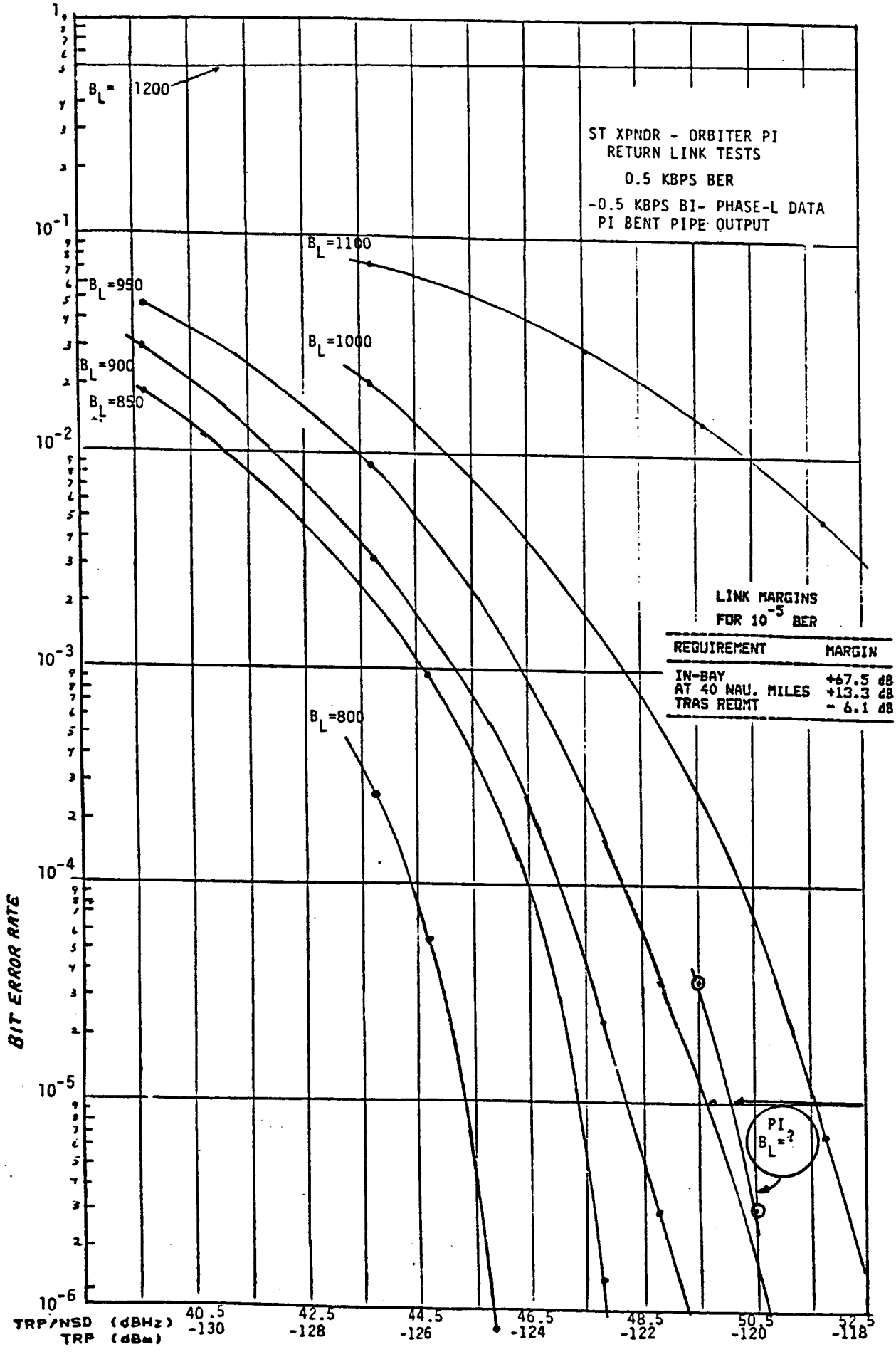

Figure 5. BER for Various Values of B_L

3.0 CONCLUSIONS

We have shown that the BER at 500 bps is strongly dependent on the actual value that the PI carrier loop bandwidth is set at. Furthermore, the communication link is subject to catastrophic performance. That is, at a particular value of loop bandwidth the BER approaches either 1/4 or 1/2, and for any greater value of B_L the BER gets worse.

We believe that utilizing 500 bps would be very dangerous, since slight parameter changes could result in a useless data link. However, the 4 kbps, 32 kbps, or 1 Mbps data rates would not be a problem.

Reference

[1] Jack Holmes, "Space Telescope Data Rate and Modulation Index Selection Report", Axiomatix Report No. 8505-1, Rev. 1, May 21, 1985.

Appendix A

"BER" Basic Program

```
86 REM computes ber for (1-h(s))*d(t) with d(t) Bi-Ø-L
88 REM bl=1000,r=500,wn=1885.7,z=.707
95 INPUT "E/No=";E1
97 E=10^(E1/10)
99 DIM S(5)
100 Z=.707
101 DIM P(1000)
102 DIM PP(1000)
110 INPUT "bl=";BL
115 W=BL*1.8857
120 S(1)=0:S(2)=0:S(3)=0:S(4)=0
130 INPUT "number of points per half=";N
149 REM D1-D2 combinations
150 FOR I=1 TO 4 :REM chg second 4 to a 4----------
155 PRINT "i=";I
160 IF I=1 THEN D1=1:IF I=1 THEN D2=1
162 IF I=2 THEN D1=1:IF I=2 THEN D2=-1
164 IF I=3 THEN D1=-1:IF I=3 THEN D2=1
166 IF I=4 THEN D1=-1:IF I=4 THEN D2=-1
170 DT=.001/N
180 FOR M=1 TO N
185 Y1=Z*W*M*DT
200 S11=(COS(Y1)-SIN(Y1))*EXP(-Y1)
220 Y2=Z*W*(M*DT+.002)
230 Y3=Z*W*(M*DT+.001)
240 S21=D1*(COS(Y2)-SIN(Y2))*EXP(-Y2)
250 S31=-2*D1*(COS(Y3)-SIN(Y3))*EXP(-Y3)
260 S41=D1*(COS(Y1)-SIN(Y1))*EXP(-Y1)
270 Y4=Z*W*(M*DT+.004)
280 Y5=Z*W*(M*DT+.003)
290 S51=D2*(COS(Y4)-SIN(Y4))*EXP(-Y4)
300 S61=-2*D2*(COS(Y5)-SIN(Y5))*EXP(-Y5)
310 S71=D2*(COS(Y2)-SIN(Y2))*EXP(-Y2)
315 P(M)=S11+S21+S31+S41+S51+S61+S71
317 REM LPRINT M;P(M)
318 REM LPRINT S11;S21;S31;S41;S51;S61;S71
320 S(I)=S(I)+S11+S21+S31+S41+S51+S61+S71
322 REM LPRINT "s(i)=";S(I)
330 NEXT M
333 IF I=1 THEN S1=S(1)/N/2
334 IF I=2 THEN S2=S(2)/N/2
336 IF I=3 THEN S3=S(3)/N/2
338 IF I=4 THEN S4=S(4)/N/2
340 SS(1)=0:SS(2)=0:SS(3)=0:SS(4)=0
350 FOR M1= 1 TO N
360 Y1= Z*W*(M1*DT+.001)
370 Y2=Z*W*(M1*DT)
380 S12=+(COS(Y1)-SIN(Y1))*EXP(-Y1)
390 S22=-2*(COS(Y2)-SIN(Y2))*EXP(-Y2)
400 Y3=Z*W*(M1*DT+.003)
410 Y4=Z*W*(M1*DT+.002)
420 Y5=Z*W*(M1*DT+.001)
430 S32=D1*(COS(Y3)-SIN(Y3))*EXP(-Y3)
440 S42=-2*D1*(COS(Y4)-SIN(Y4))*EXP(-Y4)
450 S52=D1*(COS(Y5)-SIN(Y5))*EXP(-Y5)
460 Y6=Z*W*(M1*DT+.005)
470 Y7=Z*W*(M1*DT+.004)
480 Y8=Z*W*(M1*DT+.003)
490 S62=D2*(COS(Y6)-SIN(Y6))*EXP(-Y6)
500 S72=-2*D2*(COS(Y7)-SIN(Y7))*EXP(-Y7)
```

"BER" Basic Program

```
510 S82=D2*(COS(Y8)-SIN(Y8))*EXP(-Y8)
520 SS(I)=SS(I)+S12+S22+S32+S42+S52+S62+S72+S82
523 REM pp(m1)=S12+S22+S32+S42+S52+S62+S72+S82 :REM---------
524 REM LPRINT M1;PP(M1)
526 REM LPRINT S12;S22;S32;S42;S52;S62;S72;S82
527 REM LPRINT "ss(i)=";SS(I)
530 NEXT M1
531 IF I=1 THEN SS1=SS(1)/N/2
532 IF I=2 THEN SS2=SS(2)/N/2
533 IF I=3 THEN SS3=SS(3)/N/2
534 IF I=4 THEN SS4=SS(4)/N/2
535 NEXT I
537 LPRINT S1;SS1;S2;SS2;S3;SS3;S4;SS4
540 ST1=-SS1+S1
550 ST2=-SS2+S2
560 ST3=-SS3+S3
570 ST4=-SS4+S4
580 X=SQR(2*ST1*E)
590 GOSUB 800
600 PE1=.25*Q
610 X=SQR(2*ST2*E)
620 GOSUB 800
630 PE2=.25*Q
640 X=SQR(2*ST3*E)
650 GOSUB 800
660 PE3=.25*Q
670 X=SQR(2*ST4*E)
680 GOSUB 800
690 PE4=.25*Q
700 PE=PE1+PE2+PE3+PE4
710 PRINT "eb/no(db)=";E1;"pe=";PE
715 LPRINT "eb/no=";E1;"pe=";PE;"wn=";W;"no. pts=";N
720 END
722 REM
723 REM
724 REM
725 REM
800 REM Q(x) subroutine-----------------------------------------------
810 PI=4*ATN(1)
820 ZZ=1/(SQR(2*PI))*EXP(-X*X/2)
830 T=1/(1+.2316419*X)
840 T2=T*T
850 T3=T2*T
860 Q=ZZ*(.31938153#*T-.356563782#*T2+1.781477937#*T3-1.821255978#*T2*T2
4429#*T2*T2)
                                                          +1.33027
870 RETURN
```

APPENDIX C

ATTITUDE DETERMINATION, CONTROL, AND POINTING

ATTITUDE DETERMINATION, CONTROL, AND POINTING

Interim Report

Contract No. NAS9-17384

Prepared for

Lyndon B. Johnson Space Center
Houston, Texas 77058

Prepared by

Dr. Jack K. Holmes

Axiomatix
9841 Airport Boulevard
Suite 912
Los Angeles, California 90045

Axiomatix Report No. R8605-2
June 18, 1986

Table of Contents

List of Figures

List of Tables

1.0 INTRODUCTION

The motivation of this report is to develop the possibility of using GPS by use of interferometric means to determine and to control the attitude of a large spacecraft.

The attitude of a spacecraft is its orientation in space. Attitude determination is the process of computing the orientation of the spacecraft relative to either an inertial reference or some object of interest such as Earth. Attitude control and pointing is the process of orienting the spacecraft in a specified, predetermined direction. We will discuss attitude determination since that is necessary before attitude control can be done.

Current techniques to obtain attitude determination include Sun Sensors, Horizon Sensors, Magnetometers, Star Sensors and Gyroscopes (Rate Gyros, Rate Integrating Gyros, and Control Moment Gyros).

2.0 PRINCIPLES OF INTERFEROMETRIC ATTITUDE DETERMINATION

One potential application of GPS is to perform space vehicle attitude control and pointing by use of radio-interferometry. GPS signals from a particular Navstar satellite can be simultaneously received by three (or more) antennas aboard the host vehicle. Phase comparison of two received signals can yield the angle of the baseline between the two antennas and the transmitting Navstar. If the angles are measured with respect to different Navstars, the absolute orientation of the spacecraft can be determined. Through observation of the attitude or attitude rates (or some combination thereof) experienced by the baselines between antennas, the vehicle can be stabilized or re-oriented. Two orthogonal baselines, one along the attitude and one perpendicular to it, can be used to determine the attitude and rotational position. Attitude without regard to rotational position can be obtained by using only one baseline with two antennas, in principle. However, due to obscuration, two pairs of antennas may be needed, one pair for the top, and one pair for the bottom.

Figure 1 illustrates the concept of using GPS signals for space-vehicle orientation determination. For convenience of illustration, the two-dimensional problem is first considered. Suppose the line segment L is used to designate the orientation of the space-vehicle. Two antennas are placed at the ends of the segment L respectively, and the length of the baseline L is measured and known. Two GPS receivers will be used, connected to antennas at the endpoints, respectively, to track the same signal from a Navstar satellite. Each receiver will be able to track the GPS PN code (either the 1 MHz C/A code or the 10 MHz P code) to a small fraction of a chip, depending on the received signal-to-noise ratio, receiver resolution, and vehicle dynamics. Thus, the differential path delay to points A and B from the same Navstar can be measured by comparison of the two recovered PN code phases of the receivers fairly accurately. Knowing the differential delay (line segment ΔR in Figure 1) and the baseline L, the angle of orientation of the space-

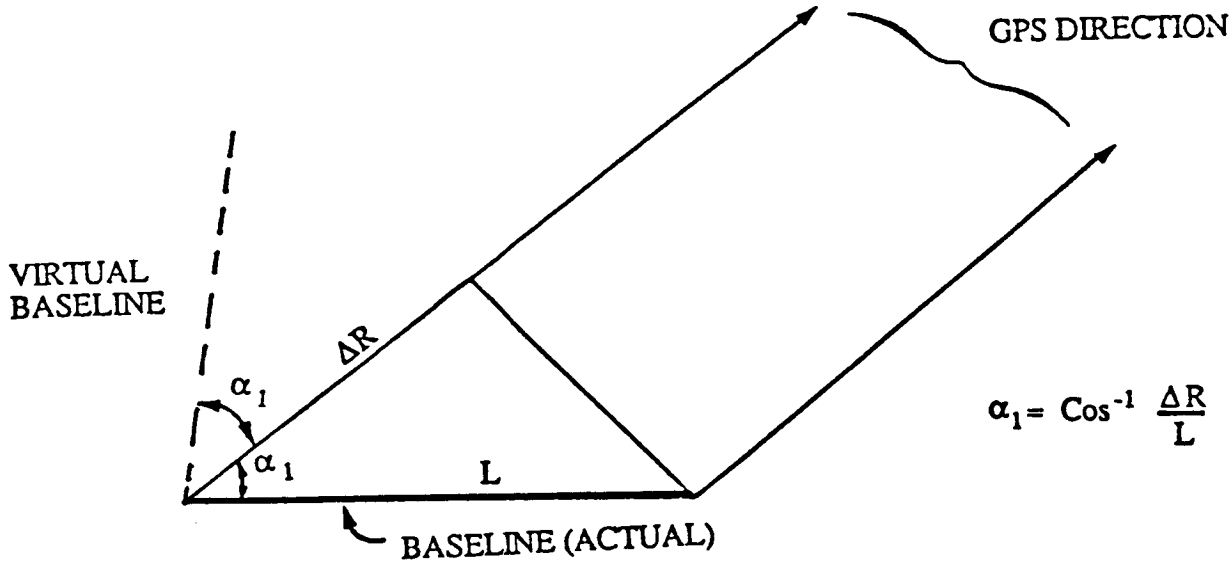

Figure 1 Measurement of Angle Orientation Using Radio Interferometry

vehicle (bold line of length L) can be obtained by calculating the angle α_1 relative to the GPS, shown in the same figure.

Knowledge of the angle α_1 can only determine the orientation of line segment L to be on the surface of a cone, (or two possible lines in the two-dimensional case), as illustrated in Figure 2. In order to select between the actual and virtual baselines, measurement of the inclination angle (α_2) between line L and another Navstar is necessary to resolve the two-fold ambiguity in this simplified two-dimensional situation. A line will be common among the two sets of lines thus determined. And the common line will be the true orientation or attitude of the space vehicle.

In the three-dimensional case, the first angle (α_1) determination will only determine the space-vehicle orientation to be on a conical surface, as shown in Figure 3. Angle measurement (α_2), with respect to another satellite, will reduce the ambiguity to the possibilities of two vector orientations. The final resolution, in the three-dimensional case, will require the measurement with respect to a third Navstar. A spacecraft centered unit celestial sphere illustrates the three circles corresponding to the intersection of the three cones and the celestial sphere shown in Figure 4. The common intersection of three circles defines the attitude (which is a point on the celestial sphere).

The possible attitude lines in three dimension form dots in two dimensions as projected in Figure 4. In Figure 4a, we see that assuming perfect errorless measurements, the six lines (dots) have the property that three of them coalesce into one point.

If, as in the normal case, the cones are measured with some pseudorange error, then the three cones will not have a common intersection line but instead three lines that are closely located as seen Figure 4b. Figure 5 illustrates the three dimensional case when there is no error in the differential range so that only one attitude line is common to all three cones.

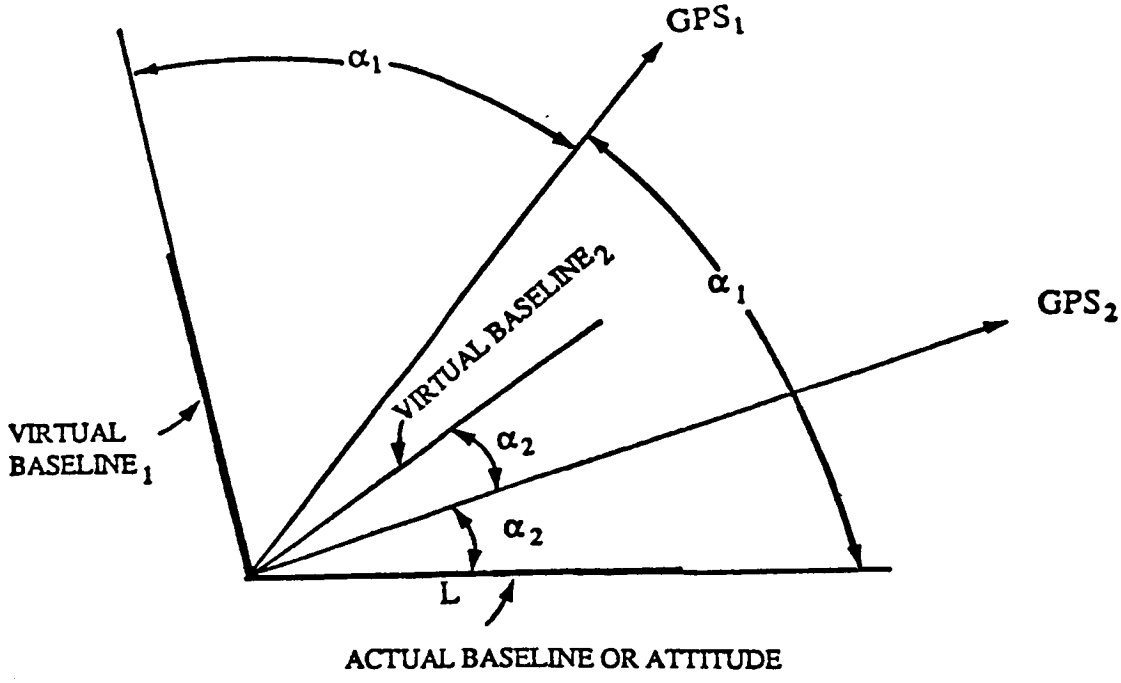

Figure 2 Two dimensional illustration of attitude determination

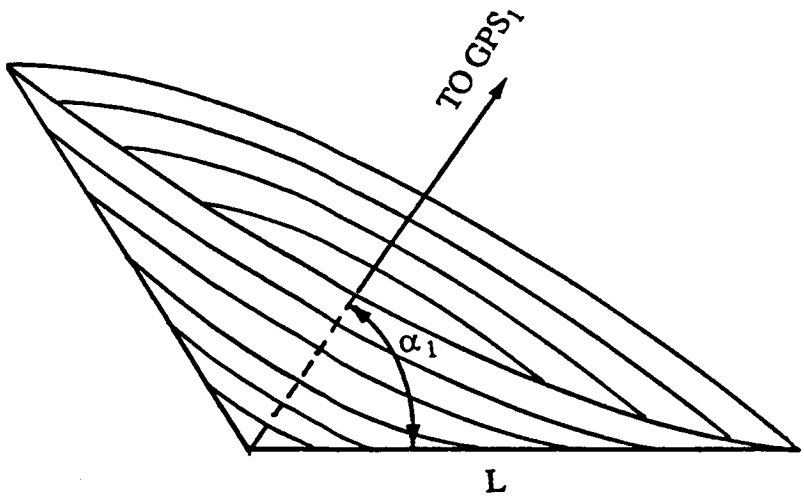

Figure 3 Conical Surface of First Angle α_1

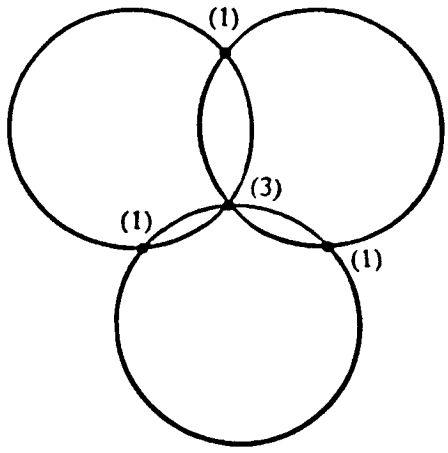

(a) No Error in Each Cone Measurement

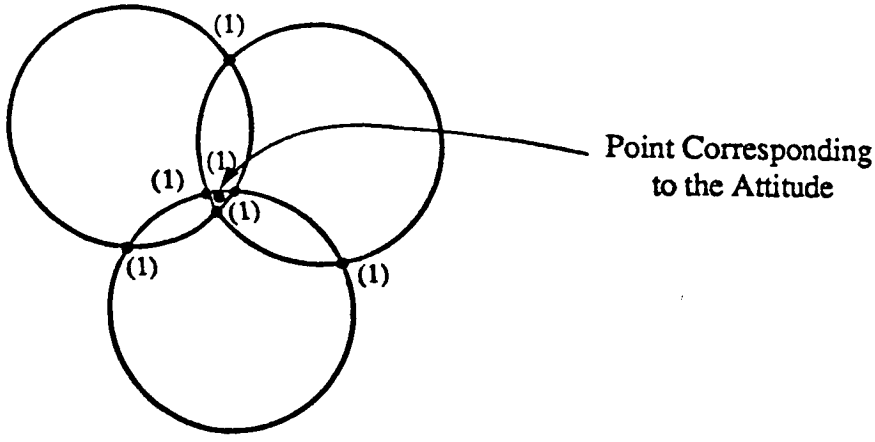

(b) Errors in Each Cone Measurement

Figure 4 Three Dimensional Example--Projection on the Celestial Sphere

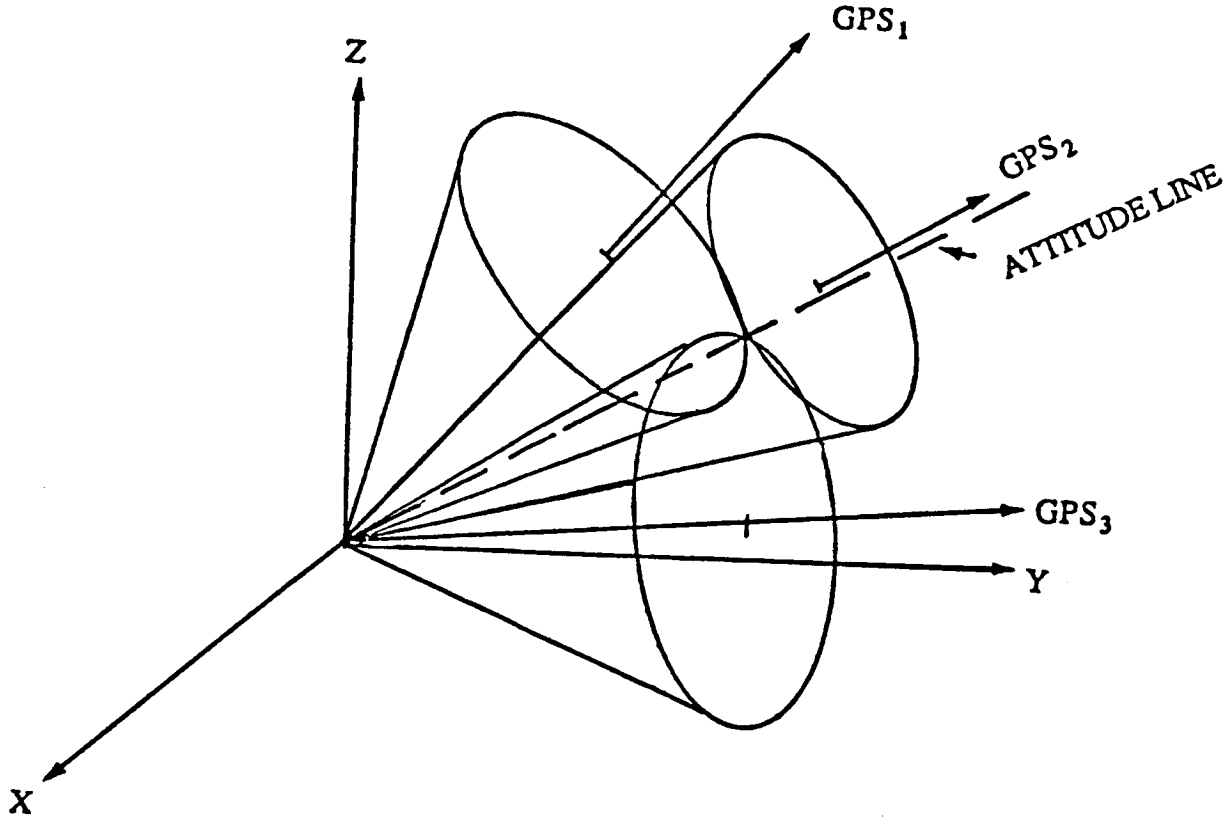

Figure 5 Three Dimensional Example--Common Intersection is the Attitude

3.0 ATTITUDE ACCURACY ESTIMATE--SINGLE AXIS ATTITUDE

The angle determination of say α_1 in Figure 1 is dependent upon the differential delay, ΔR in the figure through the equation

$$\alpha_1 = \cos^{-1}\left(\frac{\Delta R}{L}\right) \tag{1}$$

The distance ΔR depends upon the actual difference in delay as well as the noise induced errors in delay associated with each measurement. Since the two antennas are very close, the differential ionospheric or tropospheric delays would be similar and, hence, cancel out. Basically, this is a differential measurement technique.

At a given code loop bandwidth (B_L), noise bandwidth B, received signal power P_s, noise spectral density N_o (one sided), and filtering loss due to B and α, the relative code tracking error is given by

$$\left(\frac{\sigma}{T_c}\right)^2 = \frac{N_o B_L}{2\alpha P_s}\left[1 + \frac{2N_o B}{\alpha P_s}\right] \quad , \text{chips}^2 \tag{2}$$

Where T_c is the code chip time which is 1μs with the C/A code and 0.1μs with the P code. The attitude pointing performance will depend on a number of factors which include

(a) Received SNR

(b) Receiver resolution (if digital)

(c) Vehicle dynamics

(d) Calibration of the electrical path delay calibration between antennas and receivers and between the receivers.

(e) Accuracy in measuring code phase differences between the pair of PN codes.

(f) Time tagging if the measurements are done sequentially.

The receiver SNR affects each measurement at each antenna with independent noise induced errors. The mean squared timing error at each antenna is given

by (2) so that the differential distance mean squared timing error is $\sqrt{2}$ larger than the standard deviation, defined by (2).

Table 1
TYPICAL LINK BUDGET

P_s	-163 dBW
NF	1.5 dB
RF LOSSES	1 dB
KT	-204dBW/Hz
REC'D C/N_o	38.5 dB-Hz

A typical link budget is illustrated in Table 1. Using a value of $B_L = 0.1$Hz, B = 100Hz, $\alpha \cong 1$, and $P_s/N_o = 38.5$dB-Hz yield the result $\frac{\sigma}{T_c} = 2.69 \times 10^{-3}$ chips. To convert this measurement into an attitude angular error, we can differentiate Equation (1) to yield the relationship between standard deviation errors:

$$\sigma\alpha_1 = \frac{\sqrt{2}\,\sigma_{\Delta PR}}{L \sin \alpha_1} \tag{3}$$

which relates the accuracy in angular one-axis angle error to a single receiver (one end) noise induced distance error, $\sigma_{\Delta PR}$, where

$$\sigma_{\Delta PR} = \sigma C \tag{4}$$

with C is the speed of light and σ is obtained from Equation (2). Hence, we obtain

$$\sigma\alpha_1 = \frac{\sqrt{2}\,\sigma C}{L \sin \alpha_1} \tag{5}$$

Using L = 35 meters, $\alpha_1 = 45°$, $C = 3 \times 10^8$ m/sec, we obtain $\sigma\alpha_1 = 2.6°$ for the C/A code and $\sigma\alpha_1 = 0.26°$ for the P code. From (5), it is seen that a broadside measurement to a GPS provides the greatest sensitivity to angle measurement since $\alpha_1 = 90°$ implies the denominator is maximum.

Now a general solution for the attitude requires three GPS satellites to be viewed resulting in three cones that intersect in space. For the non-ideal (real) case with errors in the measurement, there does not exist a unique solution to the intersection of three

cones. The reason is clear from the observation of Figure 4a and 4b. In Figure 4a, the ideal case, there is a unique intersection. While in Figure 4b, the practical case, it is seen that there is no common line to three cones.

However, it is possible to obtain a solution to the intersection of two cones. Grubin [1] has provided a solution for the two cone-case. Consider Figure 6 which illustrates two cones. Let Θ be the angle between the two-cone centers (center lines) as shown in the figure. Also let $\bar{e}_1$ be the vector pointing towards the second GPS, then the direction of the attitude (common line to the two cones) is given by one of the two lines specified

$$\bar{U} = A\,\bar{e}_1 + B\,\bar{e}_2 \pm C\,\bar{n} \tag{6}$$

where n is given by

$$\bar{n} = \bar{e}_1 \times \bar{e}_2 \tag{7}$$

where the three coefficients are given by

$$A = \frac{\cos\alpha_1 - \cos\alpha_2 \cos\Theta}{\sin^2\Theta} \tag{8}$$

$$B = \frac{\cos\alpha_2 - \cos\Theta \cos\alpha_1}{\sin^2\Theta} \tag{9}$$

$$C = \pm\,(1 - A^2 - B^2 - 2AB\cos\Theta)^{1/2} \tag{10}$$

Since the attitude line takes on two possible vectors, we see that we have an attitude ambiguity that must be resolved a priori or,as will be discussed later, by solving three pairs and using the midline of the three closely packed solutions.

Now we consider the error in the attitude line due to the errors in α_1 and α_2 because of imperfect pseudo noise measurements.

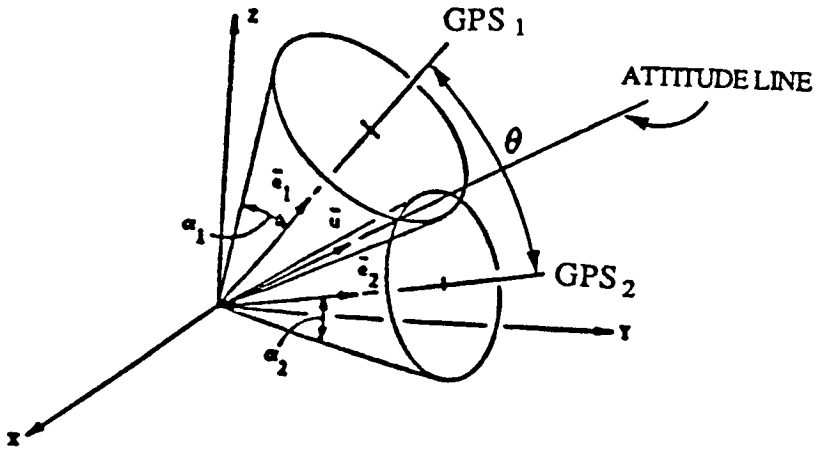

Figure 6 Two Cone Geometry

We can write the solutions to the attitude vector as:

$$\bar{U} = \frac{\cos\alpha_1 - \cos\Theta\ \cos\alpha_2}{\sin^2\Theta}\,\bar{e}_1 + \frac{\cos\alpha_2 - \cos\Theta\ \cos\alpha_1}{\sin^2\Theta}\,\bar{e}_2$$

$$\pm \frac{\bar{e}_1 \times \bar{e}_2}{|\bar{e}_1 \times \bar{e}_2|}\left(1 - \frac{(\cos\alpha_1 - \cos\Theta\ \cos\alpha_2)}{\sin^2\Theta}\cos\alpha_1 - \frac{(\cos\alpha_2 - \cos\Theta\ \cos\alpha_1)}{\sin^2\Theta}\cos\alpha_2\right) \tag{11}$$

Of course only one solution is the attitude, the other is its image. In order to measure the error between the attitude line with no errors on it and the attitude line with errors, we need a measure of "error". Thus, we consider the error measure

$$\phi = \cos^{-1}\left(\frac{\bar{U} \cdot \bar{U}_e}{|\bar{U}|\ |\bar{U}_e|}\right) \tag{12}$$

Where U is the true attitude and U_e is the measured attitude. In order to evaluate ϕ, it is convenient to express U and U_e in an orthogonal coordinate system. We use the transformation (see Figure 7):

$$\begin{aligned} \bar{e}_2 &= \bar{e}_x \\ \bar{e}_1 &= \bar{e}_y \sin\Theta + \bar{e}_x \cos\Theta \\ \bar{e}_z &= \bar{e}_1 \times \bar{e}_2 = \bar{e}_y \times \bar{e}_x \end{aligned} \tag{13}$$

Using (13) in (11) and simplifying produces

$$\bar{U} = \cos\alpha_2\,\bar{e}_x + \frac{\cos\alpha_1 - \cos\Theta\ \cos\alpha_2}{\sin\Theta}\,\bar{e}_y \pm \left[1 - \left(\frac{\cos^2\alpha_1 + \cos^2\alpha_2 - 2\cos\Theta\ \cos\alpha_2\cos\alpha_1}{\sin^2\Theta}\right)\right]\bar{e}_z \tag{14}$$

Now that we have $\bar{U}$ in an orthogonal vector representation, we can determine a perturbed vector, $\bar{U}_e$, which has errors in the measurement of α_1 and α_2 and thus is not pointing in the same direction as $\bar{U}$.

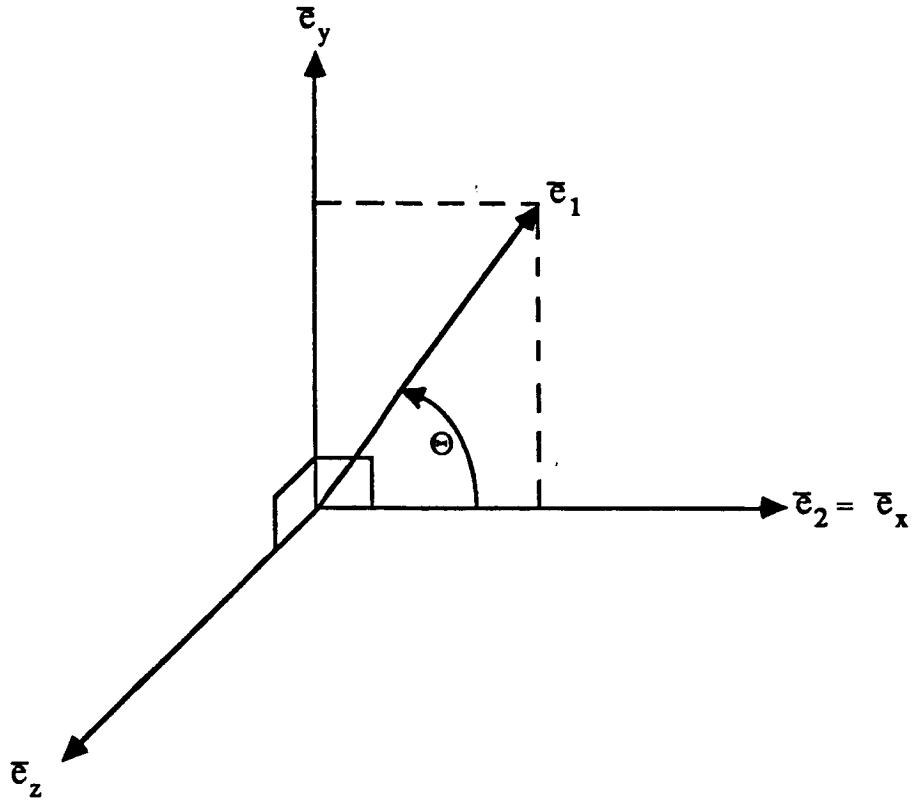

Figure 7 Transformation for Orthogonal Coordinate System

C-2

Now the perturbed vector $\bar{U}_e$ is given by

$$\bar{U}_e = \bar{U} + d\bar{U} \tag{15}$$

Then one can determine the error in the attitude by solving for the minimum positive ϕ (the angle from $\bar{U}$ to $\bar{U}_e$) from the equation

$$\cos \phi = \frac{\bar{U} \cdot \bar{U}_e}{|\bar{U}|\ |\bar{U}_e|} \tag{16}$$

Now let us determine $d\bar{U}$. Recall for a function of two variables that

$$dF = \frac{\partial F}{\partial \alpha_1} d\alpha_1 + \frac{\partial F}{\partial \alpha_2} d\alpha_2 \tag{17}$$

So that from (14) $d\bar{U}$ becomes

$$d\bar{U} = -\sin\alpha_2\, d\alpha_2\, \bar{e}_x + \left(\frac{\cos\Theta_1\, \sin\alpha_2\, d\alpha_2 - \sin\alpha_1\, d\alpha_1}{\sin\Theta}\right)\bar{e}_y \tag{18}$$

$$\pm\left(\frac{2\cos\alpha_1\sin\alpha_1 d\alpha_1 + 2\cos\alpha_2\sin\alpha_2 d\alpha_2 - 2\cos\Theta\,(\cos\alpha_1\sin\alpha_2 d\alpha_2 + \cos\alpha_2\sin\alpha_1 d\alpha_2)}{\sin^2\Theta}\right)\bar{e}_z$$

Therefore, the perturbed vector $\bar{U}_e$ is given by

$$\bar{U}_e = (\cos\alpha_2 - \sin\alpha_2\, d\alpha_2)\bar{e}_x$$

$$+ \left(\frac{\cos\alpha_1 - \cos\Theta\cos\alpha_2}{\sin\Theta} + \frac{\cos\Theta\, \sin\alpha_2\, d\alpha_2 - \sin\alpha_1\, d\alpha_1}{\sin\Theta}\right)\bar{e}_y$$

$$\pm\left[1 - \left(\frac{\cos^2\alpha_1 + \cos^2\alpha_2 - 2\cos\Theta\cos\alpha_2\cos\alpha_1}{\sin^2\Theta}\right)\right]\bar{e}_z \tag{19}$$

$$\pm\left(\frac{2\cos\alpha_1\sin\alpha_1 d\alpha_1 + 2\cos\alpha_2\sin\alpha_2 d\alpha_2 - 2\cos\Theta\,(\cos\alpha_1\sin\alpha_2 d\alpha_2 + \cos\alpha_2\sin\alpha_1 d\alpha_2)}{\sin^2\Theta}\right)e_z$$

The smallest positive ϕ such that (16) is satisfied is the pointing error. Hence, Equations (14), (16), and (19) form the general solution to attitude pointing for a single axis system.

In order to get a feel of the accuracy capability of this system, we assume that $\alpha_1 = \alpha_2 = 45°$ then we obtain (the primes denote $\alpha_1 = \alpha_2 = 45°$)

$$\bar{U}' = \frac{1}{\sqrt{2}}\bar{e}_x + \frac{1-\cos\Theta}{\sqrt{2}\sin\Theta}\bar{e}_y \pm \left[1 - \frac{1-\cos\Theta}{\sin^2\Theta}\right]\bar{e}_z \tag{20}$$

and

$$\bar{U}'_e = \frac{1-d\alpha_2}{\sqrt{2}}\bar{e}_x + \left(\frac{(1-\cos\Theta)}{\sqrt{2}\sin\Theta} + \frac{(\cos\Theta\, d\alpha_2 - d\alpha_1)}{\sqrt{2}\sin\Theta}\right)\bar{e}_y \pm \left[1 - \frac{(1-\cos\Theta)(1-(d\alpha_1 + d\alpha_2))}{\sin^2\Theta}\right]\bar{e}_z \tag{21}$$

Since ϕ is small, we may (from 16) solve for ϕ^2 via

$$\phi^2 = 2\left(1 - \frac{\bar{U}_e \cdot \bar{U}}{|\bar{U}_e|\,|\bar{U}|}\right) \tag{22}$$

so that the second moment can be obtained from (by letting $d\alpha_1 = x_1$ and $d\alpha_2 = x_2$ and $\underline{x} = (x_1, x_2)$)

$$\phi^2 = 2\int_{-\infty}^{\infty}\int_{-\infty}^{\infty}\left(1 - \frac{\bar{U}_e(\underline{x})\cdot\bar{U}_e(\underline{x})}{|\bar{U}_e(\underline{x})|\,|U(\underline{x})|}\right)\rho(x_1, x_2)\,dx_1 dx_2 \tag{23}$$

Assuming the errors are statistically and identically and normally distributed, we can write

$$\bar{\phi}^2 = 2\int_{-\infty}^{\infty}\int_{-\infty}^{\infty}\left(1 - \frac{\bar{U}_e(\underline{x})\cdot\bar{U}_e(\underline{x})}{|\bar{U}_e(\underline{x})|\,|U(\underline{x})|}\right)\frac{1}{2\pi\sigma^2}\bar{e}^{\frac{x_1}{2\sigma^2}}\bar{e}^{\frac{x_2}{2\sigma^2}}\,dx_1 dx_2 \tag{24}$$

as the mean squared attitude error. This equation can be discretized and evaluated by a digital computer. The results are indicated in Table 2 where θ_α is the noise induced angle error of each cone ($\alpha_1 = \alpha_1 = 45°$), Θ is the angle between both viewed Navstars, and $\sqrt{\bar{\phi}^2}$ is the resulting root mean squared attitude angle error.

We conclude that C/A code operation would yield attitude angle errors of about 5 degrees and P code operation would yield errors of about 0.5 degrees. Of course

Table 2

Mean Squared Attitude Angle Error ($\alpha_1 = \alpha_2 = 45°$)

CODE	Θ_α DEGR	Θ DEGR	$\sqrt{\overline{\phi}^2}$ DEGR
C/A CODE	2.6	10	1.59
	2.6	20	8.7
	2.6	30	6.3
	2.6	40	5.1
	2.6	50	4.6
	2.6	60	4.3
	2.6	70	4.2
	2.6	80	4.1
P CODE	0.26	10	1.7
	0.26	20	0.87
	0.26	30	0.63
	0.26	40	0.52
	0.26	50	0.46
	0.26	60	0.43
	0.26	70	0.42
	0.26	80	0.41

the angular error in the roll angle was not considered in this analysis, but it would be about four times larger since attitude error is inversely proportional to baseline length and the transverse length would be about one fourth the longitudinal length.

References

[1] C. Grubin, "Simple Algorithm for Intersecting Two Conical Surfaces," J. Spacecraft, Vol 14, No. 4, April 1977.

4.0 UNIQUE ATTITUDE DETERMINATION

The above solution from the work of Grubin is based on two GPS measurements assuming that the two solutions for the attitude can be resolved by outside knowledge. In the general case, if this assumption is not correct, Grubin's method can be used pairwise as discussed below.

The projections of the three cones are circles on the celestial sphere. When there are no errors in all three measurements then there will be six pairwise solutions with three of them defining identical attitudes as shown in Figure 4a.

When the measurements are not perfect corresponding to the real world case, then all six solutions are distinct as shown in Figure 4b. However, with small angular perturbations, the angular separation of the center three would be small. Thus, the centroid or some other appropriate measure could be used to locate the best estimate of the attitude.

If multiple GPS observations (>2) were made, then locating the centroid may well improve the averaging effect and, therefore, improve the attitude determination accuracy.

5.0 RECEIVER FOR INTERFEROMETRIC DETERMINATION OF THE ATTITUDE

The receiver for the computation of the pseudorange difference measurement does not have to be a full-up GPS receiver, once acquisition is completed. It has to process data sufficient to acquire either the C/A code or both the C/A code and the P-code and then track it. Also, the carrier may have to be tracked for very high accuracy requirements. Once the Navstar satellites have been acquired, as long as they are in view, they can be tracked continuously so that delta range can be output continuously .

Similar to GPS range measurements, the angle determination process can also be performed in a sequential manner, receiving signals from one Navstar at a time. In this process, only two GPS receivers are required, even though for 3-dimensional orientation determination at least four separated antennas are required. The two receivers will be sequentially connected to a pair of antennas. Each time signals from three Navstars are received so as to determine the orientation of that axis. The feasibility of this sequential approach will depend, of course, on the dynamics of the space-vehicle and its orientation.

Figure 8a illustrates how six antennas may be used on the Shuttle to obtain both attitude and rotation position. Consider the top or the bottom set of three antennas and receivers, the front and one wing antenna will determine a line between the two in space when each views three GPS Navstars. Another line can be constructed between the front antenna and the other wing antenna. From these lines, the attitude line can be constructed at the midpoint of the two wing antennas and at the nose antenna suitably adjusted to the same height as the wing antennas. The same construction can be performed for the other three antennas adjusted to the same level as the orginal three antennas so that a common attitude line is constructed.

Once each of the two wing antennas have observed three GPS satellites, then a line between the two determines the roll or angular rotation of the Shuttle. Thus, the complete attitude is determined.

Figure 8b illustrates an alternate configuration that allows the determination of attitude but not roll orientation using four antennas. On the either side only two antennas (and receivers) need view three GPS satellites each to determine the attitude. However, in this case, the two antenna pairs (front and rear) must line up in a line parallel to the attitude.

As another application consider the Space Station, which is illustrated in Figure 9. Four GPS antennas can be located on the top of the station so that the complete attitude can be determined.

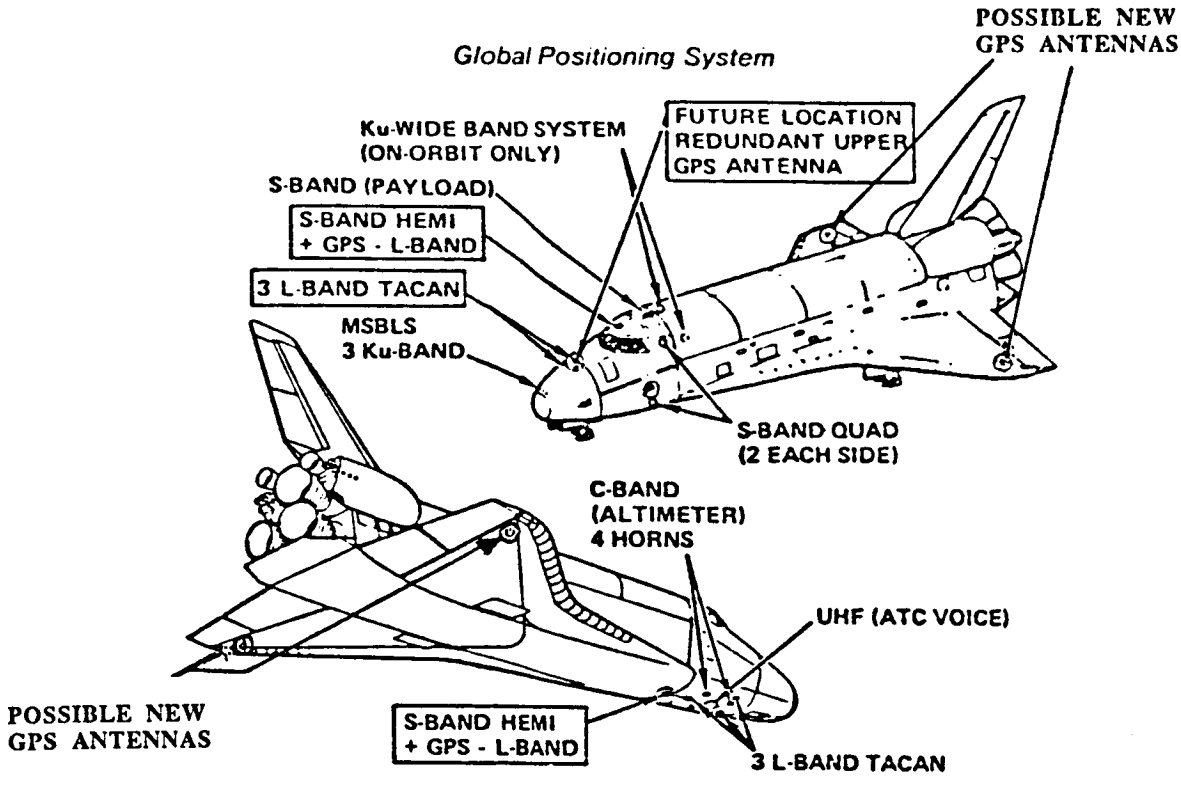

Figure 8a Antenna Locations Using Six Antennas

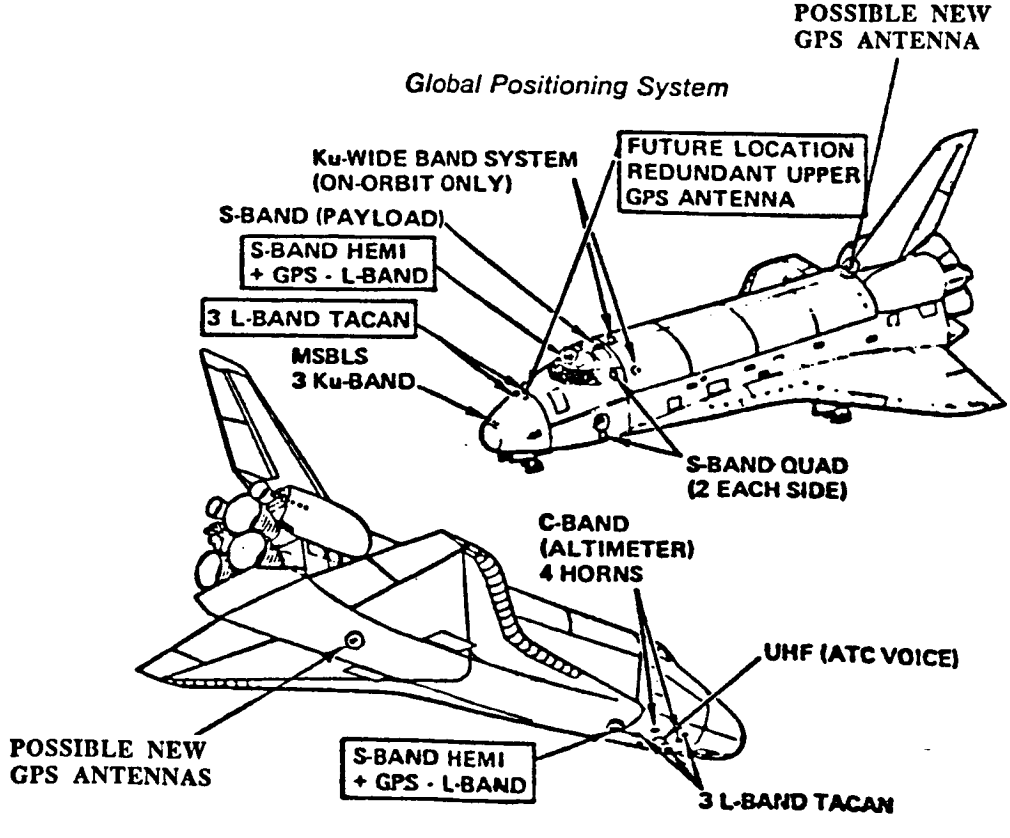

Figure 8b Antenna Locations Using Four Antennas

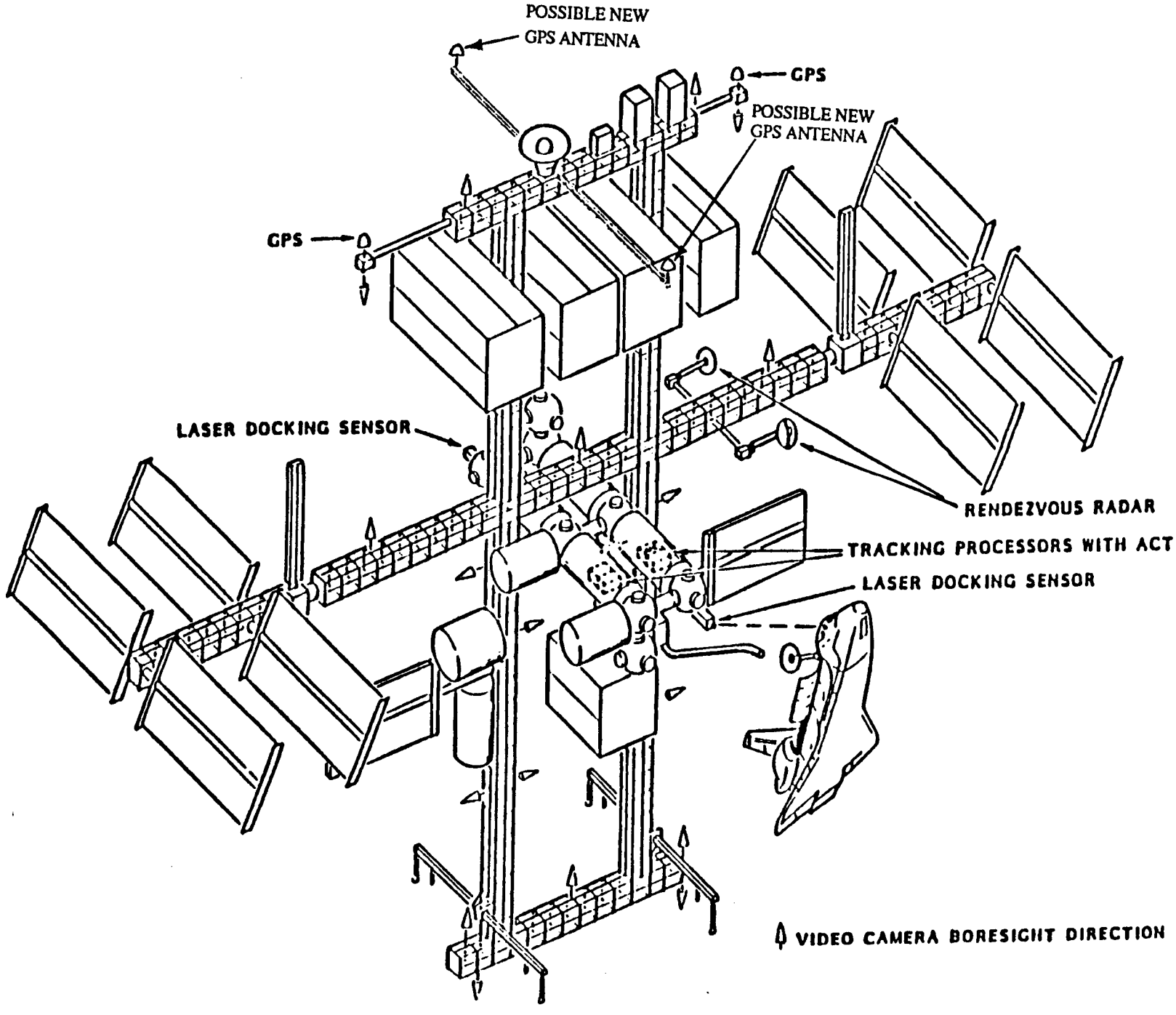

Figure 9 Space Station Dual Keel Configuration with Tracking Subsystem Locations Using Four GPS antennas

6.0 FUTURE WORK

The problem of orientation, pointing, and stabilization is important to almost all space platforms. Obvious examples are the Space Station and space-borne solar array systems.

During the remaining course of the study, a number of performance analyses and system design issues will be performed related to the problem of Spacecraft Attitude Control and Pointing. They can be summarized as follows:

(a) Obtain the three axis attitude determination accuracy

(b) Define the signal processing requirements for phase comparison measurements between received GPS Signals by receivers connected to different antennas on the same spacecraft; and to determine the resultant accuracy in attitude control and pointing, as a function of SNR, receiver resolution, vehicle dynamics, electrical path delay calibration accuracies between antennas, the measurement errors caused by the phase comparison measurement implementation, and other error sources that can be identified.

(c) Study the feasibility of using two receivers only, connected to a pair of antennas at a time, to determine the spacecraft's directional inclination in a sequential manner. If the spacecraft is relatively stationary, this approach should be feasible. The receivers would have to be switched to the differential antennas sequentially. Each time the different electrical path delays are involved, they must be taken into account in the processing algorithm. Practical limits of this approach will be investigated in the course of this study.

(d) In the above discussions, it was assumed that the differential code phase of the two receivers is used to determine the inclination angle between the baseline connecting two antennas and the Navstar. This results in a differential path delay measurement error. If better accuracy is desired, it is possible to measure the phase difference between the L-band carrier phase received by the two receivers. This can improve the measurement accuracy by a large factor ($\approx$100), so that differential delay measurement errors can be reduced to the centimeter range. This approach will required ambiguity resolution between cycles, which is feasible with the GPS signal structure.

7.0 CONCLUSIONS

A initial look at attitude determination has been made and it appears that standard links would produce a mean squared attitude tracking error of about 0.5° using the P code. Tracking the carrier would yield errors of about 0.003°.

APPENDIX D

SERVO TEST SCANS

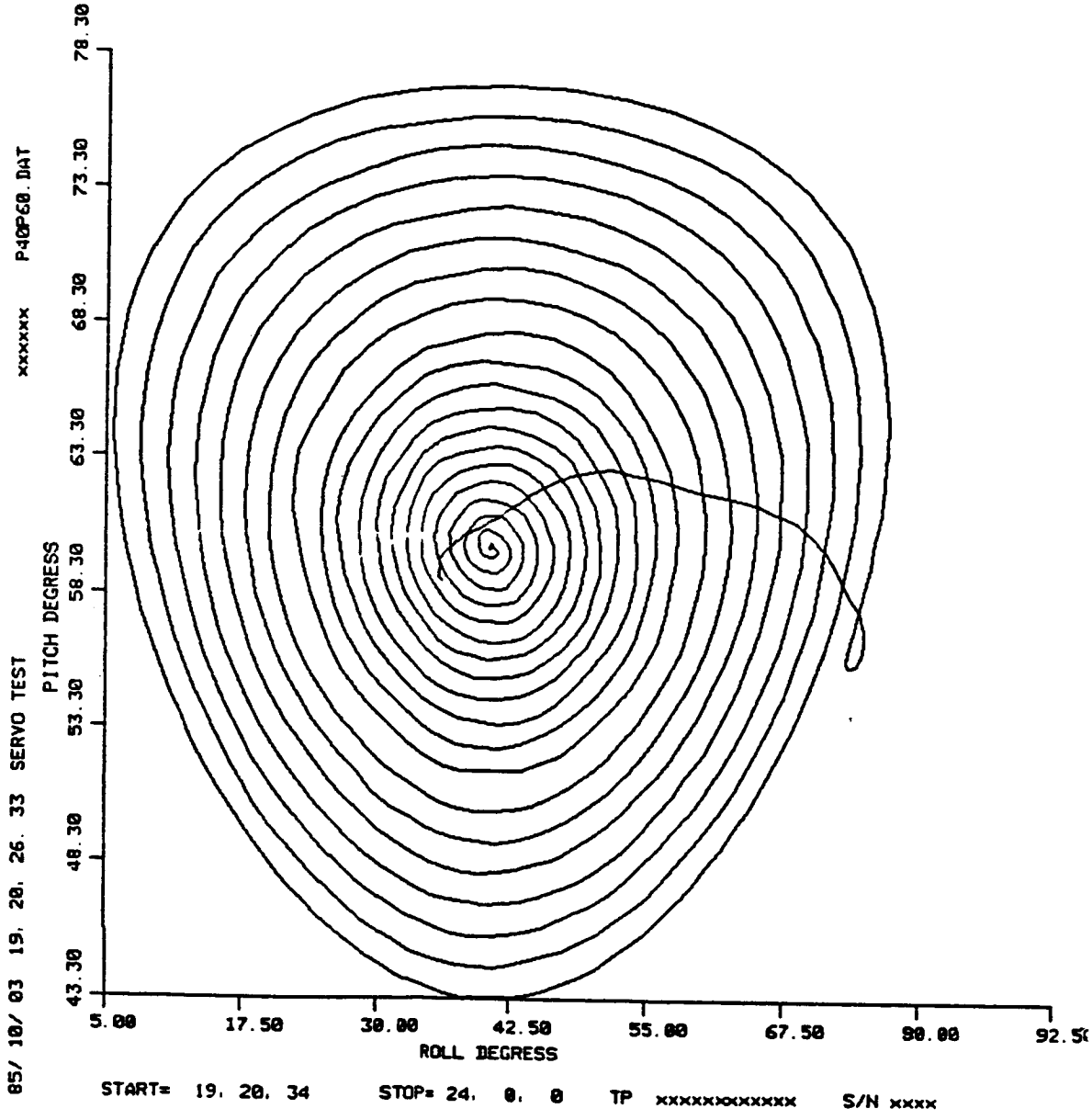
85/ 10/ 03 19. 20. 26. 33 SERVO TEST
xxxxxx P40P60.DAT
PITCH DEGRESS
78.30
73.30
68.30
63.30
58.30
53.30
48.30
43.30
5.00
17.50
30.00
42.50
55.00
67.50
80.00
92.5(
ROLL DEGRESS
START= 19. 20. 34
STOP= 24. 0. 0
TP xxxxxxxxxxx
S/N xxxx

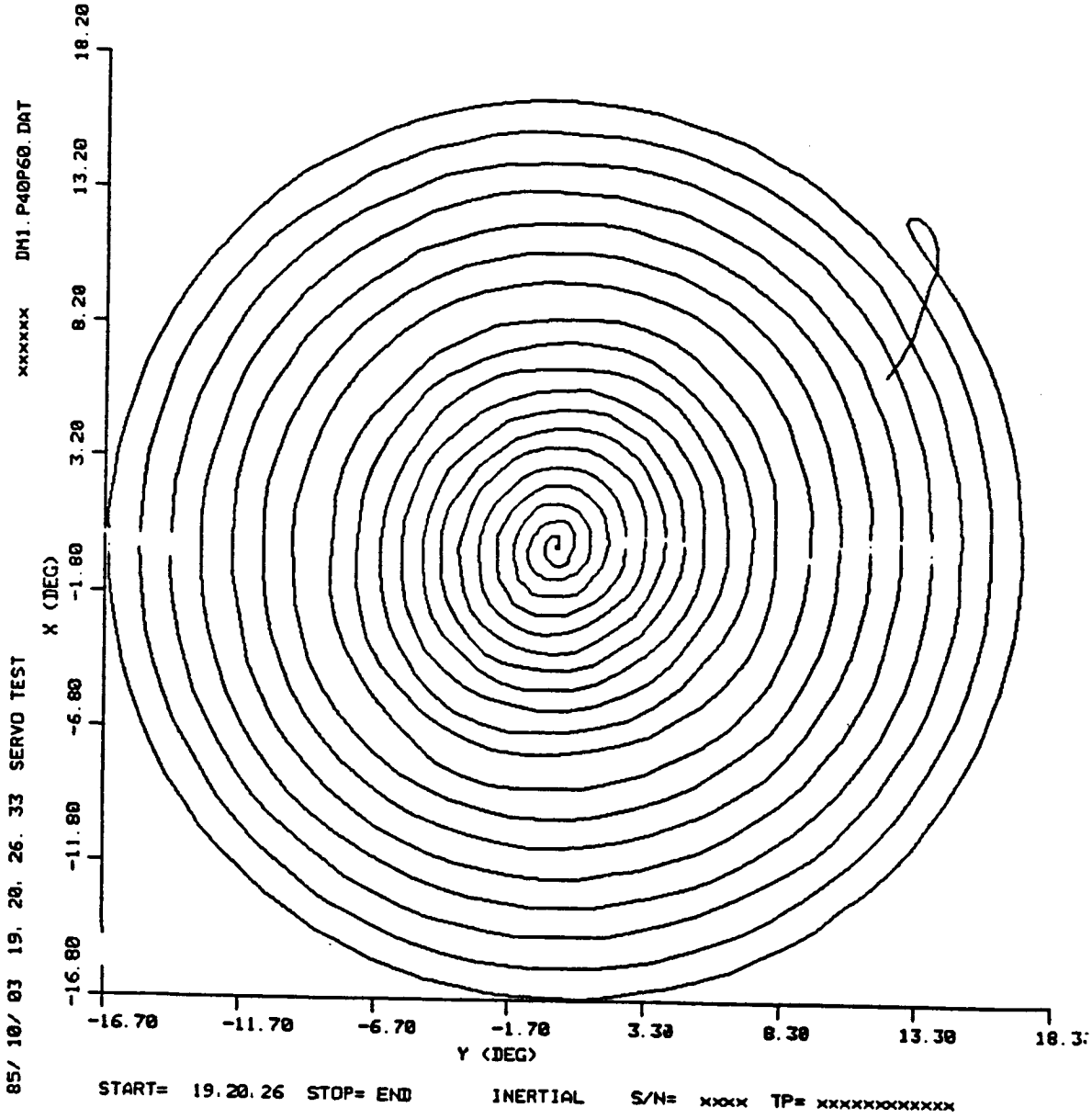
85/ 10/ 03 19. 20. 26. 33 SERVO TEST
xxxxxx DM1.P40P60.DAT
X (DEG)
18.20
13.20
8.20
3.20
-1.80
-6.80
-11.80
-16.80
-16.70
-11.70
-6.70
-1.70
3.30
8.30
13.30
18.3
Y (DEG)
START= 19.20.26 STOP= END
INERTIAL
S/N= xxxx TP= xxxxxxxxxxx

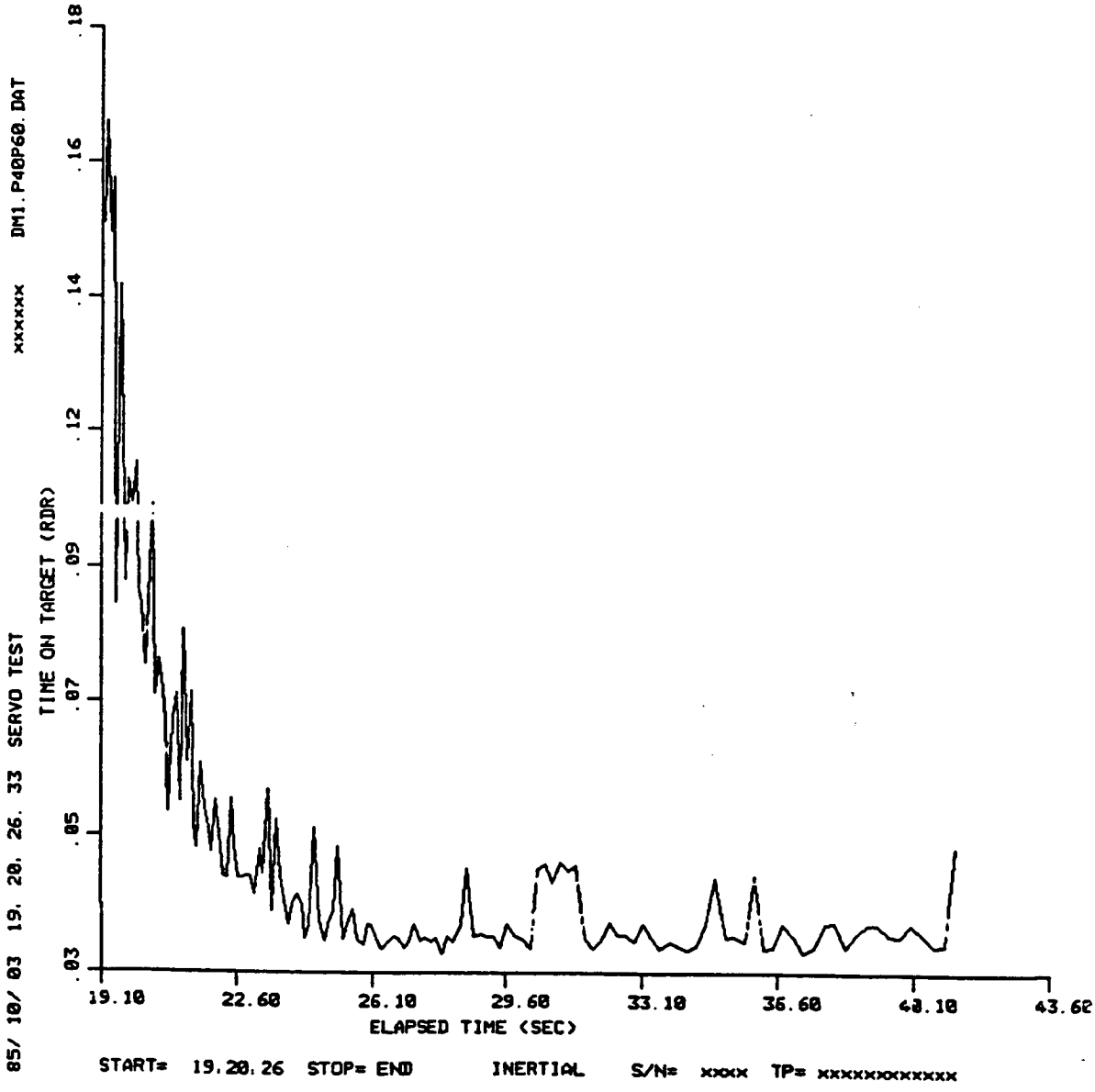
85/ 10/ 03 19. 20. 26. 33 SERVO TEST
xxxxxx DM1.P40P60.DAT
TIME ON TARGET (RDR)
.18
.16
.14
.12
.09
.07
.05
.03
19.10
22.60
26.10
29.60
33.10
36.60
40.10
43.60
ELAPSED TIME (SEC)
START= 19.20.26 STOP= END INERTIAL S/N= xxxx TP= xxxxxxxxxxx

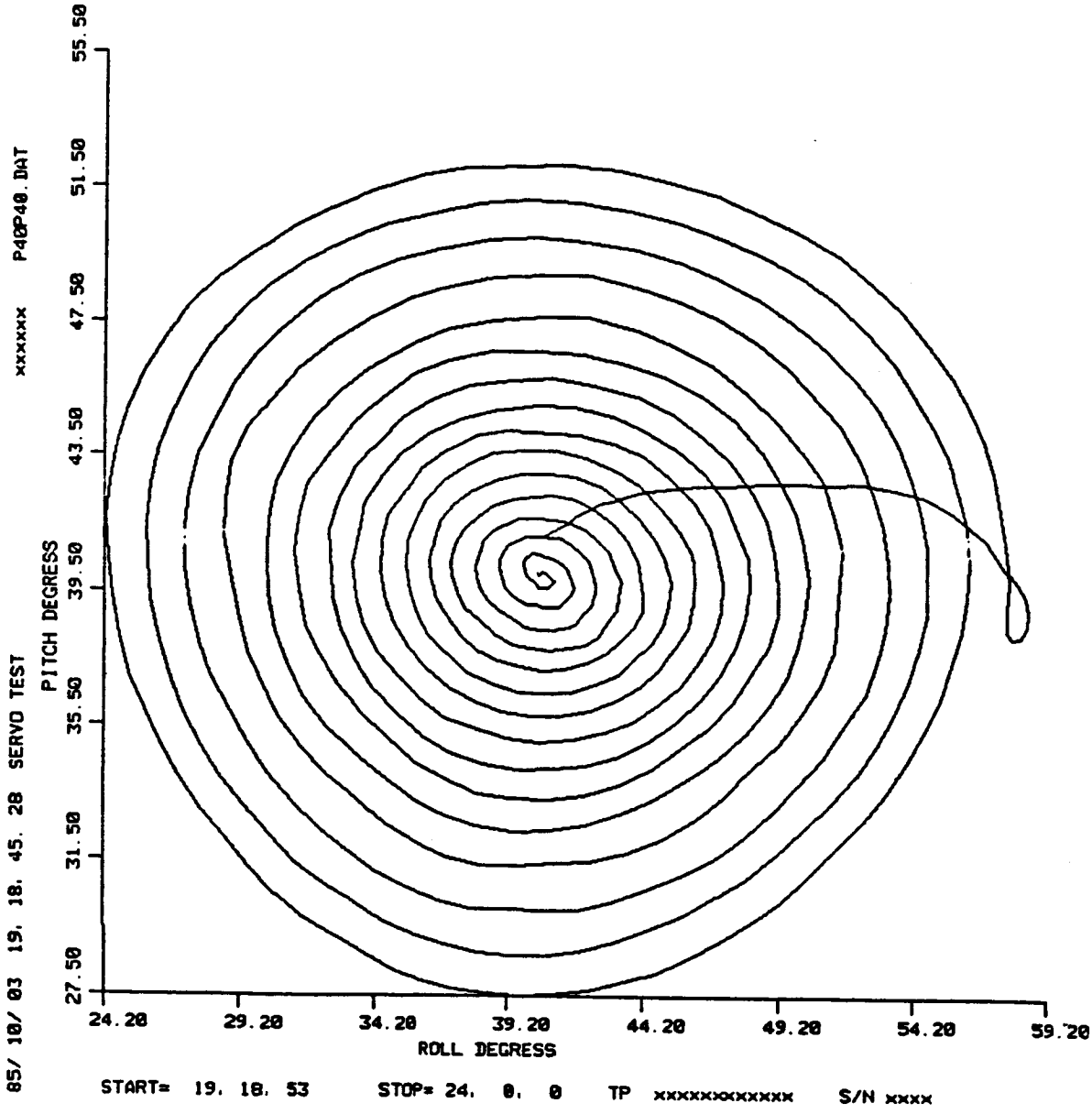
85/ 10/ 03 19. 18. 45. 28 SERVO TEST
xxxxxx P40P40.DAT
PITCH DEGRESS
55.50
51.50
47.50
43.50
39.50
35.50
31.50
27.50
24.20
29.20
34.20
39.20
44.20
49.20
54.20
59.20
ROLL DEGRESS
START= 19. 18. 53
STOP= 24. 0. 0
TP xxxxxxxxxxx
S/N xxxx

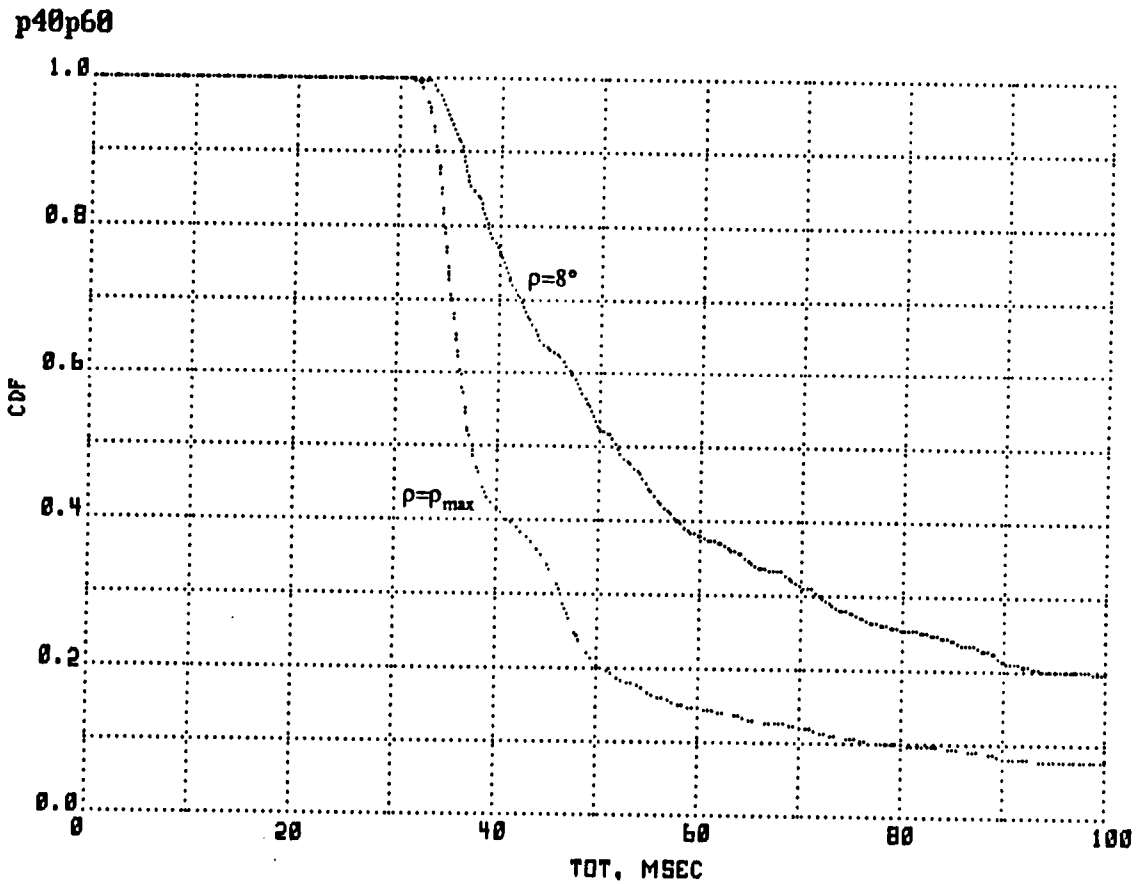
p40p60
1.0
0.8
0.6
0.4
0.2
0.0
CDF
ρ=8°
ρ=ρmax
0
20
40
60
80
100
TOT, MSEC

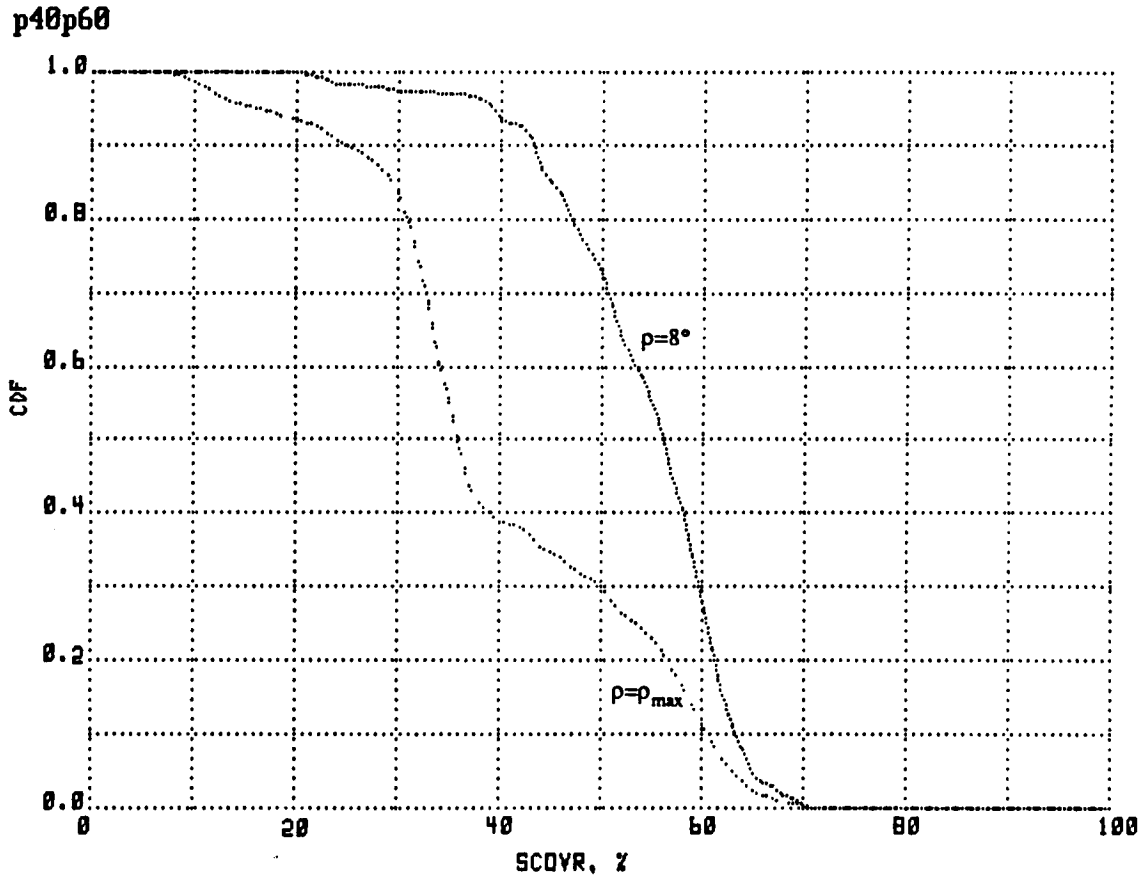
p40p60
1.0
0.8
0.6
0.4
0.2
0.0
CDF
ρ=8°
ρ=ρmax
0
20
40
60
80
100
SCOVR, %

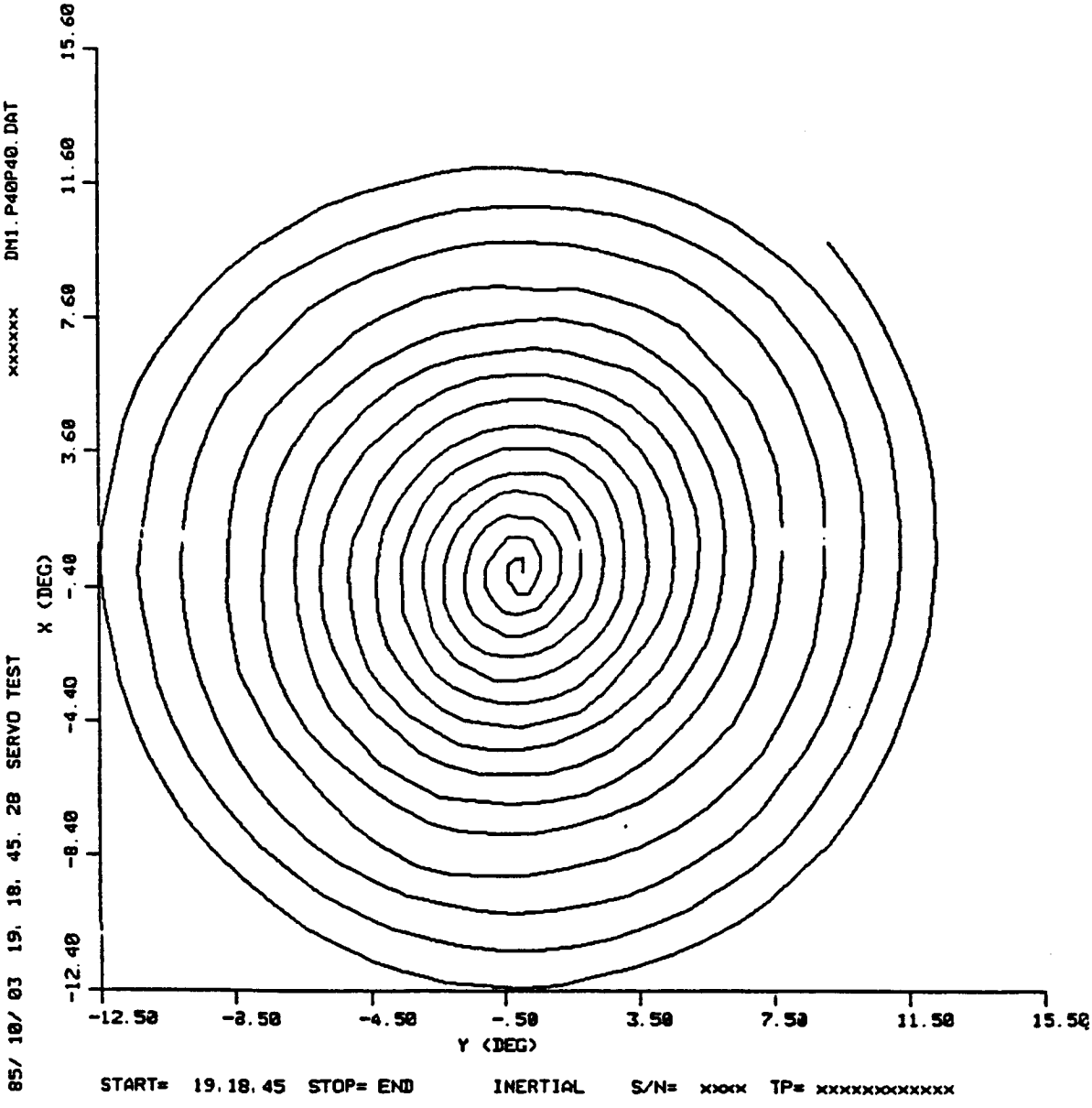
85/ 10/ 03 19. 18. 45. 28 SERVO TEST
XXXXXX DN1.P40P40.DAT
X (DEG)
15.60
11.60
7.60
3.60
-.40
-4.40
-8.40
-12.40
-12.50
-8.50
-4.50
-.50
3.50
7.50
11.50
15.50
Y (DEG)
START= 19.18.45 STOP= END INERTIAL S/N= xxxx TP= xxxxxxxxxxx

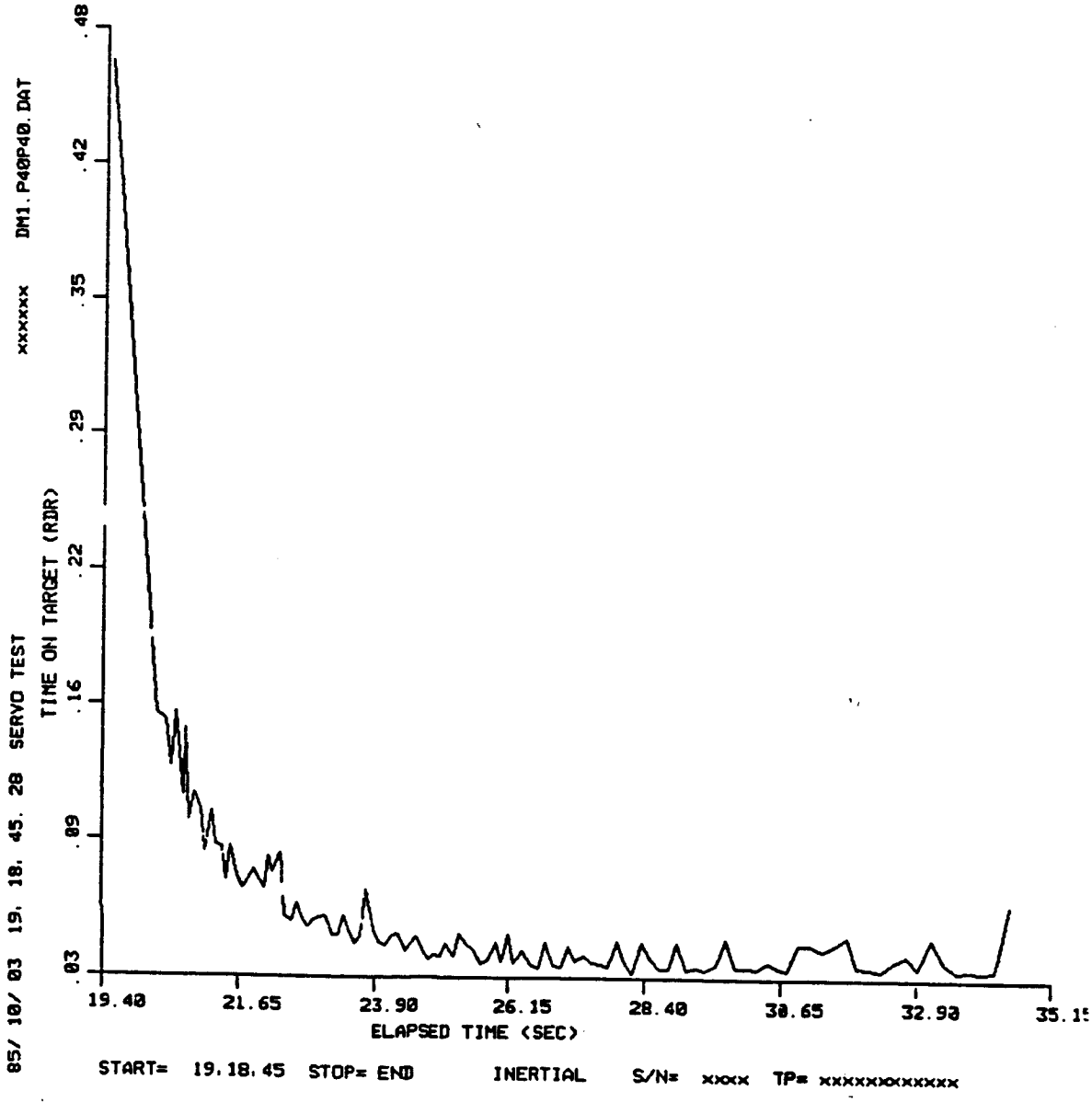
85/ 10/ 03 19. 18. 45. 28 SERVO TEST
xxxxxx DM1.P40P40.DAT
TIME ON TARGET (RDR)
.03
.09
.16
.22
.29
.35
.42
.48
19.40
21.65
23.90
26.15
28.40
30.65
32.90
35.15
ELAPSED TIME (SEC)
START= 19.18.45 STOP= END INERTIAL S/N= xxxx TP= xxxxxxxxxxx

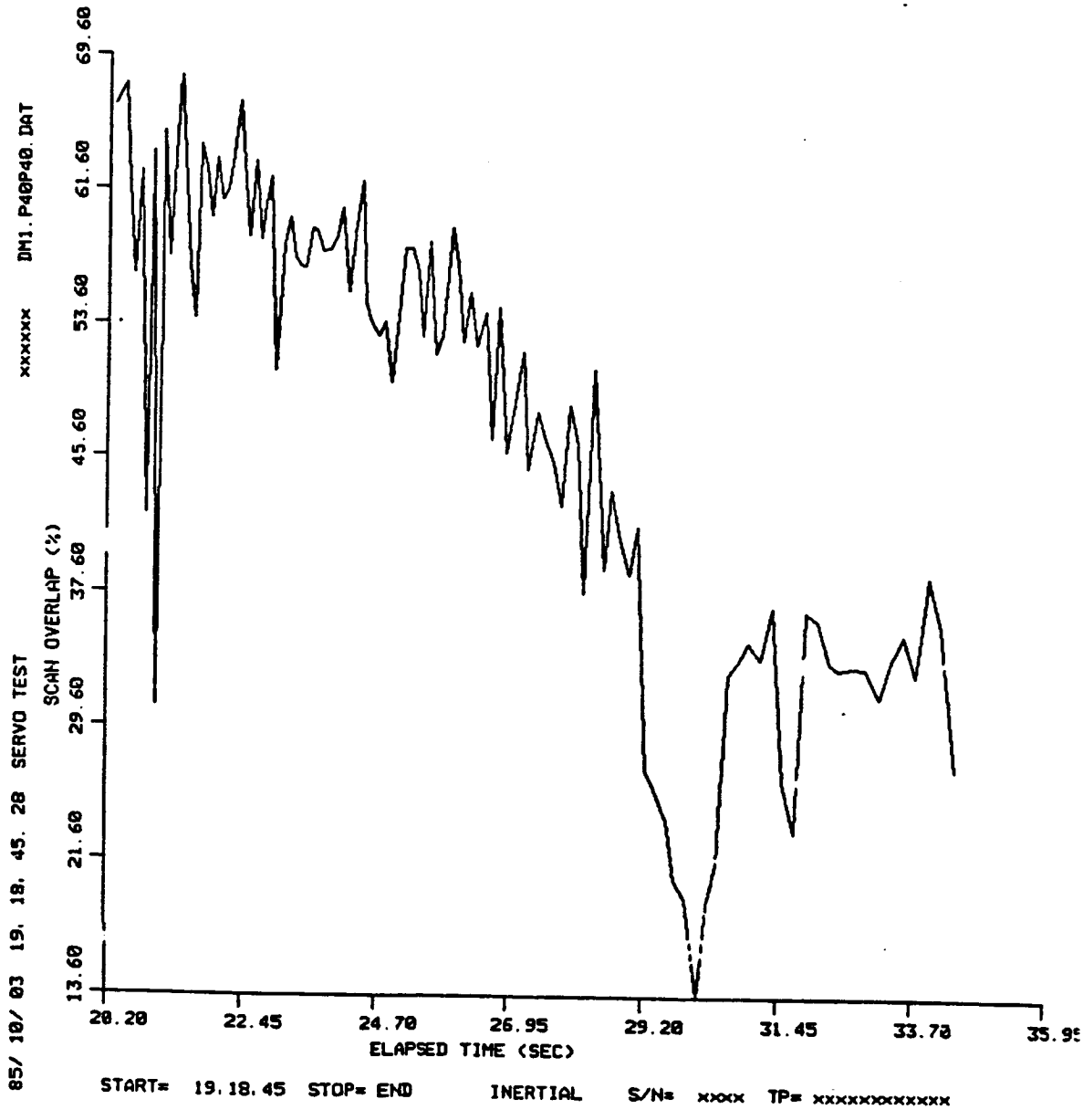
85/ 10/ 03 19. 18. 45. 28 SERVO TEST
xxxxxx DH1.P40P40.DAT
SCAN OVERLAP (%)
69.60
61.60
53.60
45.60
37.60
29.60
21.60
13.60
20.20
22.45
24.70
26.95
29.20
31.45
33.70
35.9
ELAPSED TIME (SEC)
START= 19.18.45 STOP= END
INERTIAL
S/N= xxxx TP= xxxxxxxxxxx

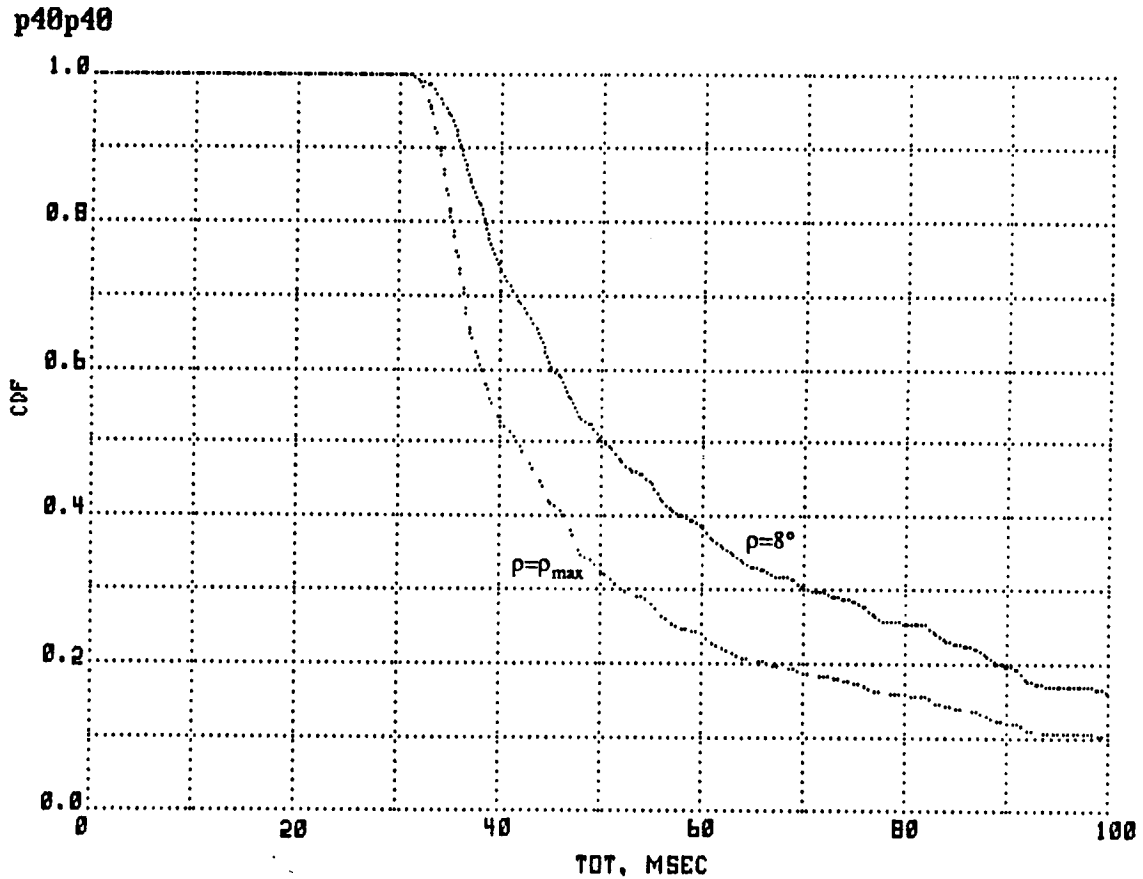
p40p40
1.0
0.8
0.6
0.4
0.2
0.0
CDF
0
20
40
60
80
100
TOT, MSEC
ρ=ρmax
ρ=8°

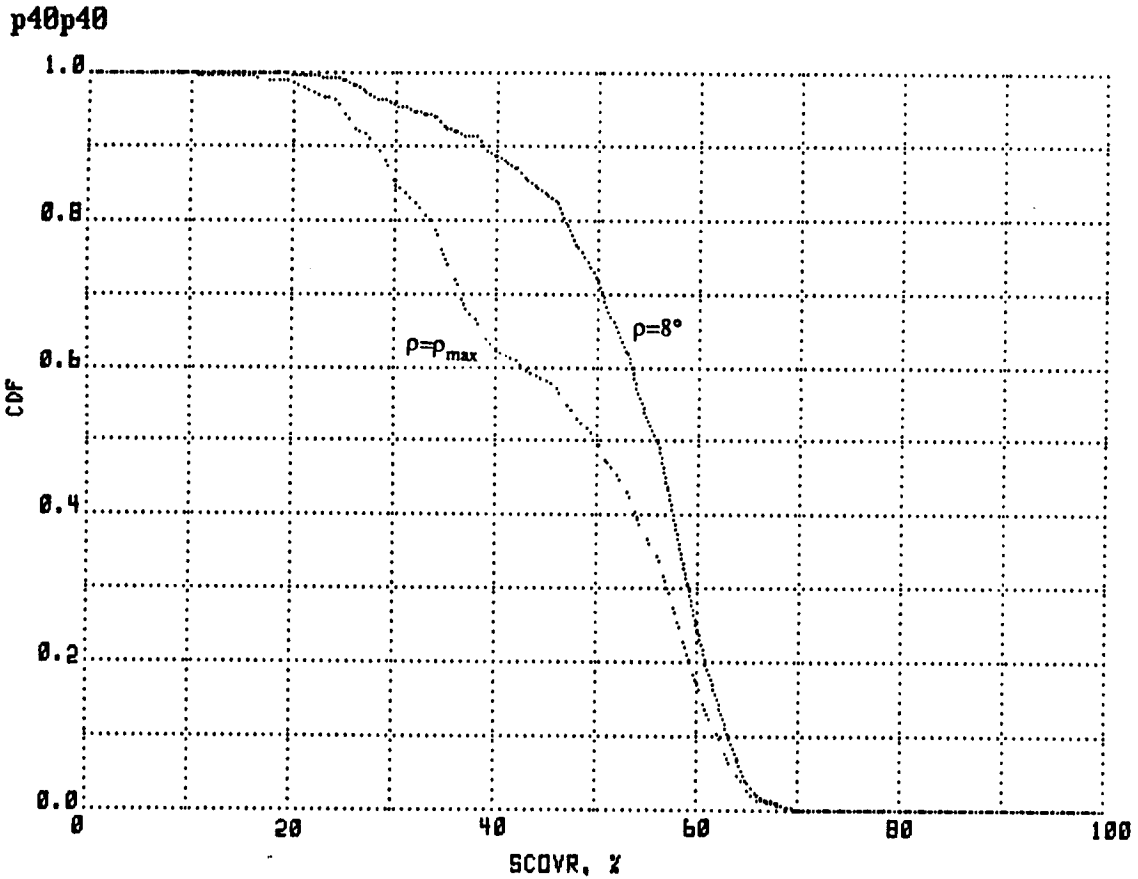
p40p40
1.0
0.8
0.6
0.4
0.2
0.0
CDF
0
20
40
60
80
100
SCOVR, %
ρ=ρmax
ρ=8°

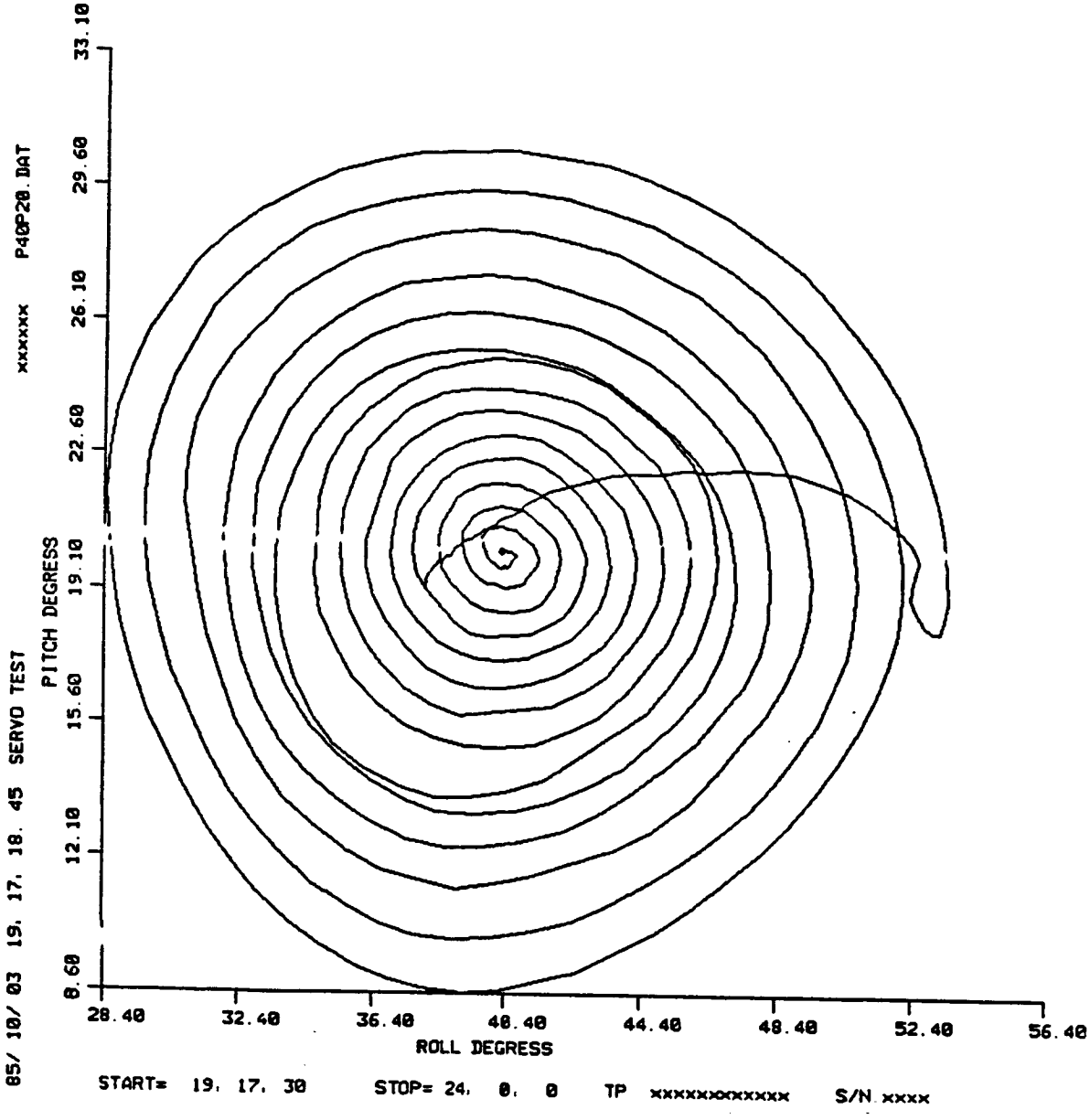
85/ 10/ 03 19. 17. 18. 45 SERVO TEST
xxxxxx P40P20.DAT
PITCH DEGRESS
33.10
29.60
26.10
22.60
19.10
15.60
12.10
8.60
28.40
32.40
36.40
40.40
44.40
48.40
52.40
56.40
ROLL DEGRESS
START= 19. 17. 30
STOP= 24. 0. 0
TP xxxxxxxxxxx
S/N xxxx

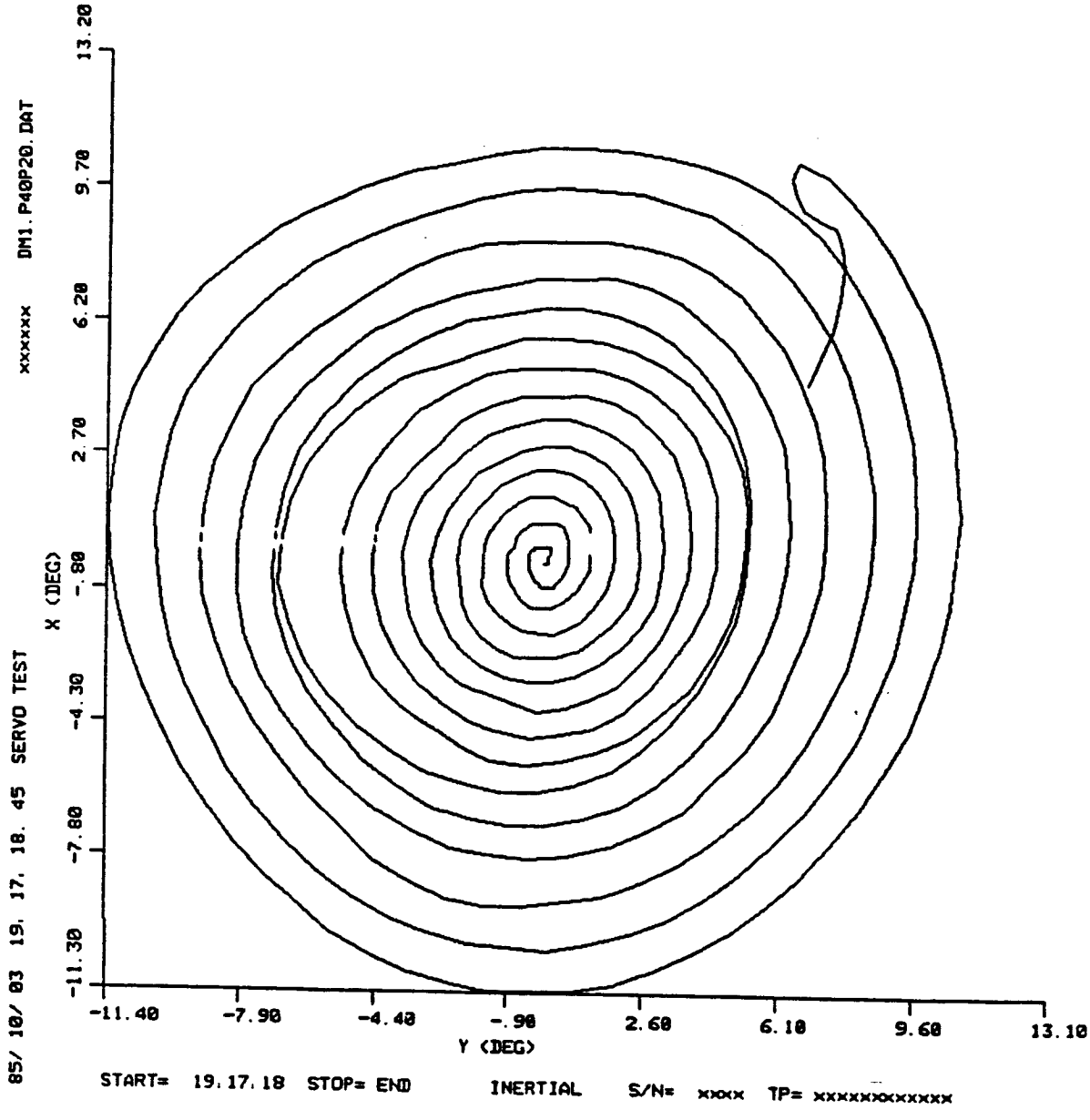
85/ 10/ 03 19. 17. 18. 45 SERVO TEST
XXXXXX DM1.P40P20.DAT
X (DEG)
13.20
9.70
6.20
2.70
-.80
-4.30
-7.80
-11.30
-11.40
-7.90
-4.40
-.90
2.60
6.10
9.60
13.10
Y (DEG)
START= 19.17.18 STOP= END
INERTIAL
S/N= xxxx TP= xxxxxxxxxxx

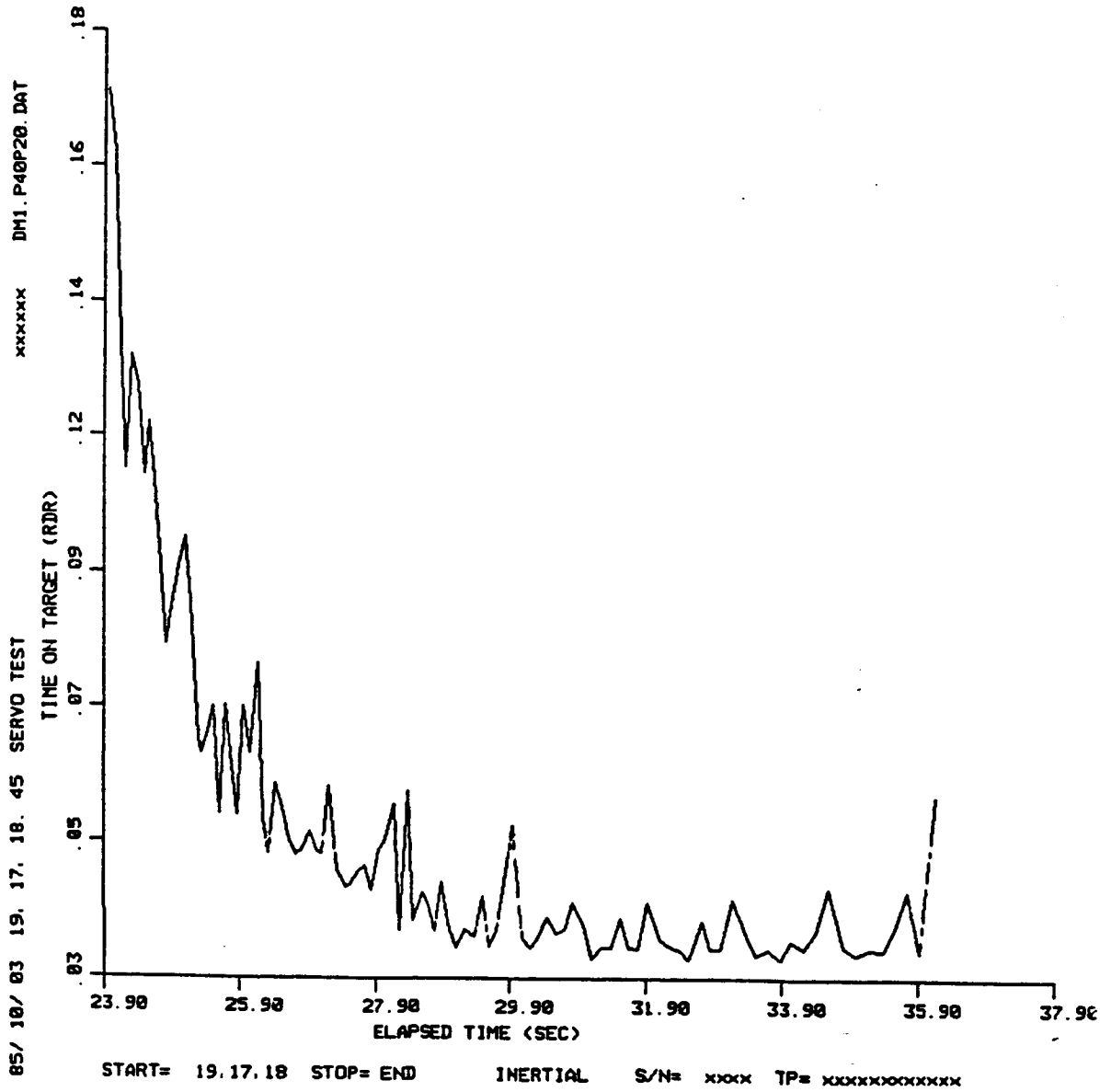
85/ 10/ 03 19. 17. 18. 45 SERVO TEST
xxxxxx DM1.P40P20.DAT
TIME ON TARGET (RDR)
.18
.16
.14
.12
.09
.07
.05
.03
23.90
25.90
27.90
29.90
31.90
33.90
35.90
37.90
ELAPSED TIME (SEC)
START= 19.17.18 STOP= END INERTIAL S/N= xxxx TP= xxxxxxxxxxx

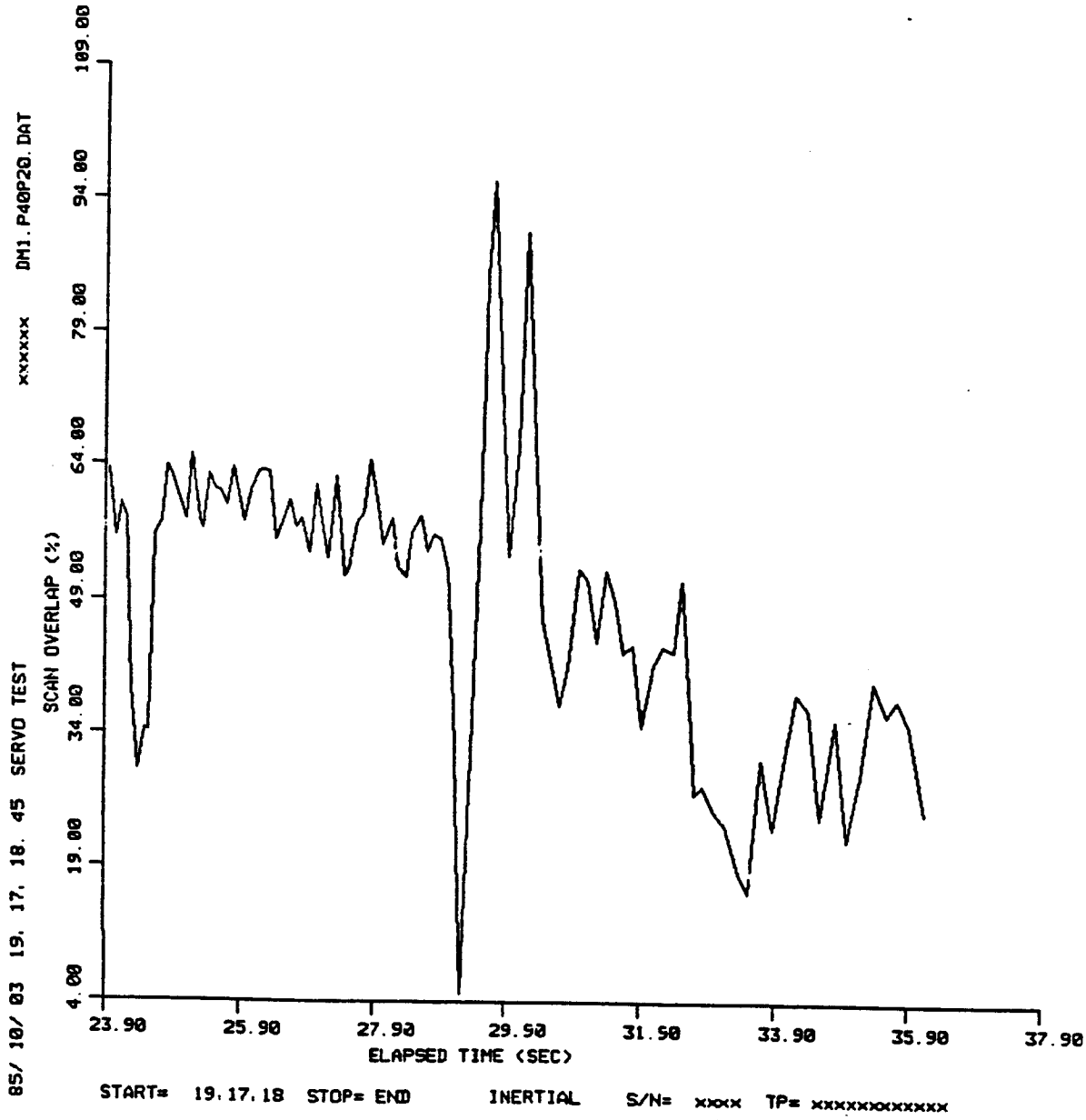
85/ 10/ 03 19. 17. 18. 45 SERVO TEST
xxxxxx DM1.P40P20.DAT
SCAN OVERLAP (%)
4.00
19.00
34.00
49.00
64.00
79.00
94.00
109.00
23.90
25.90
27.90
29.90
31.50
33.90
35.90
37.90
ELAPSED TIME (SEC)
START= 19.17.18 STOP= END
INERTIAL
S/N= xxxx TP= xxxxxxxxxxx

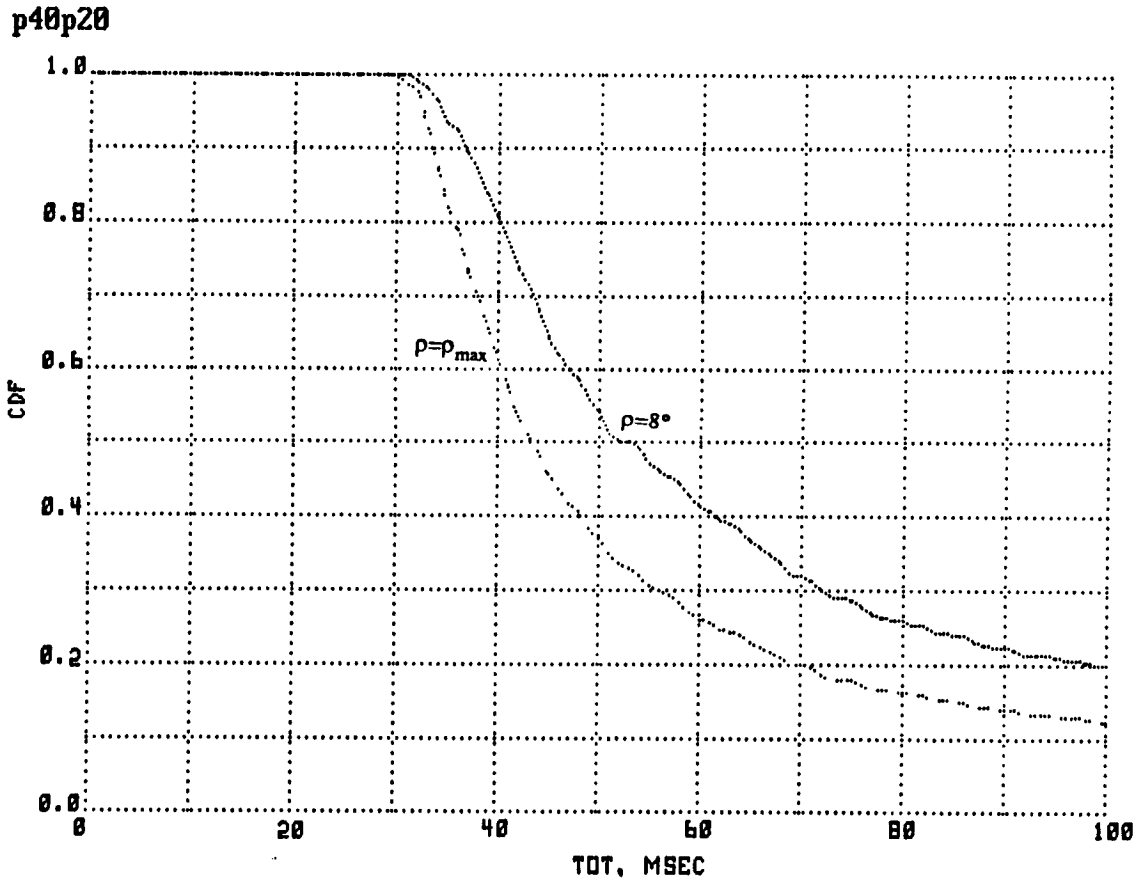
p40p20
1.0
0.8
0.6
0.4
0.2
0.0
CDF
ρ=ρmax
ρ=8°
0
20
40
60
80
100
TOT, MSEC

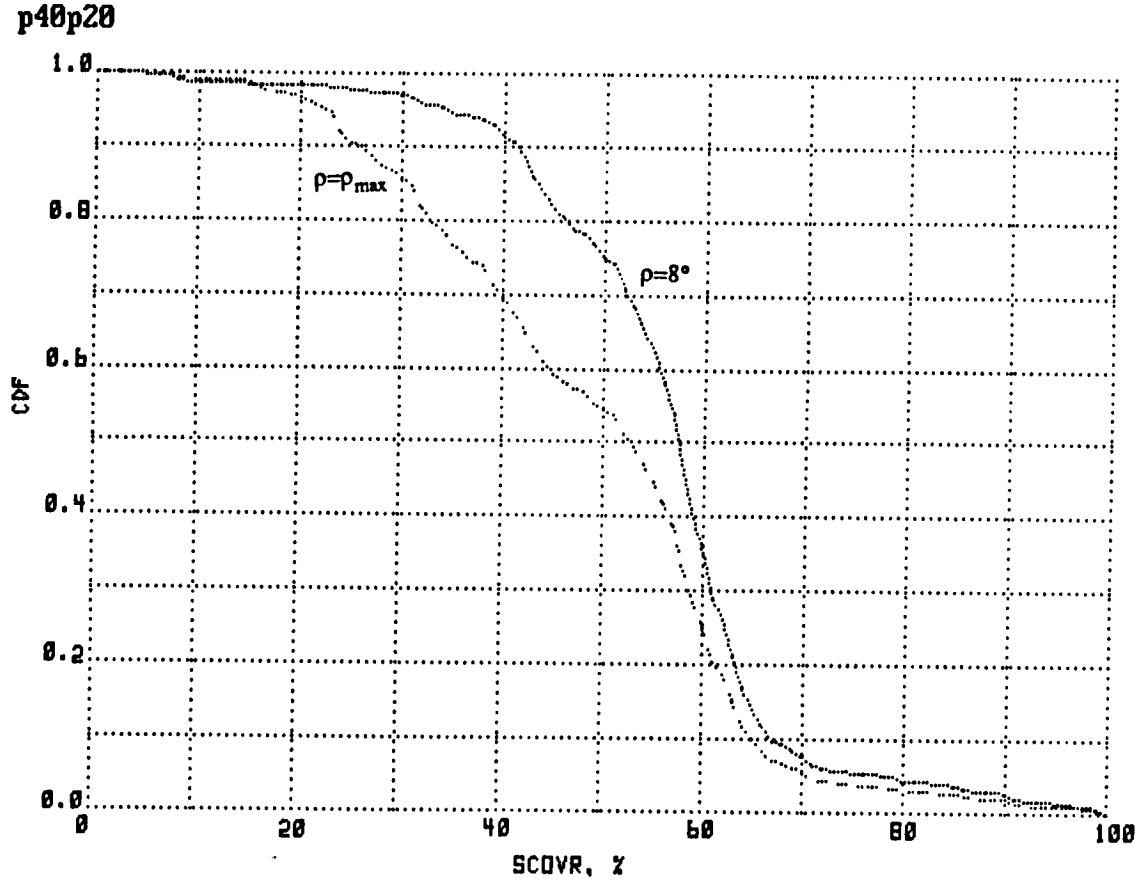
p40p20
1.0
0.8
0.6
0.4
0.2
0.0
CDF
ρ=ρmax
ρ=8°
0
20
40
60
80
100
SCOVR, %

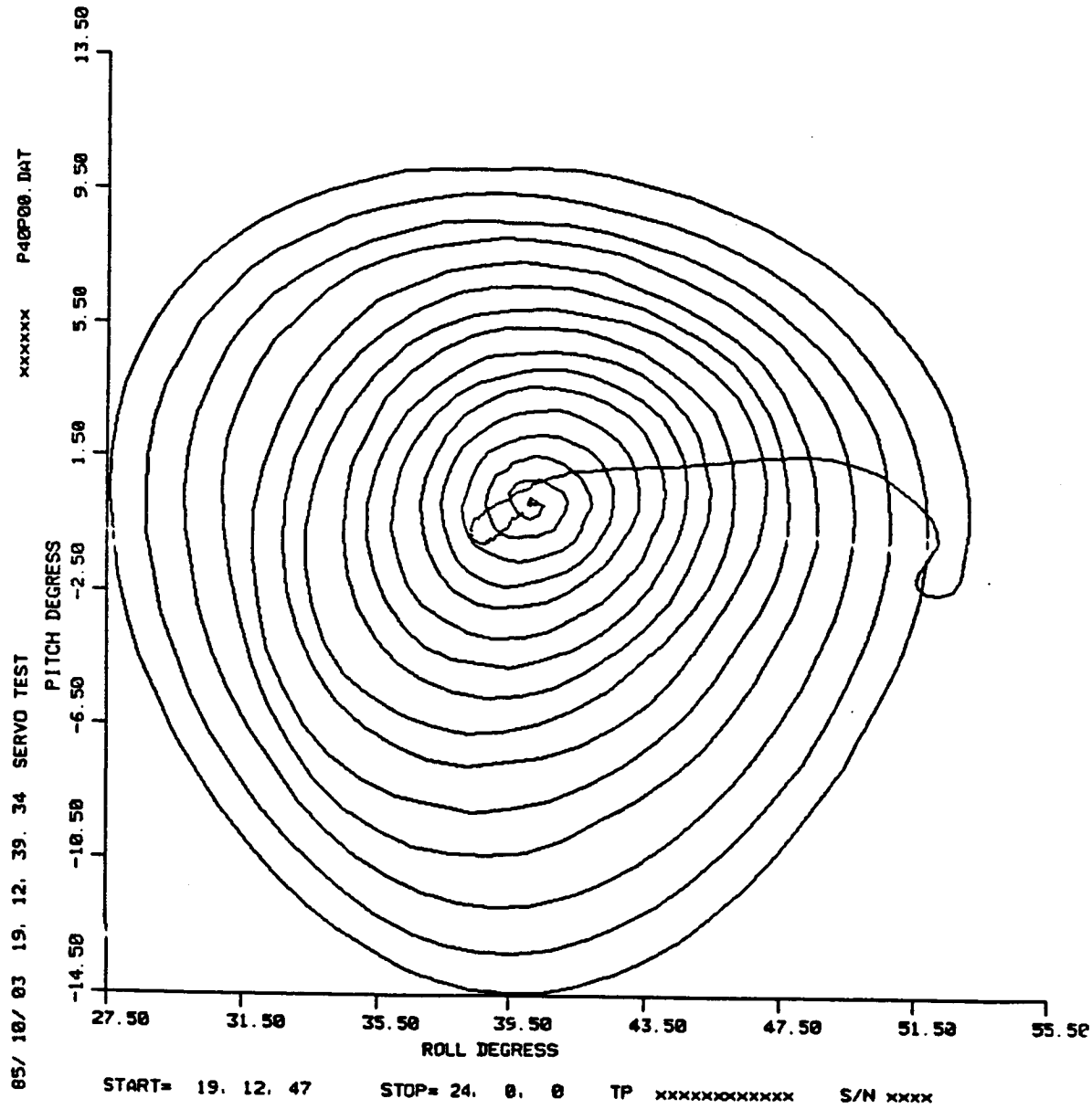
85/ 10/ 03 19. 12. 39. 34 SERVO TEST
xxxxxx P40P00.DAT
PITCH DEGRESS
13.50
9.50
5.50
1.50
-2.50
-6.50
-10.50
-14.50
27.50
31.50
35.50
39.50
43.50
47.50
51.50
55.50
ROLL DEGRESS
START= 19. 12. 47
STOP= 24. 0. 0
TP xxxxxxxxxxx
S/N xxxx

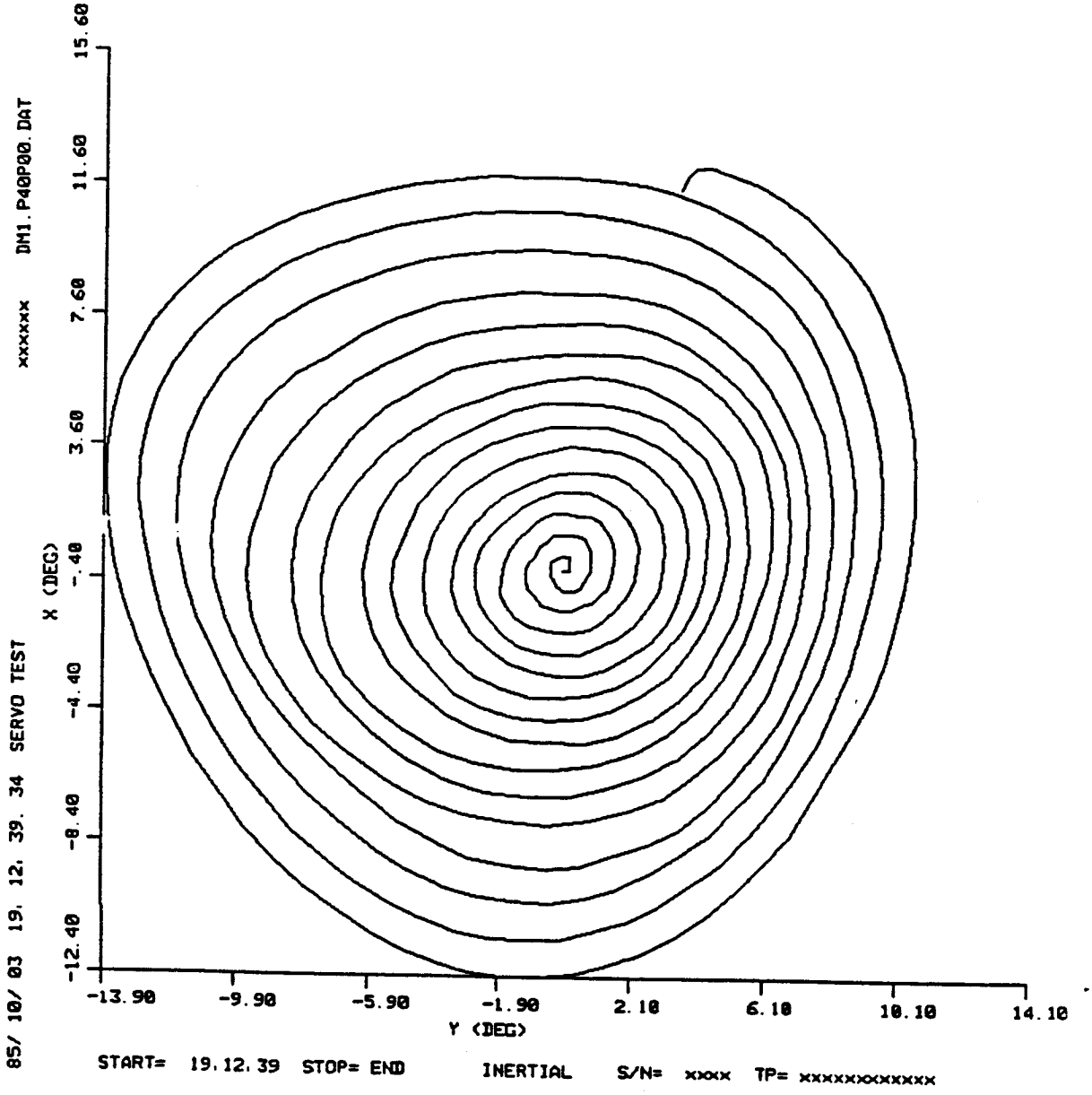
85/ 10/ 03 19. 12. 39. 34 SERVO TEST
XXXXXX DN1.P40P00.DAT
X (DEG)
15.60
11.60
7.60
3.60
-.40
-4.40
-8.40
-12.40
-13.90
-9.90
-5.90
-1.90
2.10
6.10
10.10
14.10
Y (DEG)
START= 19.12.39 STOP= END
INERTIAL
S/N= XXXX TP= XXXXXXXXXXX

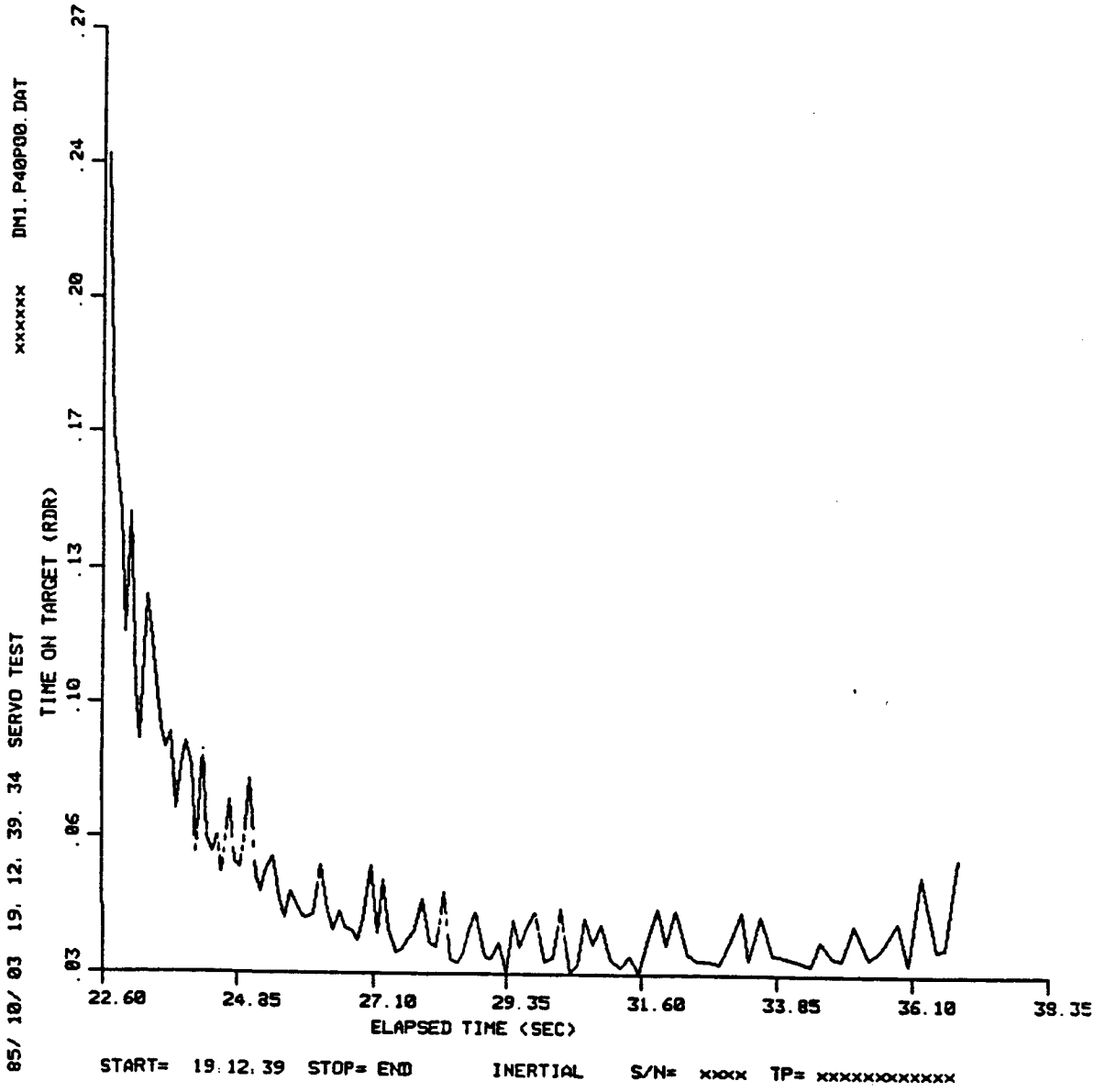
85/ 10/ 03 19. 12. 39. 34 SERVO TEST
xxxxxx DM1.P40P00.DAT
TIME ON TARGET (RDR)
.03
.06
.10
.13
.17
.20
.24
.27
22.60
24.85
27.10
29.35
31.60
33.85
36.10
38.35
ELAPSED TIME (SEC)
START= 19.12.39 STOP= END
INERTIAL
S/N= xxxx TP= xxxxxxxxxxx

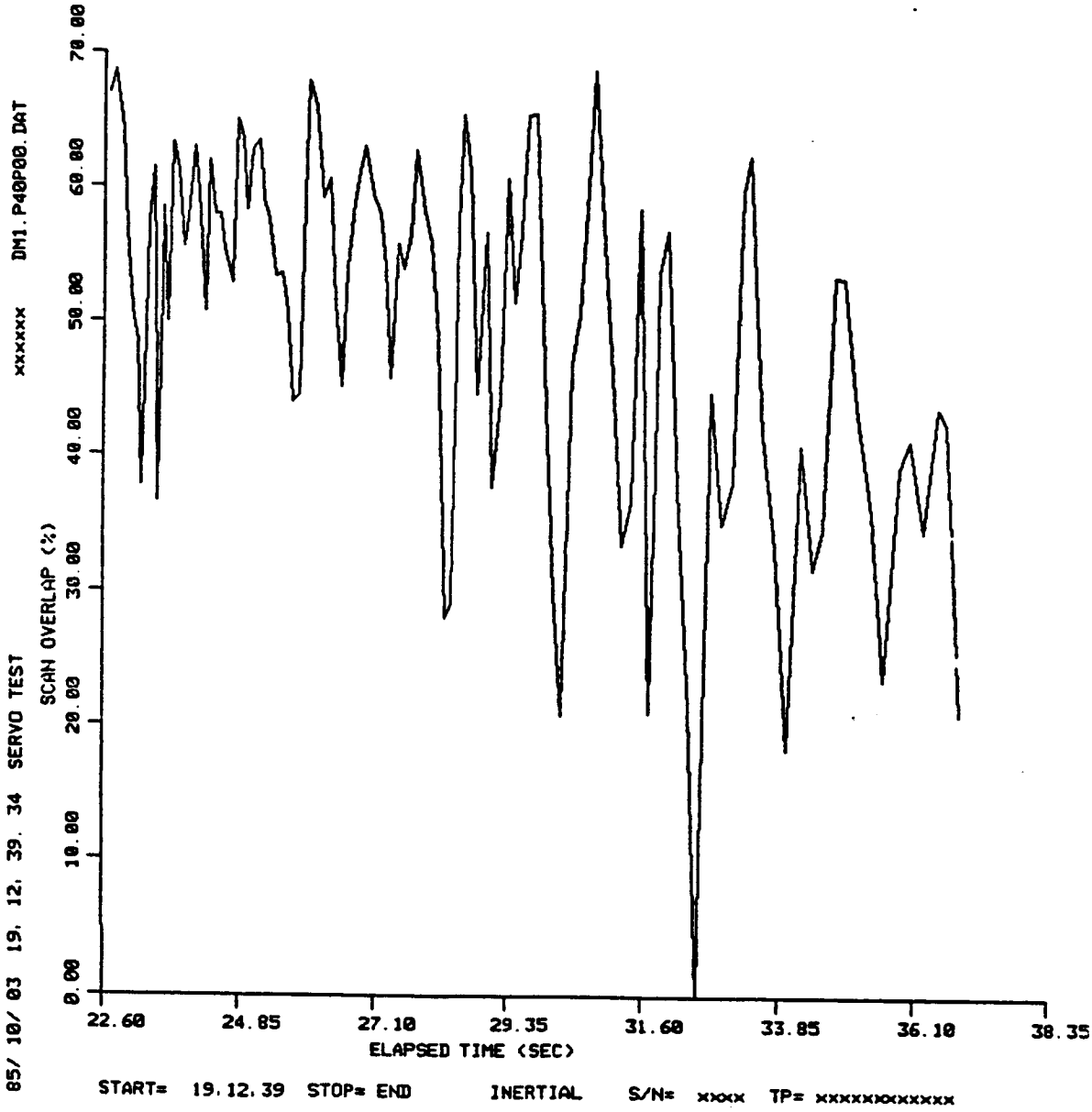
85/ 10/ 03 19. 12. 39. 34 SERVO TEST
xxxxxx DN1.P40P00.DAT
SCAN OVERLAP (%)
0.00
10.00
20.00
30.00
40.00
50.00
60.00
70.00
22.60
24.85
27.10
29.35
31.60
33.85
36.10
38.35
ELAPSED TIME (SEC)
START= 19.12.39 STOP= END INERTIAL S/N= xxxx TP= xxxxxxxxxxx

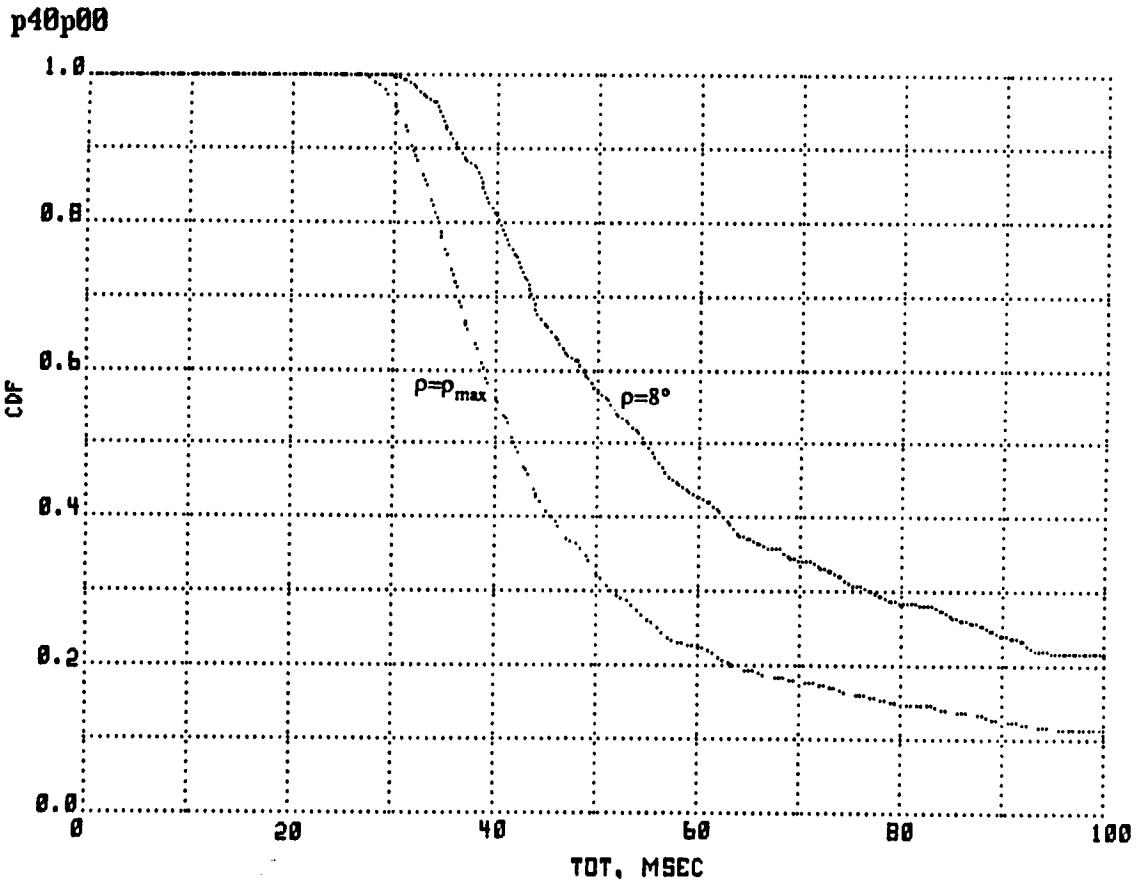
p40p00
1.0
0.8
0.6
0.4
0.2
0.0
CDF
ρ=ρmax
ρ=8°
0
20
40
60
80
100
TOT, MSEC

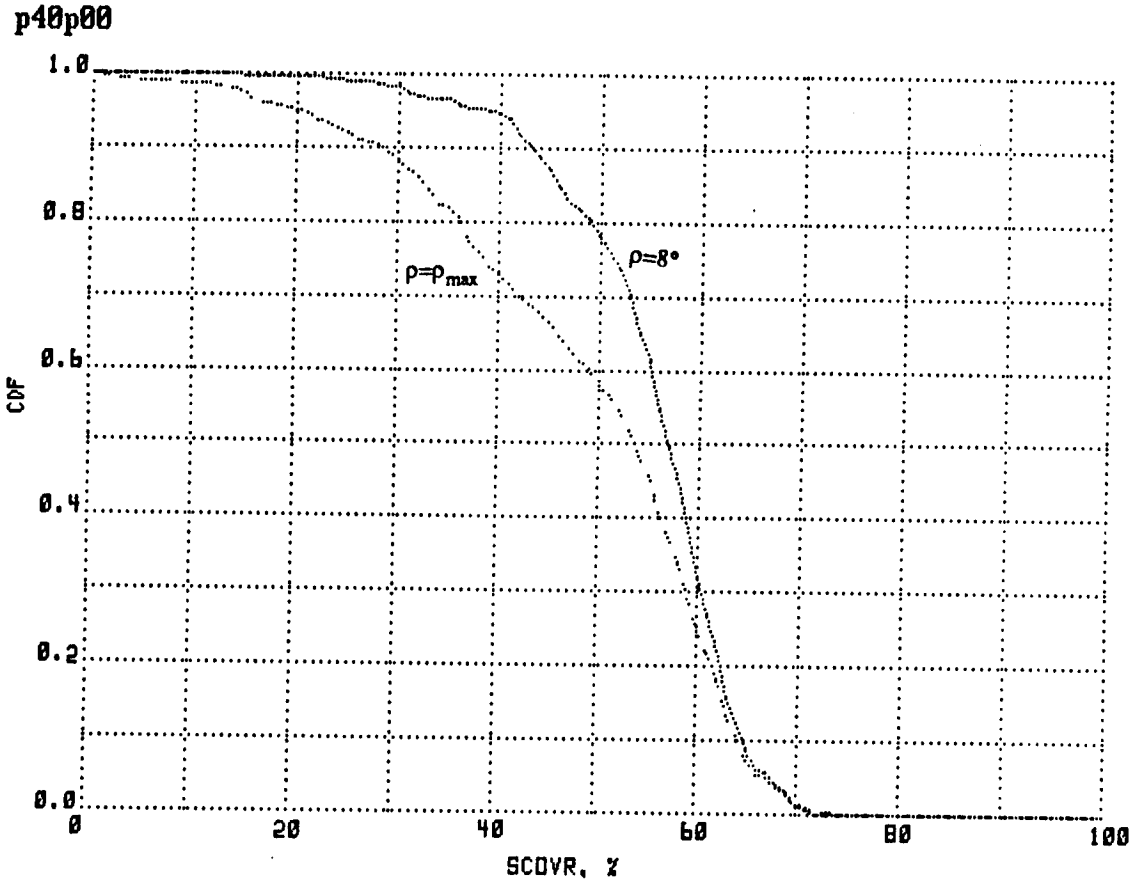
p40p00
1.0
0.8
0.6
0.4
0.2
0.0
CDF
ρ=ρmax
ρ=8°
0
20
40
60
80
100
SCOVR, %

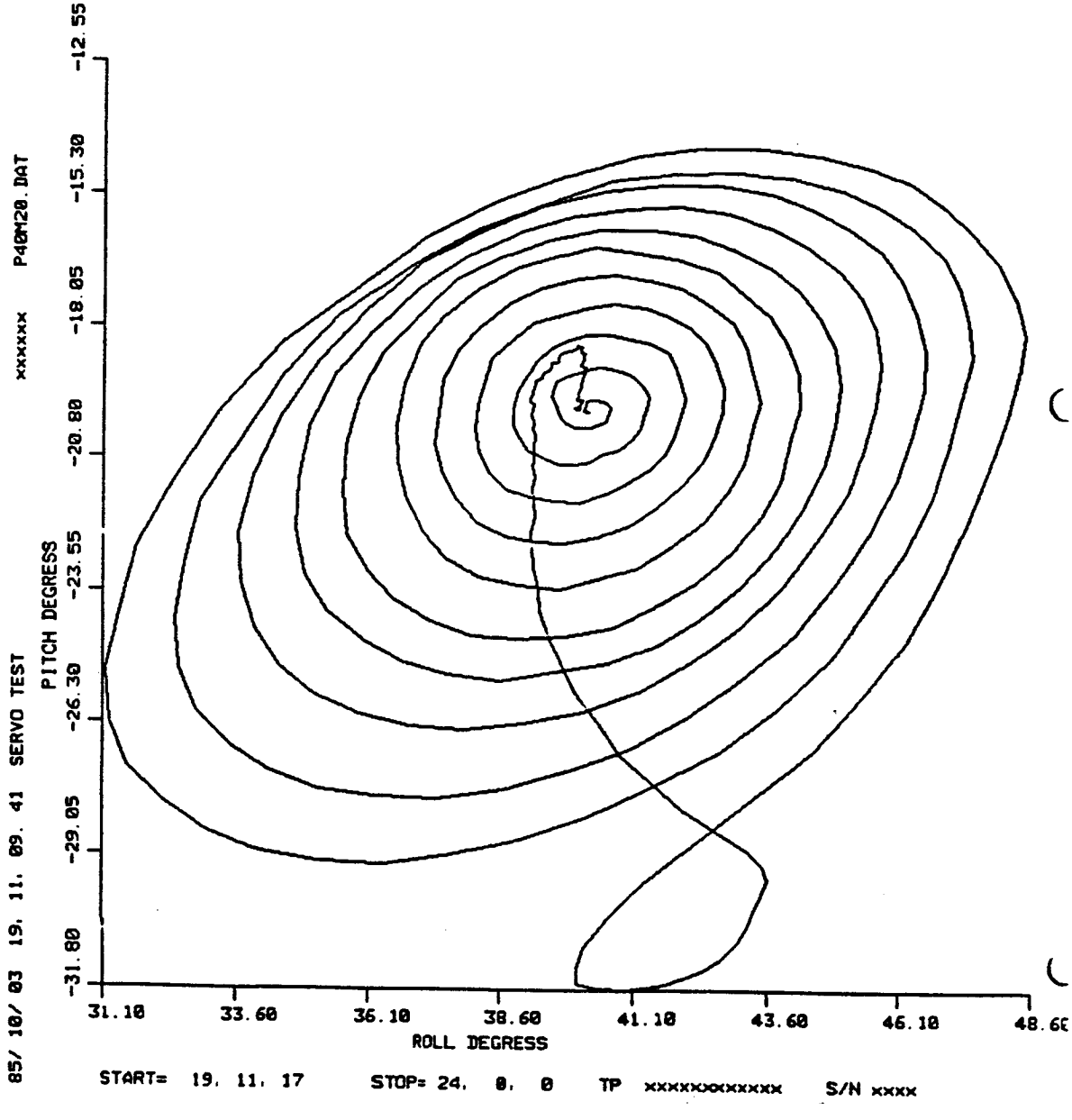
85/ 10/ 03 19. 11. 09. 41 SERVO TEST
xxxxxx P40M20.DAT
PITCH DEGRESS
-12.55
-15.30
-18.05
-20.80
-23.55
-26.30
-29.05
-31.80
31.10
33.60
36.10
38.60
41.10
43.60
46.10
48.60
ROLL DEGRESS
START= 19. 11. 17
STOP= 24. 0. 0
TP xxxxxxxxxxx
S/N xxxx

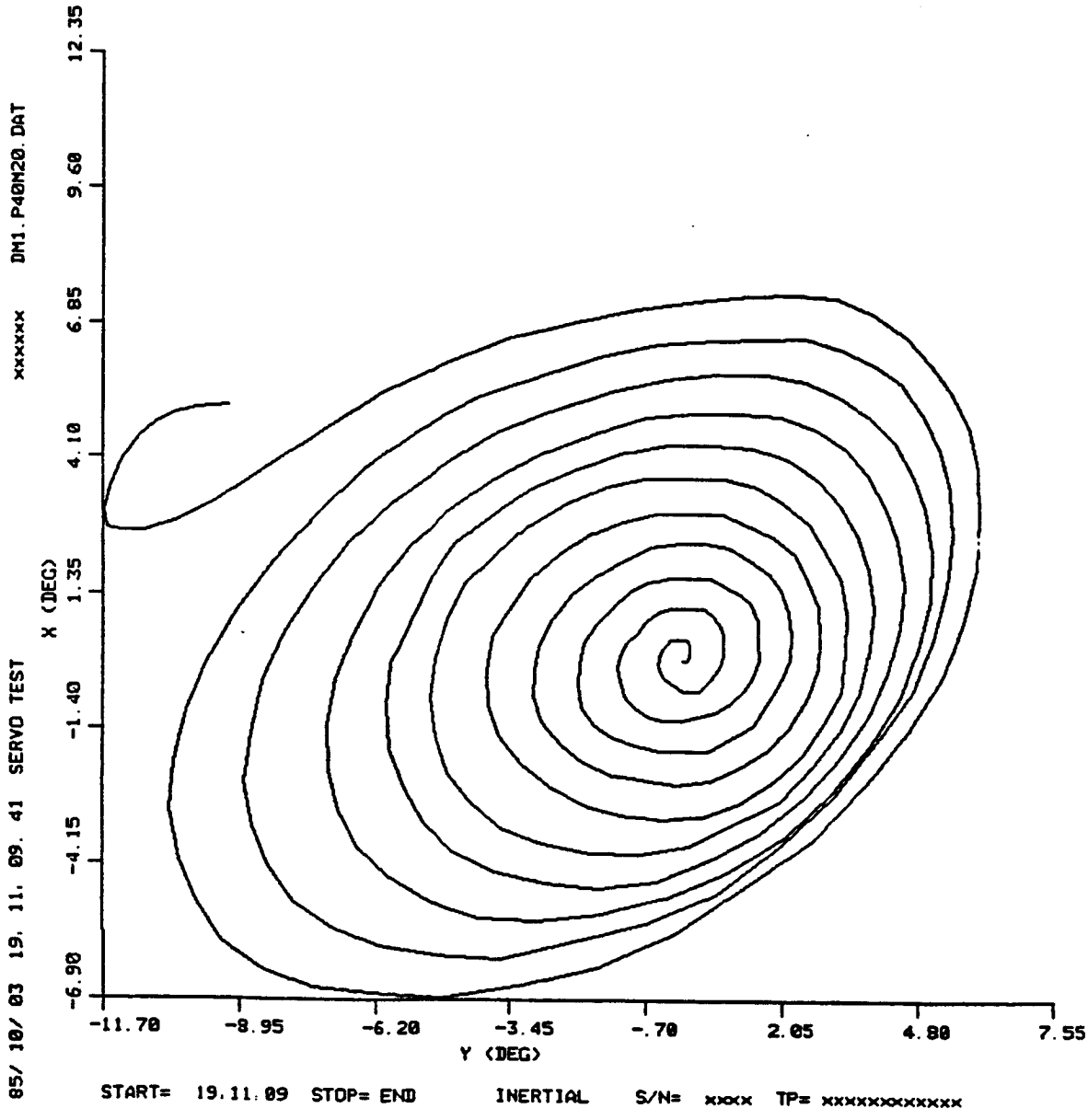
85/ 10/ 03 19. 11. 09. 41 SERVO TEST
xxxxxx DM1.P40N20.DAT
X (DEG)
12.35
9.60
6.85
4.10
1.35
-1.40
-4.15
-6.90
-11.70
-8.95
-6.20
-3.45
-.70
2.05
4.80
7.55
Y (DEG)
START= 19.11.09 STOP= END INERTIAL S/N= xxxx TP= xxxxxxxxxxx

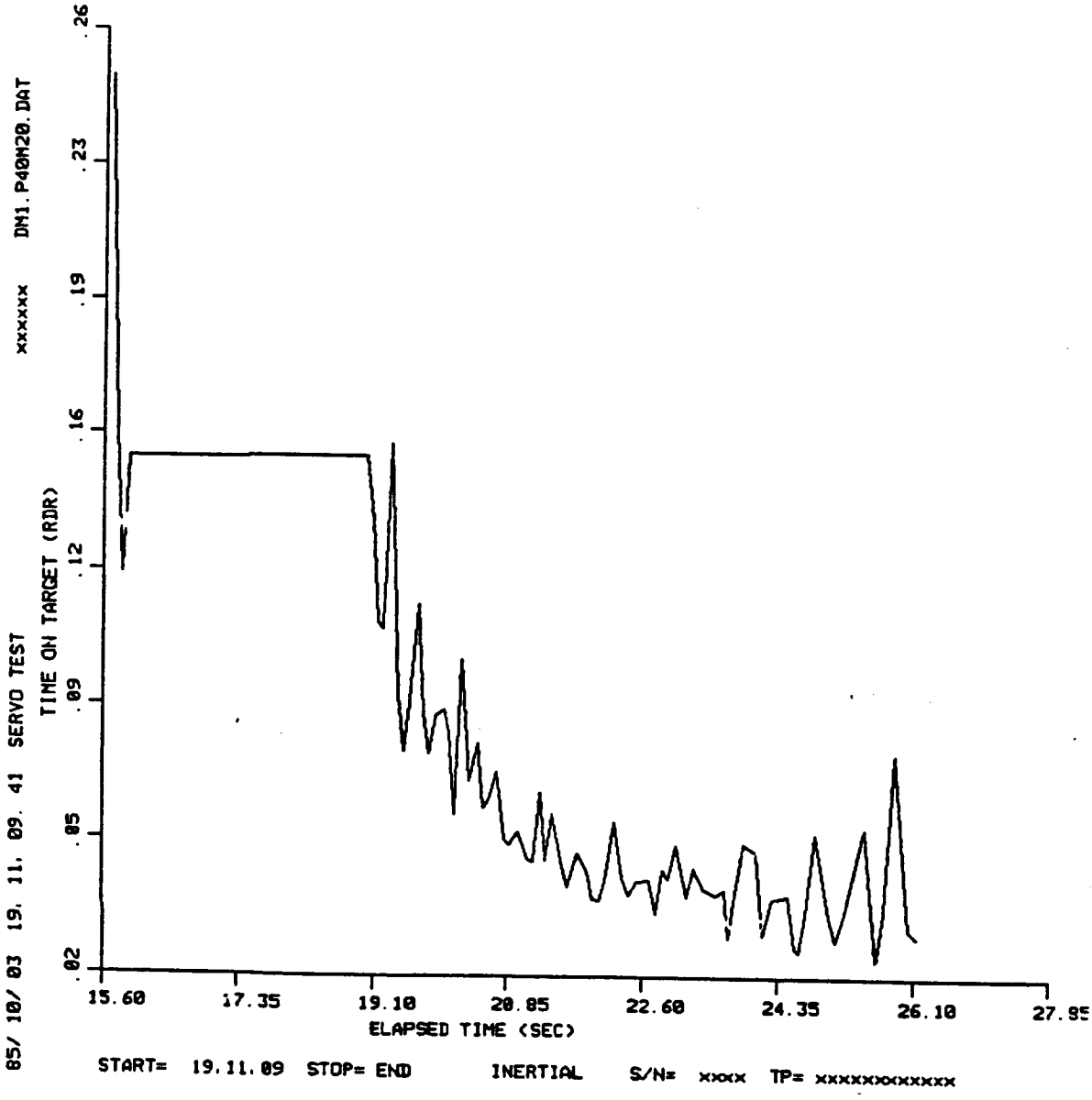
85/ 10/ 03 19. 11. 09. 41 SERVO TEST
xxxxxx DN1.P40M20.DAT
TIME ON TARGET (RDR)
.26
.23
.19
.16
.12
.09
.05
.02
15.60
17.35
19.10
20.85
22.60
24.35
26.10
27.85
ELAPSED TIME (SEC)
START= 19.11.09 STOP= END INERTIAL S/N= xxxx TP= xxxxxxxxxxx

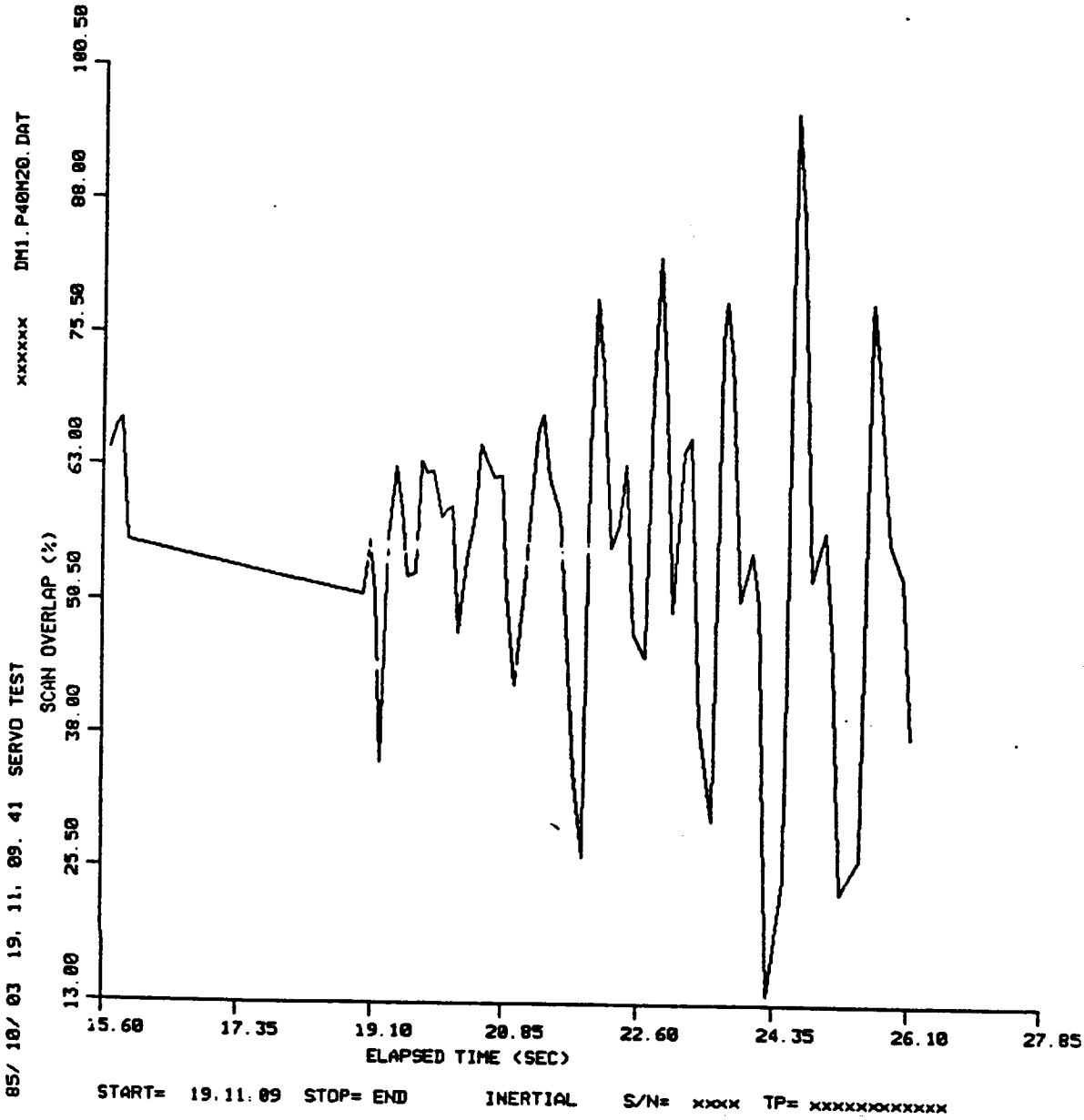
85/ 10/ 03 19. 11. 09. 41 SERVO TEST
xxxxxx DM1.P40N20.DAT
SCAN OVERLAP (%)
100.50
88.00
75.50
63.00
50.50
38.00
25.50
13.00
15.60
17.35
19.10
20.85
22.60
24.35
26.10
27.85
ELAPSED TIME (SEC)
START= 19.11.09 STOP= END
INERTIAL
S/N= xxxx TP= xxxxxxxxxxx

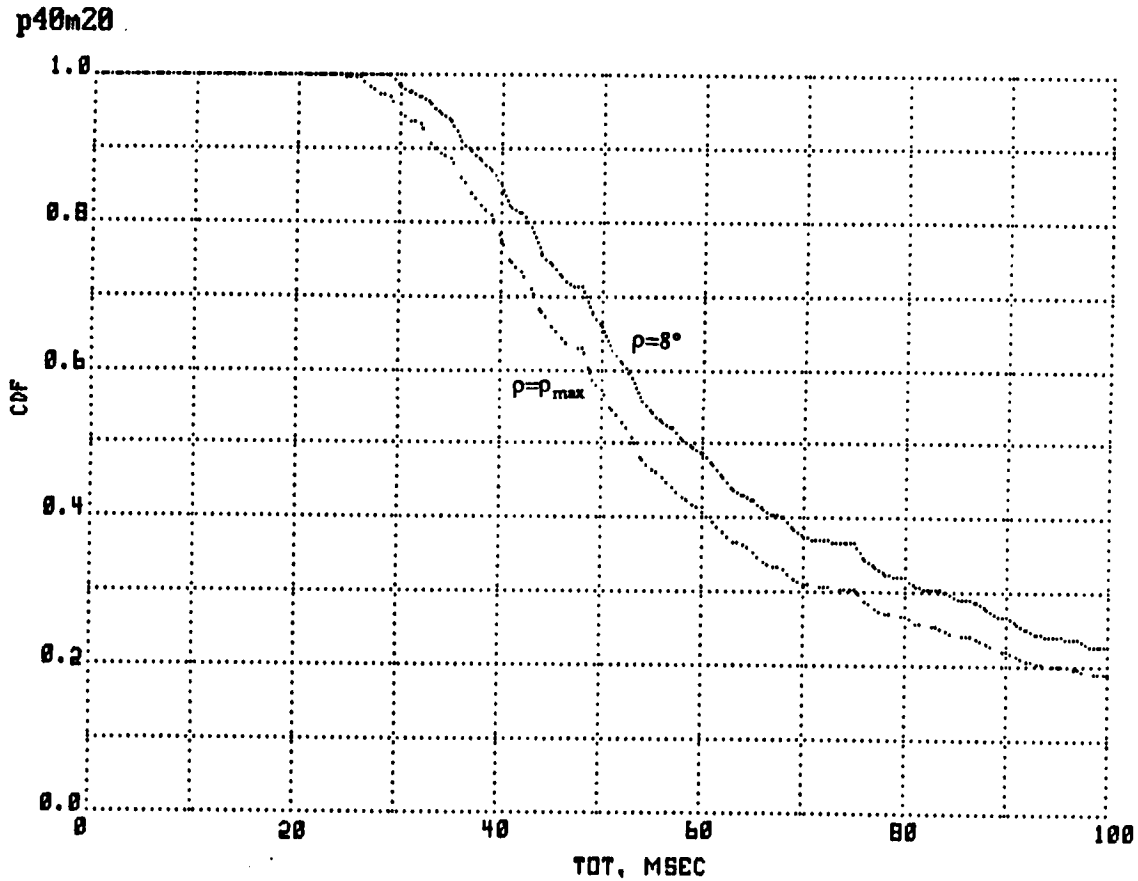
p40m20
1.0
0.8
0.6
0.4
0.2
0.0
CDF
ρ=8°
ρ=ρmax
0
20
40
60
80
100
TOT, MSEC

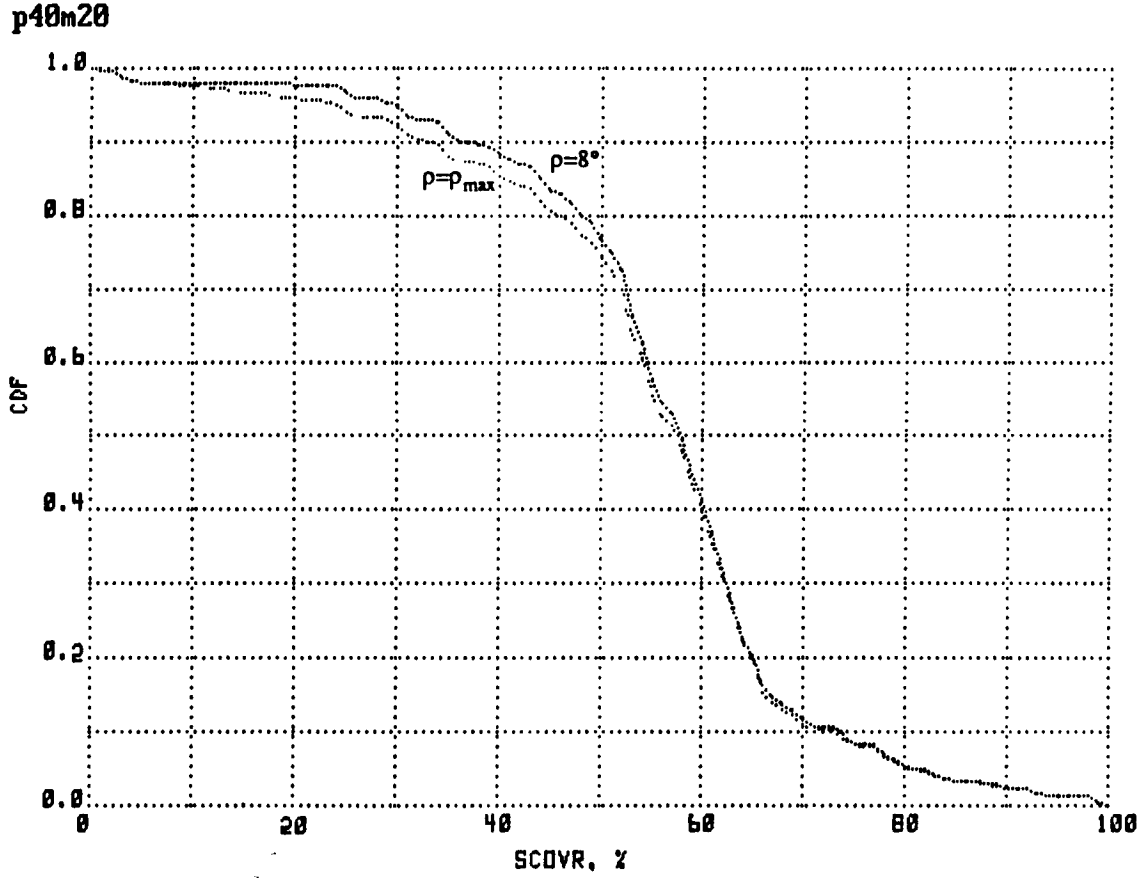
p40m20
1.0
0.8
0.6
0.4
0.2
0.0
COF
0
20
40
60
80
100
SCOVR, %
ρ=ρmax
ρ=8°

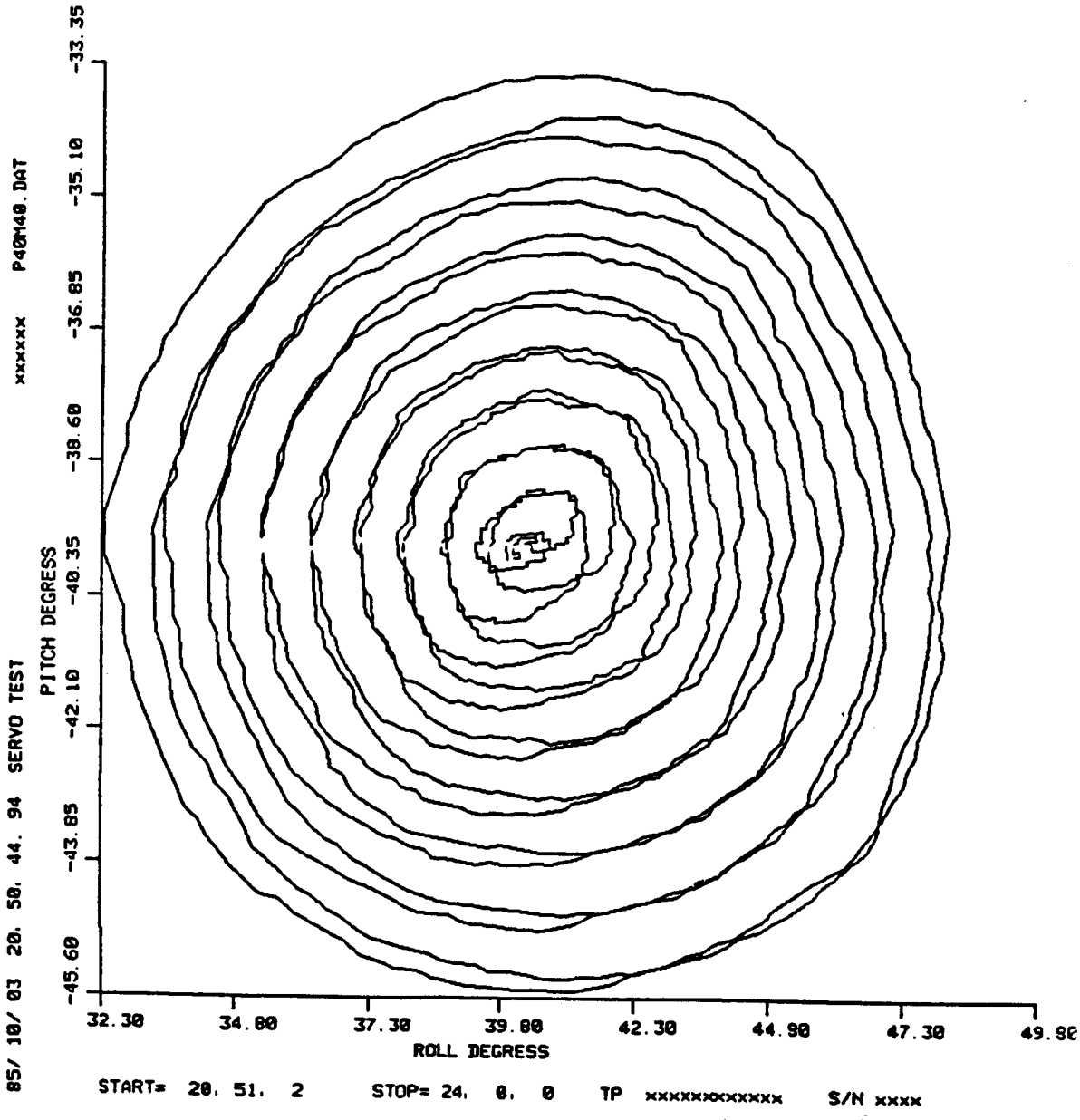
85/ 10/ 03 20. 50. 44. 94 SERVO TEST
xxxxxx P40M40.DAT
PITCH DEGRESS
-33.35
-35.10
-36.85
-38.60
-40.35
-42.10
-43.85
-45.60
32.30
34.80
37.30
39.80
42.30
44.90
47.30
49.80
ROLL DEGRESS
START= 20. 51. 2
STOP= 24. 0. 0
TP xxxxxxxxxxx
S/N xxxx

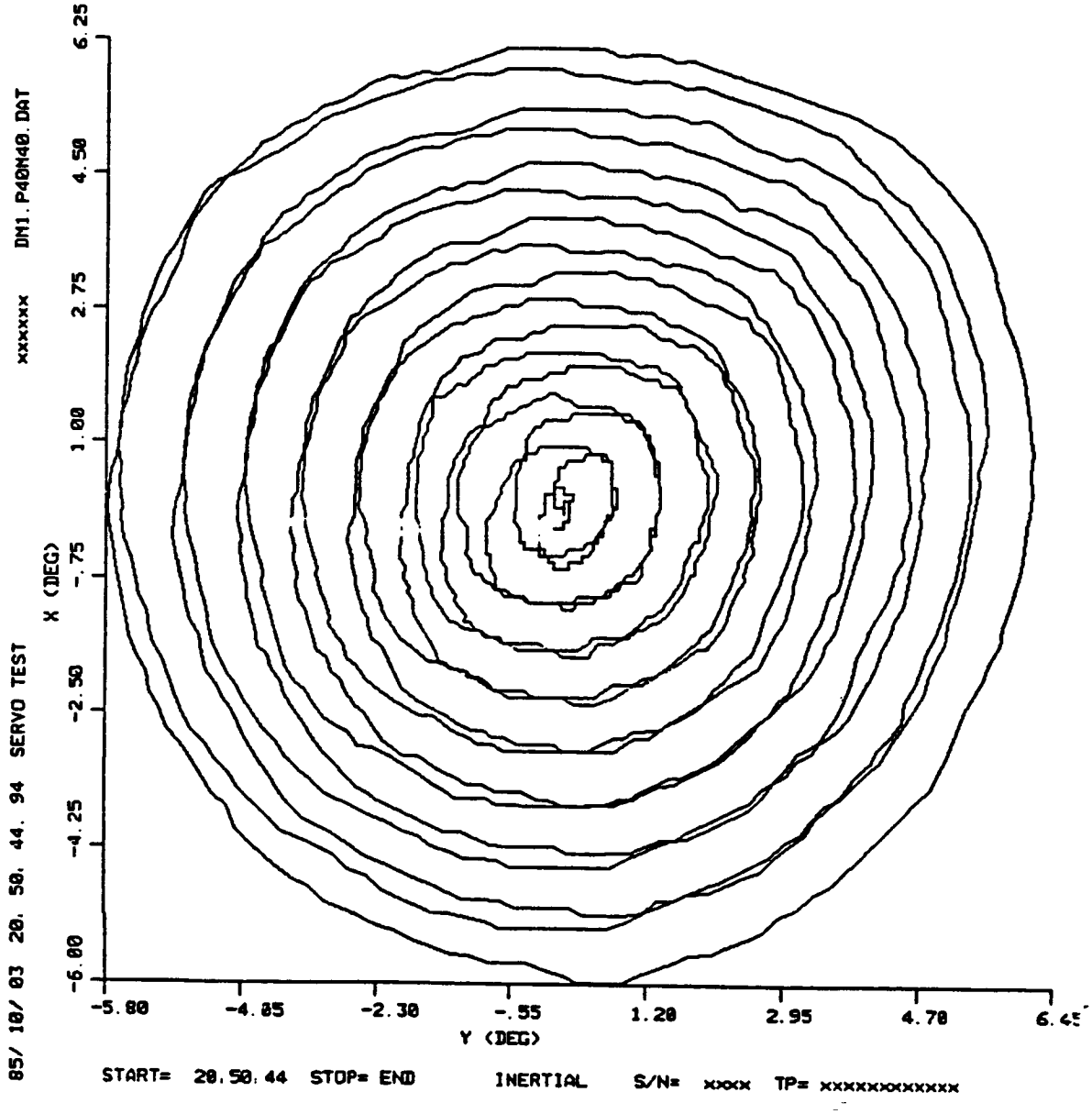
85/ 10/ 03 20. 50. 44. 94 SERVO TEST
XXXXXX DM1.P40N40.DAT
X (DEG)
6.25
4.50
2.75
1.00
-.75
-2.50
-4.25
-6.00
-5.80
-4.05
-2.30
-.55
1.20
2.95
4.70
Y (DEG)
START= 20.50.44 STOP= END
INERTIAL
S/N= xxxx TP= xxxxxxxxxxx

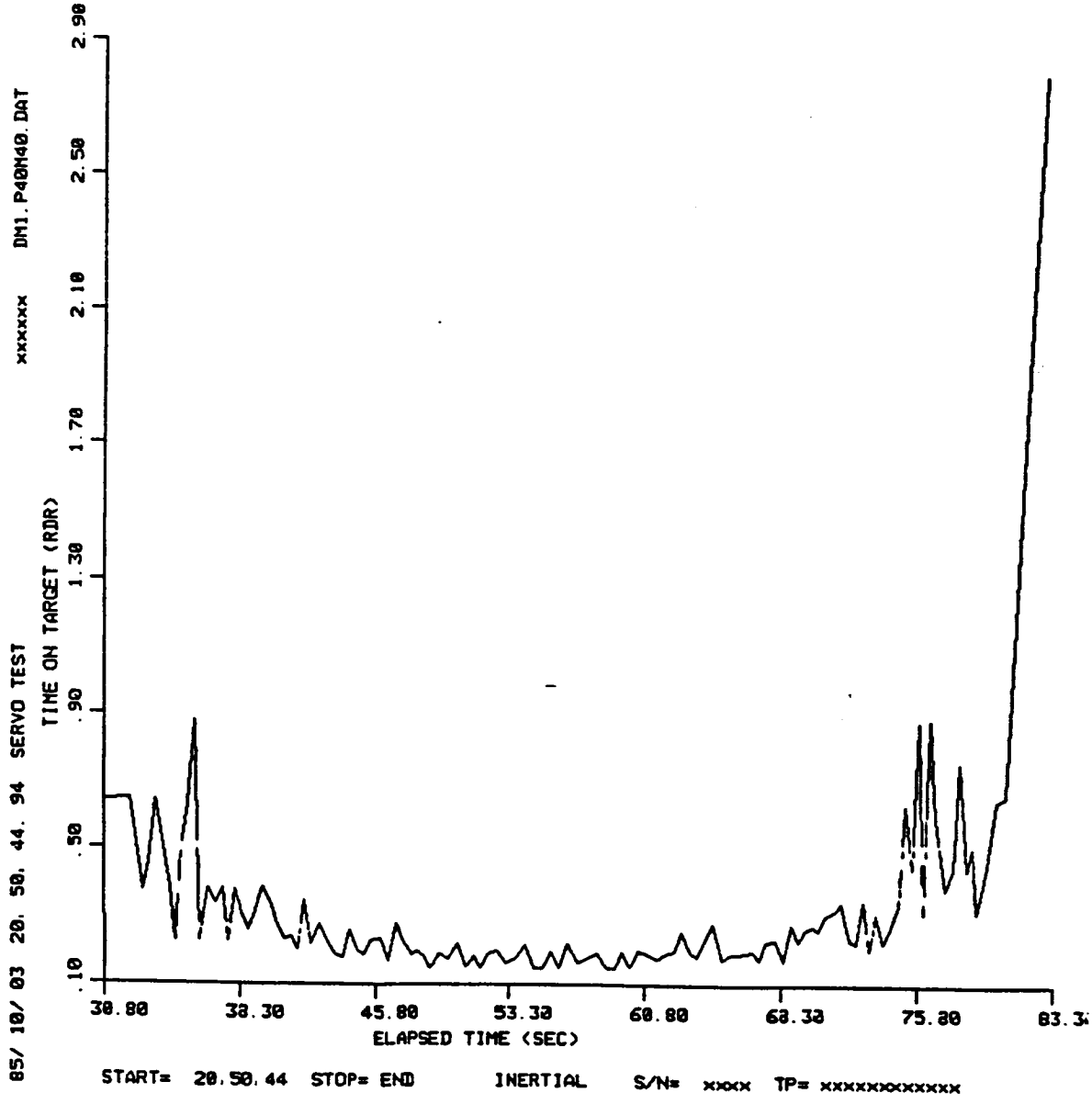
85/ 10/ 03 20. 50. 44. 94 SERVO TEST
xxxxxx DM1.P40N40.DAT
TIME ON TARGET (RDR)
.10
.50
.90
1.30
1.70
2.10
2.50
2.90
30.80
38.30
45.80
53.30
60.80
68.30
75.80
83.3
ELAPSED TIME (SEC)
START= 20.50.44 STOP= END INERTIAL S/N= xxxx TP= xxxxxxxxxxx

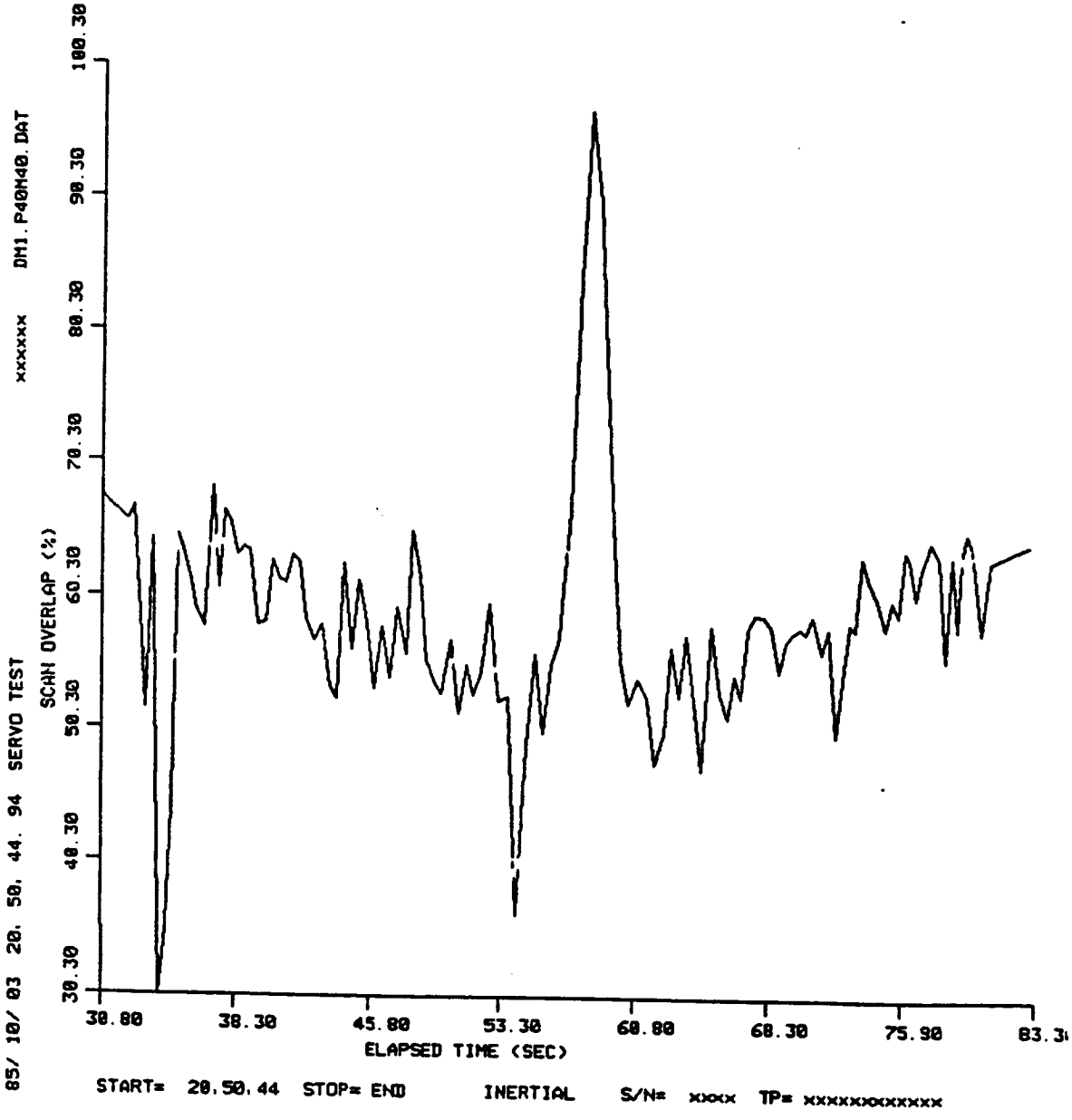
85/ 10/ 03 20. 50. 44. 94 SERVO TEST
xxxxxx DM1.P40N40.DAT
SCAN OVERLAP (%)
100.30
90.30
80.30
70.30
60.30
50.30
40.30
30.30
30.80
38.30
45.80
53.30
60.80
68.30
75.90
83.3
ELAPSED TIME (SEC)
START= 20.50.44 STOP= END INERTIAL S/N= xxxx TP= xxxxxxxxxxx

575 p40m60

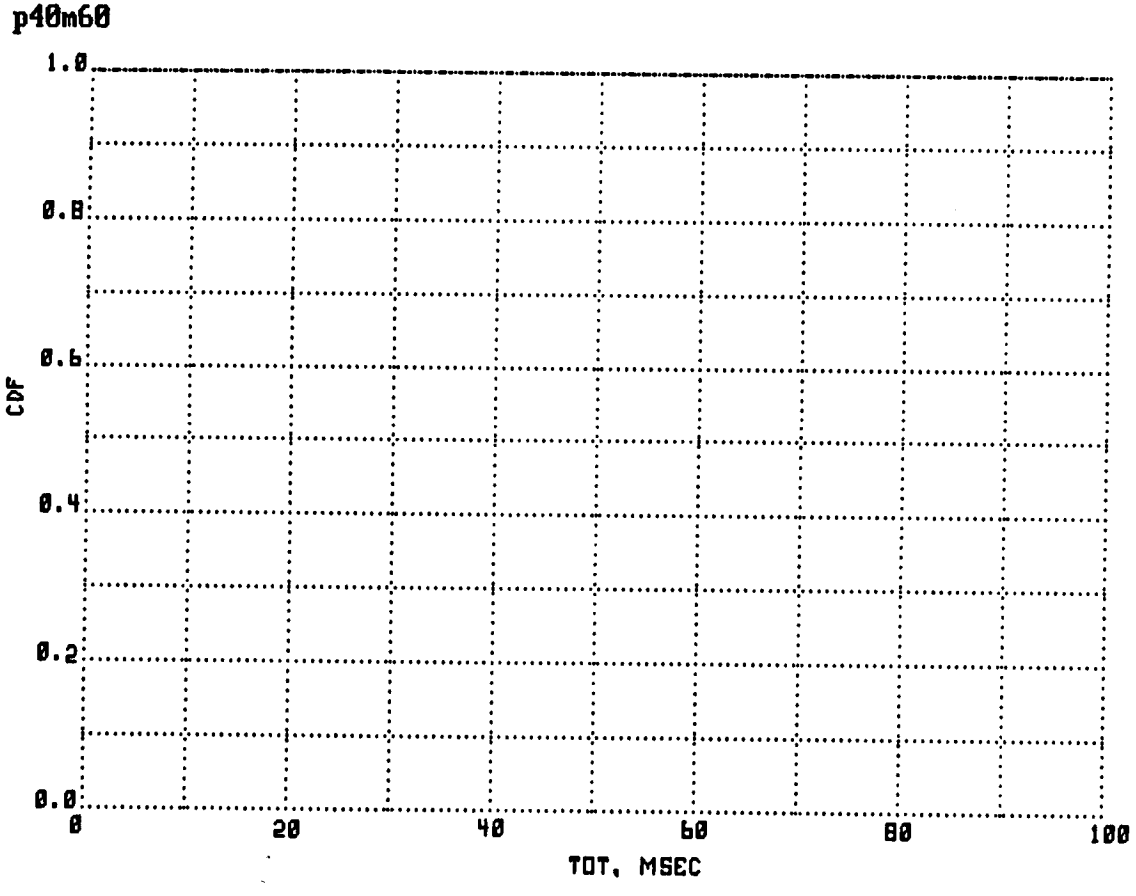
p40m60
1.0
0.8
0.6
0.4
0.2
0.0
CDF
0
20
40
60
80
100
TOT, MSEC

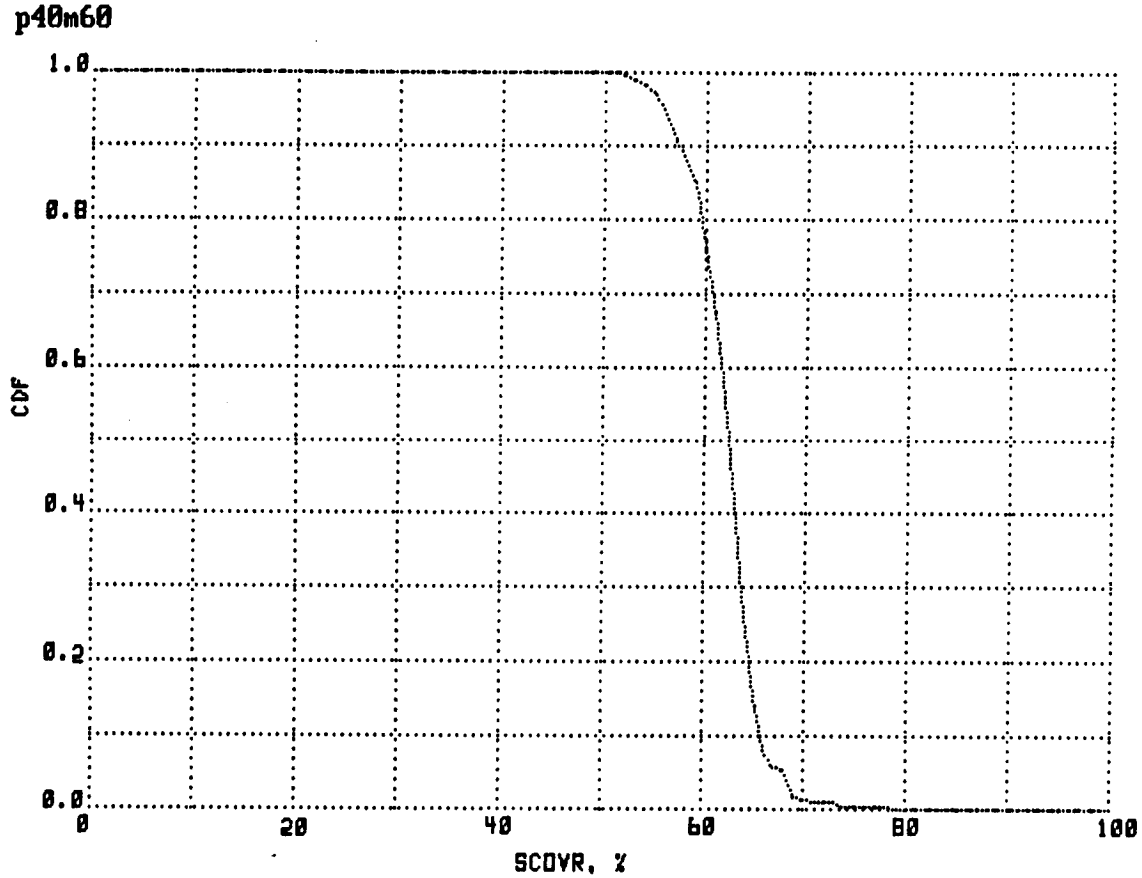
p40m60
1.0
0.8
0.6
0.4
0.2
0.0
CDF
0
20
40
60
80
100
SCOVR, %

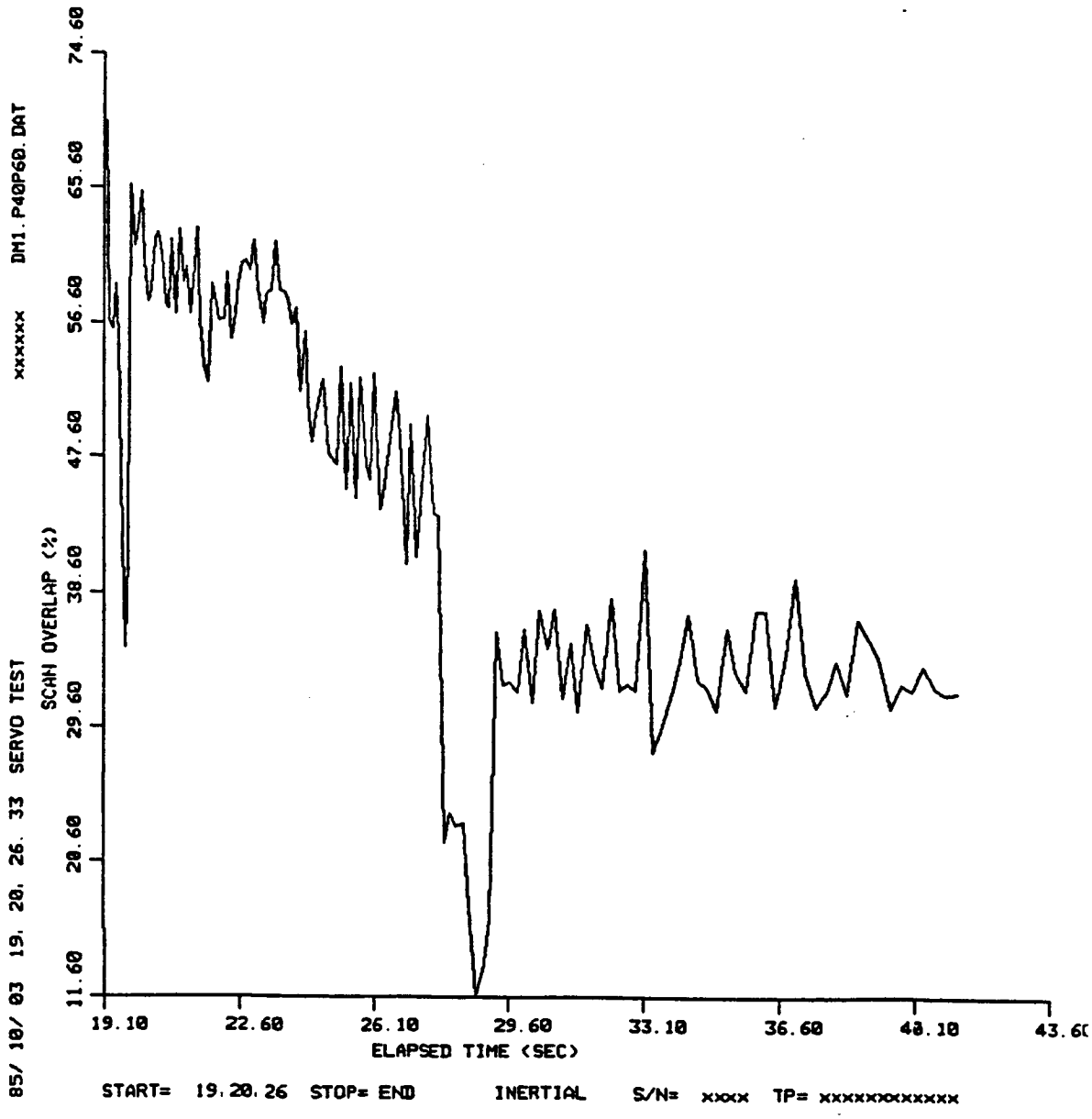
85/ 10/ 03 19. 20. 26. 33 SERVO TEST
xxxxxx DM1.P40P60.DAT
SCAN OVERLAP (%)
74.60
65.60
56.60
47.60
38.60
29.60
20.60
11.60
19.10
22.60
26.10
29.60
33.10
36.60
40.10
43.6(
ELAPSED TIME (SEC)
START= 19.20.26 STOP= END INERTIAL S/N= xxxx TP= xxxxxxxxxxx

p20m60

p20m40

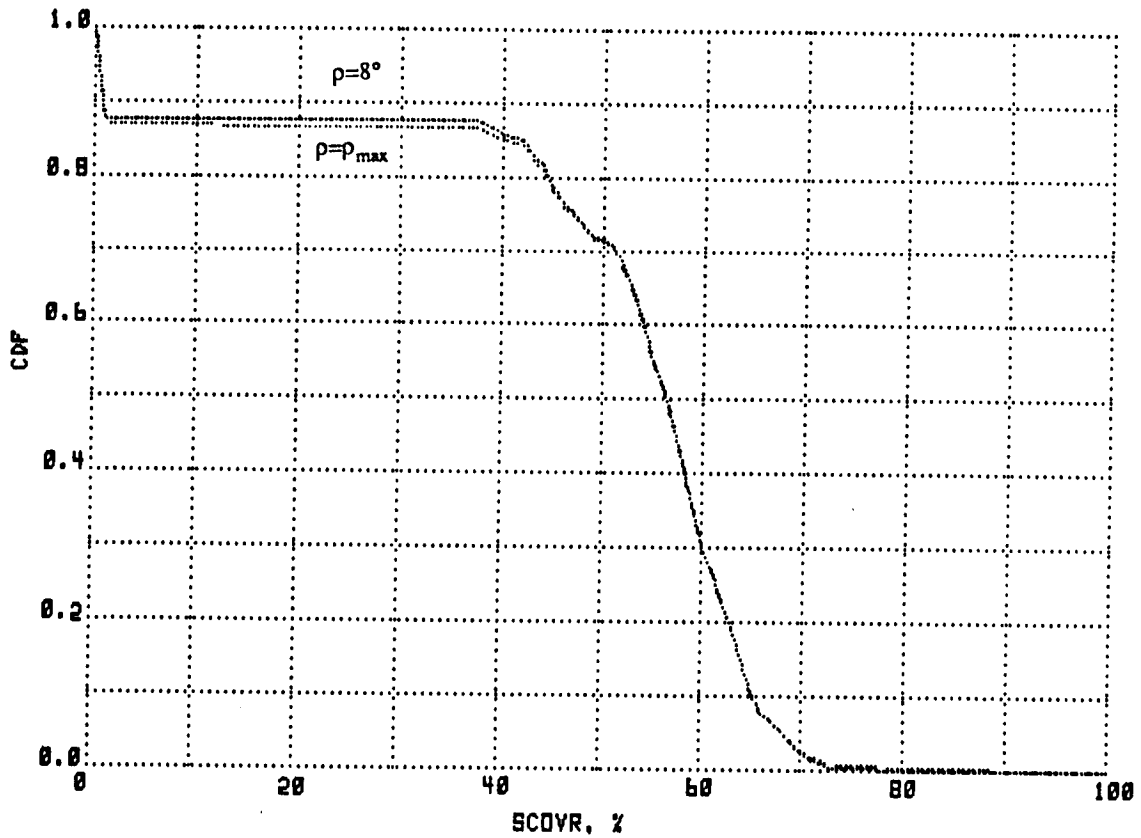

p20m40

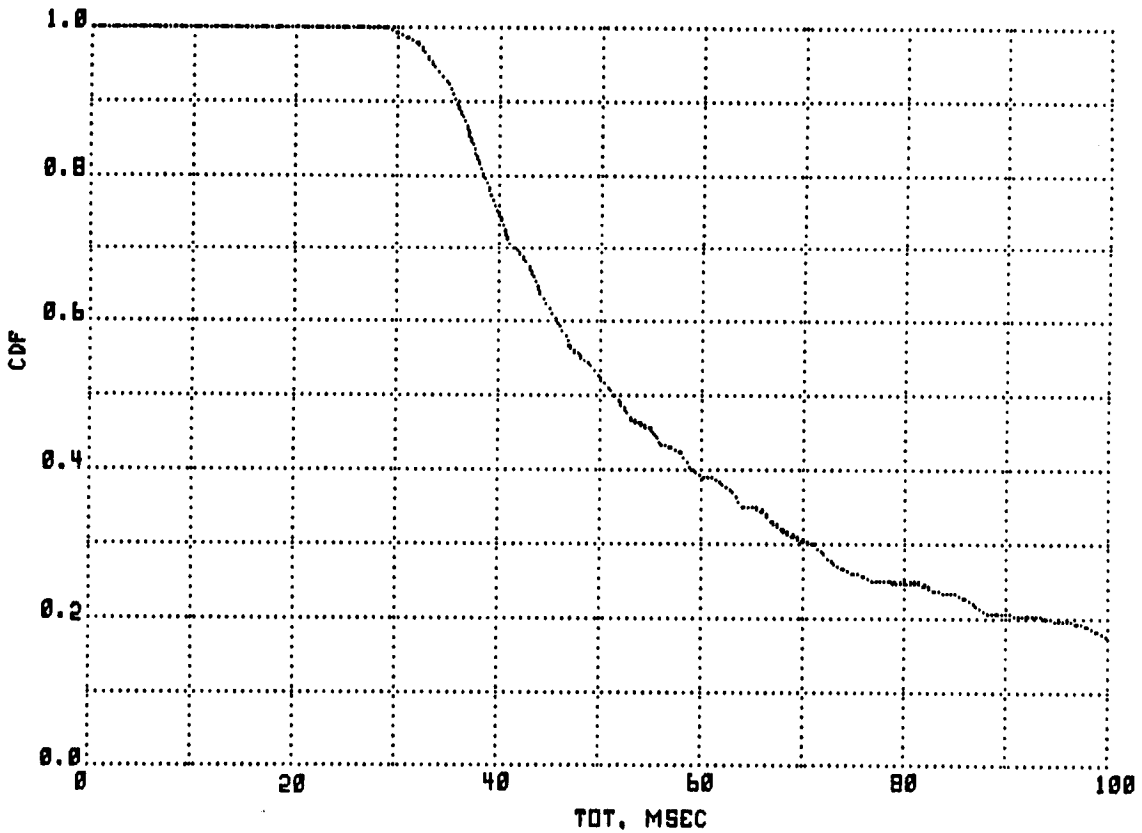

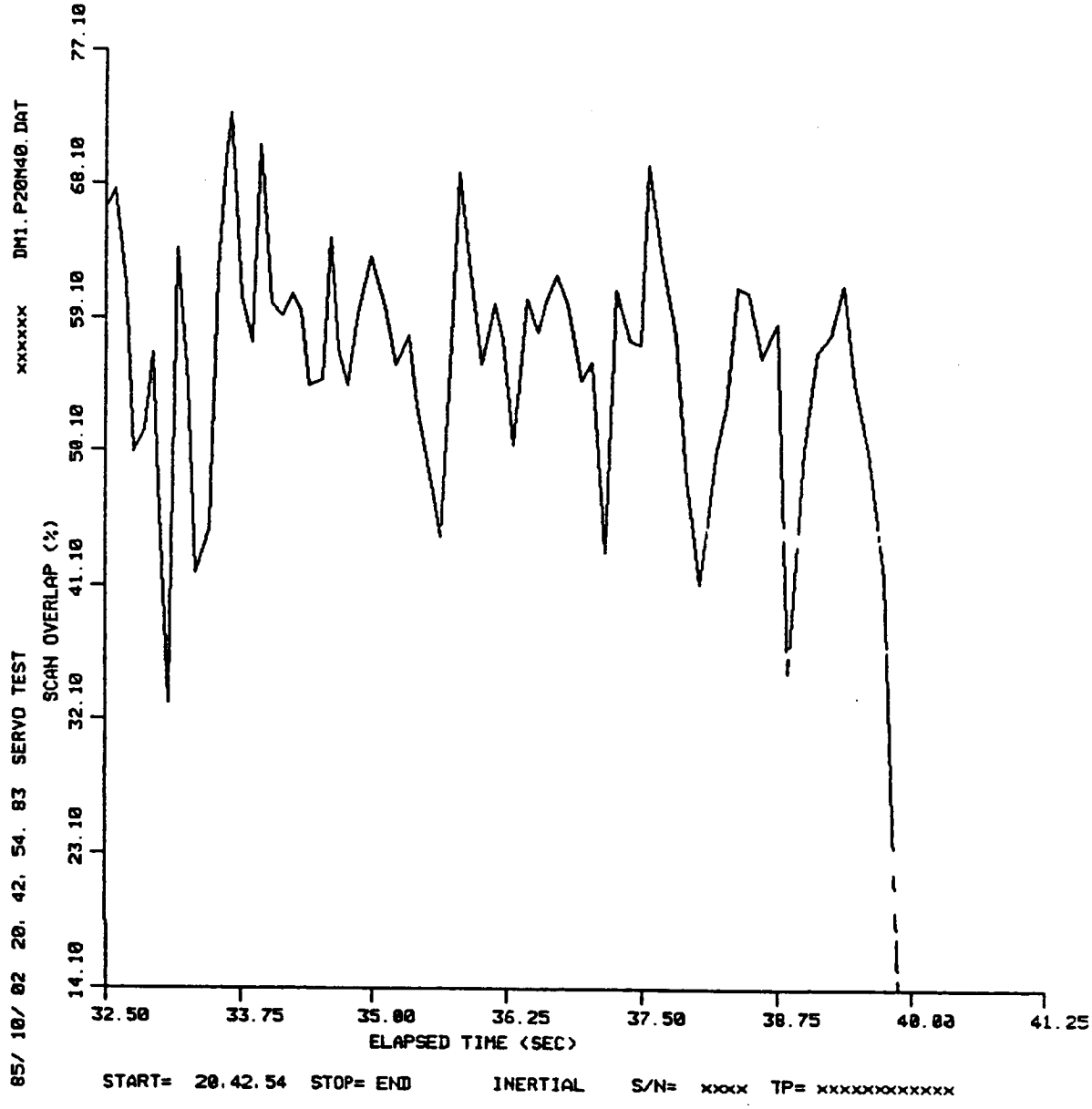
85/ 10/ 02 20. 42. 54. 83 SERVO TEST
xxxxxx DM1.P20N40.DAT
SCAN OVERLAP (%)
14.10
23.10
32.10
41.10
50.10
59.10
68.10
77.10
32.50
33.75
35.00
36.25
37.50
38.75
40.00
41.25
ELAPSED TIME (SEC)
START= 20.42.54 STOP= END
INERTIAL
S/N= xxxx TP= xxxxxxxxxxx

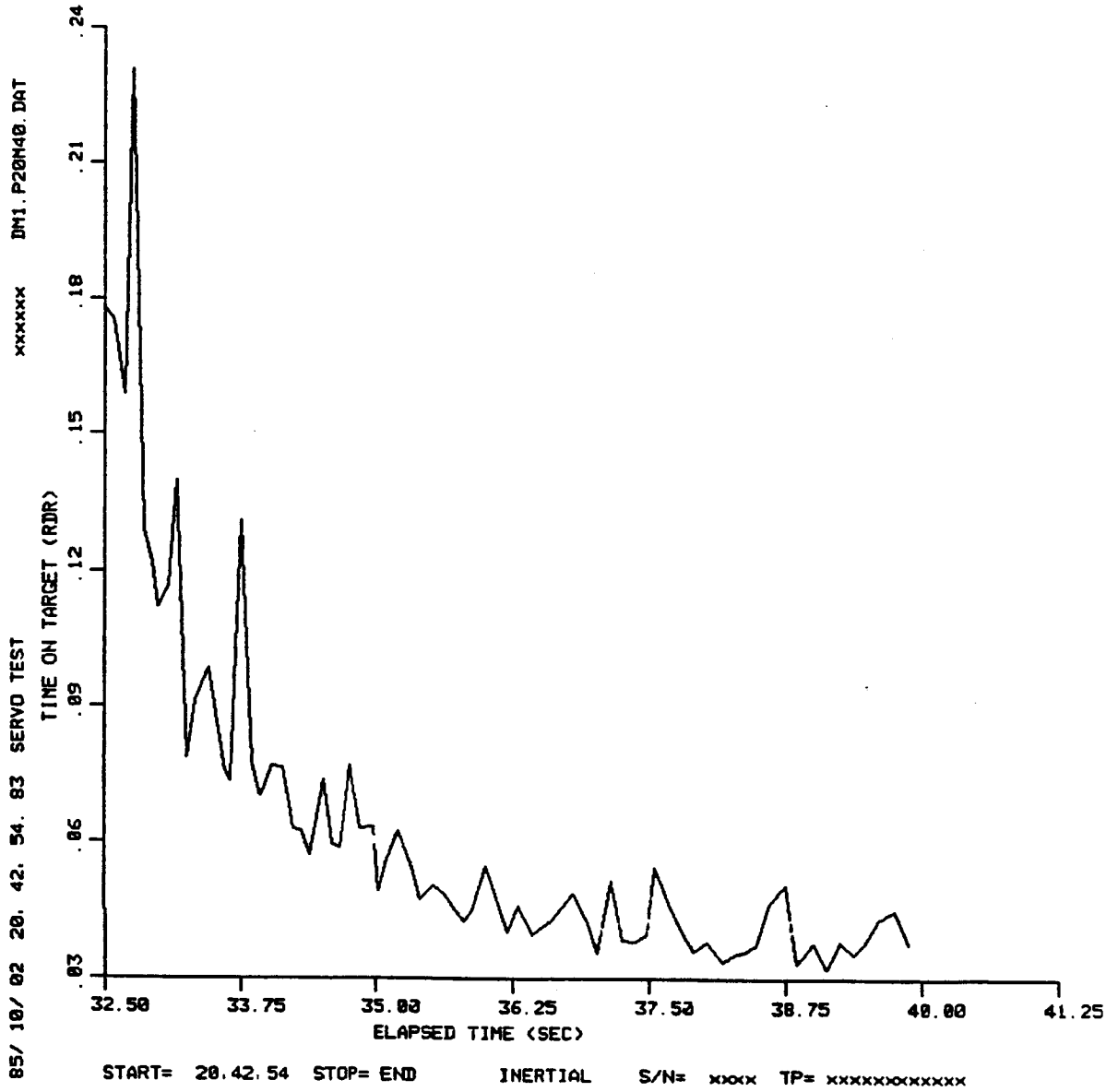
85/ 10/ 02 20. 42. 54. 83 SERVO TEST
xxxxxx DM1.P20H40.DAT
TIME ON TARGET (RDR)
.03
.06
.09
.12
.15
.18
.21
.24
32.50
33.75
35.00
36.25
37.50
38.75
40.00
41.25
ELAPSED TIME (SEC)
START= 20.42.54 STOP= END
INERTIAL
S/N= xxxx TP= xxxxxxxxxxx

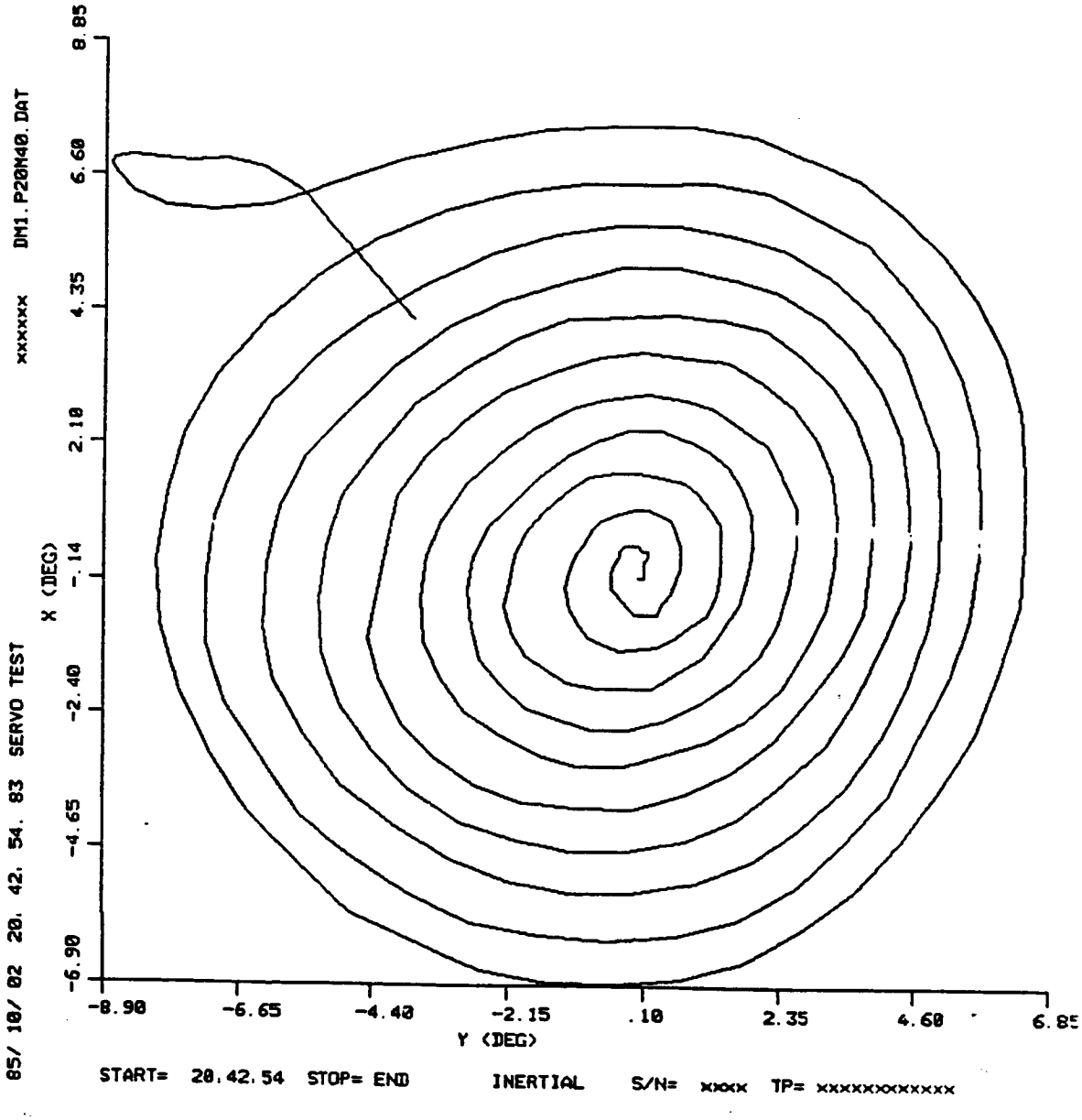
85/ 10/ 02 20. 42. 54. 83 SERVO TEST
xxxxxx DM1.P20M40.DAT
X (DEG)
8.85
6.60
4.35
2.10
-.14
-2.40
-4.65
-6.90
-8.90
-6.65
-4.40
-2.15
.10
2.35
4.60
6.85
Y (DEG)
START= 20.42.54 STOP= END
INERTIAL
S/N= xxxx TP= xxxxxxxxxxx

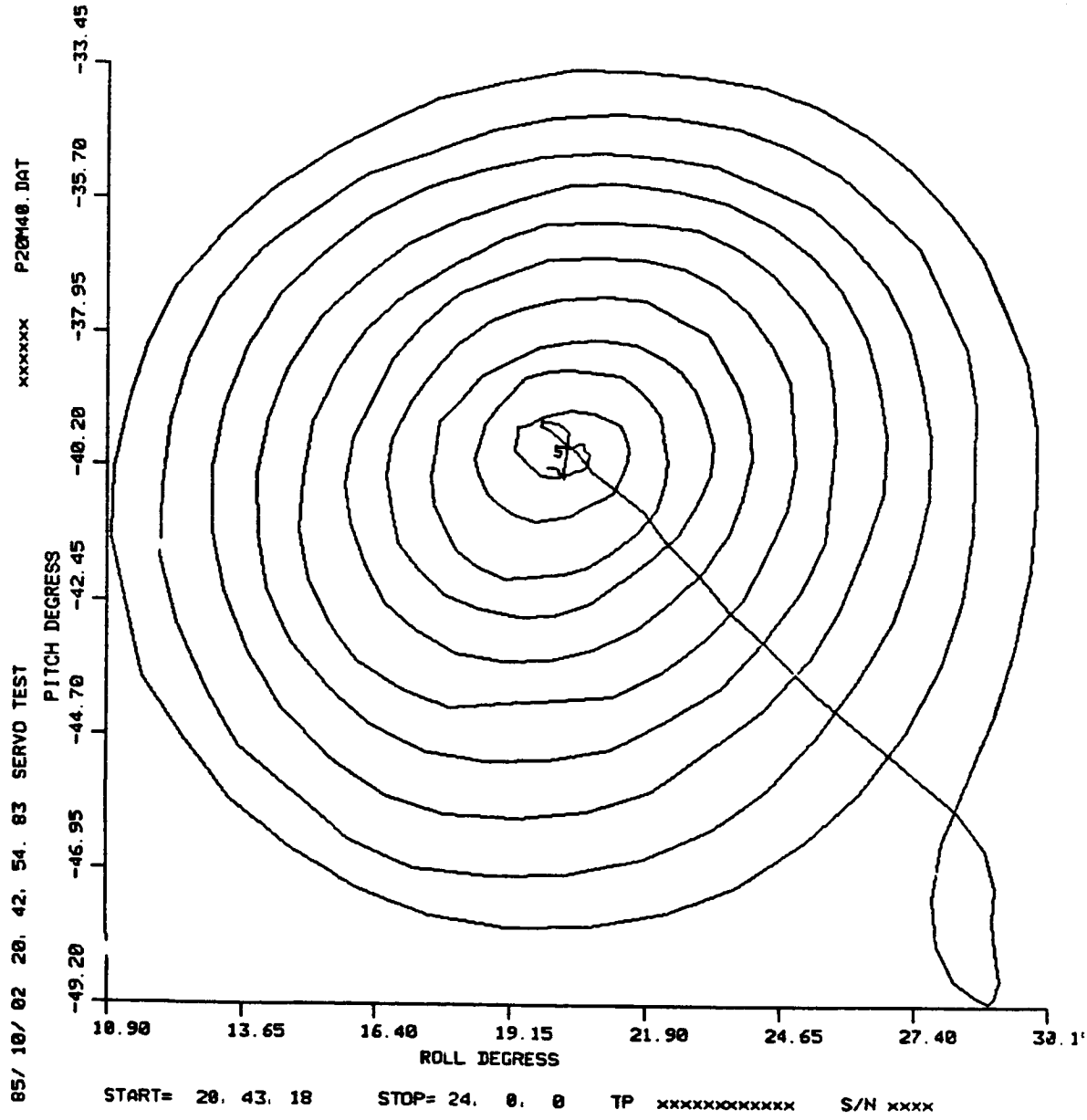
85/ 10/ 02 20, 42, 54. 83 SERVO TEST
xxxxxx P20M40.DAT
PITCH DEGRESS
-33.45
-35.70
-37.95
-40.20
-42.45
-44.70
-46.95
-49.20
10.90
13.65
16.40
19.15
21.90
24.65
27.40
ROLL DEGRESS
START= 20, 43, 18
STOP= 24, 0, 0
TP xxxxxxxxxxx
S/N xxxx

p20m20

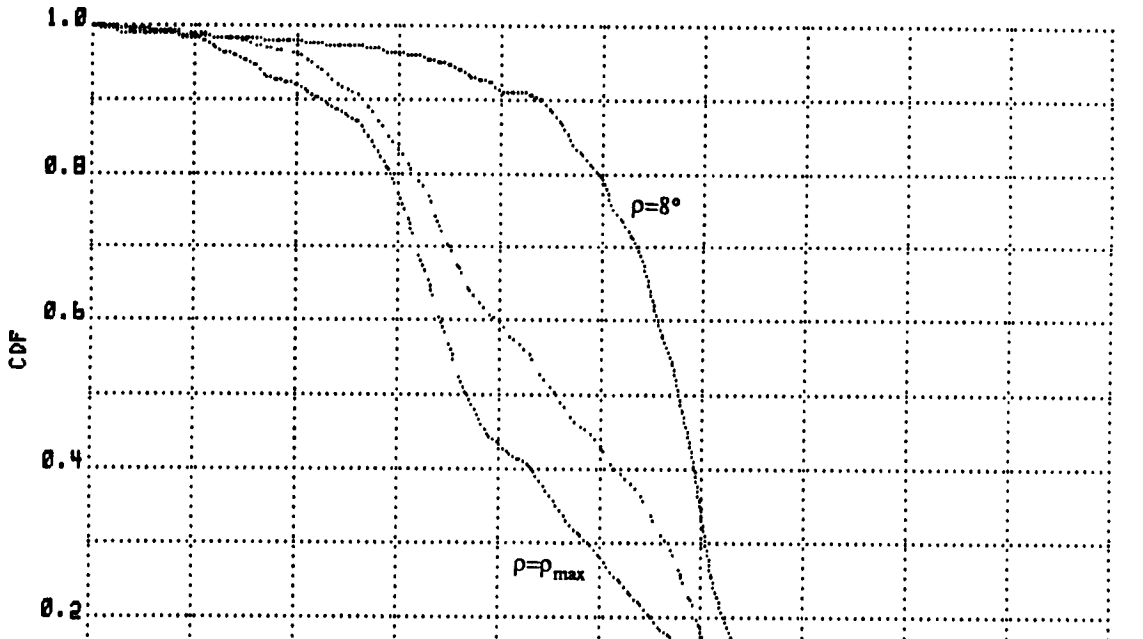

p20m20

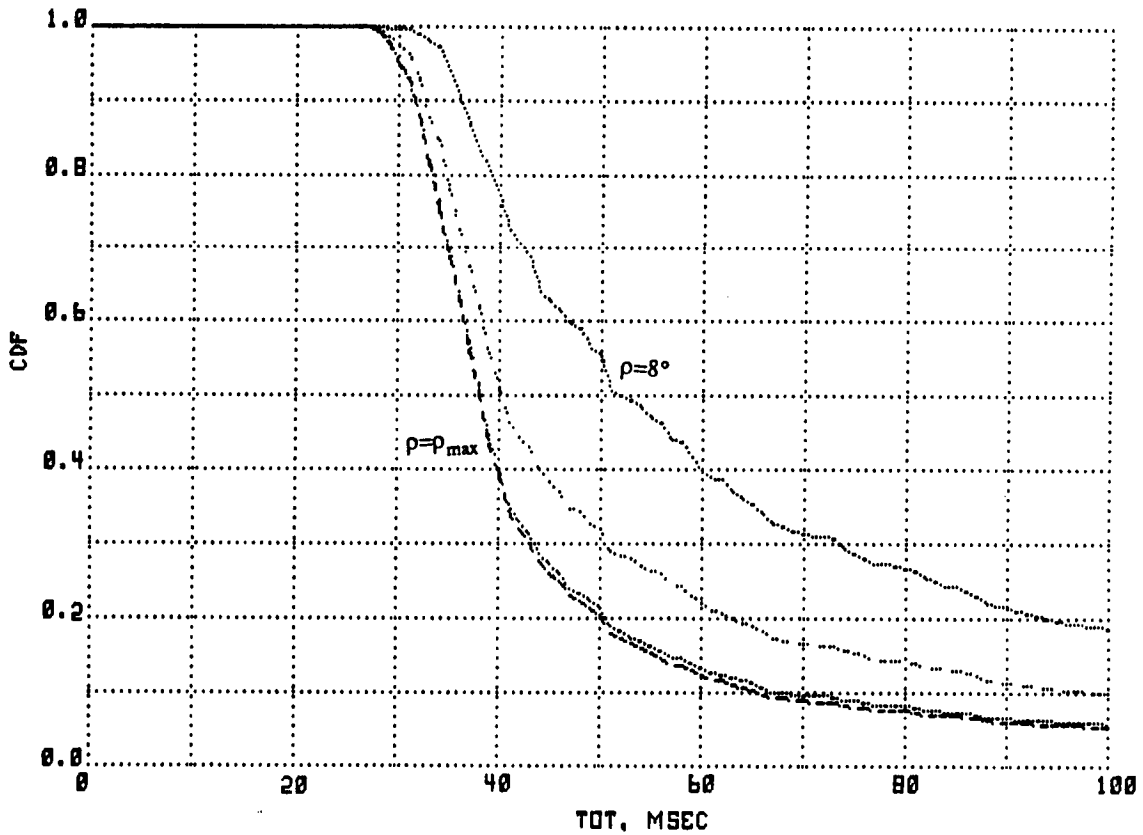

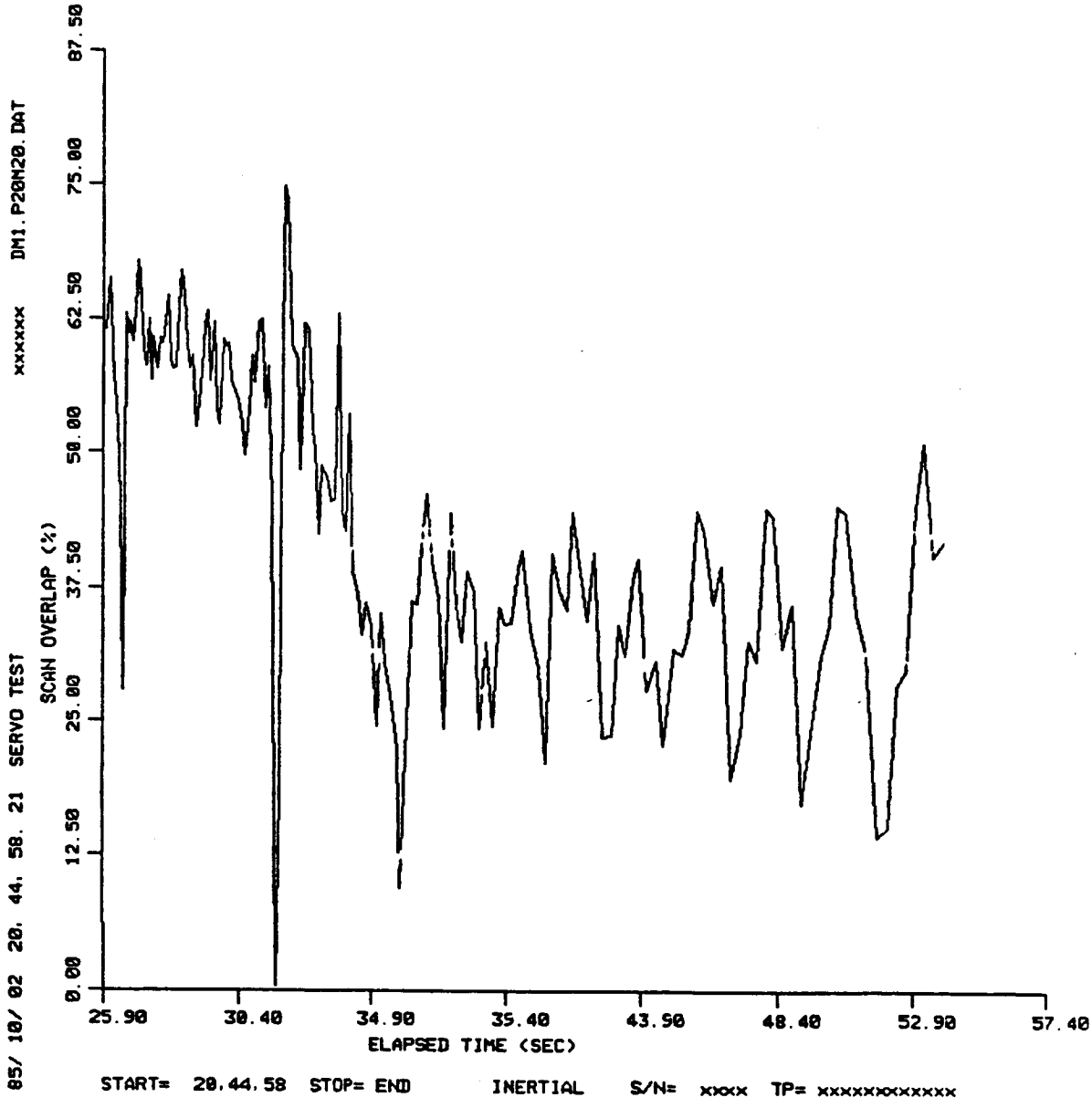
85/ 10/ 02 20. 44. 58. 21 SERVO TEST
xxxxxx DM1.P20N20.DAT
SCAN OVERLAP (%)
0.00
12.50
25.00
37.50
50.00
62.50
75.00
87.50
25.90
30.40
34.90
35.40
43.90
48.40
52.90
57.40
ELAPSED TIME (SEC)
START= 20.44.58 STOP= END INERTIAL S/N= xxxx TP= xxxxxxxxxxx

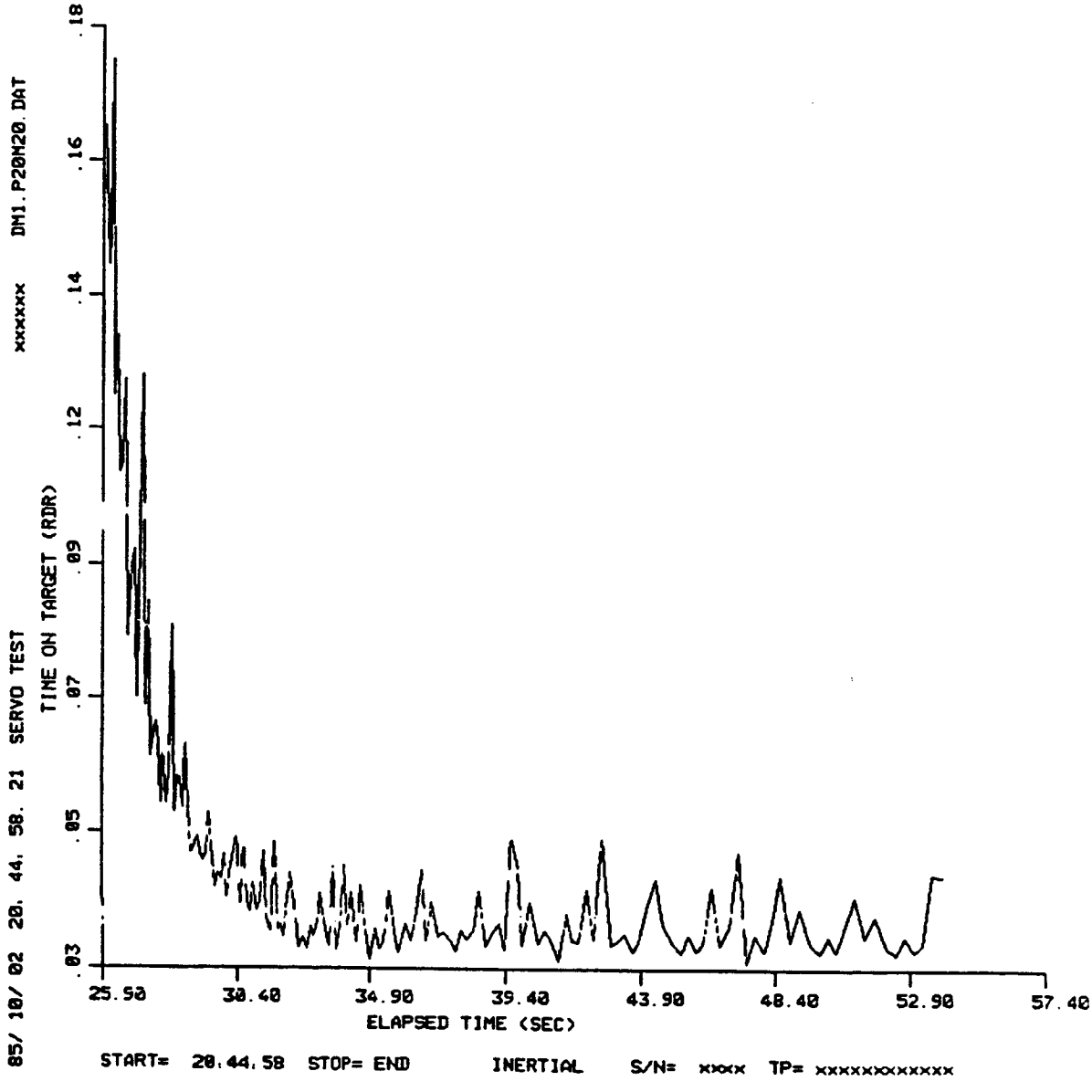
85/ 10/ 02 20. 44. 58. 21 SERVO TEST
xxxxxx DM1.P20N20.DAT
TIME ON TARGET (RDR)
.03
.05
.07
.09
.12
.14
.16
.18
25.90
30.40
34.90
39.40
43.90
48.40
52.90
57.40
ELAPSED TIME (SEC)
START= 20.44.58 STOP= END
INERTIAL
S/N= xxxx TP= xxxxxxxxxxx

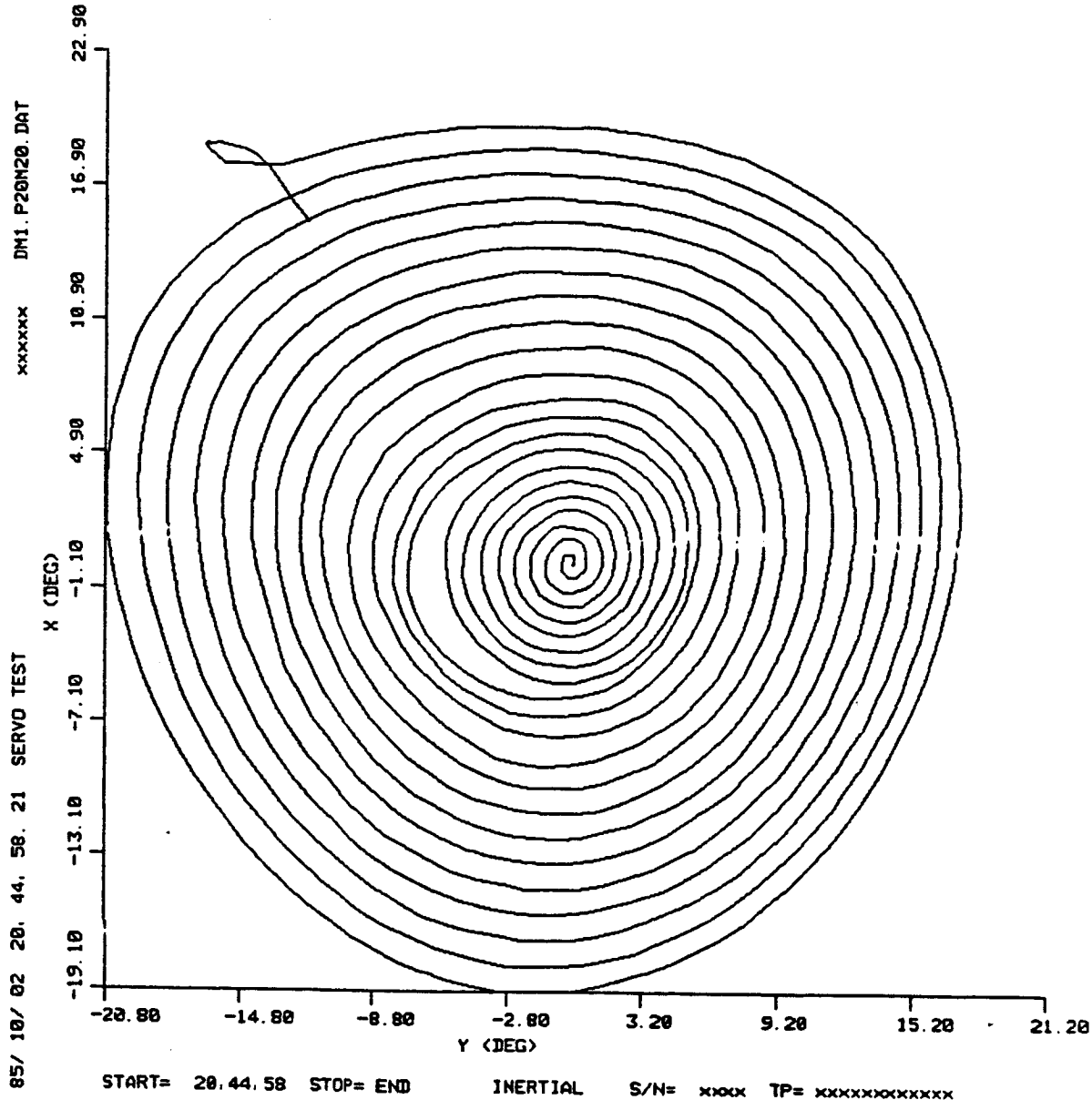
85/ 10/ 02 20. 44. 58. 21 SERVO TEST
xxxxxx DM1.P20N20.DAT
X (DEG)
22.90
16.90
10.90
4.90
-1.10
-7.10
-13.10
-19.10
-20.80
-14.80
-8.80
-2.80
3.20
9.20
15.20
21.20
Y (DEG)
START= 20.44.58 STOP= END
INERTIAL
S/N= xxxx TP= xxxxxxxxxxx

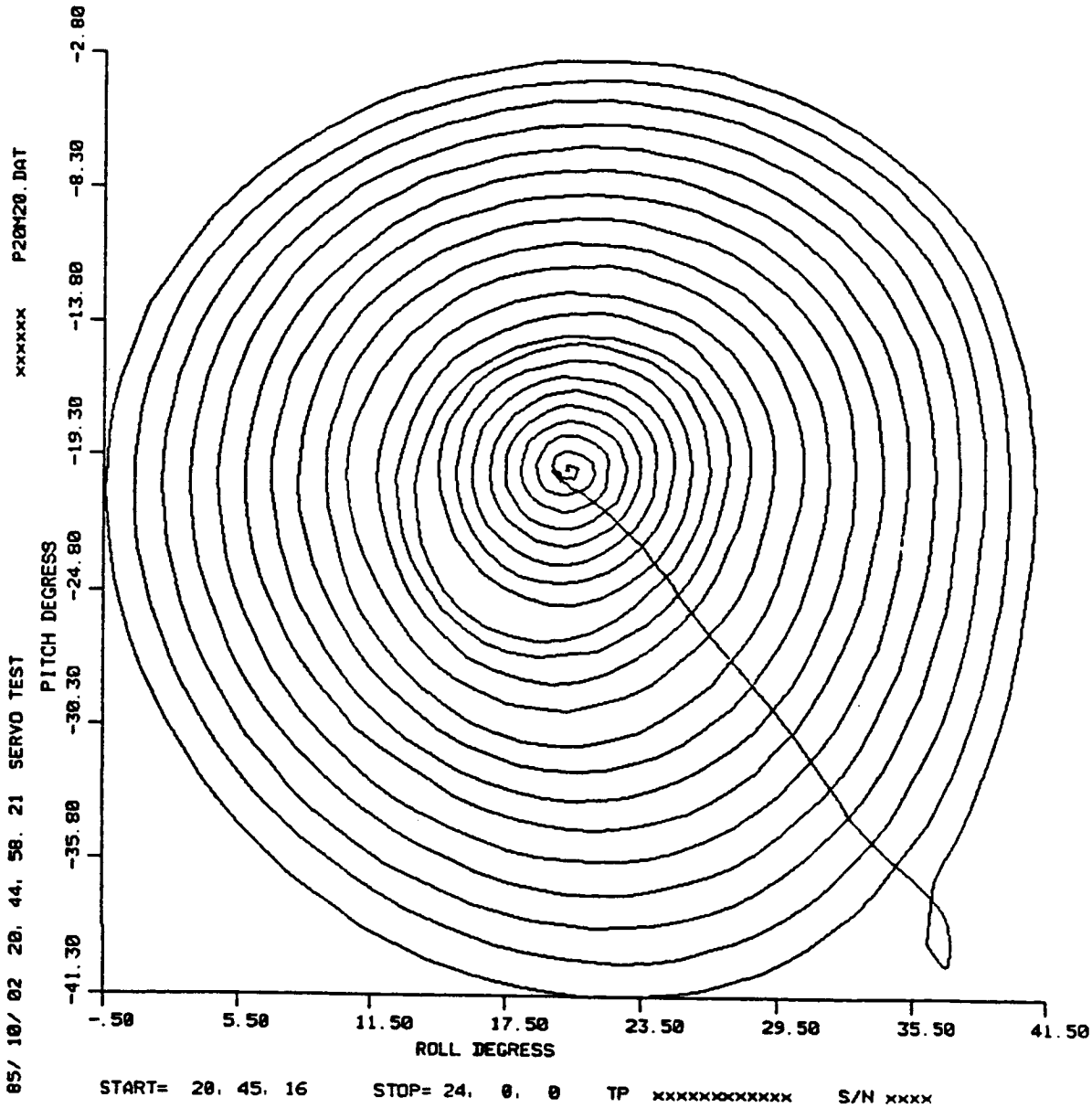
85/ 10/ 02 20. 44. 58. 21 SERVO TEST
xxxxxx P20120.DAT
PITCH DEGRESS
-2.80
-8.30
-13.80
-19.30
-24.80
-30.30
-35.80
-41.30
-.50
5.50
11.50
17.50
23.50
29.50
35.50
41.50
ROLL DEGRESS
START= 20. 45. 16
STOP= 24. 0. 0
TP xxxxxxxxxxx
S/N xxxx

p20p00

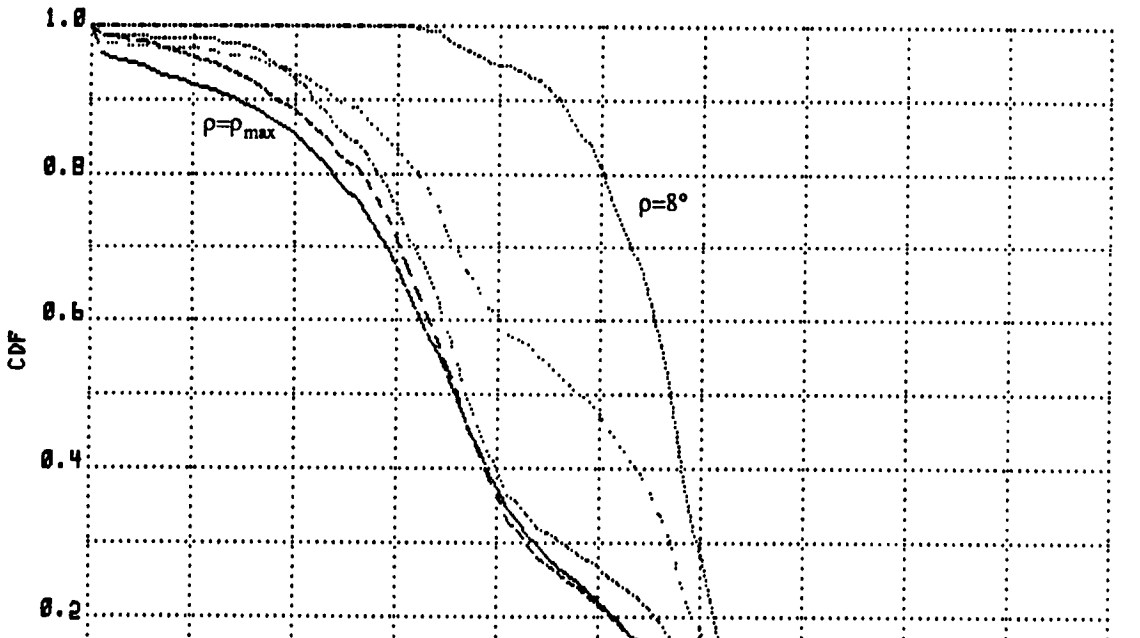

p20p00

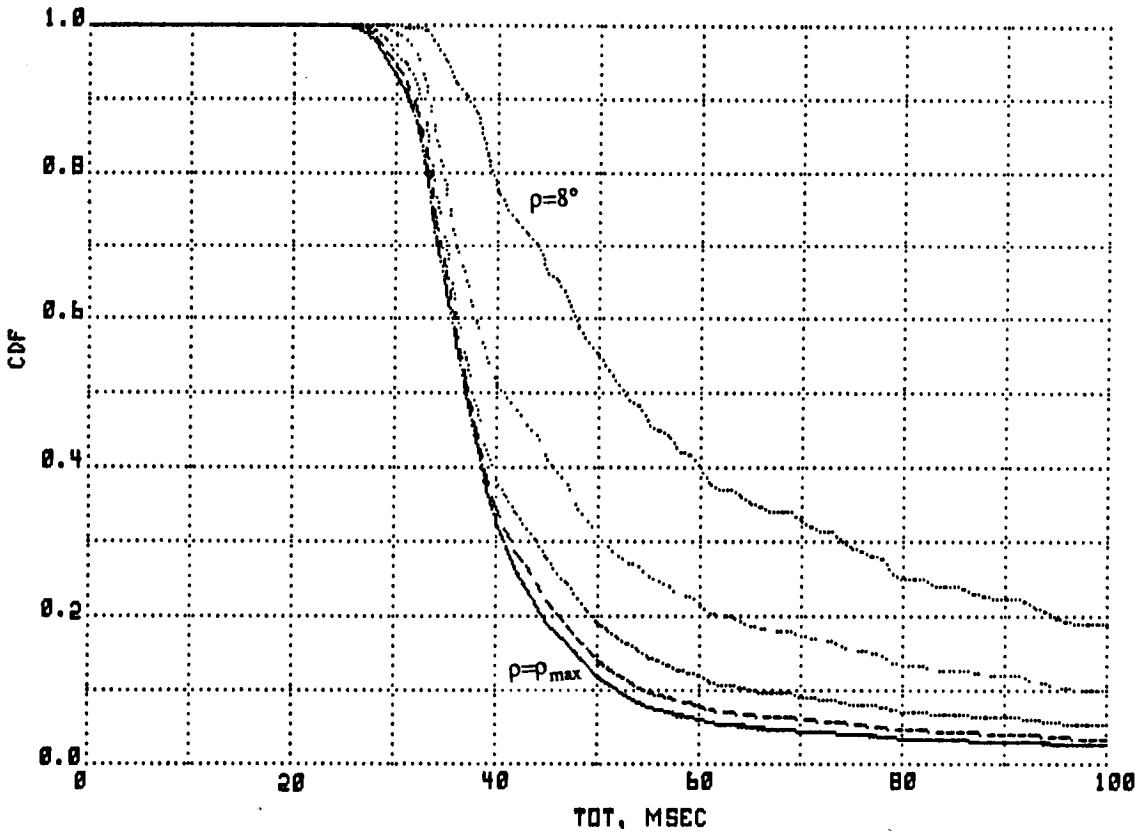

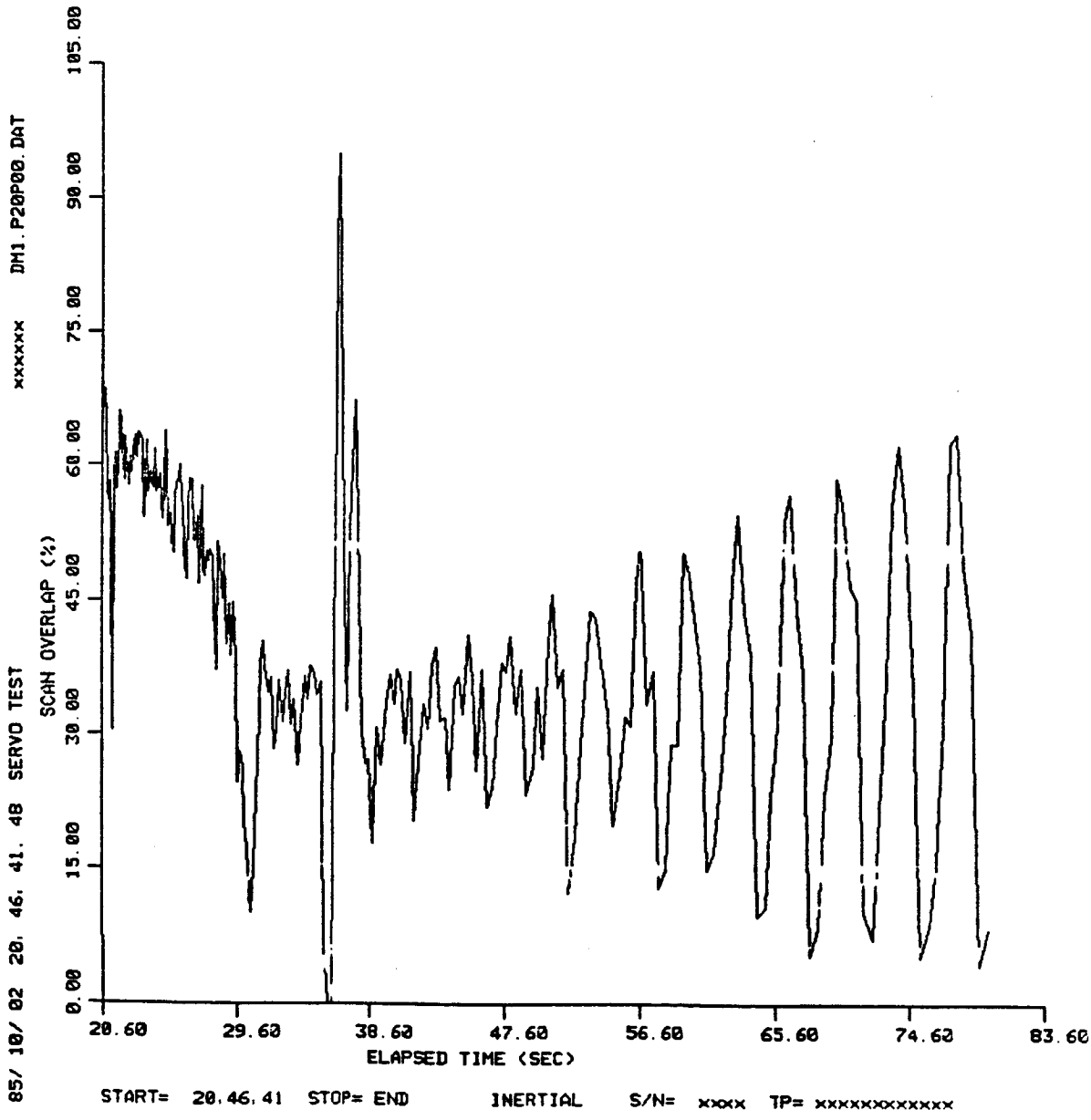
85/ 10/ 02 20. 46. 41. 48 SERVO TEST
xxxxxx DM1.P20P00.DAT
SCAN OVERLAP (%)
0.00
15.00
30.00
45.00
60.00
75.00
90.00
105.00
20.60
29.60
38.60
47.60
56.60
65.60
74.60
83.60
ELAPSED TIME (SEC)
START= 20.46.41 STOP= END
INERTIAL
S/N= xxxx TP= xxxxxxxxxxxx

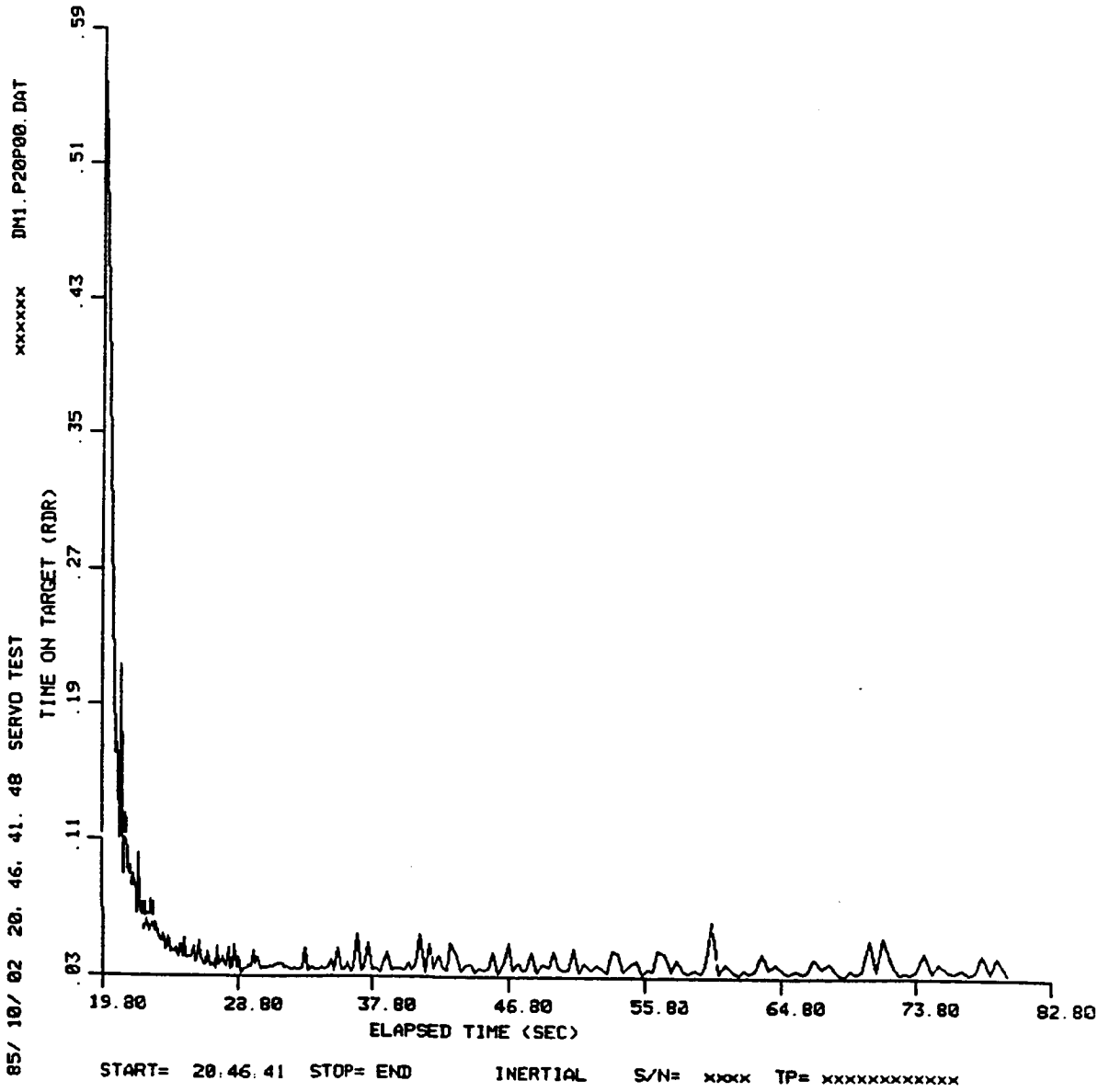
85/ 10/ 02 20. 46. 41. 48 SERVO TEST
xxxxxx DM1.P20P00.DAT
TIME ON TARGET (RDR)
.03
.11
.19
.27
.35
.43
.51
.59
19.80
28.80
37.80
46.80
55.80
64.80
73.80
82.80
ELAPSED TIME (SEC)
START= 20:46:41 STOP= END
INERTIAL
S/N= xxxx TP= xxxxxxxxxxx

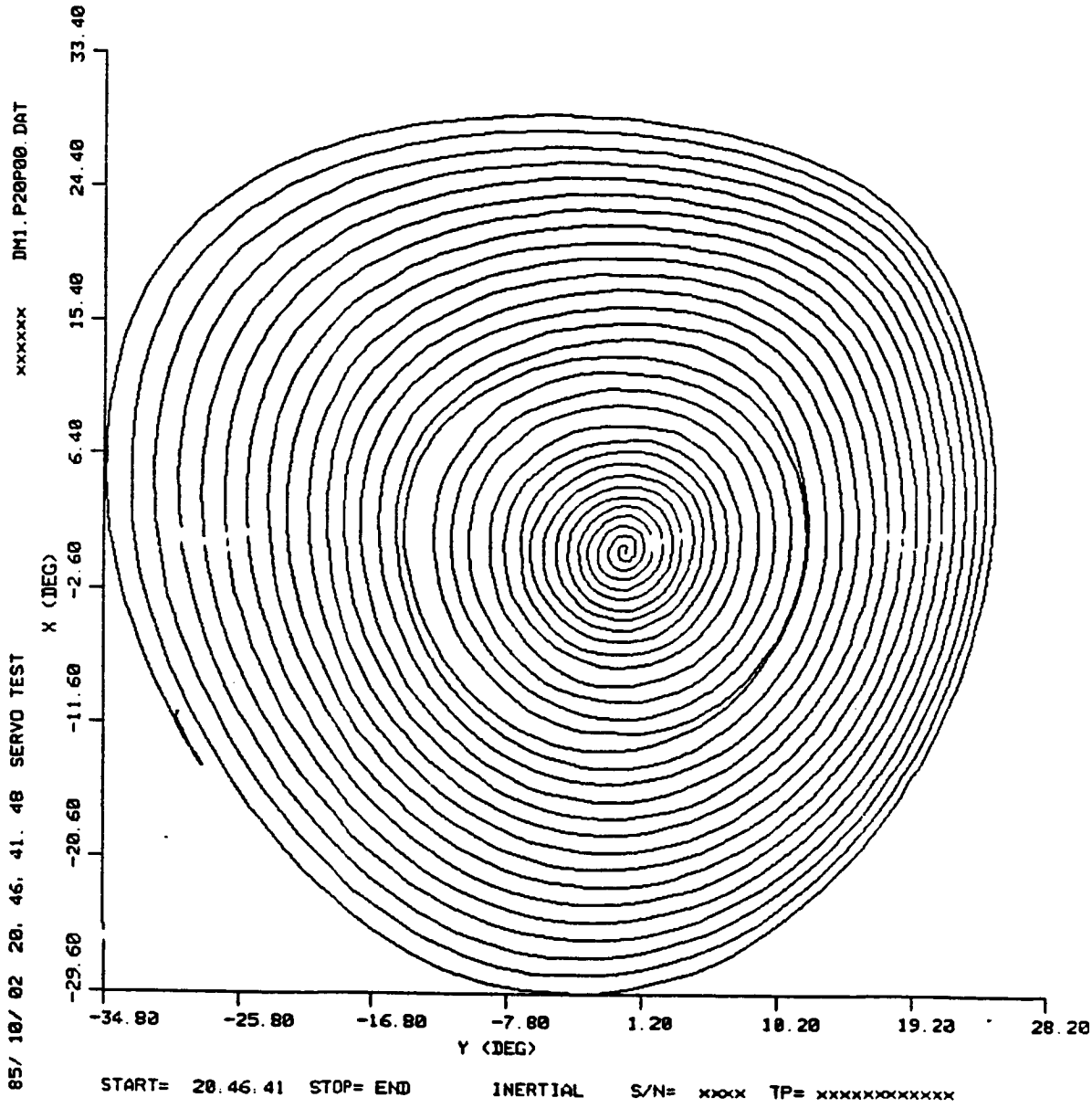
85/ 10/ 02 20. 46. 41. 48 SERVO TEST
xxxxxx DM1.P20P00.DAT
X (DEG)
33.40
24.40
15.40
6.40
-2.60
-11.60
-20.60
-29.60
-34.80
-25.80
-16.80
-7.80
1.20
10.20
19.20
28.20
Y (DEG)
START= 20.46.41 STOP= END
INERTIAL
S/N= xxxx TP= xxxxxxxxxxx

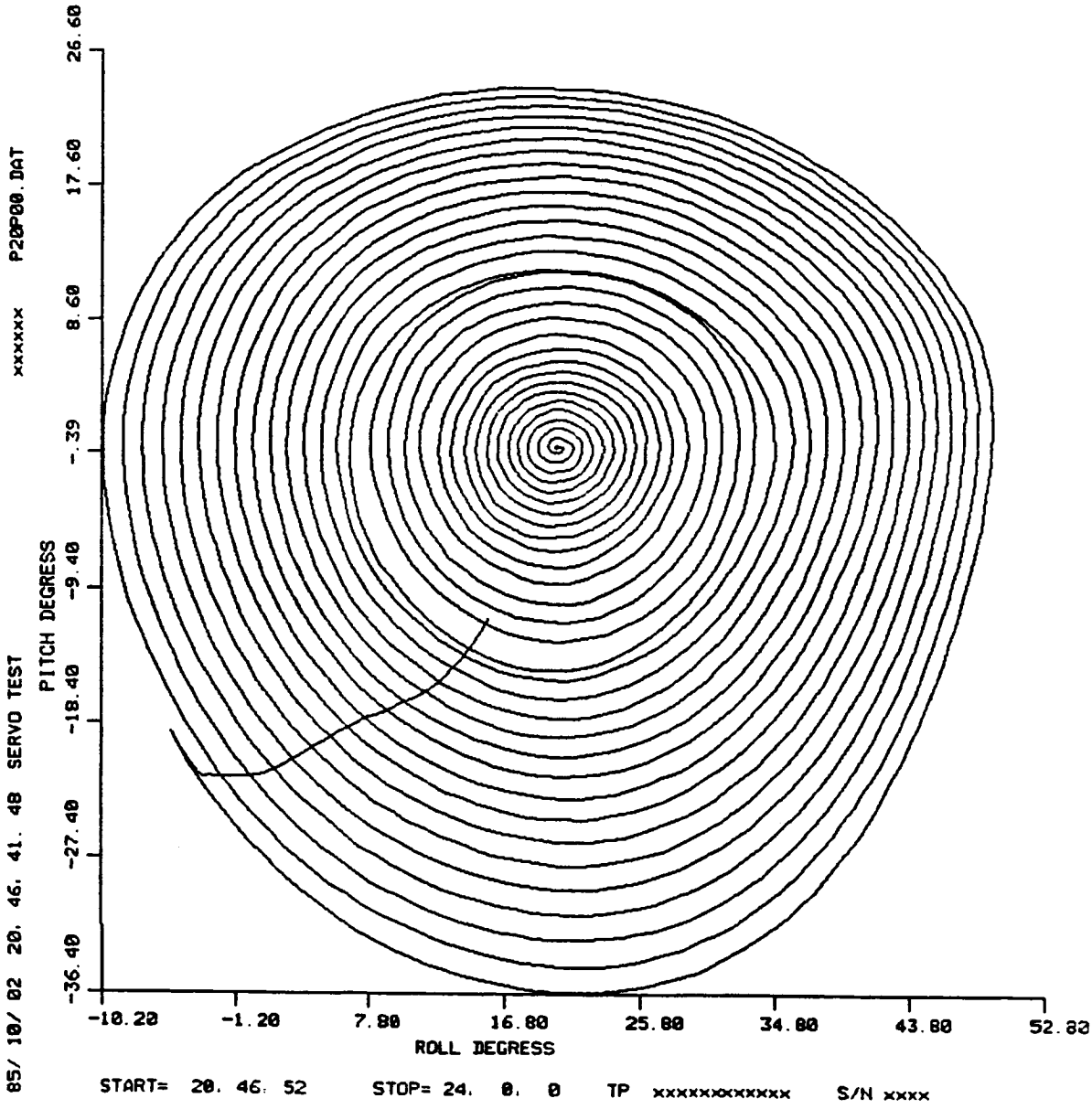
85/ 10/ 02 20. 46. 41. 48 SERVO TEST
xxxxxx P20P00.DAT
PITCH DEGRESS
26.60
17.60
8.60
-.39
-9.40
-18.40
-27.40
-36.40
-10.20
-1.20
7.80
16.80
25.80
34.80
43.80
52.80
ROLL DEGRESS
START= 20. 46. 52
STOP= 24. 0. 0
TP xxxxxxxxxxx
S/N xxxx

p20p20

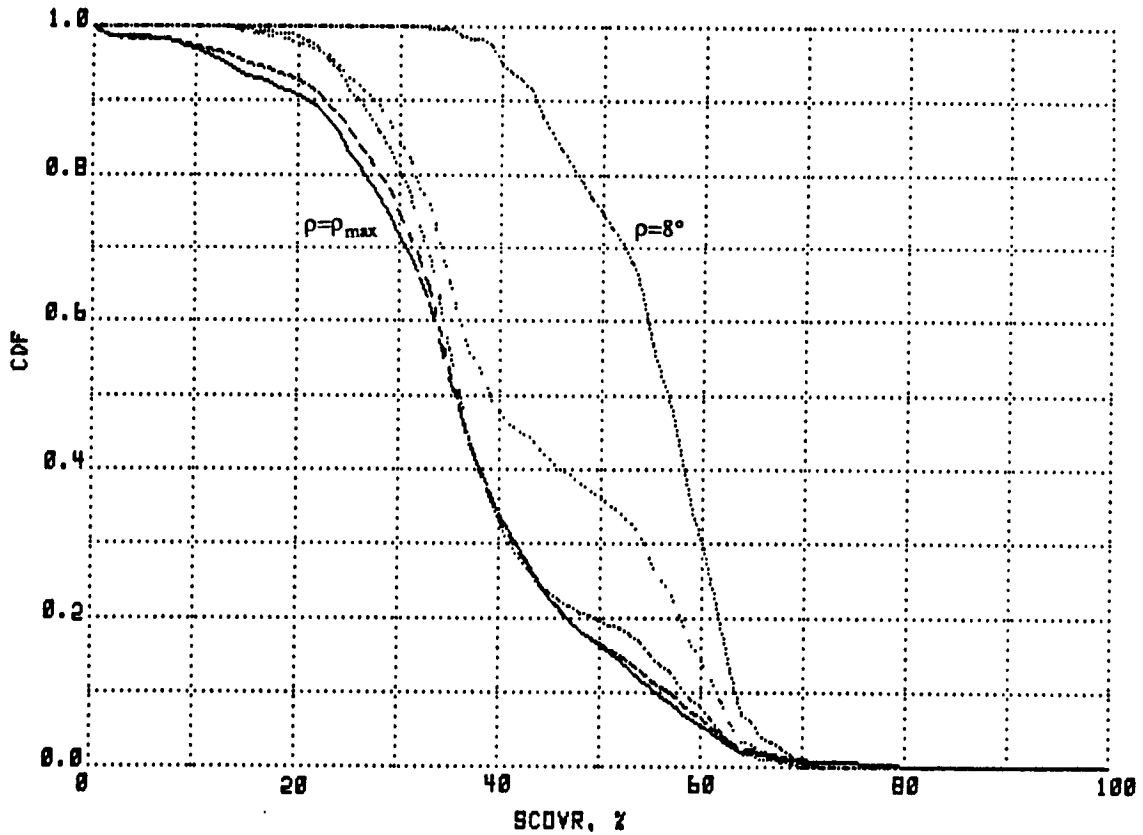

p20p20

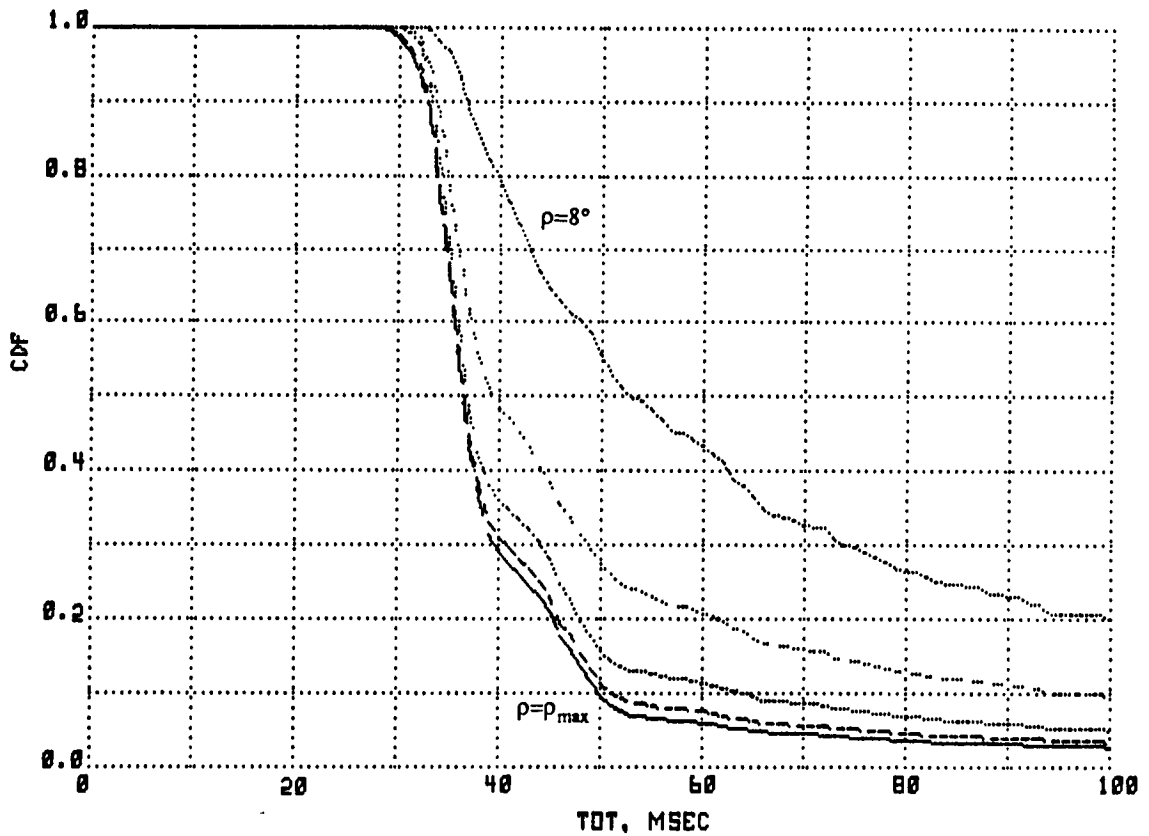

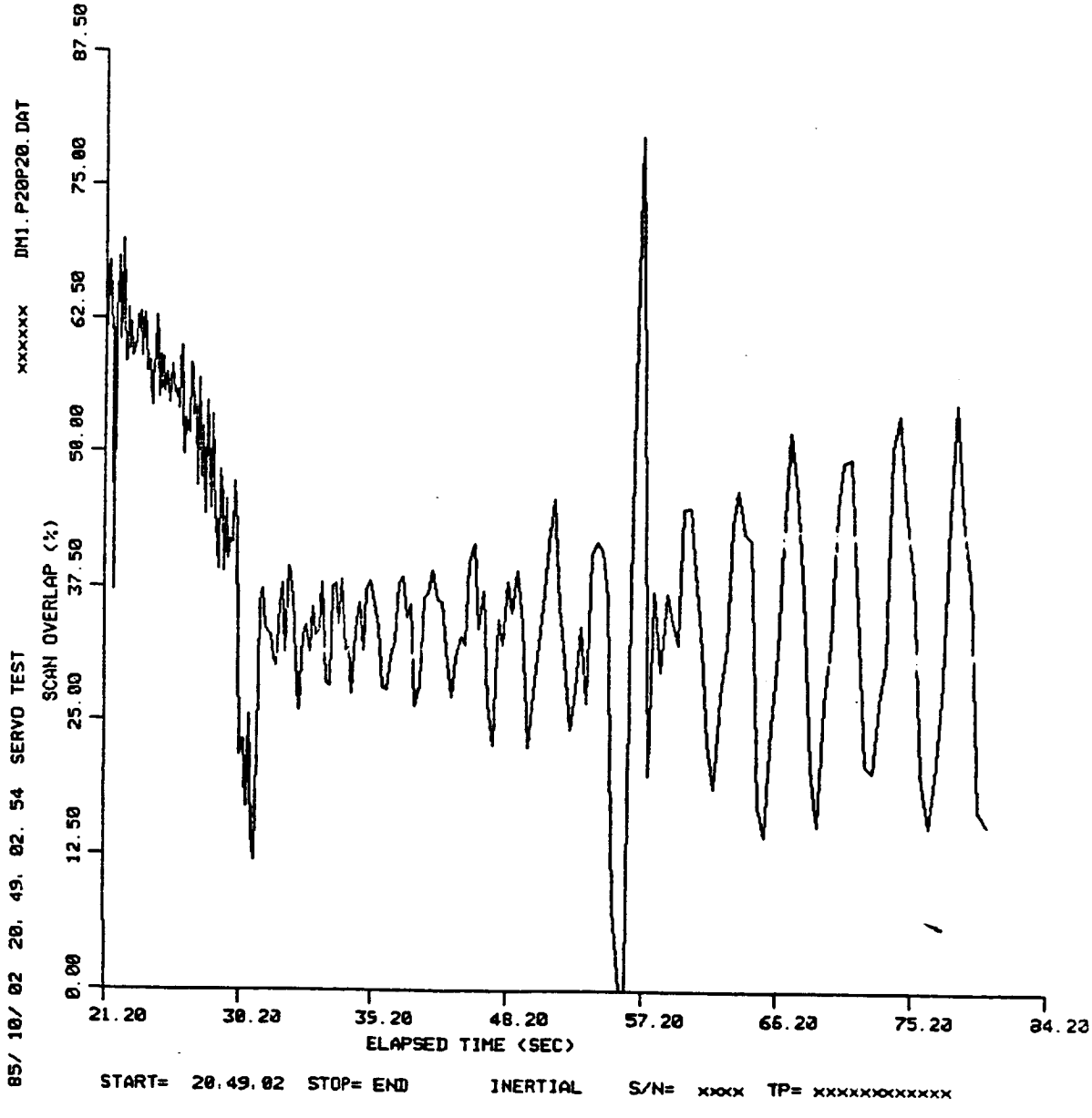
85/ 10/ 02 20. 49. 02. 54 SERVO TEST
xxxxxx DM1.P20P20.DAT
SCAN OVERLAP (%)
0.00
12.50
25.00
37.50
50.00
62.50
75.00
87.50
21.20
30.20
39.20
48.20
57.20
66.20
75.20
84.20
ELAPSED TIME (SEC)
START= 20.49.02 STOP= END
INERTIAL
S/N= xxxx TP= xxxxxxxxxxx

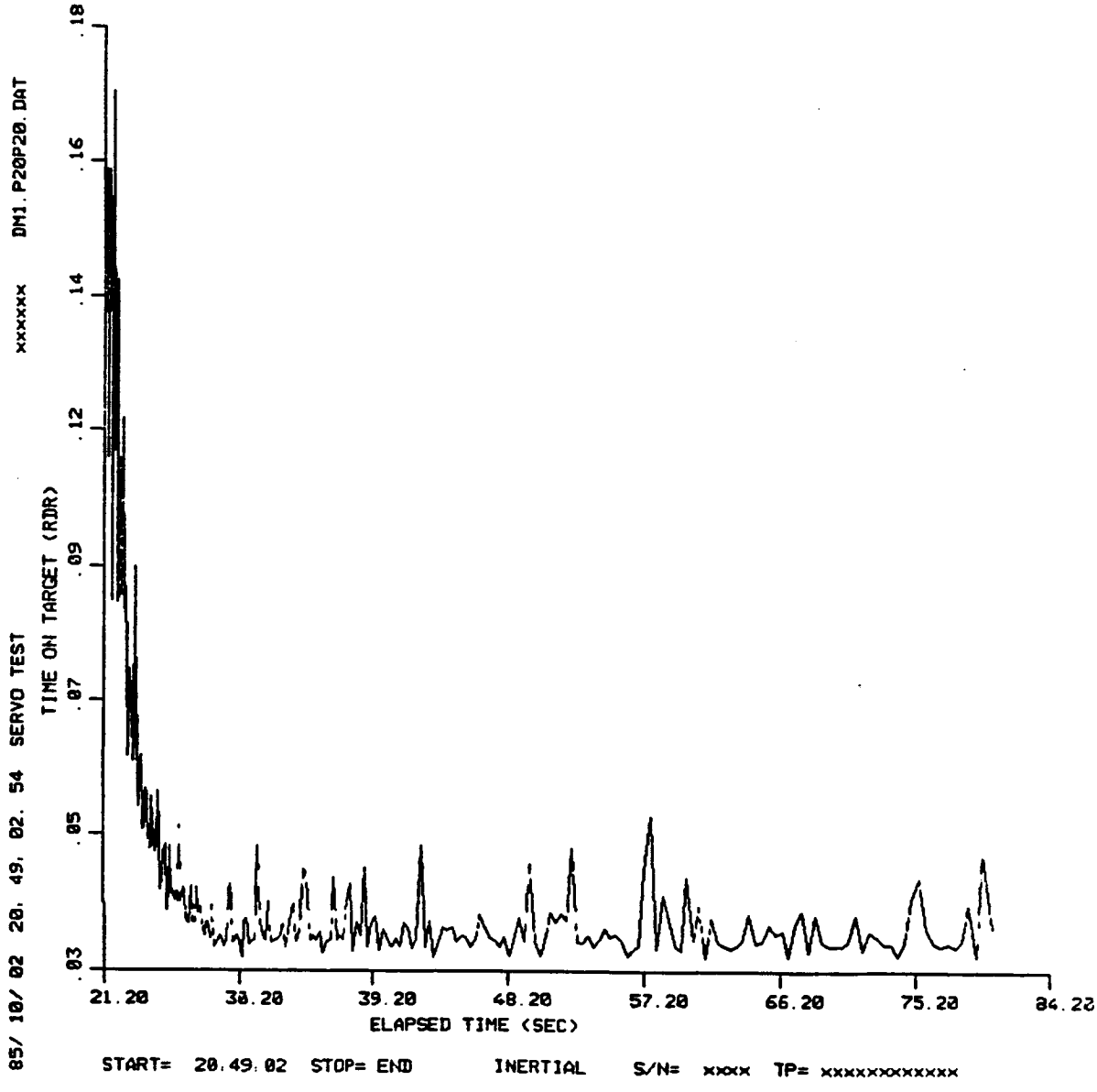
85/ 10/ 02 20: 49: 02. 54 SERVO TEST
xxxxxx DM1.P20P20.DAT
TIME ON TARGET (RDR)
.03
.05
.07
.09
.12
.14
.16
.18
21.20
30.20
39.20
48.20
57.20
66.20
75.20
84.22
ELAPSED TIME (SEC)
START= 20:49:02 STOP= END
INERTIAL
S/N= xxxx TP= xxxxxxxxxxx

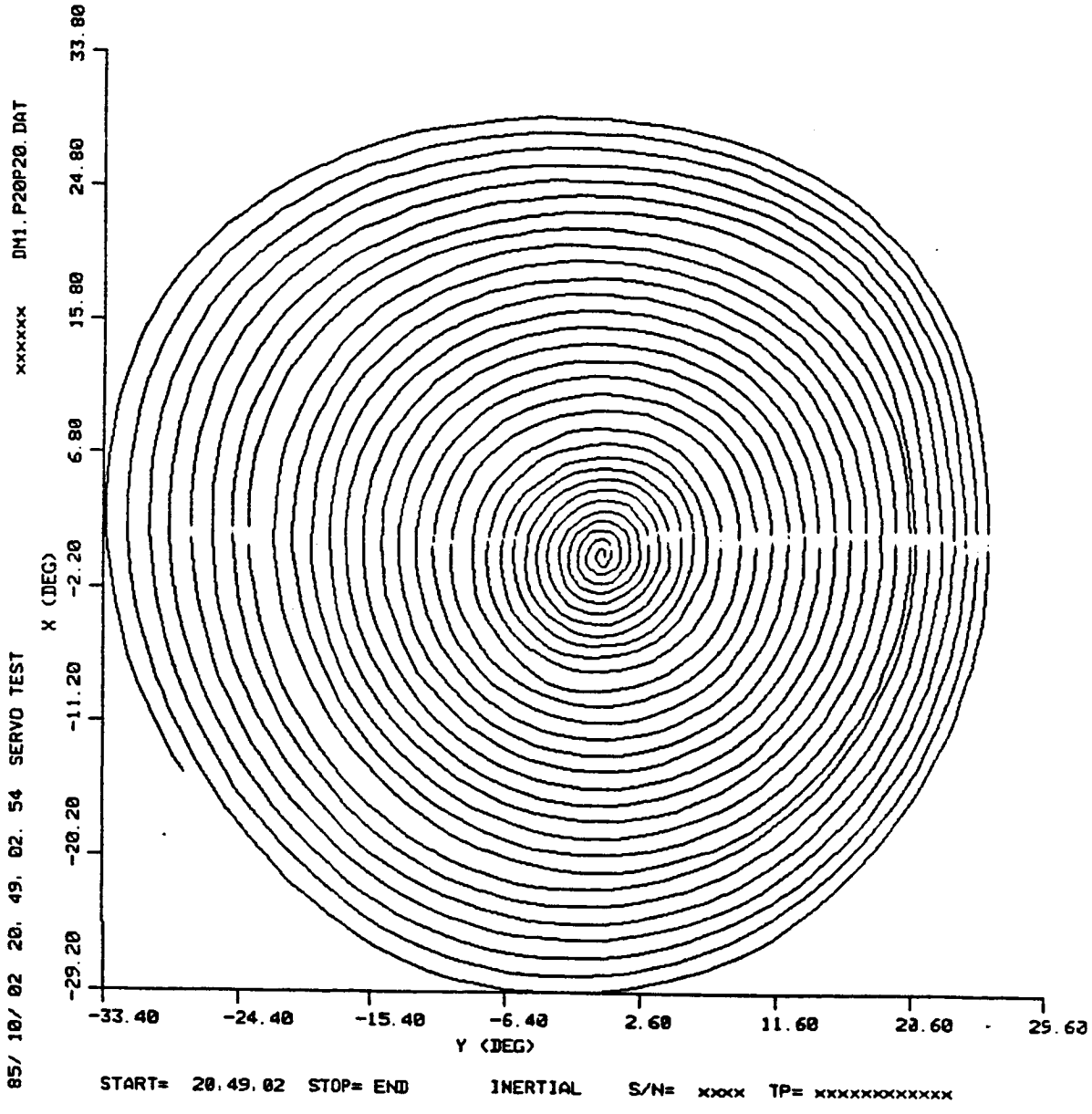
85/ 10/ 02 20. 49. 02. 54 SERVO TEST
XXXXXX DM1.P20P20.DAT
X (DEG)
33.80
24.80
15.80
6.80
-2.20
-11.20
-20.20
-29.20
-33.40
-24.40
-15.40
-6.40
2.60
11.60
20.60
29.60
Y (DEG)
START= 20.49.02 STOP= END
INERTIAL
S/N= XXXX TP= XXXXXXXXXXX

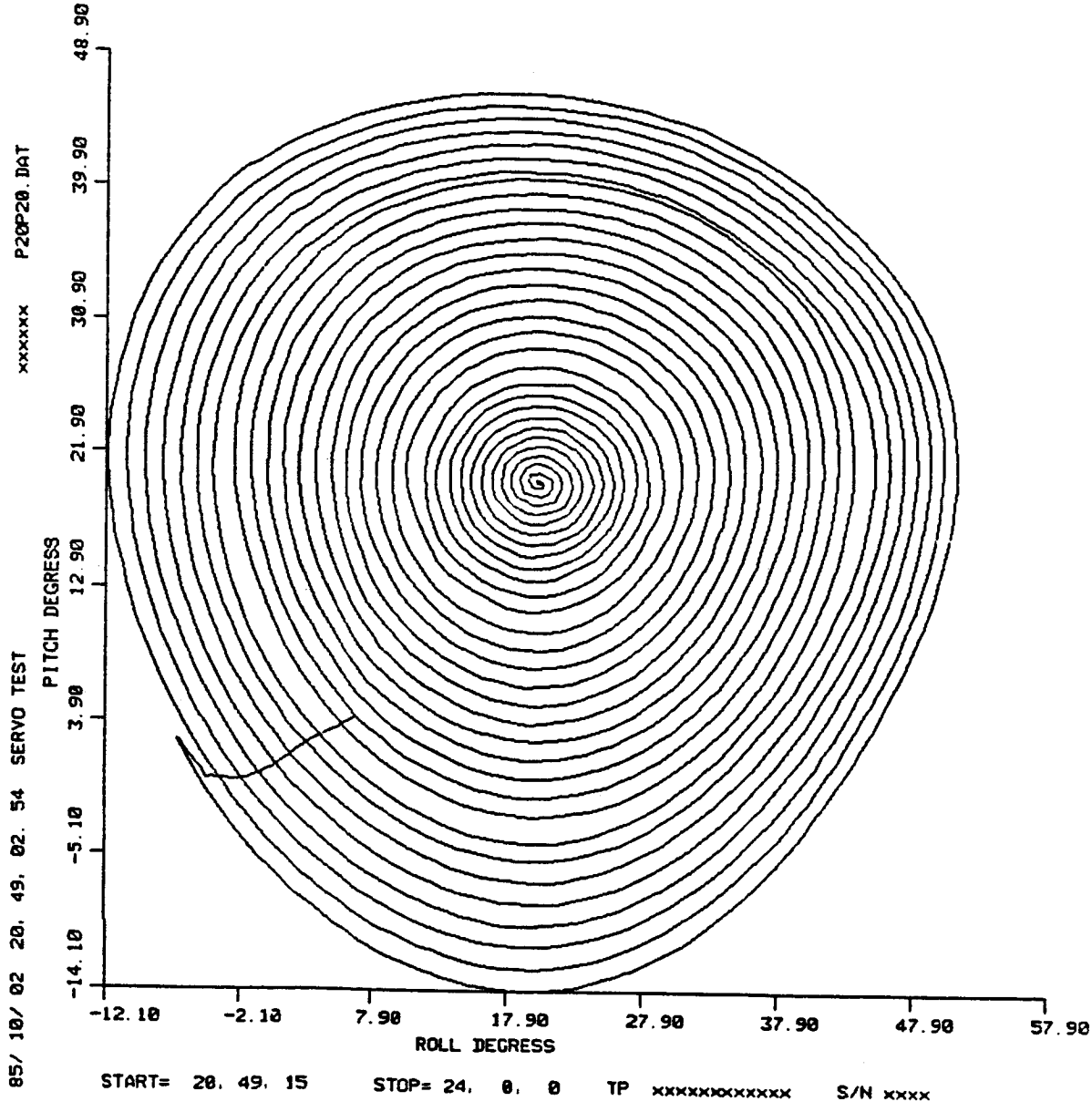
85/ 10/ 02 20. 49. 02. 54 SERVO TEST
xxxxxx P20P20.DAT
PITCH DEGRESS
48.90
39.90
30.90
21.90
12.90
3.90
-5.10
-14.10
-12.10
-2.10
7.90
17.90
27.90
37.90
47.90
57.90
ROLL DEGRESS
START= 20. 49. 15
STOP= 24. 0. 0
TP xxxxxxxxxxx
S/N xxxx

p20p20

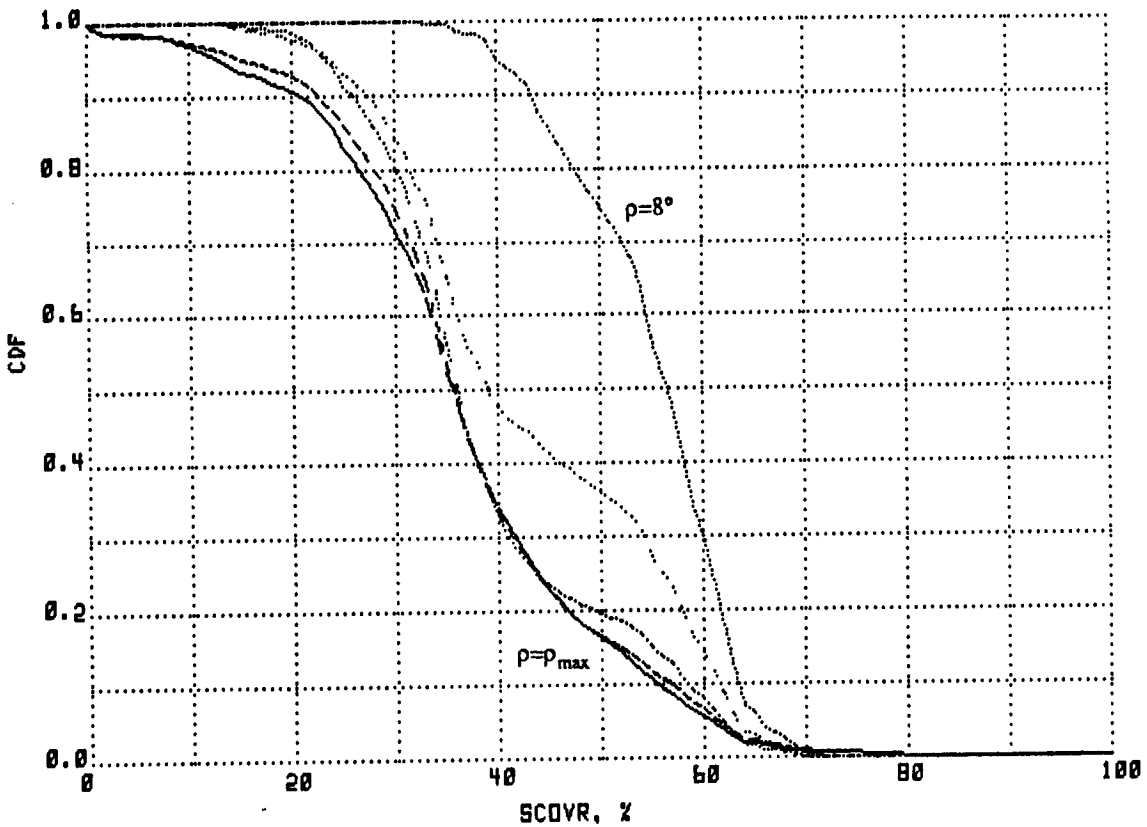

p20p40

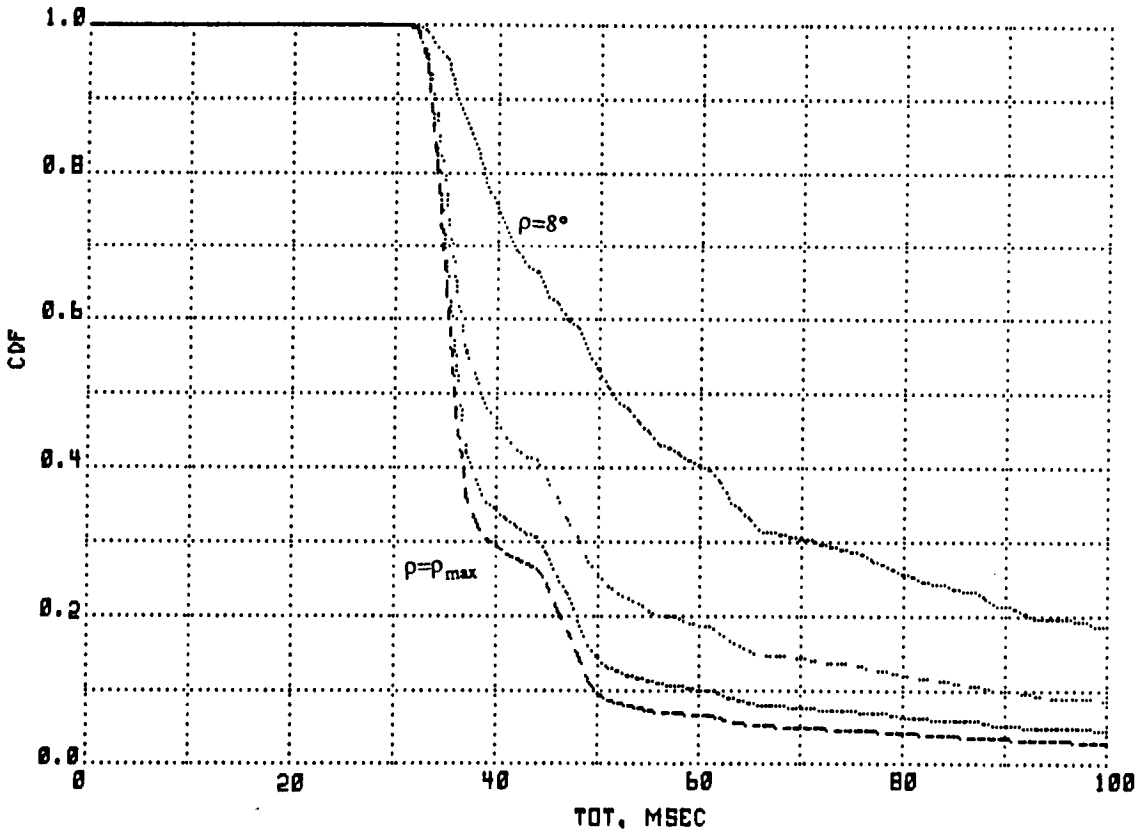

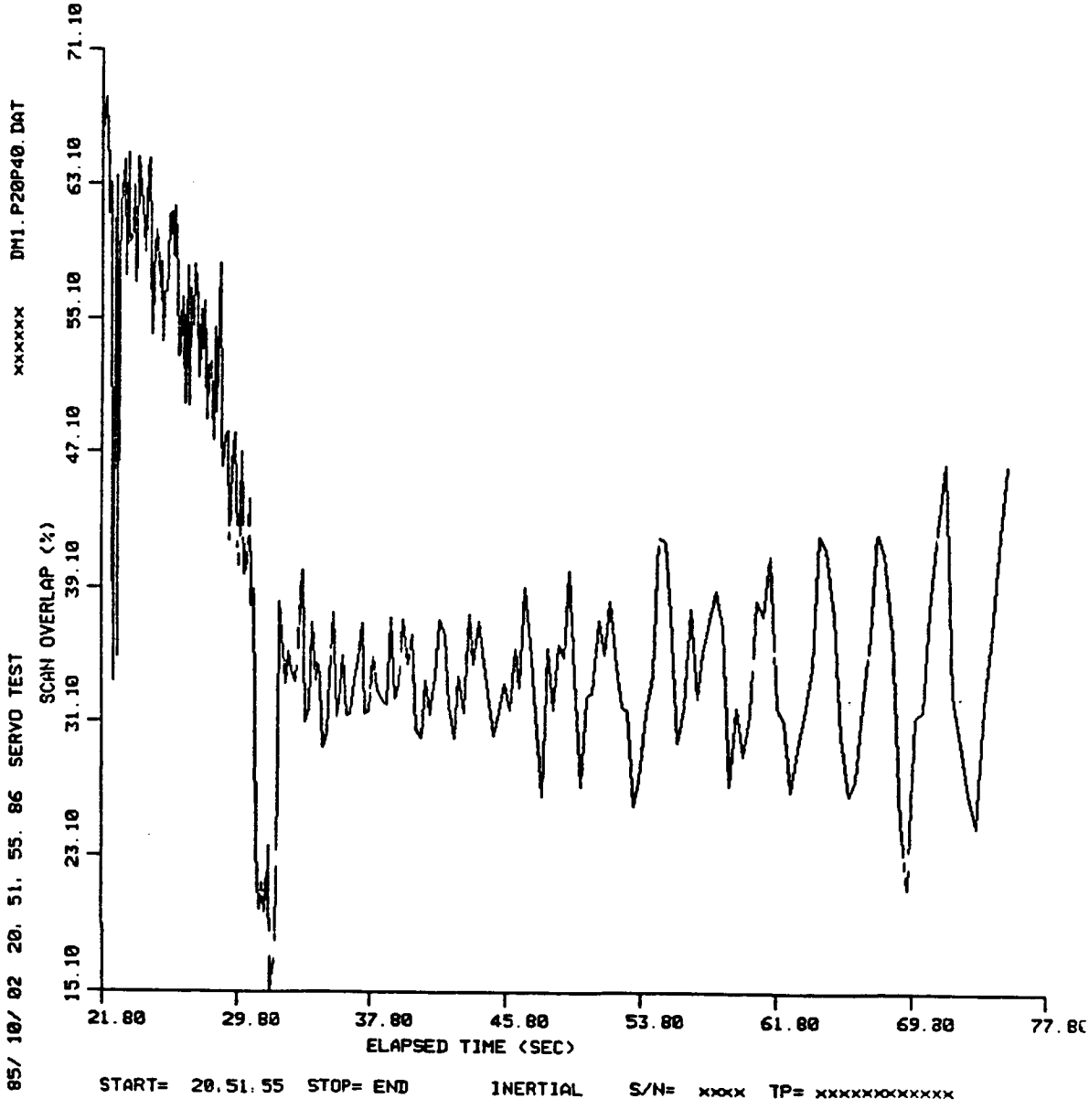
85/ 10/ 02 20. 51. 55. 86 SERVO TEST
xxxxxx DM1.P20P40.DAT
SCAN OVERLAP (%)
15.10
23.10
31.10
39.10
47.10
55.10
63.10
71.10
21.80
29.80
37.80
45.80
53.80
61.80
69.80
77.80
ELAPSED TIME (SEC)
START= 20.51.55 STOP= END
INERTIAL
S/N= xxxx TP= xxxxxxxxxxx

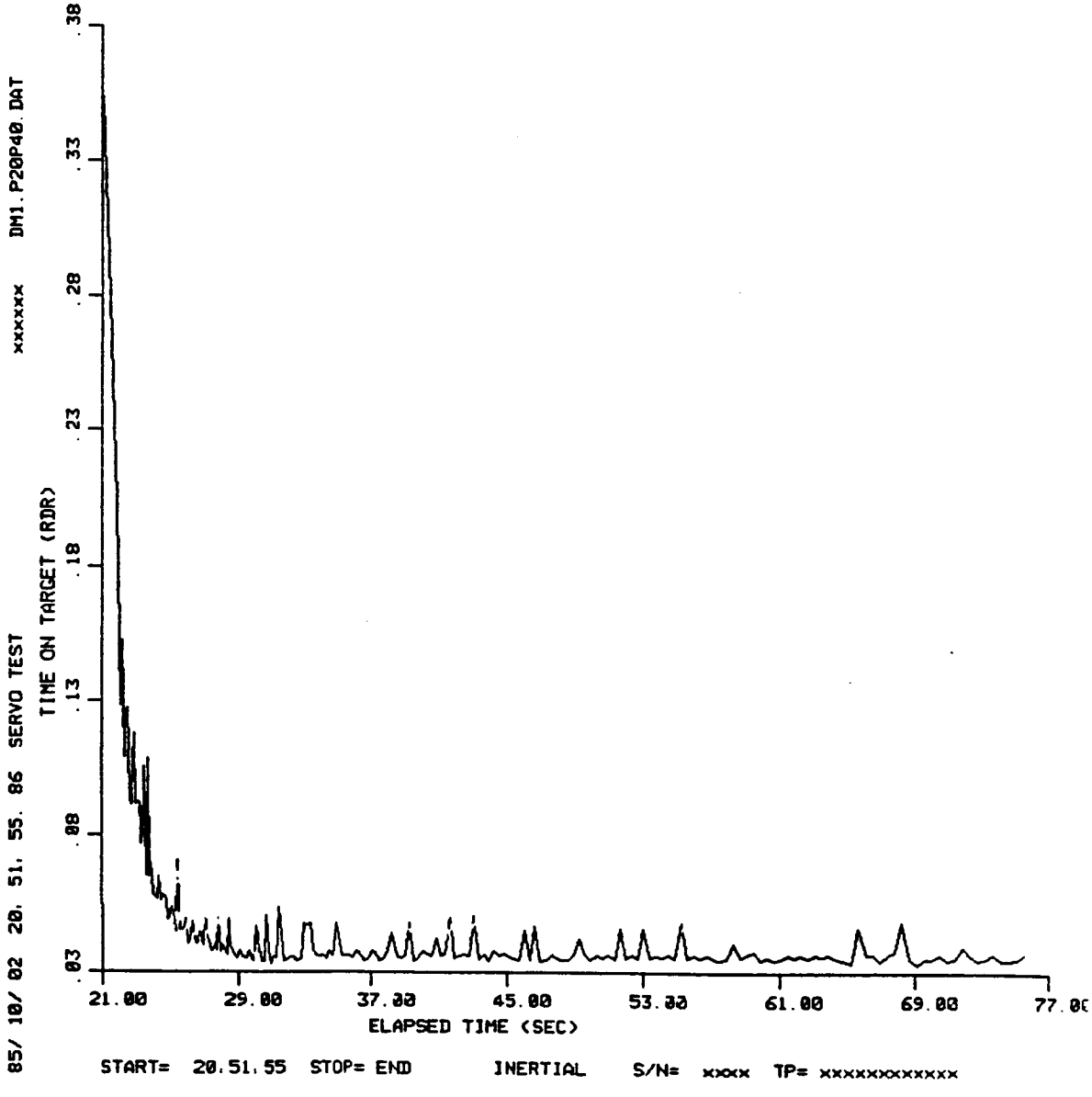
85/ 10/ 02 20. 51. 55. 86 SERVO TEST
xxxxxx DM1.P20P40.DAT
TIME ON TARGET (RDR)
.03
.08
.13
.18
.23
.28
.33
.38
21.00
29.00
37.00
45.00
53.00
61.00
69.00
77.00
ELAPSED TIME (SEC)
START= 20.51.55 STOP= END INERTIAL S/N= xxxx TP= xxxxxxxxxxx

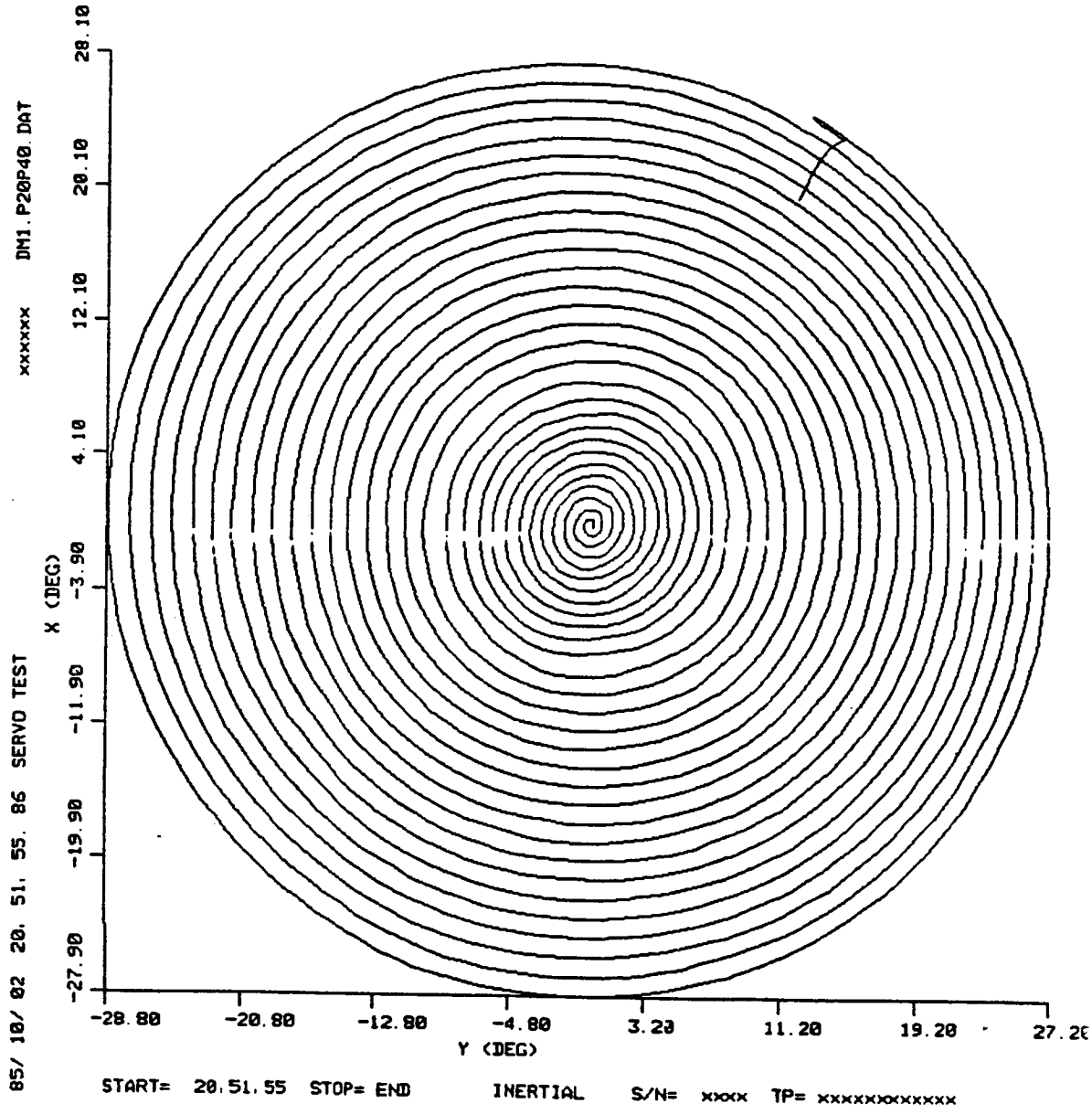
85/ 10/ 02 20. 51. 55. 86 SERVO TEST
xxxxxx DM1.P20P40.DAT
X (DEG)
28.10
20.10
12.10
4.10
-3.90
-11.90
-19.90
-27.90
-28.80
-20.80
-12.80
-4.80
3.20
11.20
19.20
27.20
Y (DEG)
START= 20:51:55 STOP= END
INERTIAL
S/N= xxxx TP= xxxxxxxxxxx

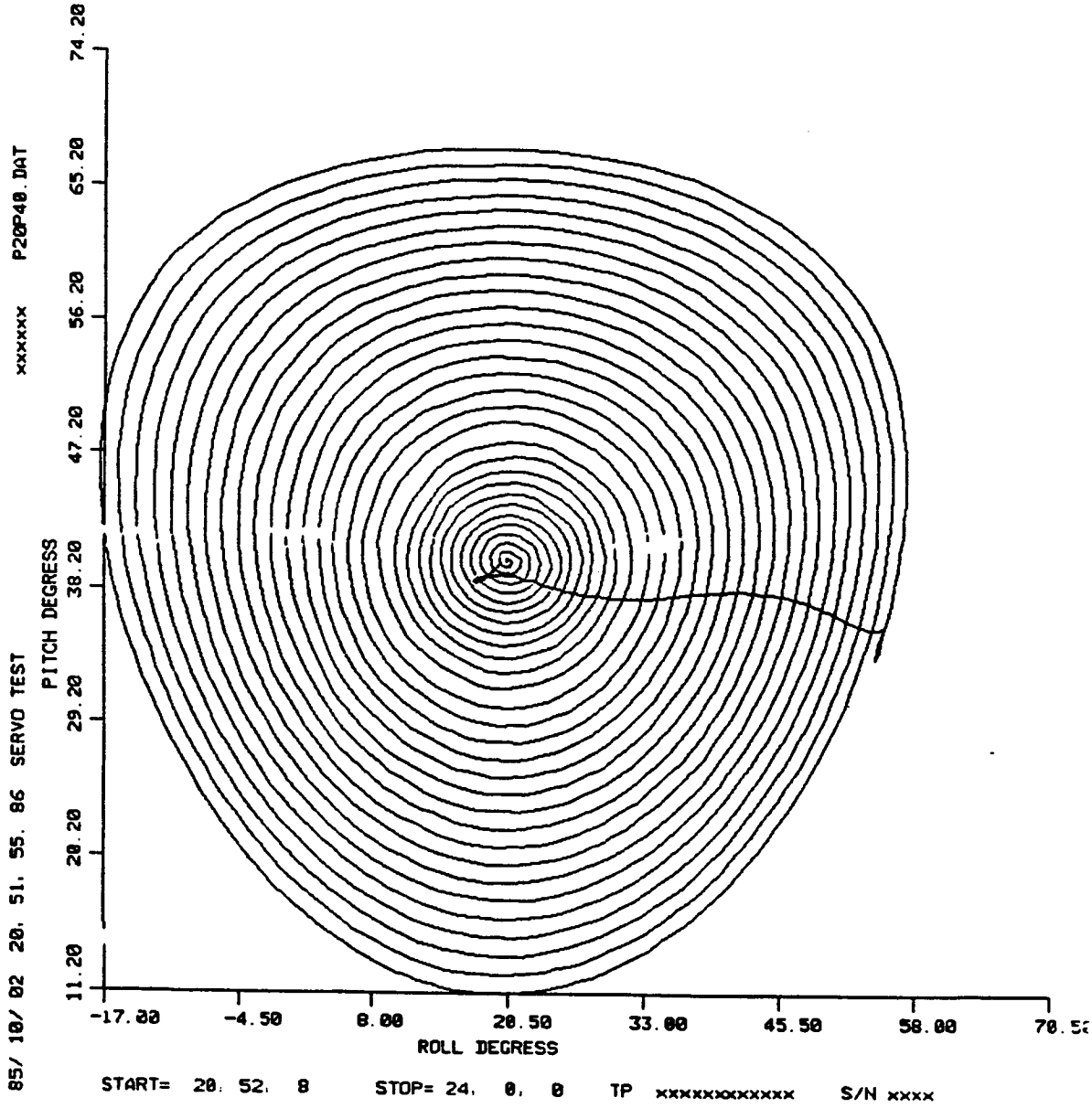
85/ 10/ 02 20: 51: 55. 86 SERVO TEST
xxxxxx P20P40.DAT
PITCH DEGRESS
74.20
65.20
56.20
47.20
38.20
29.20
20.20
11.20
-17.00
-4.50
8.00
20.50
33.00
45.50
58.00
ROLL DEGRESS
START= 20: 52: 8
STOP= 24, 0, 0
TP xxxxxxxxxxxx
S/N xxxx

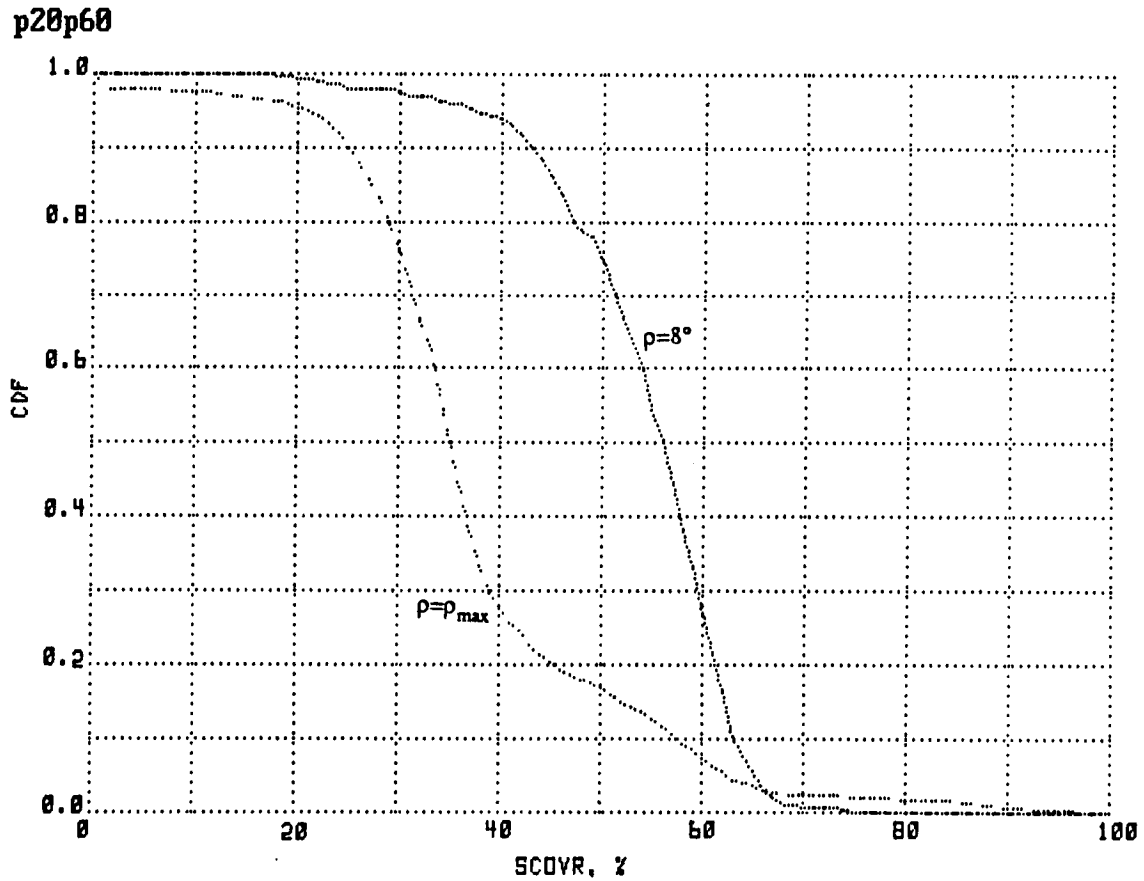
p20p60
1.0
0.8
0.6
0.4
0.2
0.0
CDF
ρ=8°
ρ=ρmax
0
20
40
60
80
100
SCOVR, %

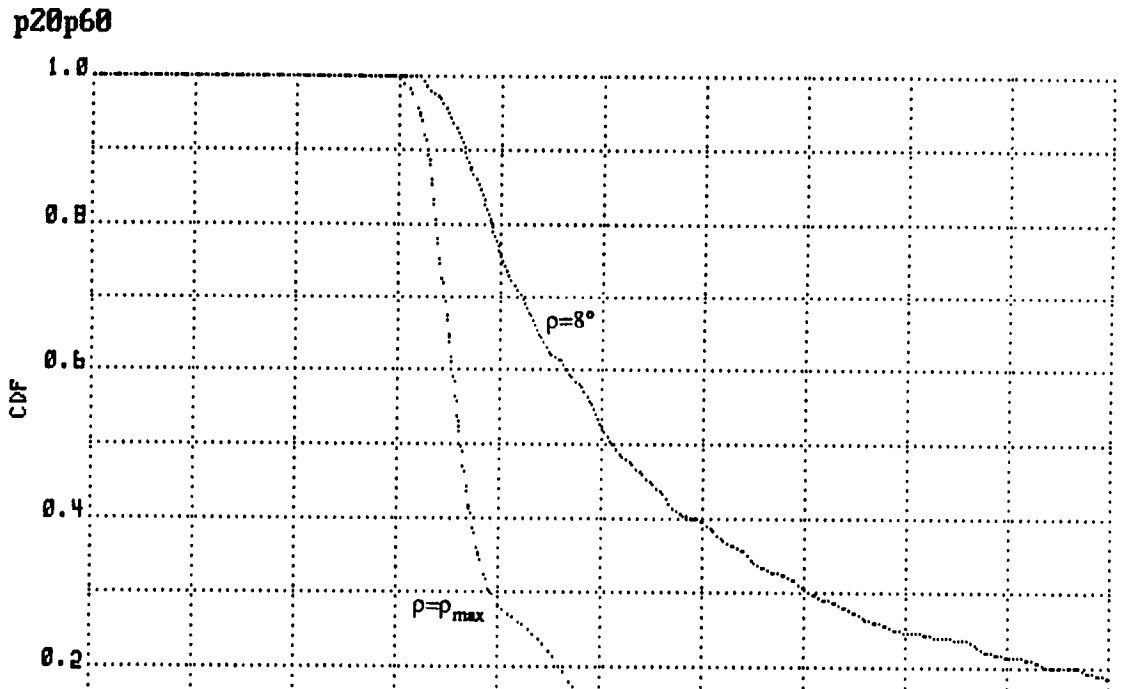
p20p60
1.0
0.8
0.6
0.4
0.2
0.0
CDF
ρ=8°
ρ=ρmax
0
20
40
60
80
100
TOT, MSEC

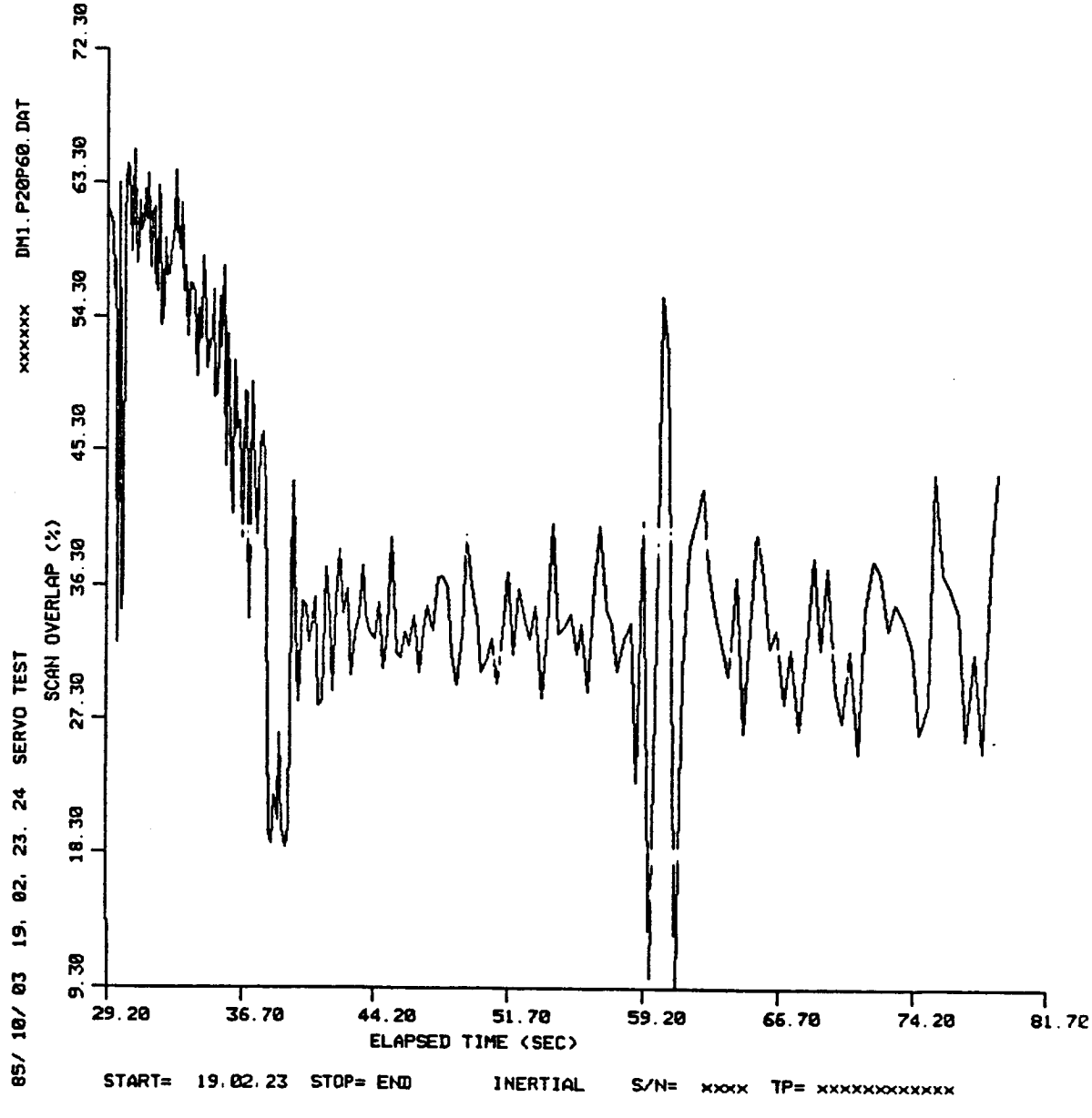
85/ 10/ 03 19. 02. 23. 24 SERVO TEST
xxxxxx DM1.P20P60.DAT
SCAN OVERLAP (%)
72.30
63.30
54.30
45.30
36.30
27.30
18.30
9.30
29.20
36.70
44.20
51.70
59.20
66.70
74.20
81.70
ELAPSED TIME (SEC)
START= 19.02.23 STOP= END
INERTIAL
S/N= xxxx TP= xxxxxxxxxxxx

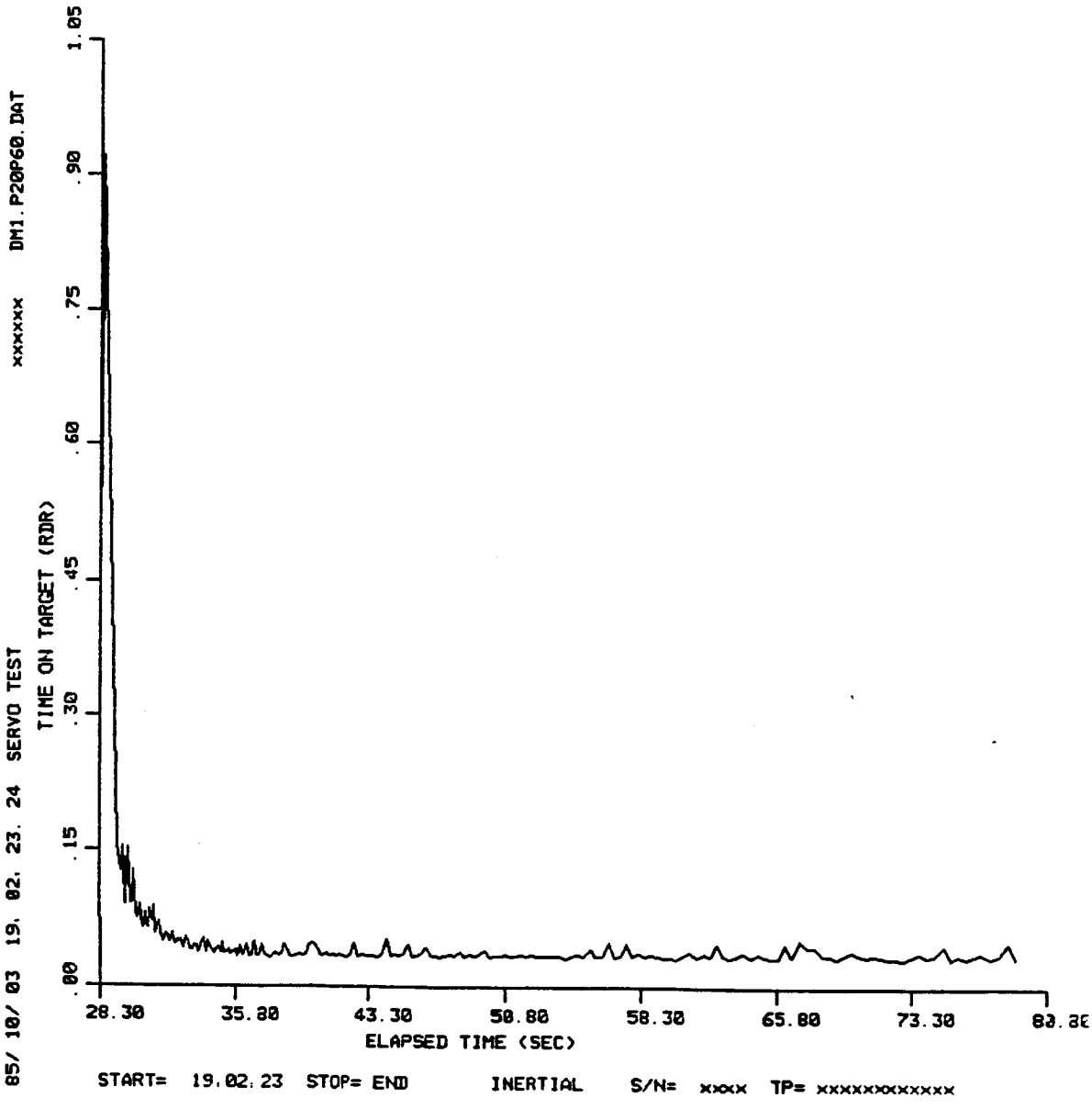
85/ 10/ 03 19. 02. 23. 24 SERVO TEST xxxxxx DM1.P20P60.DAT
TIME ON TARGET (RDR)
.00
.15
.30
.45
.60
.75
.90
1.05
28.30
35.80
43.30
50.80
58.30
65.80
73.30
80.80
ELAPSED TIME (SEC)
START= 19.02.23 STOP= END INERTIAL S/N= xxxx TP= xxxxxxxxxxx

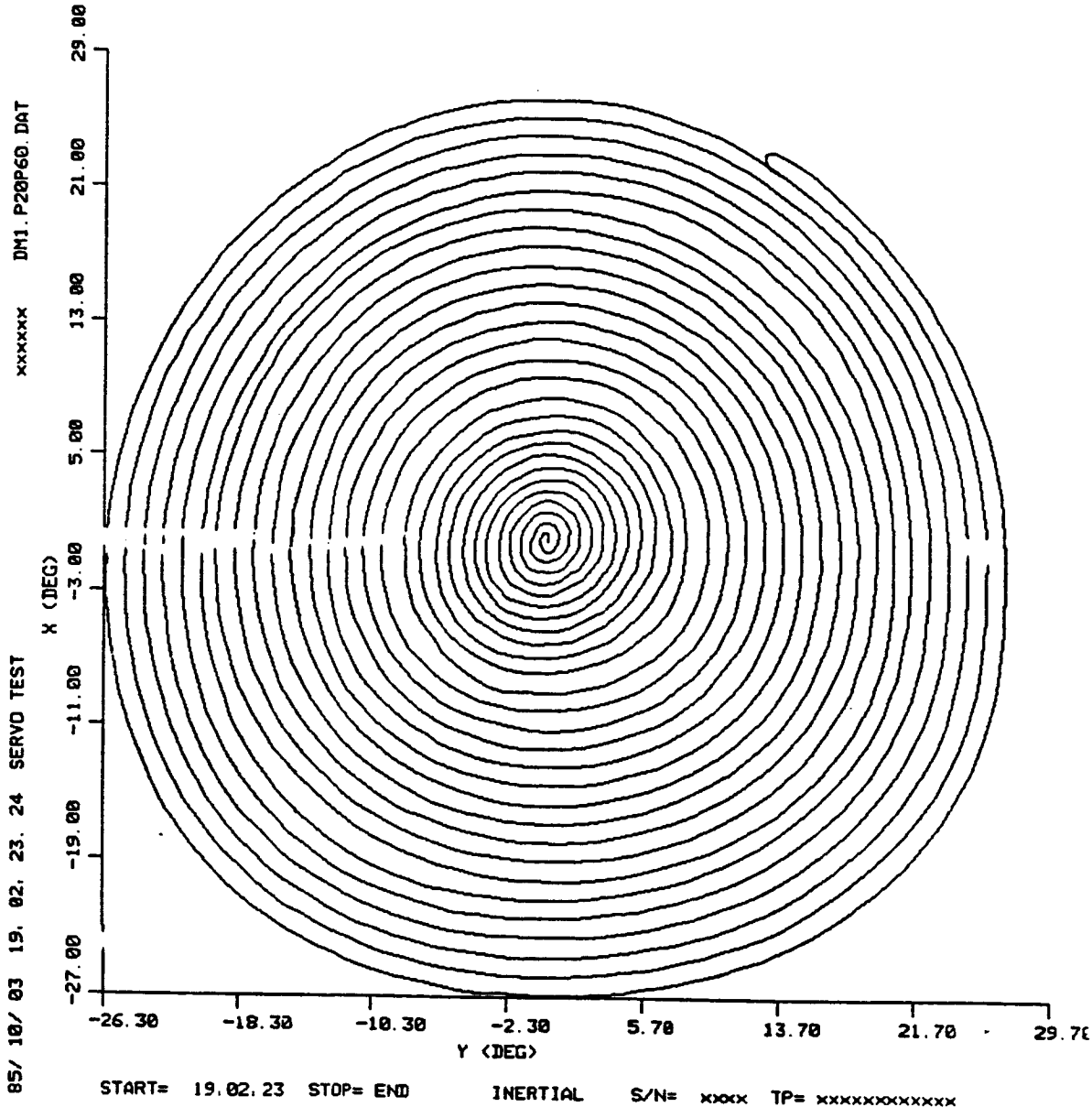
85/ 10/ 03 19. 02. 23. 24 SERVO TEST
XXXXXX DM1.P20P60.DAT
X (DEG)
29.00
21.00
13.00
5.00
-3.00
-11.00
-19.00
-27.00
-26.30
-18.30
-10.30
-2.30
5.70
13.70
21.70
Y (DEG)
START= 19.02.23 STOP= END
INERTIAL
S/N= xxxx TP= xxxxxxxxxxx

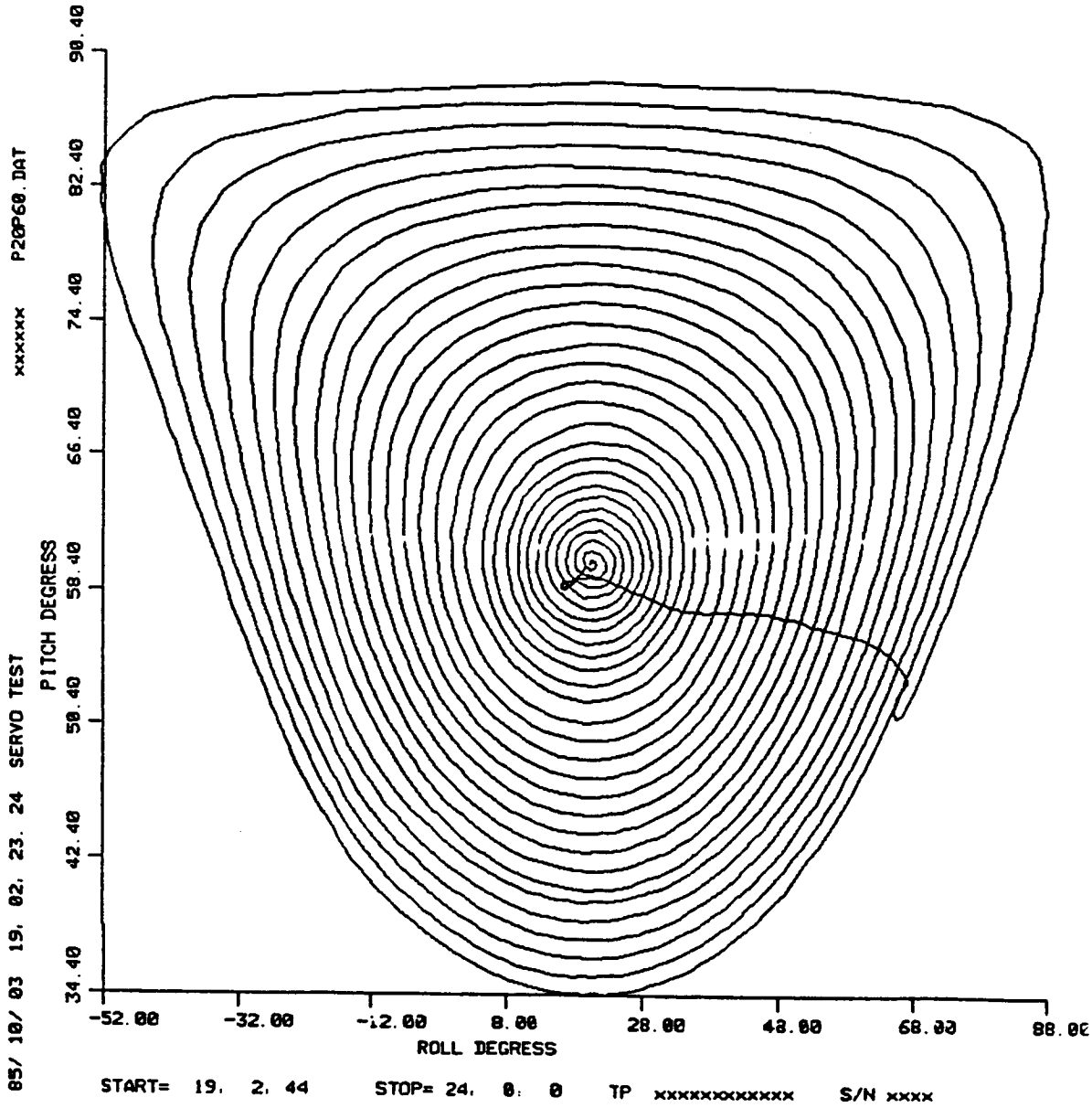
85/ 10/ 03 19, 02, 23. 24 SERVO TEST
xxxxxx P20P60.DAT
PITCH DEGRESS
90.40
82.40
74.40
66.40
58.40
50.40
42.40
34.40
-52.00
-32.00
-12.00
8.00
28.00
48.00
68.00
88.00
ROLL DEGRESS
START= 19, 2, 44
STOP= 24, 0: 0
TP xxxxxxxxxxxx
S/N xxxx

P00P60

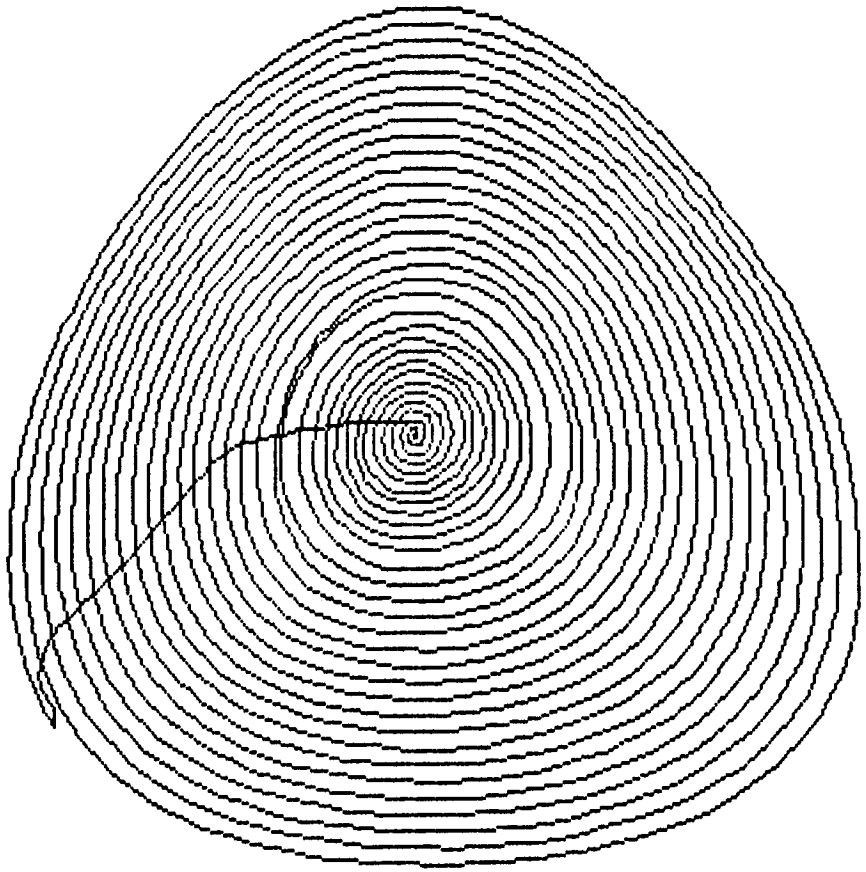

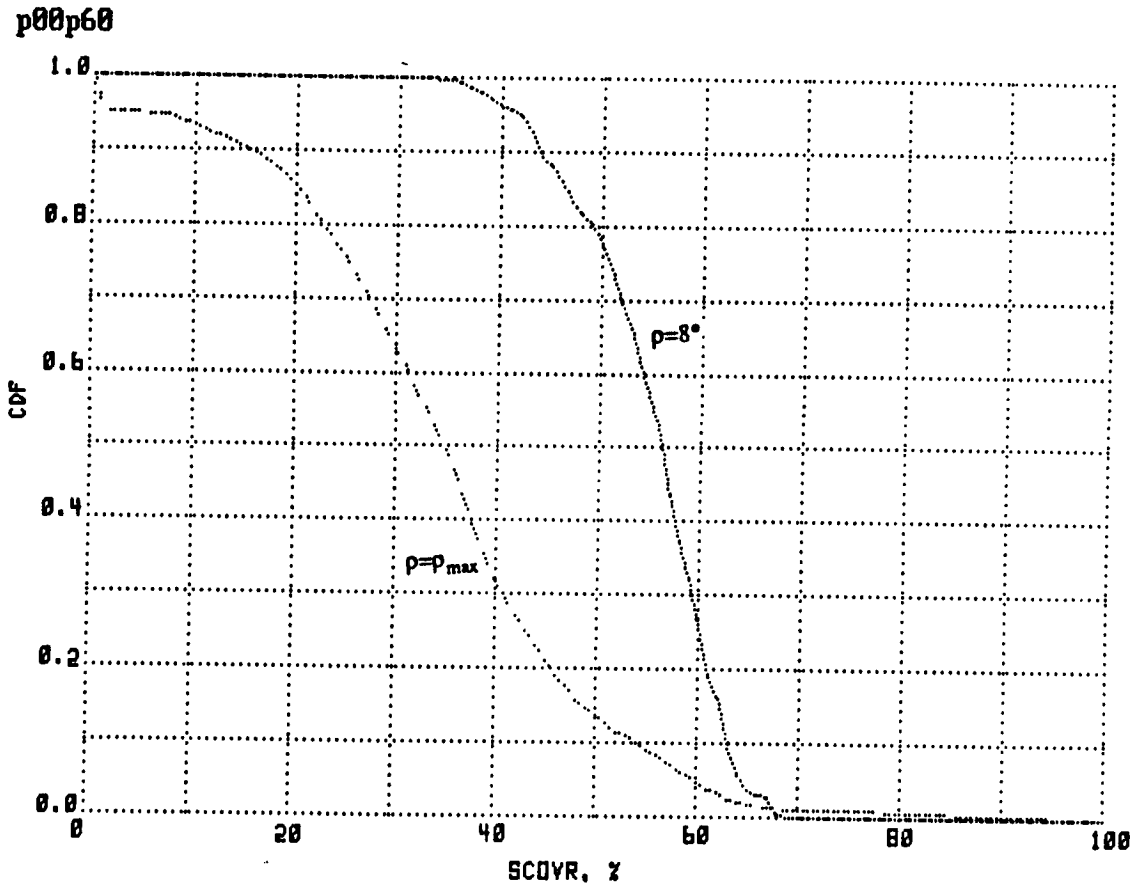
p00p60
1.0
0.8
0.6
0.4
0.2
0.0
CDF
0
20
40
60
80
100
SCOVR, %
ρ=8°
ρ=ρmax

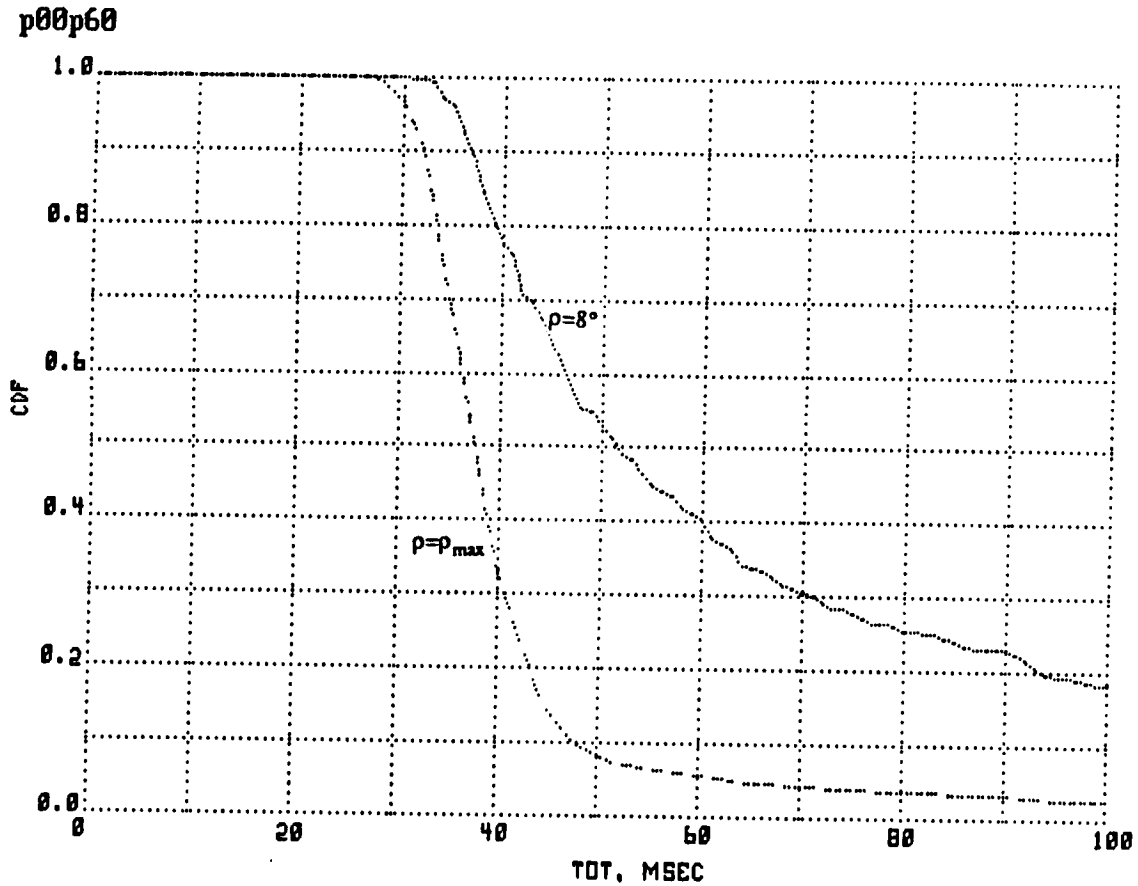
p00p60
1.0
0.8
0.6
0.4
0.2
0.0
CDF
ρ=8°
ρ=ρmax
0
20
40
60
80
100
TOT, MSEC

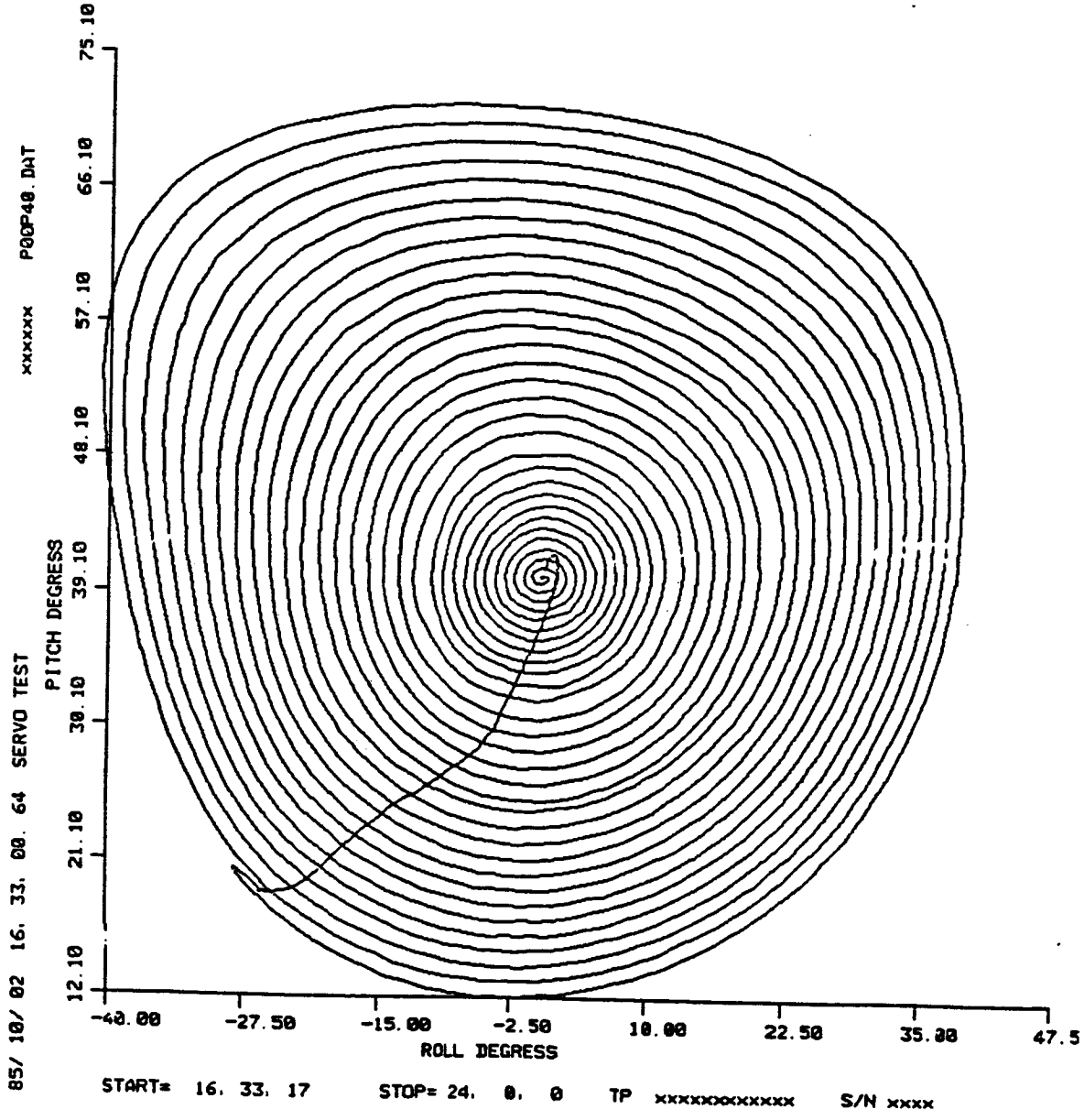
85/ 10/ 02 16. 33. 00. 64 SERVO TEST
xxxxxx P00P40.DAT
PITCH DEGRESS
75.10
66.10
57.10
48.10
39.10
30.10
21.10
12.10
-40.00
-27.50
-15.00
-2.50
10.00
22.50
35.00
47.5
ROLL DEGRESS
START= 16. 33. 17
STOP= 24. 0. 0
TP xxxxxxxxxxx
S/N xxxx

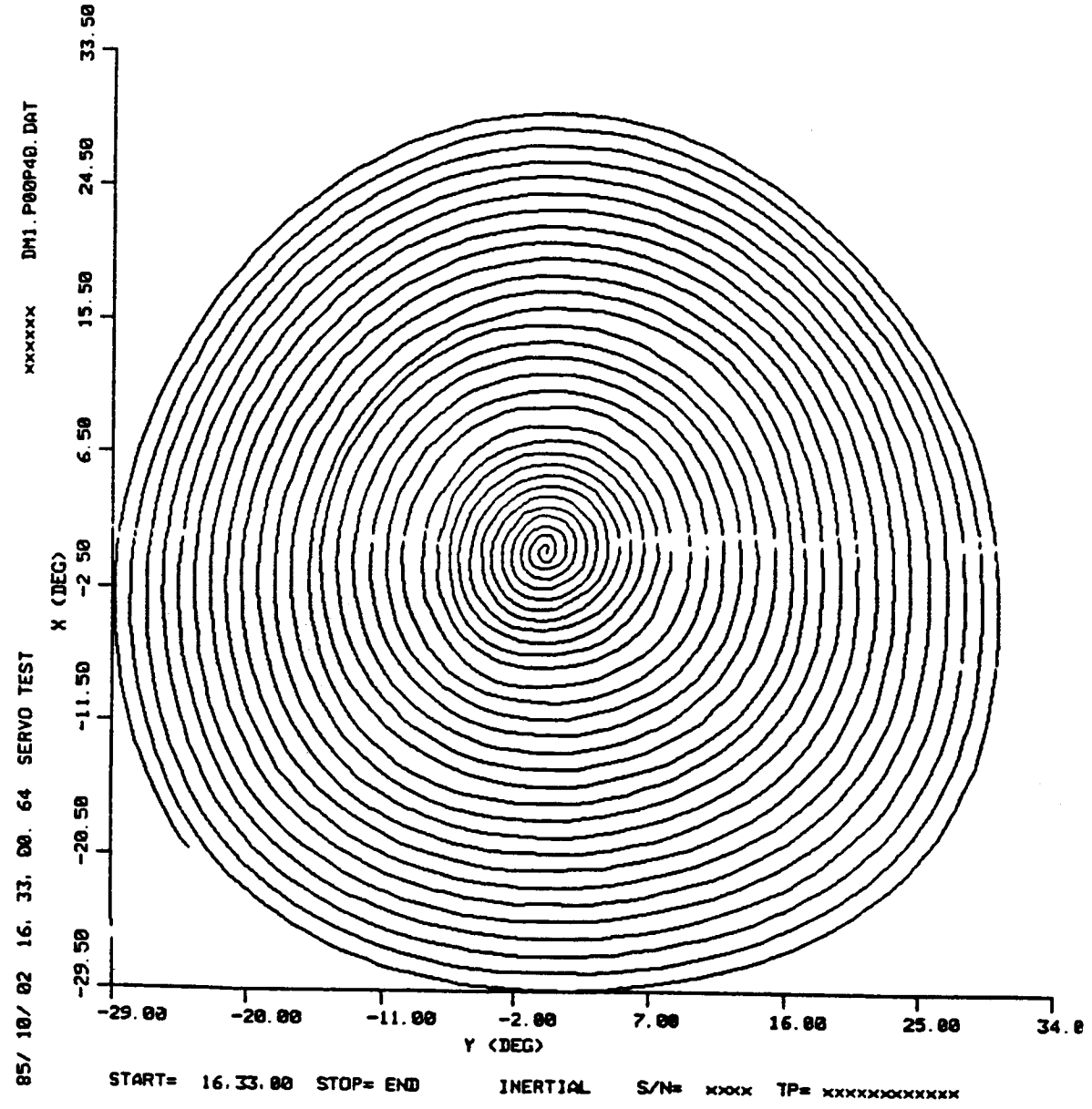
85/ 10/ 02 16. 33. 00. 64 SERVO TEST
xxxxxx DM1.P00P40.DAT
X (DEG)
33.50
24.50
15.50
6.50
-2.50
-11.50
-20.50
-29.50
-29.00
-20.00
-11.00
-2.00
7.00
16.00
25.00
34.0
Y (DEG)
START= 16.33.00 STOP= END
INERTIAL
S/N= xxxx TP= xxxxxxxxxxx

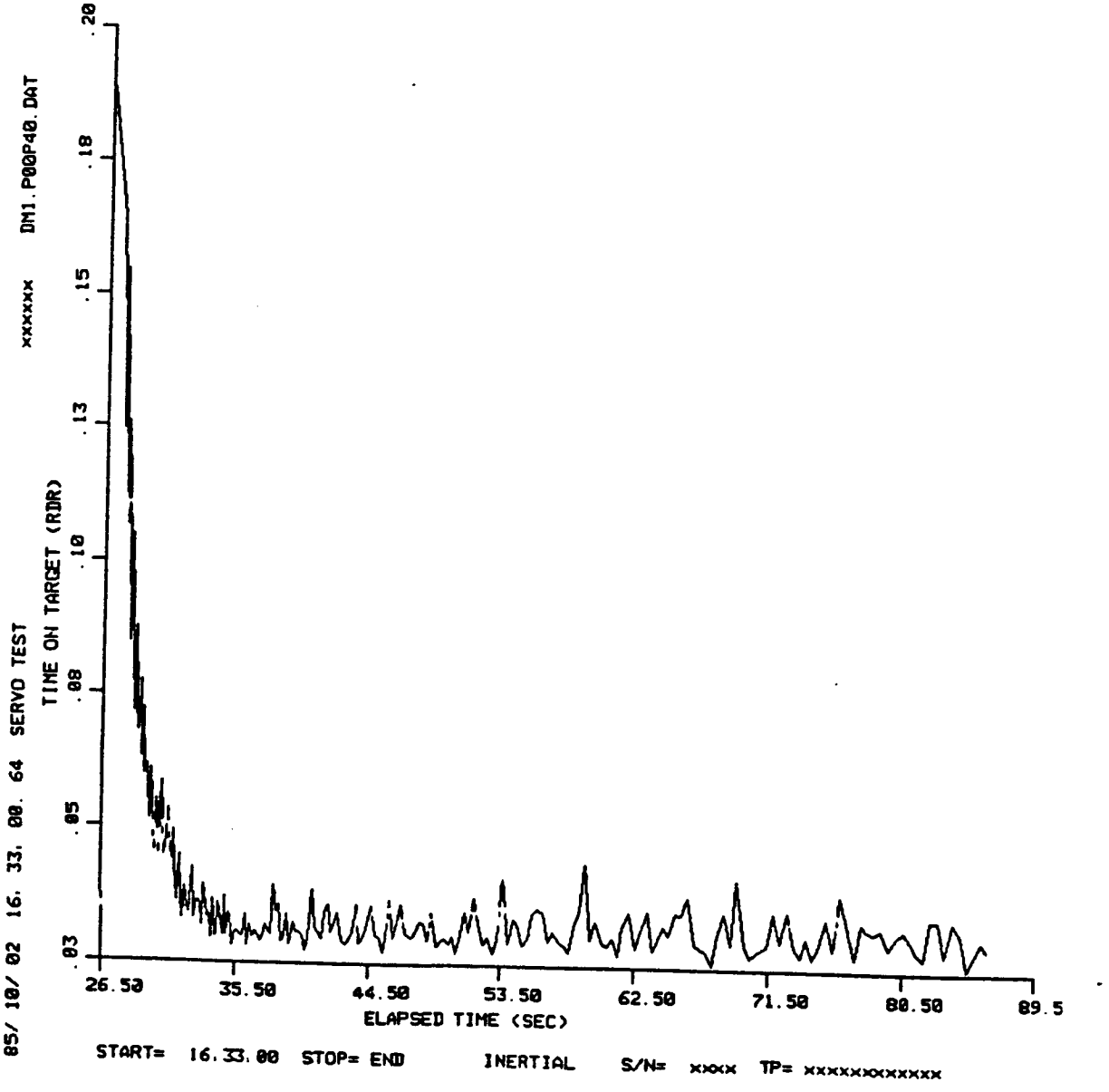
85/ 10/ 02 16. 33. 00. 64 SERVO TEST
xxxxxx DM1.P00P40.DAT
TIME ON TARGET (RDR)
.03
.05
.08
.10
.13
.15
.18
.20
26.50
35.50
44.50
53.50
62.50
71.50
80.50
89.5
ELAPSED TIME (SEC)
START= 16.33.00 STOP= END
INERTIAL
S/N= xxxx TP= xxxxxxxxxxx

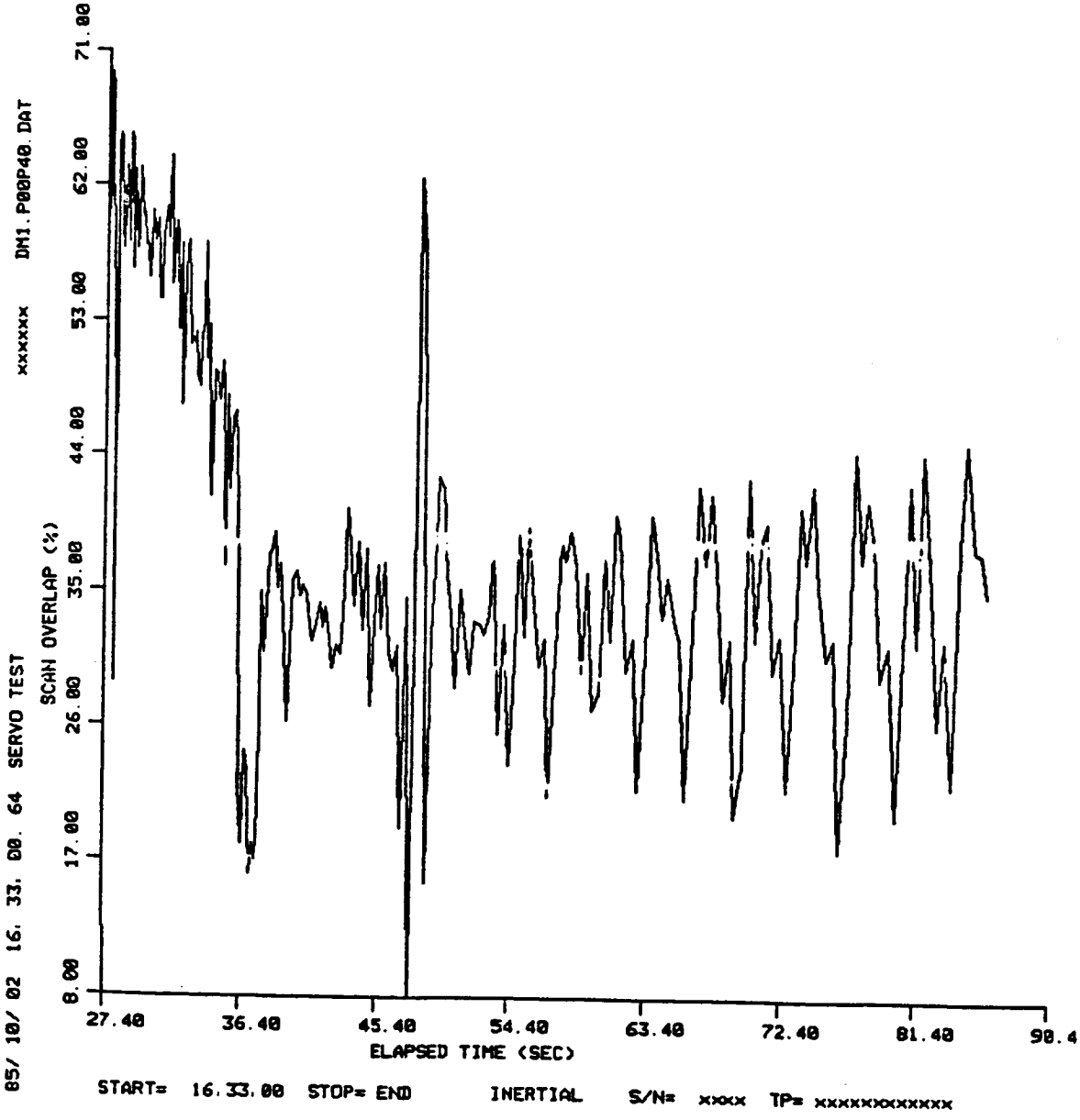
85/ 10/ 02 16. 33. 00. 64 SERVO TEST
xxxxxx DM1.P00P40.DAT
SCAN OVERLAP (%)
71.00
62.00
53.00
44.00
35.00
26.00
17.00
8.00
27.40
36.40
45.40
54.40
63.40
72.40
81.40
90.4
ELAPSED TIME (SEC)
START= 16.33.00 STOP= END INERTIAL S/N= xxxx TP= xxxxxxxxxxx

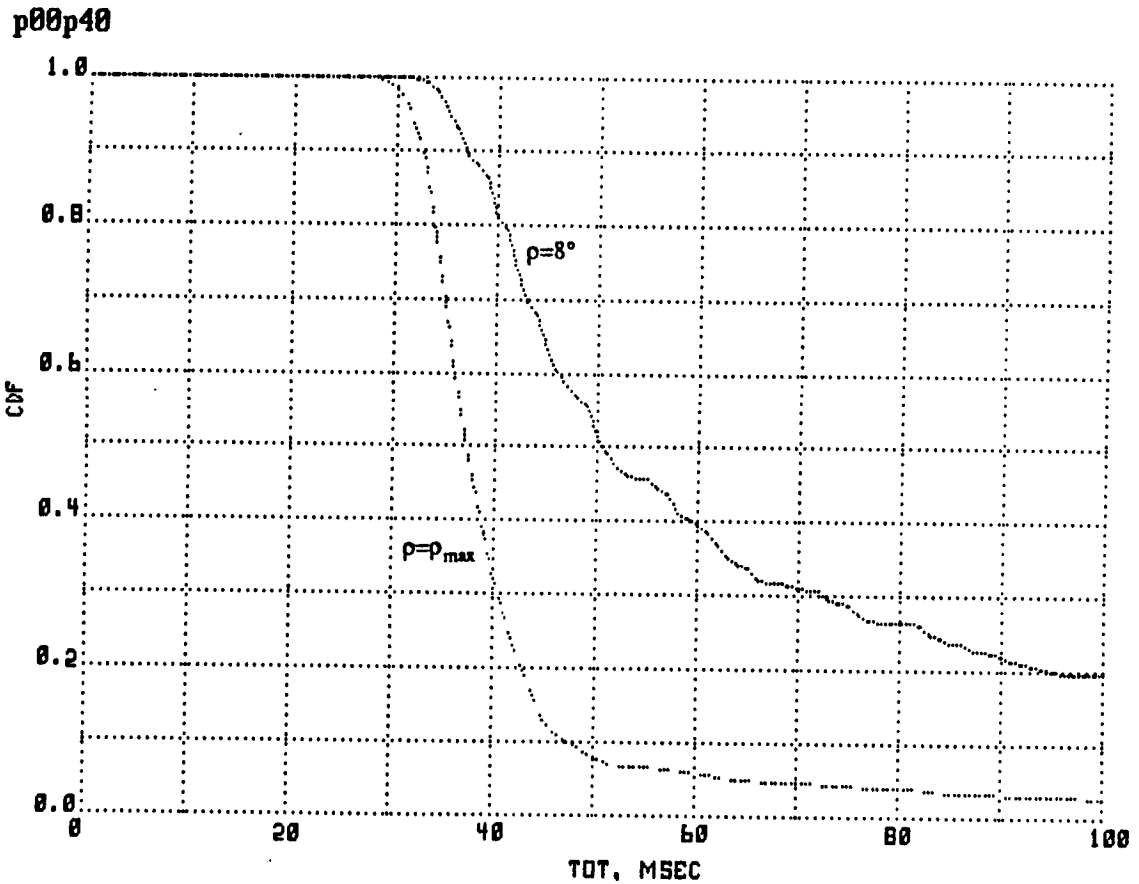
p00p40
1.0
0.8
0.6
0.4
0.2
0.0
CDF
ρ=8°
ρ=ρmax
0
20
40
60
80
100
TOT, MSEC

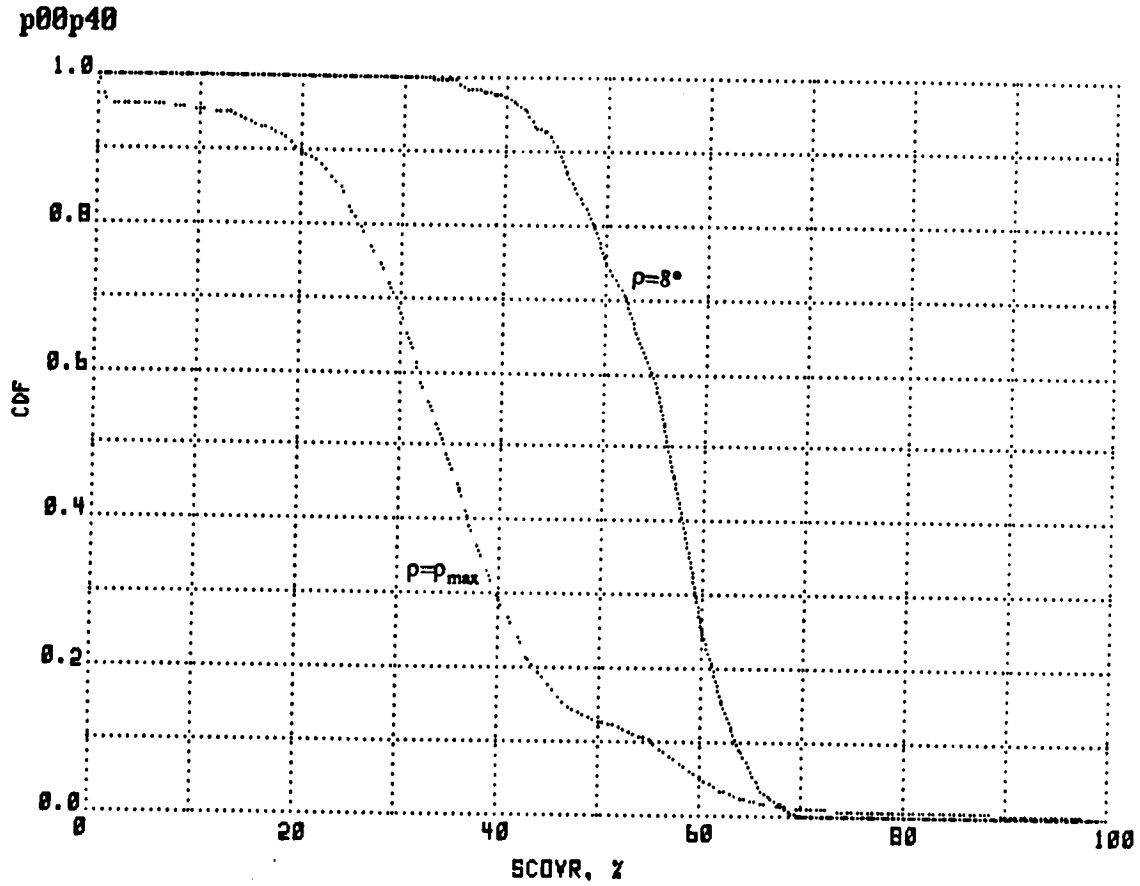
p00p40
1.0
0.8
0.6
0.4
0.2
0.0
CDF
ρ=8°
ρ=ρmax
0
20
40
60
80
100
SCOVR, %

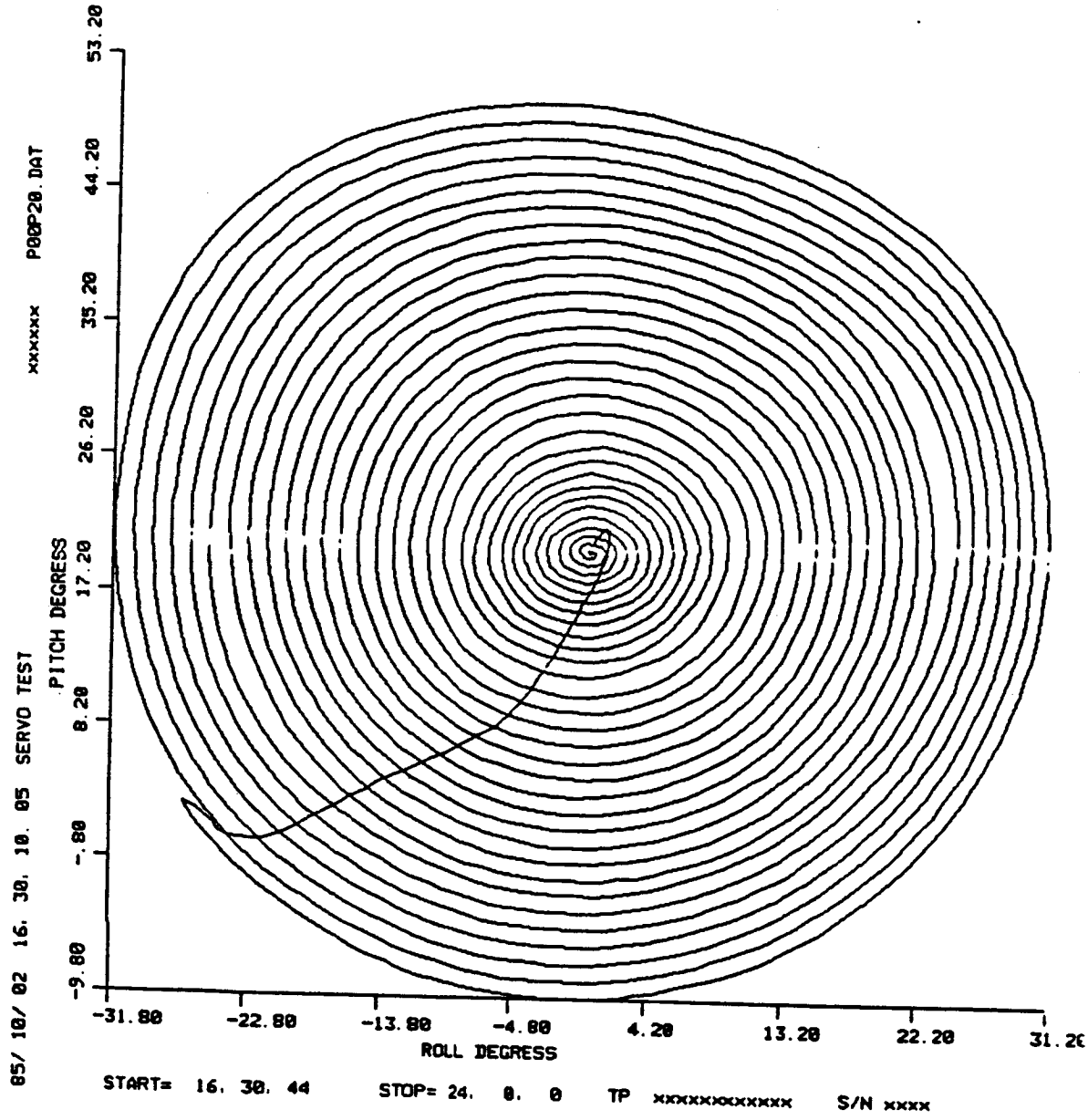
85/ 10/ 02 16. 30. 10. 05 SERVO TEST
xxxxxx P00P20.DAT
PITCH DEGRESS
53.20
44.20
35.20
26.20
17.20
8.20
-.80
-9.80
-31.80
-22.80
-13.80
-4.80
4.20
13.20
22.20
31.20
ROLL DEGRESS
START= 16. 30. 44
STOP= 24. 0. 0
TP xxxxxxxxxxx
S/N xxxx

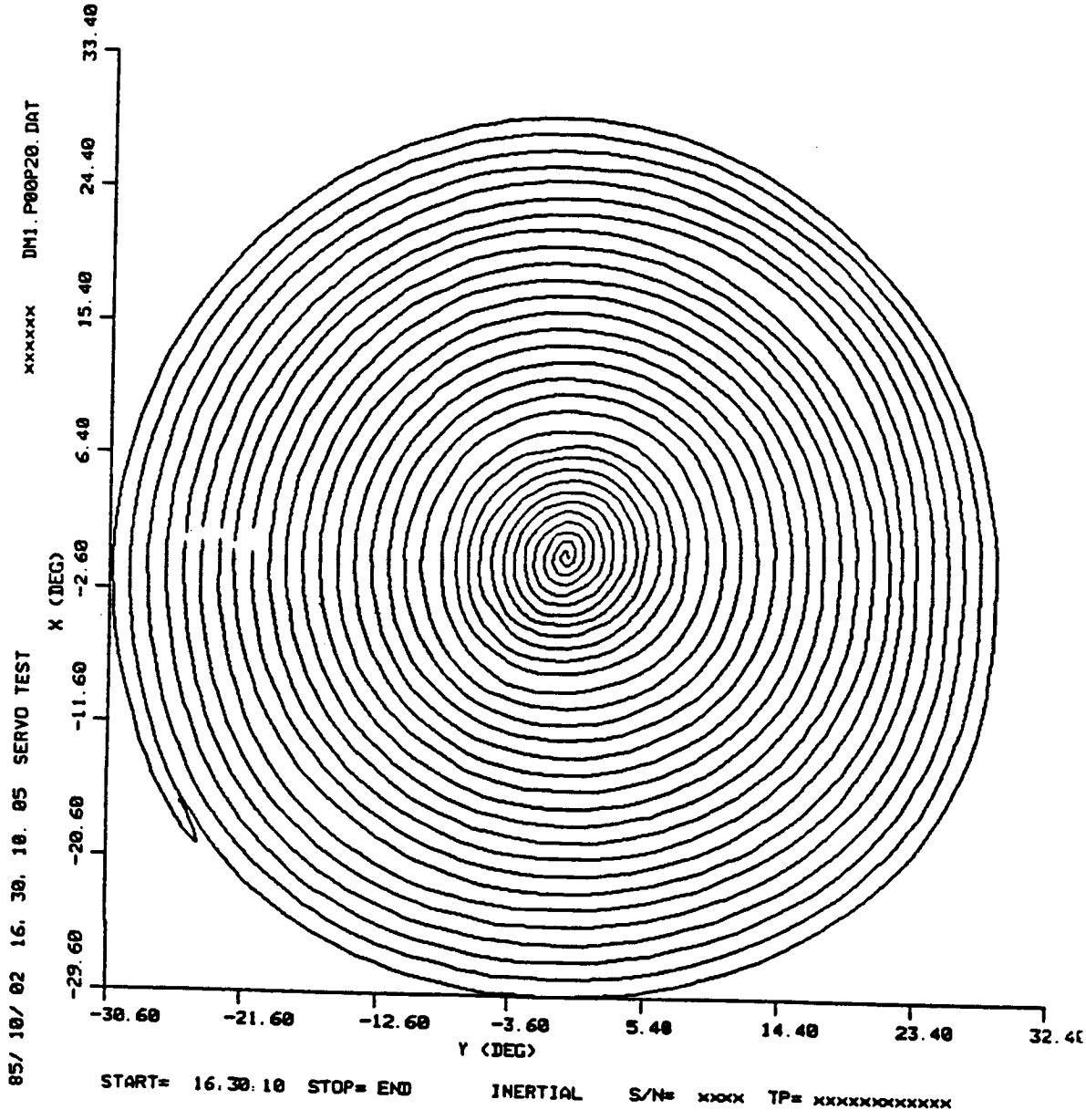
85/ 10/ 02 16. 30. 10. 05 SERVO TEST
xxxxxx DM1.P00P20.DAT
X (DEG)
33.40
24.40
15.40
6.40
-2.60
-11.60
-20.60
-29.60
-30.60
-21.60
-12.60
-3.60
5.40
14.40
23.40
32.4
Y (DEG)
START= 16.30.10 STOP= END
INERTIAL
S/N= xxxx TP= xxxxxxxxxxx

C-3

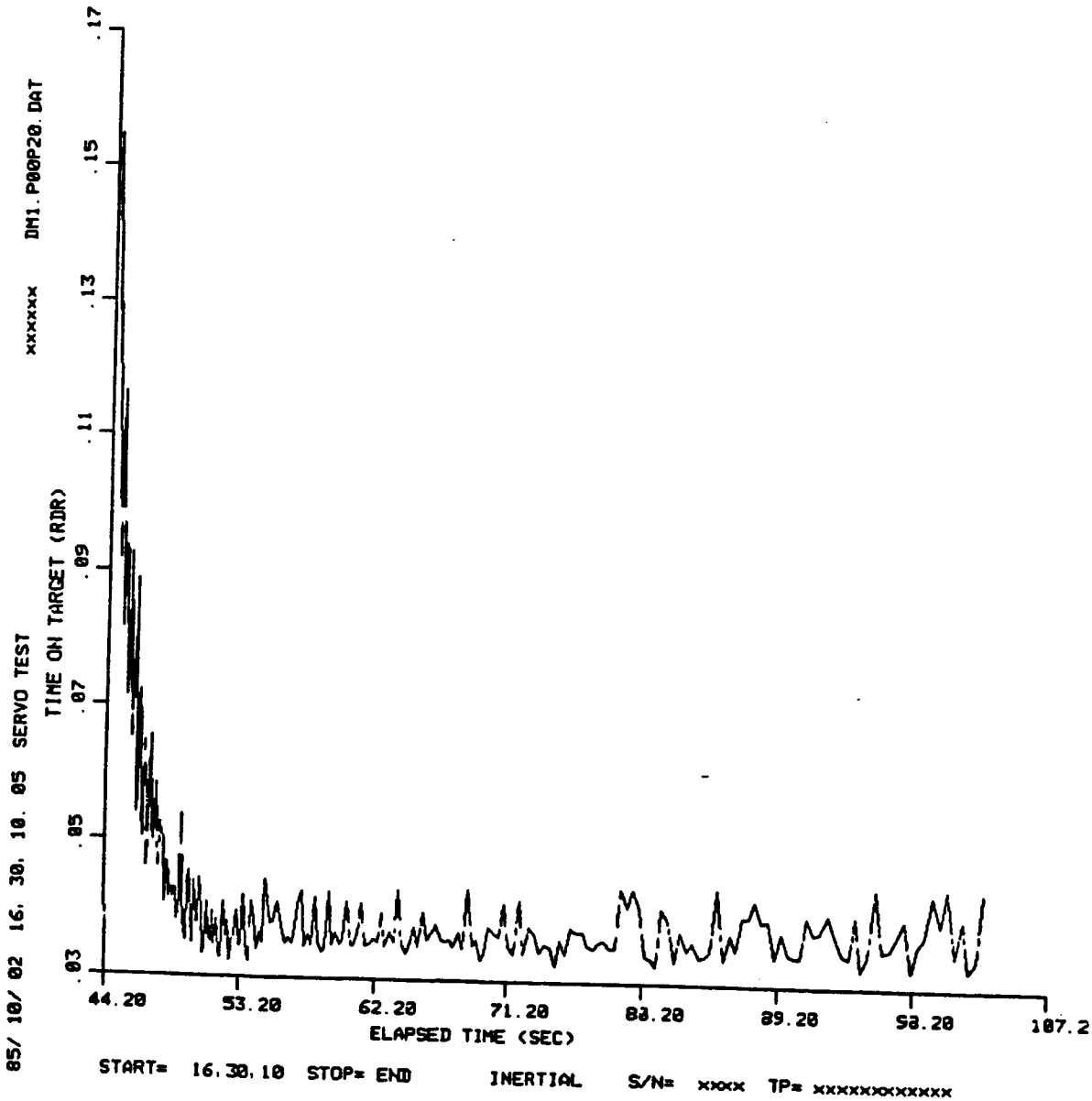
85/ 10/ 02 16. 30. 10. 05 SERVO TEST
TIME ON TARGET (RDR)
xxxxxx DM1.P00P20.DAT
.03
.05
.07
.09
.11
.13
.15
.17
44.20
53.20
62.20
71.20
80.20
89.20
98.20
107.2
ELAPSED TIME (SEC)
START= 16.30.10 STOP= END INERTIAL S/N= xxxx TP= xxxxxxxxxxx

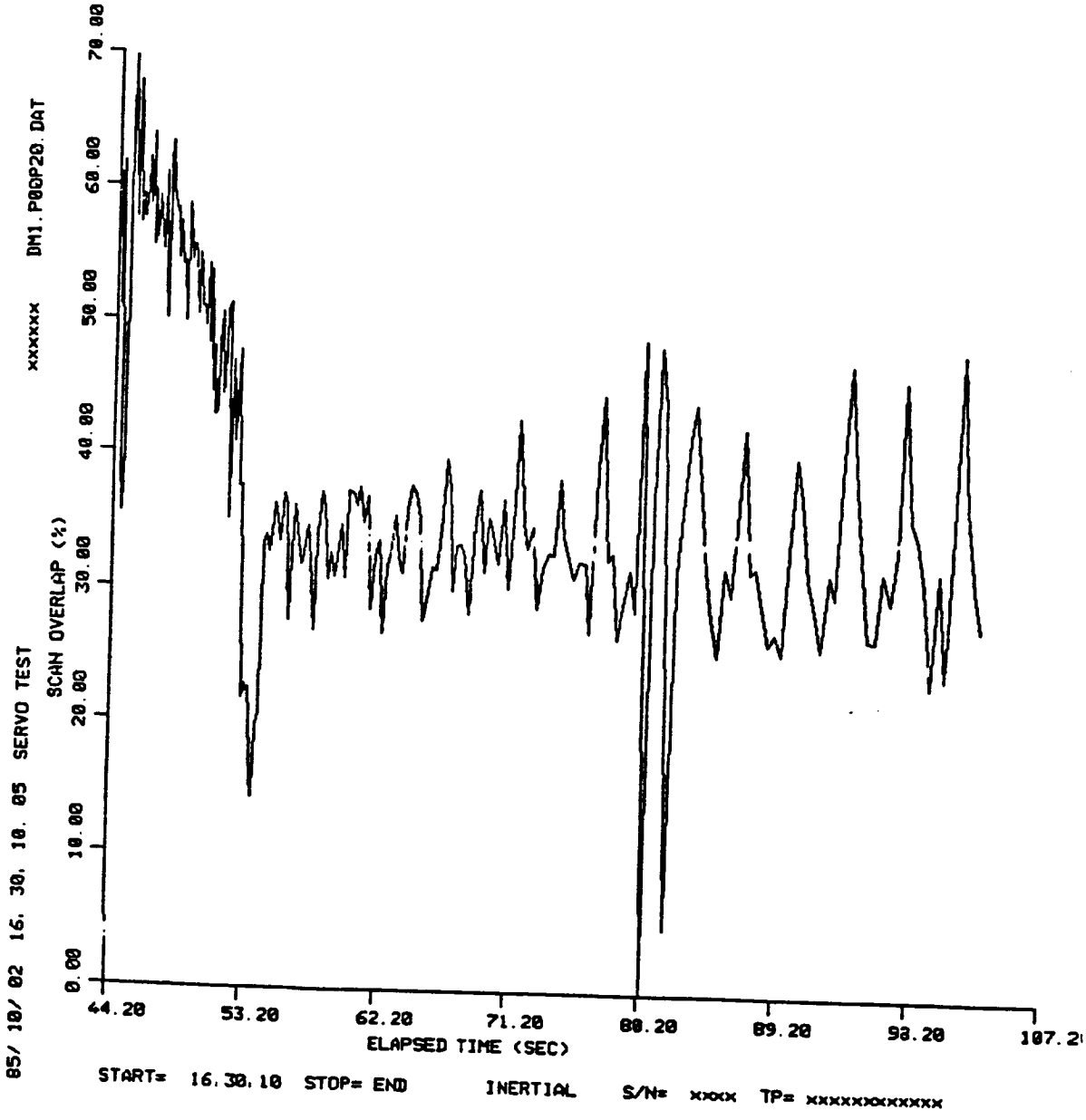
85/ 10/ 02 16. 30. 10. 05 SERVO TEST
SCAN OVERLAP (%)
xxxxxx DM1.P00P20.DAT
0.00
10.00
20.00
30.00
40.00
50.00
60.00
70.00
44.20
53.20
62.20
71.20
80.20
89.20
98.20
107.2
ELAPSED TIME (SEC)
START= 16.30.10 STOP= END INERTIAL S/N= xxxx TP= xxxxxxxxxxx

p00p20

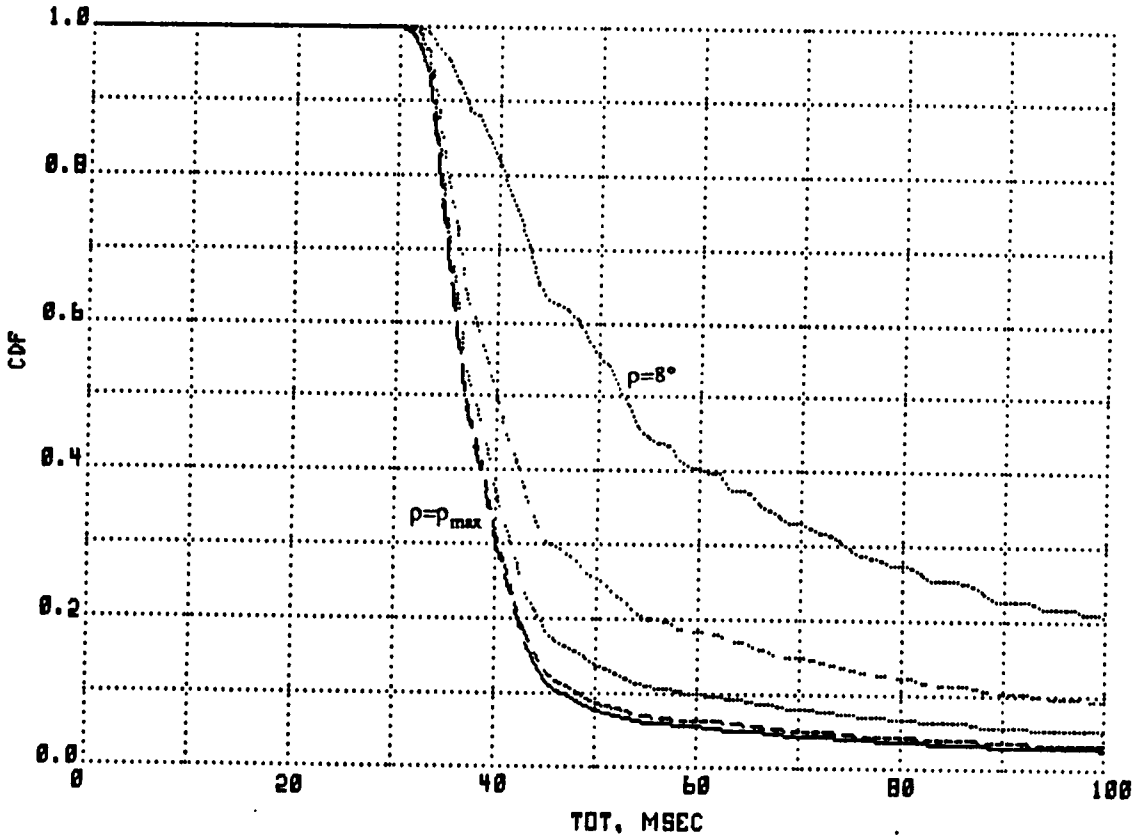

p00p20

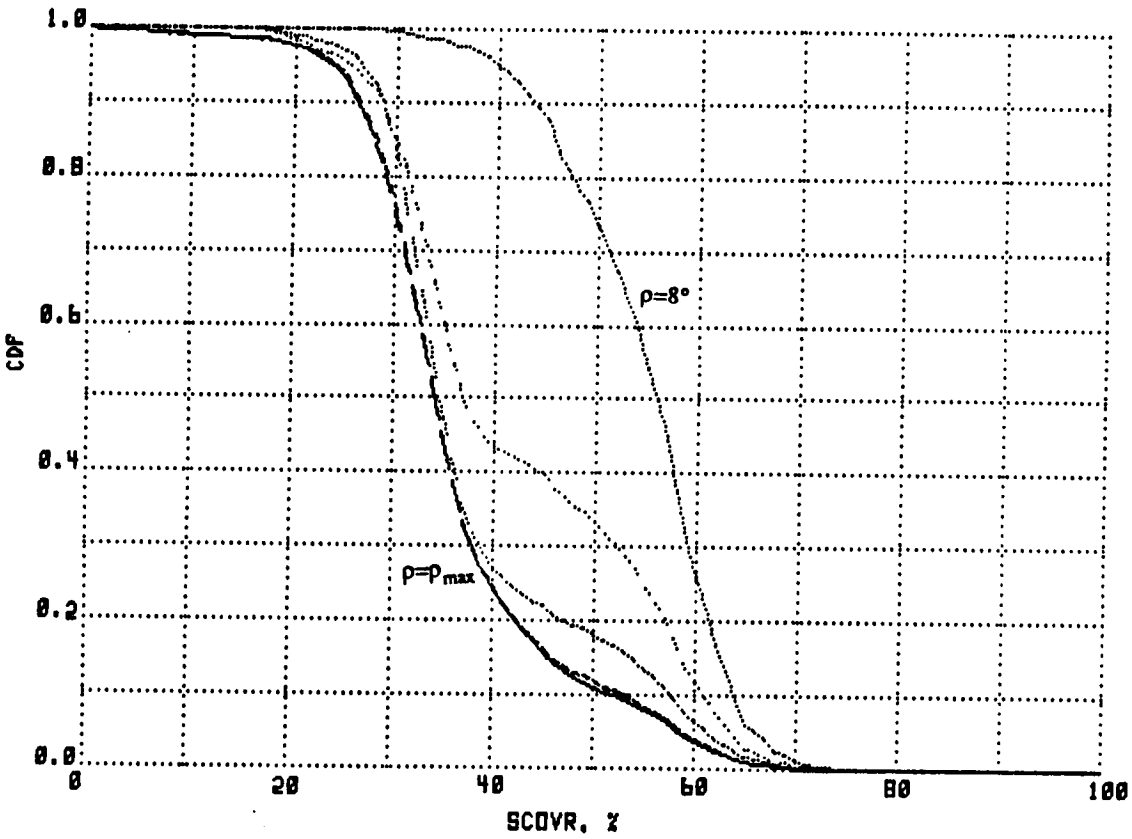

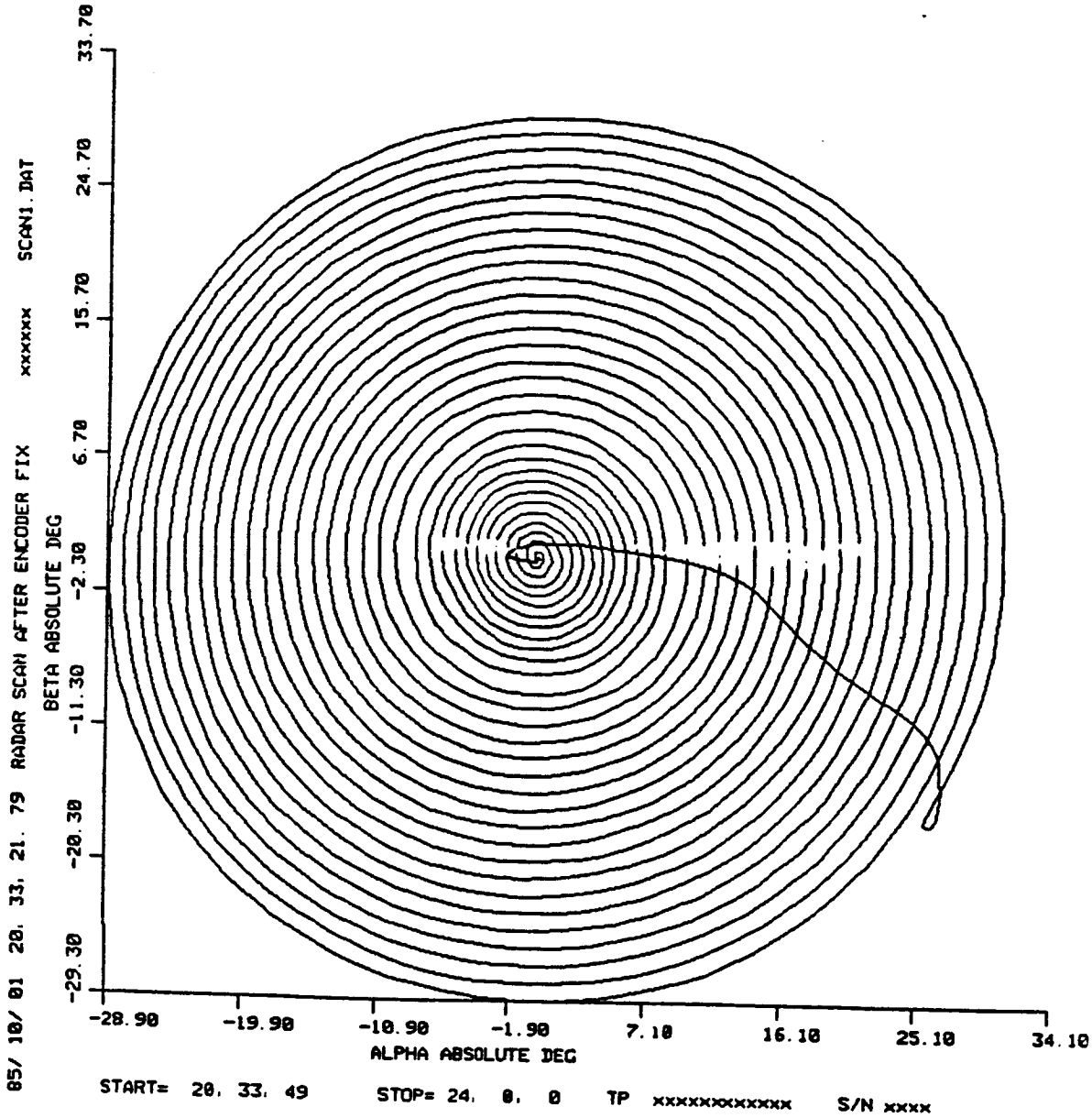
85/ 10/ 01 20. 33. 21. 79 RADAR SCAN AFTER ENCODER FIX xxxxxx SCAN1.DAT
BETA ABSOLUTE DEG
33.70
24.70
15.70
6.70
-2.30
-11.30
-20.30
-29.30
-28.90
-19.90
-10.90
-1.90
7.10
16.10
25.10
34.10
ALPHA ABSOLUTE DEG
START= 20. 33. 49
STOP= 24. 0. 0
TP xxxxxxxxxxx
S/N xxxx

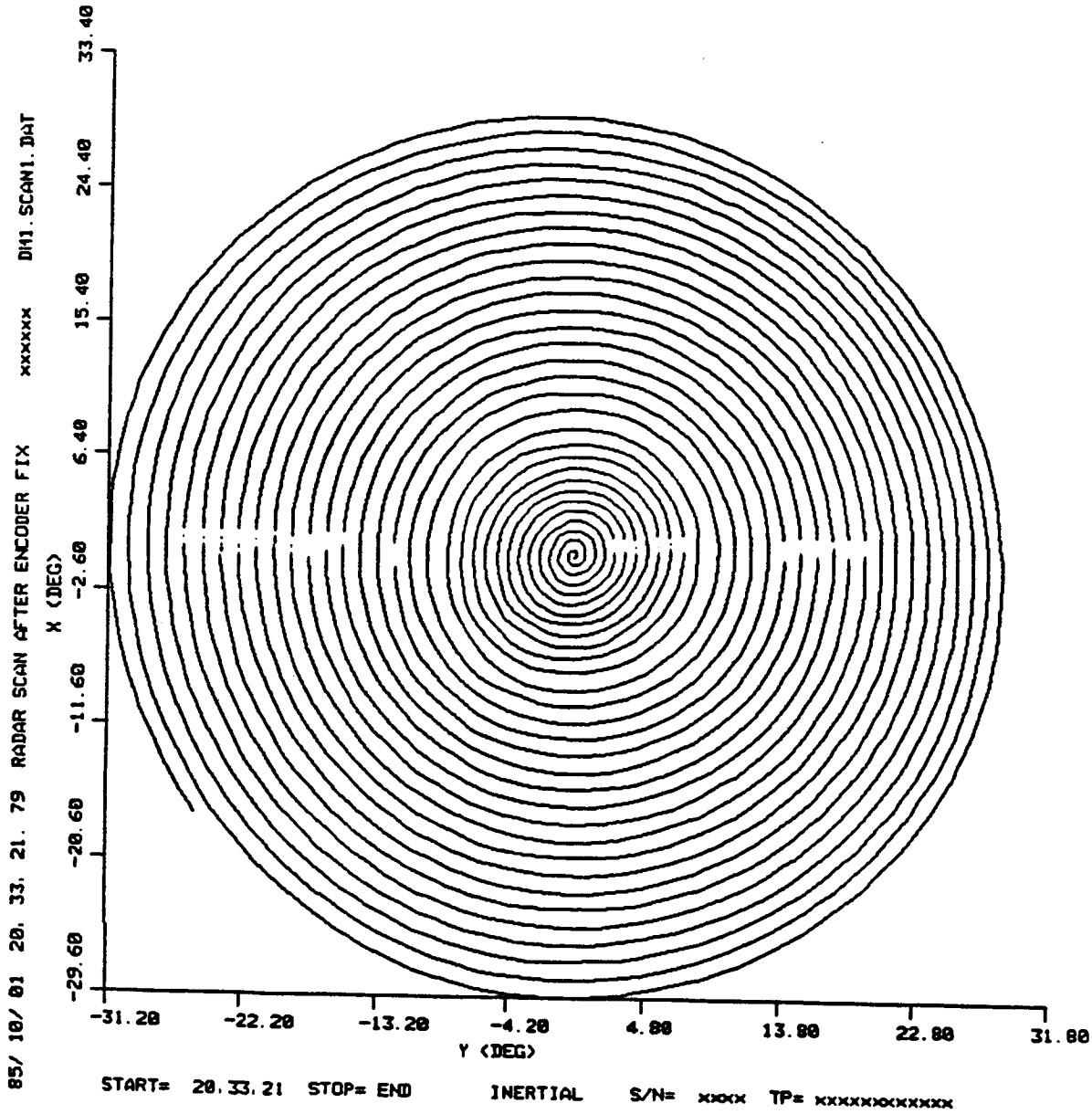
85/ 10/ 01 20. 33. 21. 79 RADAR SCAN AFTER ENCODER FIX xxxxxx DH1.SCAN1.DAT
X (DEG)
33.40
24.40
15.40
6.40
-2.60
-11.60
-20.60
-29.60
-31.20
-22.20
-13.20
-4.20
4.80
13.80
22.80
31.80
Y (DEG)
START= 20.33.21 STOP= END INERTIAL S/N= xxxx TP= xxxxxxxxxxx

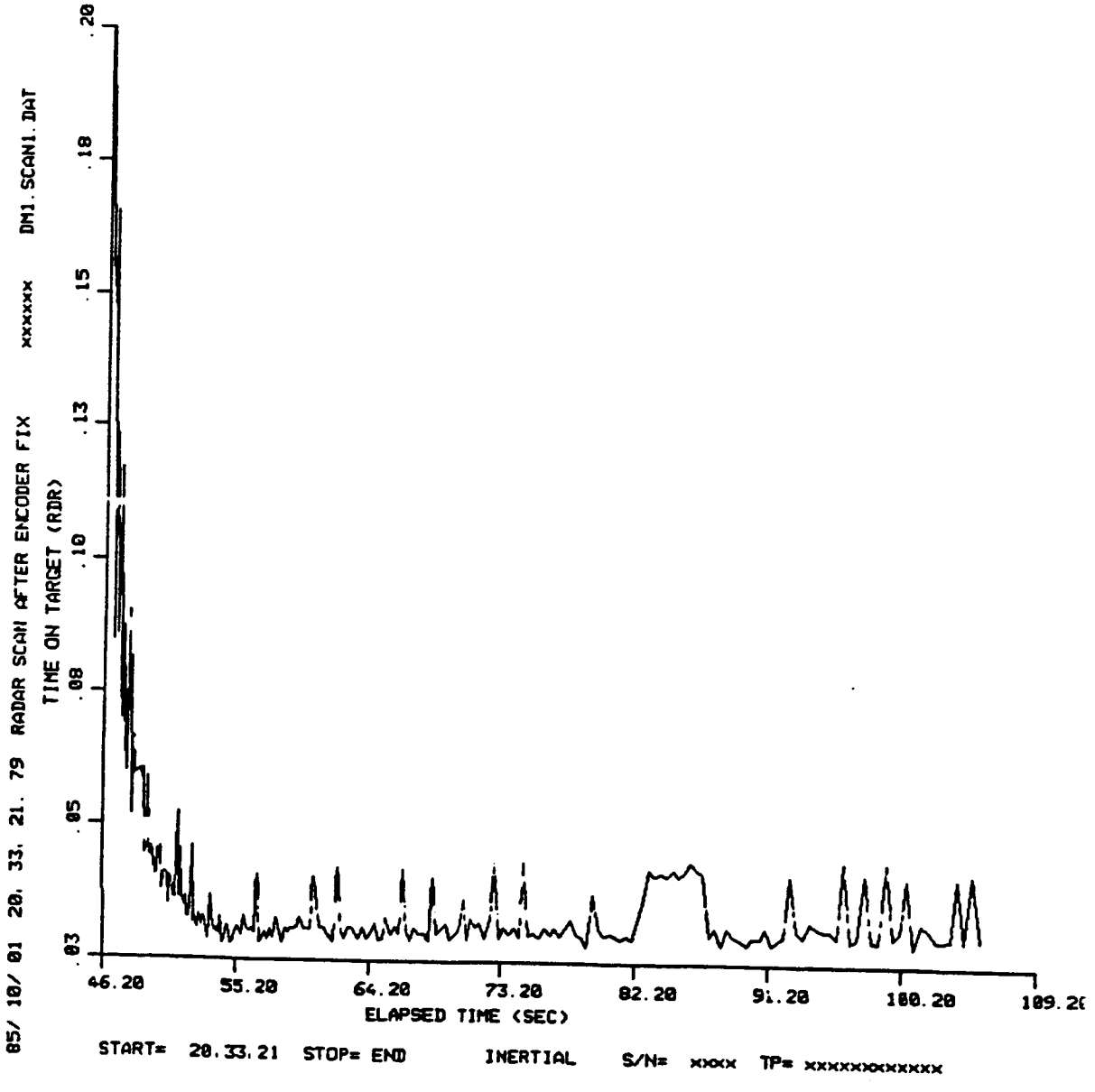
85/ 10/ 01 20. 33. 21. 79 RADAR SCAN AFTER ENCODER FIX xxxxxx DM1.SCAN1.DAT
TIME ON TARGET (RDR)
.03
.05
.08
.10
.13
.15
.18
.20
46.20
55.20
64.20
73.20
82.20
91.20
100.20
109.20
ELAPSED TIME (SEC)
START= 20.33.21 STOP= END INERTIAL S/N= xxxx TP= xxxxxxxxxxx

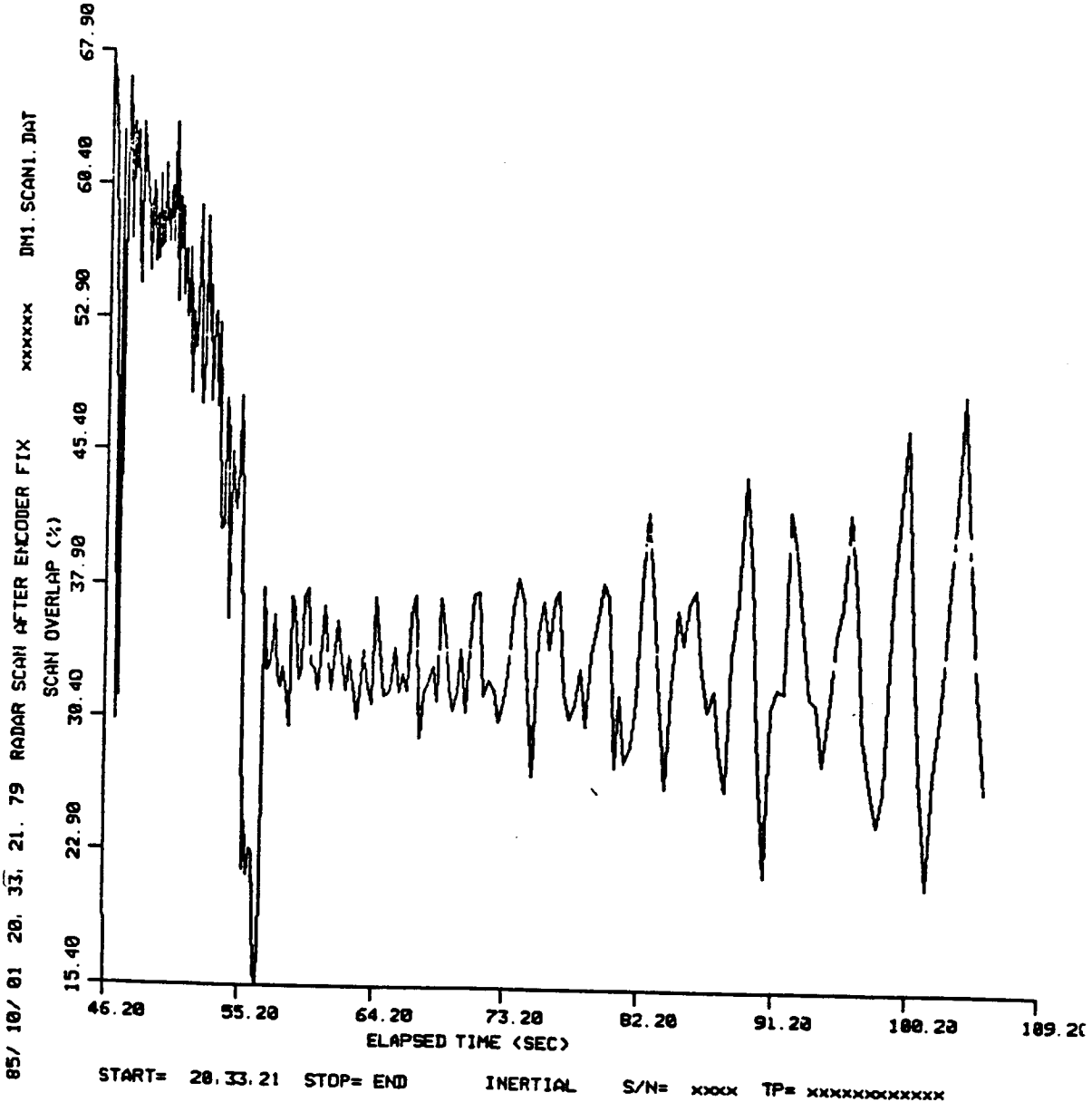
85/ 10/ 01 20. 33. 21. 79 RADAR SCAN AFTER ENCODER FIX xxxxxx DM1.SCAN1.DAT
SCAN OVERLAP (%)
67.90
60.40
52.90
45.40
37.90
30.40
22.90
15.40
46.20
55.20
64.20
73.20
82.20
91.20
100.20
109.20
ELAPSED TIME (SEC)
START= 20.33.21 STOP= END INERTIAL S/N= xxxx TP= xxxxxxxxxxx

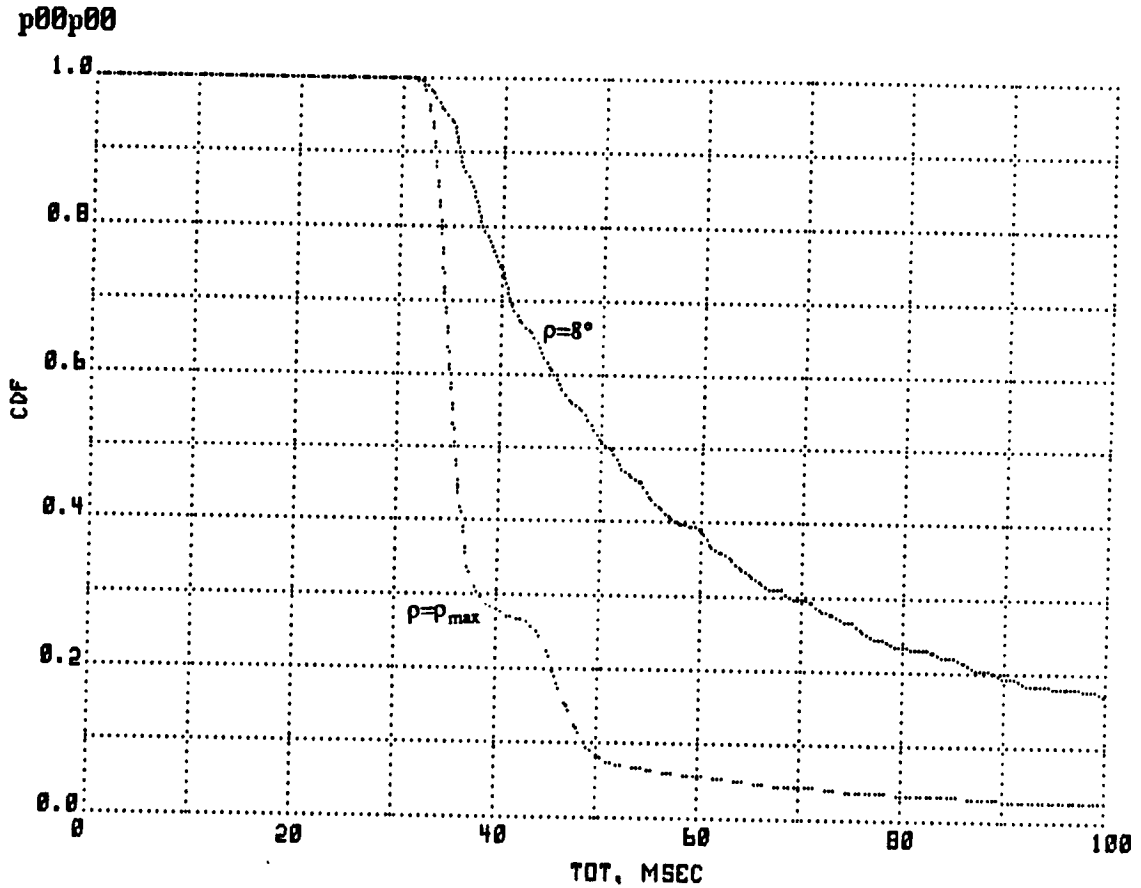
p00p00
1.0
0.8
0.6
0.4
0.2
0.0
CDF
ρ=8°
ρ=ρmax
0
20
40
60
80
100
TOT, MSEC

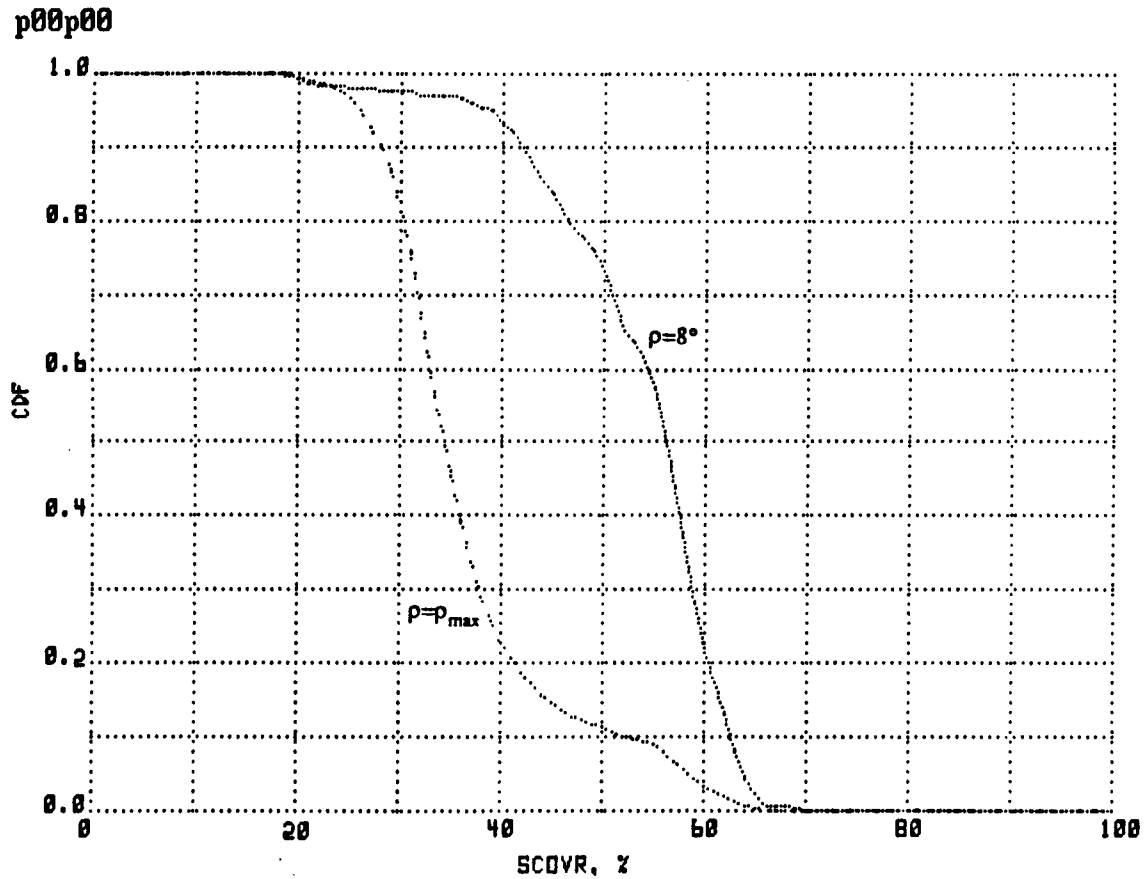
p00p00
1.0
0.8
0.6
0.4
0.2
0.0
CDF
ρ=8°
ρ=ρmax
0
20
40
60
80
100
SCOVR, %

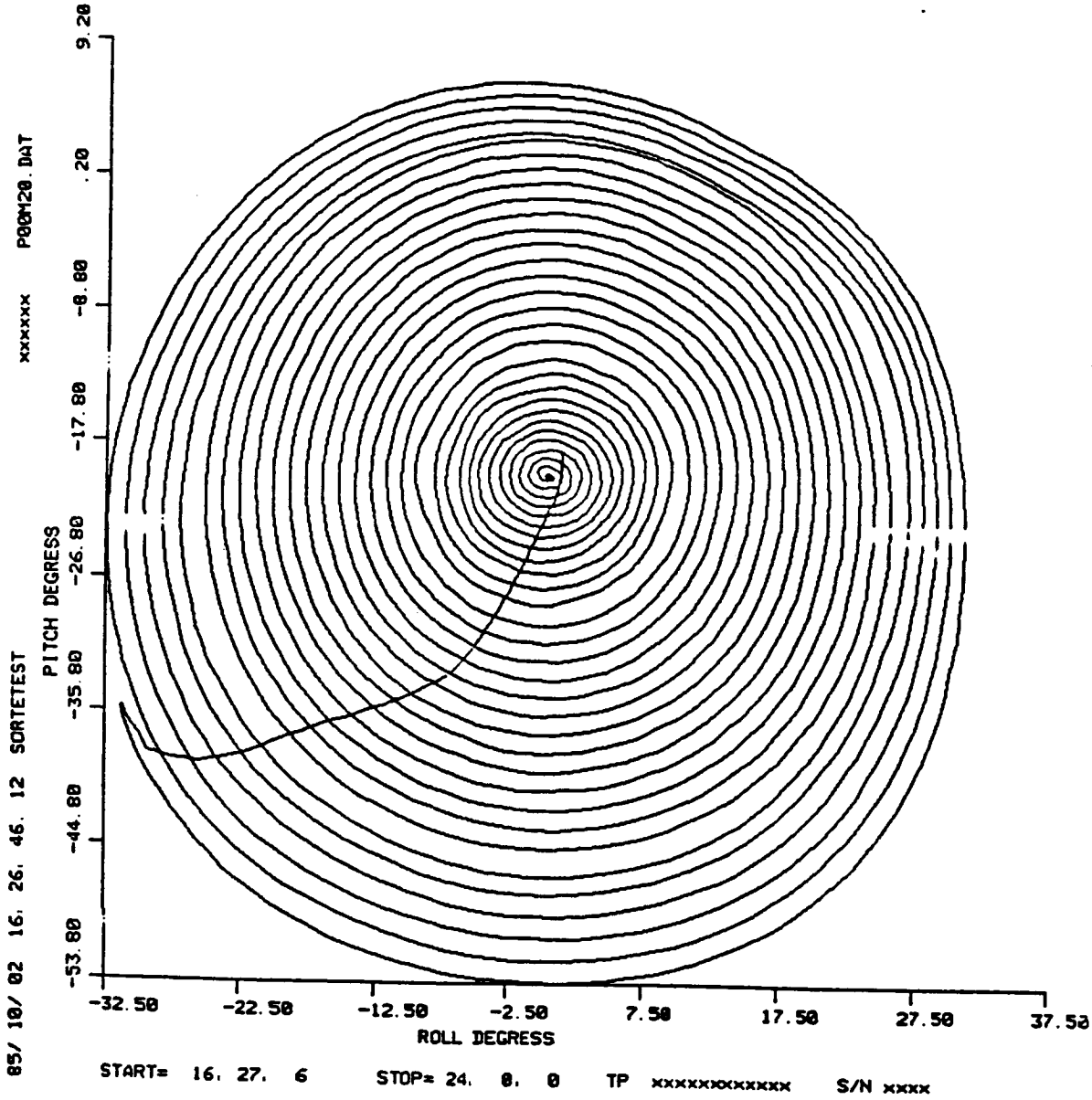
85/ 10/ 02 16. 26. 46. 12 SORTETEST
xxxxxx P00M20.DAT
PITCH DEGRESS
9.20
.20
-8.80
-17.80
-26.80
-35.80
-44.80
-53.80
-32.50
-22.50
-12.50
-2.50
7.50
17.50
27.50
37.50
ROLL DEGRESS
START= 16. 27. 6
STOP= 24. 0. 0
TP xxxxxxxxxxx
S/N xxxx

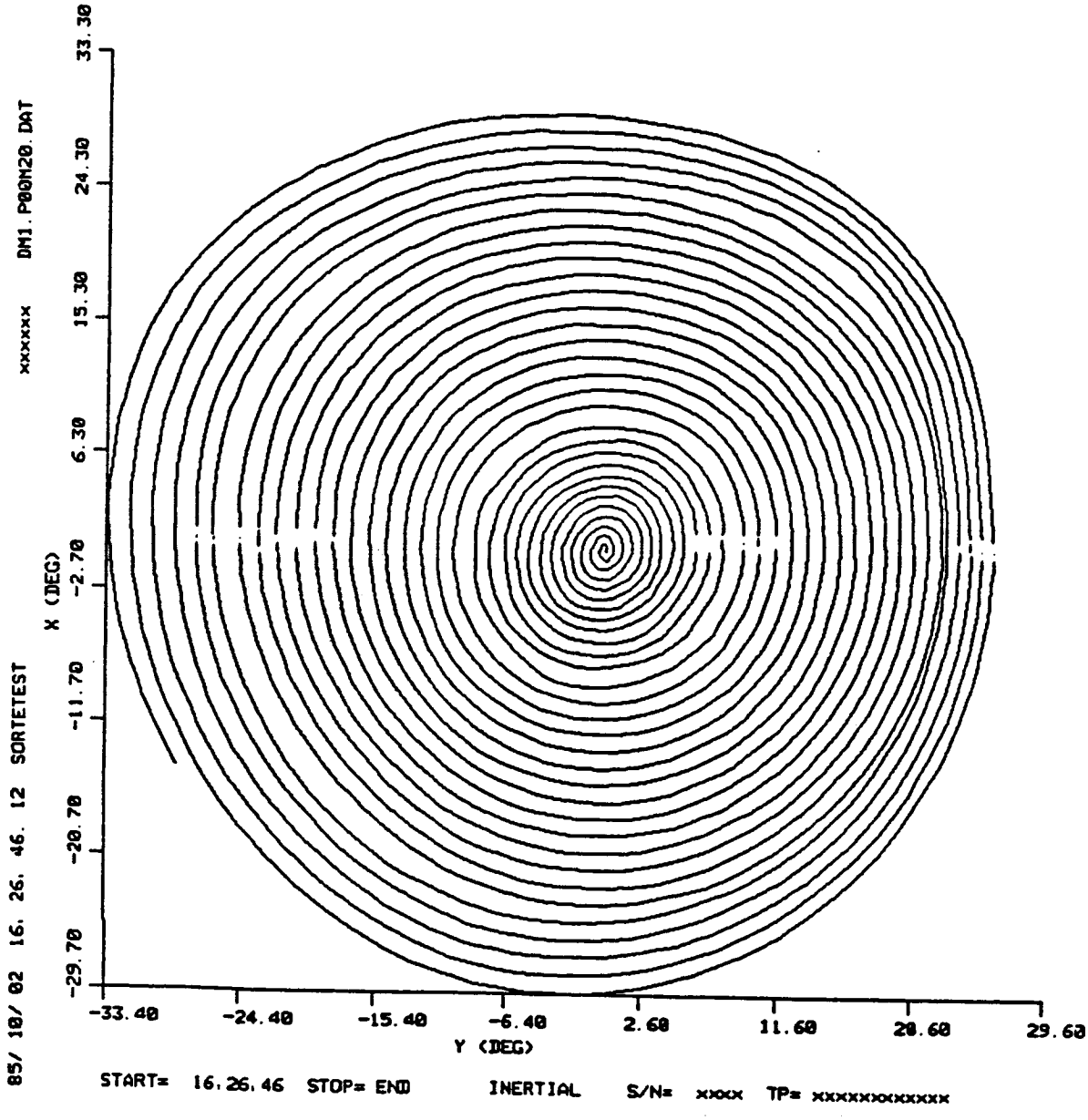
85/ 10/ 02 16. 26. 46. 12 SORTETEST
XXXXXX DM1.P00M20.DAT
X (DEG)
33.30
24.30
15.30
6.30
-2.70
-11.70
-20.70
-29.70
-33.40
-24.40
-15.40
-6.40
2.60
11.60
20.60
29.60
Y (DEG)
START= 16.26.46 STOP= END
INERTIAL
S/N= xxxx TP= xxxxxxxxxxx

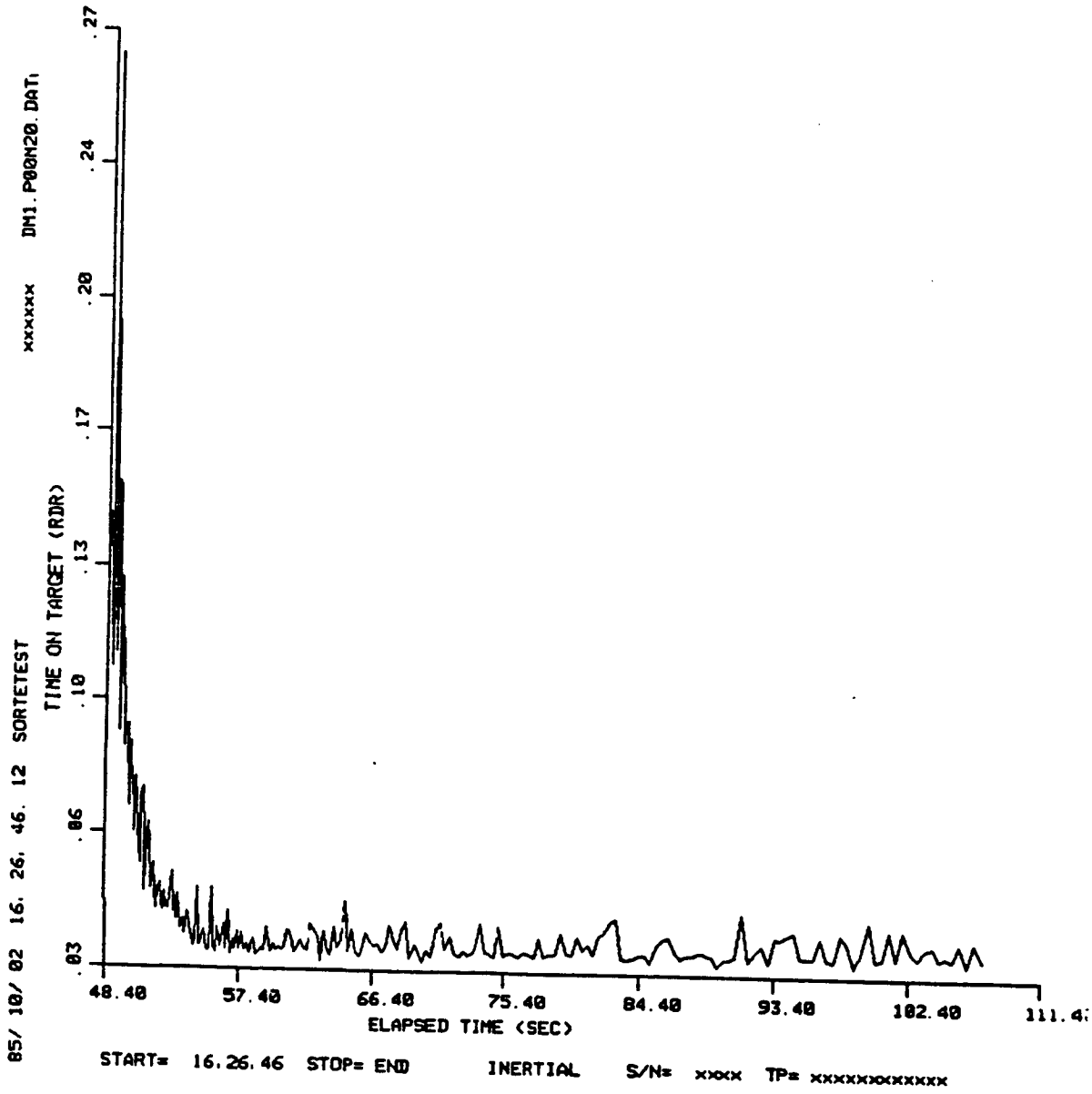
85/ 10/ 02 16. 26. 46. 12 SORTETEST
TIME ON TARGET (RDR)
.03
.06
.10
.13
.17
.20
.24
.27
xxxxxx DM1.P00N20.DAT
48.40
57.40
66.40
75.40
84.40
93.40
102.40
111.4
ELAPSED TIME (SEC)
START= 16.26.46 STOP= END INERTIAL S/N= xxxx TP= xxxxxxxxxxx

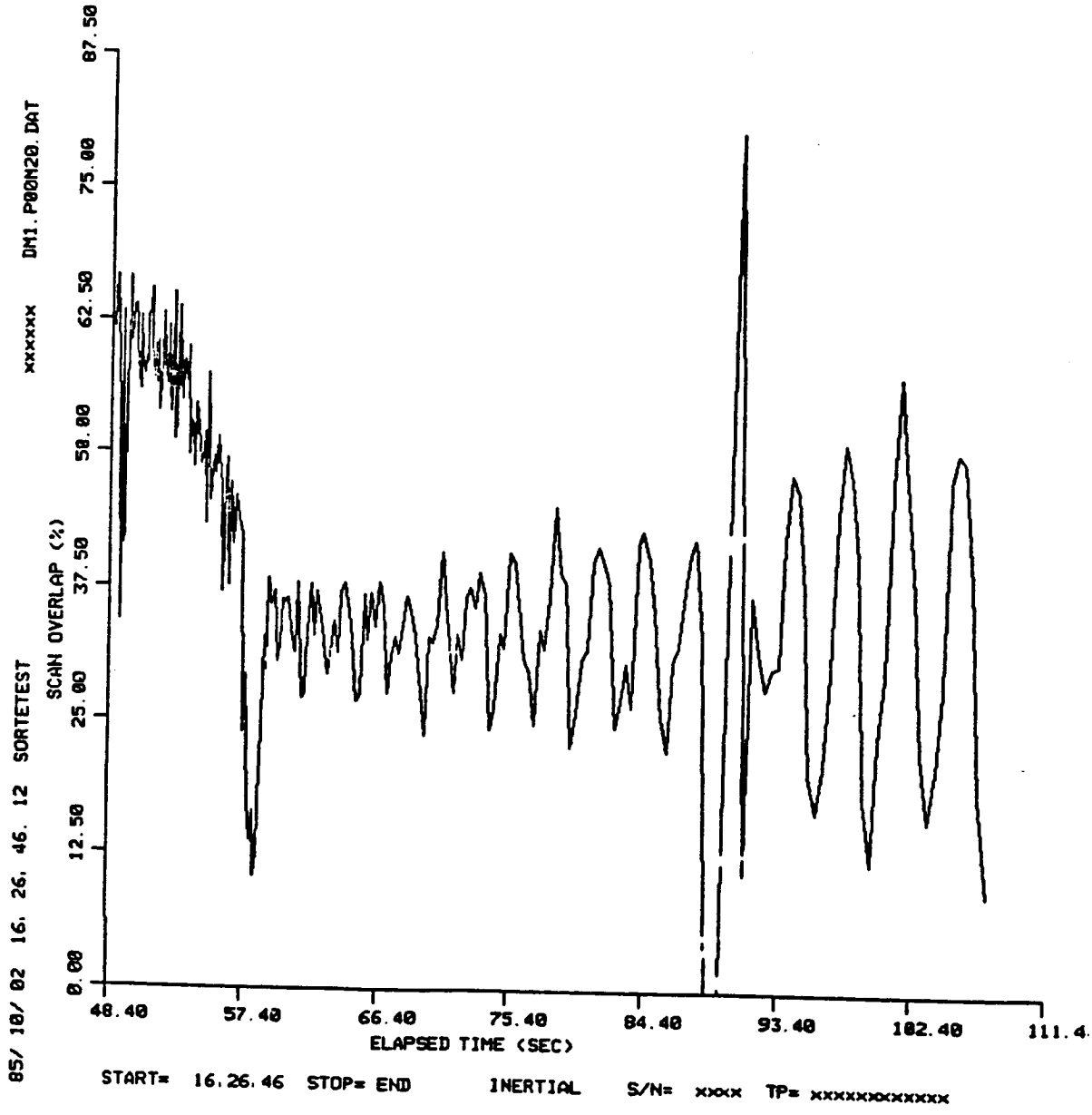
85/ 10/ 02 16. 26. 46. 12 SORTETEST
xxxxxx DM1.P00N20.DAT
SCAN OVERLAP (%)
0.00
12.50
25.00
37.50
50.00
62.50
75.00
87.50
48.40
57.40
66.40
75.40
84.40
93.40
102.40
111.4
ELAPSED TIME (SEC)
START= 16.26.46 STOP= END
INERTIAL
S/N= xxxx TP= xxxxxxxxxxx

p00m20

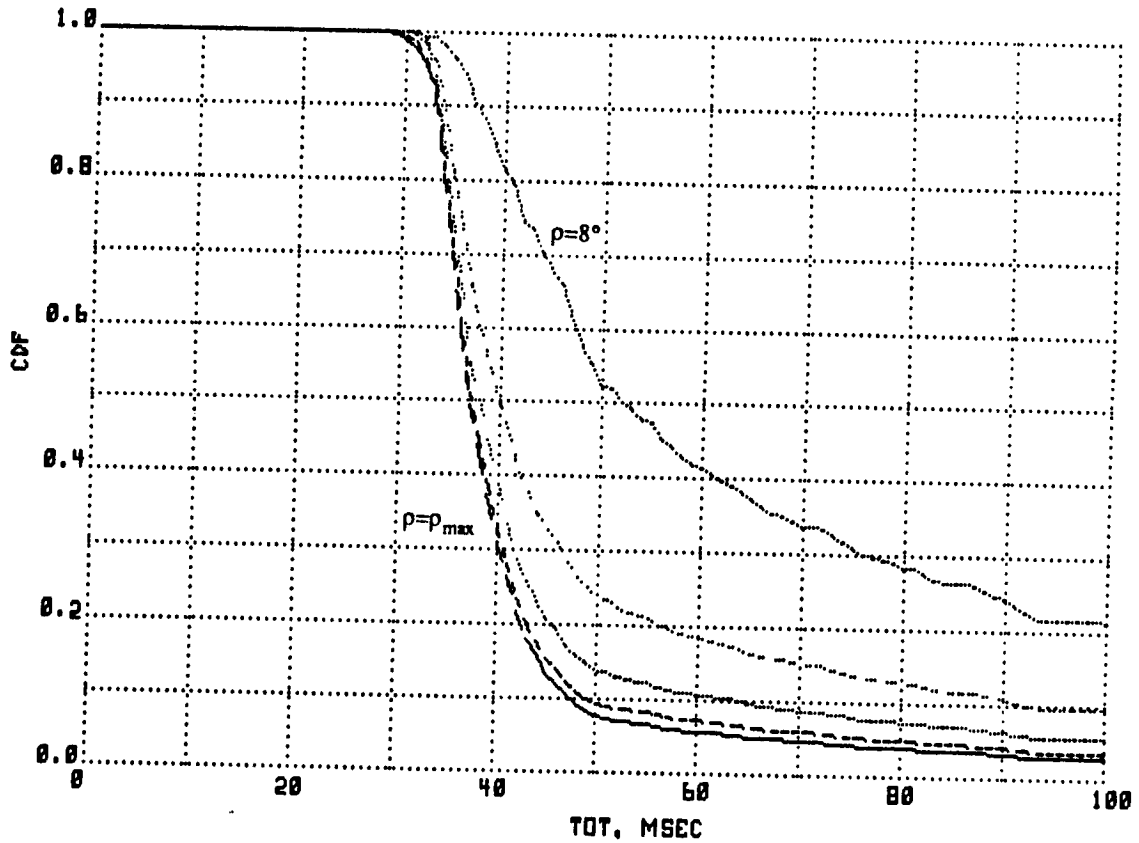

p00m20

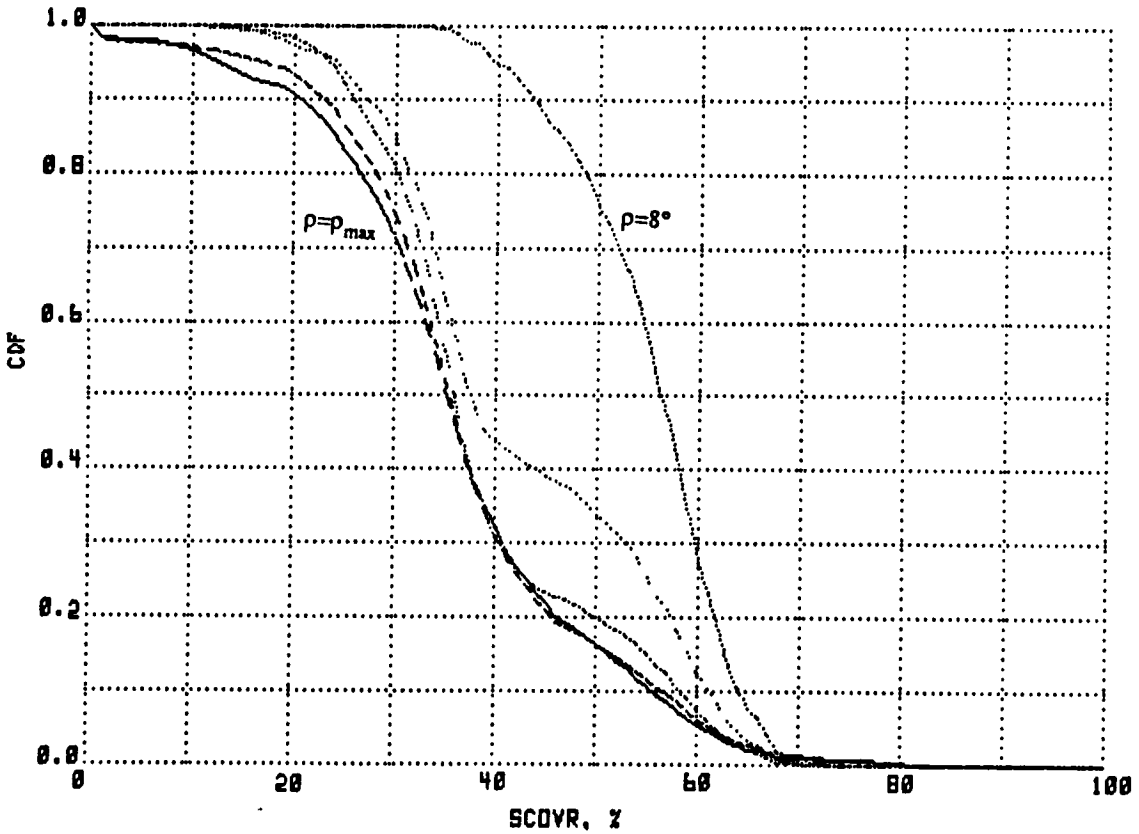

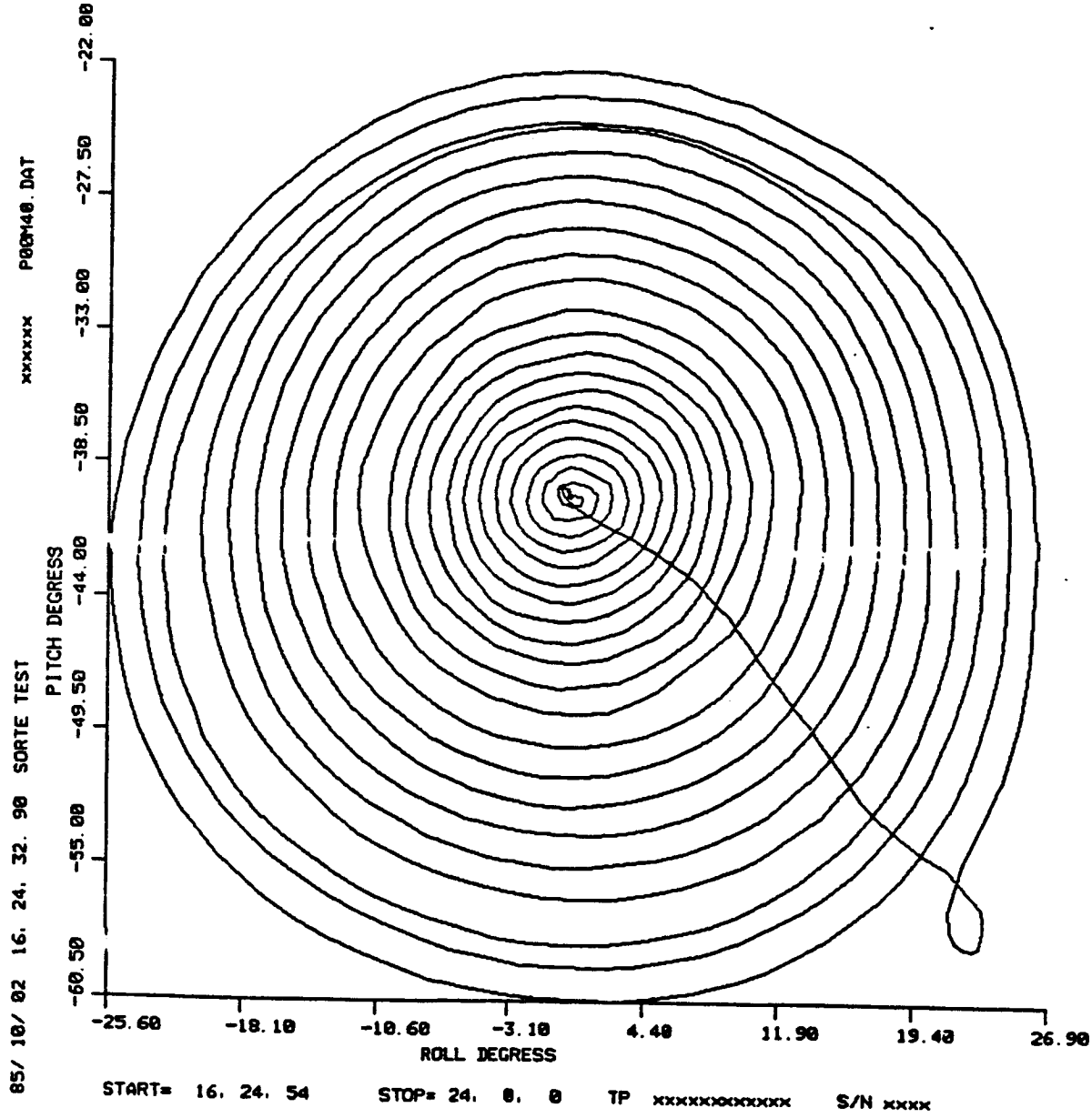
85/ 10/ 02 16. 24. 32. 90 SORTE TEST
xxxxxx P00M40.DAT
PITCH DEGRESS
-22.00
-27.50
-33.00
-38.50
-44.00
-49.50
-55.00
-60.50
-25.60
-18.10
-10.60
-3.10
4.40
11.90
19.40
26.90
ROLL DEGRESS
START= 16. 24. 54
STOP= 24. 0. 0
TP xxxxxxxxxxx
S/N xxxx

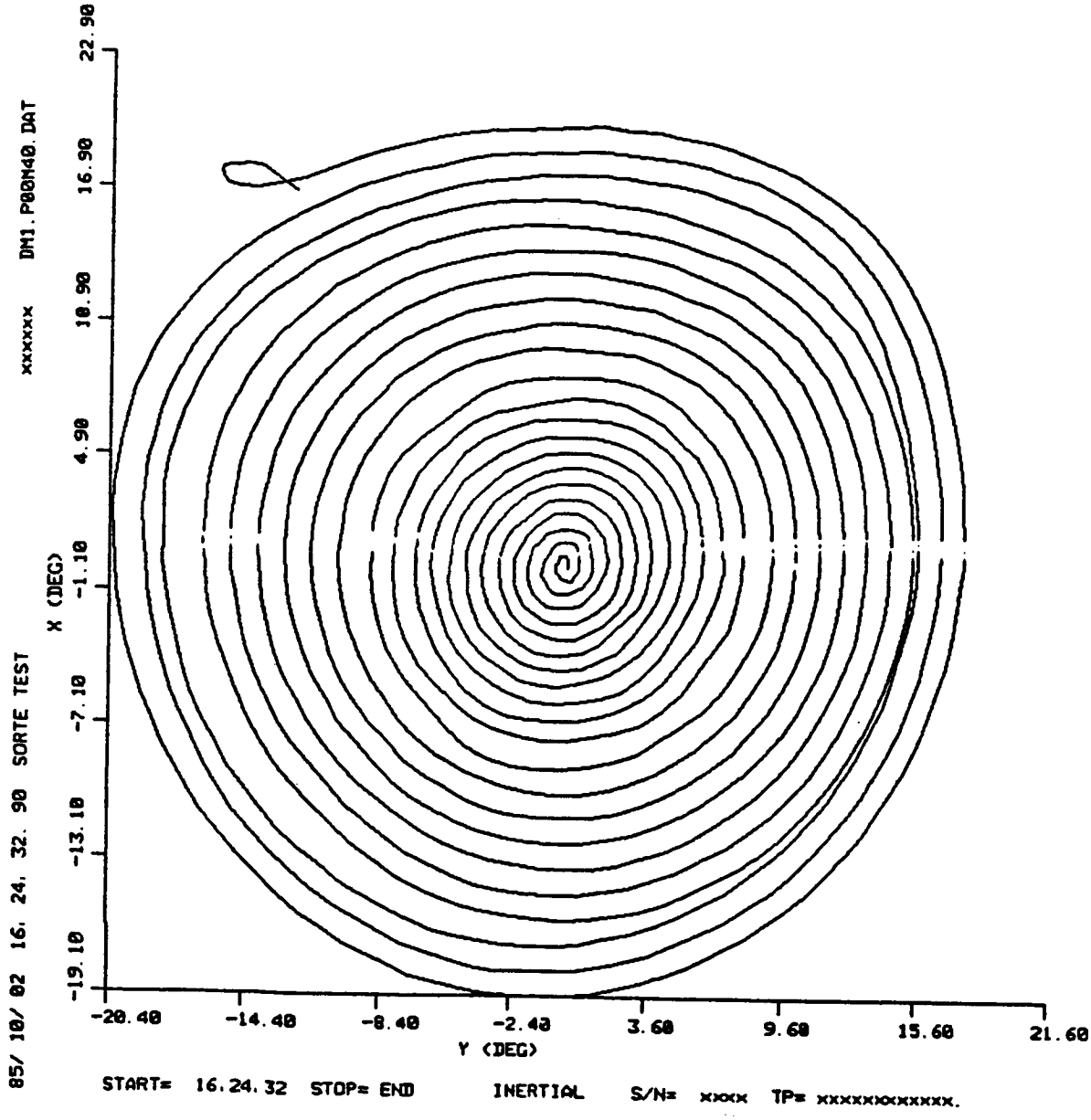
85/ 10/ 02 16. 24. 32. 90 SORTE TEST
XXXXXX DM1.P00N40.DAT
X (DEG)
22.90
16.90
10.90
4.90
-1.10
-7.10
-13.10
-19.10
-20.40
-14.40
-8.40
-2.40
3.60
9.60
15.60
21.60
Y (DEG)
START= 16.24.32 STOP= END
INERTIAL
S/N= XXXX TP= XXXXXXXXXXX.

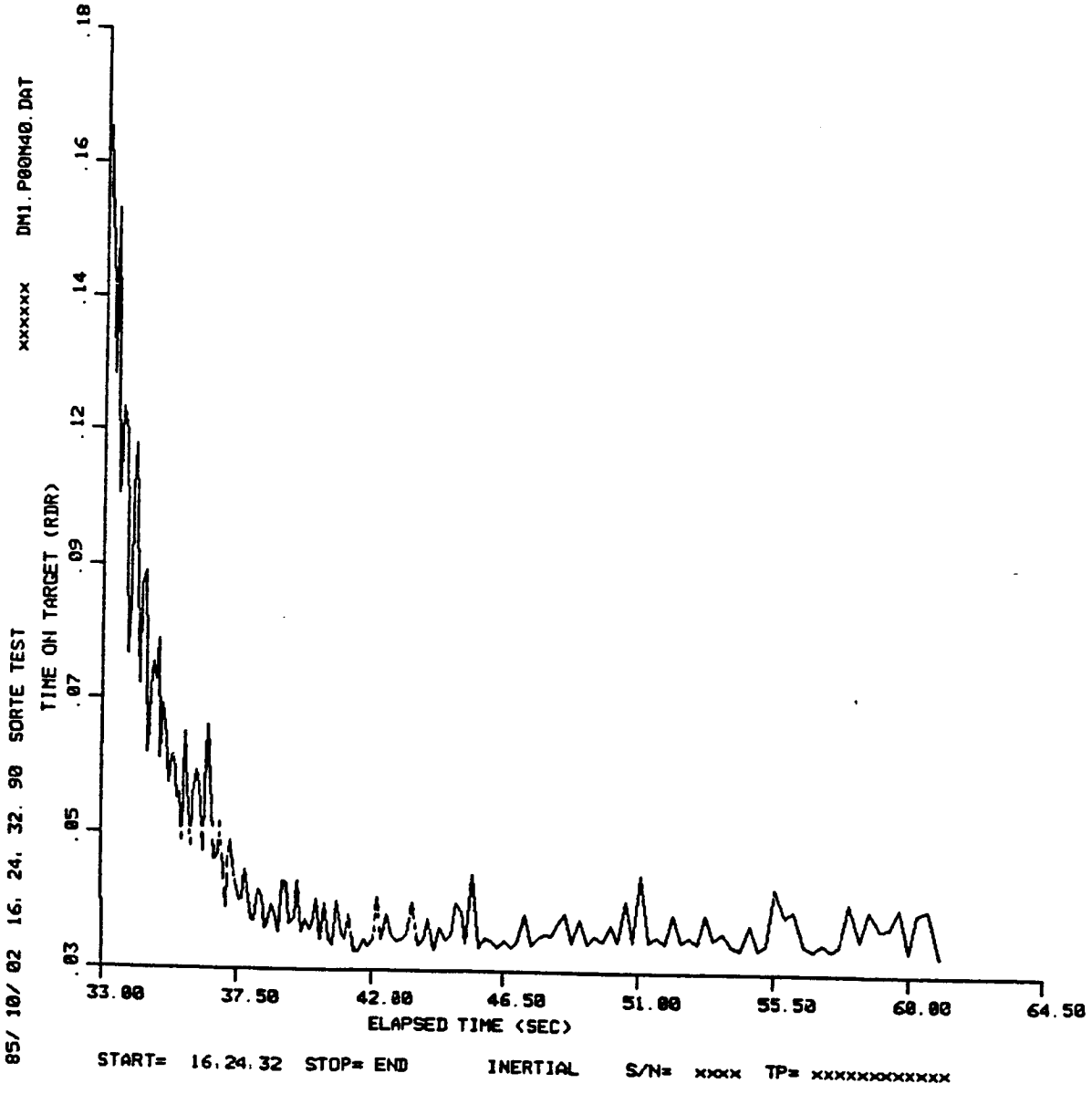
85/ 10/ 02 16. 24. 32. 90 SORTE TEST
xxxxxx DM1.P00M40.DAT
TIME ON TARGET (RDR)
.03
.05
.07
.09
.12
.14
.16
.18
33.00
37.50
42.00
46.50
51.00
55.50
60.00
64.50
ELAPSED TIME (SEC)
START= 16.24.32 STOP= END
INERTIAL
S/N= xxxx TP= xxxxxxxxxxx

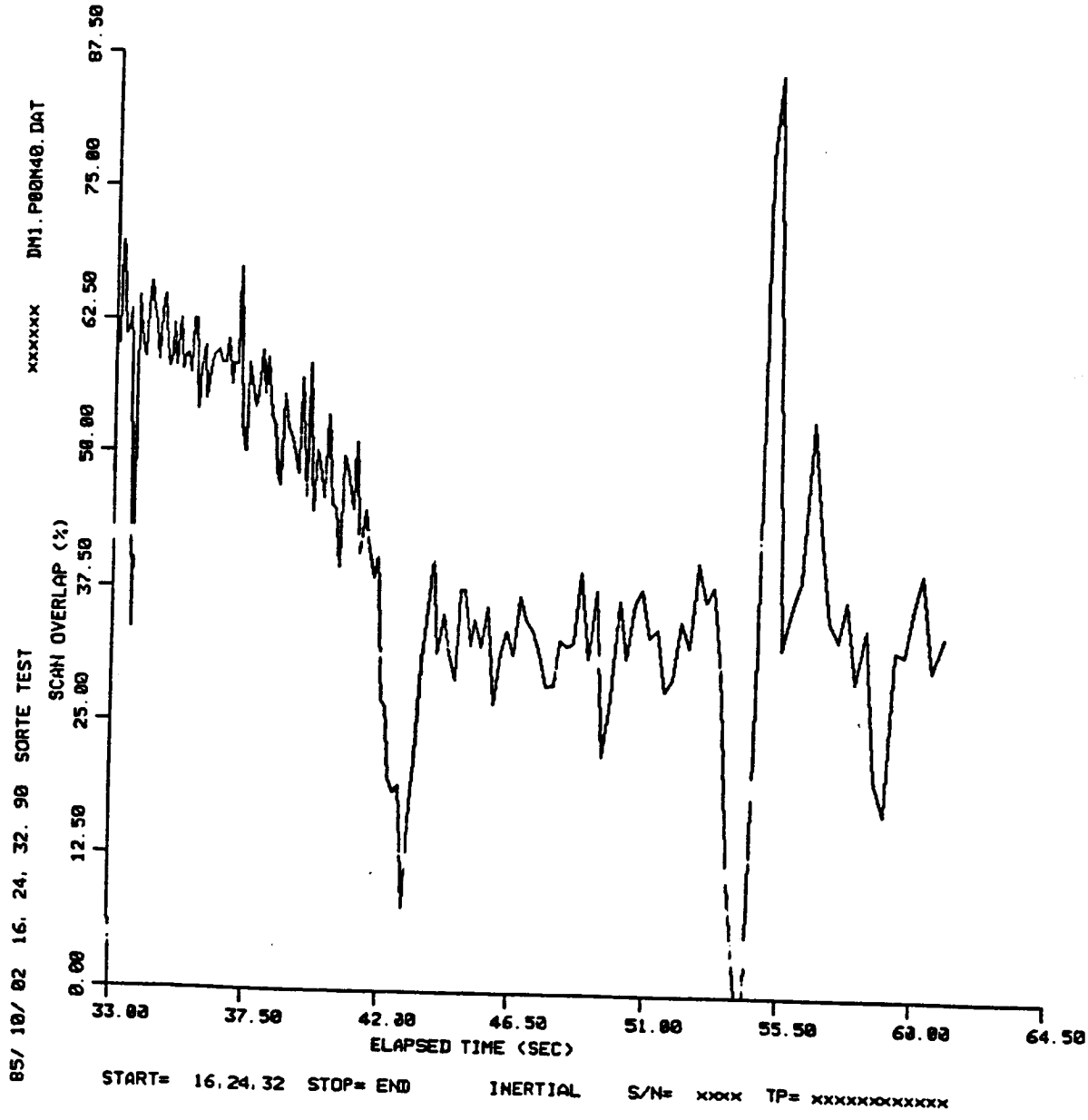
87.50
75.00
62.50
50.00
37.50
25.00
12.50
0.00
SCAN OVERLAP (%)
xxxxxx DM1.P00N40.DAT
85/ 10/ 02 16. 24. 32. 90 SORTE TEST
33.00
37.50
42.00
46.50
51.00
55.50
60.00
64.50
ELAPSED TIME (SEC)
START= 16.24.32 STOP= END INERTIAL S/N= xxxx TP= xxxxxxxxxxx

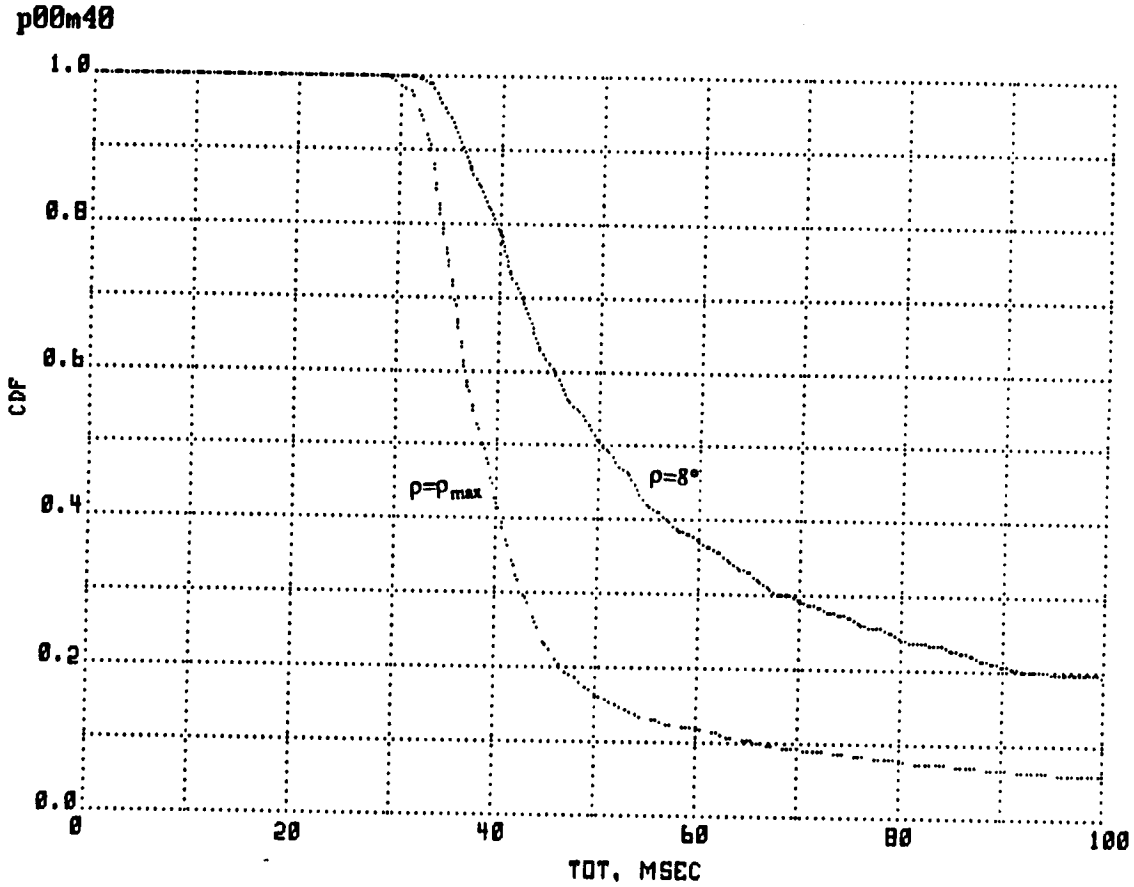
p00m40
1.0
0.8
0.6
0.4
0.2
0.0
CDF
0
20
40
60
80
100
TOT, MSEC
ρ=ρmax
ρ=8°

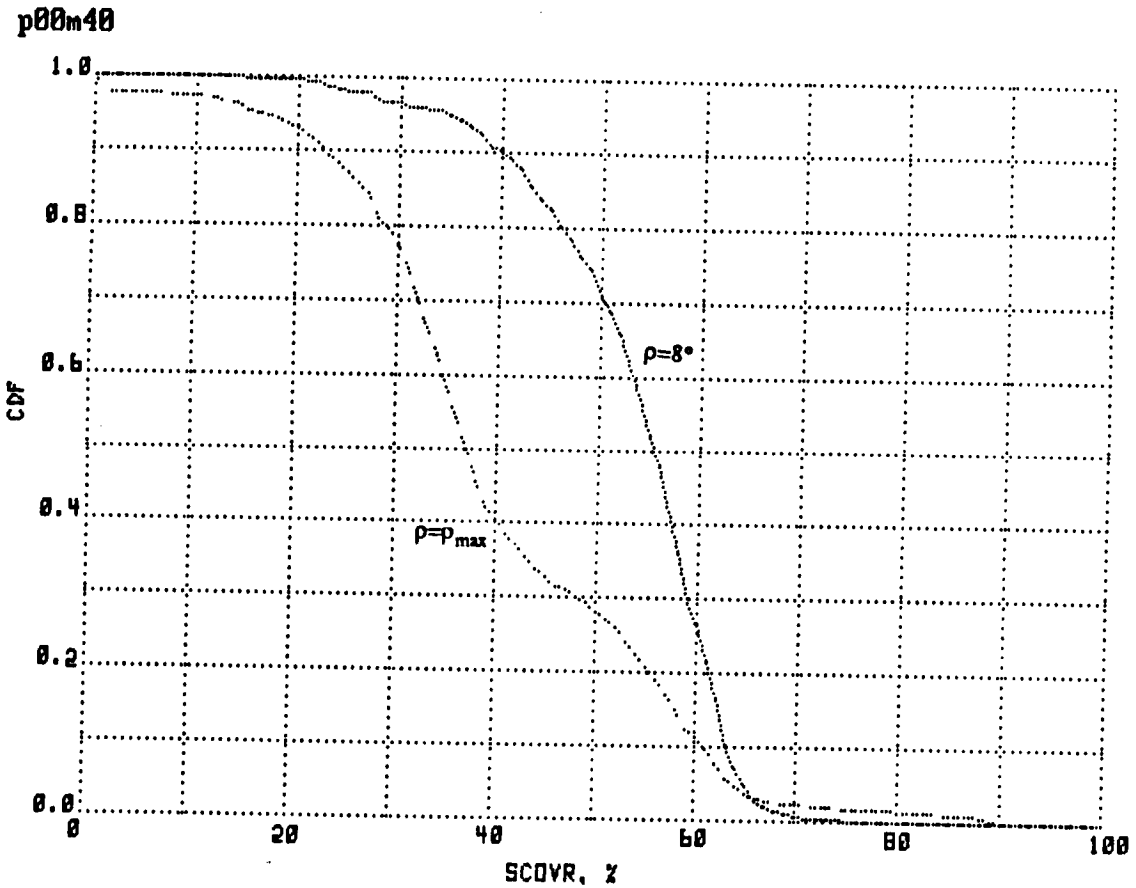
p00m40
1.0
0.8
0.6
0.4
0.2
0.0
CDF
ρ=8°
ρ=ρmax
0
20
40
60
80
100
SCOVR, %

p00m40

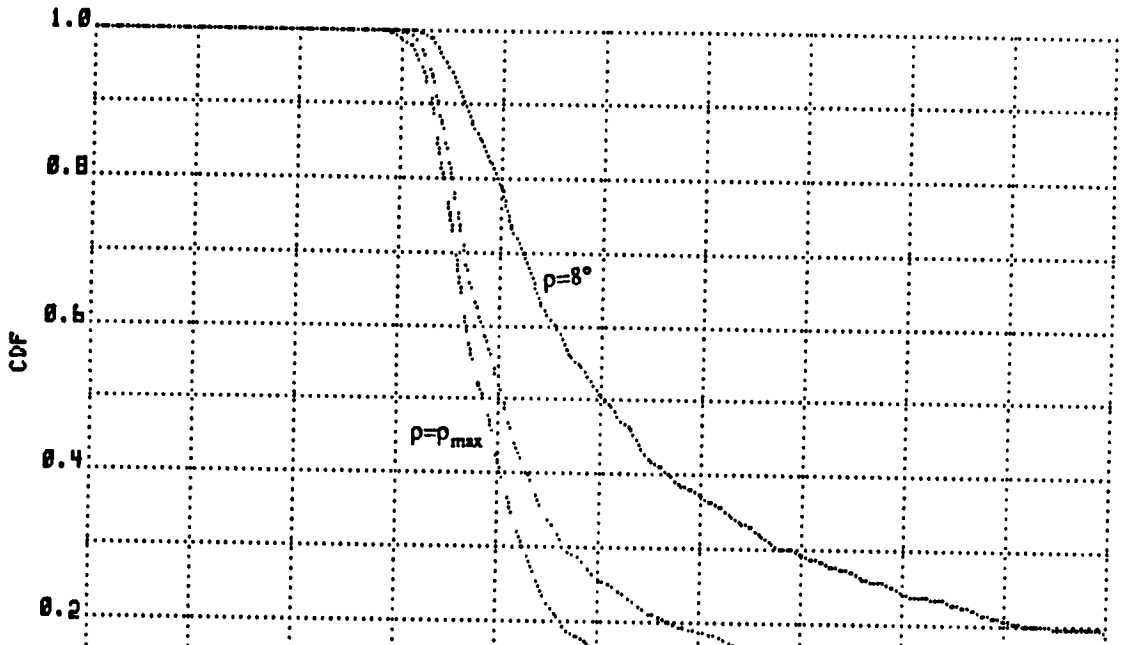

p00m40

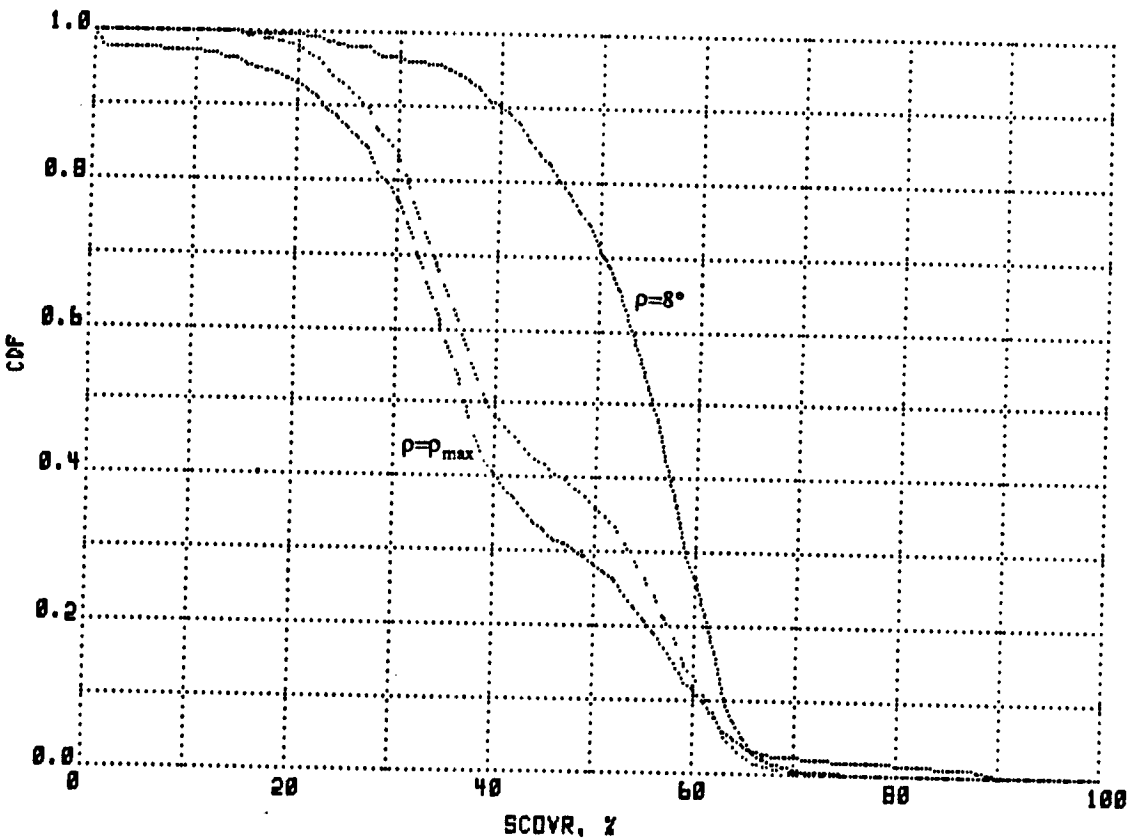

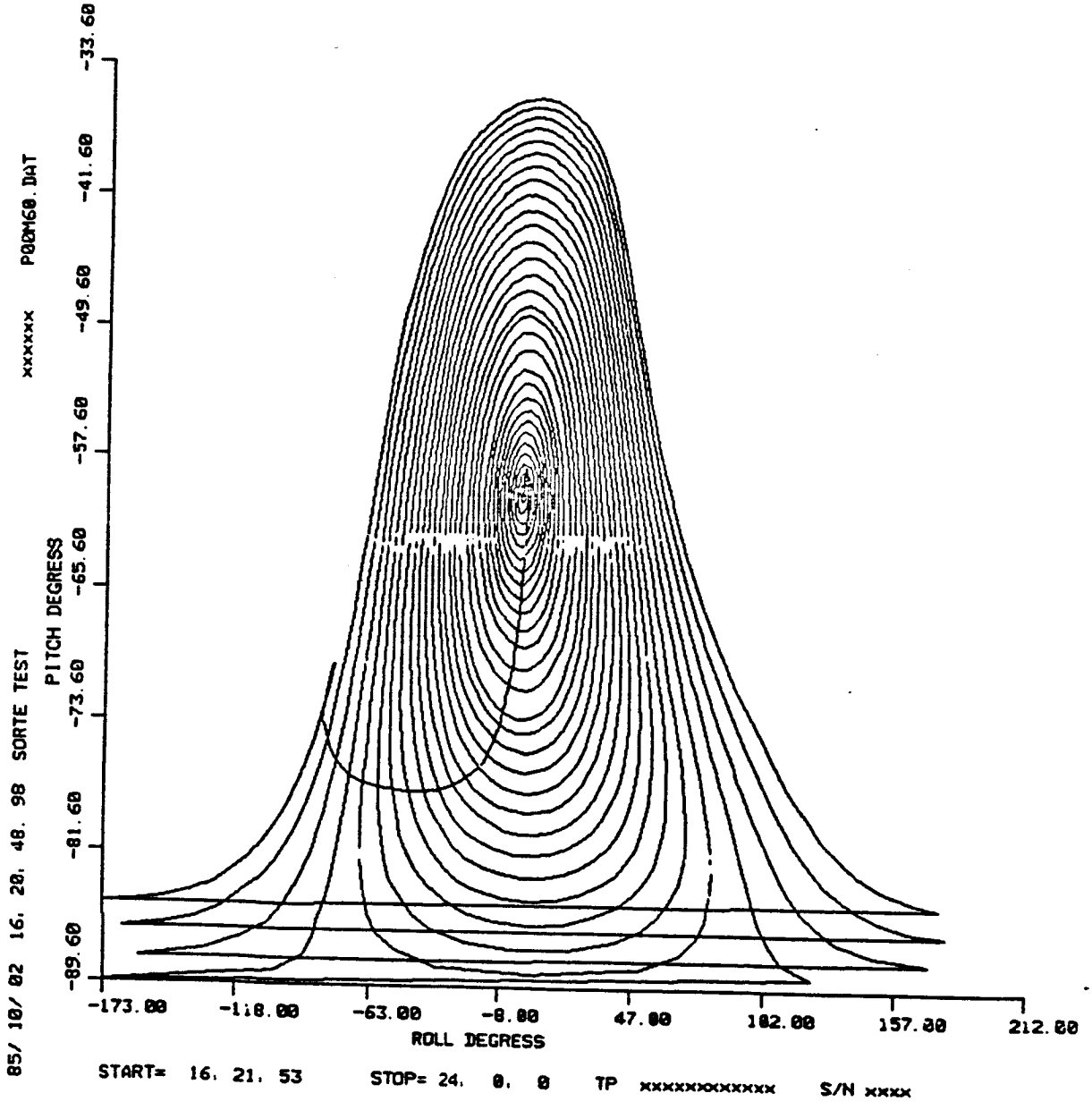
85/ 10/ 02 16. 20. 48. 98 SORTE TEST
xxxxxx P00M60.DAT
PITCH DEGRESS
-33.60
-41.60
-49.60
-57.60
-65.60
-73.60
-81.60
-89.60
-173.00
-118.00
-63.00
-8.00
47.00
102.00
157.00
212.00
ROLL DEGRESS
START= 16. 21. 53
STOP= 24. 0. 0
TP xxxxxxxxxxx
S/N xxxx

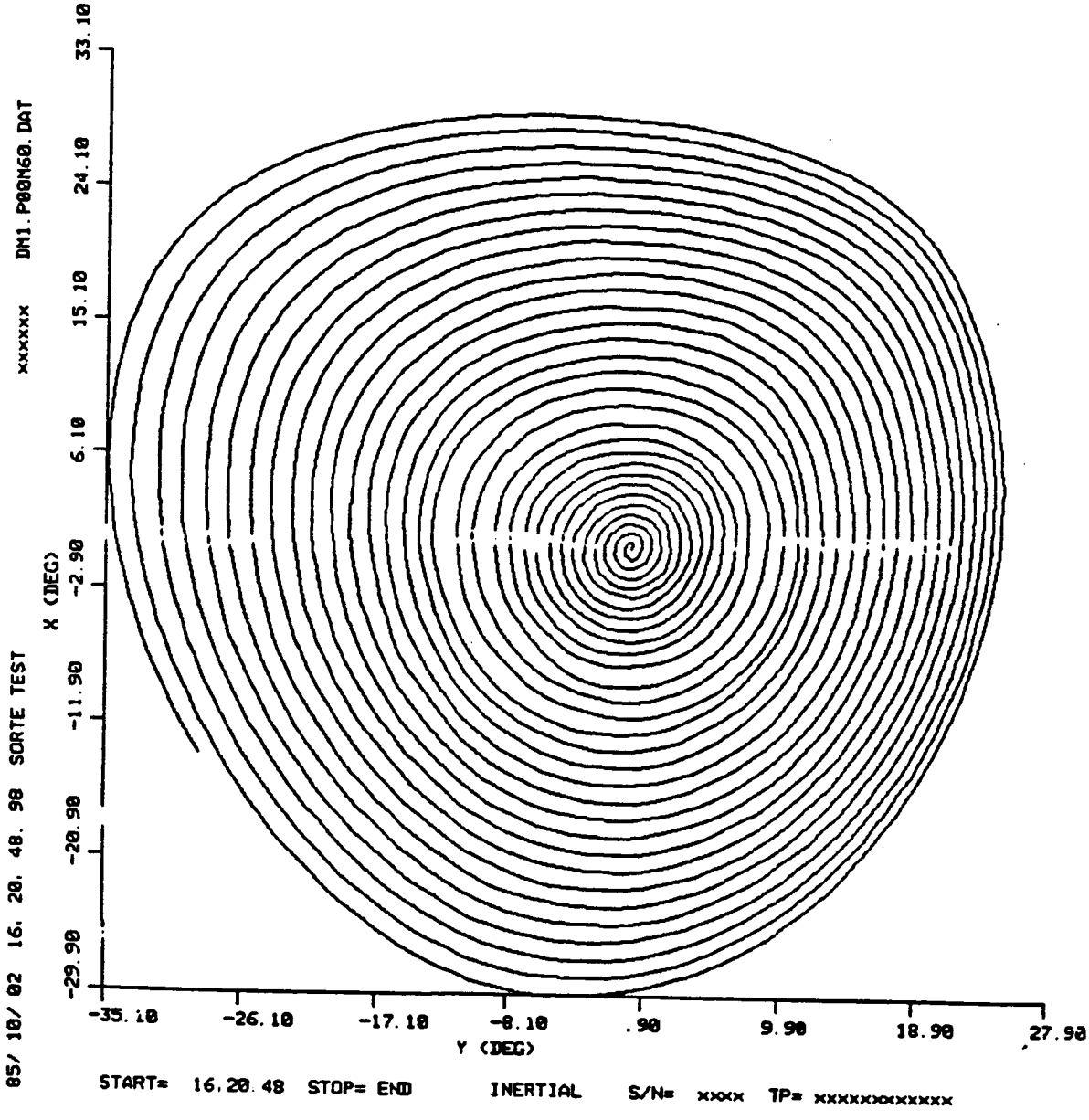
85/ 10/ 02 16. 20. 48. 98 SORTE TEST
xxxxxx DM1.P00N60.DAT
X (DEG)
33.10
24.10
15.10
6.10
-2.90
-11.90
-20.90
-29.90
-35.10
-26.10
-17.10
-8.10
.90
9.90
18.90
27.90
Y (DEG)
START= 16.20.48 STOP= END
INERTIAL
S/N= xxxx TP= xxxxxxxxxxx

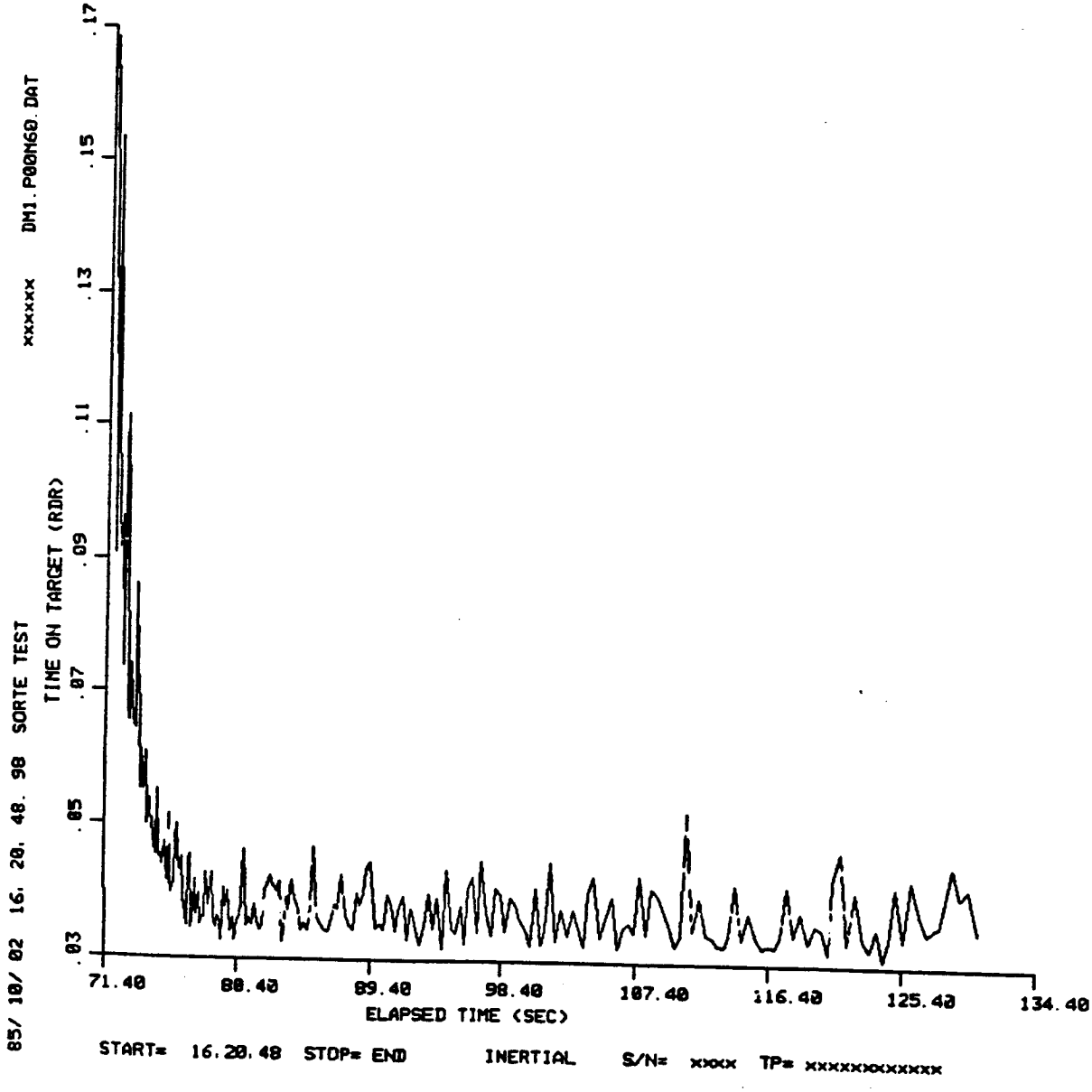
85/ 10/ 02 16. 20. 48. 98 SORTE TEST
xxxxxx DM1.P00N60.DAT
TIME ON TARGET (RDR)
.03
.05
.07
.09
.11
.13
.15
.17
71.40
80.40
89.40
98.40
107.40
116.40
125.40
134.40
ELAPSED TIME (SEC)
START= 16.20.48 STOP= END
INERTIAL
S/N= xxxx TP= xxxxxxxxxxx

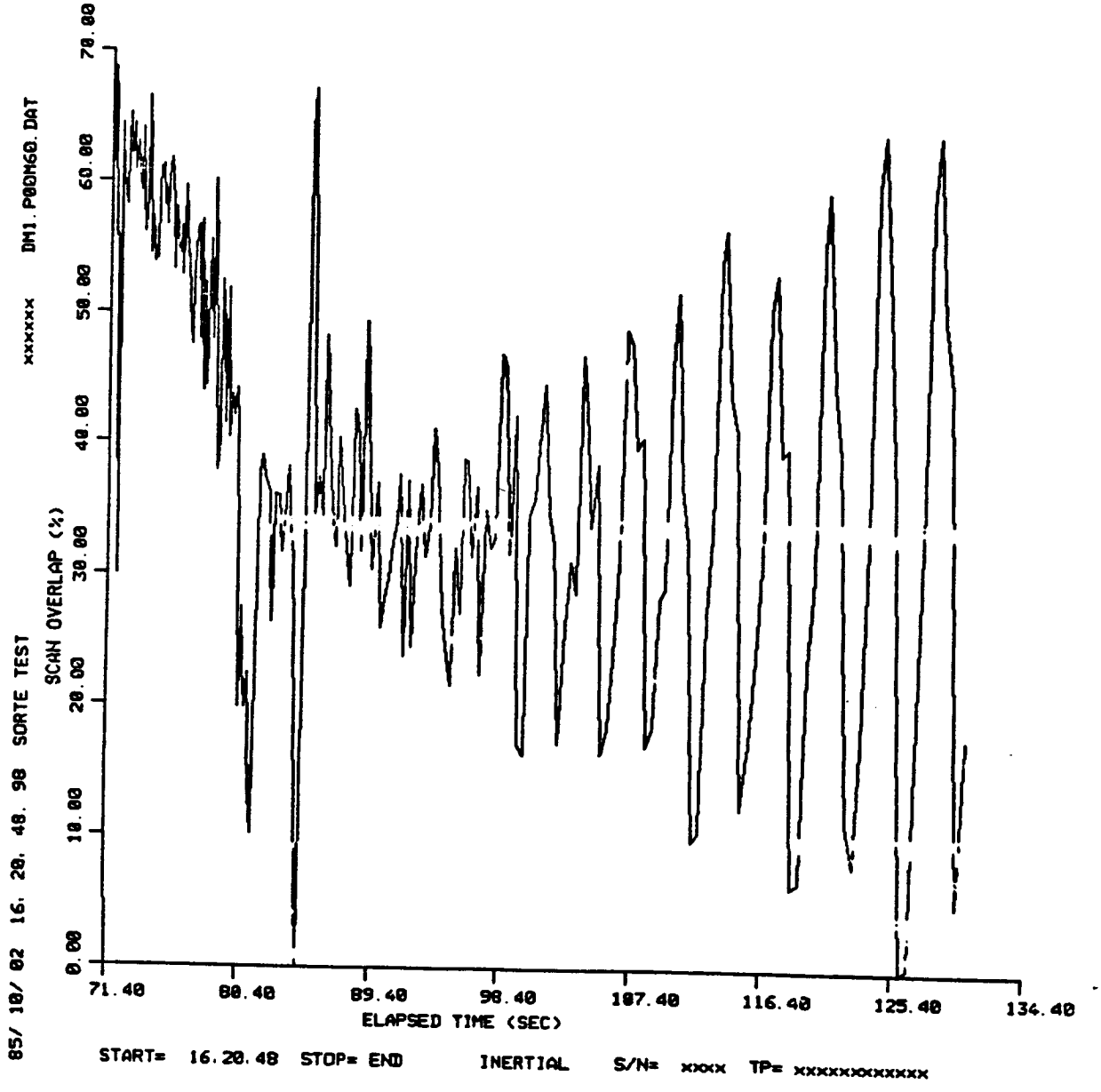
85/ 10/ 02 16. 20. 48. 98 SORTE TEST
SCAN OVERLAP (%)
xxxxxx DM1.P00N60.DAT
0.00
10.00
20.00
30.00
40.00
50.00
60.00
70.00
71.40
80.40
89.40
98.40
107.40
116.40
125.40
134.40
ELAPSED TIME (SEC)
START= 16.20.48 STOP= END INERTIAL S/N= xxxx TP= xxxxxxxxxxx

p00m60

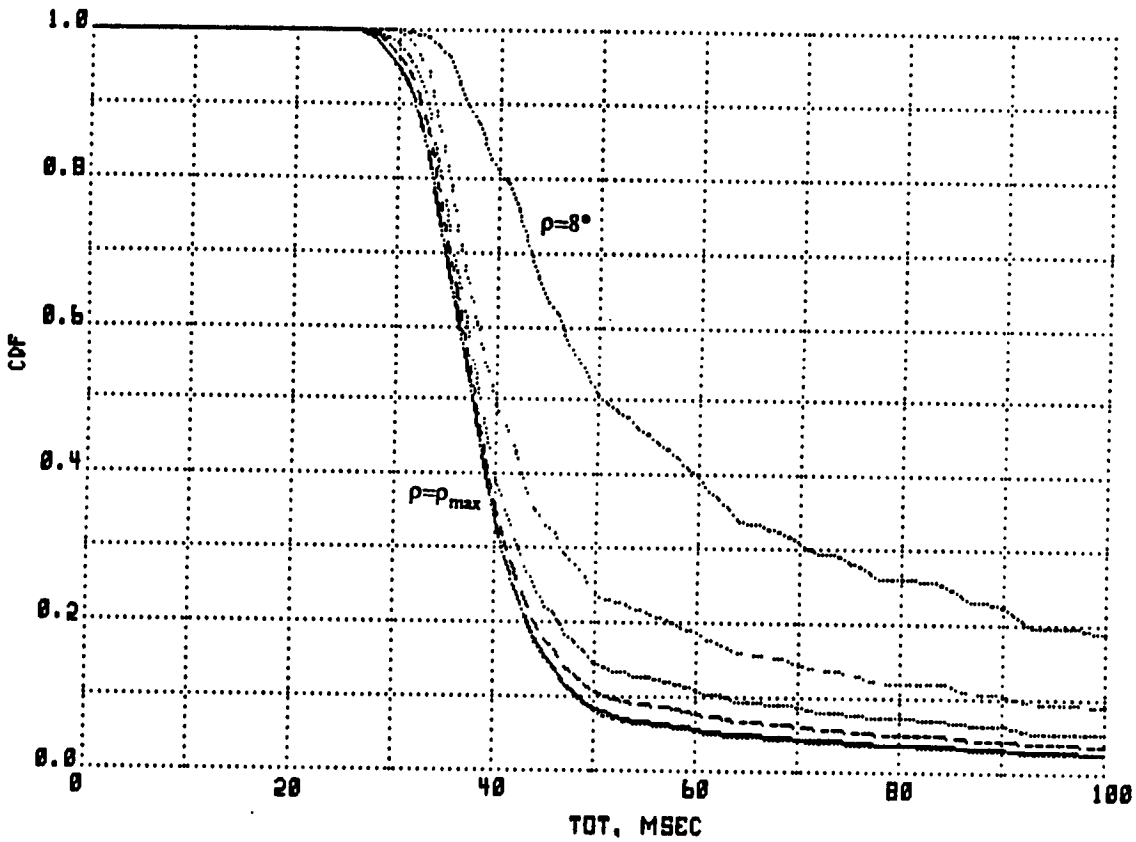

p00m60

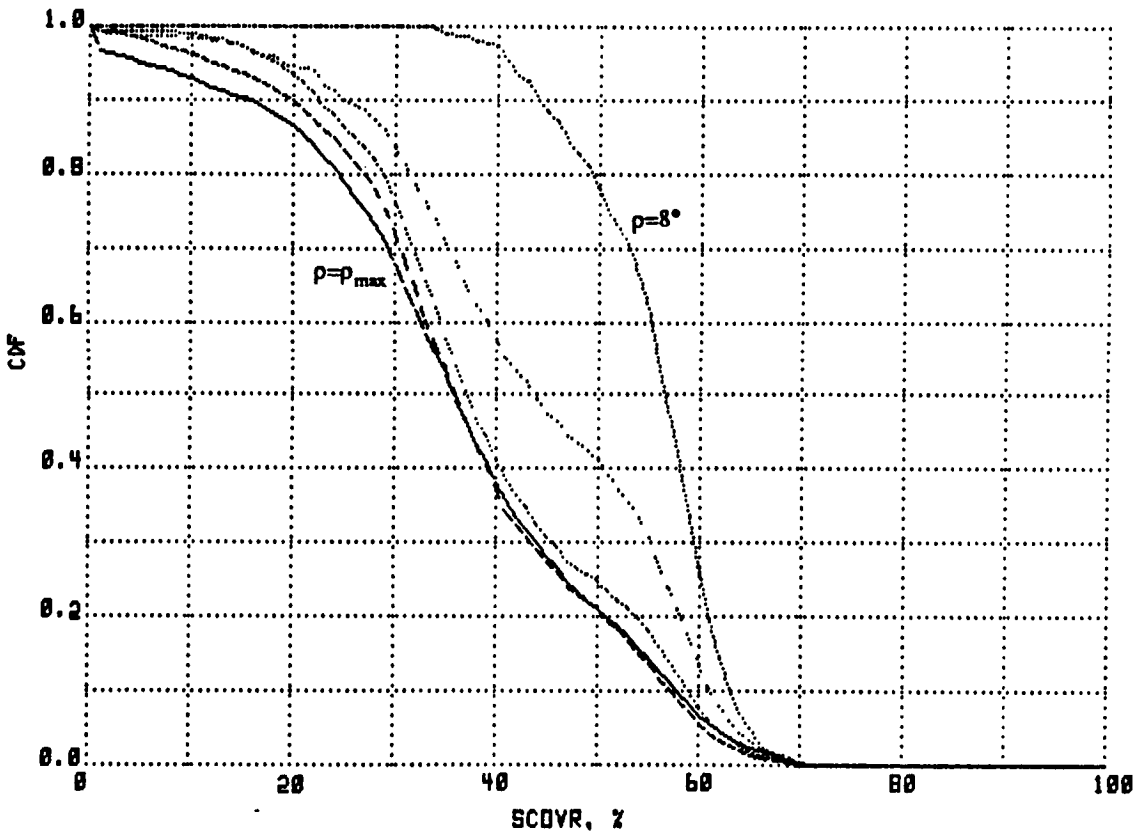

M20P60

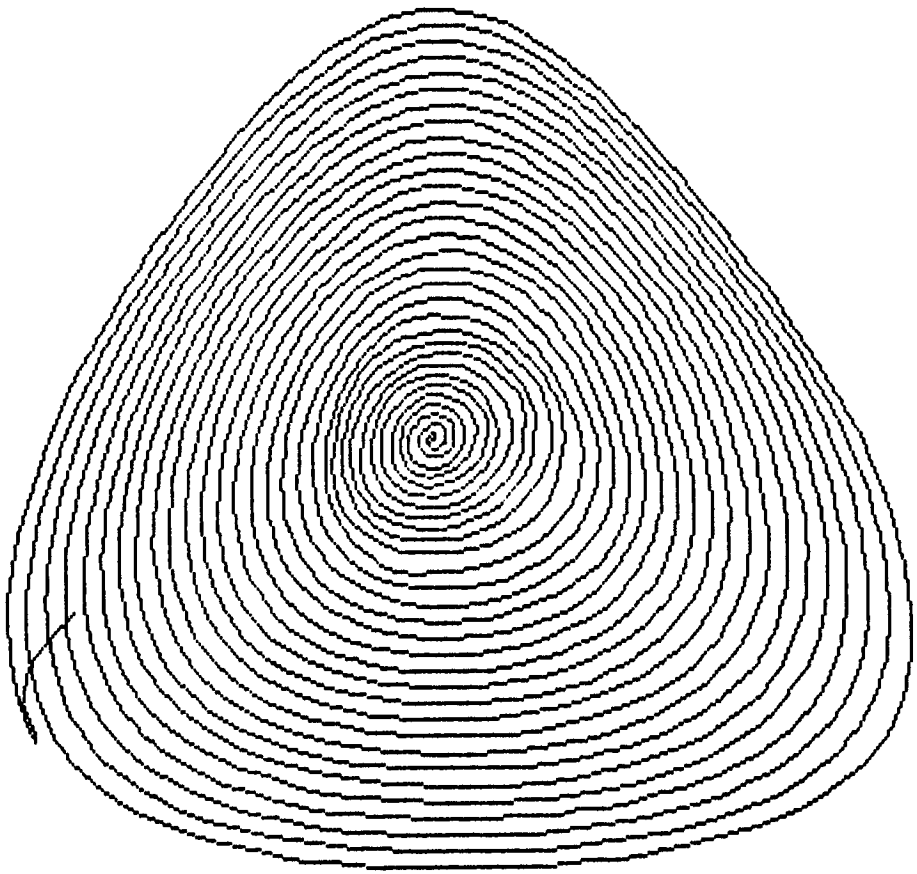

m20p60

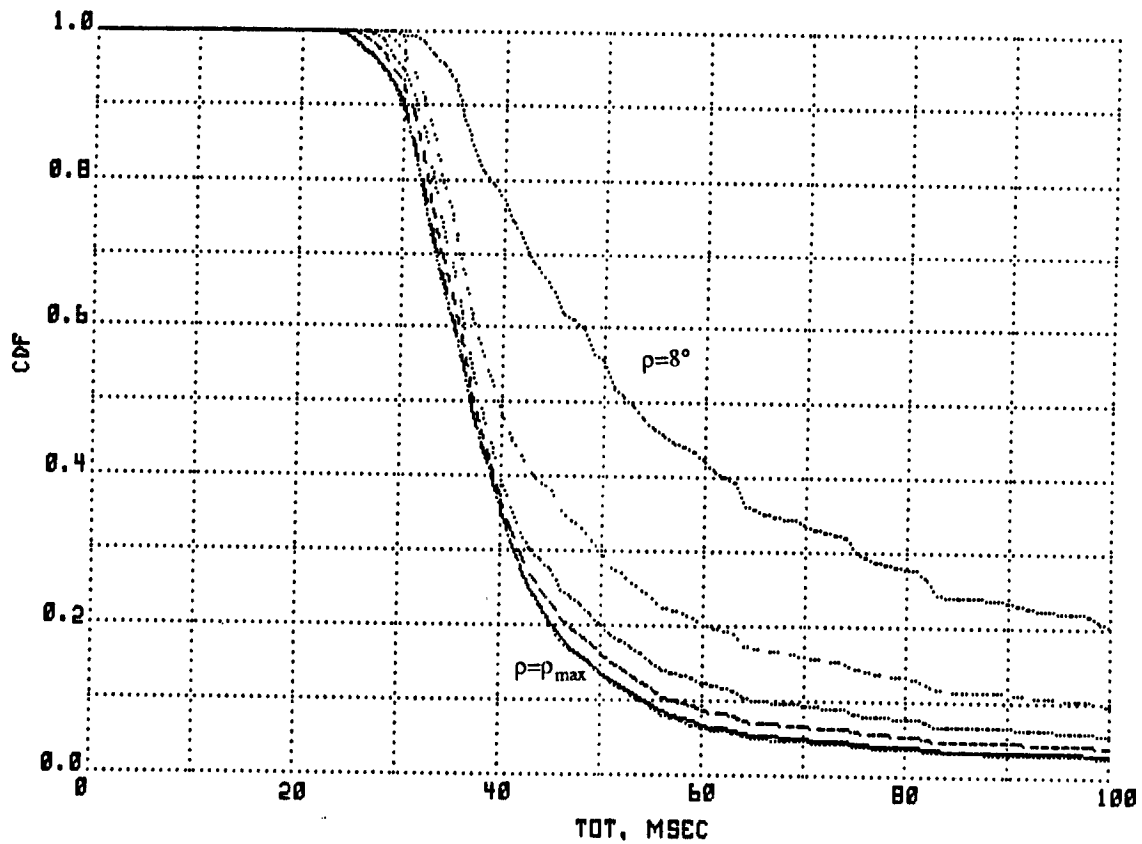

m20p60

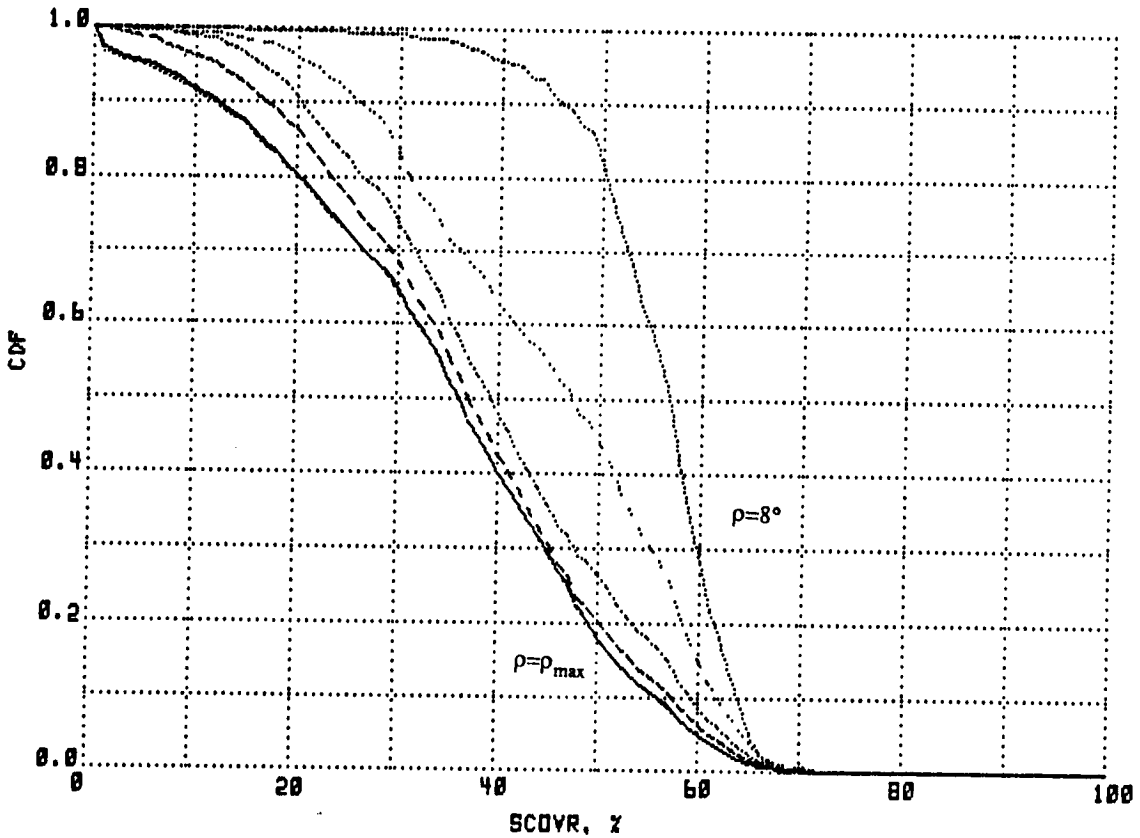

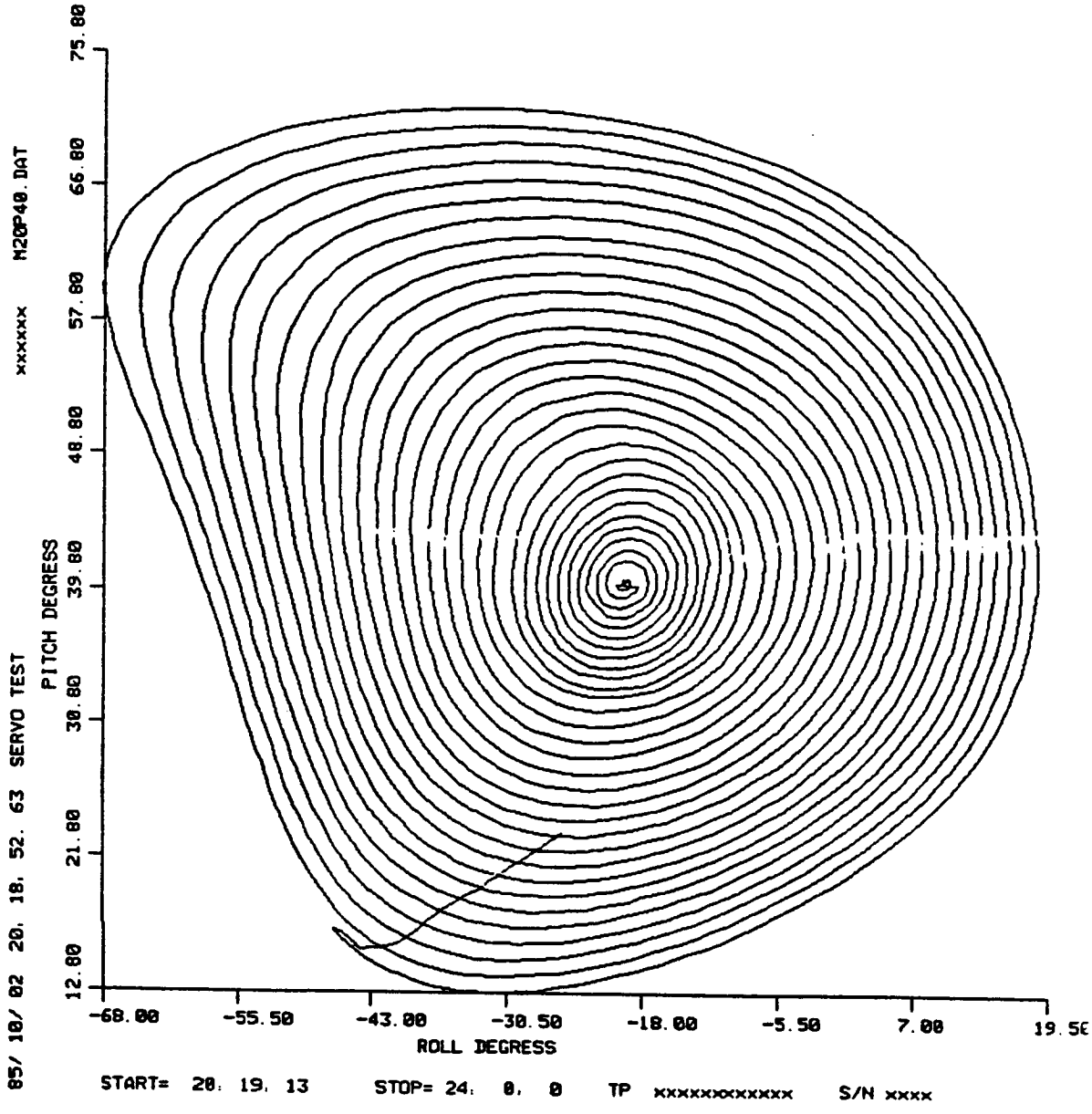
85/ 10/ 02 20: 18: 52. 63 SERVO TEST
xxxxxx M20P40.DAT
PITCH DEGRESS
75.00
66.00
57.00
48.00
39.00
30.00
21.00
12.00
-68.00
-55.50
-43.00
-30.50
-18.00
-5.50
7.00
19.50
ROLL DEGRESS
START= 20: 19: 13
STOP= 24: 0: 0
TP xxxxxxxxxxx
S/N xxxx

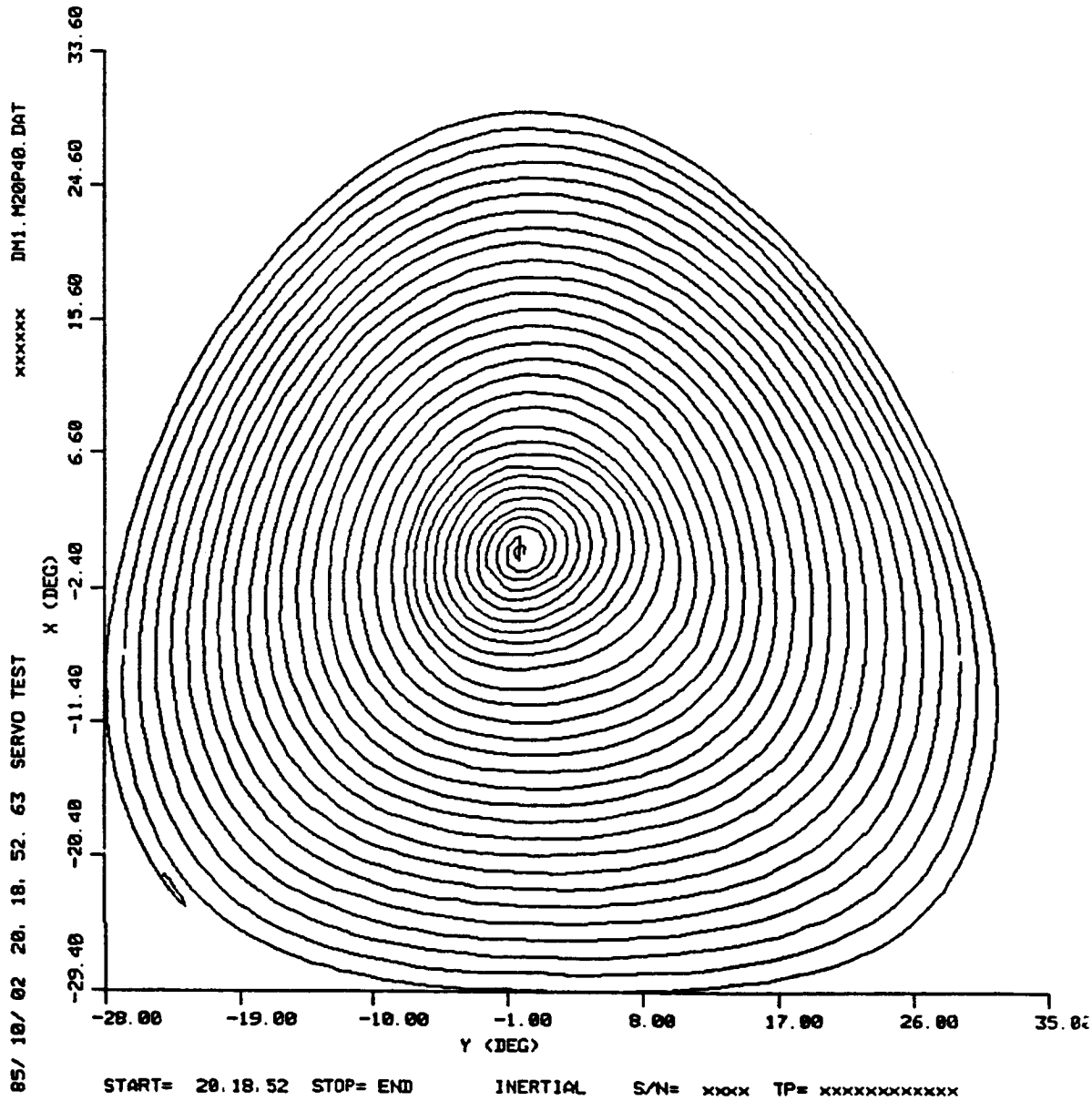
85/ 10/ 02 20. 18. 52. 63 SERVO TEST
xxxxxx DM1.M20P40.DAT
X (DEG)
33.60
24.60
15.60
6.60
-2.40
-11.40
-20.40
-29.40
-28.00
-19.00
-10.00
-1.00
8.00
17.00
26.00
Y (DEG)
START= 20.18.52 STOP= END
INERTIAL
S/N= xxxx TP= xxxxxxxxxxx

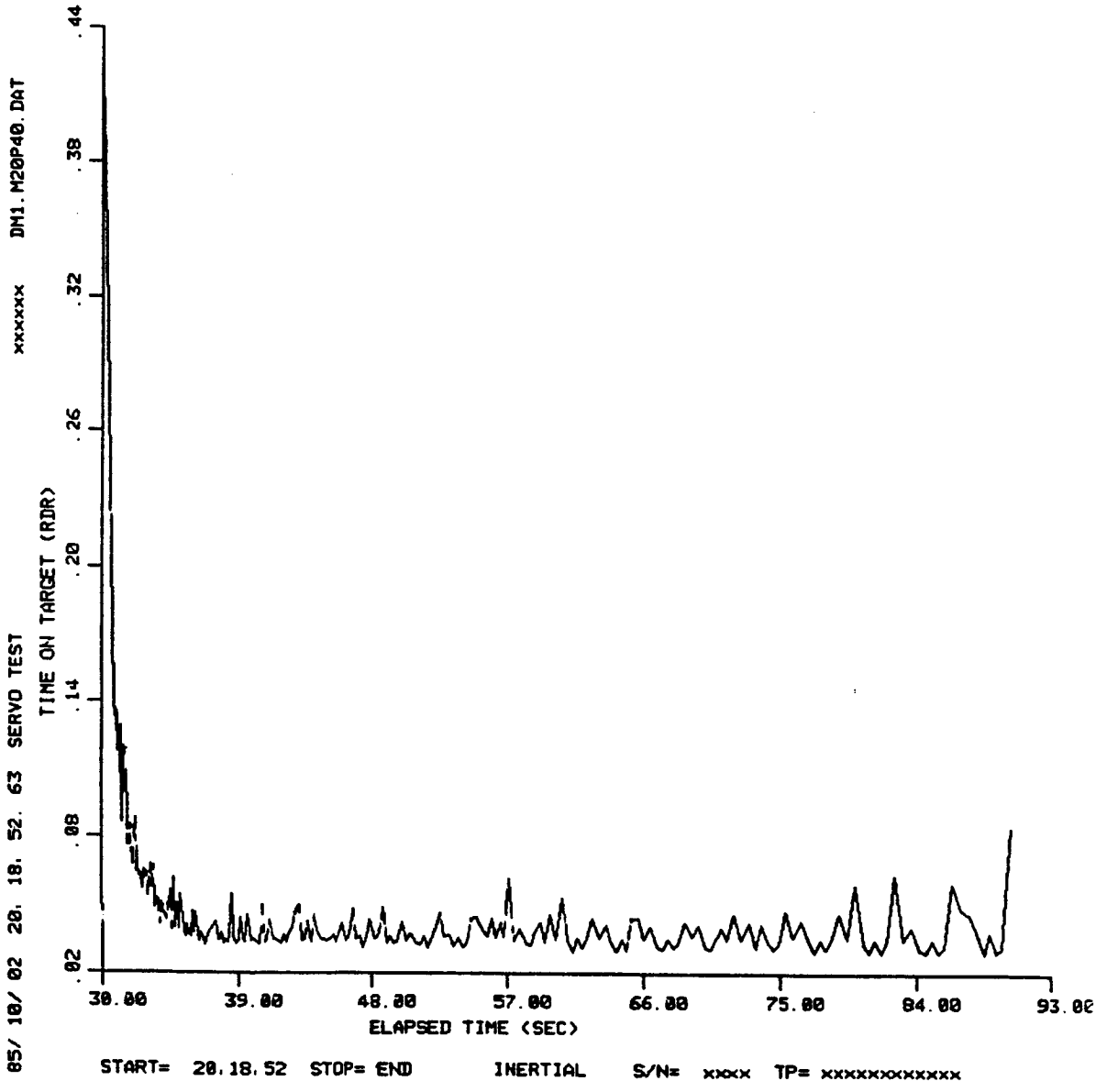
85/ 10/ 02 20. 18. 52. 63 SERVO TEST
xxxxxx DM1.M20P40.DAT
TIME ON TARGET (RDR)
.02
.08
.14
.20
.26
.32
.38
.44
30.00
39.00
48.00
57.00
66.00
75.00
84.00
93.00
ELAPSED TIME (SEC)
START= 20.18.52 STOP= END INERTIAL S/N= xxxx TP= xxxxxxxxxxx

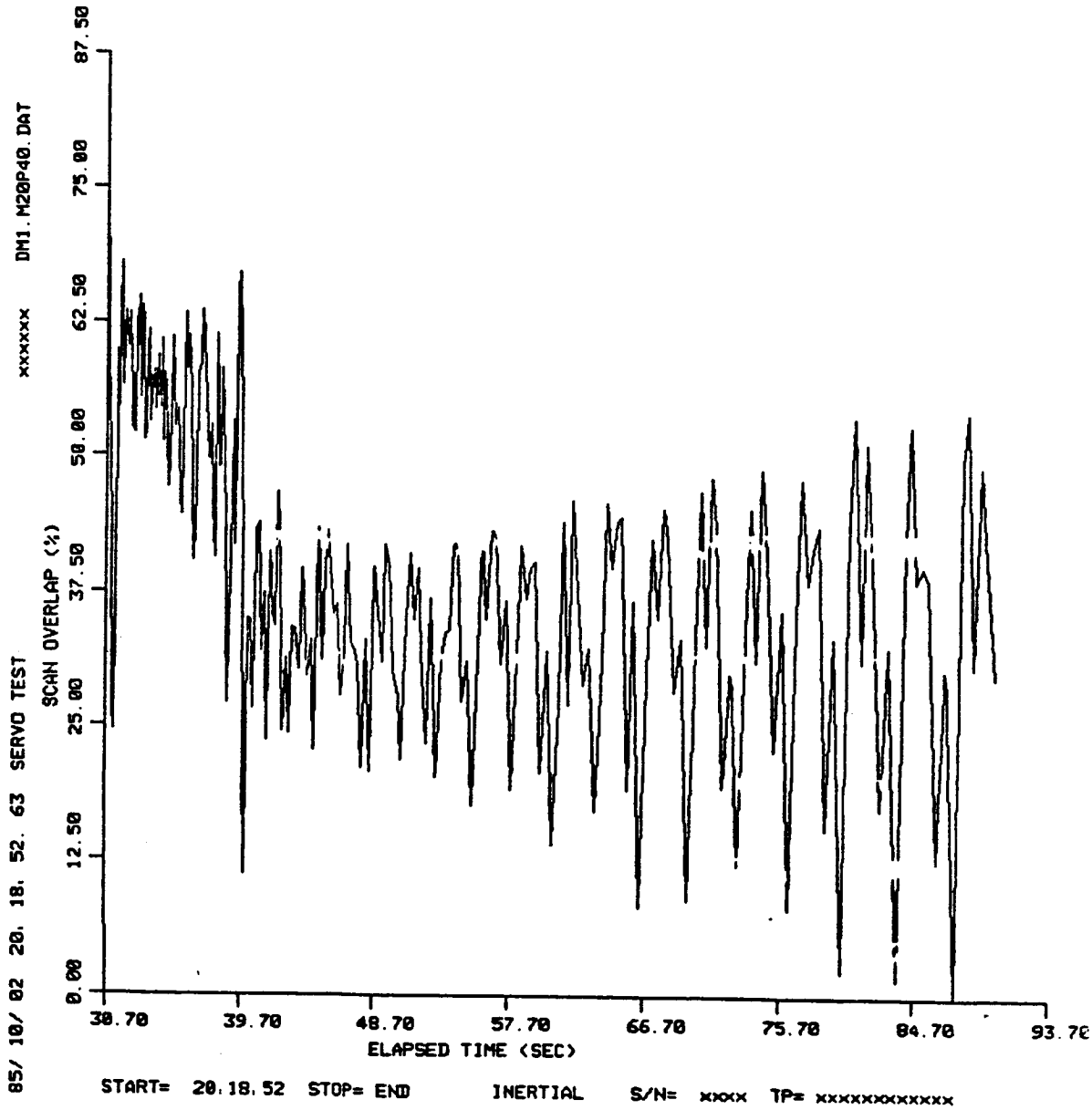
85/ 10/ 02 20. 18. 52. 63 SERVO TEST
xxxxxx DM1.M20P40.DAT
SCAN OVERLAP (%)
0.00
12.50
25.00
37.50
50.00
62.50
75.00
87.50
30.70
39.70
48.70
57.70
66.70
75.70
84.70
93.70
ELAPSED TIME (SEC)
START= 20.18.52 STOP= END
INERTIAL
S/N= xxxx TP= xxxxxxxxxxx

m20p40

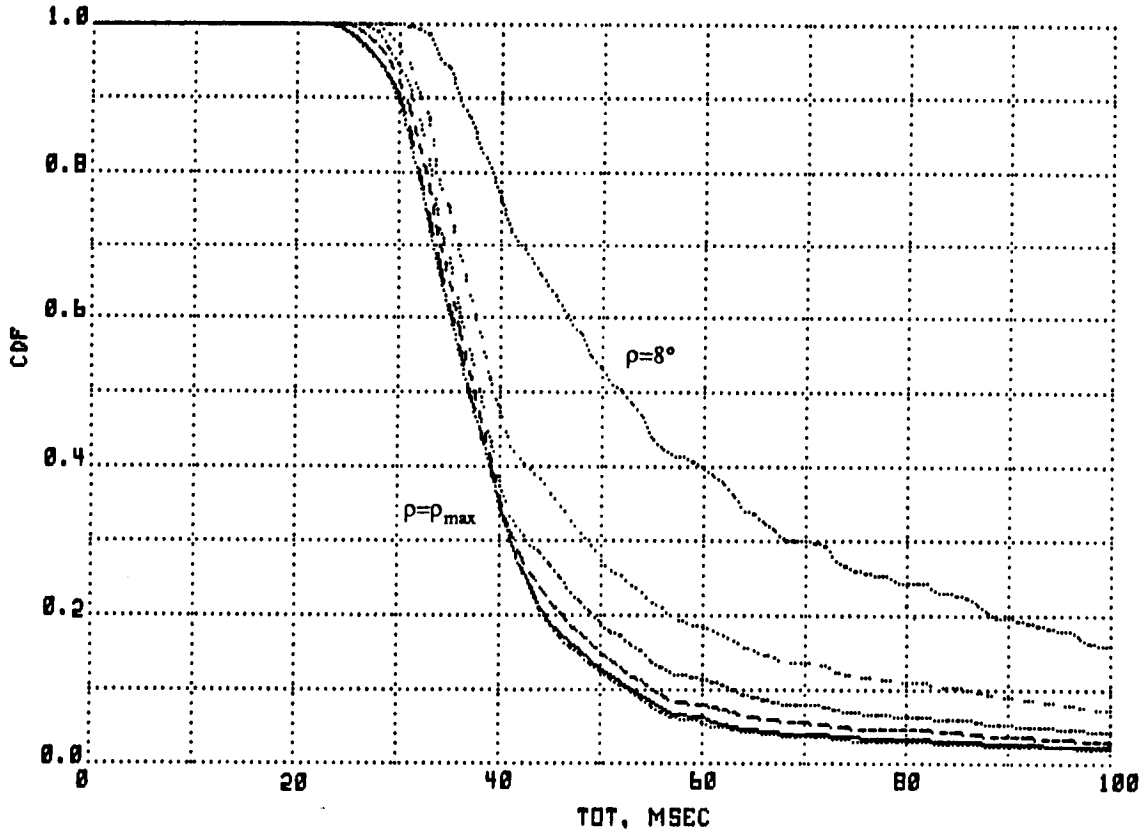

m20p40

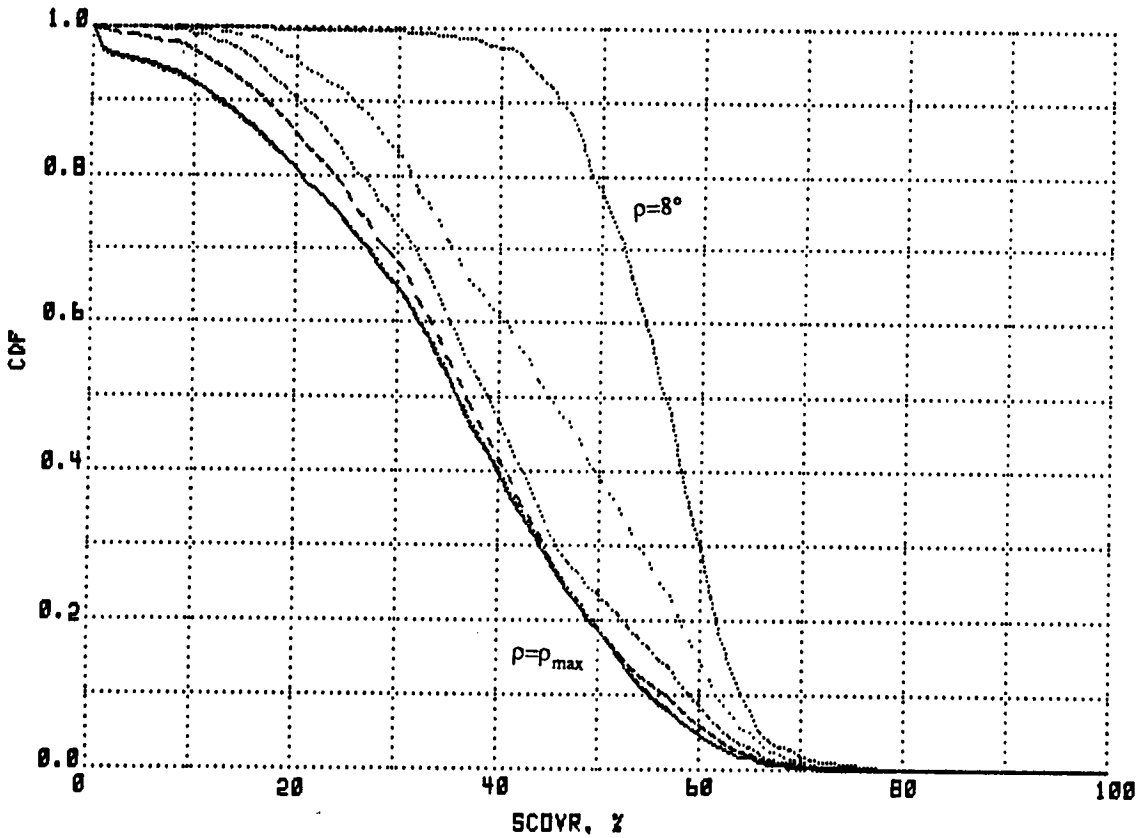

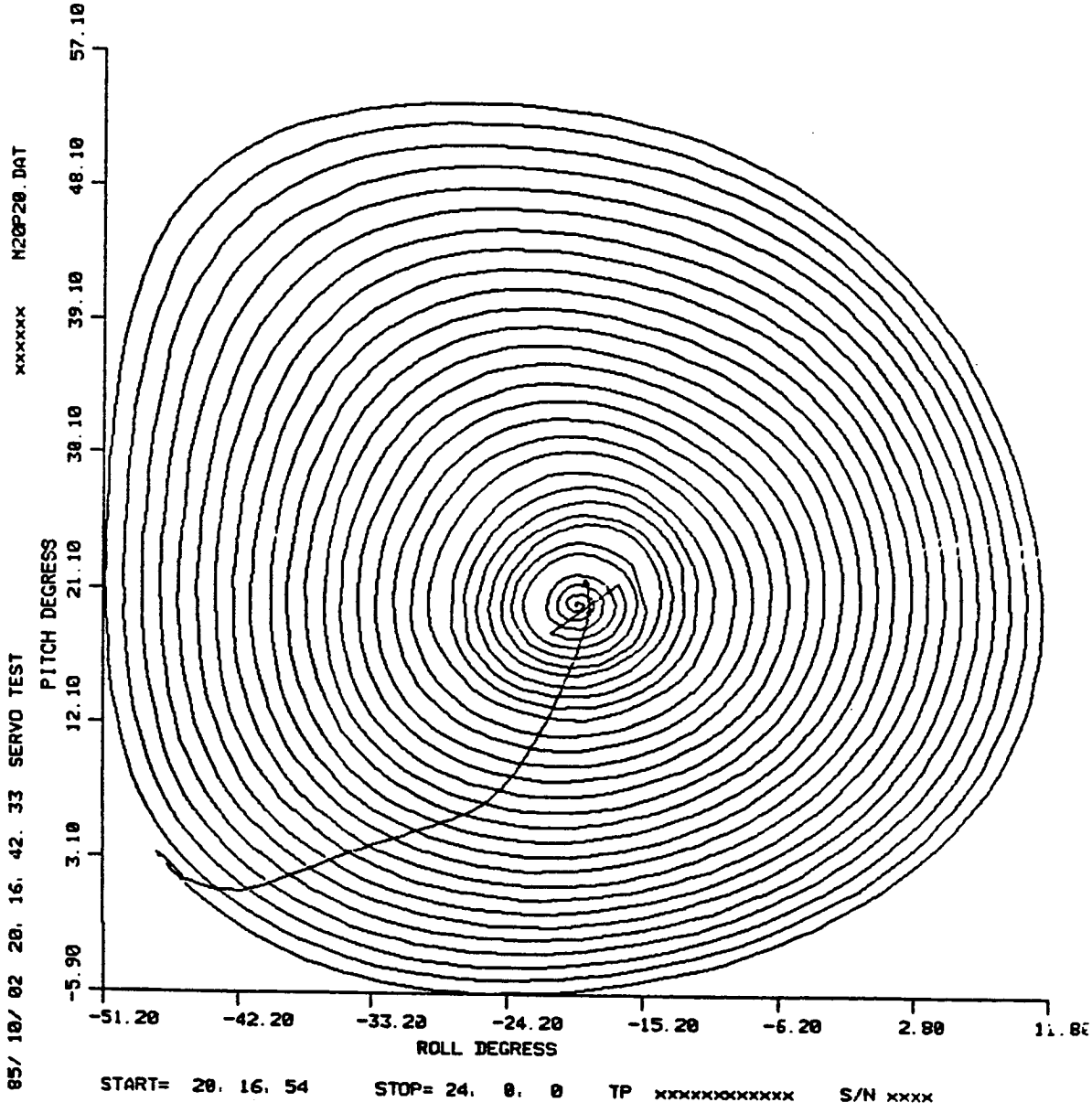
85/ 10/ 02 20. 16. 42. 33 SERVO TEST
xxxxxx M20P20.DAT
PITCH DEGRESS
57.10
48.10
39.10
30.10
21.10
12.10
3.10
-5.90
-51.20
-42.20
-33.20
-24.20
-15.20
-6.20
2.80
ROLL DEGRESS
START= 20. 16. 54
STOP= 24. 0. 0
TP xxxxxxxxxxx
S/N xxxx

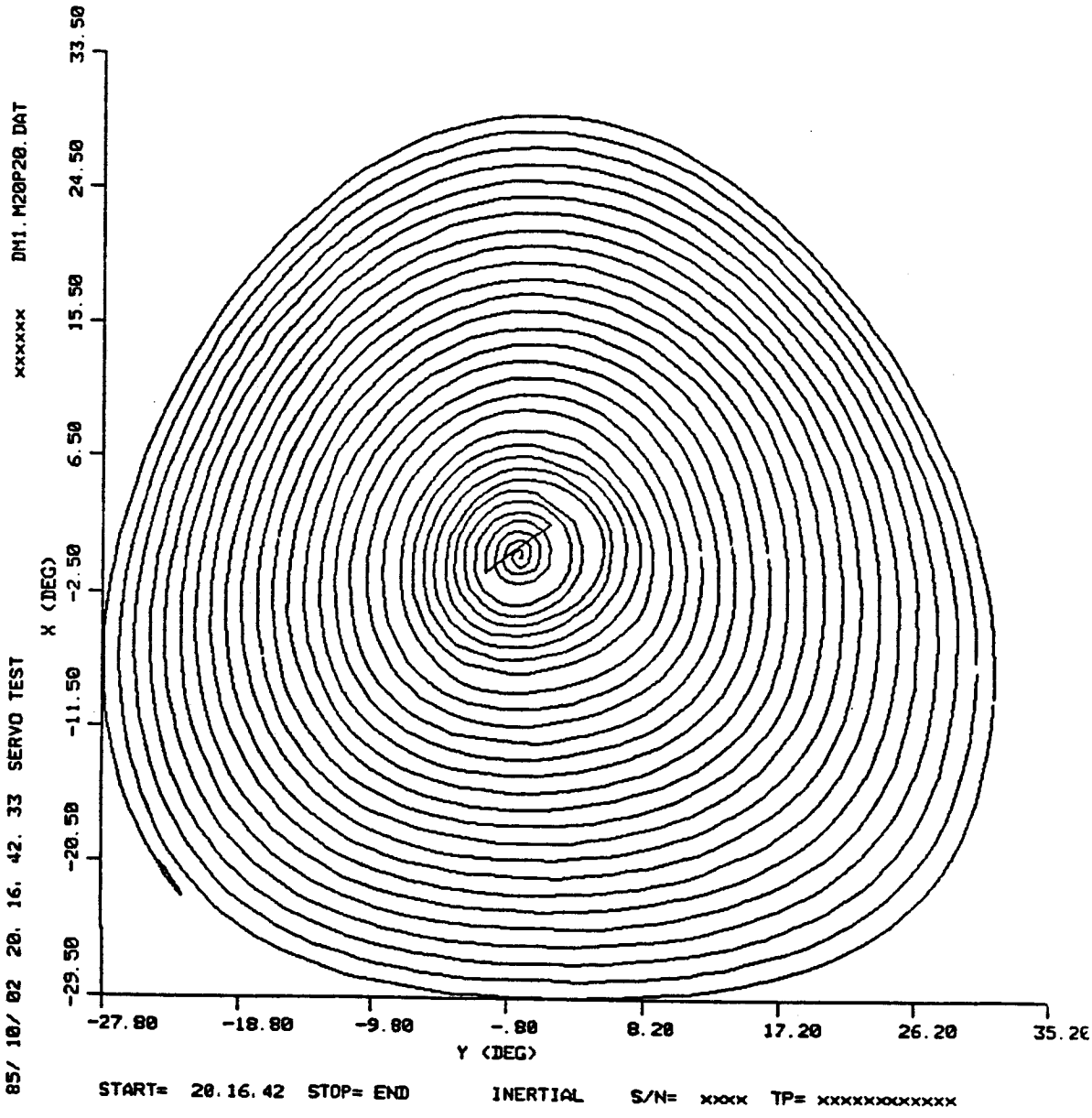
85/ 10/ 02 20. 16. 42. 33 SERVO TEST
XXXXXX DN1.M20P20.DAT
X (DEG)
33.50
24.50
15.50
6.50
-2.50
-11.50
-20.50
-29.50
-27.80
-18.80
-9.80
-.80
8.20
17.20
26.20
35.20
Y (DEG)
START= 20.16.42 STOP= END
INERTIAL
S/N= xxxx TP= xxxxxxxxxxx

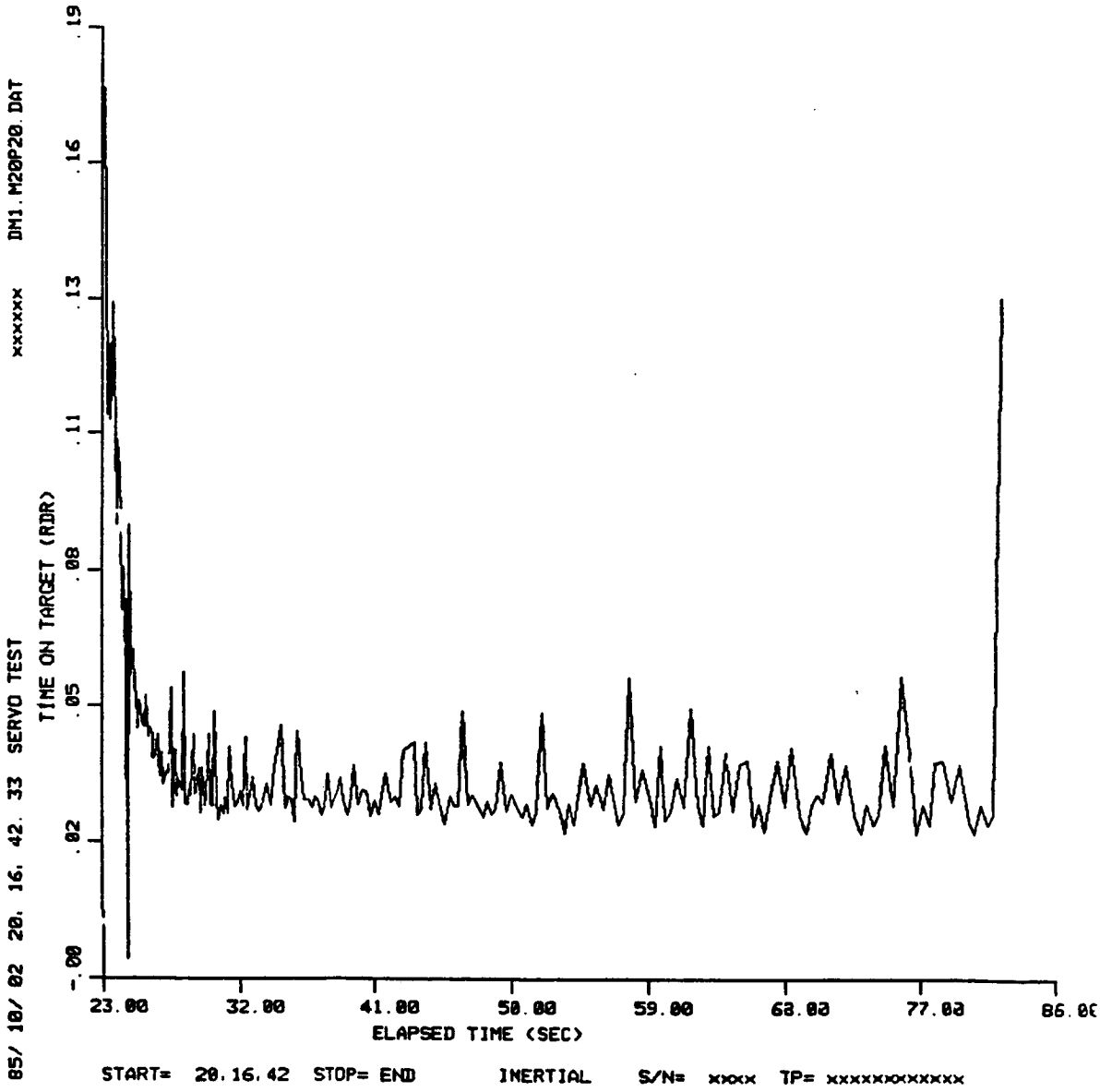
85/ 10/ 02 20. 16. 42. 33 SERVO TEST
xxxxxx DM1.M20P20.DAT
TIME ON TARGET (RDR)
-.00
.02
.05
.08
.11
.13
.16
.19
23.00
32.00
41.00
50.00
59.00
68.00
77.00
86.00
ELAPSED TIME (SEC)
START= 20.16.42 STOP= END INERTIAL S/N= xxxx TP= xxxxxxxxxxx

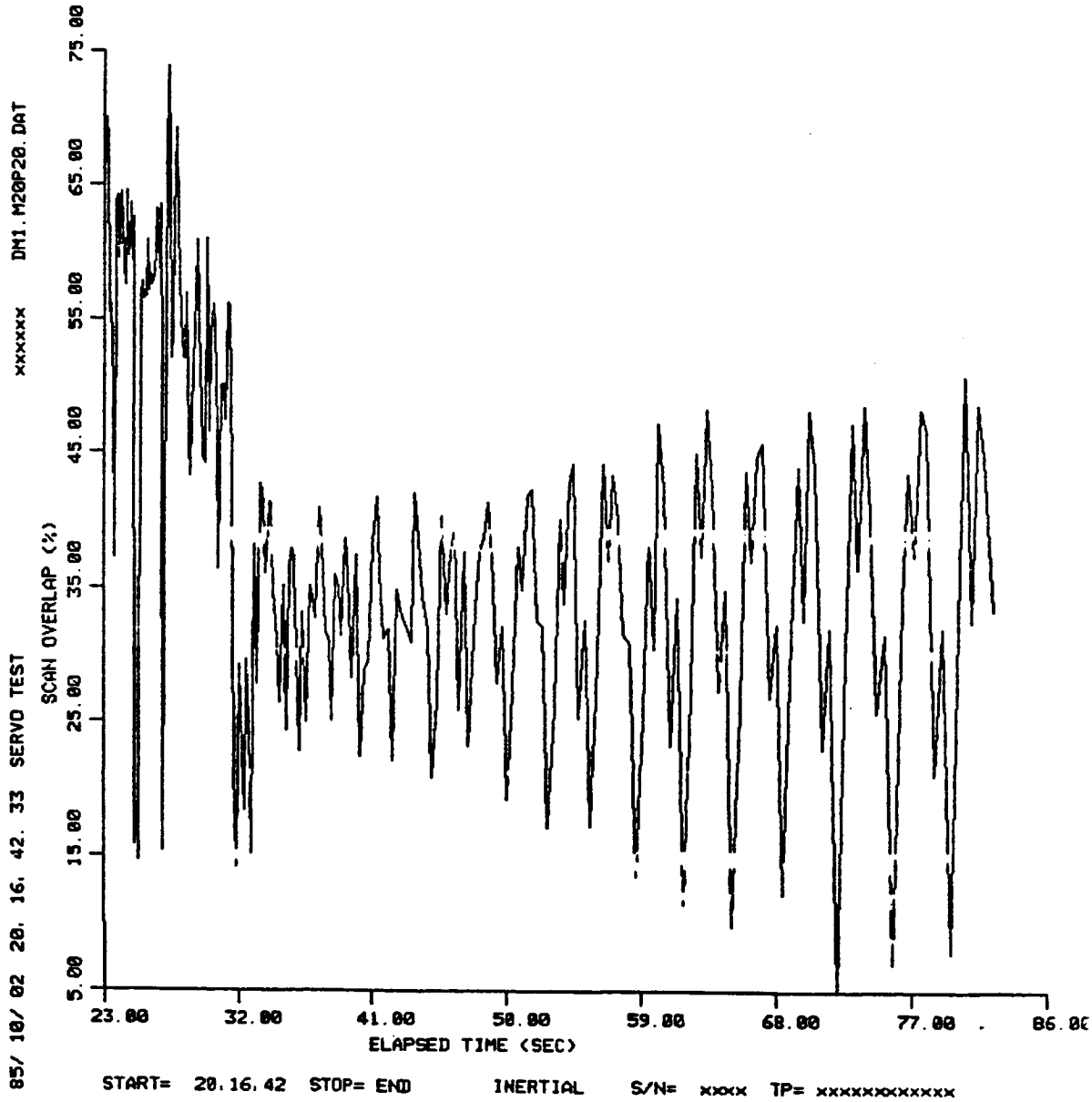
85/ 10/ 02 20. 16. 42. 33 SERVO TEST
xxxxxx DM1.M20P20.DAT
SCAN OVERLAP (%)
5.00
15.00
25.00
35.00
45.00
55.00
65.00
75.00
23.00
32.00
41.00
50.00
59.00
68.00
77.00
86.00
ELAPSED TIME (SEC)
START= 20.16.42 STOP= END
INERTIAL
S/N= xxxx TP= xxxxxxxxxxx

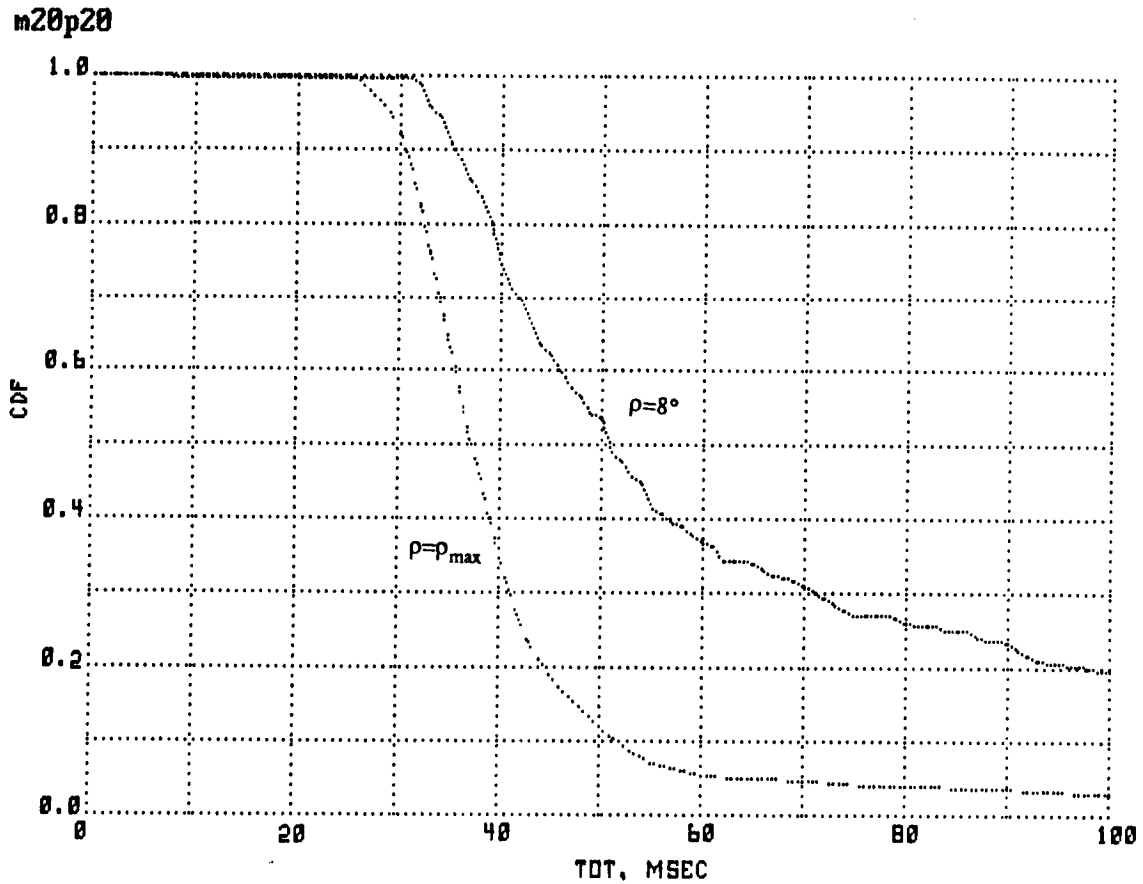
m20p20
1.0
0.8
0.6
0.4
0.2
0.0
CDF
ρ=8°
ρ=ρmax
0
20
40
60
80
100
TOT, MSEC

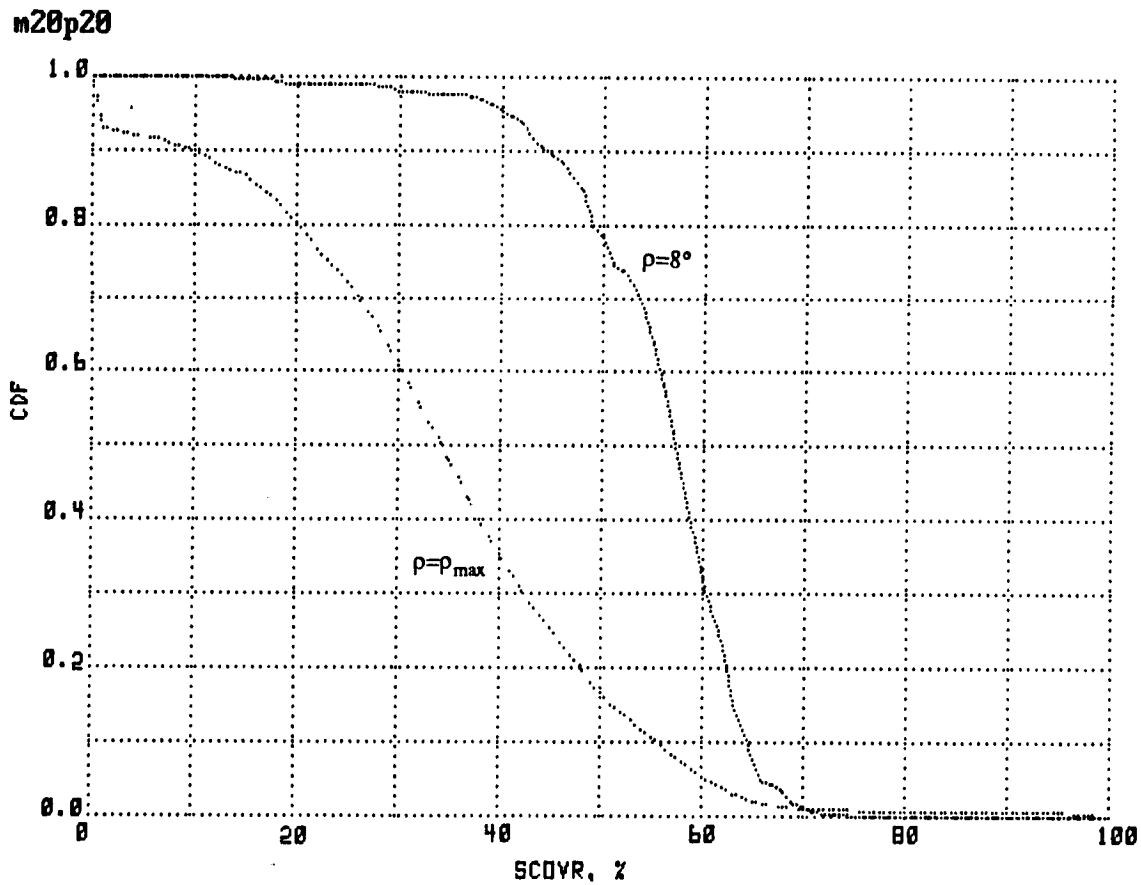
m20p20
1.0
0.8
0.6
0.4
0.2
0.0
CDF
ρ=8°
ρ=ρmax
0
20
40
60
80
100
SCOVR, %

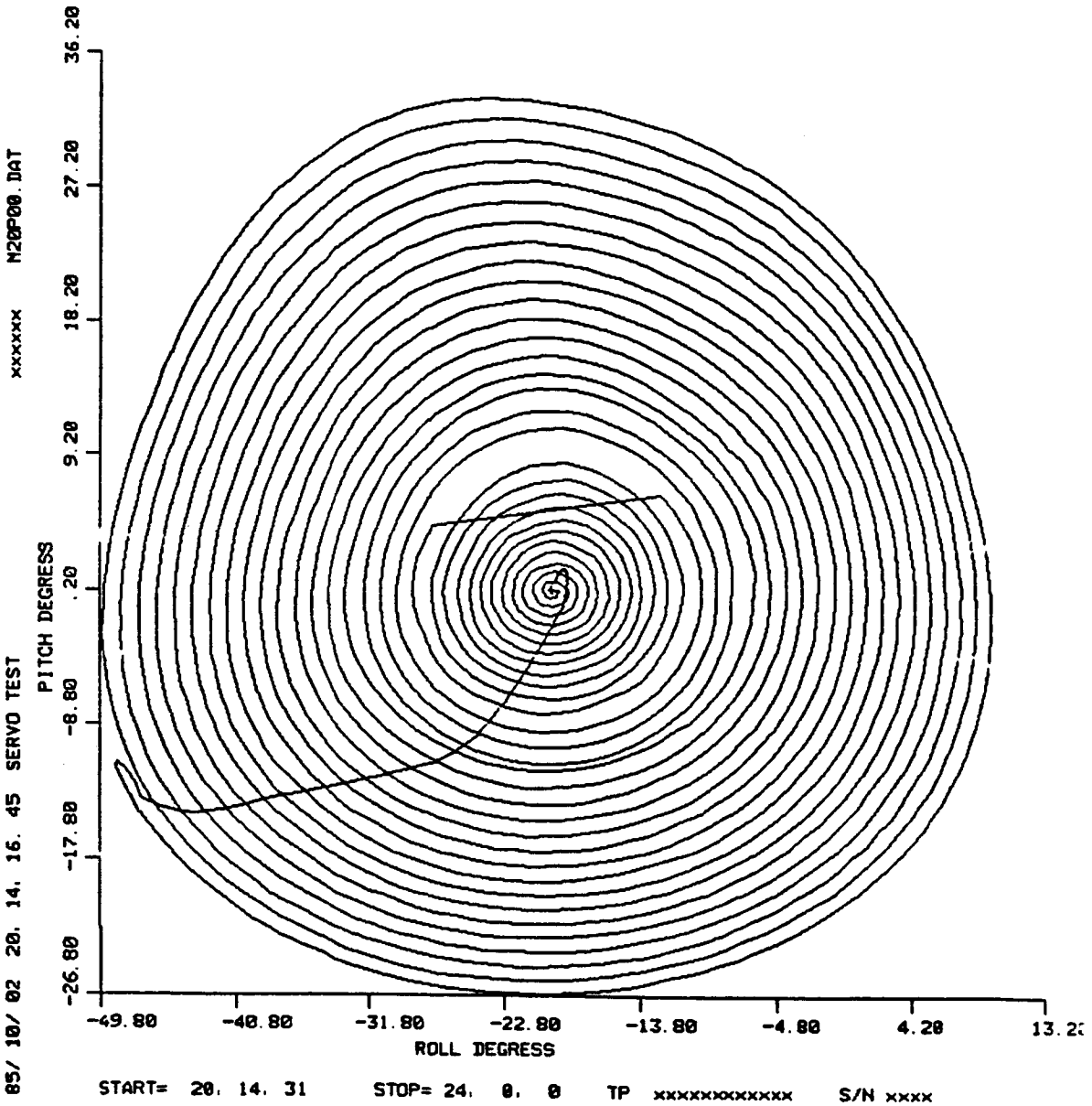
85/ 10/ 02 20. 14. 16. 45 SERVO TEST
xxxxxx N20P00.DAT
PITCH DEGRESS
36.20
27.20
18.20
9.20
.20
-8.80
-17.80
-26.80
-49.80
-40.80
-31.80
-22.80
-13.80
-4.80
4.20
ROLL DEGRESS
START= 20. 14. 31
STOP= 24. 0. 0
TP xxxxxxxxxxx
S/N xxxx

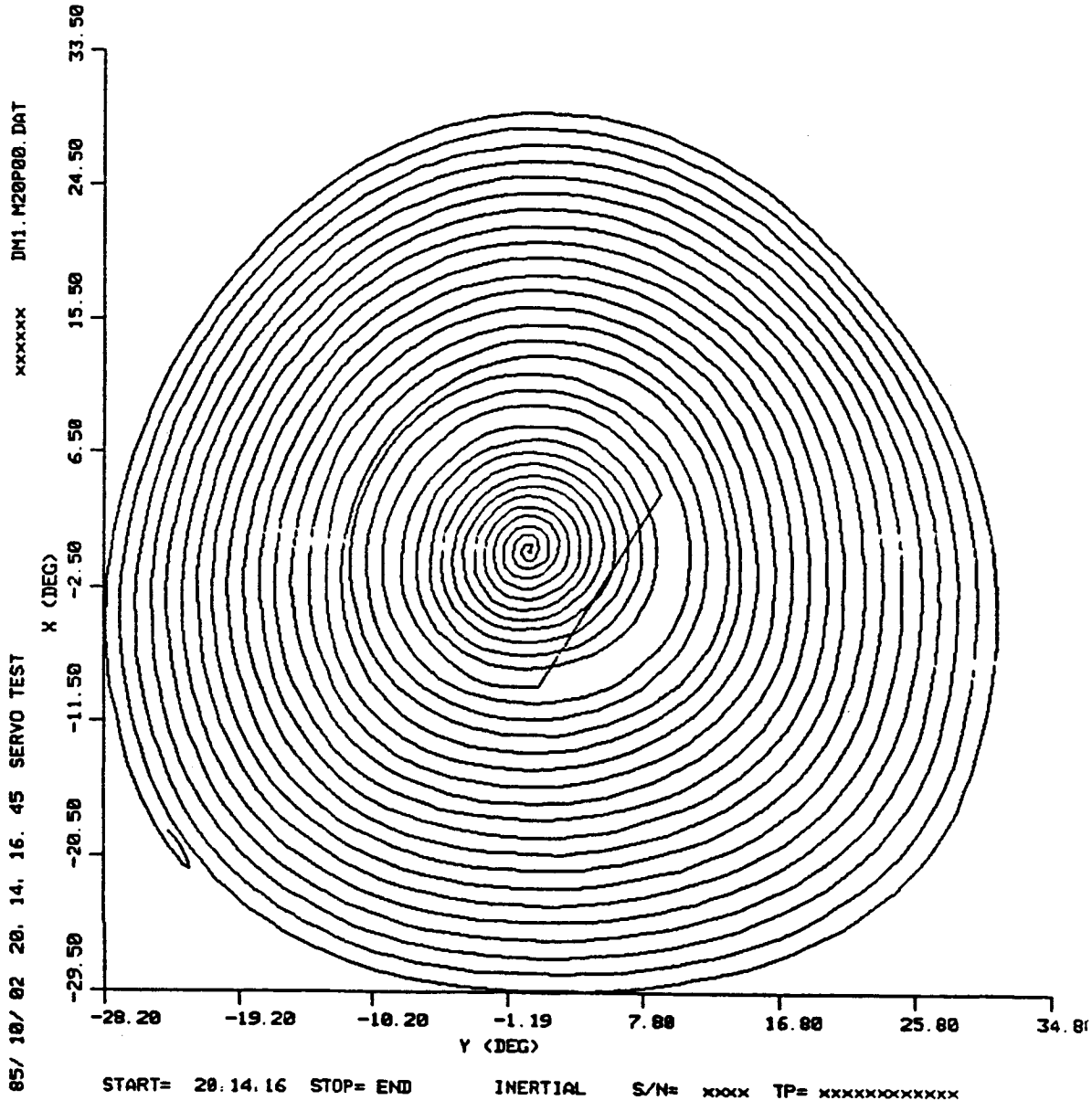
85/ 10/ 02 20. 14. 16. 45 SERVO TEST
XXXXXX DM1.M20P00.DAT
X (DEG)
33.50
24.50
15.50
6.50
-2.50
-11.50
-20.50
-29.50
-28.20
-19.20
-10.20
-1.19
7.80
16.80
25.80
34.8
Y (DEG)
START= 20:14:16 STOP= END
INERTIAL
S/N= XXXX TP= XXXXXXXXXXX

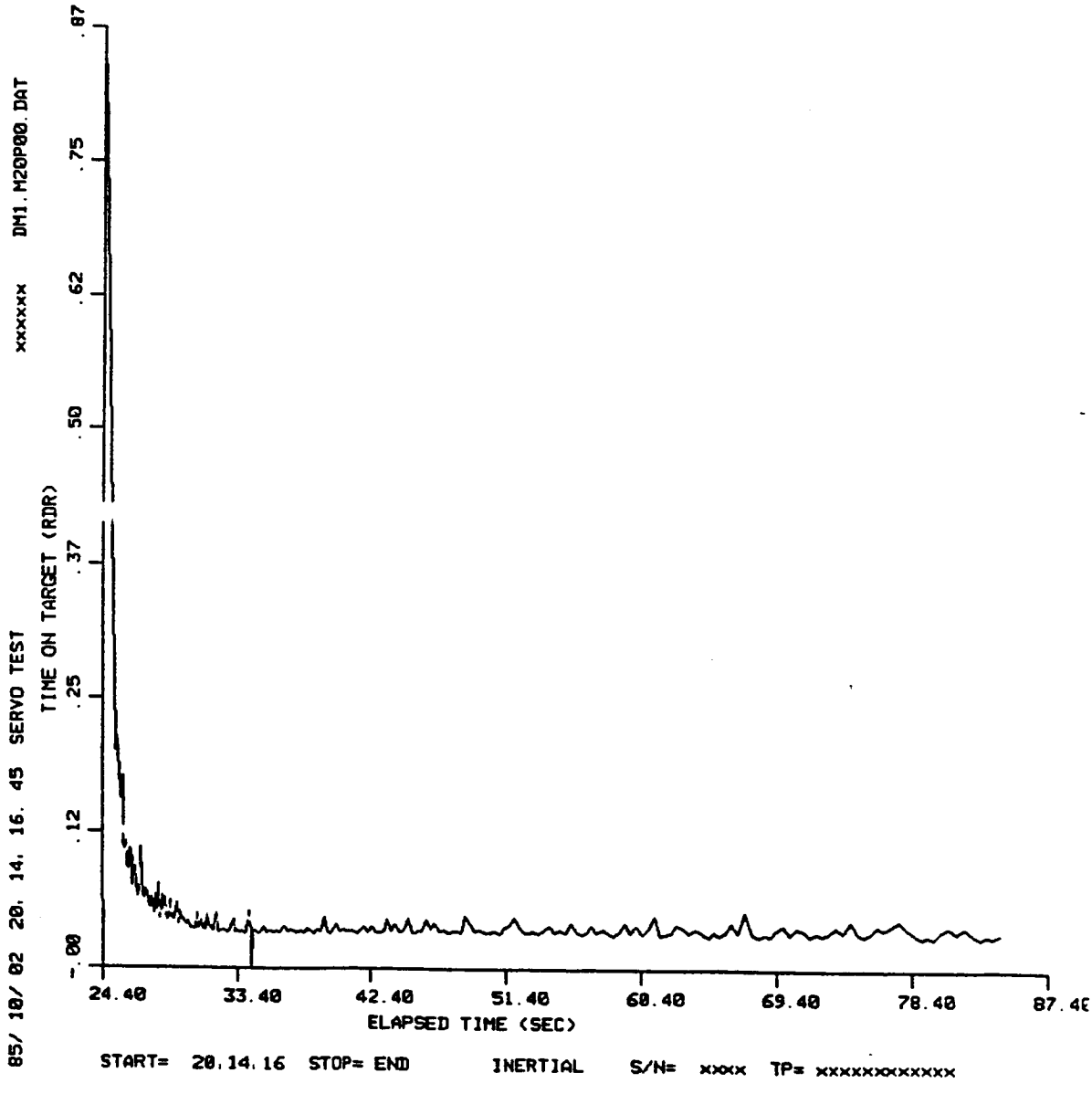
85/ 10/ 02 20. 14. 16. 45 SERVO TEST
xxxxxx DM1.M20P00.DAT
TIME ON TARGET (RDR)
-.00
.12
.25
.37
.50
.62
.75
.87
24.40
33.40
42.40
51.40
60.40
69.40
78.40
87.40
ELAPSED TIME (SEC)
START= 20.14.16 STOP= END INERTIAL S/N= xxxx TP= xxxxxxxxxxx

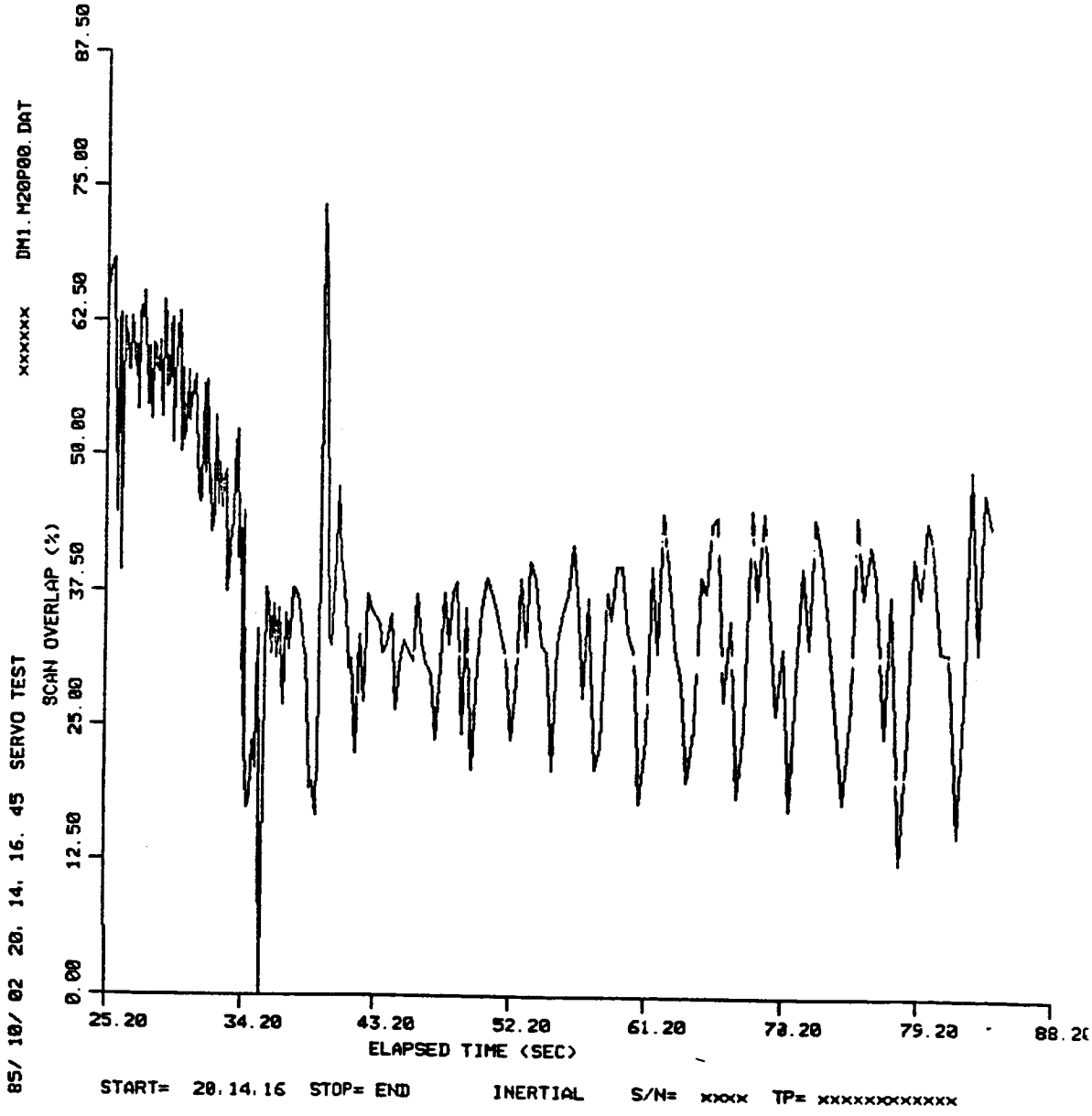
85/ 10/ 02 20. 14. 16. 45 SERVO TEST
xxxxxx DM1.M20P00.DAT
SCAN OVERLAP (%)
0.00
12.50
25.00
37.50
50.00
62.50
75.00
87.50
25.20
34.20
43.20
52.20
61.20
70.20
79.20
88.20
ELAPSED TIME (SEC)
START= 20.14.16 STOP= END
INERTIAL
S/N= xxxx TP= xxxxxxxxxxx

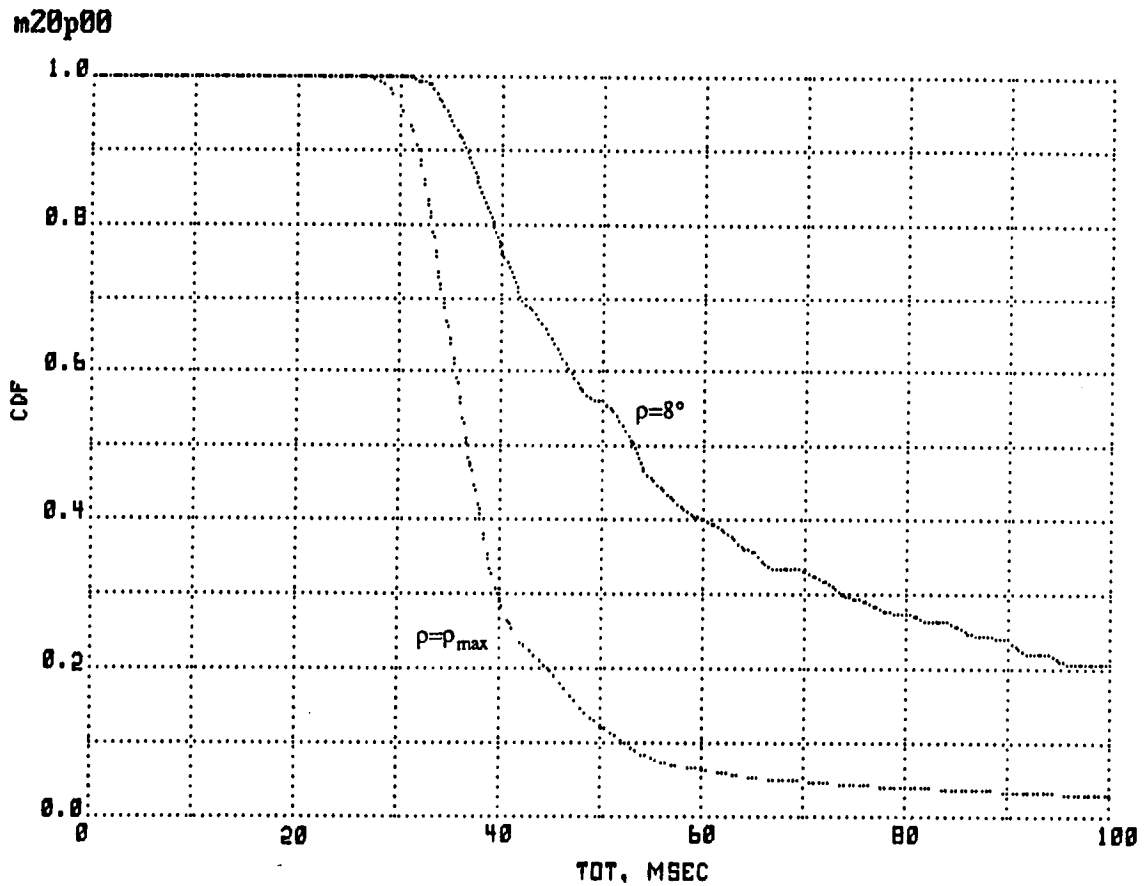
m20p00
1.0
0.8
0.6
0.4
0.2
0.0
CDF
ρ=8°
ρ=ρmax
0
20
40
60
80
100
TOT, MSEC

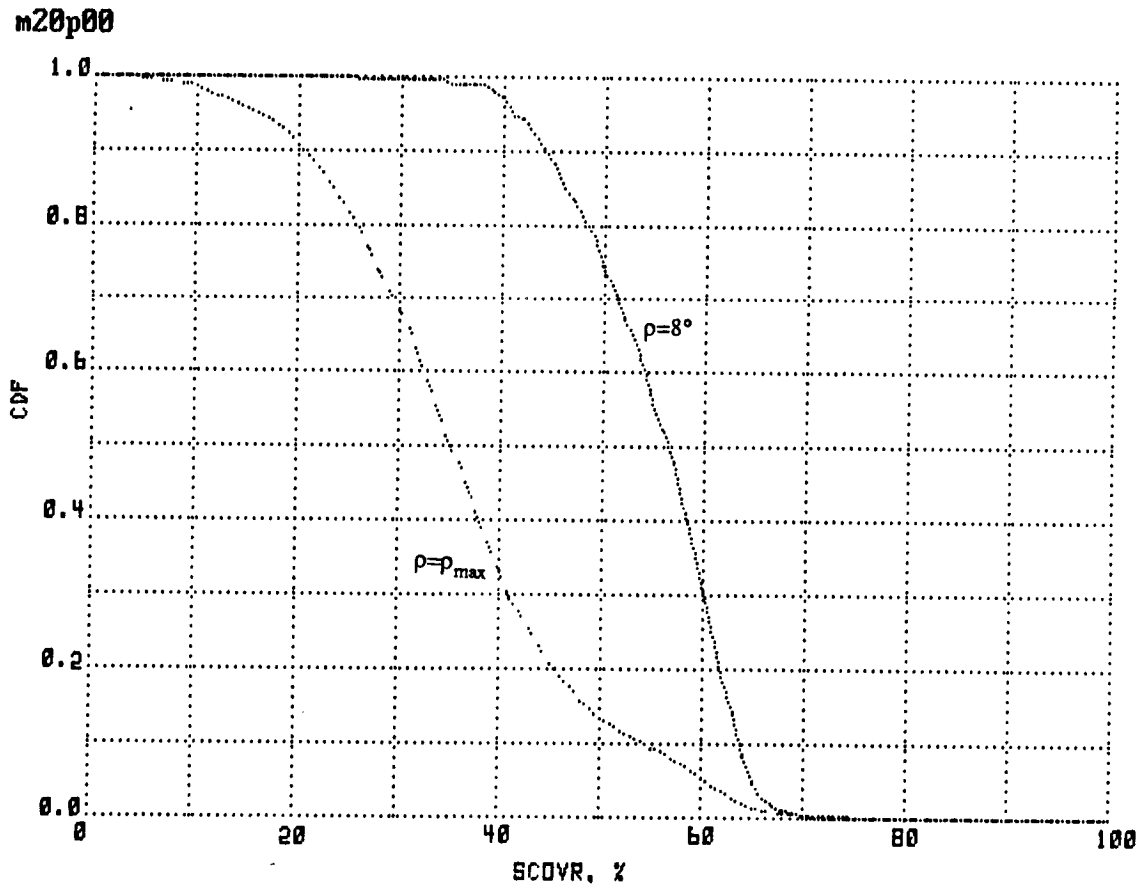
m20p00
1.0
0.8
0.6
0.4
0.2
0.0
CDF
0
20
40
60
80
100
SCOVR, %
ρ=8°
ρ=ρmax

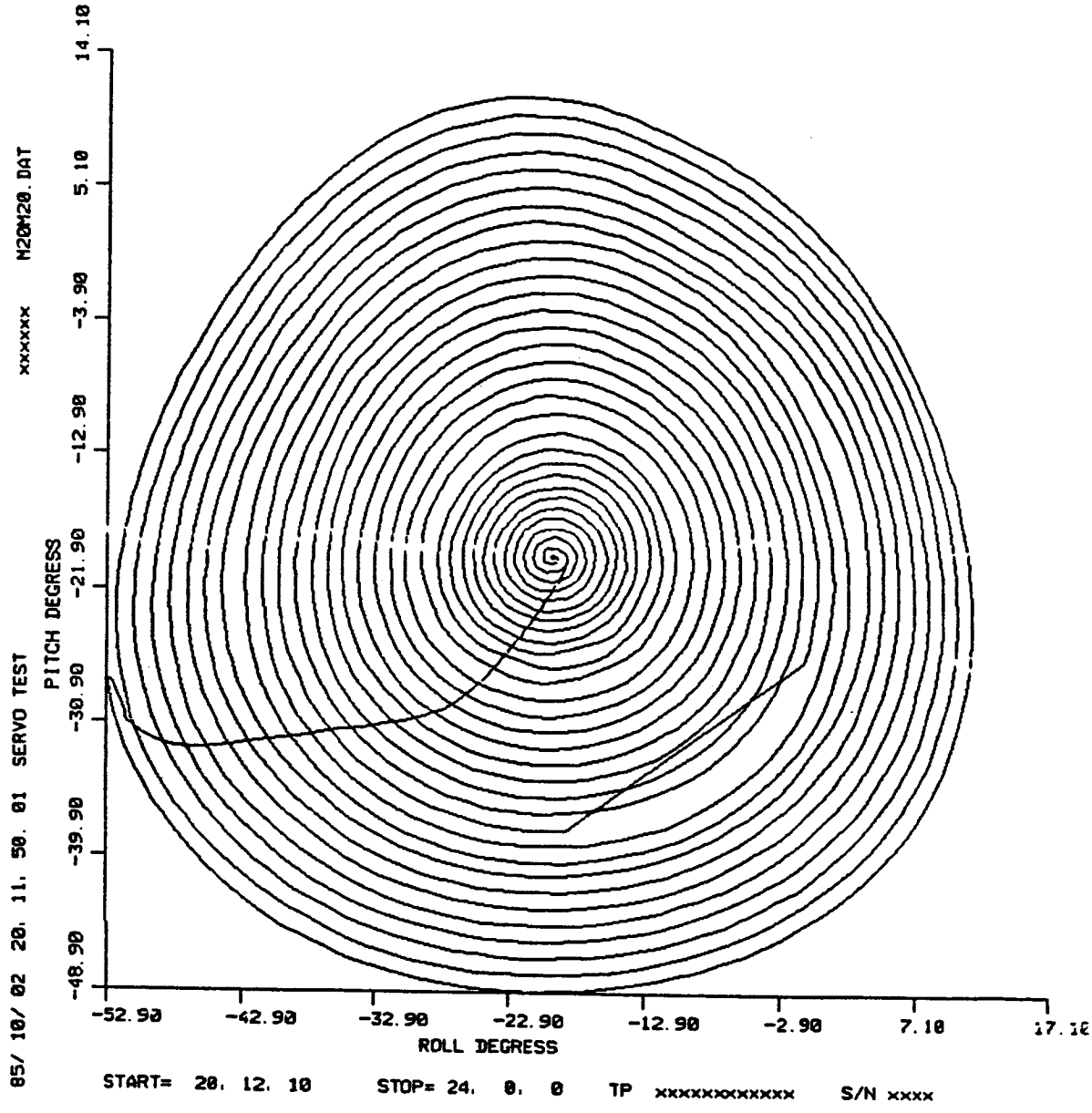
85/ 10/ 02 20. 11. 50. 01 SERVO TEST
xxxxxx M20M20.DAT
PITCH DEGRESS
14.10
5.10
-3.90
-12.90
-21.90
-30.90
-39.90
-48.90
-52.90
-42.90
-32.90
-22.90
-12.90
-2.90
7.10
17.10
ROLL DEGRESS
START= 20. 12. 10
STOP= 24. 0. 0
TP xxxxxxxxxxx
S/N xxxx

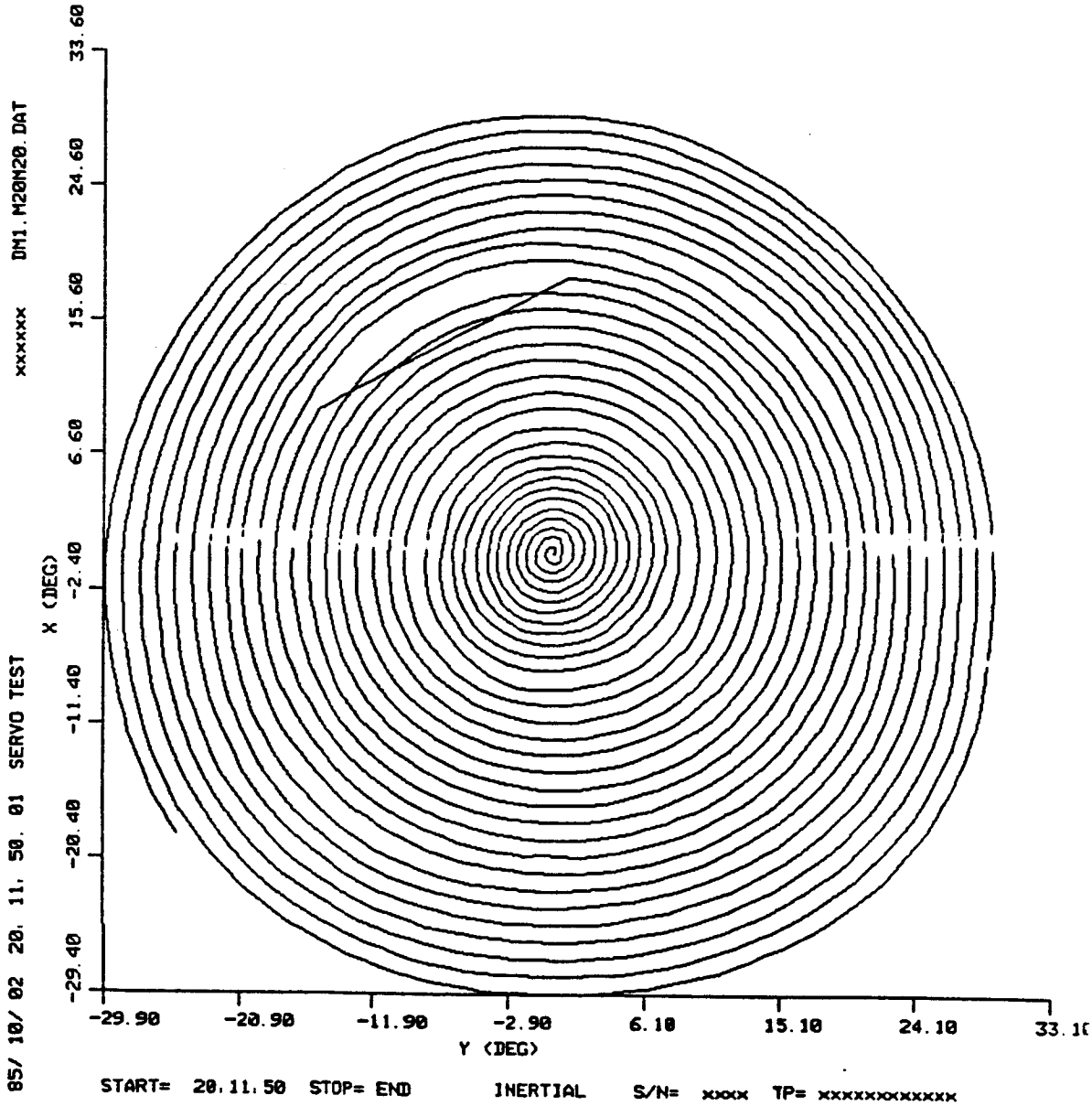
85/ 10/ 02 20. 11. 50. 01 SERVO TEST
xxxxxx DM1.M20N20.DAT
X (DEG)
33.60
24.60
15.60
6.60
-2.40
-11.40
-20.40
-29.40
-29.90
-20.90
-11.90
-2.90
6.10
15.10
24.10
33.1
Y (DEG)
START= 20.11.50 STOP= END
INERTIAL
S/N= xxxx TP= xxxxxxxxxxx

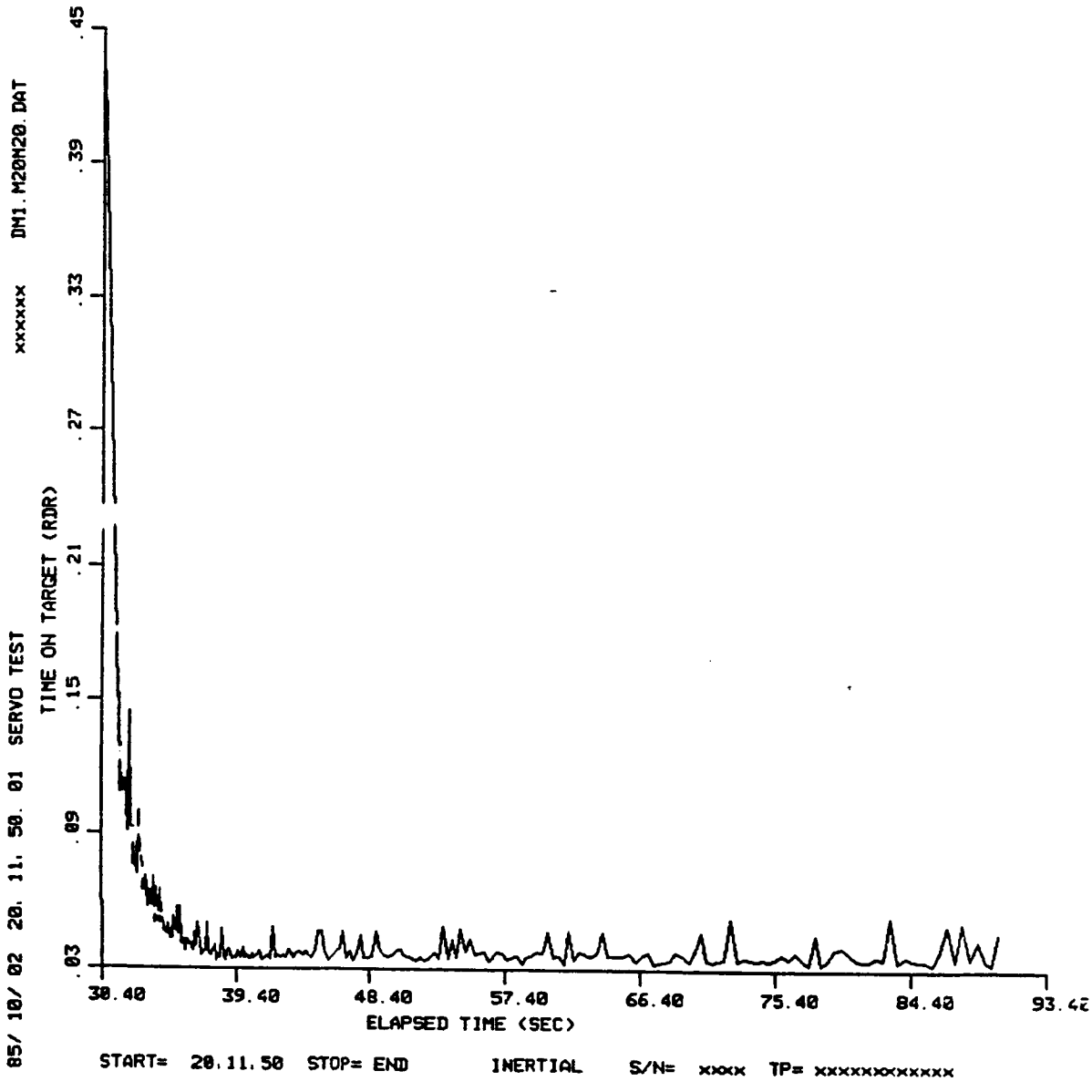
85/ 10/ 02 20. 11. 50. 01 SERVO TEST
TIME ON TARGET (RDR)
xxxxxx DM1.M20M20.DAT
.03
.09
.15
.21
.27
.33
.39
.45
30.40
39.40
48.40
57.40
66.40
75.40
84.40
93.42
ELAPSED TIME (SEC)
START= 20.11.50 STOP= END INERTIAL S/N= xxxx TP= xxxxxxxxxxx

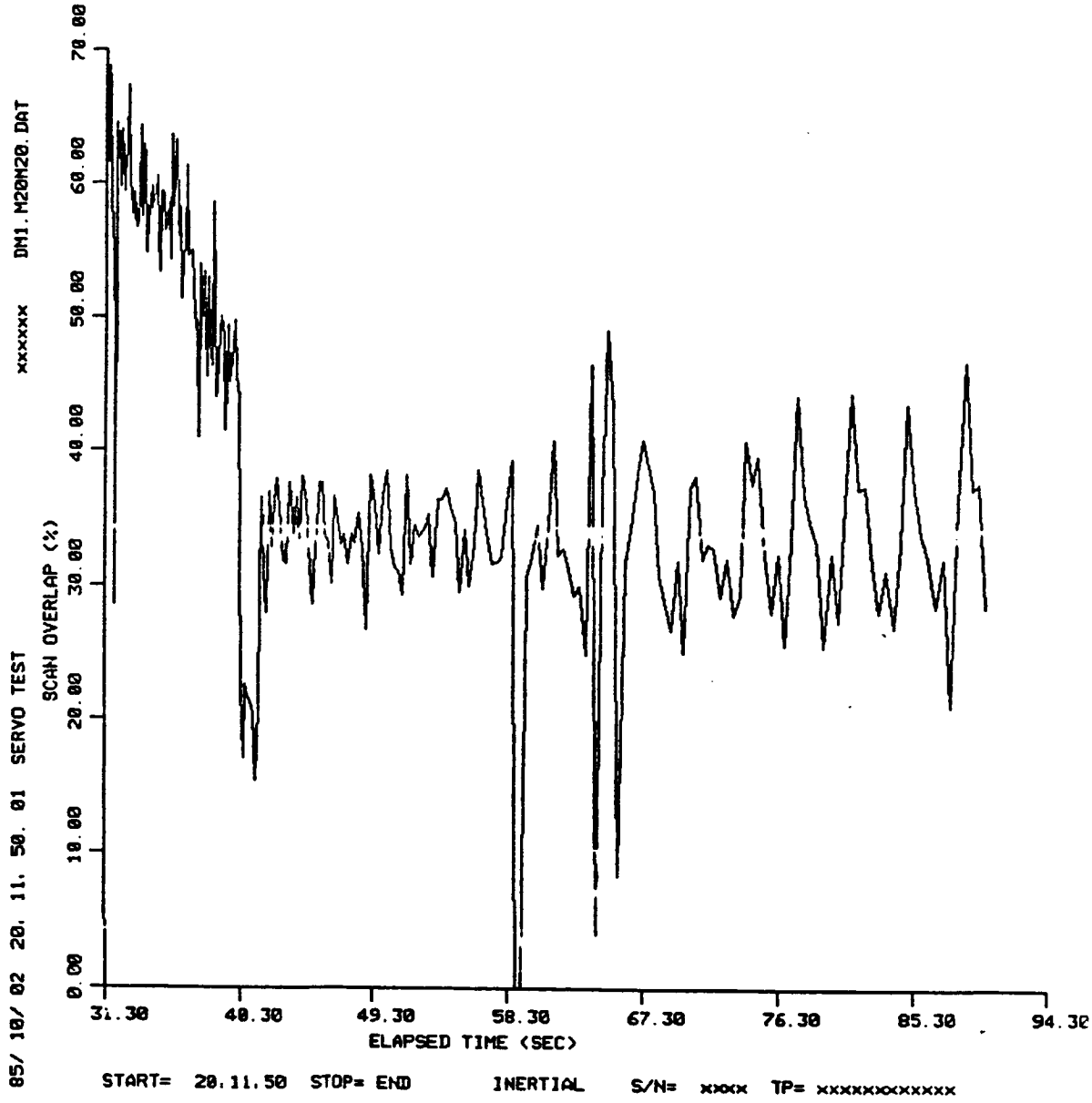
85/ 10/ 02 20. 11. 50. 01 SERVO TEST
xxxxxx DM1.M20M20.DAT
SCAN OVERLAP (%)
0.00
10.00
20.00
30.00
40.00
50.00
60.00
70.00
31.30
40.30
49.30
58.30
67.30
76.30
85.30
94.30
ELAPSED TIME (SEC)
START= 20.11.50 STOP= END
INERTIAL
S/N= xxxx TP= xxxxxxxxxxx

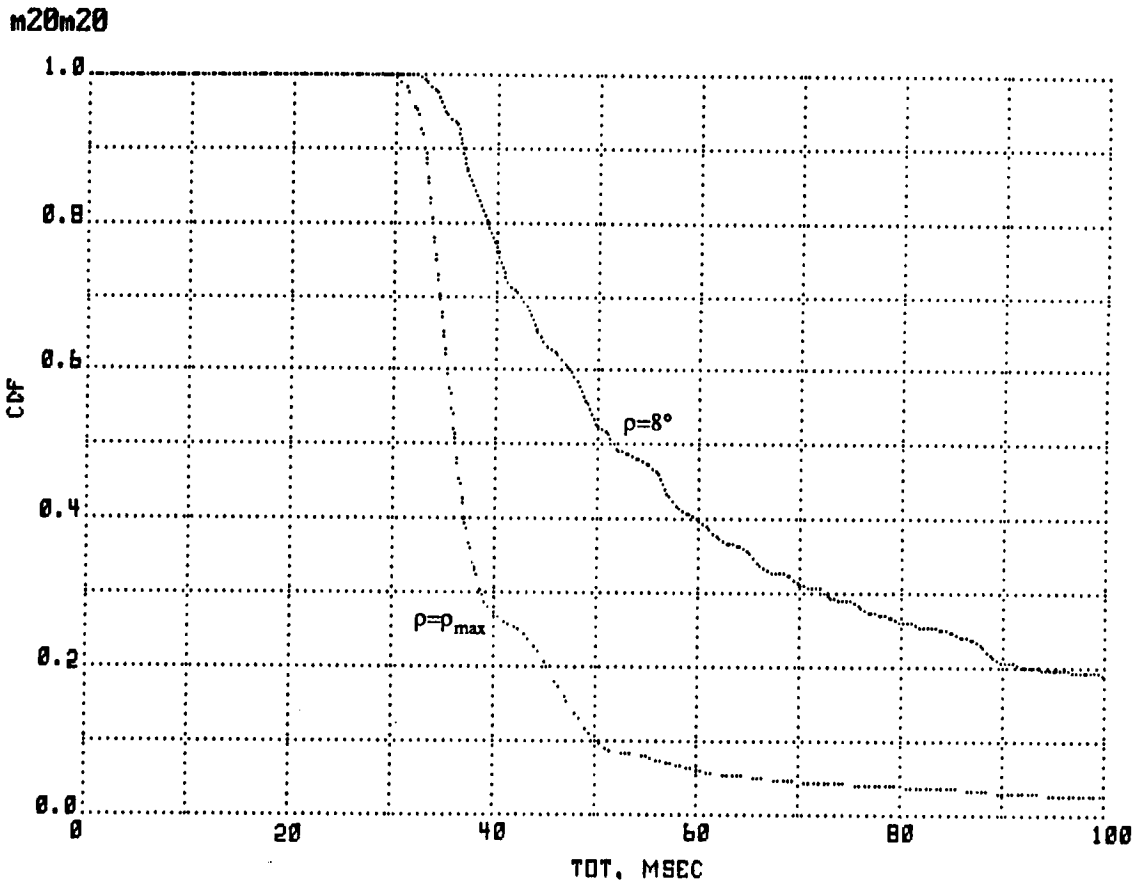
m20m20
1.0
0.8
0.6
0.4
0.2
0.0
CDF
ρ=8°
ρ=ρmax
0
20
40
60
80
100
TOT, MSEC

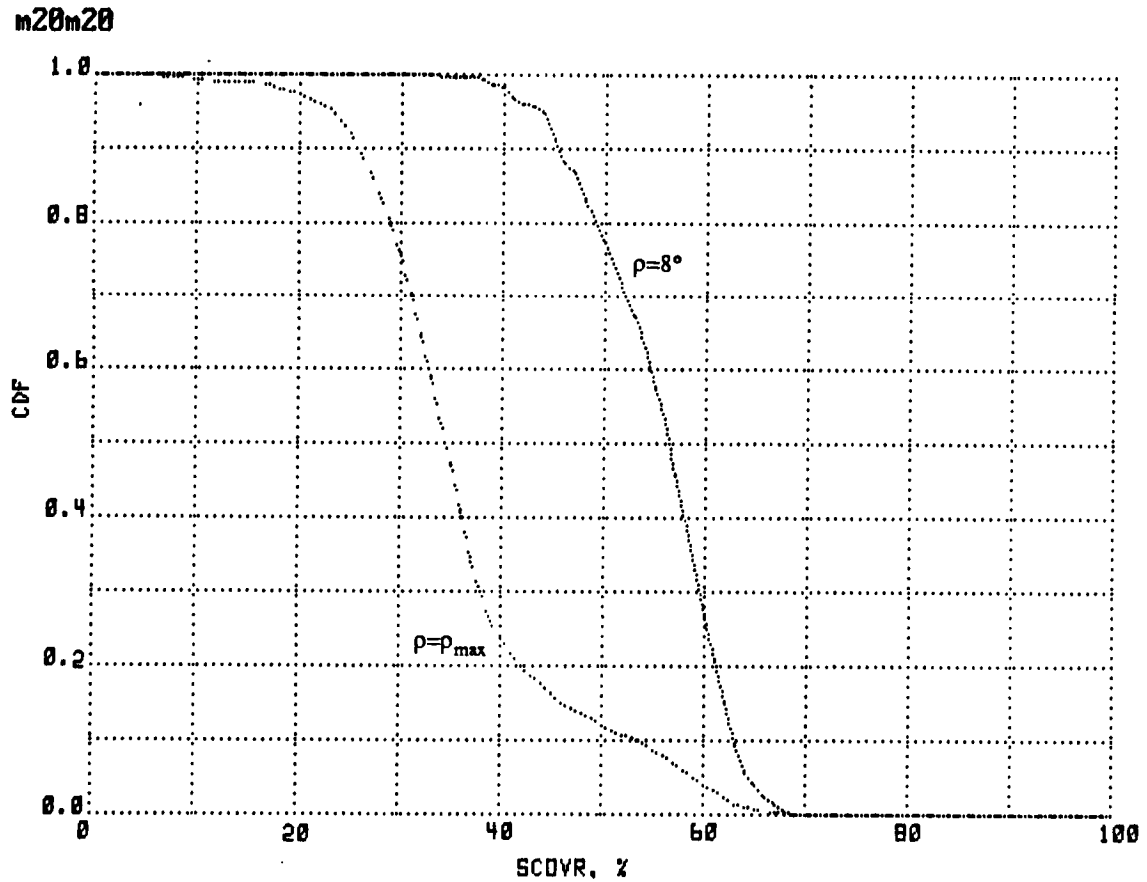
m20m20
1.0
0.8
0.6
0.4
0.2
0.0
CDF
ρ=8°
ρ=ρmax
0
20
40
60
80
100
SCOVR, %

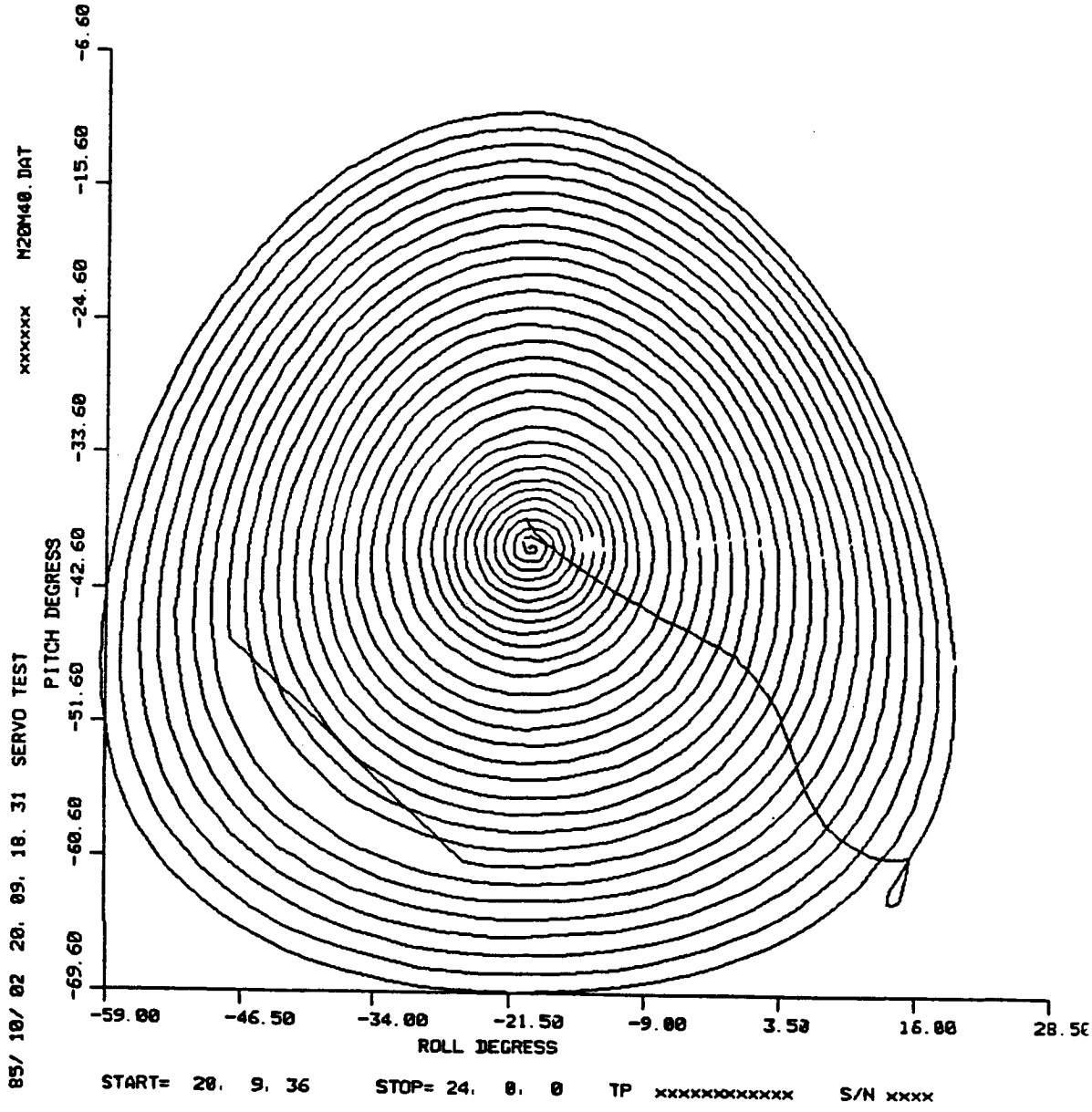
85/ 10/ 02 20. 09. 18. 31 SERVO TEST
xxxxxx N20M40.DAT
PITCH DEGRESS
-6.60
-15.60
-24.60
-33.60
-42.60
-51.60
-60.60
-69.60
-59.00
-46.50
-34.00
-21.50
-9.00
3.50
16.00
28.50
ROLL DEGRESS
START= 20. 9. 36
STOP= 24. 0. 0
TP xxxxxxxxxxxx
S/N xxxx

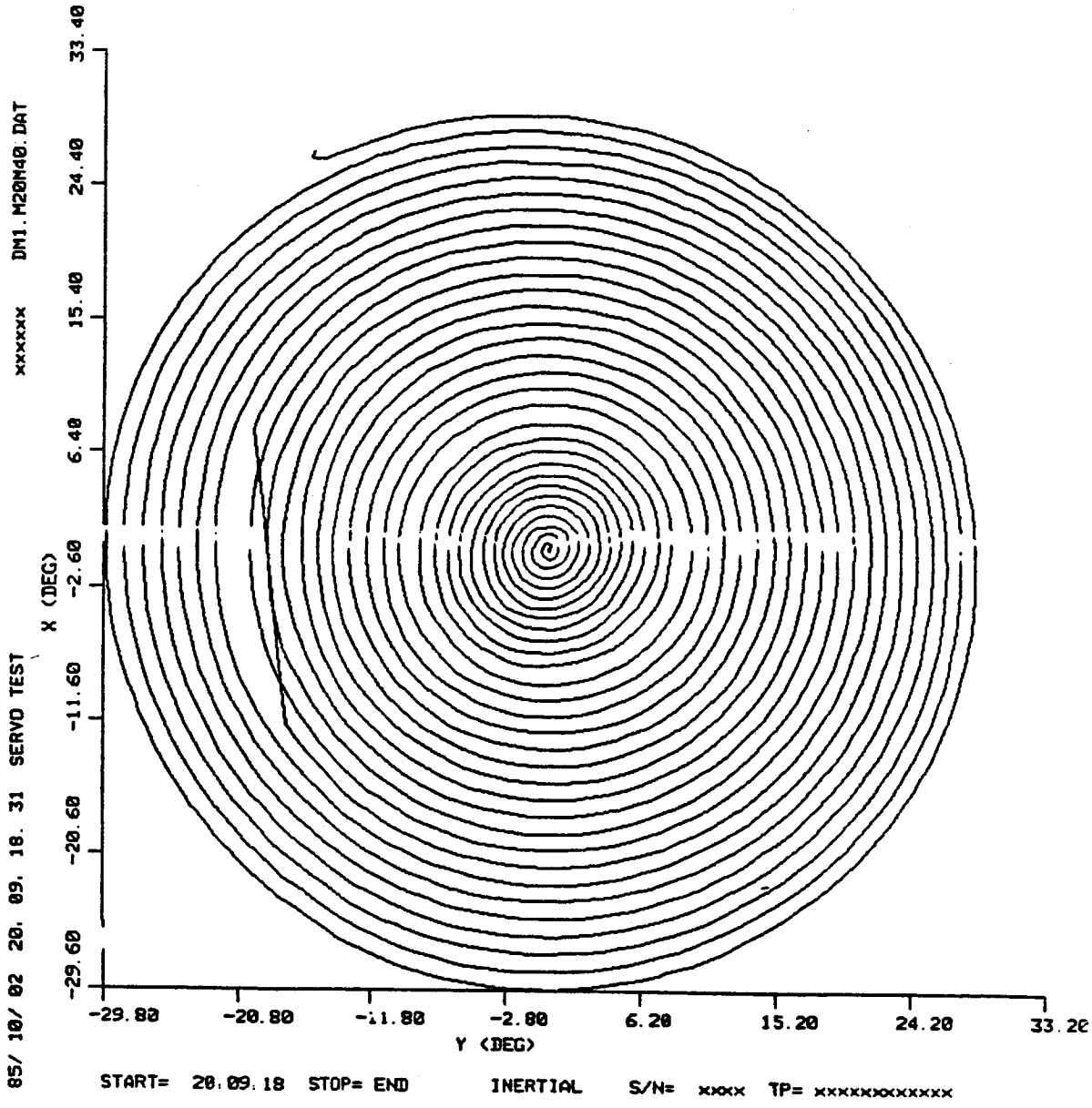
85/ 10/ 02 20. 09. 18. 31 SERVO TEST
xxxxxx DN1.M20N40.DAT
X (DEG)
33.40
24.40
15.40
6.40
-2.60
-11.60
-20.60
-29.60
-29.80
-20.80
-11.80
-2.80
6.20
15.20
24.20
33.20
Y (DEG)
START= 20:09:18 STOP= END INERTIAL S/N= xxxx TP= xxxxxxxxxxx

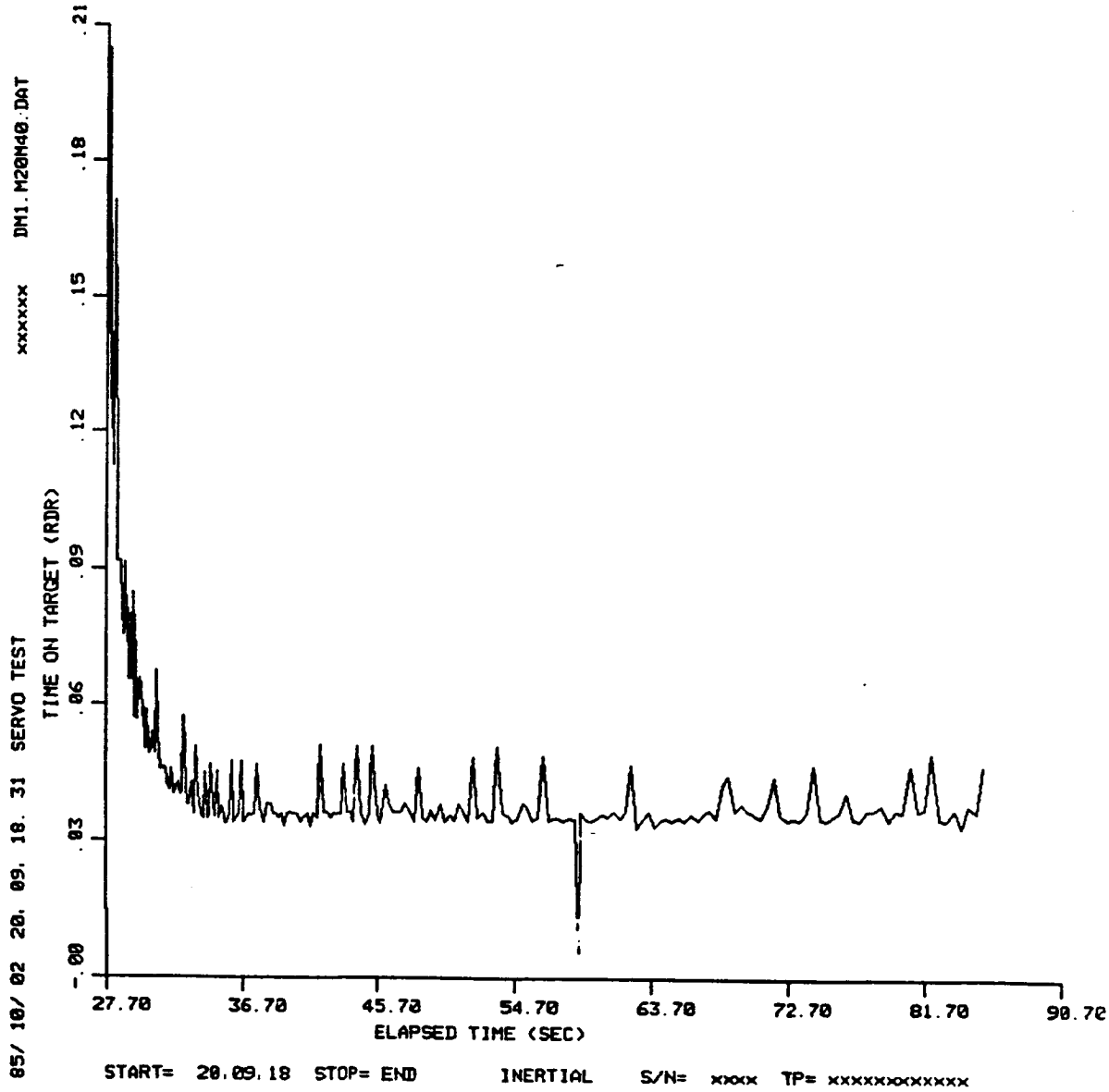
85/ 10/ 02 20. 09. 18. 31 SERVO TEST
xxxxxx DM1.M20M40.DAT
TIME ON TARGET (RDR)
-.00
.03
.06
.09
.12
.15
.18
.21
27.70
36.70
45.70
54.70
63.70
72.70
81.70
90.70
ELAPSED TIME (SEC)
START= 20.09.18 STOP= END
INERTIAL
S/N= xxxx TP= xxxxxxxxxxx

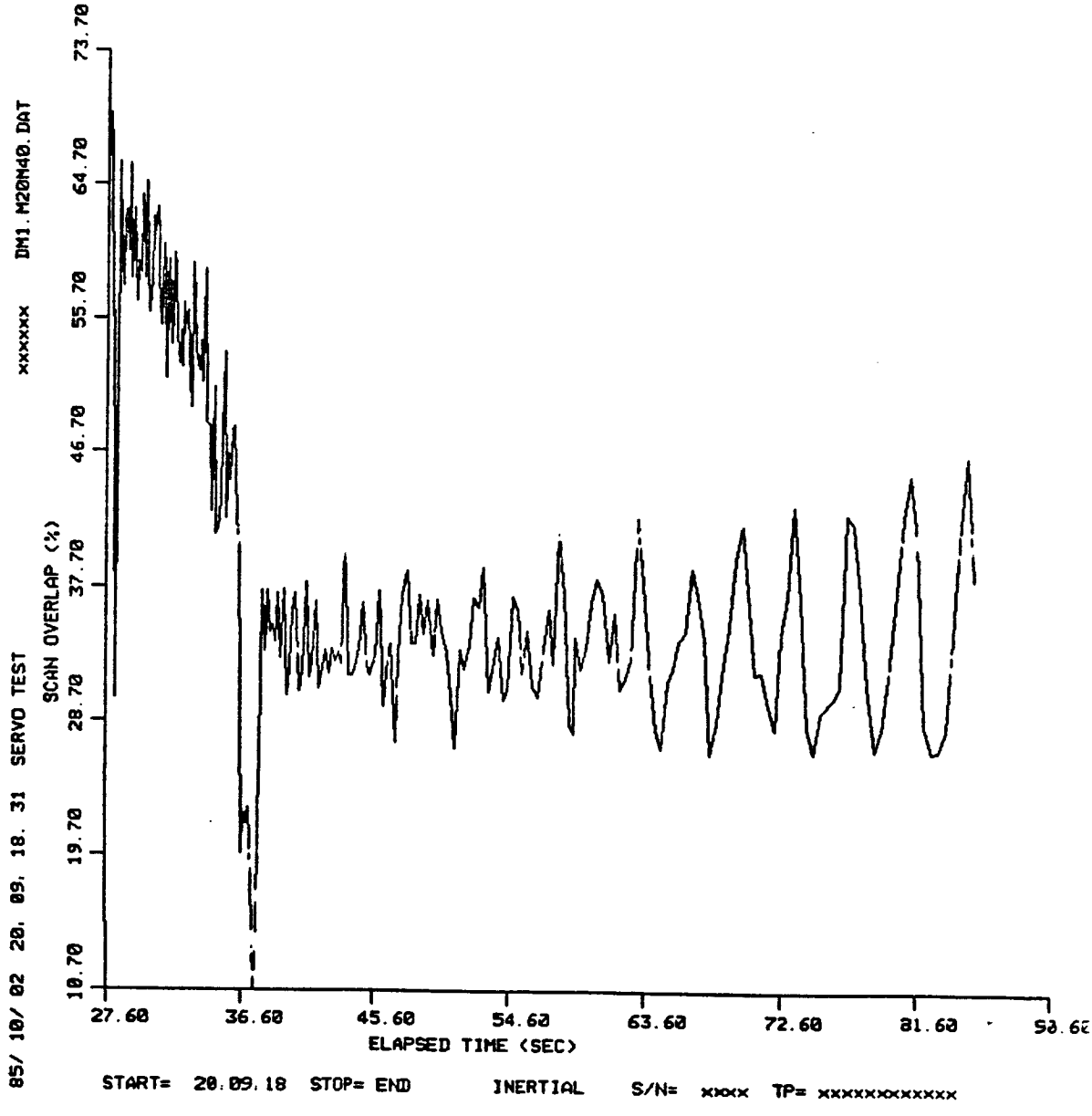
85/ 10/ 02 20. 09. 18. 31 SERVO TEST
xxxxxx DM1.M20M40.DAT
SCAN OVERLAP (%)
73.70
64.70
55.70
46.70
37.70
28.70
19.70
10.70
27.60
36.60
45.60
54.60
63.60
72.60
81.60
ELAPSED TIME (SEC)
START= 20:09:18 STOP= END
INERTIAL
S/N= xxxx TP= xxxxxxxxxxx

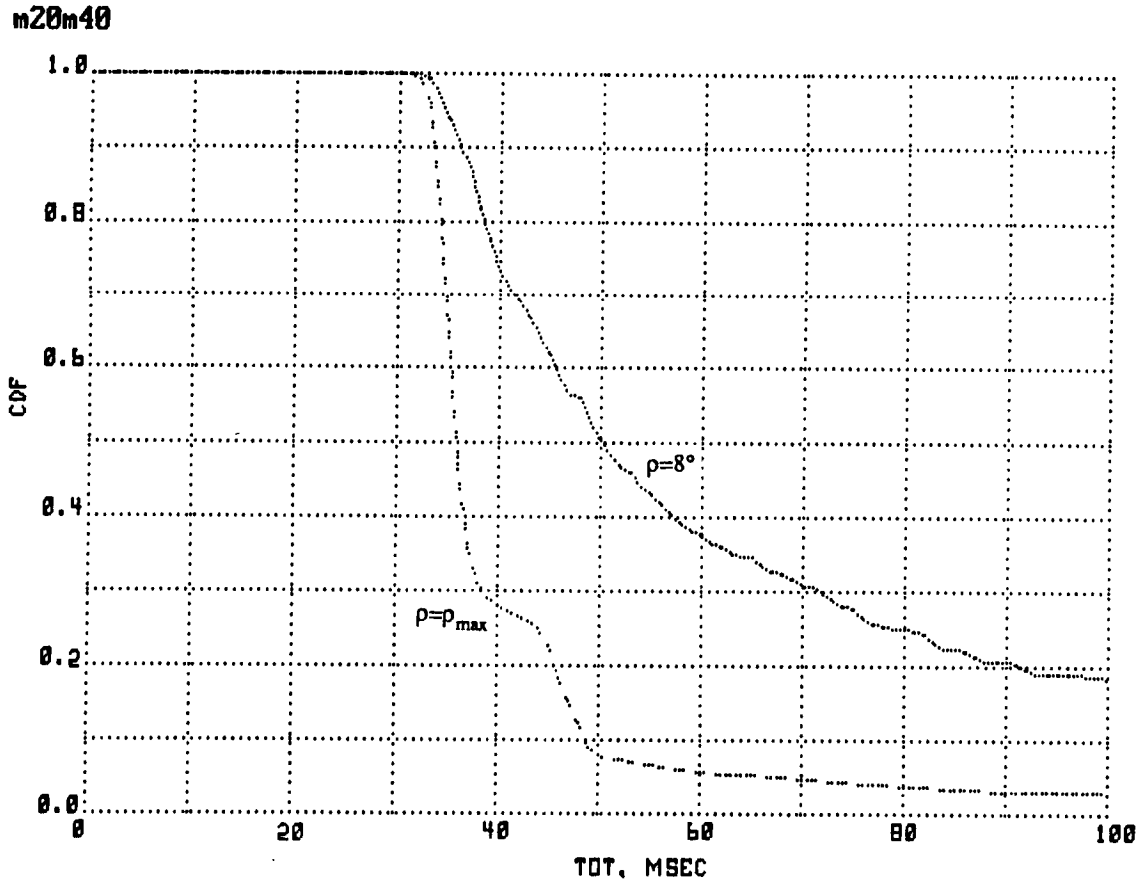
m20m40
1.0
0.8
0.6
0.4
0.2
0.0
CDF
0
20
40
60
80
100
TOT, MSEC
ρ=8°
ρ=ρmax

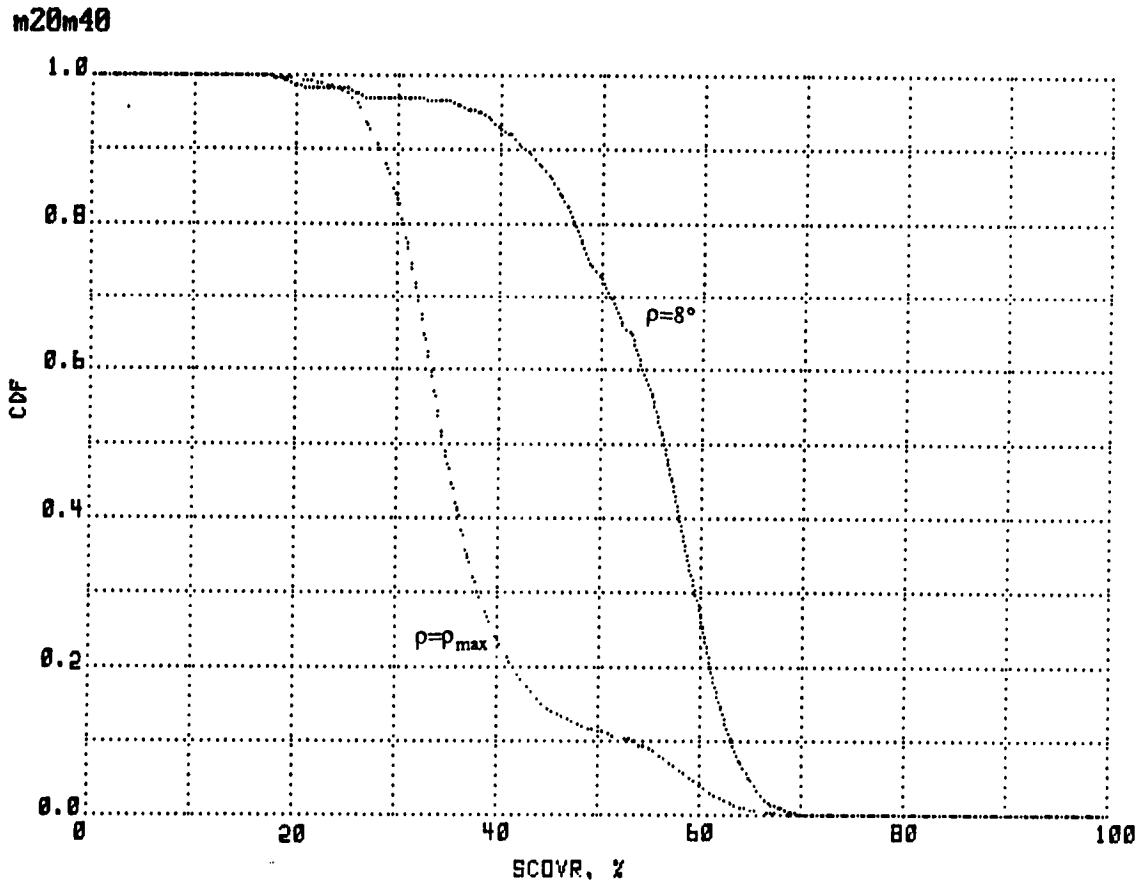
m20m40
1.0
0.8
0.6
0.4
0.2
0.0
CDF
0
20
40
60
80
100
SCOVR, %
ρ=8°
ρ=ρmax

2399 m20m60

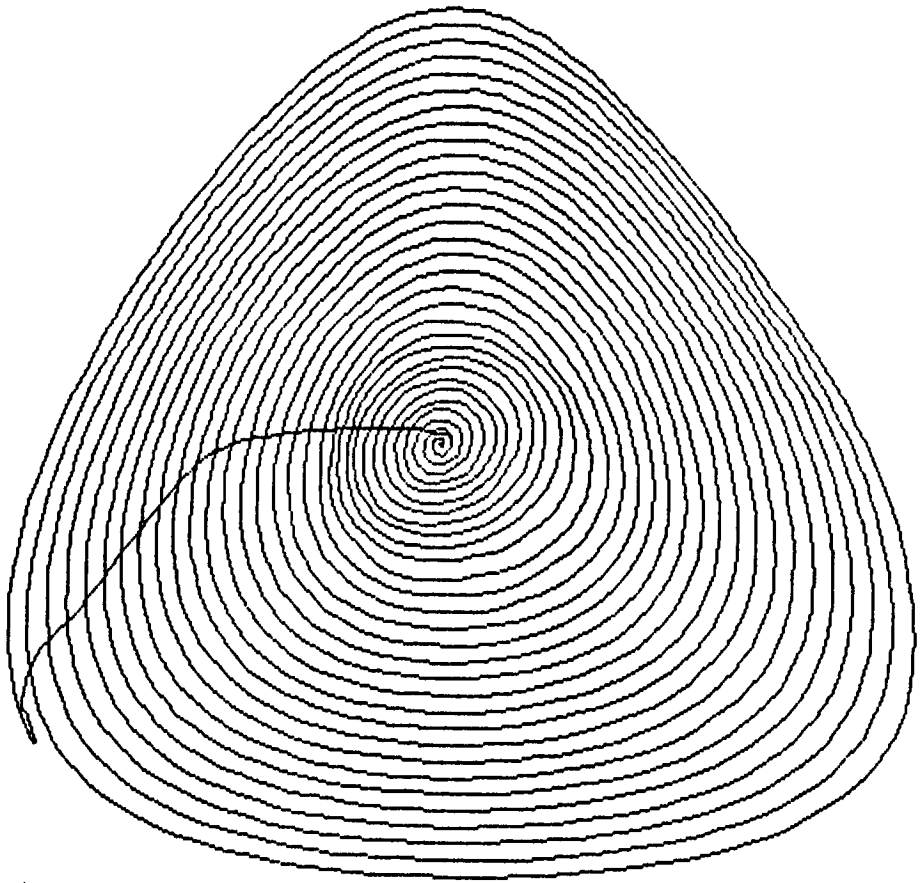

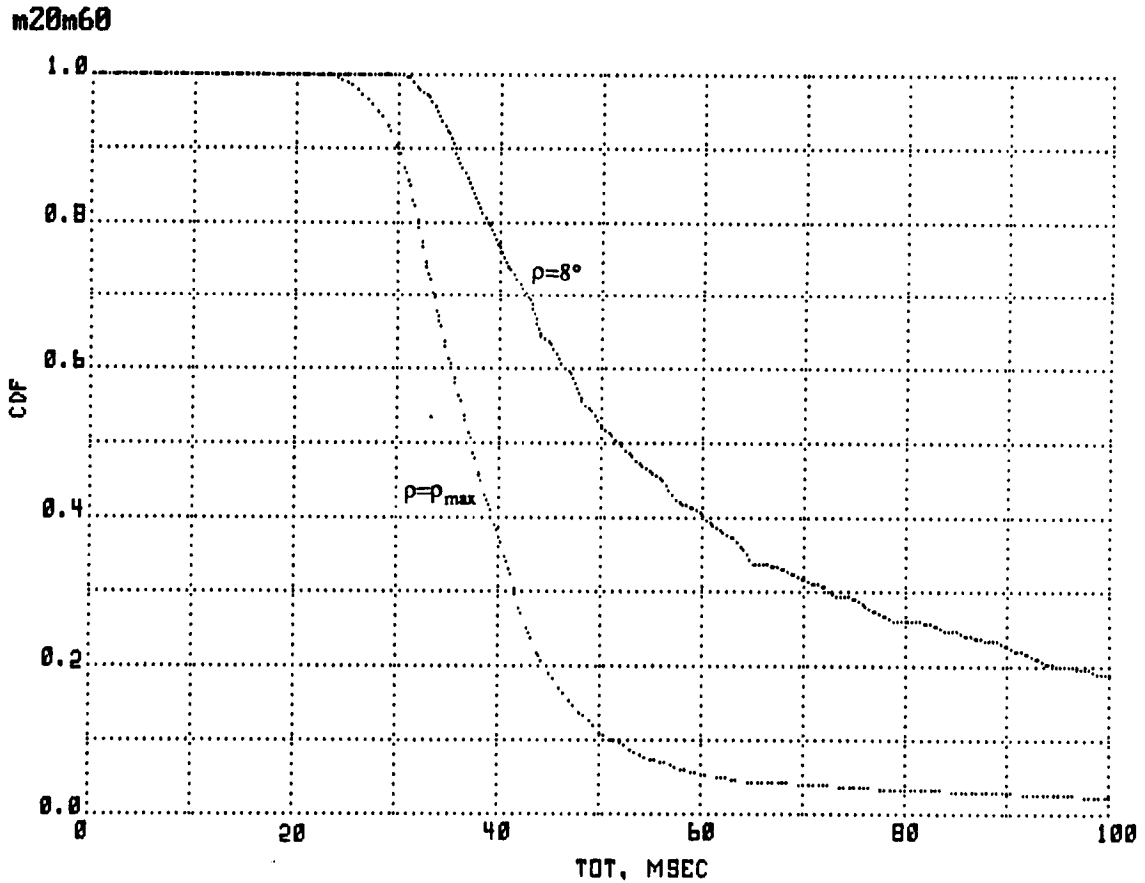
m20m60
1.0
0.8
0.6
0.4
0.2
0.0
CDF
ρ=8°
ρ=ρmax
0
20
40
60
80
100
TOT, MSEC

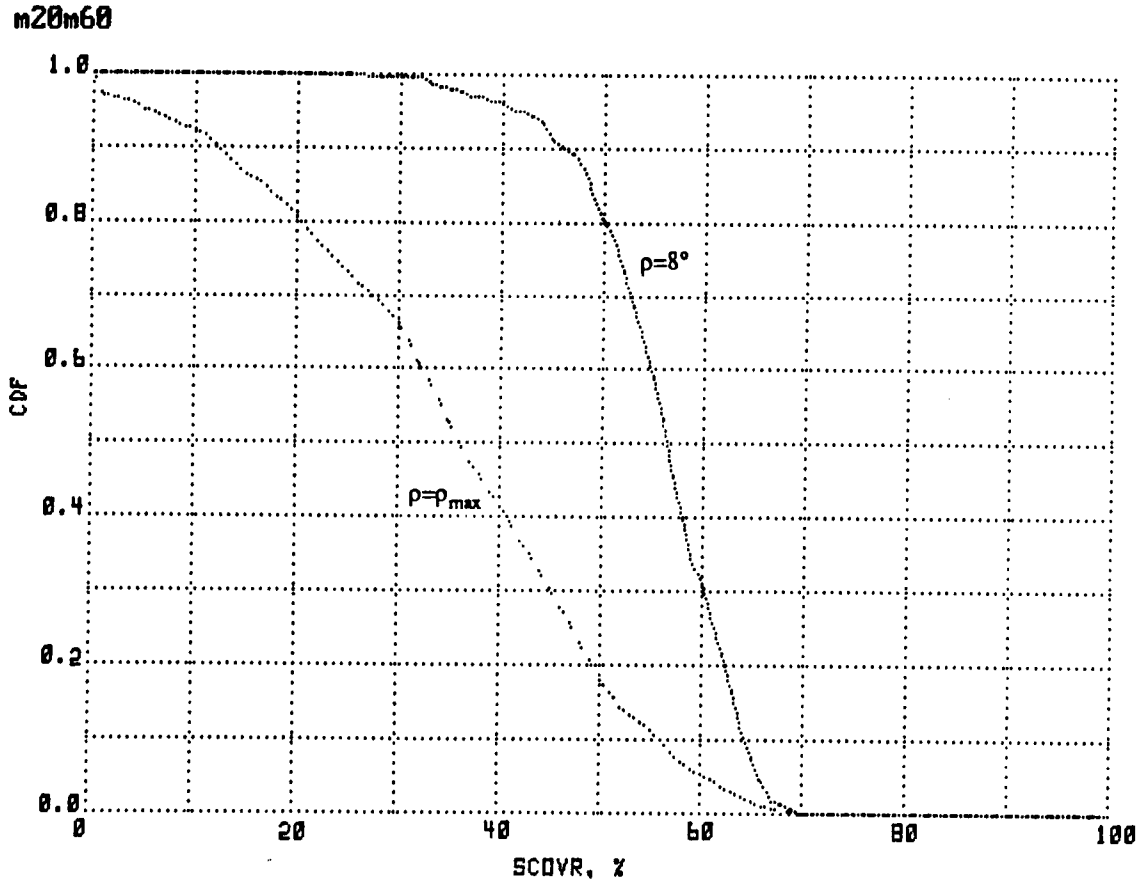
m20m60
1.0
0.8
0.6
0.4
0.2
0.0
CDF
ρ=8°
ρ=ρmax
0
20
40
60
80
100
SCOVR, %

M40P60

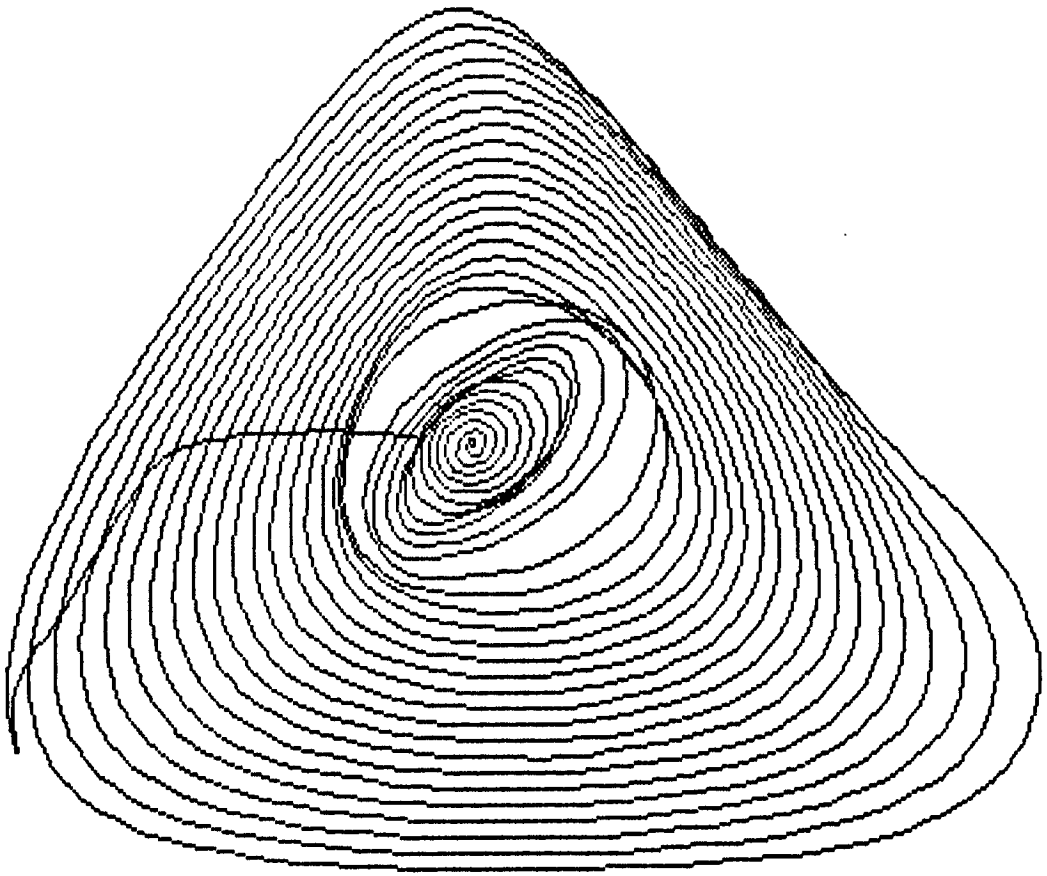

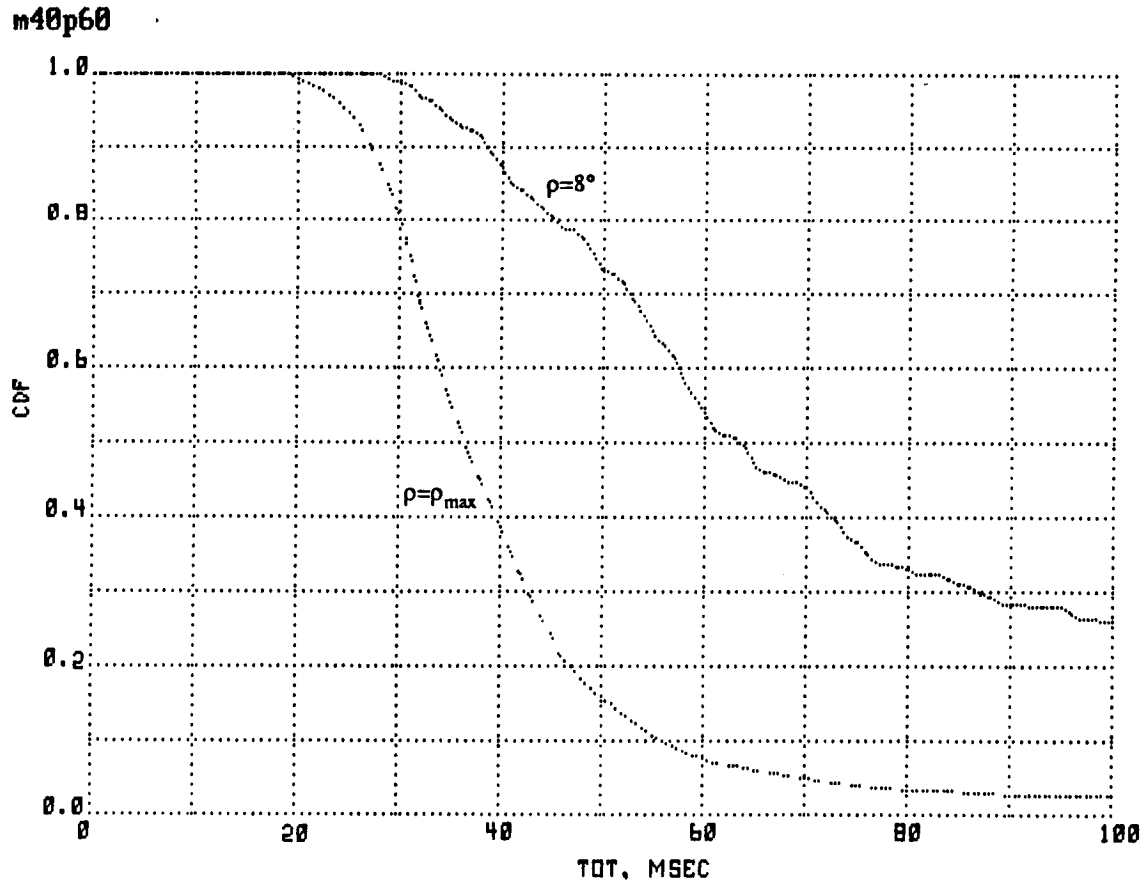
m40p60
1.0
0.8
0.6
0.4
0.2
0.0
CDF
ρ=8°
ρ=ρmax
0
20
40
60
80
100
TOT, MSEC

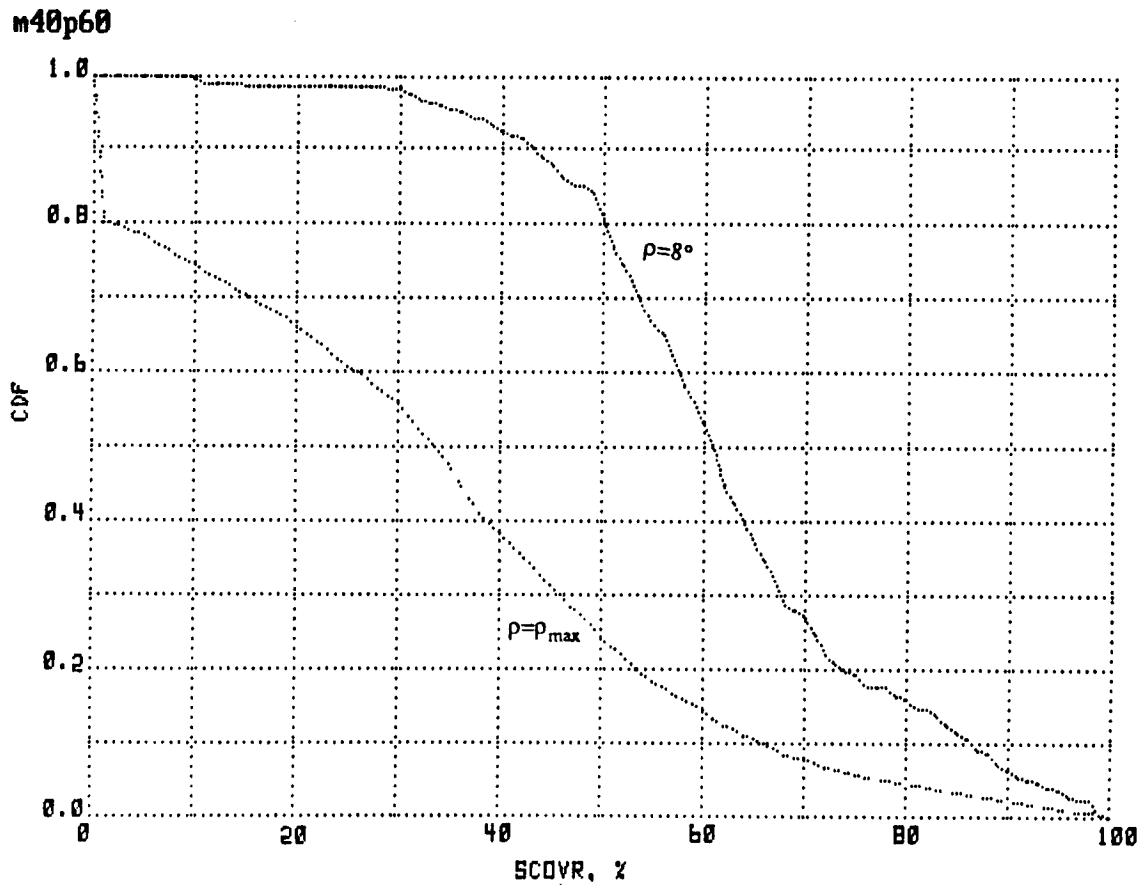
m40p60
1.0
0.8
0.6
0.4
0.2
0.0
CDF
ρ=8°
ρ=ρmax
0
20
40
60
80
100
SCOVR, %

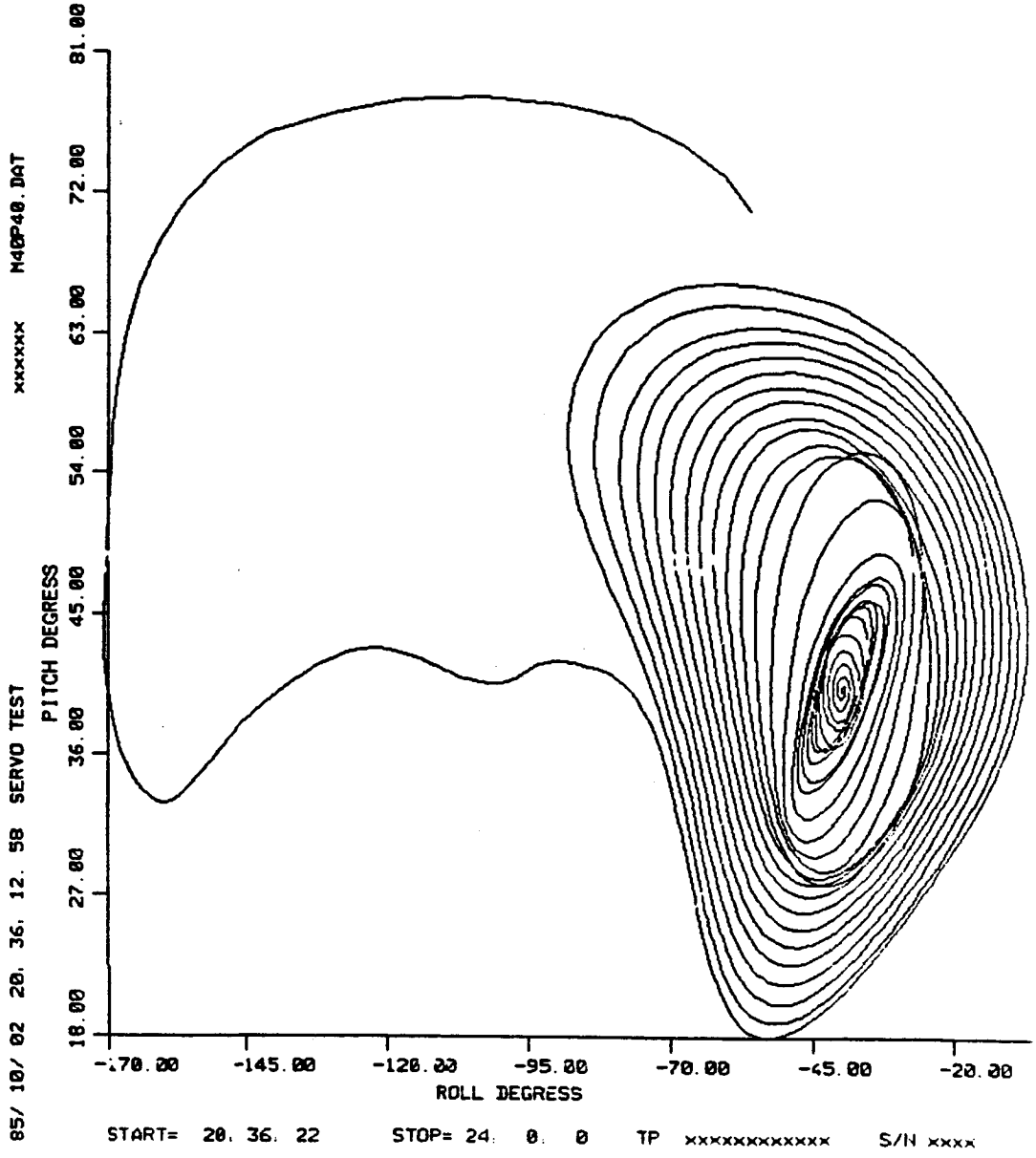
81.00
72.00
63.00
54.00
45.00
36.00
27.00
18.00
PITCH DEGRESS
xxxxxx M40P40.DAT
-170.00
-145.00
-120.00
-95.00
-70.00
-45.00
-20.00
ROLL DEGRESS
85/ 10/ 02 20. 36. 12. 58 SERVO TEST
START= 20. 36. 22
STOP= 24. 0. 0
TP xxxxxxxxxxxx
S/N xxxx

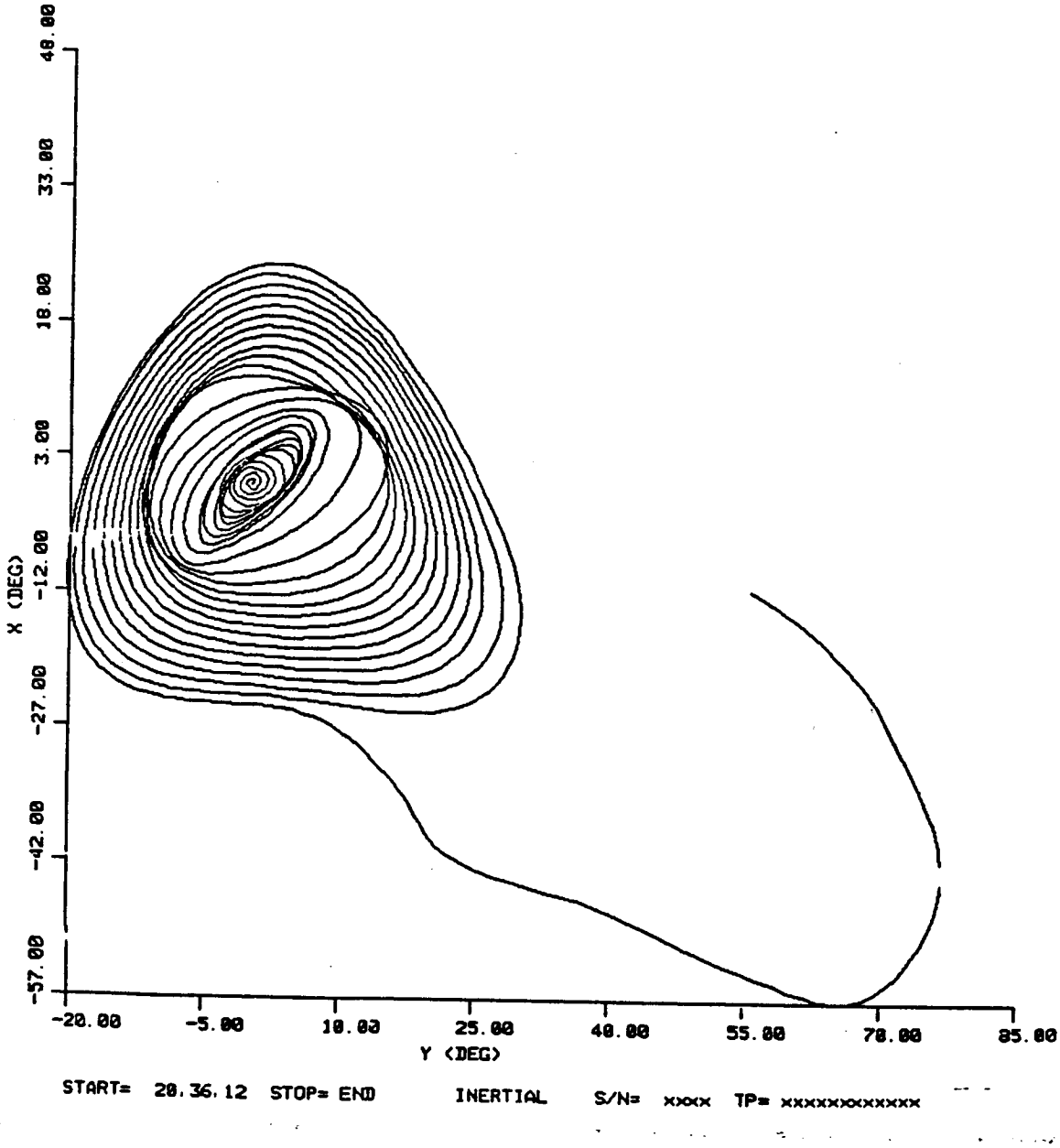
48.00
33.00
18.00
3.00
-12.00
-27.00
-42.00
-57.00
X (DEG)
-20.00
-5.00
10.00
25.00
40.00
55.00
70.00
85.00
Y (DEG)
START= 20.36.12 STOP= END
INERTIAL
S/N= xxxx TP= xxxxxxxxxxx

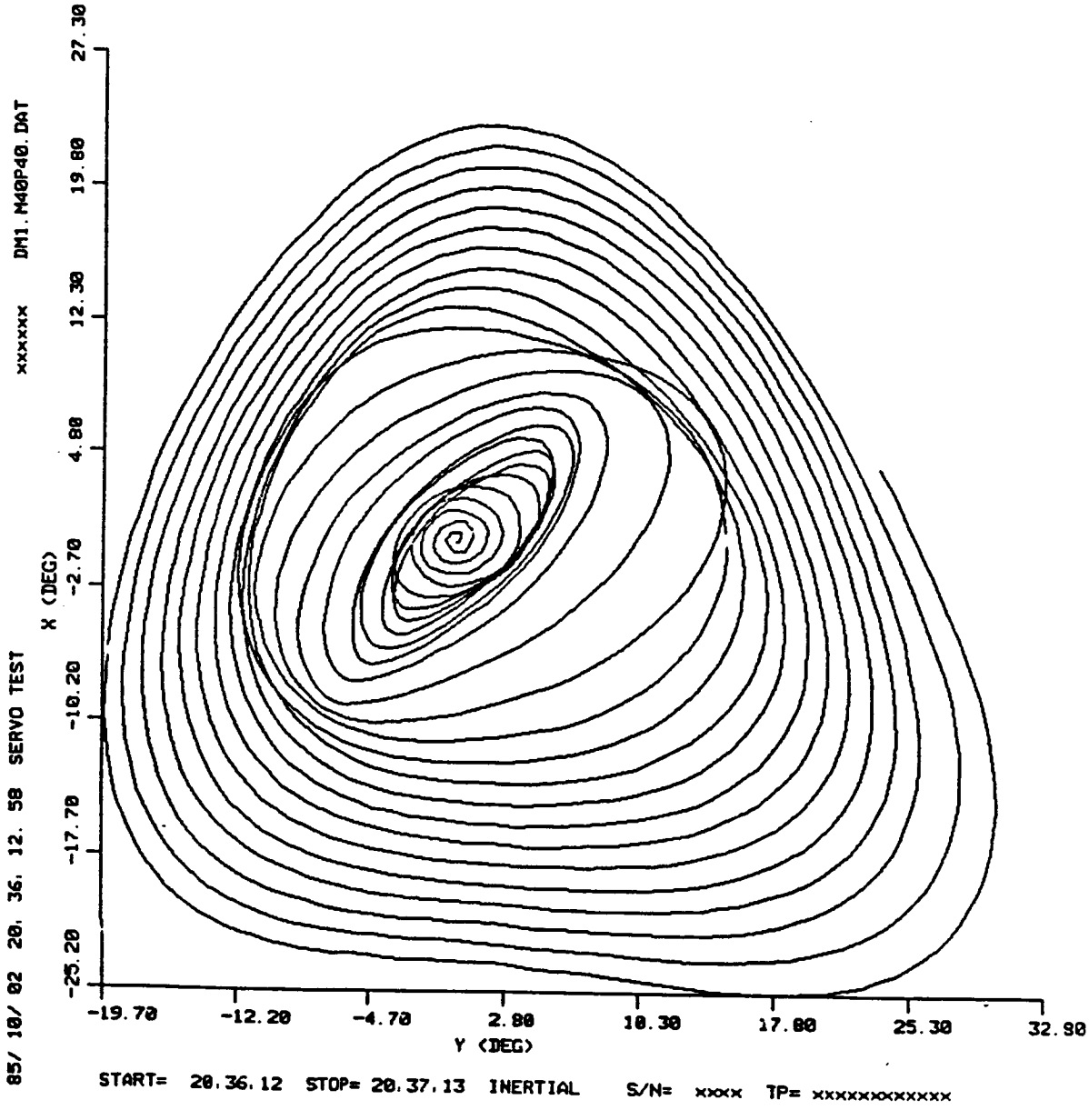
85/ 10/ 02 20. 36. 12. 58 SERVO TEST
XXXXXX DM1.M40P40.DAT
X (DEG)
27.30
19.80
12.30
4.80
-2.70
-10.20
-17.70
-25.20
-19.70
-12.20
-4.70
2.80
10.30
17.80
25.30
32.80
Y (DEG)
START= 20.36.12 STOP= 20.37.13 INERTIAL S/N= XXXX TP= XXXXXXXXXXX

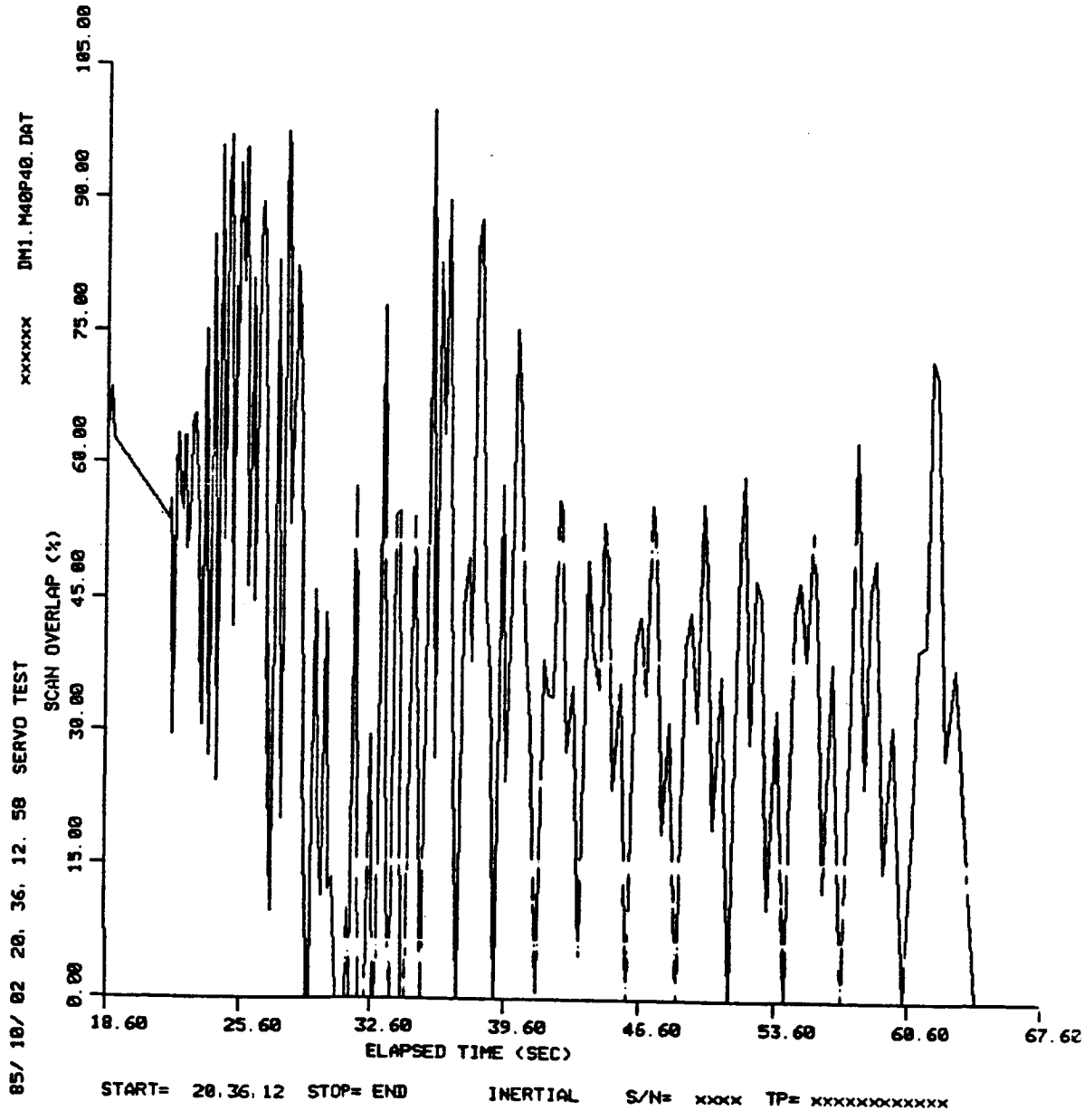
85/ 10/ 02 20. 36. 12. 58 SERVO TEST
xxxxxx DM1.M40P40.DAT
SCAN OVERLAP (%)
0.00
15.00
30.00
45.00
60.00
75.00
90.00
105.00
18.60
25.60
32.60
39.60
46.60
53.60
60.60
67.62
ELAPSED TIME (SEC)
START= 20.36.12 STOP= END
INERTIAL
S/N= xxxx TP= xxxxxxxxxxx

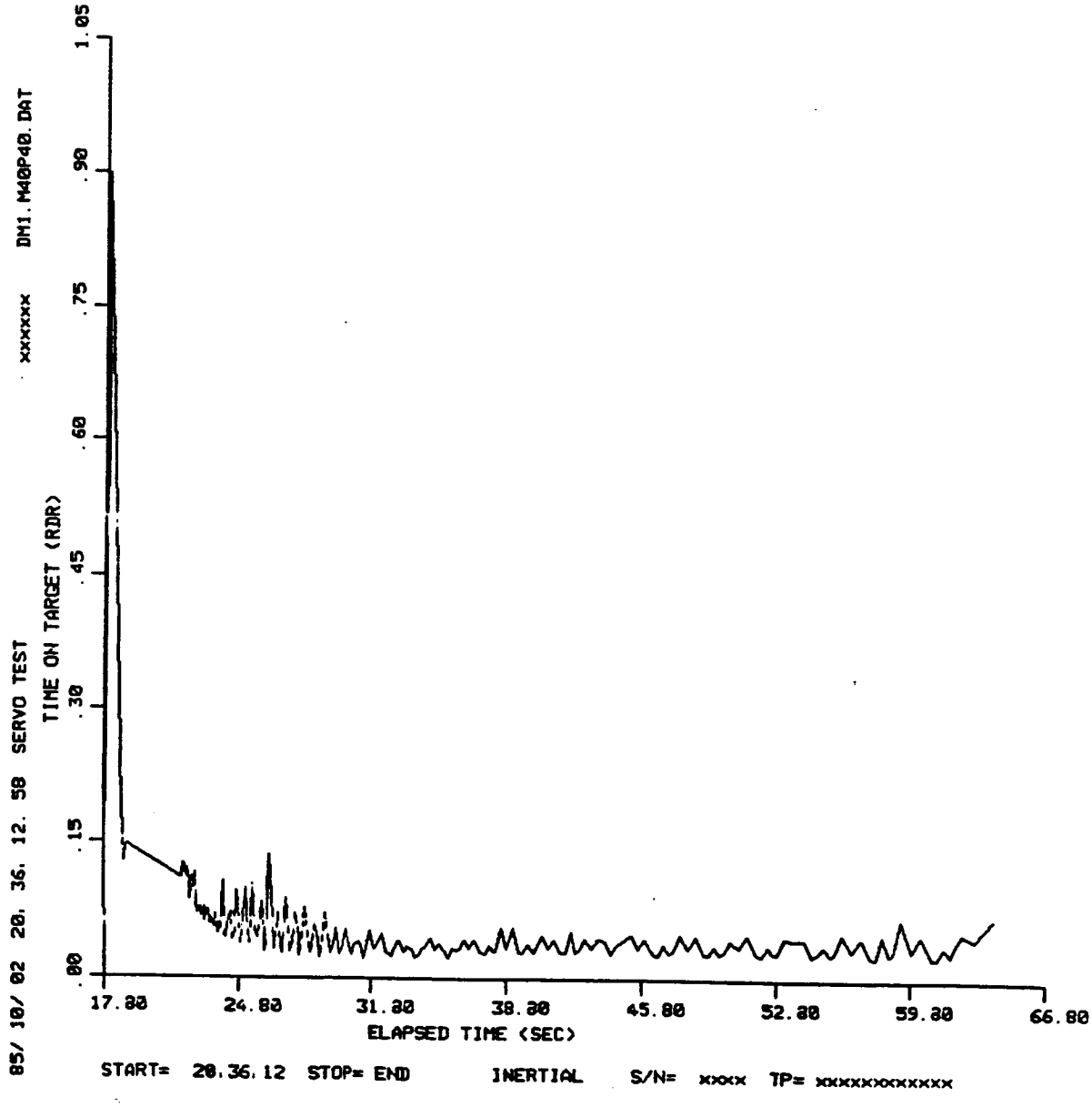
85/ 10/ 02 20. 36. 12. 58 SERVO TEST
xxxxxx DM1.M40P40.DAT
TIME ON TARGET (RDR)
.00
.15
.30
.45
.60
.75
.90
1.05
17.80
24.80
31.80
38.80
45.80
52.80
59.80
66.80
ELAPSED TIME (SEC)
START= 20.36.12 STOP= END
INERTIAL
S/N= xxxx TP= xxxxxxxxxxx

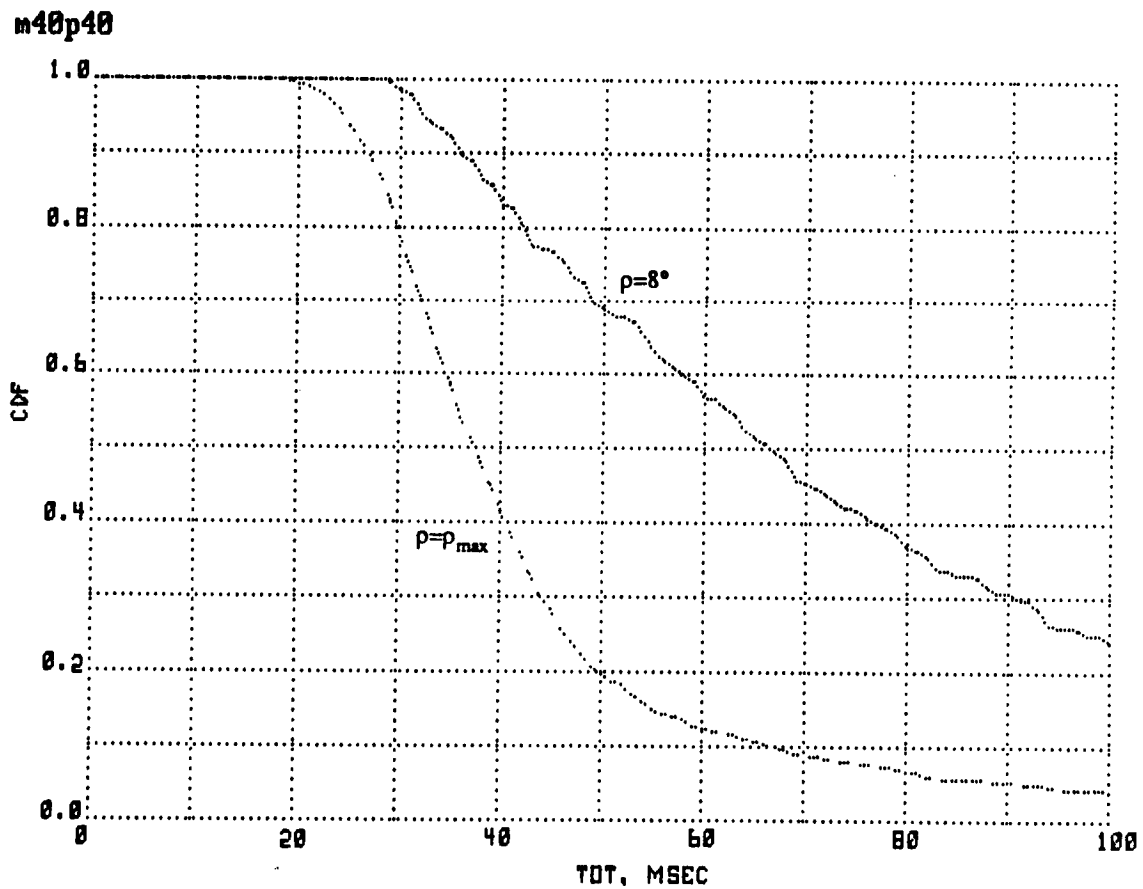
m40p40
1.0
0.8
0.6
0.4
0.2
0.0
CDF
ρ=8°
ρ=ρmax
0
20
40
60
80
100
TOT, MSEC

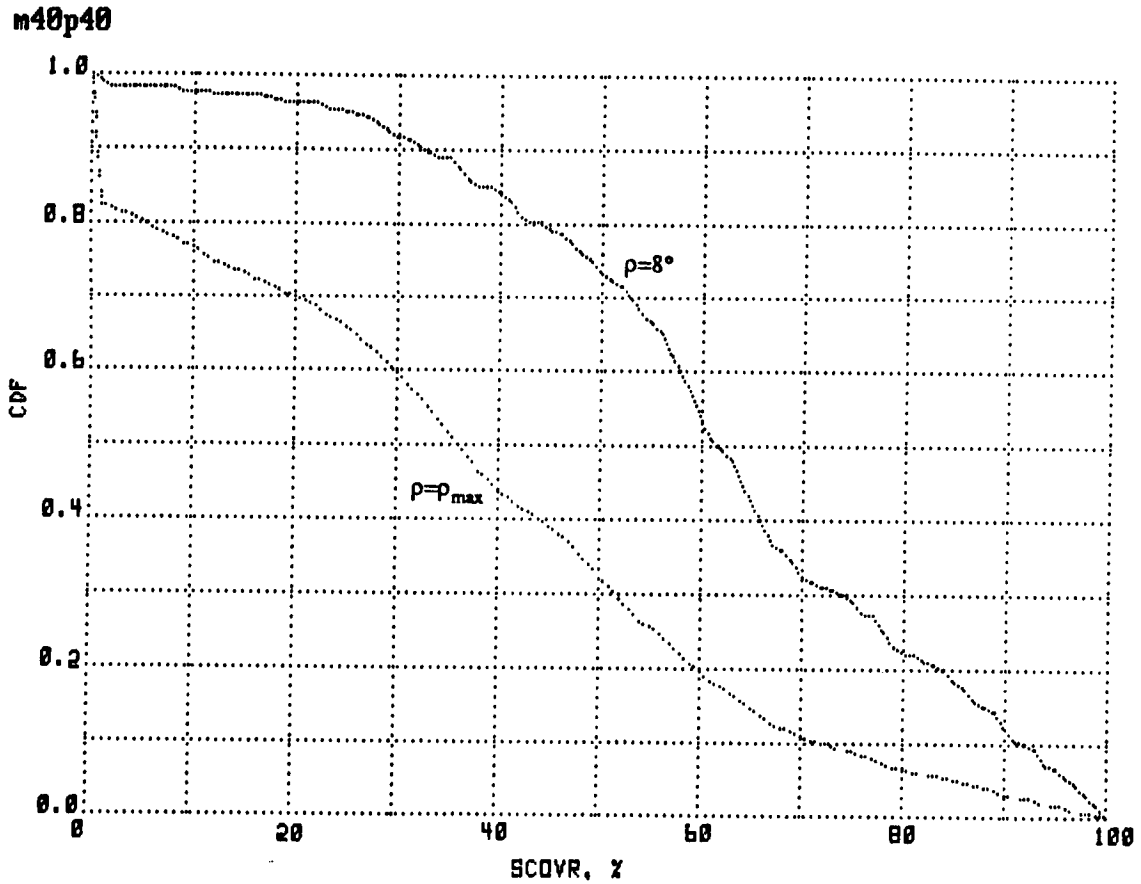
m40p40
1.0
0.8
0.6
0.4
0.2
0.0
CDF
ρ=8°
ρ=ρmax
0
20
40
60
80
100
SCOVR, %

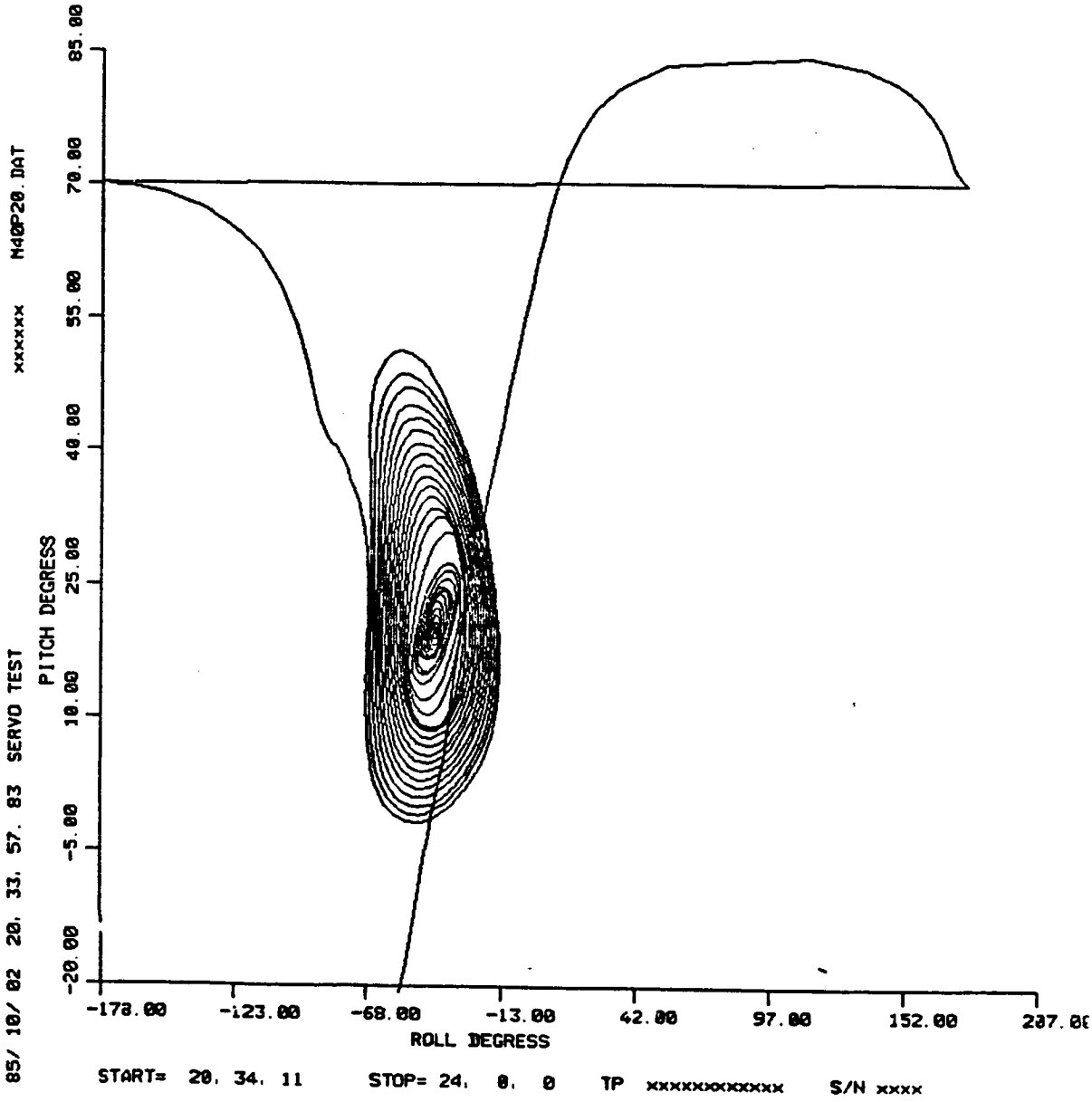
85/ 10/ 02 20. 33. 57. 83 SERVO TEST
xxxxxx N40P20.DAT
PITCH DEGRESS
85.00
70.00
55.00
40.00
25.00
10.00
-5.00
-20.00
-178.00
-123.00
-68.00
-13.00
42.00
97.00
152.00
ROLL DEGRESS
START= 20. 34. 11
STOP= 24. 0. 0
TP xxxxxxxxxxx
S/N xxxx

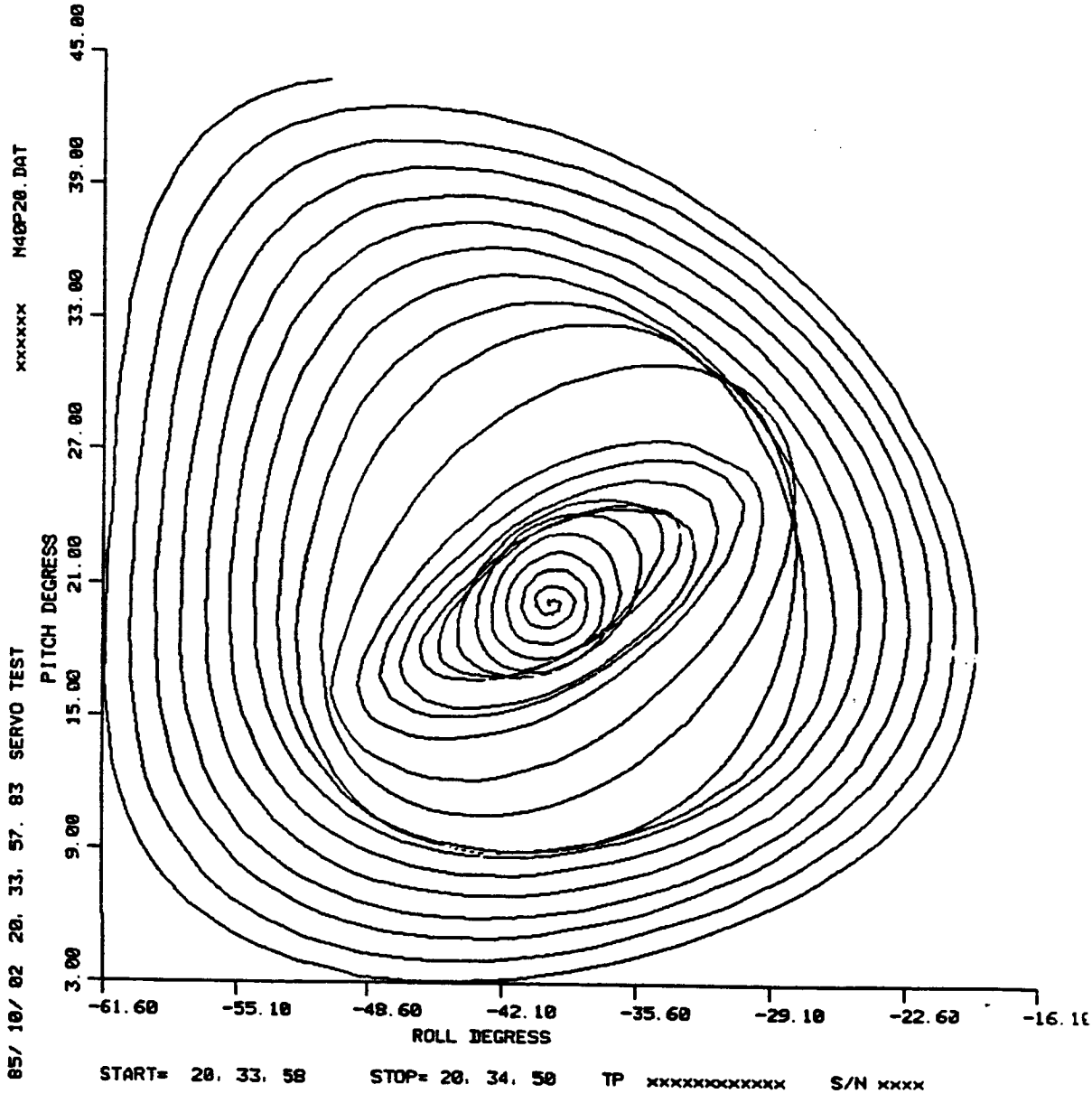
85/ 10/ 02 20. 33. 57. 83 SERVO TEST
xxxxxx M40P20.DAT
PITCH DEGRESS
45.00
39.00
33.00
27.00
21.00
15.00
9.00
3.00
-61.60
-55.10
-48.60
-42.10
-35.60
-29.10
-22.60
-16.1
ROLL DEGRESS
START= 20. 33. 58
STOP= 20. 34. 50
TP xxxxxxxxxxx
S/N xxxx

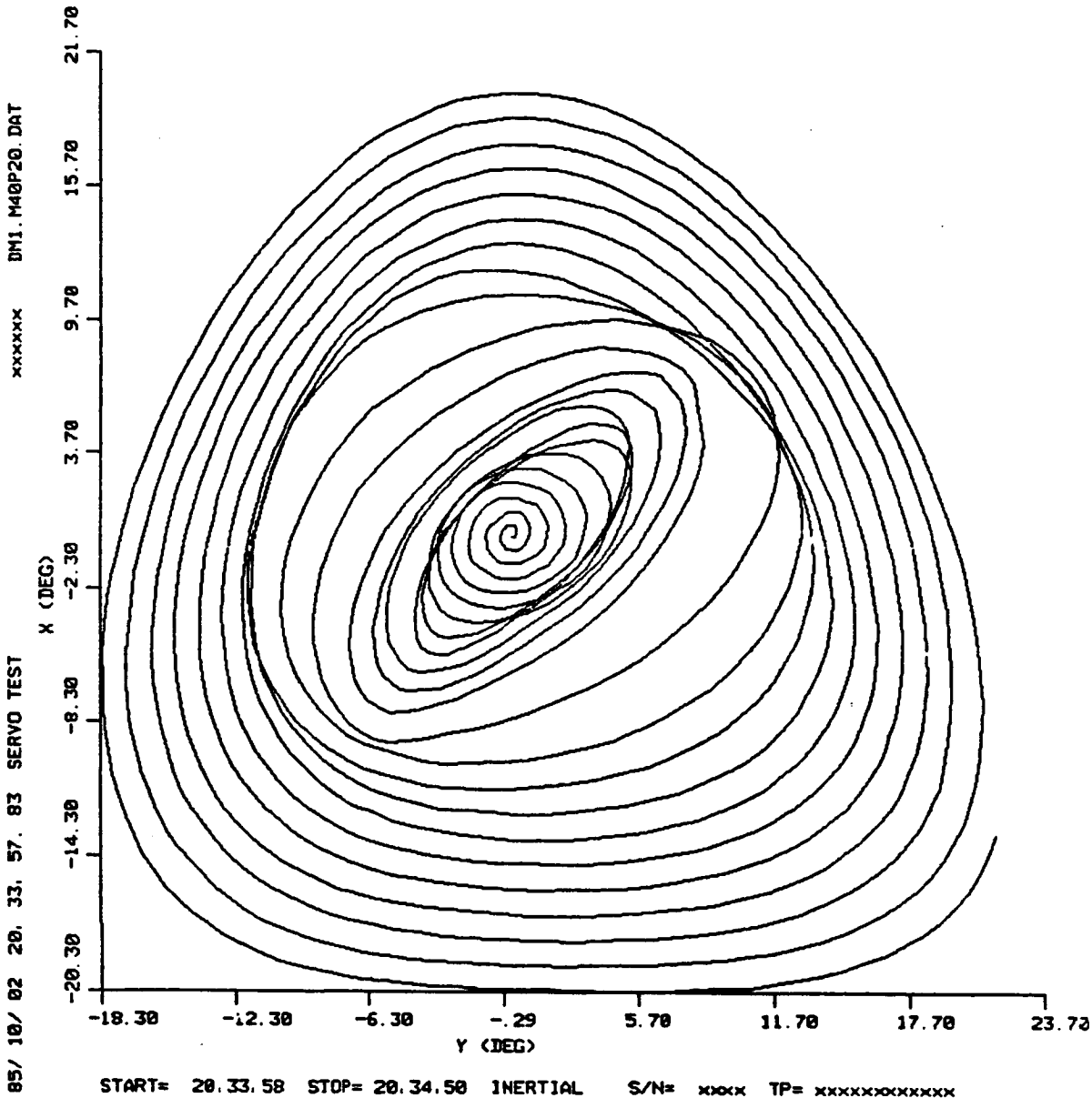
85/ 10/ 02 20. 33. 57. 83 SERVO TEST
xxxxxx DM1.M40P20.DAT
X (DEG)
21.70
15.70
9.70
3.70
-2.30
-8.30
-14.30
-20.30
-18.30
-12.30
-6.30
-.29
5.70
11.70
17.70
23.70
Y (DEG)
START= 20.33.58 STOP= 20.34.50 INERTIAL S/N= xxxx TP= xxxxxxxxxxx

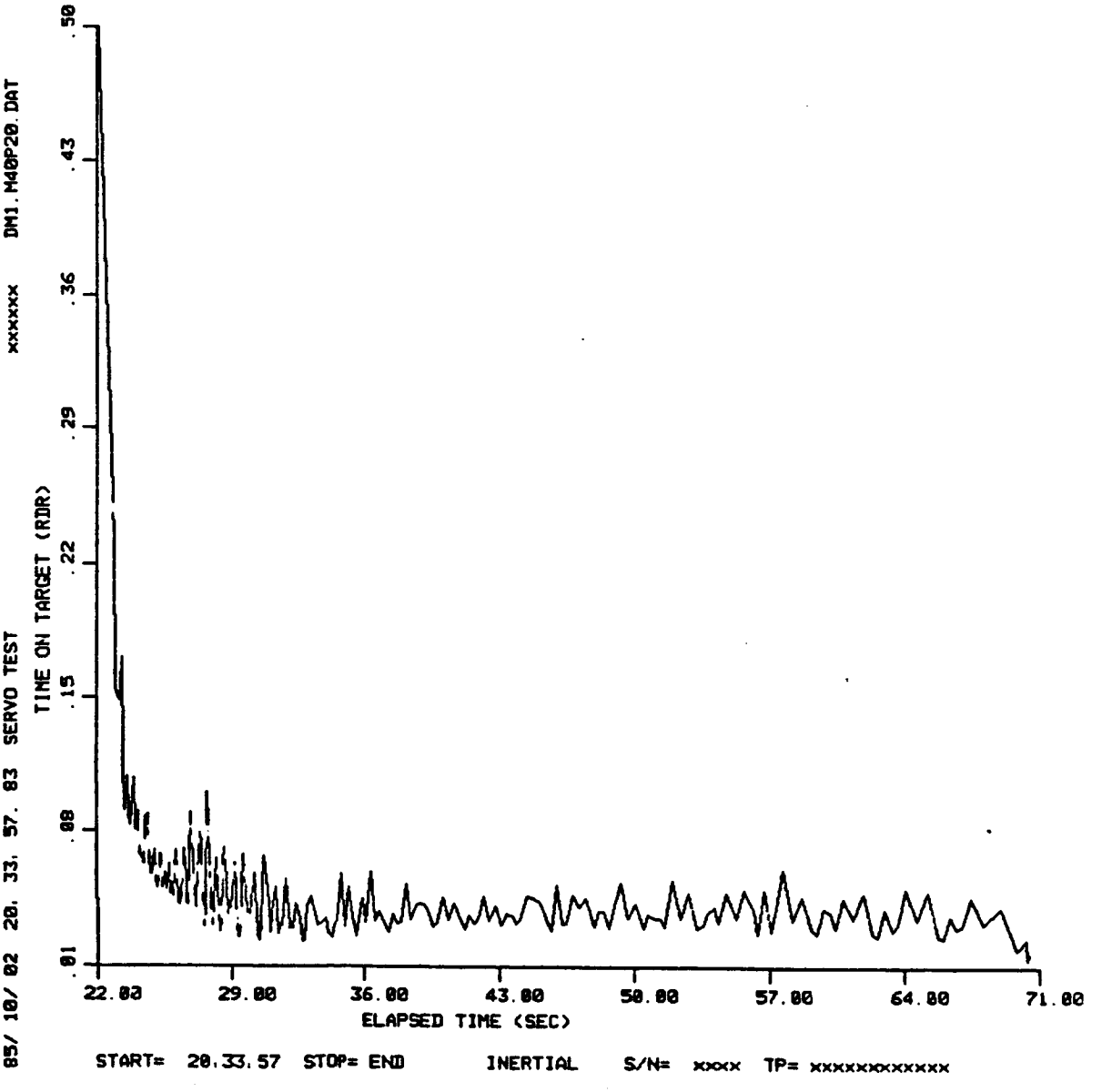
85/ 10/ 02 20. 33. 57. 83 SERVO TEST xxxxxx DM1.M40P20.DAT
TIME ON TARGET (RDR)
.01
.08
.15
.22
.29
.36
.43
.50
22.00
29.00
36.00
43.00
50.00
57.00
64.00
71.00
ELAPSED TIME (SEC)
START= 20.33.57 STOP= END INERTIAL S/N= xxxx TP= xxxxxxxxxxx

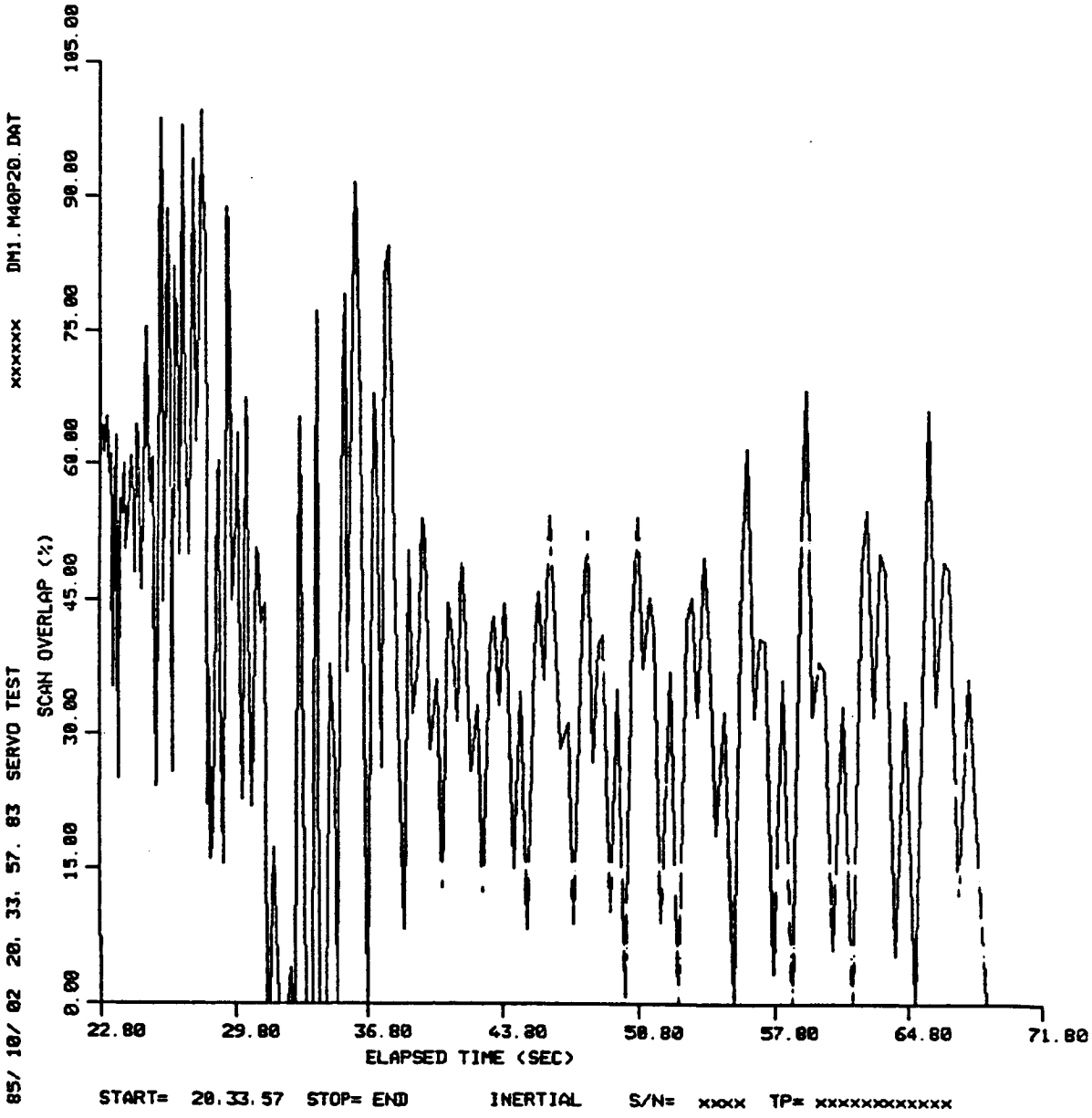
85/ 10/ 02 20. 33. 57. 83 SERVO TEST
xxxxxx DM1.M40P20.DAT
SCAN OVERLAP (%)
0.00
15.00
30.00
45.00
60.00
75.00
90.00
105.00
22.00
29.00
36.00
43.00
50.00
57.00
64.00
71.00
ELAPSED TIME (SEC)
START= 20.33.57 STOP= END INERTIAL S/N= xxxx TP= xxxxxxxxxxx

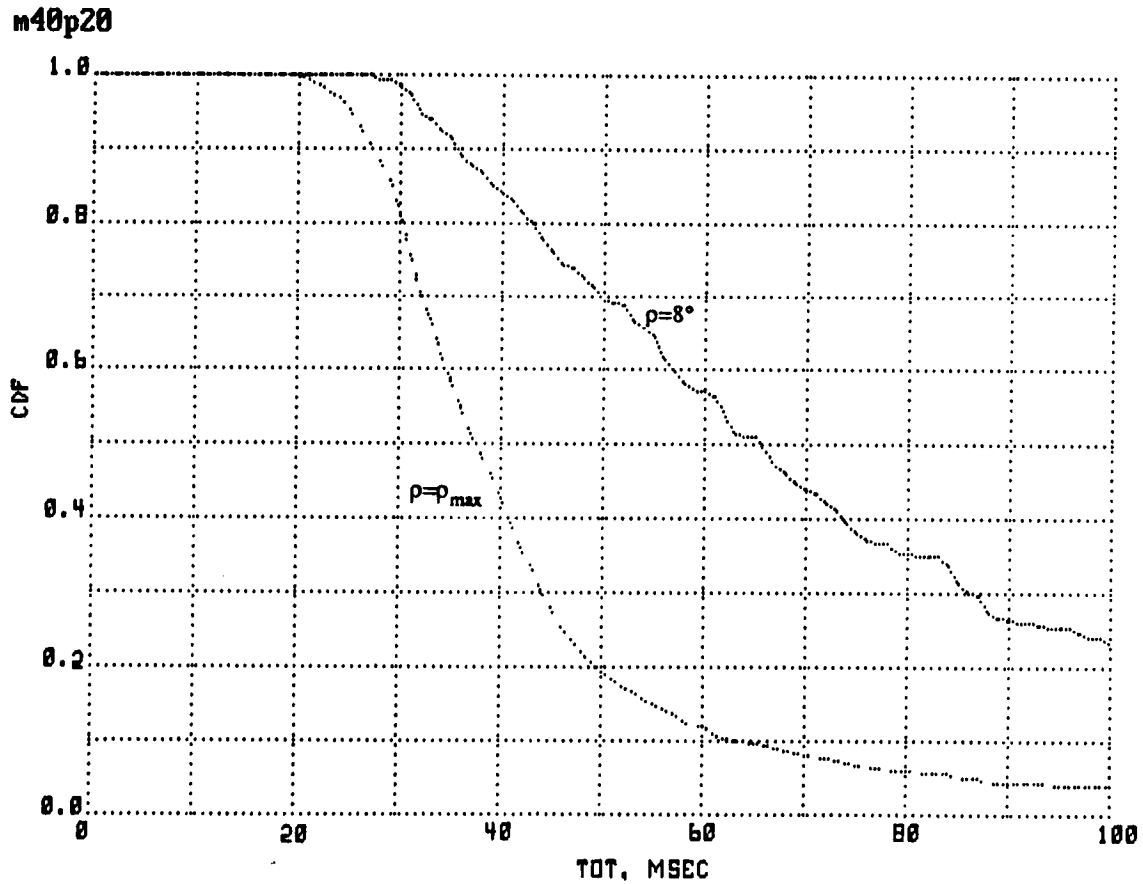
m40p20
1.0
0.8
0.6
0.4
0.2
0.0
CDF
ρ=8°
ρ=ρmax
0
20
40
60
80
100
TOT, MSEC

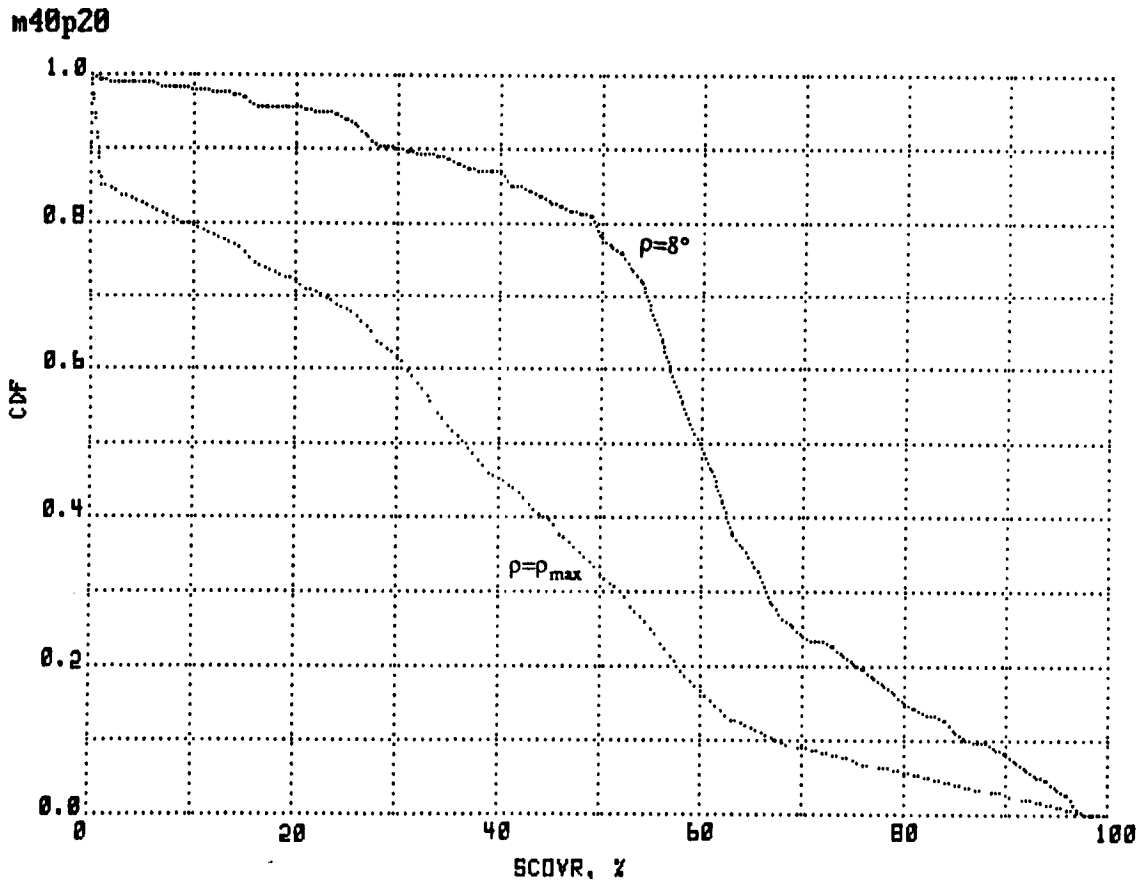
m40p20
1.0
0.8
0.6
0.4
0.2
0.0
CDF
ρ=8°
ρ=ρmax
0
20
40
60
80
100
SCOVR, %

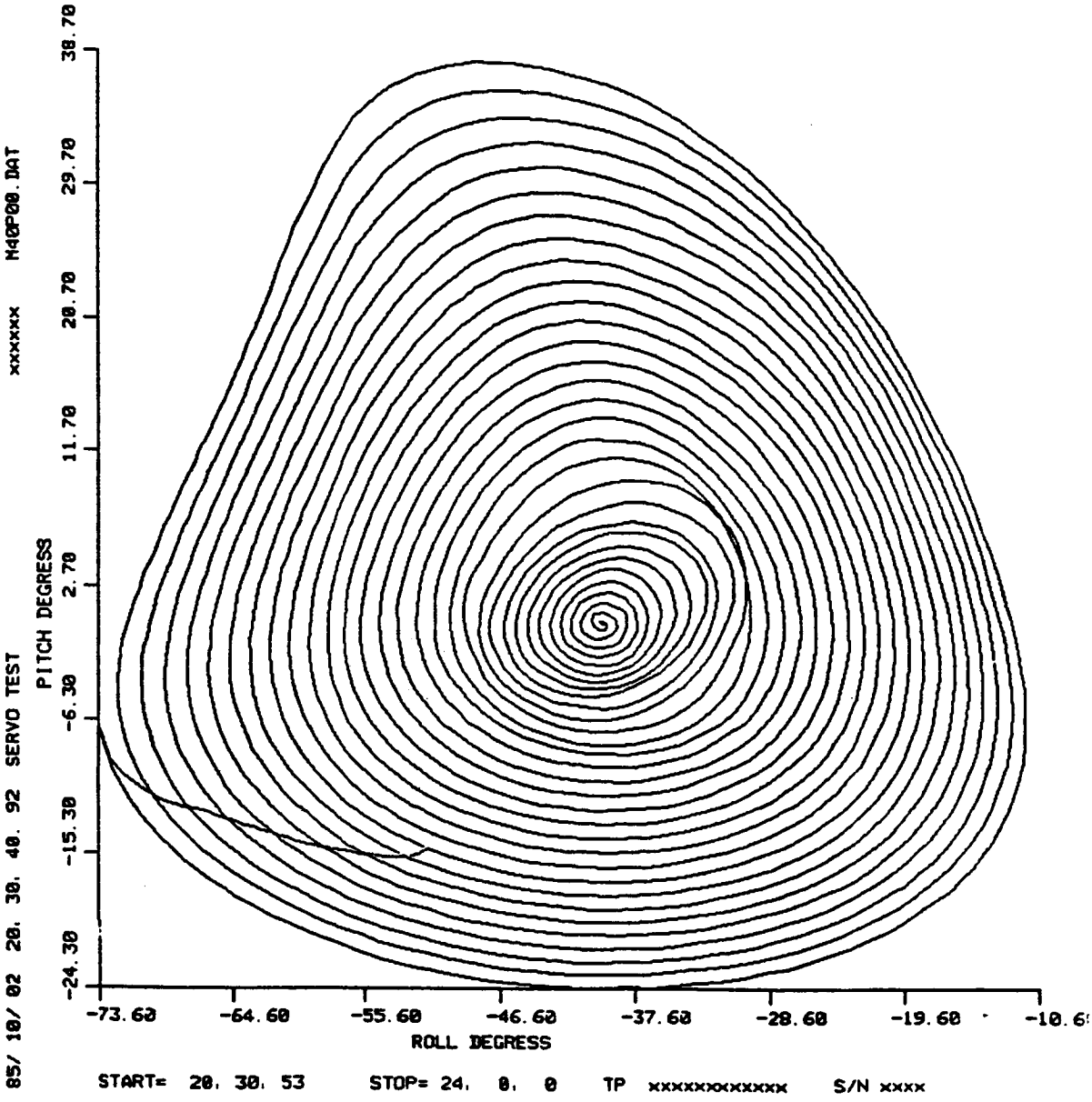
85/ 10/ 02 20. 30. 40. 92 SERVO TEST
xxxxxx M40P00.DAT
PITCH DEGRESS
38.70
29.70
20.70
11.70
2.70
-6.30
-15.30
-24.30
-73.60
-64.60
-55.60
-46.60
-37.60
-28.60
-19.60
-10.6
ROLL DEGRESS
START= 20. 30. 53 STOP= 24. 0. 0 TP xxxxxxxxxxx S/N xxxx

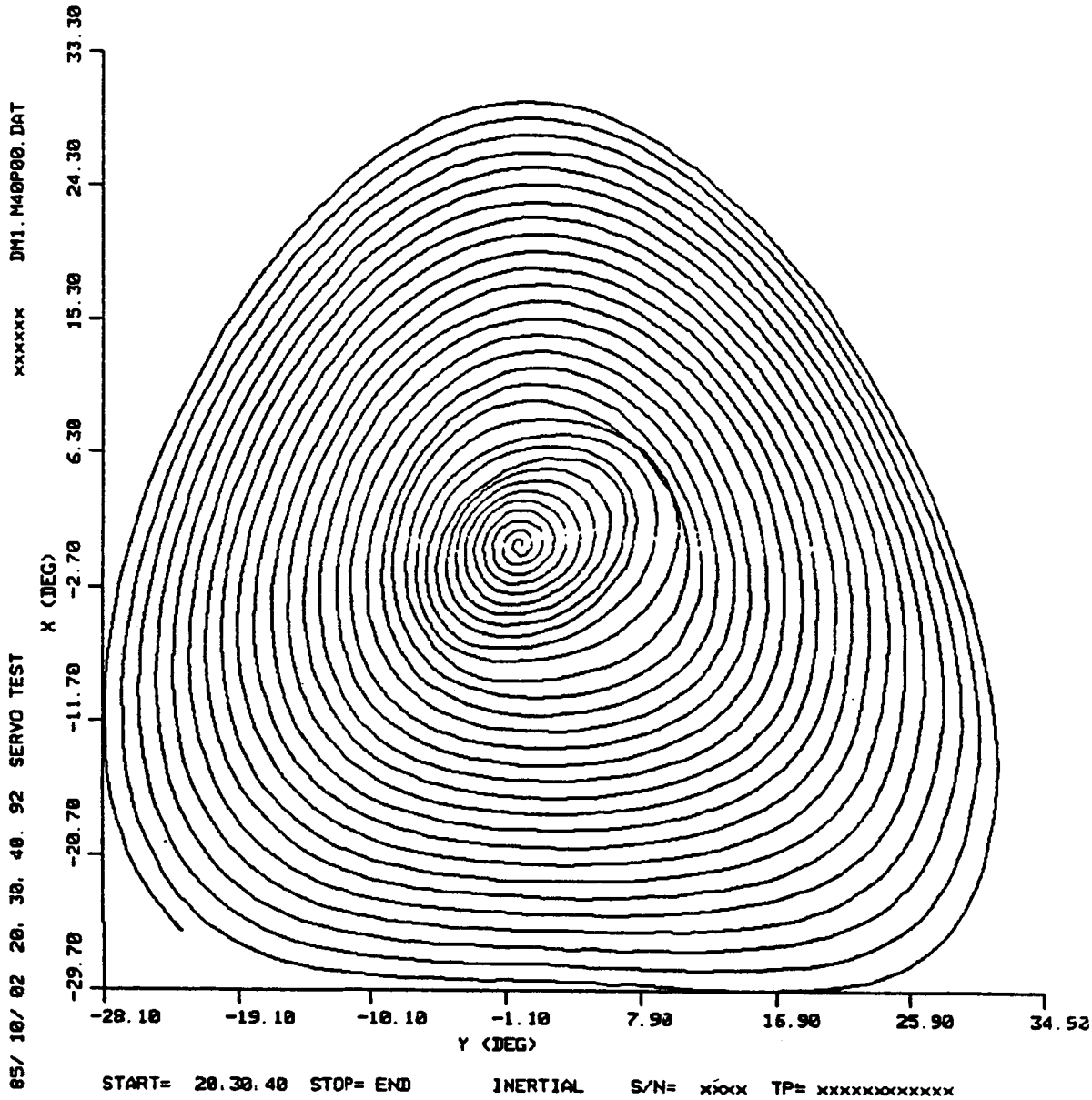
xxxxxx DM1.M40P00.DAT
X (DEG)
33.30
24.30
15.30
6.30
-2.70
-11.70
-20.70
-29.70
-28.10
-19.10
-10.10
-1.10
7.90
16.90
25.90
34.52
Y (DEG)
05/ 10/ 02 20. 30. 40. 92 SERVO TEST
START= 20.30.40 STOP= END
INERTIAL
S/N= xxxx TP= xxxxxxxxxxx

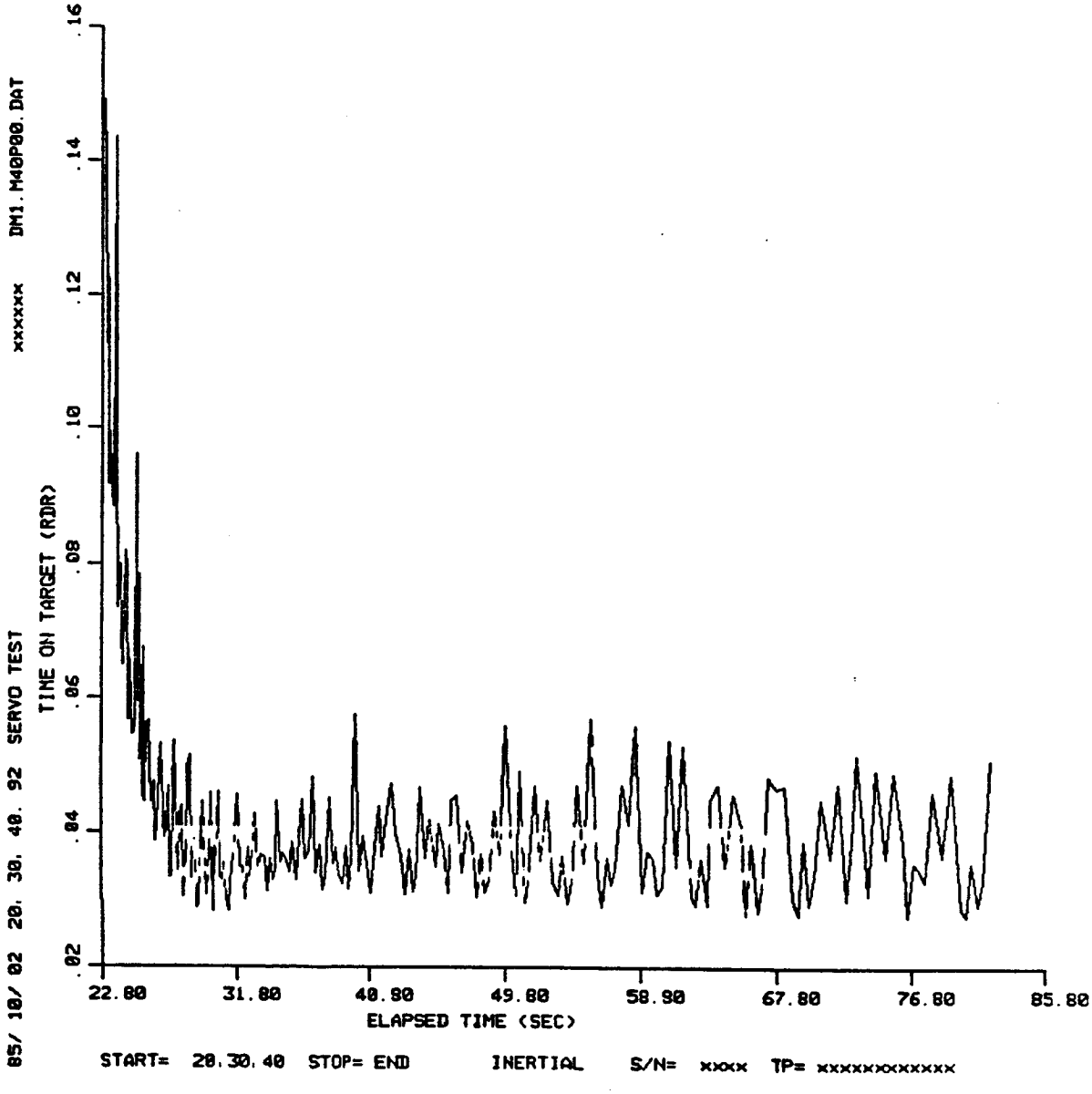
85/ 10/ 02 20. 30. 40. 92 SERVO TEST
xxxxxx DM1.M40P00.DAT
TIME ON TARGET (RDR)
.02
.04
.06
.08
.10
.12
.14
.16
22.80
31.80
40.80
49.80
58.90
67.80
76.80
85.80
ELAPSED TIME (SEC)
START= 20.30.40 STOP= END INERTIAL S/N= xxxx TP= xxxxxxxxxxx

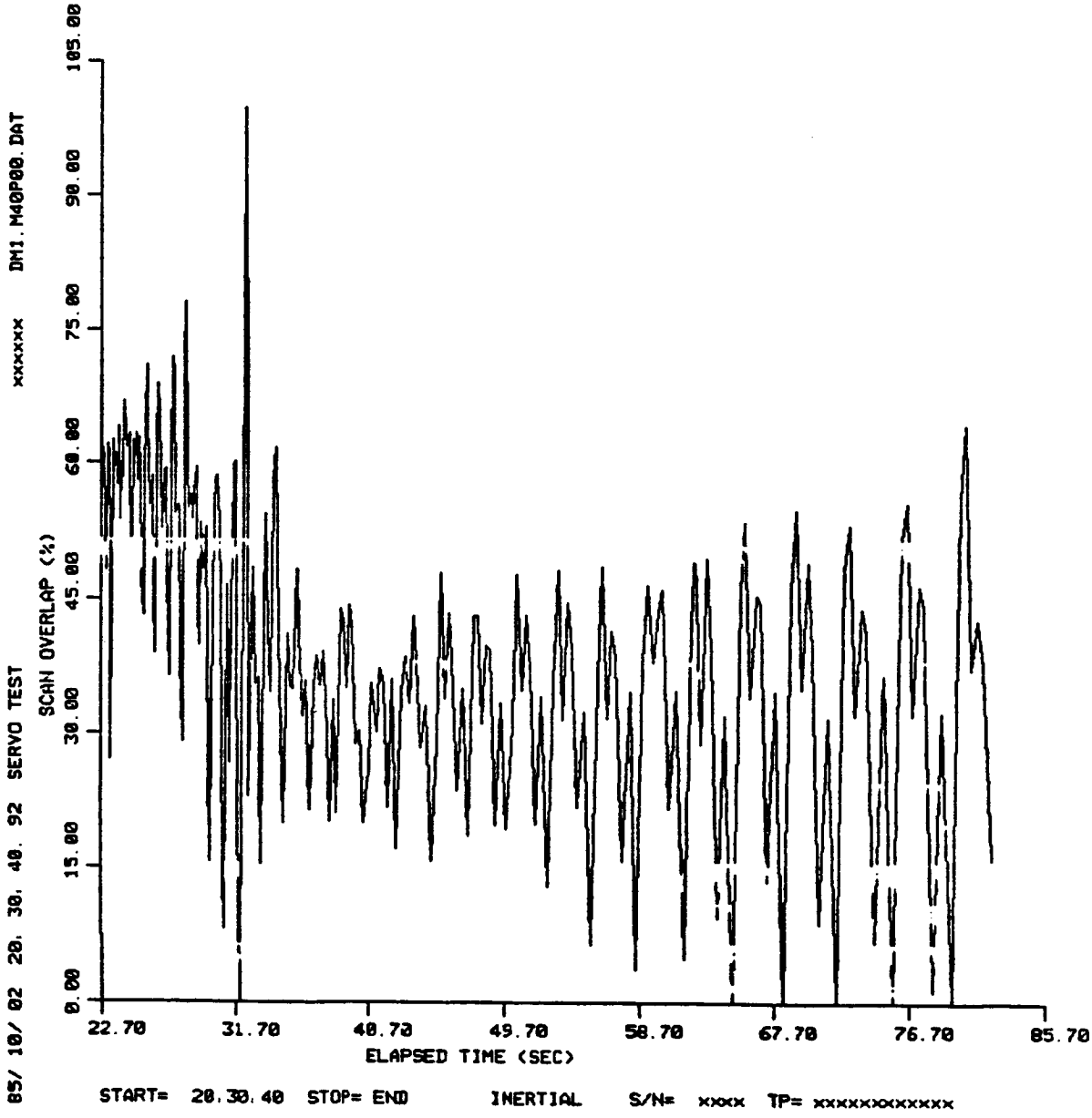
85/ 10/ 02 20. 30. 40. 92 SERVO TEST
xxxxxx DM1.M40P00.DAT
SCAN OVERLAP (%)
0.00
15.00
30.00
45.00
60.00
75.00
90.00
105.00
22.70
31.70
40.70
49.70
58.70
67.70
76.70
85.70
ELAPSED TIME (SEC)
START= 20.30.40 STOP= END INERTIAL S/N= xxxx TP= xxxxxxxxxxx

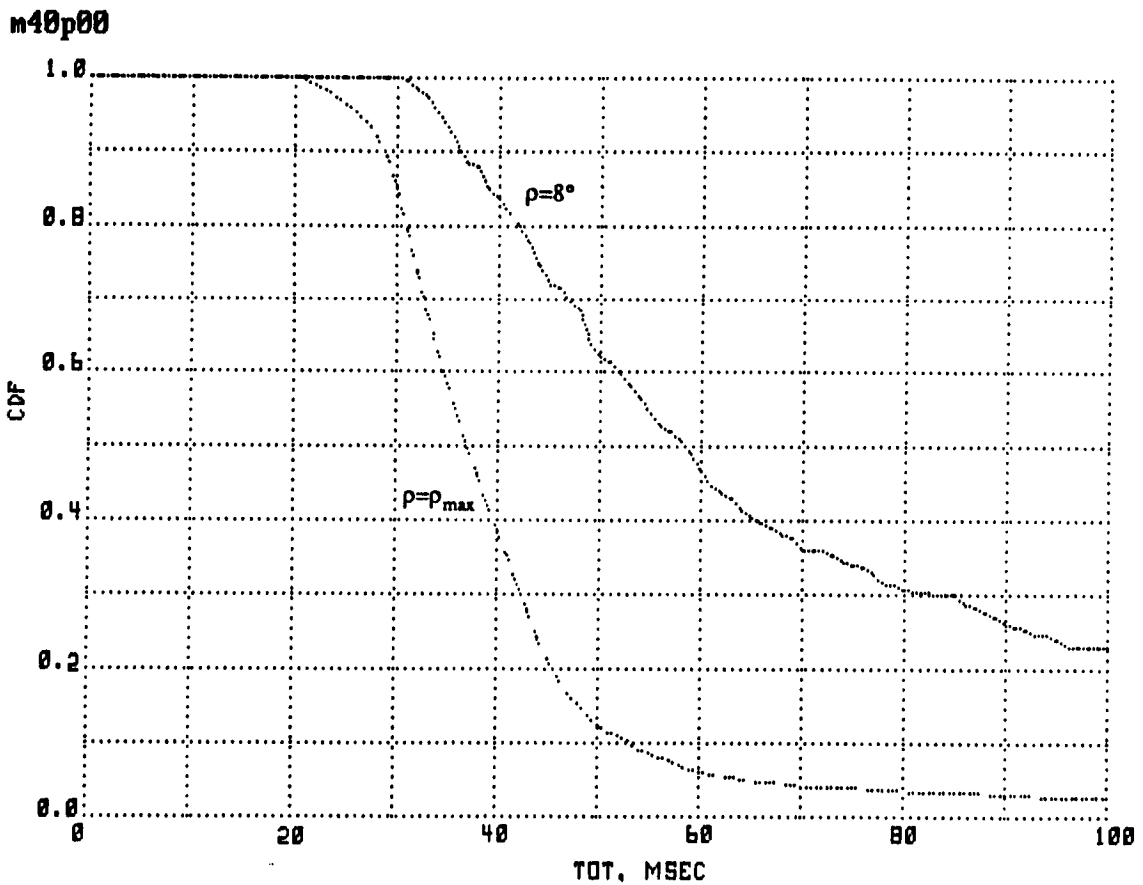
m40p00
1.0
0.8
0.6
0.4
0.2
0.0
CDF
ρ=8°
ρ=ρmax
0
20
40
60
80
100
TOT, MSEC

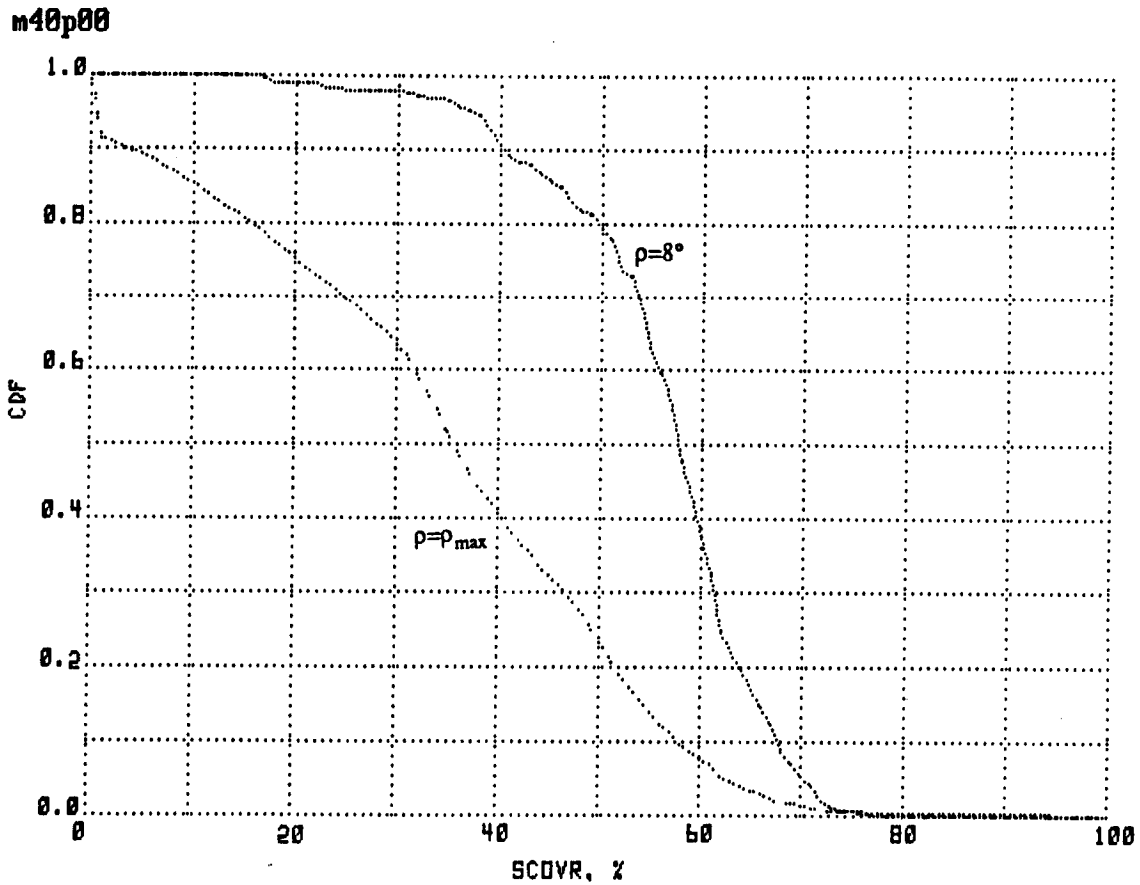
m40p00
1.0
0.8
0.6
0.4
0.2
0.0
CDF
0
20
40
60
80
100
SCOVR, %
ρ=8°
ρ=ρmax

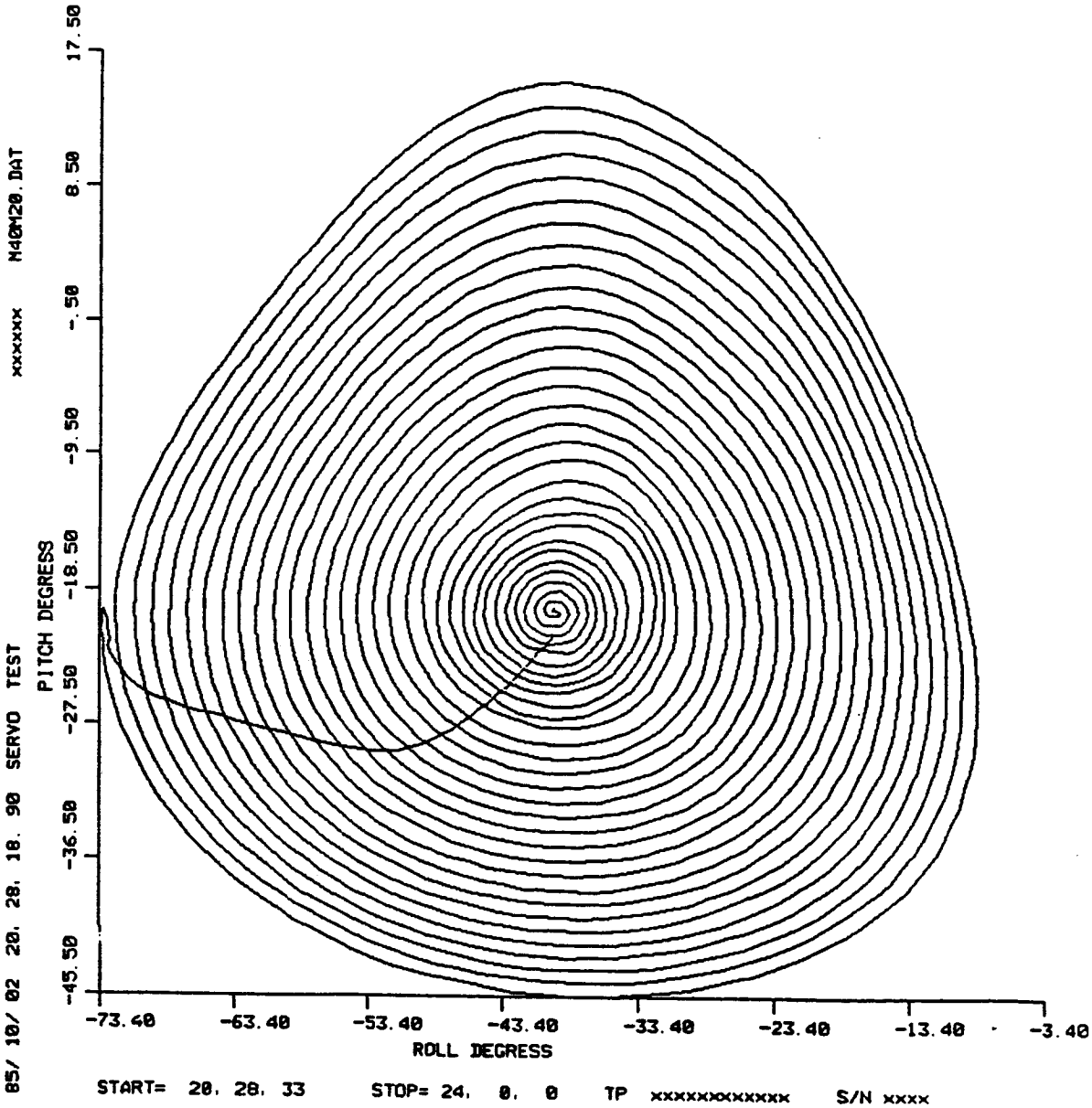
85/ 10/ 02 20. 28. 18. 90 SERVO TEST
xxxxxx N40M20.DAT
PITCH DEGRESS
17.50
8.50
-.50
-9.50
-18.50
-27.50
-36.50
-45.50
-73.40
-63.40
-53.40
-43.40
-33.40
-23.40
-13.40
-3.40
ROLL DEGRESS
START= 20. 28. 33
STOP= 24. 0. 0
TP xxxxxxxxxxx
S/N xxxx

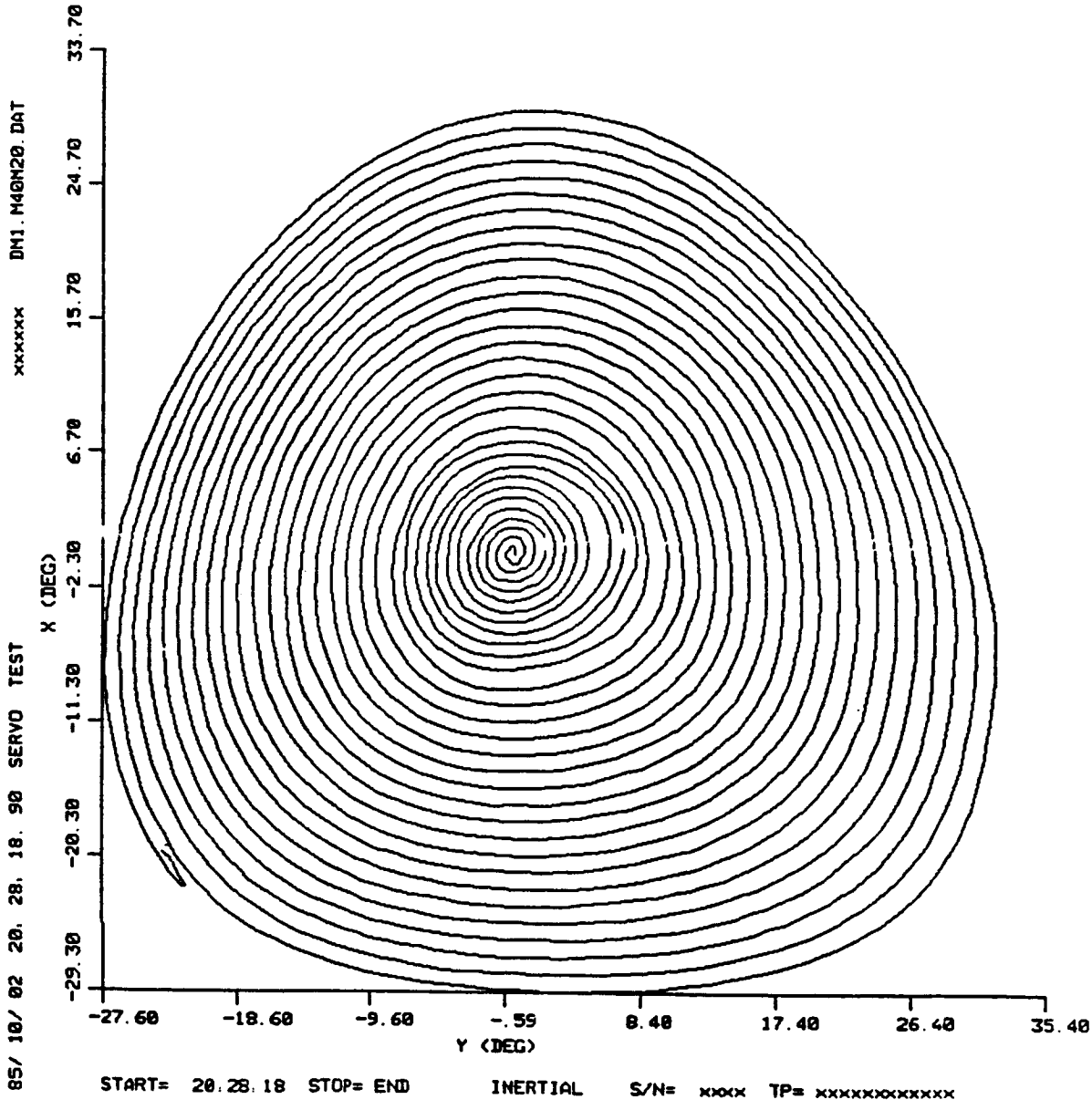
85/ 10/ 02 20. 28. 18. 90 SERVO TEST
xxxxxx DM1.M40N20.DAT
X (DEG)
33.70
24.70
15.70
6.70
-2.30
-11.30
-20.30
-29.30
-27.60
-18.60
-9.60
-.59
8.40
17.40
26.40
35.40
Y (DEG)
START= 20.28.18 STOP= END
INERTIAL
S/N= xxxx TP= xxxxxxxxxxx

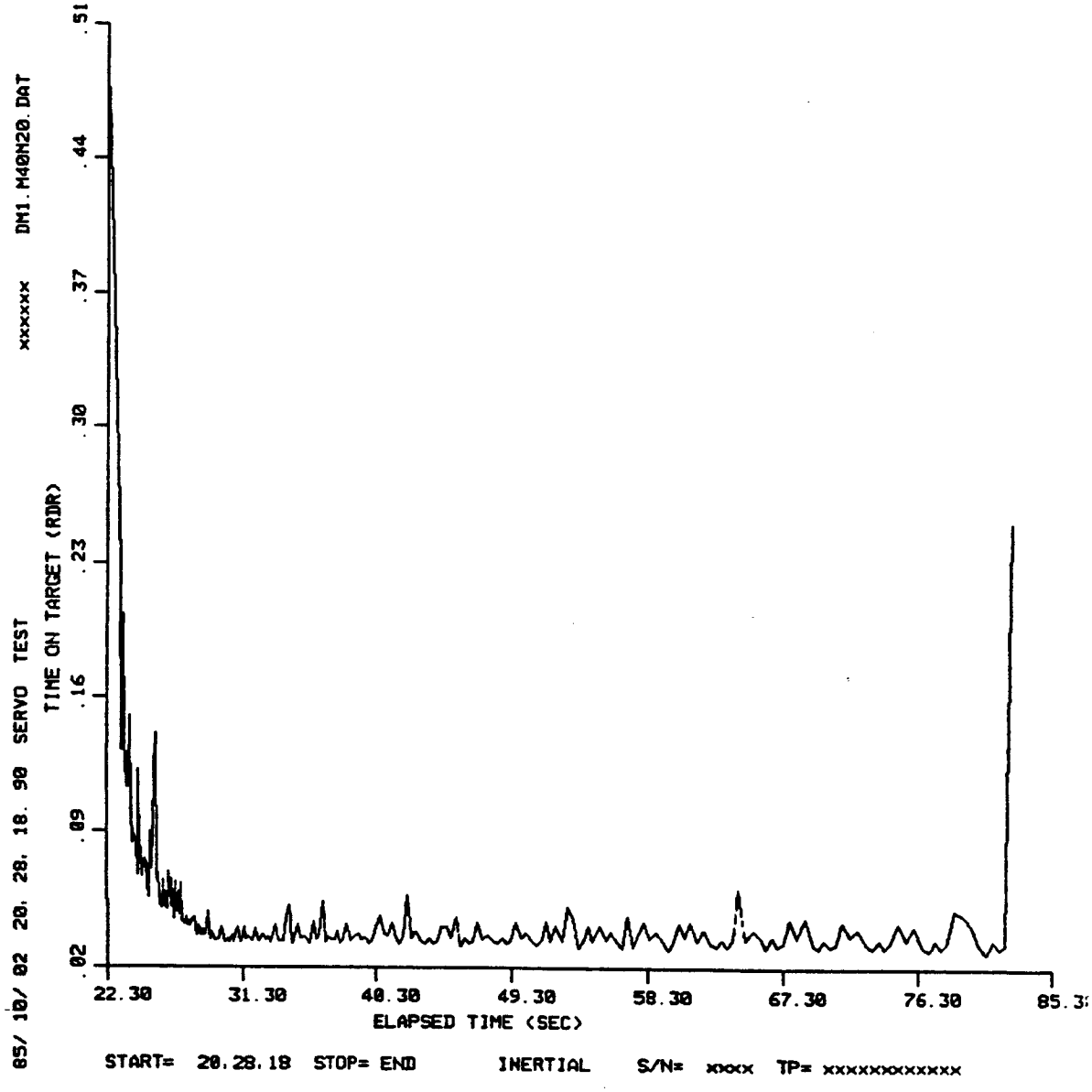
85/ 10/ 02 20. 28. 18. 90 SERVO TEST
xxxxxx DM1.M40M20.DAT
TIME ON TARGET (RDR)
.02
.09
.16
.23
.30
.37
.44
.51
22.30
31.30
40.30
49.30
58.30
67.30
76.30
85.3
ELAPSED TIME (SEC)
START= 20.28.18 STOP= END
INERTIAL
S/N= xxxx TP= xxxxxxxxxxx

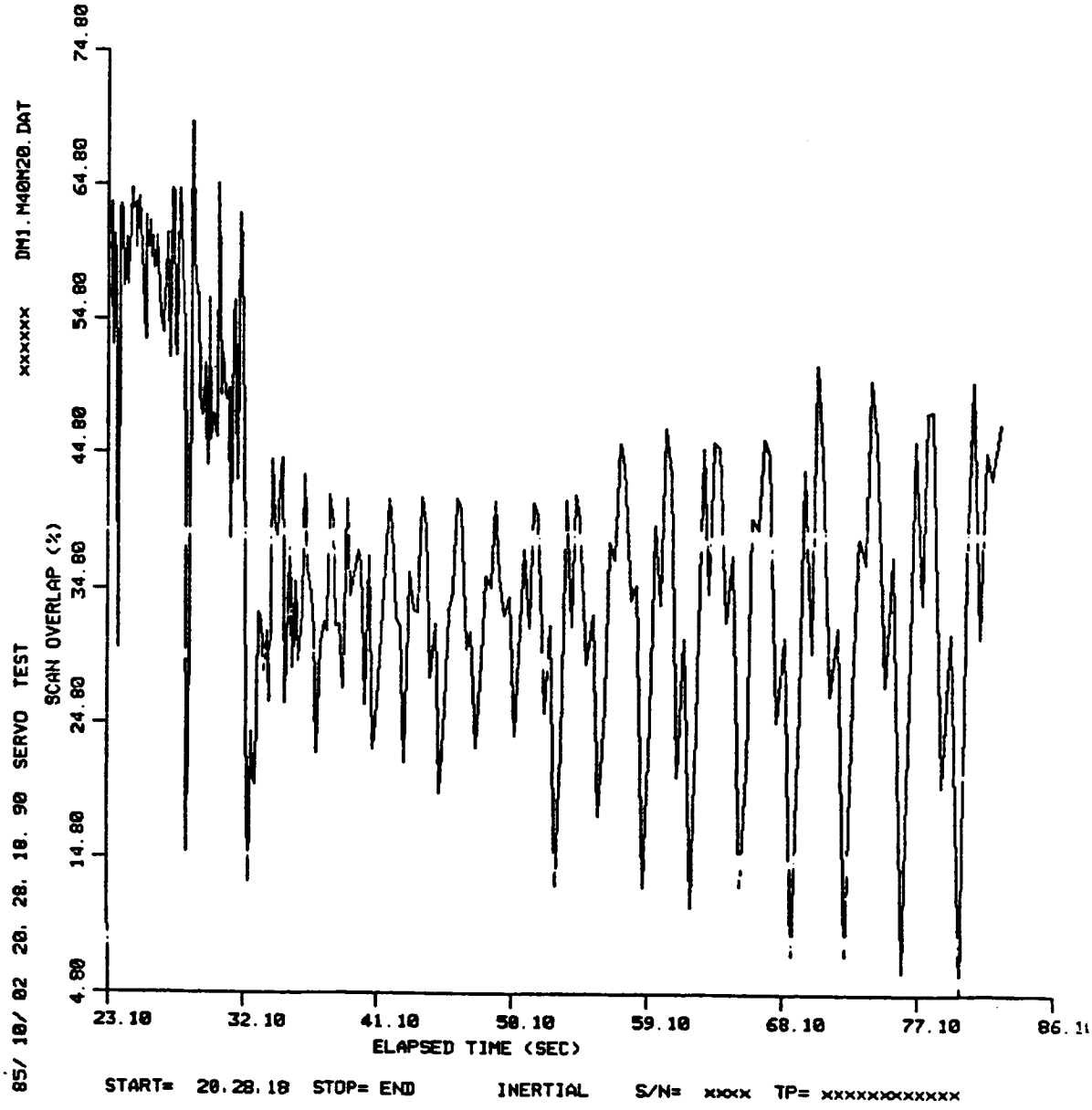
85/ 10/ 02 20. 28. 18. 90 SERVO TEST
xxxxxx DM1.M40N20.DAT
SCAN OVERLAP (%)
4.80
14.80
24.80
34.80
44.80
54.80
64.80
74.80
23.10
32.10
41.10
50.10
59.10
68.10
77.10
ELAPSED TIME (SEC)
START= 20.28.18 STOP= END INERTIAL S/N= xxxx TP= xxxxxxxxxxx

m40m20

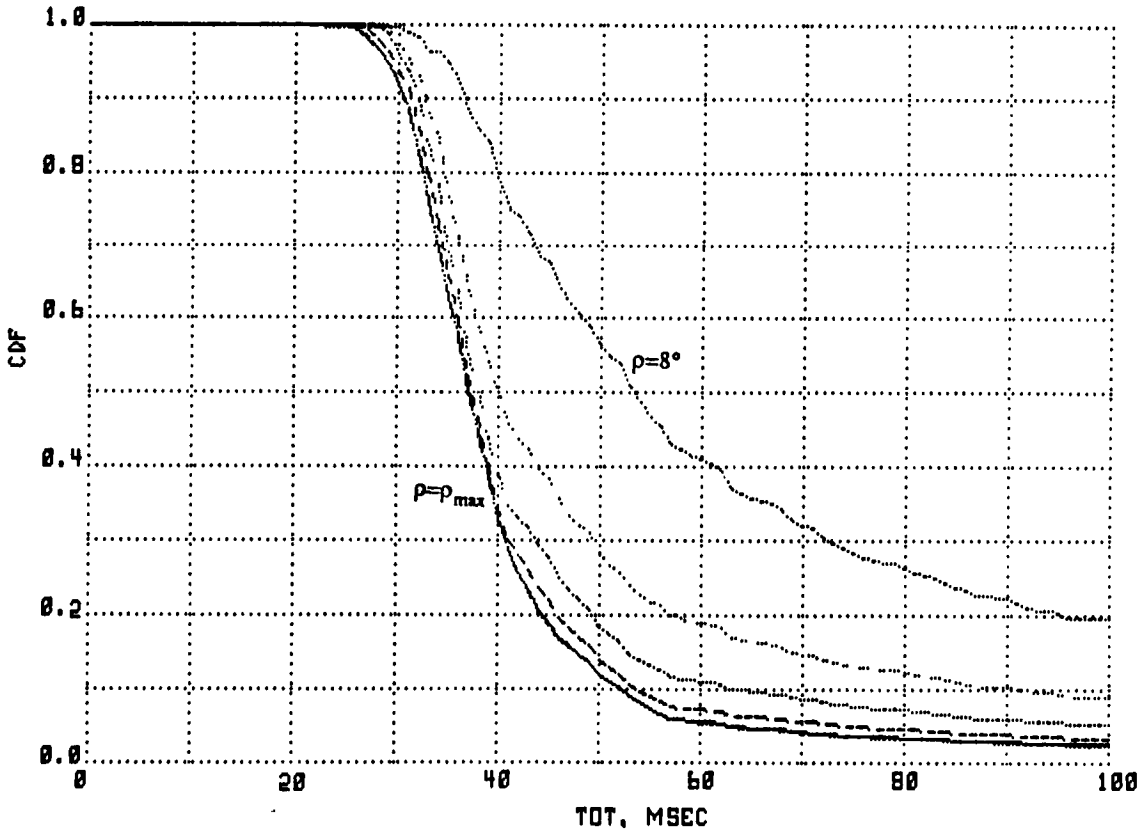

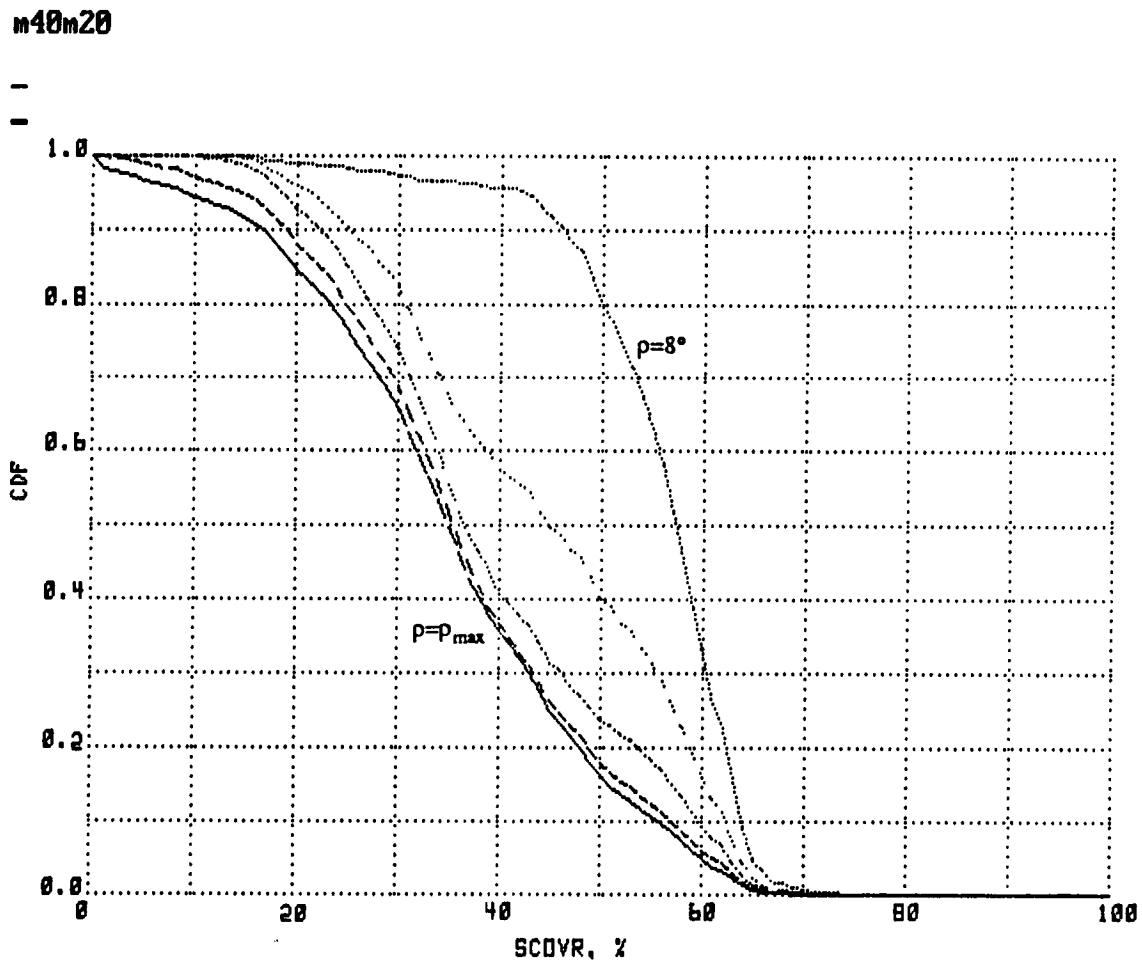
m40m20
1.0
0.8
0.6
0.4
0.2
0.0
CDF
ρ=8°
ρ=ρmax
0
20
40
60
80
100
SCOVR, %

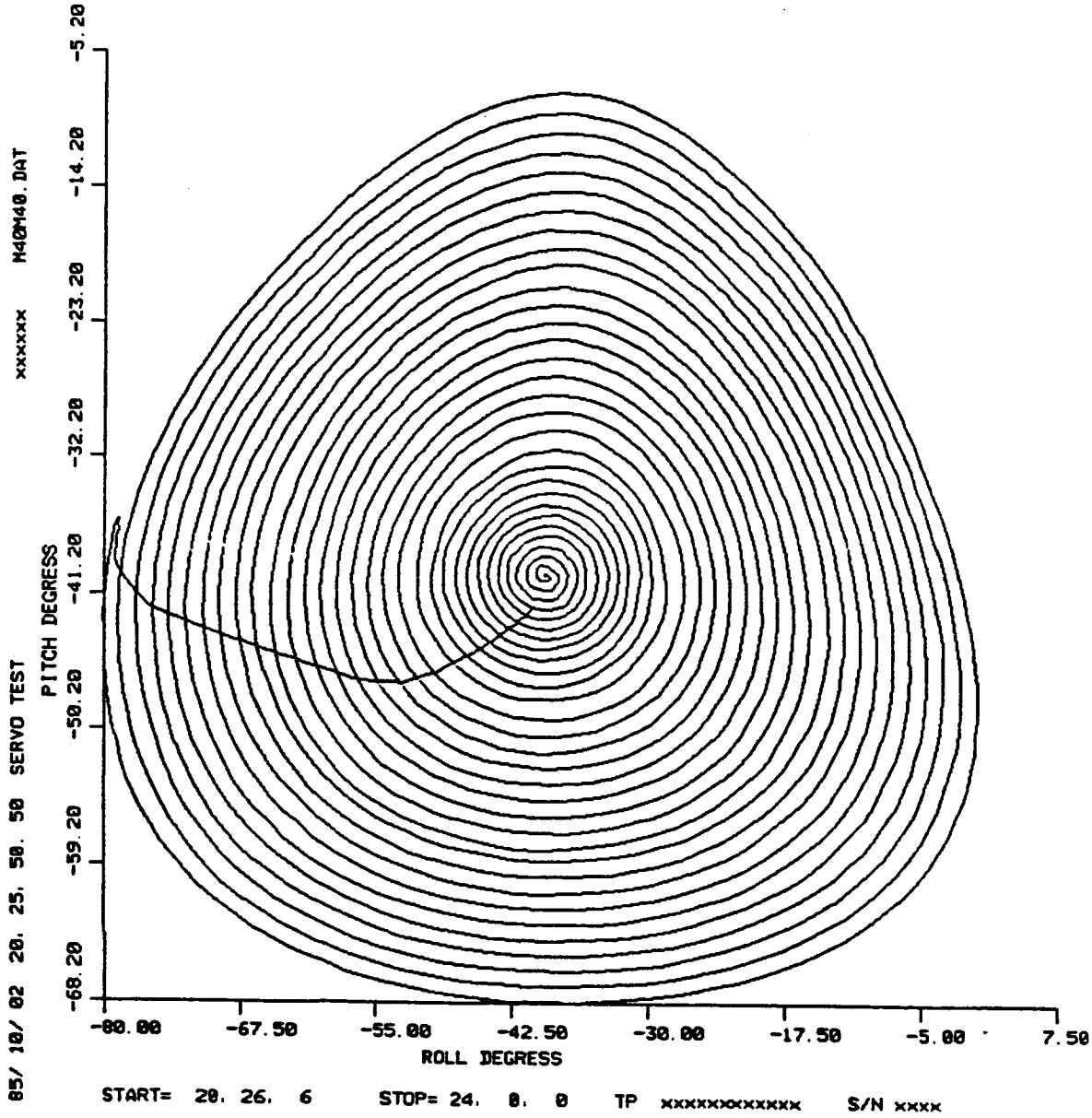
85/ 10/ 02 20. 25. 50. 50 SERVO TEST
xxxxxx N40N40.DAT
PITCH DEGRESS
-5.20
-14.20
-23.20
-32.20
-41.20
-50.20
-59.20
-68.20
-80.00
-67.50
-55.00
-42.50
-30.00
-17.50
-5.00
7.50
ROLL DEGRESS
START= 20. 26. 6
STOP= 24. 0. 0
TP xxxxxxxxxxx
S/N xxxx

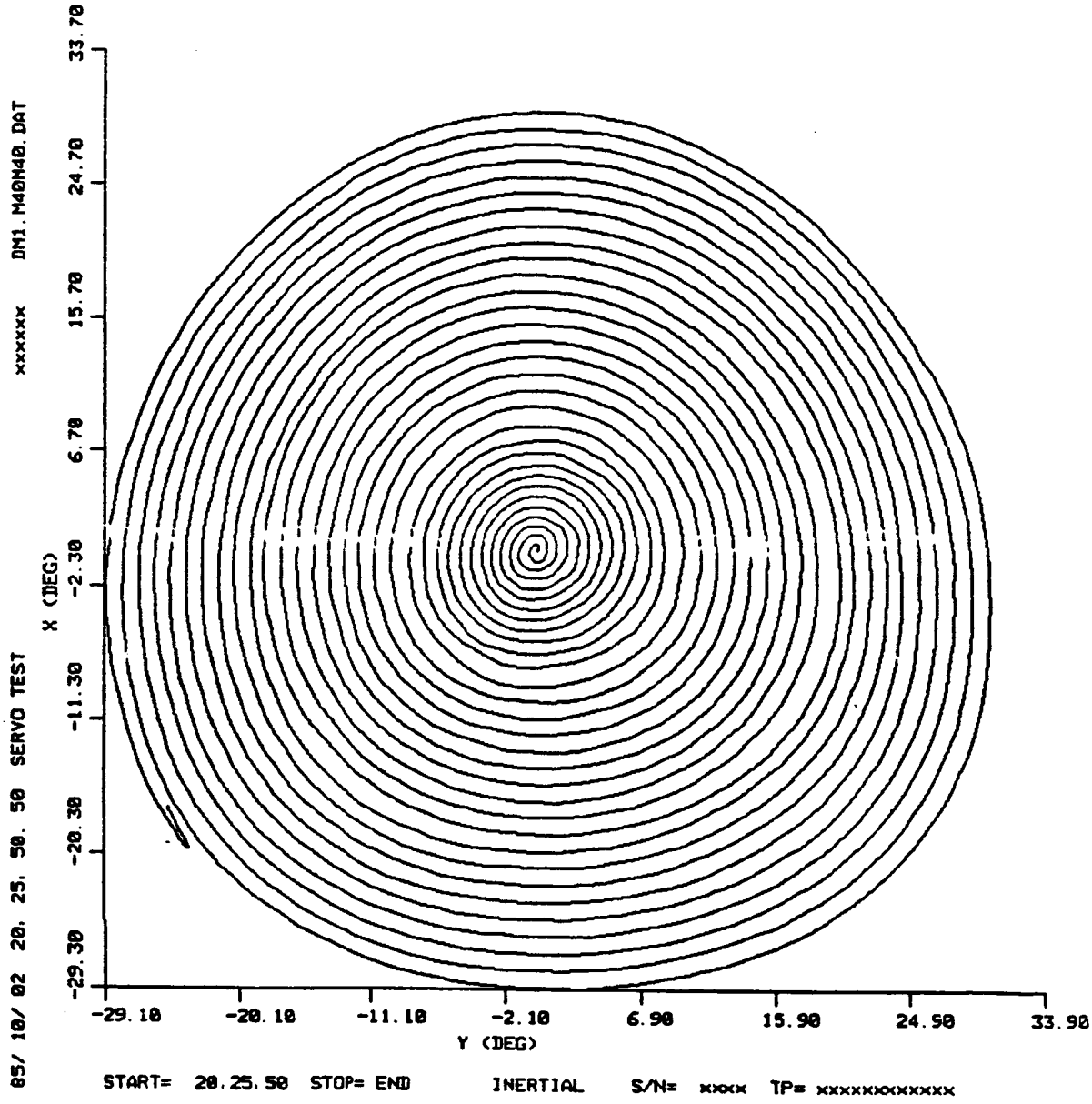
xxxxxx DM1.M40N40.DAT
X (DEG)
33.70
24.70
15.70
6.70
-2.30
-11.30
-20.30
-29.30
-29.10
-20.10
-11.10
-2.10
6.90
15.90
24.90
33.90
Y (DEG)
05/ 10/ 02 20. 25. 50. 50 SERVO TEST
START= 20.25.50 STOP= END
INERTIAL
S/N= xxxx TP= xxxxxxxxxxx

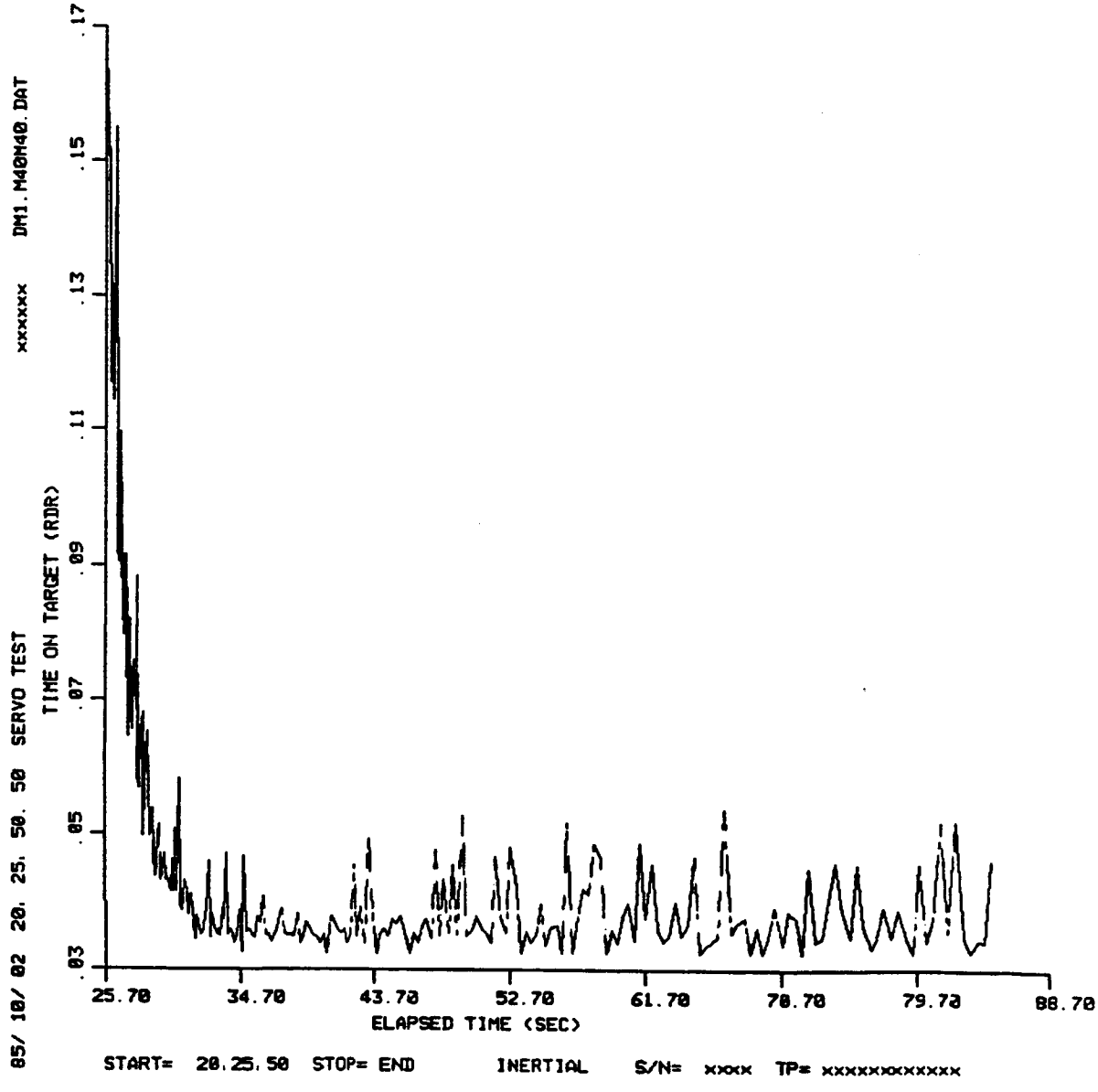
85/ 10/ 02 20. 25. 50. 50 SERVO TEST
xxxxxx DM1.M40N40.DAT
TIME ON TARGET (RDR)
.03
.05
.07
.09
.11
.13
.15
.17
25.70
34.70
43.70
52.70
61.70
70.70
79.70
88.70
ELAPSED TIME (SEC)
START= 20.25.50 STOP= END
INERTIAL
S/N= xxxx TP= xxxxxxxxxxx

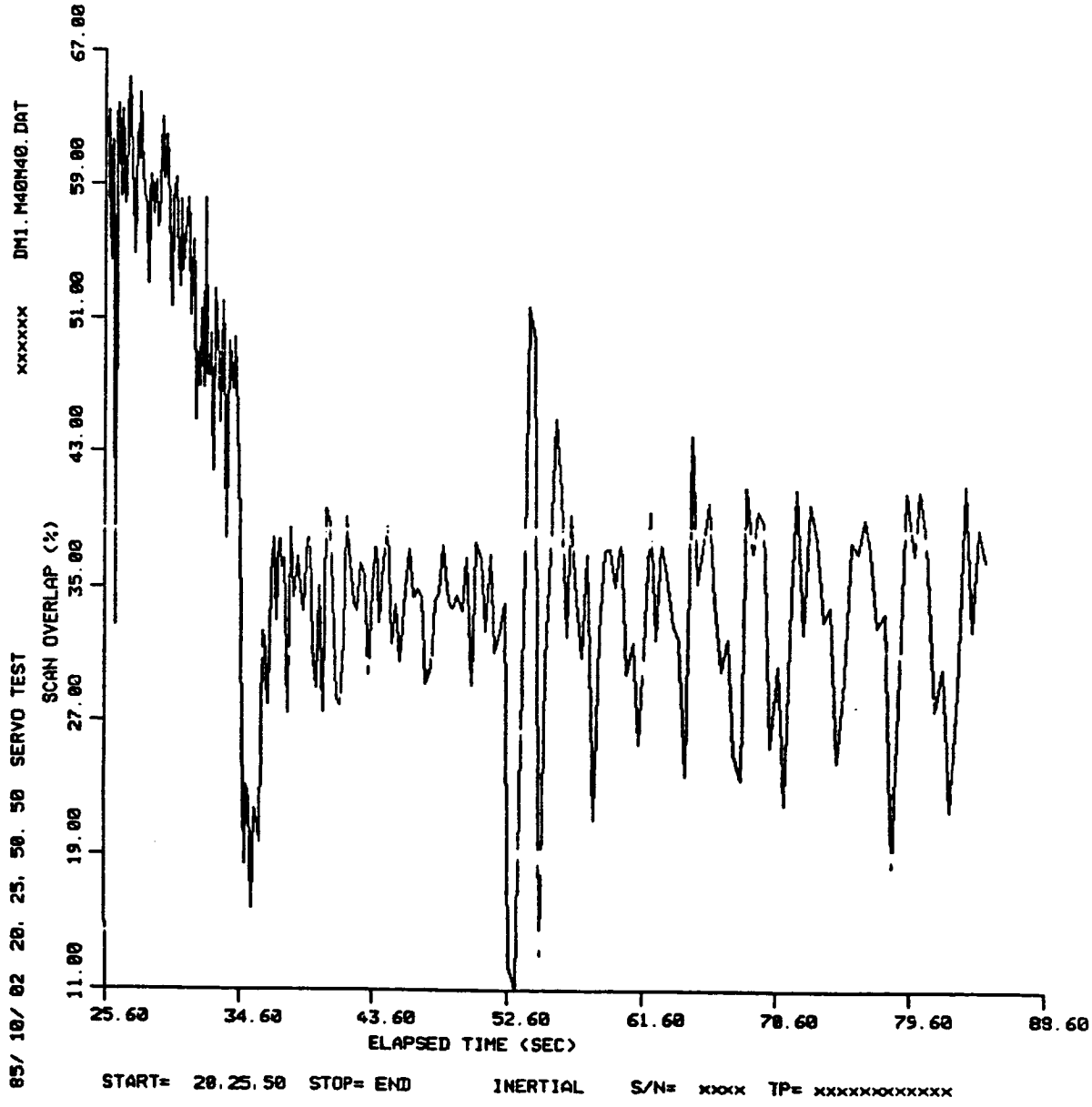
85/ 10/ 02 20. 25. 50. 50 SERVO TEST
SCAN OVERLAP (%)
xxxxxx DM1.M40N40.DAT
67.00
59.00
51.00
43.00
35.00
27.00
19.00
11.00
25.60
34.60
43.60
52.60
61.60
70.60
79.60
88.60
ELAPSED TIME (SEC)
START= 20.25.50 STOP= END
INERTIAL
S/N= xxxx TP= xxxxxxxxxxx

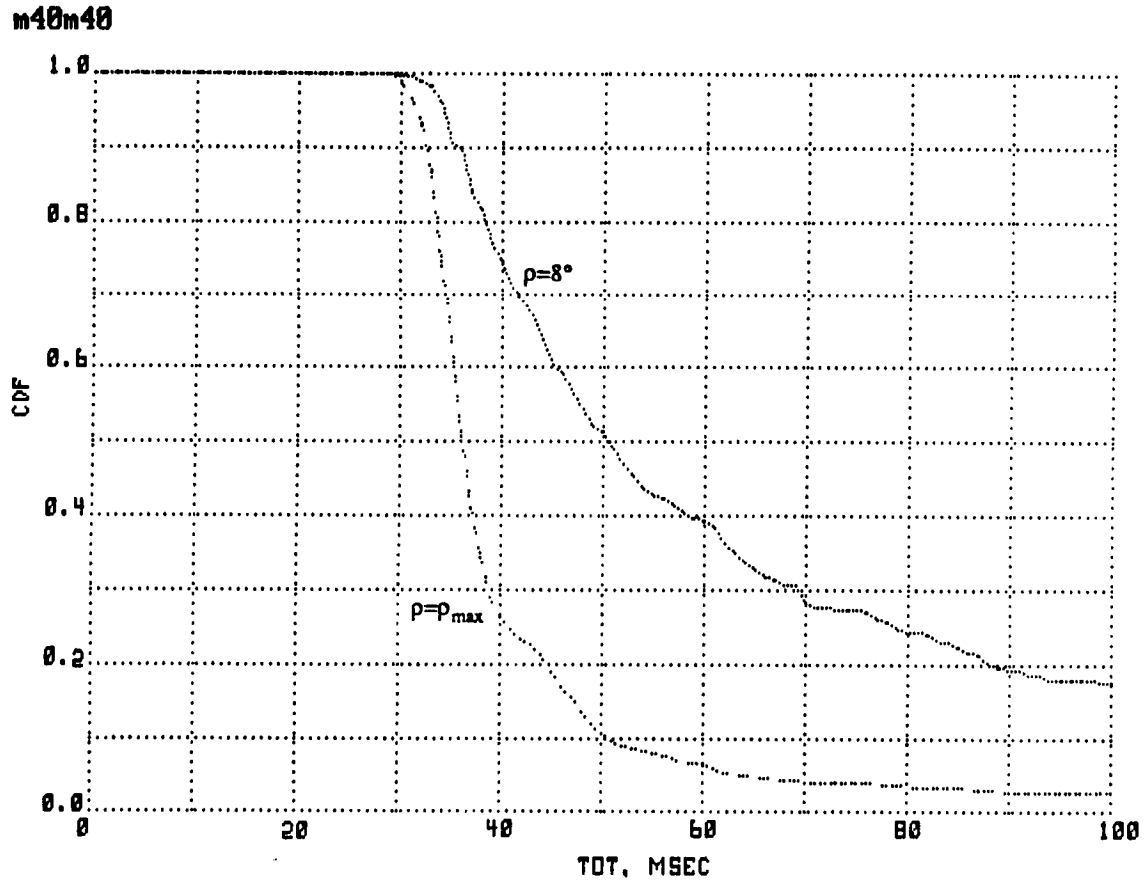
m40m40
1.0
0.8
0.6
0.4
0.2
0.0
CDF
ρ=8°
ρ=ρmax
0
20
40
60
80
100
TOT, MSEC

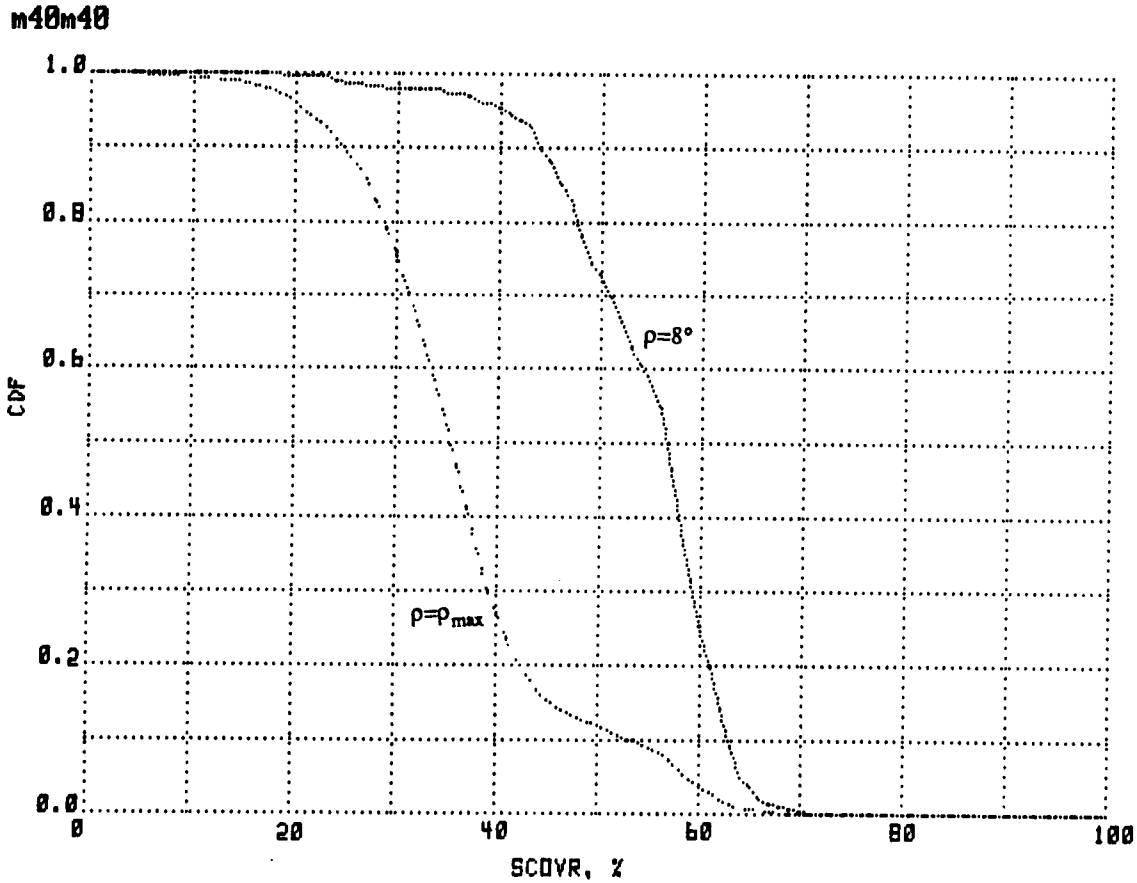
m40m40
1.0
0.8
0.6
0.4
0.2
0.0
CDF
ρ=8°
ρ=ρmax
0
20
40
60
80
100
SCOVR, %

917 m40m60

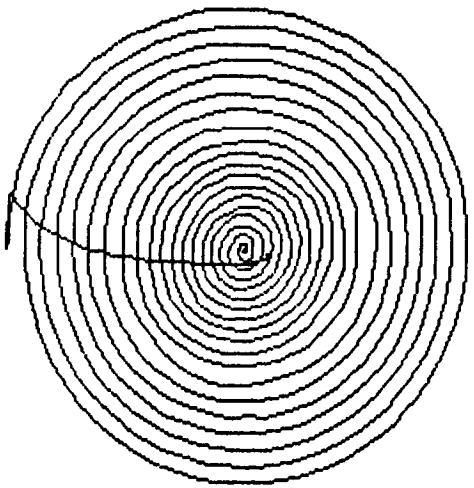

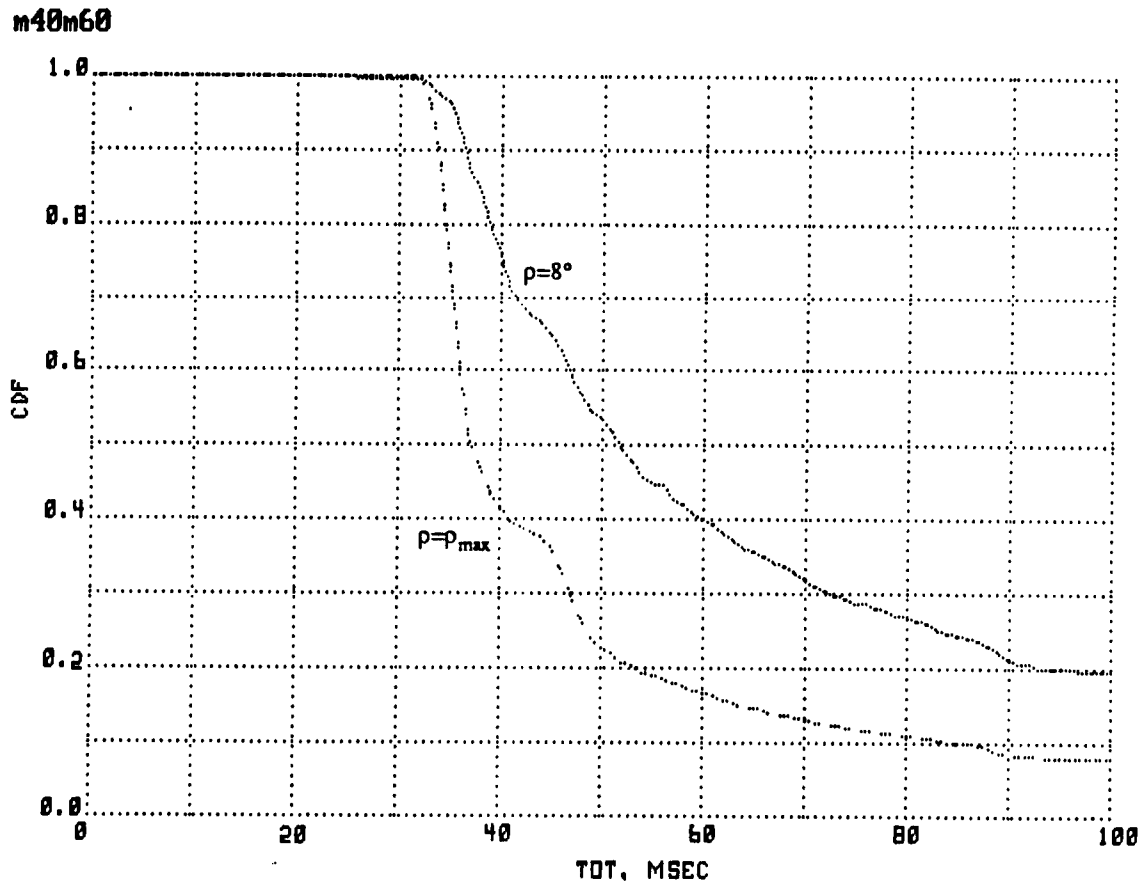
m40m60
1.0
0.8
0.6
0.4
0.2
0.0
CDF
ρ=8°
ρ=ρmax
0
20
40
60
80
100
TOT, MSEC

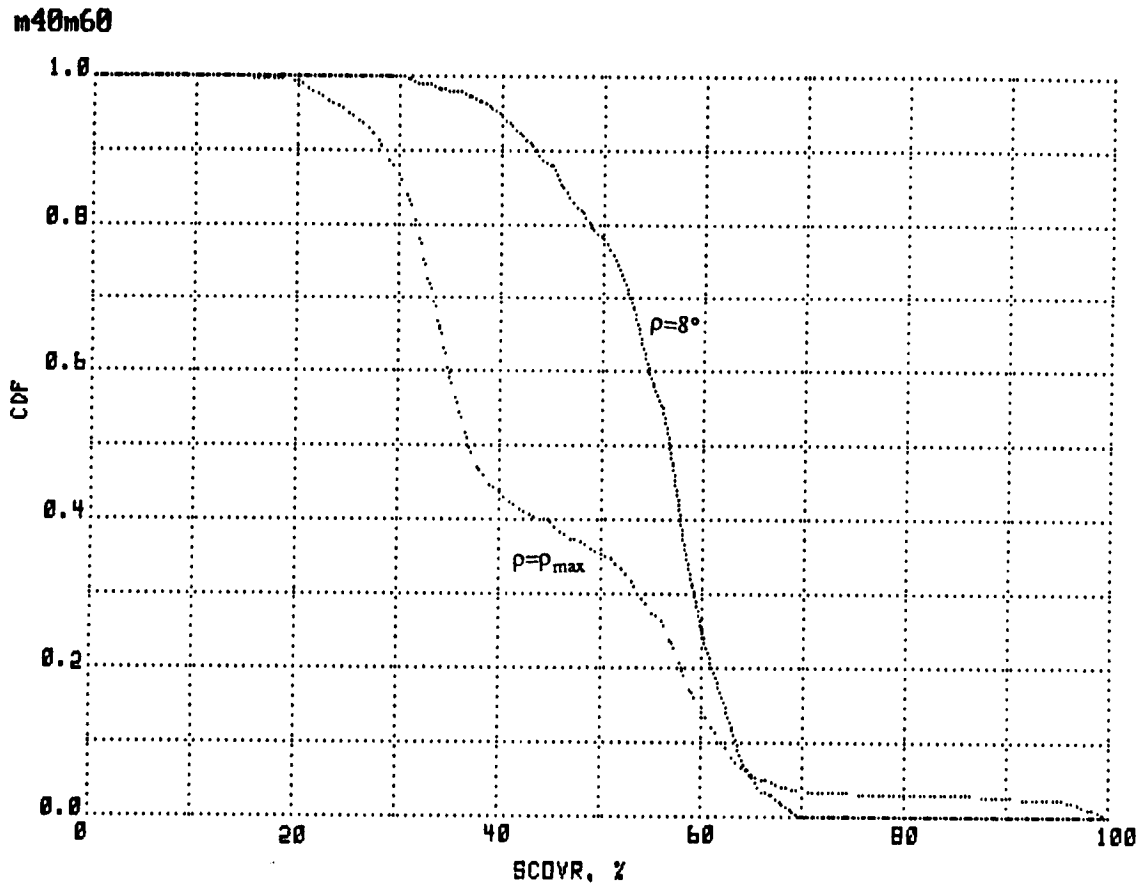
m40m60
1.0
0.8
0.6
0.4
0.2
0.0
CDF
ρ=8°
ρ=ρmax
0
20
40
60
80
100
SCOVR, %

APPENDIX E

RADAR CROSS SECTION OF A TETHER

Axiomatix

9841 Airport Boulevard • Suite 912 • Los Angeles, California 90045 • Phone (213) 641-8600

TO: JIM DODDS

FROM: CHUCK WEBER

SUBJECT: RADAR CROSS-SECTION OF A TETHER

DATE: January 30, 1985

SUMMARY

It is concluded that the tether does not significantly effect the capability of the the Ku-band radar to track the tethered satellite.

The only situation in which the tether has a significant radar cross section (RCS) is when a significant length of tether is perfectly straight and at a normal incidence ($\theta = 90°$) to the boresight axis of the mainbeam. This is a most unlikely event.

EVALUATION OF THE EFFECT OF THE TETHER

The effect that the tether has on the satellite, with RCS of $\sigma \approx 1m^2$, is determined by deciding the worst case scenario, and showing that all other situations are negligible.

We assume that the tether is a perfectly conducting wire which is many wavelengths long, but only a fraction of a wavelength thick.

In the computation below, the radius a is set at

$$a = .2 \text{ cm} = .002 \text{ m}$$

at 15 GHz, the wavelength λ is

$$\lambda = 2 \text{ cm} = .02 \text{ m}$$

---

1. J.W. Crispin, Jr. and K.M. Siegel, "Methods of Radar Cross-Section Analysis", Academic Press, New York, 1968, p. 107.

In addition, we examine a length of tether L = 1,000 m. long. Therefore, the above assumptions are satisfied. A distance of L = 1,000 m. is used since that is approximately the length of the tether that can be exposed at normal incidence (θ=90° in Figure 1) by the mainbeam of the Ku-band (λ=.02m) at 20nmi, (θ_β=3 dB beamwidth 1.6°).

If the actual tether is not perfectly conducting, its RCS will be less than those determined here.

Given the above assumption, an expression for the RCS of a long perfectly conducting wire, which is in good agreement with the experiment, is Chu's formula (1)

$$\sigma = \frac{\pi L^2 \sin^2\theta \left\{ \frac{\sin\left[\frac{2\pi L \cos\theta}{\lambda}\right]}{\left[\frac{2\pi L \cos\theta}{\lambda}\right]} \right\}^2 \cos^4\phi}{\left(\frac{\pi}{2}\right)^2 + \left[\ell n\left(\frac{\lambda}{\gamma\pi\, a \sin\theta}\right)\right]^2}$$

where the wire is assumed straight, ϕ is the angle between the polarization direction and the plane formed by the wire and the direction of incidence, and γ = 1.78. The other variables are as defined above. We set ϕ = 0°, as that is clearly the worst case.

RESULTS

Chu's formula was evaluated as a function of the incidence angle θ at L = 1,000 m., λ = .02m., a = 2 mm, and ϕ =0. This adequately upper bounds the RCS that can be anticipated from the tether. The results shown in Figure 2, where the reflected (monostatic radar) tether RCS is plotted in $dB/(meter)^2$. The wild variation would smooth out, if the computation were averaged overall 5 Ku-band RF's. It would smooth out more so it a variety of lengths were also averaged. The general shape of the curve would remain unchanged, however. As the relative angle,θ, increases and the wire approaches normal incidence, there is a gradual increase in σ. Note however, that θ must be greater than$\approx$89°, before there is a real problem. (The scale between 89° and 90° is expanded). It is most unlikely that a length of tether will be exactly normally incident(within 1°, Or $89° \leqslant \theta \leqslant 90°$), at any time, and therefore, this event is not considered a problem.

At all angles below 89°, the upper bound on the reflected tether RCS, and therefore, the reflected tether RCS itself is very small, and will not hinder the acquistion and tracking of the tether satellite.

CW:dd

cc: Alice Lewton, JSC

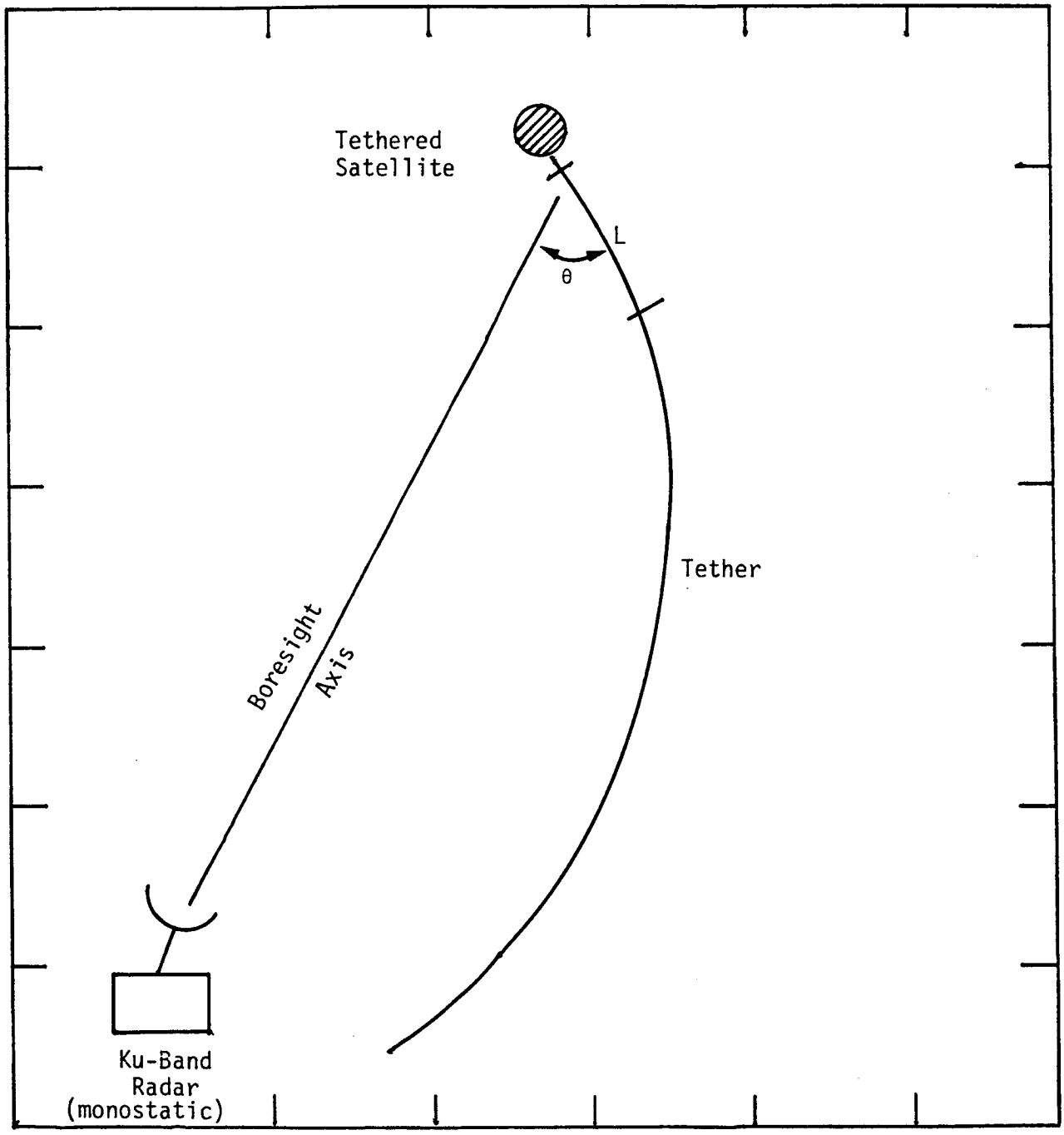

Figure 1. Specification of θ for Determining RCS of the Tether

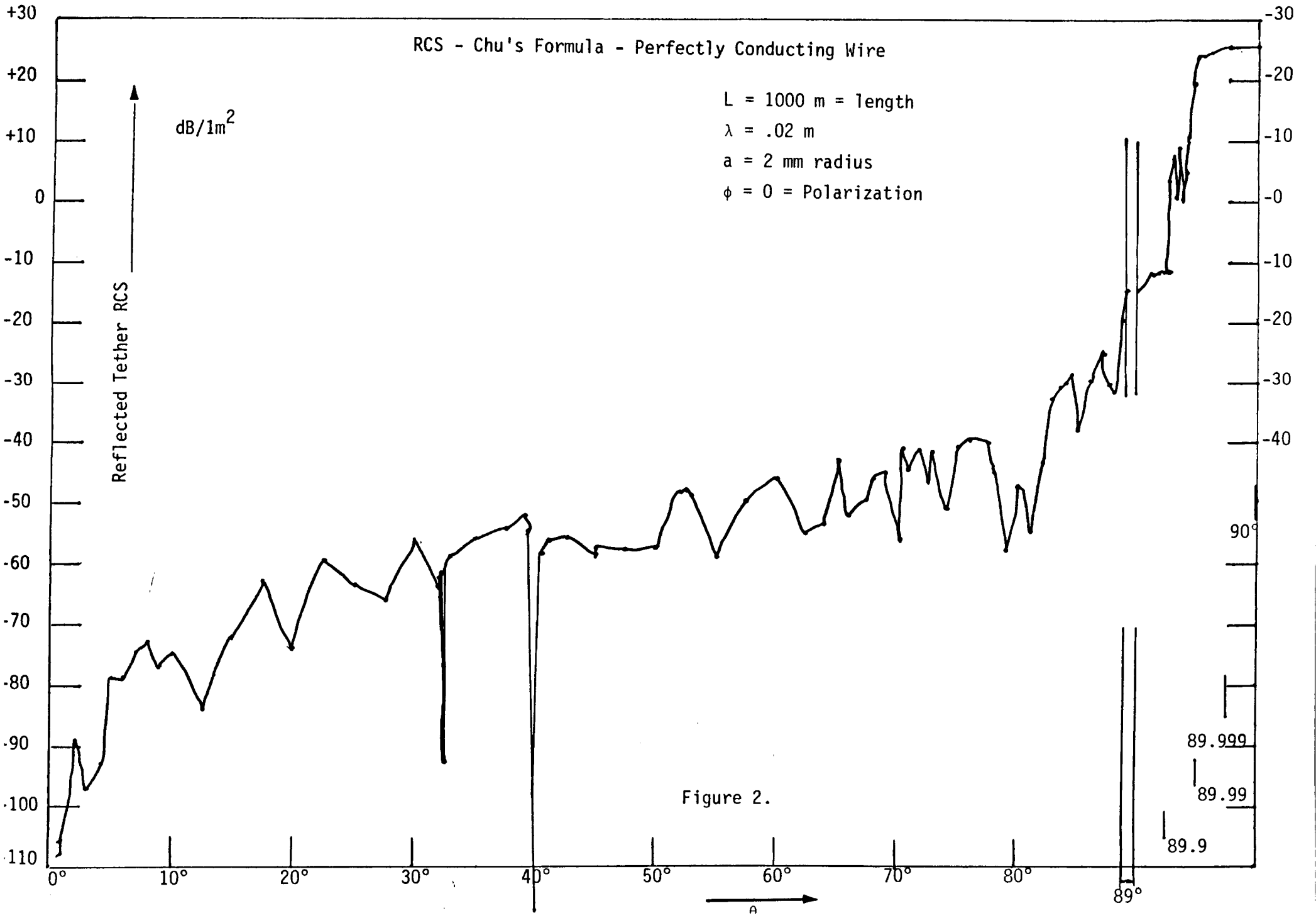
RCS - Chu's Formula - Perfectly Conducting Wire
L = 1000 m = length
λ = .02 m
a = 2 mm radius
ϕ = 0 = Polarization
dB/1m²
Reflected Tether RCS
+30
+20
+10
0
-10
-20
-30
-40
-50
-60
-70
-80
-90
-100
-110
0°
10°
20°
30°
40°
50°
60°
70°
80°
89°
90°
89.999
89.99
89.9
θ

Figure 2.